PATHOGENESIS OF ANTI-HIV DRUG (TENOFOVIR) INDUCED RENAL DAMAGE: POSSIBLE ROLES OF OXIDATIVE STRESS, NITROSATIVE STRESS AND NF-κB PATHWAY

A THESIS TO BE SUBMITTED TO

THE TAMILNADU DR. M.G.R MEDICAL UNIVERSITY, CHENNAI

FOR THE DEGREE OF
DOCTOR OF PHILOSOPHY

By

R.HEMALATHA

Department Of Biochemistry

Christian Medical College

Vellore 632 002, Tamil Nadu, India

OCTOBER 2013

INSTITUTIONAL ANIMAL ETHICS COMMITTEE
CHRISTIAN MEDICAL COLLEGE, VELLORE. INDIA

Dr. Alfred Job Daniel
Principal & Chairman

Dr. Solomon Sathishkumar
Secretary

July 25th 2013

TO WHOMSOEVER IT MAY CONCERN

This is to certify that the animal studies done by **R. HEMALATHA** as part of her PhD thesis titled "PATHOGENESIS OF ANTI- HIV DRUG (TENOFOVIR) INDUCED RENAL DAMAGE: POSSIBLE ROLES OF OXIDATIVE STRESS, NITROSATIVE STRESS AND NFkB PATHWAY", was approved by the Institutional Animal Ethics Committee of Christian Medical College, Vellore (IAEC Approval Number 14/ 2008).

Dr. Solomon Sathishkumar
Secretary, IAEC
Associate Professor of Physiology

Professor
Department of Physiology
Christian Medical College,
Vellore - 632 002, Tamilnadu, India.

CERTIFICATE

I, **HEMALATHA. R** hereby declare that the thesis entitled **" Pathogenesis of anti-HIV drug (Tenofovir) induced renal damage: Possible roles of Oxidative stress, Nitrosative stress and NF-κB pathway"** is a record of research work done by me during the period of my study under the guidance of **Dr. Premila Abraham**, Professor, Department of Biochemistry, Christian Medical College, Vellore – 632002, India. This work has not previously formed the basis for the award of any degree, diploma, associate ship, fellowship or other similar title of any other university.

R.HEMALATHA
Senior Research Fellow,
Department of Biochemistry,
Christian Medical College,
Vellore, India.

OCTOBER 2013

Vellore

DEPARTMENT OF BIOCHEMISTRY
CHRISTIAN MEDICAL COLLEGE, VELLORE – 632002, INDIA

MOLLY JACOB, M.B.B.S., M.D., Ph. D.
DHAYAKANI SELVAKUMAR, M.Sc., Ph.D.
PREMILA ABRAHAM, M.Sc., Ph.D.
MINNIE FAITH K., M.B.B.S., M.D.
JOE VARGHESE, M.B.B.S., M.D., D.N.B.

Telephone : 91-416-2284267
: 91-416-2284458
Fax : 91-416-2262268
E-mail: biochemistry@cmcvellore.ac.in

CERTIFICATE

This is to certify that the thesis entitled **" Pathogenesis of anti-HIV drug (Tenofovir) induced renal damage: Possible role of Oxidative stress, Nitrosative stress and NFkB pathway"** is based on the results of the work carried out by **Ms. R. HEMALATHA** for the Ph.D. degree under my supervision. This work has not been submitted for any degree, diploma, associateship,fellowship or other similar title of any other university.

Dr. Premila Abraham, M.Sc., Ph.D.
Professor of Biochemistry
(Supervisor)

Dr. PREMILA ABRAHAM, Ph.D.
PROFESSOR IN BIOCHEMISTRY,
CHRISTIAN MEDICAL COLLEGE,
BAGAYAM, VELLORE - 632 002.

OCTOBER 1, 2013
Vellore

DEPARTMENT OF BIOCHEMISTRY
CHRISTIAN MEDICAL COLLEGE, VELLORE – 632002, INDIA

MOLLY JACOB, M.B.B.S., M.D., Ph. D.
DHAYAKANI SELVAKUMAR, M.Sc., Ph.D.
PREMILA ABRAHAM, M.Sc., Ph.D.
MINNIE FAITH K., M.B.B.S., M.D.
JOE VARGHESE, M.B.B.S., M.D., D.N.B.

Telephone : 91-416-2284267
: 91-416-2284458
Fax : 91-416-2262268
E-mail: biochemistry@cmcvellore.ac.in

CERTIFICATE

This is to certify that the thesis entitled **" Pathogenesis of anti-HIV drug (Tenofovir) induced renal damage: Possible role of Oxidative stress, Nitrosative stress and NFkB pathway"** is based on the results of the work carried out by **Ms. R. HEMALATHA** for the Ph.D. degree under my coguidance. This work has not been submitted for any degree, diploma, associateship,fellowship or other similar title of any other university.

Dhayakani Selvakumar

Dr. Dhayakani Selvakumar, M.Sc., Ph.D.
Professor of Biochemistry
(Co-guide)

Dr. DHAYAKANI SELVAKUMAR, Ph.D.,
PROFESSOR OF BIOCHEMISTRY
DEPARTMENT OF BIOCHEMISTRY,
CHRISTIAN MEDICAL COLLEGE,
VELLORE -632 002. INDIA.

OCTOBER 1, 2013
Vellore

ACKNOWLEDGEMENT

I owe my heartfelt gratitude and sincere appreciation for the enthusiastic supervision of **Dr. Premila Abraham, Professor in Biochemistry**, who, despite being a very busy scientist, always made time for discussions which proved invaluable guaidance and helpful suggestions in accomplishing this work.

I convey my special thanks to my co-guide **Dr. Dhayakani Selvakumar** for unfailing support and encouragement during my research work.

I wish to express my sincere thanks to **Dr. Molly Jacob,** Head and Professor, Department of Biochemistry, for providing me the necessary facilities in the department to carry out my work effectively.

I would like to thank **Dr. Bina, Dr. Indirani and Dr. Suganthy Rabi,** Department of Anatomy for helping me to execute histological work.

I wish to express my sincere thanks to all the Members of Biochemistry Department for their support.

My thanks are also due to **Mr. Srinivasan** and **Mrs. Rita Bascal** for the Electron Microscopy and Photographic work for my project work.

I am very grateful to the Principal and the administrative authorities of the Christian Medical College, Vellore and the Tamilnadu Dr. M.G.R Medical University, Chennai for giving me the opportunity to pursue my doctoral studies in this institution.

I express my gratitude to Dr. R. Selvakumar , Professor and Head, Department of Clinical Biochemistry for helping me to carry out the clinical assays.

I extend my thanks to Dr. Solomon Sathishkumar , secretary IAEC, animal house faculty, Mr. Antony, Mr. Samuel and Mr. Ramesh, for providing me with rats for my experimental work.

Finally, I gratefully acknowledge the Council of Scientific and Industrial Research, New Delhi, India for their financial Support.

I would like to thank my mother and brother for the moral support, constant encouragement and optimism in getting through the bad patches in research.

I would like to thank the God Almighty for giving me the knowledge and enabling me to keep good health throughout this project.

CONTENTS

LIST OF ABBREVIATIONS

ALP	Alkaline phosphatase
ADP	Adenosine diphosphate
AQP2	Aquaporin 2
ATP	Adenosine triphosphate
BSA	Bovine serum albumin
COX	Cyclooxygenase
DAB	3,3’-diaminobenzidine
DCT	Distal convoluted tubules
DTT	Dithiothreitol
DNPH	2,4 dinitrophenyl hydrazine
DTNB	5,5'-Dithiobis (2-nitrobenzoic acid)
DMSO	Dimethyl sulphoxide
EDTA	Ethylenediamine tetra acetic acid
ETC	Electron transport chain
GSH	Reduced glutathione
GSSG	Oxidized glutathione
GAPDH	Glyceraldehyde 3-phosphate dehydrogenase
HSP	Heat shock protein
HO-1	Heme oxygenase-1
IKB-α	Inhibitory kinase-B alpha
iNOS	Inducible nitric oxide synthase

NF-κB	Nuclear factor kappa B
MDA	Malondialdehyde
MMP	Matrix metalloproteinase
MPO	Myeloperoxidase
MPTP	Mitochondrial permeability transition pore
MTT	3-(4, 5-dimethylthiazole-2yl)-2, 5-diphenyl tetrazolium
NAD/NADP	Nicotinamide adenine dinucleotide/ Nicotinamide adenine dinucleotide phosphate (oxidized form)
NADH/NADPH	Nicotinamide adenine dinucleotide/ Nicotinamide adenine dinucleotide phosphate (reduced form)
NO	Nitric oxide
NOS	Nitric oxide synthase
PARP	Poly-ADP ribose polymerase
PCT	Proximal convoluted tubules
PLA2	Phospholipase A2
RCR	Respiratory control ratio
ROS	Reactive oxygen species
RNS	Reactive nitrogen species
SOD	Superoxide dismutase
SDS	Sodium dodecyl sulfate
TBA	Thiobarbituric acid
TCA	Trichloroacetic acid
TDF	Tenofovir Disoproxil Fumarate
TRIS	Tris (hydroxyl methyl) aminomethane
XO	Xanthine oxidase

Introduction

Tenofovir is one of the most commonly used drugs for the treatment of HIV. Tenofovir disoproxil fumarate (TDF) (Viread) is an analog of adenosine monophosphate, manufactured by Gilead Sciences (San Francisco, California, USA) and it was approved by the US, Food and Drug Administration (FDA) on October 26th, 2001 for treatment against Human Immunodeficiency Virus (HIV) infection (1,2). Tenofovir disoproxil fumarate is a fumaric acid salt of bis-isopropoxycarbonyloxymethyl ester derivative of tenofovir and it was also formerly called as bis(POC)-PMPA (9-(R)-{2-(phosphonomethoxy) propyl}adenine. Recently, tenofovir was also approved for the treatment of chronic hepatitis B infection on August 11th, 2008.

Tenofovir disoproxil fumarate (TDF) is the preferred drug to treat patients with HIV disease as it has several advantages such as utility (one pill a day), potency, safety, low resistance profile, and tolerability over other anti-retroviral drugs (1). Tenofovir, a close analogue of adefovir, in the recommended dose of 300 mg daily is rarely associated with nephrotoxicity during the first year (3). Recently, however, renal dysfunction has been reported in patients with human immunodeficiency virus (HIV) infection treated with tenofovir for several years (2-9 years). Numerous case reports and case series have described severe cases of renal tubular toxicity associated with TDF exposure. Several case reports, observational studies, and animal models, support the notion that tenofovir is a proximal tubular toxin (4–9). As the target of TDF toxicity is the proximal tubule, patients can develop Fanconi syndrome (characterized by phosphaturia, glycosuria, bicarbonate wasting, tubular proteinuria, and aminoaciduria) which may persist even after discontinuation of the drug (10–13). Several human and animal studies have shown damage to specifically renal proximal tubular mitochondria (14,15). In the TDF treated HIV patients who underwent kidney biopsy, the main abnormality on light microscopy was acute proximal tubule injury, and the presence of intracytoplasmic inclusions. Electron microscopy showed morphologic abnormalities in the proximal tubule mitochondria, with marked variations in size and shape,

disruption of cristae, mitochondrial swelling, and intra-mitochondrial deposits (16,17). Identifying a prophylactic/therapeutic agent that can prevent/minimize TDF nephrotoxicity can lead to better tolerance of the drug and improve its therapeutic efficacy. The key to prevent/minimize TDF nephrotoxicity lies in the elucidation of the mechanism by which it causes renal injury. Therefore, there is an urgent need to unravel the mechanism of TDF tubulopathy.

The well known target of TDF is the proximal tubular mitochondria. Mitochondria are the power house of the cell, and the components in the electron transport chain, which play the central role in ATP synthesis, are found in the cristae. The major function of electron transport chain which is present in the inner mitochondrial membrane is to convert the redox energy into electrochemical proton gradient by transfer of a series of electron carriers of complexes namely complex I (NADH ubiquinone reductase), complex II (succinate ubiquinone reductase), complex III (ubiquinol cytochrome-c reductase) and complex IV (cytochrome c oxidase) causes the production of ATP from ADP by ATP synthase. Thus, damage to the cristae can result in the disruption of electron transport chain, decreased activity of the electron chain complexes and hence decrease ATP production by the mitochondria.

Proximal tubules are being intrinsically vulnerable to mitochondrial dysfunction because of limited anaerobic ATP-generating capacity (10). They have a high- requirement for ATP (and mitochondria) for driving sodium-potassium pumps in order to reabsorb the filtered nutrients such as glucose and amino acids as well as ions such as sodium, chloride, phosphate and bicarbonate (9). Damage to proximal tubular mitochondria can limit the availability of ATP for proximal tubular function resulting in the loss of the nutrients and ions in urine (Fanconi syndrome). Mitochondrial swelling and disruption of cristae are considered to be a characteristic feature of deteriorated function of this organelle (8).

Damaged mitochondria are a major source of ROS and RNS. Accumulation of ROS and RNS can cause oxidative and nitrosative damage to the lipids, proteins, and DNA (18) resulting in cellular dysfunction and ultimately cell death.

Inflammation is a constant companion of oxidative stress, and NF-κB is an important proinflammatory transcription factor that plays a pivotal role in the cellular signaling mechanism for oxidative stress-induced inflammation in various conditions (19). NF-κB signaling pathway is shown to play a role in the pathogenesis of renal injury caused by various agents (20).

Melatonin is a naturally occurring compound in animals, plants and microbes. It is a hormone produced by the pineal gland. It is characterized as a dietary supplement, but not as a drug by US Food and Drug Administration (FDA). It was approved for the prescription by the European Medicines Agency in 2007 and in 2009 in Australia (21,22). During the last decade, a number of studies have demonstrated that melatonin plays an effective role in regulating mitochondrial homeostasis by multiple mechanisms. In addition to being a free radical scavenger, melatonin reduces nitric oxide (NO) generation within mitochondria. It maintains the electron flow, efficiency of oxidative phosphorylation, ATP production and bioenergetic function of the cell by regulating respiratory complex activities, Ca^{2+} influx, and mitochondrial permeability transition pore opening (23–26). Recently, many studies confirmed that melatonin exerts anti-inflammatory effect through inhibition of NF-κB. (27–30).

The mechanism of nephrotoxicity of tenofovir is not fully explored. The present study elucidates the mechanism of tenofovir nephrotoxicity, and also proves that melatonin pretreatment can attenuate TDF nephrotoxicity.

PURPOSE OF THE STUDY

The purpose of our study is to elucidate the mechanism of TDF nephrotoxicity. An animal model is required to study the mechanism of nephrotoxicity of tenofovir. **Therefore our first objective was to standardize a rat model of TDF induced renal damage.**

Several human and animal studies have shown that TDF damages renal proximal tubular mitochondria (14,31,32). Human kidney biopsies and kidneys obtained after chronic TDF treatment showed severe morphologic abnormalities in proximal tubule mitochondria, with marked variations in size and shape and disruption of cristae, mitochondrial swelling, and intra-mitochondrial paracrystals and sometimes decreased number of mitochondria (14,33). Mitochondrial swelling and disruption of cristae are considered to be a characteristic feature of deteriorated function of this organelle (34). Damage to proximal tubular mitochondria can limit the availability of ATP for proximal tubular function resulting in the loss of the nutrients and ions in urine (Fanconi syndrome). We hypothesized that TDF induced proximal tubular damage and dysfunction may be due to the impairment of mitochondrial function and lowering of the activities of the electron chain complexes that are required for ATP synthesis. **Our second objective was to assess the effect of TDF administration on mitochondrial structure, and function.**

Oxidative stress is closely linked to mitochondrial dysfunction as mitochondria are both generators of and targets for reactive species, which include reactive oxygen species (ROS) and reactive nitrogen species (RNS) (35,36). Accumulation of ROS and RNS can cause oxidative and nitrosative damage to the lipids, proteins, and DNA (36,37) resulting in cellular dysfunction and ultimately cell death. Because of the deleterious effects of ROS and RNS, the cell is equipped with several antioxidant systems in order to detoxify these reactive species. Cellular damage is shown to

occur when the antioxidants are depleted (38). **Our third objective was to determine the role of oxido-nitrosative stress and antioxidant enzyme system in TDF nephrotoxicity.**

ROS-dependent activation of the NF-κB pathway promotes apoptosis in proximal tubular cells (39). Cisplatin and gentamicin , both of which are predominantly proximal tubular toxins, cause apoptosis and inflammation of epithelial cells lining the tubular structures via induction of NF-κB signaling (40,41). **Therefore, we hypothesized that tenofovir may act through similar mechanism. This served as our fourth objective.**

Pharmacological doses of melatonin suppress the production of inflammatory cytokines and iNOS via inhibition of NF-κB. The underlying mechanisms may be through inhibition of NF-κB expression, reduction of IκB-α degradation and NF-κB translocation, or suppression of the DNA binding activity of NF-κB (42,43). **Therefore, our final objective was to study the effect of melatonin pretreatment on tenofovir nephrotoxicity.**

RESEARCH HYPOTHESIS

Our research hypothesis is that damage to the mitochondria of proximal tubules may play a vital role in tenofovir nephrotoxicity. This hypothesis is based on the previously reported findings that

1. TDF administration results in severe damage to the proximal tubular mitochondria
2. TDF causes mt DNA damage
3. Mitochondria are major sources as well as targets of ROS and RNS
4. Excess ROS and RNS cause mitochondrial dysfunction
4. ROS and RNS are activators of NF-κB inflammatory signalling pathway
5. NF-κB activation and PARP overactivation can result in cellular necrosis

The hypothesis proposed for the mechanism of tenofovir nephrotoxicity is shown in Fig.1.1

FIGURE: 1.1.

PROPOSED MECHANISMS FOR THE ROLES OF OXIDO-NITROSATIVE STRESS, NEUTROPHIL INFILTRATION, AND NF-κB SIGNALLING PATHWAY IN TENOFOVIR INDUCED RENAL DAMAGE

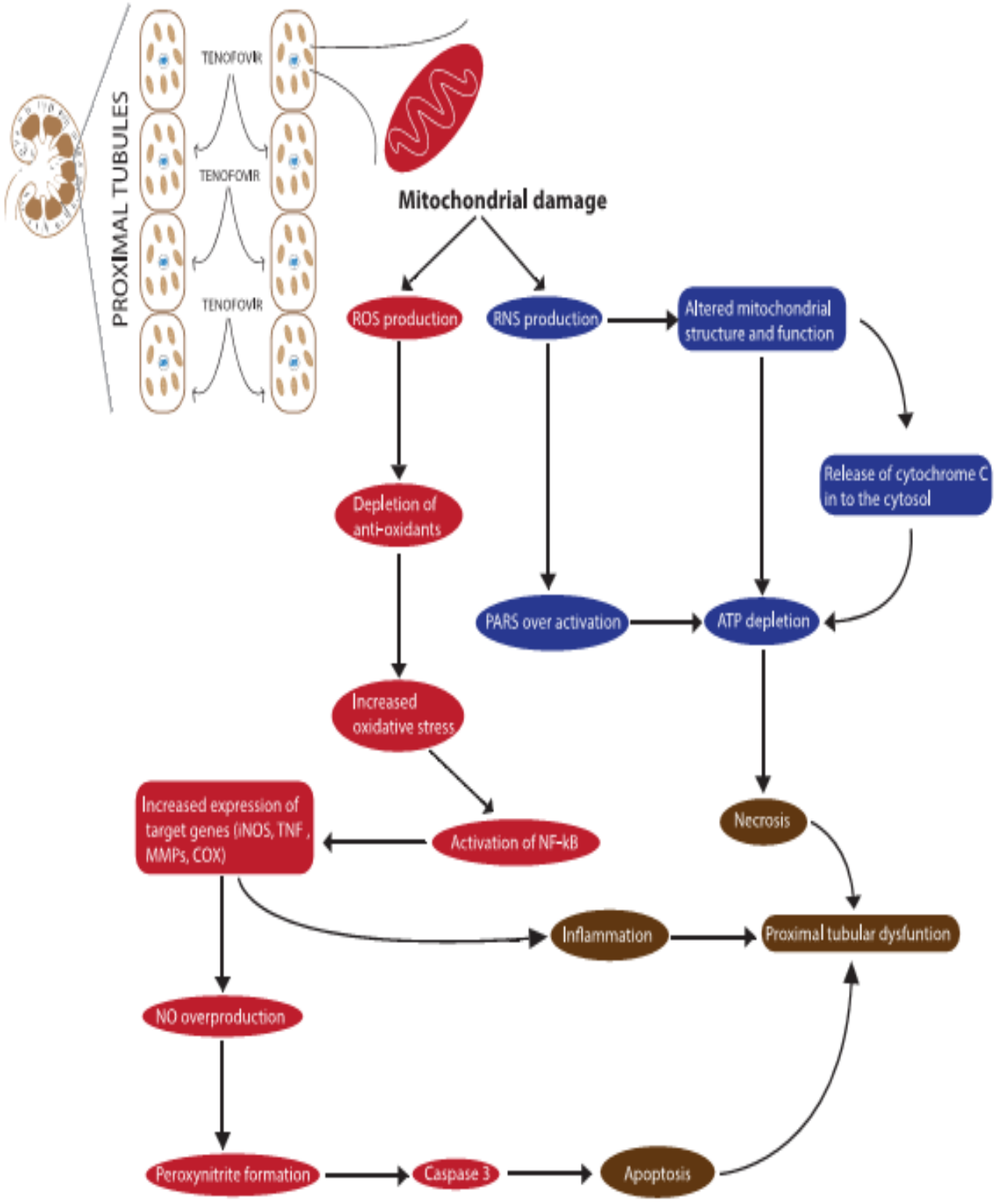

Aims and Objectives

The present study is aimed at elucidation of mechanism of Tenofovir induced renal damage and methods to minimize the damage, using a rat model.

The objectives are to

1. Standardize a rat model of Tenofovir nephrotoxicity
2. Assess the effect of tenofovir on mitochondrial structure and function in the kidney.
3. Investigate the roles of oxidative stress and nitrosative stress in tenofovir induced renal damage.
4. Investigate the role of NF-κB activation and its target genes, PARP activation in tenofovir induced renal damage.
5. Study the effect of melatonin, a potent anti-oxidant, anti-inflammatory agent and NF-κB inhibitor on tenofovir - induced renal damage.

Review of Literature

TENOFOVIR DISOPROXIL FUMARATE (TDF)

The presence of Acquired Immunodeficiency Syndrome (AIDS) was not noticed in Asia and India until the late 1980s (44). However, South-East Asia has now become the epicenter of theHIV/AIDS pandemic. Current evidence indicates that the doubling time of this epidemic in India is less than 2 years. The 5.1 million of people infected in India make it the second largest HIV infected population in the world. Experts say that the number could quadruple in upcoming years (44).

About 37-45% of HIV patients on the antiviral drugs suffer from some kind of renal lesions. The introduction of more effective and powerful antiviral drugs (eg., protease inhibitors, acyclic nucleotide phosphonate analogues) (45) and the necessity to combine several potentially toxic drugs are well known causes of increase in the antiviral drug nephrotoxicity (45). Drug induced kidney injury is a major side effect in clinical practice, frequently leading to acute renal failure (7,46–48) The exact frequency of nephrotoxicity induced by antiviral drugs is difficult to determine. VIREAD is the brand name for Tenofovir disoproxil fumarate (a prodrug) of tenofovir that inhibits the activity of HIV-1 reverse transcriptase and hepatitis B virus (HBV) polymerase by competing with deoxyadenosine 5'-triphosphate and by DNA chain termination after incorporation into DNA (47). Tenofovir disoproxil fumarate was approved for the treatment of HIV infection by FDA on October 26, 2001, only six months after Gilead Sciences Inc. submitted the new drug application (NDA). It is indicated for the treatment of HIV-1 infection when used in combination with other antiretroviral medicines. Tenofovir was also approved for treatment of chronic hepatitis B in adults in 2008 (2).

Tenofovir disoproxil fumarate (TDF) is the preferred drug to treat patients with HIV disease as it has several advantages such as utility (one pill a day), potency, safety, low resistance profile, and tolerability over other anti-retroviral drugs (1). Tenofovir is now a widely used component of

antiretroviral regimens for both treatment of naïve and experienced patients on the basis of its efficacy and tolerability in clinical trials. In HIV-infected patients, treatment with TDF has been associated with excellent virological suppression and favorable clinical outcomes. (313). Tenofovir has less adverse effects on blood lipids, fat accumulation, and mitochondrial toxicity than nucleoside phosphonate reverse transcriptase inhibitors (13). US HIV treatment guidelines considered tenofovir as part of all preferred regimens for antiretroviral-naive adults and adolescents (6). Tenofovir is available in fixed-dose combination with emtricitabine and efavirenz (49).

1. Chemistry

Tenofovir disoproxil fumarate is [[(1R)-2(6-Amino- 9H-purin-9-yl)-1-methylethoxy] methyl] phosphonate, bis(isopropyloxycarbonyloxymethyl ester), fumarate (1:1) with a molecular formula of $C_{19}H_{30}N_5O_{10}P,C_4H_4O_4$ and its molecular weight of 635.52. It is a white to off-white crystalline powder with a solubility of 13.4mg/ml in distilled water at 25°C, soluble in methanol and slightly solube in dichloromethane (50).

Figure 2.1 Chemical Structure Of Tenofovir Disoproxil Fumarate (47)

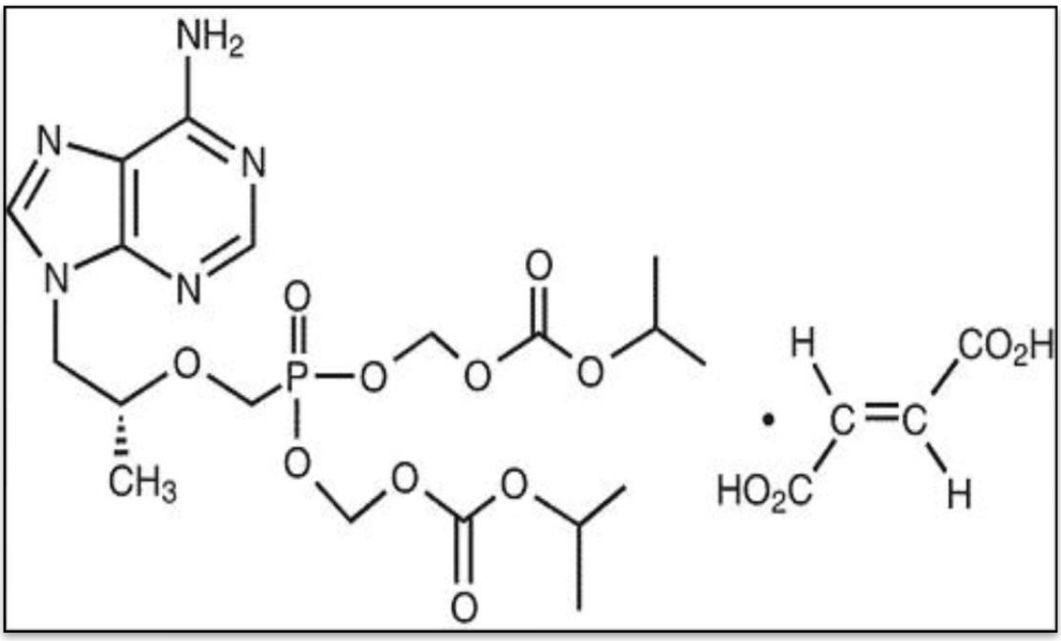

TDF tablets are prescribed for oral administration in HIV patients. Each tablet contains 300 mg of tenofovir disoproxil fumarate, which is equivalent to 245 mg of tenofovir disoproxil, and the following inactive ingredients: croscarmellose sodium, lactose monohydrate, magnesium stearate, microcrystalline cellulose, and pre gelatinized starch. The tablets are coated with Opadry II Y–30–10671–A, which contains aluminum lake, hydroxypropyl methylcellulose , lactose monohydrate, titanium dioxide, and triacetin.

2. Mechanism of action

Tenofovir disoproxil fumarate is an acyclic nucleotide phosphonate diester and it is a structural analog of adenosine monophosphate. Initially tenofovir disoproxil fumarate requires initial diester hydrolysis by non-specific esterases in blood and tissues for conversion to tenofovir and subsequent phosphorylations by cellular enzymes to form tenofovir diphosphate, which is an obligate chain terminator of the reaction. Tenofovir diphosphate inhibits the activity of HIV reverse transcriptase and HBV polymerase by competing with the natural substrate deoxyadenosine 5'-triphosphate and, after incorporation into DNA, by DNA chain termination. It is a weak inhibitor of mammalian DNA polymerase α, β and mitochondrial DNA polymerase ɣ. Tenofovir diphosphate is a structural analog of deoxyadenosine-5′-triphosphate, the usual substrate for viral RNA-directed DNA polymerase, and is a weak inhibitor of mammalian DNA α- and β-polymerases and mitochondrial DNA γ-polymerase. Therefore, following the phosphorylation, tenofovir is converted to active metabolite tenofovir diphosphate, which latter acts as an obligate chain terminator by constitutively expressed cellular enzyme reverse transcriptase reaction (50)

Figure: 2.2 Mechanism Of Action Of Tenofovir (PMPA) (51)

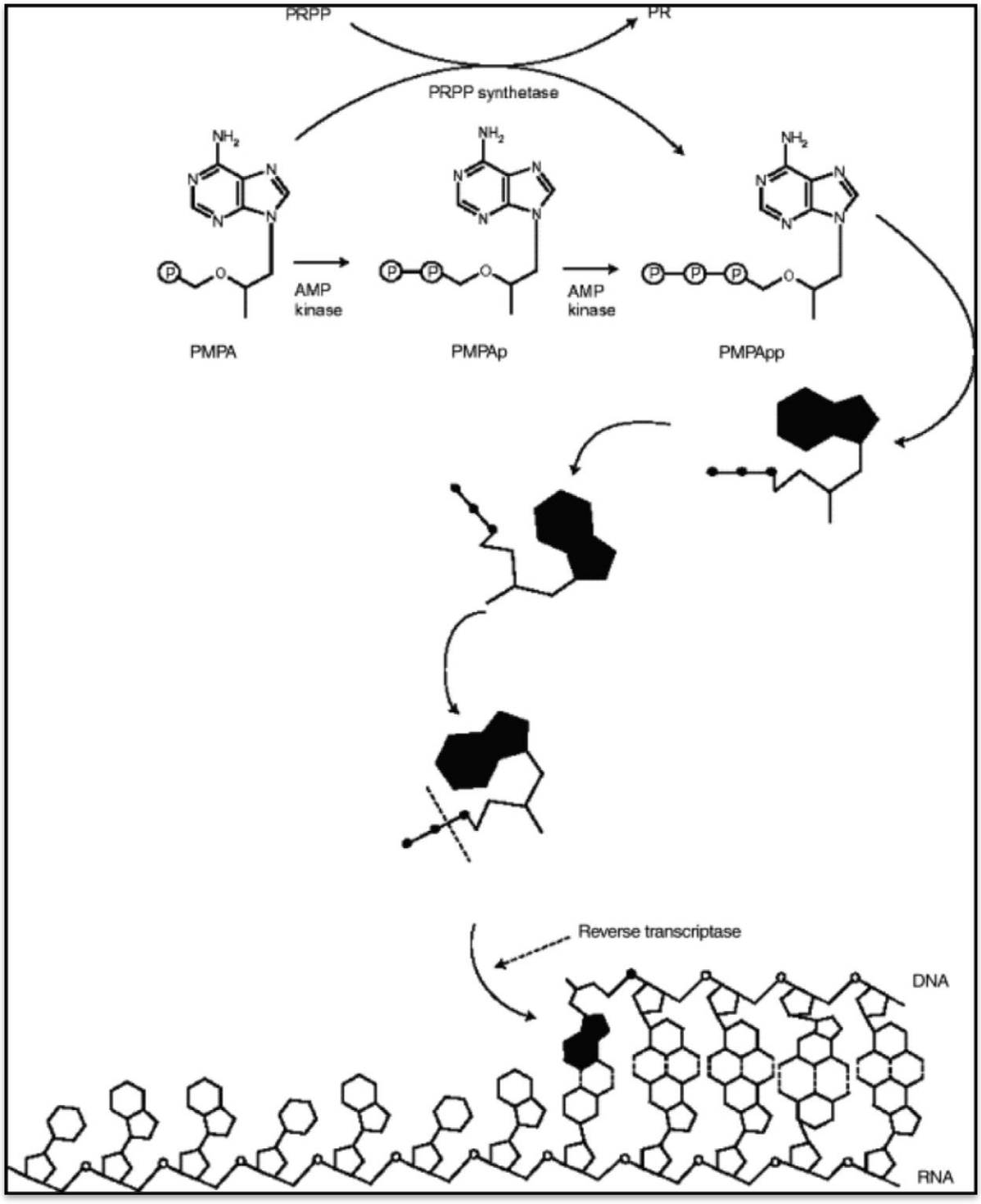

TDF (PMPA) NEEDS TO BE PHOSPHORYLATED, IN ONE OR TWO STEPS, TO THE DIPHOSPHATE FORM BEFORE IT INTERFERES, AS CHAIN TERMINATOR, WITH THE REVERSE TRANSCRIPTASE REACTION

3. Pharmacokinetics

a. Absorption

TDF is a water soluble diester prodrug of the active ingredient tenofovir. The oral bioavailability of tenofovir in fasting patients is approximately 25%. Following oral administration of a single dose of TDF 300 mg to HIV-1 infected patients in the fasted state, maximum serum concentrations (Coax) is 0.3 ± 0.09 µg/ml. The pharmacokinetics of tenofovir are dose proportional over a TDF dose range of 75 to 600 mg. It is not affected by repeated dosing.

Administration of tenofovir following a high-fat meal (~700 to 1000 kcal containing 40 to 50% fat) increases the oral bioavailability, with an increase in tenofovir AUC of approximately 40% and an increase in Cmax of approximately 14%. However, administration of tenofovir with a light meal did not have a significant effect on the pharmacokinetics of tenofovir when compared to fasted administration of the drug. Food delays the time to tenofovir Cmax by approximately 1 hour. Cmax and AUC of tenofovir are 0.33 ± 0.12 µg/ml and 3.32 ± 1.37 µg/hr/ml respectively following multiple doses of tenofovir 300 mg once daily in the fed state, when meal content was not controlled. Thus Tmax is approximately 1h, and bioavailability is approximately 25%.

b. Metabolism

Following administration of tenofovir, approximately 70-80% of the dose is recovered in the urine as unchanged tenofovir within 72 hours of dosing. After multiple oral doses of tenofovir disoproxil fumarate 300 mg once daily under fed conditions, approximately 32% - 10% of the administered dose is recovered in urine over 24 hours.

c. Excretion

Tenofovir is eliminated unchanged in the urine by combination of glomerular filtration and active tubular secretion (9). 20–30% of the drug is actively transported into renal proximal tubule cells by organic anion transporters (hOAT1, and to a lesser extent, OAT3) in the basolateral membrane (10,11). Subsequently the drug is secreted to the tubular lumen by the apical membrane transporters MRP-4 and MRP-2 (multidrug resistance proteins, encoded byABCC4 and ABCC2 genes) (49). A number of drugs interact with these transporters and may cause excessive entry or reduced outflow of the drug, favoring intracellular accumulation and increasing renal toxicity.

Figure: 2.3 Mechanism of Tenofovir transport by proximal tubular cell (52)

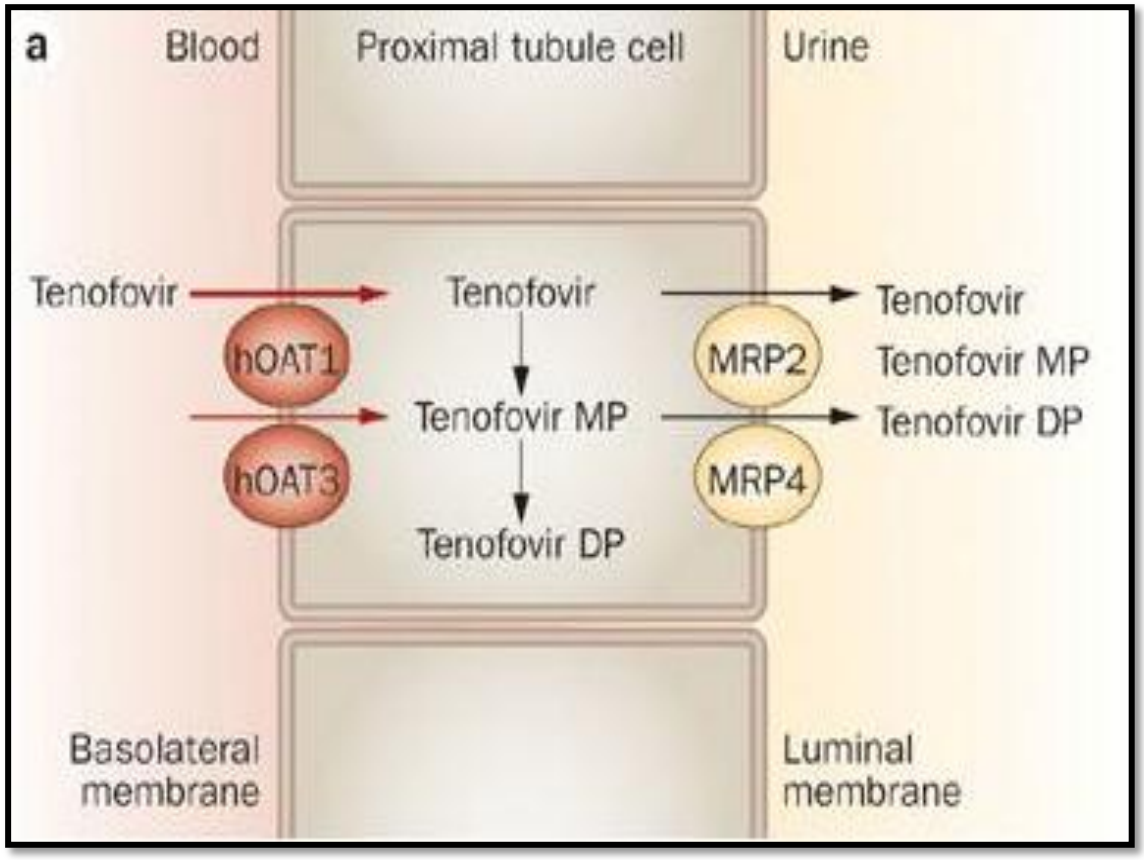

The secretory pathway of tenofovir disturbance, such as increase in the OAT-1 activity or decrease in MRP efflux transport activity may lead to increased tenofovir concentration within the cell which

causes mtDNA depletion and ultimately leads to mitochondrial dysfunction. The alteration in the transporter pathway leads to proximal tubular damage.

4. Recommended dose

For the treatment of HIV-1 infection or chronic hepatitis B in adults and adolescents with body weight ≥35 kg, the recommended dose is one 300 mg Tenofovir disoproxil fumarate tablet once daily taken orally, without regard of food.

5. Overdosage

Limited clinical experience at doses higher than the therapeutic dose of Tenofovir disoproxil fumurate is available. The effects of higher doses are not known. If overdose occurs then the patient must be monitored for evidence of toxicity, and standard supportive treatment is provided as necessary. Tenofovir is efficiently removed by hemodialysis with an extraction coefficient of approximately 54%. Following a single 300mg dose of Tenofovir disoproxil fumurate, a four-hour hemodialysis session removed approximately 10% of the administered tenofovir dose.

In recent days renal toxicity is becoming common in HIV patients treated with TDF for a long time. Numerous case reports and case series have described severe cases of renal tubular toxicity associated with TDF exposure (53–56). It is estimated that renal tubular dysfunction develops in nearly 15% of patients treated with tenofovir for 2-9 years (57). In recent years, it has been reported that TDF-associated nephrotoxicity is the most common single reason for HIV related referral to nephrologists, accounting for at least 20% of consultations (58). Kidney toxicity may lead to acute kidney injury (AKI), chronic kidney disease (CKD), and features of proximal tubular injury, including Fanconi syndrome, isolated hypophosphatemia, and decreased bone mineral density (16–18,54,59).

GENERAL MECHANISMS PROPOSED FOR ANTI-VIRAL DRUG INDUCED RENAL DAMAGE

Two mechanisms are suggested for anti-viral agent induced renal injury.

1. Transporter defects

2. Mitochondrial injury

It is proposed that increased cellular uptake of acyclic nucleotides cidofovir or adenoviral disoproxil by the human organic anion transporter 1 (OAT1) favors proximal tubular dysfunction (60,61). However, nucleoside analogues including Zidovudine, Stavudine, didanosine, and lamivudine also are substrates of OAT1, but these agents have not been associated with tubular dysfunction (62).

Recently, the human concentrative nucleoside transporter1 and the human equilibrative nucleoside transporter1 were localized to the mitochondria (63,64). These transporters are important in mediating the transport of nucleoside and nucleotide drugs (eg. antiviral and anticancer drugs) across cell membranes (65). To produce their mitochondrial toxicity, nucleoside drugs first must be transported into the cytosol or diffused into cells. Except for the few moderately lipophilic nucleoside drugs, other nucleoside drugs that cause mitochondrial toxicity is too hydrophilic to diffuse into cells in appreciable quantity. Thus, it is very likely that they are transported into cells by the nucleoside transporter. The above suggested mechanisms do not fully explain the anti-HIV drug induced renal damage, suggesting that other mechanisms may exist.

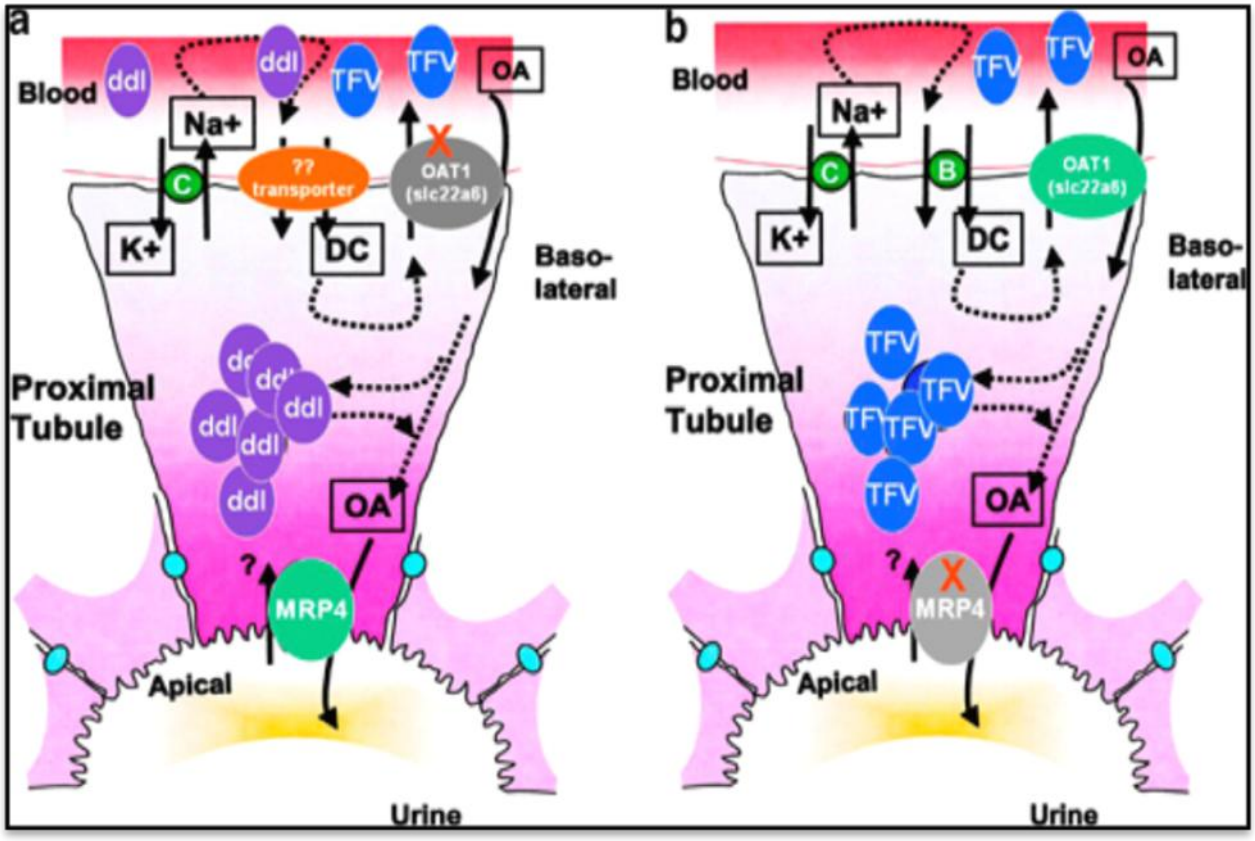

Figure:2.4.Schematic diagram of mechanisms of OAT1 and MRP4 in the transport of antiretrovirals within renal proximal tubules. (a) The potential block of tenofovir (TFV) transport across the basolateral membrane of the proximal tubule in OAT1 knockout (KO) is shown. An unidentified alternate transporter may be upregulated in the absence of OAT1. This moiety may have affinity for ddI transport, and cause accumulation of ddI in proximal tubules with mitochondrial toxicity. (b) Increased accumulation of TFV in proximal tubules results from OAT1 transport across the basolateral membrane but lack of efflux on the apical membrane in Mrp4À/À KO, leading to increased mitochondrial toxicity (31).

a. Nephrotoxicity of tenofovir

The principal side effects associated with TDF use are hypophosphatemia (60–62), renal failure (63,64) and tubular toxicity (65). The main site of toxicity appears to be the proximal tubule, and in more severe cases, patients can develop Fanconi syndrome which is characterized by tubular proteinuria, aminoaciduria, phosphaturia, glycosuria, and bicarbonate wasting (leading to metabolic

acidosis) or acute kidney injury. Several case reports, observational studies, and animal models, support the notion that tenofovir is nephrotoxic for proximal tubular cells (54–57). In a recent cross-sectional study of HIV infected patients with eGFRs in the reference range, 22% of those using TDF had evidence of abnormal proximal tubule function of glycosuria, phosphaturia, or amino aciduria compared with 6% of those on alternative forms of ART and 12% of those who were treatment naive (66). It has been suggested that TDF causes direct proximal tubular damage, which may lead to renal failure (67). Proximal tubular cells are particularly sensitive to the toxic effects of tenofovir due to their unique set of cell membrane transporters that favor entry of the drug (10).

Proximal tubule alterations induce bicarbonaturia, β2-microglobulinuria, glucosuria and aminoaciduria. Distal alterations induce tubular acidosis, hyperkalemia and sodium loss (68). Hence, the tubular toxicity induced by TDF manifests as Fanconi syndrome and renal tubular acidosis.

b. Potential molecular mechanisms of TDF nephrotoxicity

The main target for the tenofovir toxicity is proximal tubular cell due to its cell membrane transporters which supports accumulation of tenofovir. Presently the evidence has shown that the target organelle for cytoxicity of tenofovir is mitochondria. Most of the tubular transport for molecules and reabsorbing over 200g NaCl, 1kg glucose and other molecules every day from the lumen of proximal tubular cells (75). The mitochondrial cell provide the energy for the transport. Since proximal tubule has cell membrane transporters, activation of 25 dihydroxycholecalciferol by 1α hydroxylation in proximal tubule mitochondria yields a active metabolite calcitriol (vitamin D). Further, it release ammonia to secrete protons into urine by distal segments (75). Thus impairment of molecular transport in mitochondria, activation of vitamin D and urinary acidification. The mitochondria assembly required cooperation of both nuclear and mitochondrial genome which results in mitochondrial dysfunction such as defective mitochondrial genes / missing genes, relevant nuclear genes defective or missing, and normally assembled mitochondrial damage and loss of function.

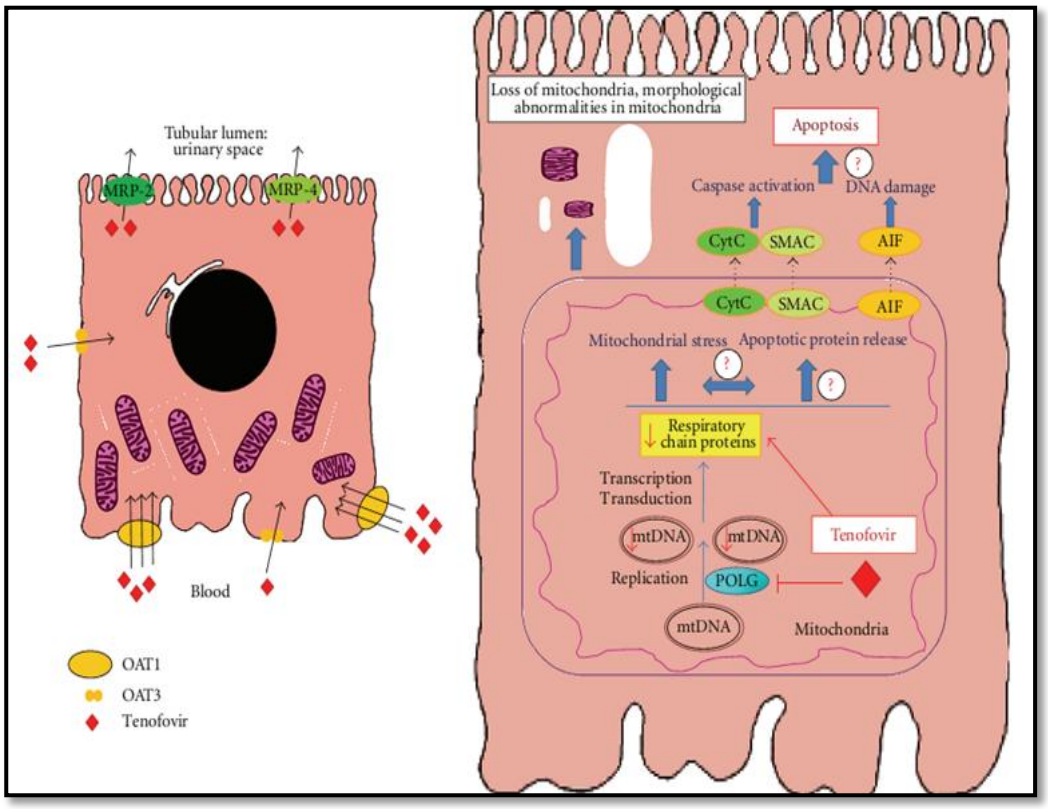

Figure:2.5. Tenofovir handling by proximal tubular cells and potential molecular mechanisms and clinical consequences of tenofovir nephrotoxicity (75)

FREE RADICALS

Free radicals can be defined as molecules or molecular fragments, capable of independent existence, which contain one or more unpaired electrons. The presence of these unpaired electrons confers them a considerable degree of reactivity, since they need another electron to fill the orbital and become stable (19). Free radicals are often reactive species, although the opposite is not always true. Hydrogen peroxide (H_2O_2), for example, although considered a reactive species, is not regarded as a free radical since it has no unpaired electrons in its structure (19). On the other hand, molecular oxygen (dioxygen, O_2) has a unique electronic configuration and it is considered a reactive species.

The most common intracellular forms of reactive oxygen and nitrogen species include radical ($O_2^{\bullet -}$, $^{\bullet}OH$, $^{\bullet}NO$, lipid peroxy radical ($LOO^{\bullet}$) among others), as well as non-radical (O_2, $ONOO^-$, H_2O_2, HOCl, O_3) moieties, that can be deleterious to cells (69).

Although molecular oxygen (O_2) has two unpaired electrons in two different orbitals, it is not a free radical. Molecular oxygen, however, reacts rapidly with most other radicals, forming other free radicals that are more reactive and cause selective oxidation of lipid, protein, or DNA molecules (70).

1.Biochemistry of ROS/RNS

The addition of one electron to molecular oxygen forms the superoxide anion radical ($O_2^{\bullet -}$), which despite being a free radical, is not highly reactive, since it lacks the ability to cross lipid membranes. In this way, it stays enclosed in the compartment where it is generated (19). It is considered the "primary" ROS,from which "secondary" ROS can be generated (71) and arises mainly through metabolic processes (electron transport chain in the mitochondria, flavoenzymes like xanthine oxidase, lipoxygenases and cyclooxygenases,and NADPH oxidase). In the presence of superoxidedismutase, two molecules of this radical can easily be transformed to hydrogen peroxide and molecular oxygen (20).

Singlet oxygen is also a very reactive ROS that induces various genotoxic, carcinogenic, and mutageniceffects through its action on polyunsaturated fatty acids(PUFAs) and DNA (20).

Hydrogen peroxide (H_2O_2) is not a free radical. Nonetheless, it is highly important, much because of its ability to penetrate biological membranes. It plays a radical forming role as an intermediate in the production of more reactive ROS molecules including HOCl (hypochlorous acid) by the action of myeloperoxidase(an enzyme present in the phagosomes of neutrophils)and, most importantly, in the formation of the hydroxyl radical via oxidation of transition metals (19,72). The hydroxyl radical ($^{\bullet}OH$) is highly reactive, being able to attack and damage all biomolecules ie.,

carbohydrates, lipids, proteins and DNA (73). Since it has a half-life in aqueous solution of less than 1 nanosecond, when produced in vivo, this radical reacts close to its site of formation. Production of $^{\bullet}OH$ close to DNA could lead to this radical reacting with DNA bases or the deoxyribosyl backbone of DNA to produce damaged bases or strand breaks. It can be generated through several mechanisms, including ionising radiation and photolytic decomposition of alkyl hydroperoxides, but the majority of the hydroxyl radicals produced in vivo comes from metal catalyzed (mainly involving iron and copper) breakdown of hydrogen peroxide, according to the Fenton reaction (19,74). Superoxide also plays an important role in these reaction, by recycling the metal ions. Transition metals thus play an important function in the formation of various free radicals, as is the case of hydroxyl radicals.

Nitric oxide ($^{\bullet}NO$) is synthesised from L-arginine by three isoforms of nitric oxide synthase (NOS): neuronal nitric oxide synthase (nNOS), endothelial nitric oxide synthase (eNOS), and inducible nitric oxide synthase (iNOS) (30). Like superoxide anion, $^{\bullet}NO$ does not readily react with most biomolecules, despite its unpaired electron. On the other hand, it easily reacts withother free radicals (e.g. peroxyl and alkyl radicals), generating mainly less reactive molecules (75), thus in fact functioning as a free radical scavenger (19).

In addition, nitric oxide seems to be also involved in neurotransmission, regulation of vascular relaxation and in inflammatory processes (30,76). However, it can react with the superoxide anion, yielding peroxynitrite ($ONOO^{-}$). Peroxynitrite can react with other compounds to form other types of reactive nitrogen species (RNS) which includes nitrogen dioxide ($^{\bullet}NO2$) and dinitrogen trioxide (N_2O_3) as well as reactive free radicals (77) . The following are the reactions of RNS:

- $ONOO^{-} + H+ \rightarrow$ ONOOH (peroxynitrous acid) $\rightarrow$ $^{\bullet}NO_2$ (nitrogen dioxide) + $^{\bullet}OH$ (hydroxyl radical)
- $ONOO^{-} + CO_2$ (carbon dioxide) $\rightarrow ONOOCO_2^{-}$ (nitrosoperoxycarbonate)
- $ONOOCO_2- \rightarrow$ $^{\bullet}NO2$ (nitrogen dioxide) + $O=C(O^{\bullet})O-$ (carbonate radical)
- $^{\bullet}NO + {}^{\bullet}NO_2$ N_2O_3 (dinitrogen trioxide)

Figure: 2.6 Overview of sources of ROS and RNS production and their consequences (78)

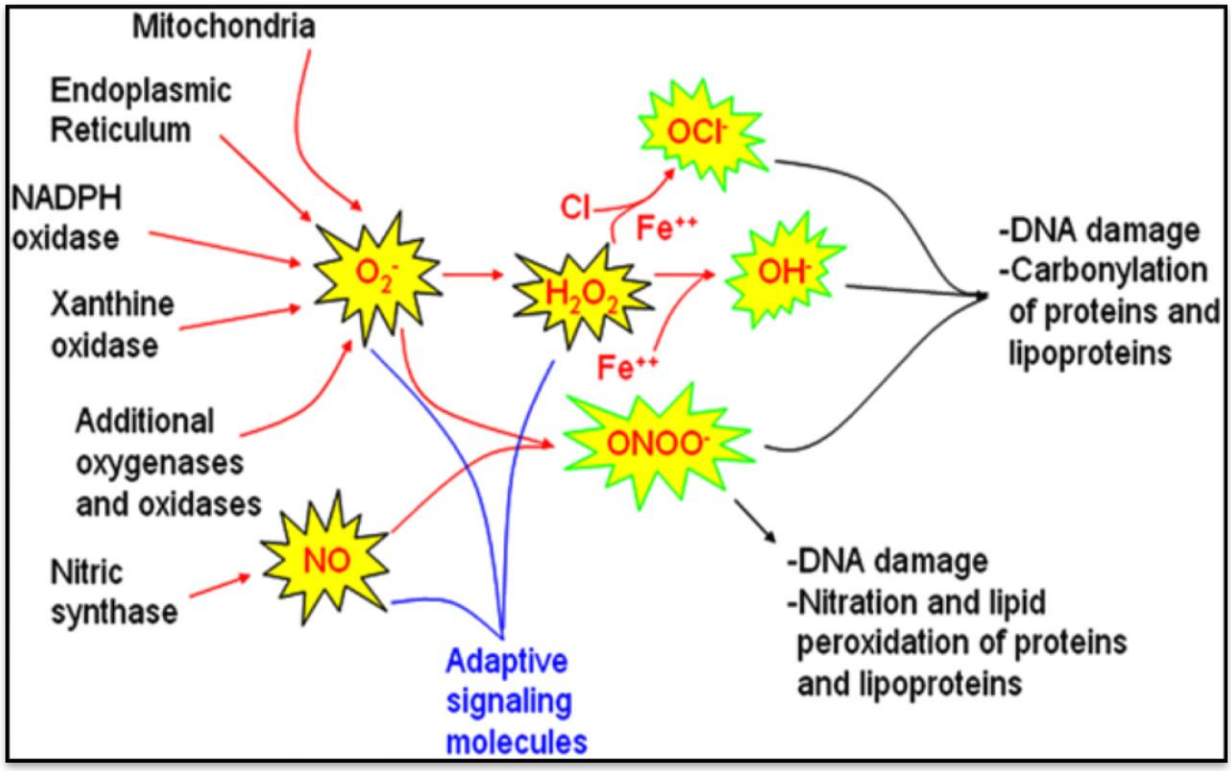

Other reactive species derived from oxygen that can be formed in living systems include peroxyl radicals ($ROO^{\bullet}$). The simplest peroxyl radical is $HOO^{\bullet}$, which is the protonated form of superoxide and is usually termed either hydroperoxyl radical or perhydroxyl radical. Its involvement in the initiation of lipid peroxidation has already been demonstrated (79).

2. Physiological functions of reactive species

Reactive species are known to play a dual role in biological systems, since they can be either harmful or beneficial to living systems. These species are maintained at low, but measurable, concentrations in the cells, through a balance between their rates of production and their rates of removal by antioxidants. Thus, each cell is characterized by a particular concentration of electrons (redox state) stored in many cellular constituents, and the redox state of a cell and its oscillation determines cellular functioning. A temporary shift of the intracellular redox state towards more

oxidising conditions results in a temporary imbalance that represents the physiological basis for redox regulation (80).

A great number of physiological functions are controlled by redox-responsive signalling pathways (80). Several evidences suggest that ROS participate in the defense against intrusion of foreign bodies (81). Activated neutrophils and macrophages produce large quantities of ROS via the phagocytic isoform of NAD(P)H oxidase, in order to kill the pathogens. This massive production of ROS during an inflammatory event is called "**oxidative burst"** and plays an important role as the first line of defence against environmental pathogens (19,79). On a smaller scale, some types of non-phagocytic cells, like fibroblasts, vascular smooth muscle cells, cardiac myocytes and endothelial cells are also known to produce ROS by NADPH oxidase to regulate intracellular signalling cascades. Thus, ROS plays an important role in the regulation of cardiac and vascular cell functioning (82).

Nitric oxide plays several regulatory functions. NO production is regulated at the transcriptional and post-transcriptional levels of signalling pathways involving redox-dependent transcription factor NF-κB or mitogen-activated protein kinases (MAPKs). In addition, $^{\bullet}NO$, in combination with H_2O_2, leads to the activation of the enzyme soluble guanylate cyclase (sGC), which catalyses the formation of cyclic guanosine monophosphate (cGMP) that, by its turn, is used as an intracellular amplifier and second messenger in a variety of physiological responses, such as modulation of protein kinases, ion channels, smooth muscle tone and inhibition of platelet adhesion (83) .

In higher organisms, oxygen homeostasis is maintained by a tight regulation of the red blood cell mass and respiratory ventilation. It has been proposed that changes in oxygen concentration are sensed independently by several different ROS-producing proteins, including a b-type cytochrome. Other studies also suggested that a change in the rate of mitochondrial ROS may play a role in this oxygen sensing by the carotid bodies, which are sensory organs that detect alterations in arterial

blood oxygen. Other responses to changes in oxygen pressure include the regulated production of certain hormones (e.g. erythropoietin) controlled by the transcription hypoxia inducible factor-1 (HIF-1) (84,85).

ROS also seem to be involved in cell adhesion, a mechanism that plays an important role in embryogenesis, cell growth, differentiation, wound repair, among other processes. The expression of cell adhesion molecules is stimulated by bacterial lipopolysaccharides and by various cytokines such as TNF-α, interleukin-1α, and interleukin-1β. The adherence of leukocytes to endothelial cells is also induced by ROS. Moreover, the oxidant-induced adherence of neutrophils is inhibited by hydroxyl radical scavengers or iron chelators, suggesting that the induction of adherence may be mediated by hydroxyl radicals generated from hydrogen peroxide within the cell (86).

Reactive oxygen and nitrogen species can directly affect the conformation and/or activities of all sulfhydryl-containing molecules, such as proteins or glutathione (GSH), by oxidation of their thiol moiety. This type of redox regulation affects many proteins important for signal transduction and carcinogenesis, such as protein kinase C, Ca^{2+}-ATPase, collagenase and tyrosine kinases, among many other enzymes and membrane receptors (87). In addition, ROS/RNS are known to trigger apoptotic cell death, by causing Bcl-2 (a protein located in the outer membranes of mitochondria) to activate a related protein, Bax, which by its turn leads to the release of cytochrome c from mitochondria (88–90). This release then results in the activation of several other proteins.

3. Reactive Oxygen Species (ROS)

The exogenous reactive oxygen species (ROS) are produced by a various sources from the environment sources such as photooxidations, emissions such as UV rays, X-rays causes increase ROS which can lead to cellular damage to the cell structure. It is also produced from pollutants, tobacco, smoke, drugs and xenobiotics. The normal cellular functions such as mitochondrial metabolism and activation of neutrophils (91) are other sources of ROS.

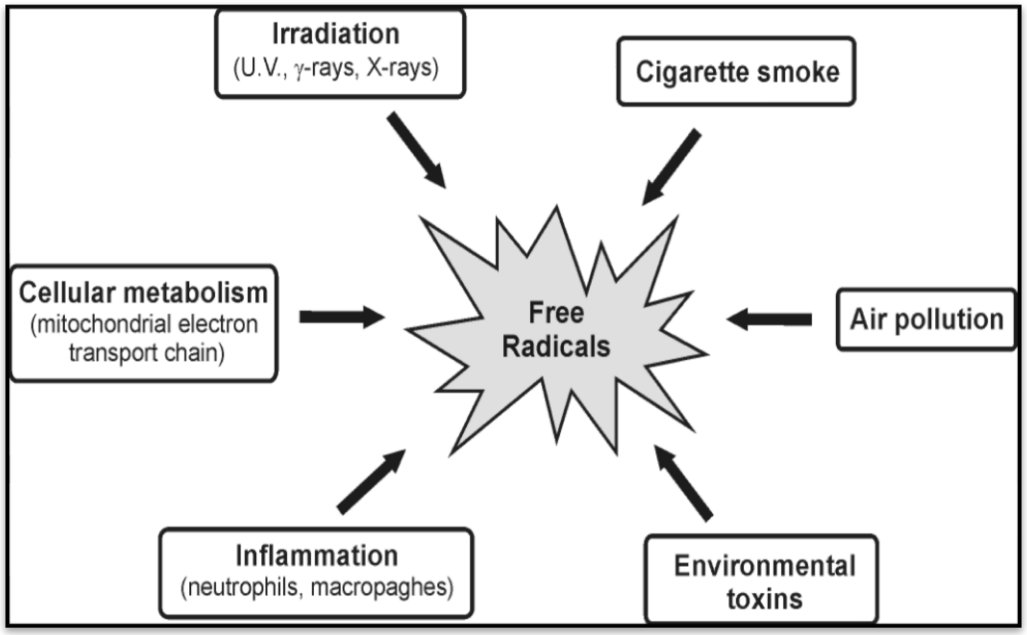

Figure: 2.7 Summary of exogenous and endogenous sources of free radicals (92)**.**

3.1. Mitochondrial sources of ROS

The mitochondrial ETC has been recognized as one of the major sites of ROS production, with superoxide anion being the first ROS produced and therefore a major source of oxidative stress (93). A defect in the activity of the respiratory complexes mainly Complex I and complex III is considered a potential source of superoxide production although specific sites of ROS generation production are controversial (94).

3.2. Extra-mitochondrial sources of ROS

Besides mitochondria, there are other endogenous sources of ROS. For example, xanthine oxidase, a widely distributed enzyme in the tissues of mammals, during the catalysation of the reaction of hypoxanthine to xanthine and xanthine to uric acid, leads to the reduction of molecular oxygen, forming the superoxide anion in the first step and hydrogen peroxide in the second one (79). Additional sources of cellular ROS are inflammatory cell activation (neutrophils, eosinophils and in particular macrophages, cytochrome P_{450} metabolism (namely following the breakdown or

uncoupling of the P_{450} catalytic cycle) (95) and peroxisomes, which mainly lead to the production of H_2O_2 (96).

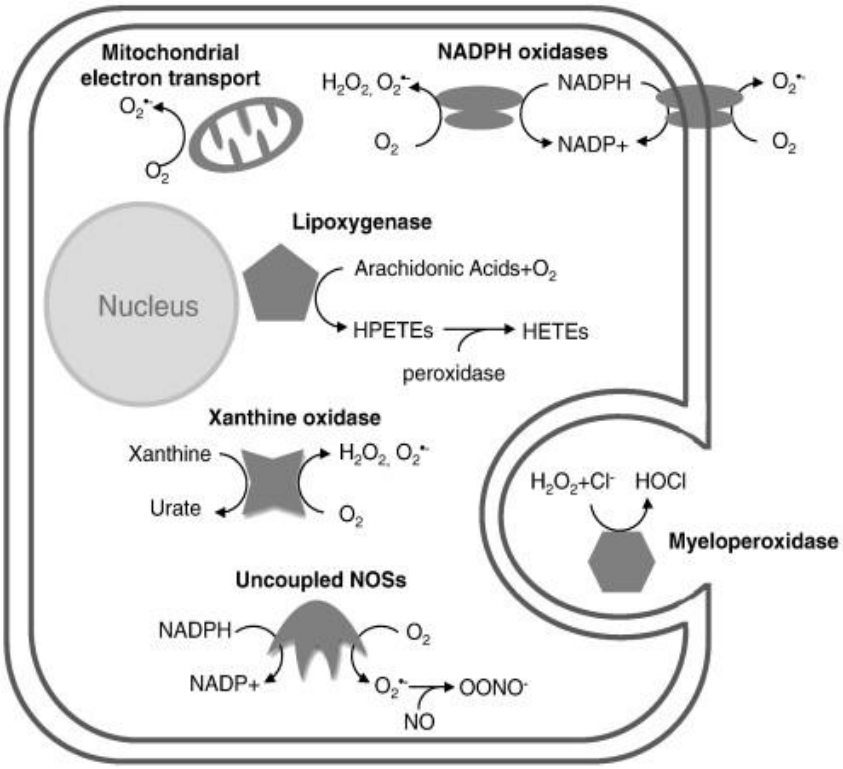

Figure: 2.8 . Different cellular sources of ROS (103)

3.3. Defense against reactive species

The free radical formation or oxidants is a physiological event in aerobic cells, which assembles both enzymatic and nonenzymatic resources are known as antioxidant defenses to exclude these oxidizing species by antioxidant enzymes. The imbalance between oxidants and antioxidants is referred as oxidative stress which leads to damage to the cell molecules for several pathophysiological states such as cancer, cardiovascular diseases, neurodegeneration, aging or mutagenesis.

Aerobic organisms defend themselves against reactive oxygen and nitrogen species through enzymatic and non-enzymatic detoxification mechanisms. The enzymatic detoxification mechanisms involve antioxidant enzymes (superoxide dismutases, catalases, and peroxidases),

small molecular-weight antioxidants (vitamin E, vitamin C, glutathione, ubiquinone, beta-carotene, etc.), and adaptive mechanism leading to an antioxidant gene expression such as HSPs and heme oxygenases.

Antioxidants can work at various levels:

- Protection of the organism from the formation of reactive oxygen species,
- Conversion to un-radical molecules or to less reactive ROS,
- Reparation of damaged molecules and cell structures,
- Removing of oxidized molecules.

a. Cellular Antioxidant Defenses

The balance between the physiological production of ROS and their detoxification is maintained in cells by effective enzymatic and non-enzymatic antioxidant systems (97). As a first line of defence, preventive antioxidants act by binding to and sequestering promoters of oxidation and transition metal ions, like iron and copper, which contain unpaired electrons and strongly accelerate the formation of free radicals. Some examples of preventive antioxidants are transferrin, lactoferrin, ceruloplasmin, haptoglobins, hemopexin, and albumin (27,98). This class of preventive antioxidants also comprises the enzymatic antioxidant defences, like superoxide dismutase (SOD), catalase (CAT), and glutathione peroxidase (GPx). These enzymes act on specific ROS following their formation and degrade them to less harmful products (27,72).

One of the most effective intracellular enzymatic antioxidants is superoxide dismutase. This enzyme catalyses the dismutation of the superoxide anion to molecular oxygen and hydrogen peroxide. The H_2O_2 formed in this reaction is then destroyed by the action of catalases and glutathione peroxidases. In humans, there are three forms of SOD: the cytosolic Cu/Zn-SOD, which contains copper and zinc in its active centre, the mitochondrial Mn-SOD (that contains manganese in the active site), and the extracellular SOD (EC-SOD) (99).

Figure: 2.9a. Some important cellular antioxidants (104)

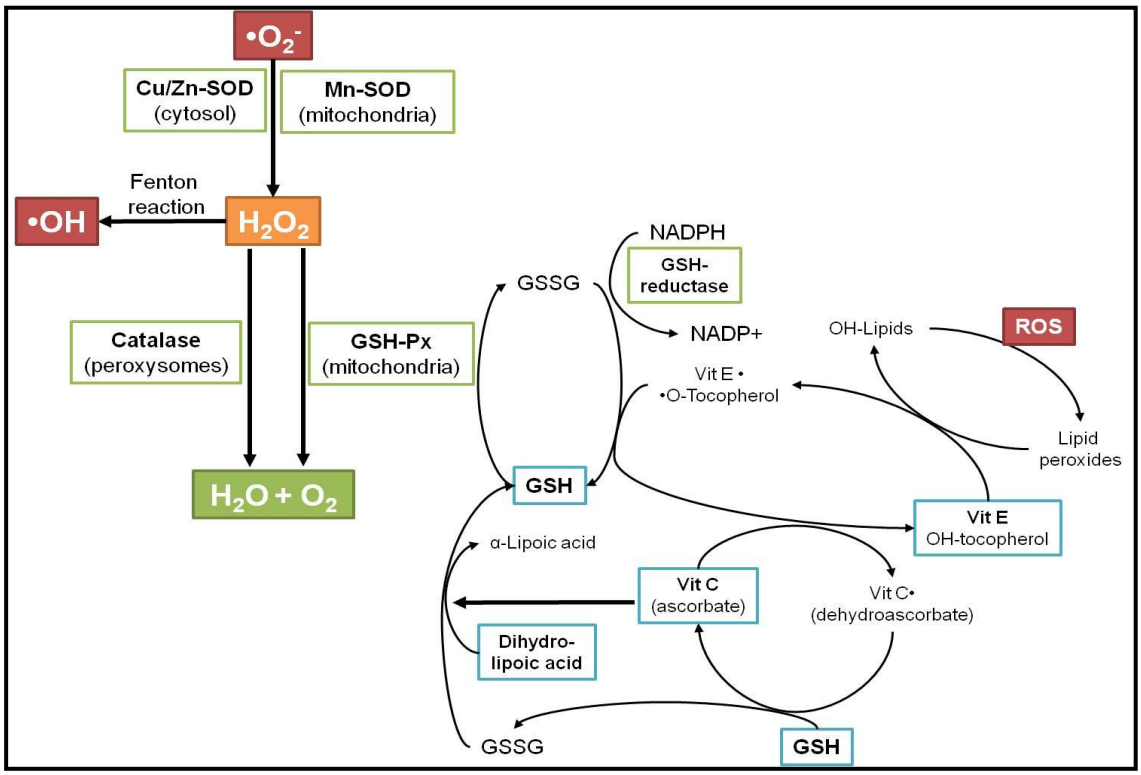

Catalase is a heme-containing enzyme, mainly localized in the peroxisomes of mammalian cells, which decomposes hydrogen peroxide to water and molecular oxygen. Thus, it lowers the risk of $OH^{\bullet}$ formation from H_2O_2, via the Fenton reaction. In addition, catalase is involved in the detoxification of other substrates that work as H^+ donors, such as phenols and alcohols (100).

The selenium-containing peroxidases, of which glutathione peroxidase may be considered the most important example, catalyse the reduction of a variety of hydroperoxides (H_2O_2 or ROOH) in the presence of the reduced form of glutathione (GSH) (100). This enzyme (for which at least four different mammalian forms are known), oxidizes two molecules of GSH toGSSG (the oxidized form of glutathione), which can subsequently be reduced to GSH again by glutathione reductase (19).

In addition to these enzymatic defenses, cells possess low molecular mass agents that also results in the production of less harmful products, acting as a second line of defense. These include, among

others, molecules like glutathione, thioredoxin, and coenzyme Q (27). The tripeptide **glutathione** exists either in the reduced (GSH) or oxidized (GSSG) form and is ubiquitously present in all cells (distributed between the nucleus, endoplasmic reticulum, and mitochondria). Its main functions include: restoration of oxidised protein sulphydryls; detoxification of hydrogen peroxide, lipid hydroperoxides, and electrophilic compounds either directly (via GPx-catalysed reactions) or indirectly (through glutathione S-transferases-catalysed conjugation reactions); transport of amino acids through the plasma membrane; direct scavenging of hydroxyl radical and singlet oxygen; regeneration of some important antioxidants, like vitamins C and E, to their active forms; and protection of brain tissue from oxidative stress (17,1 03,104).

Along with GSH, **thioredoxin**, a small and multifunctional disulphide-containing polypeptide,is also important for the maintenance of cellular thiol homeostasis, contributing to the total antioxidant protection (103,104). It mainly functions as a general protein disulfide reductant, but is also able to provide control over several transcription factors that affect cell proliferation and death (19,105).

Coenzyme Q (CoQ), or ubiquinone, is a ubiquitous electron and proton carrier, playing an important role in the mitochondrial electron-transport chain. Its reduced form, ubiquinol, can function as an antioxidant, preventing lipid peroxidation by reduction of peroxyl radicals and is also able to interact with α-tocopheroxyl radical, thus regenerating endogenous vitamin E within the lipid membrane (106).

Other cellular low molecular weight antioxidant agents include **bilirubin** (107)**, lipoic acid** (108)**, melatonin** (109)**, and uric acid** (110)**.**

Since the processes of prevention and removal of reactive species are not completely effective, damage still accumulates in biomolecules. So, adding to the several types of antioxidants mentioned

above, cells protect their critical structures by other mechanisms, such as repair and de novo synthesis of enzymes. These act as the last line of defence, by repairing or eliminating damaged molecules, reconstituting them, and even by clearing the toxic and waste products (27,111). This type of antioxidants **includes heat shock proteins, DNA repair enzymes, proteases**, lipases, and transferases (72).

Heme oxygenase plays an important role in organism defence to oxidative stress (112) and inflammation (113).HO-1 is activated by many inflammatory mediators, ROS and other stimuli (114,115). Upregulation of HO-1 is accepted as a sensitive marker of oxidative stress.

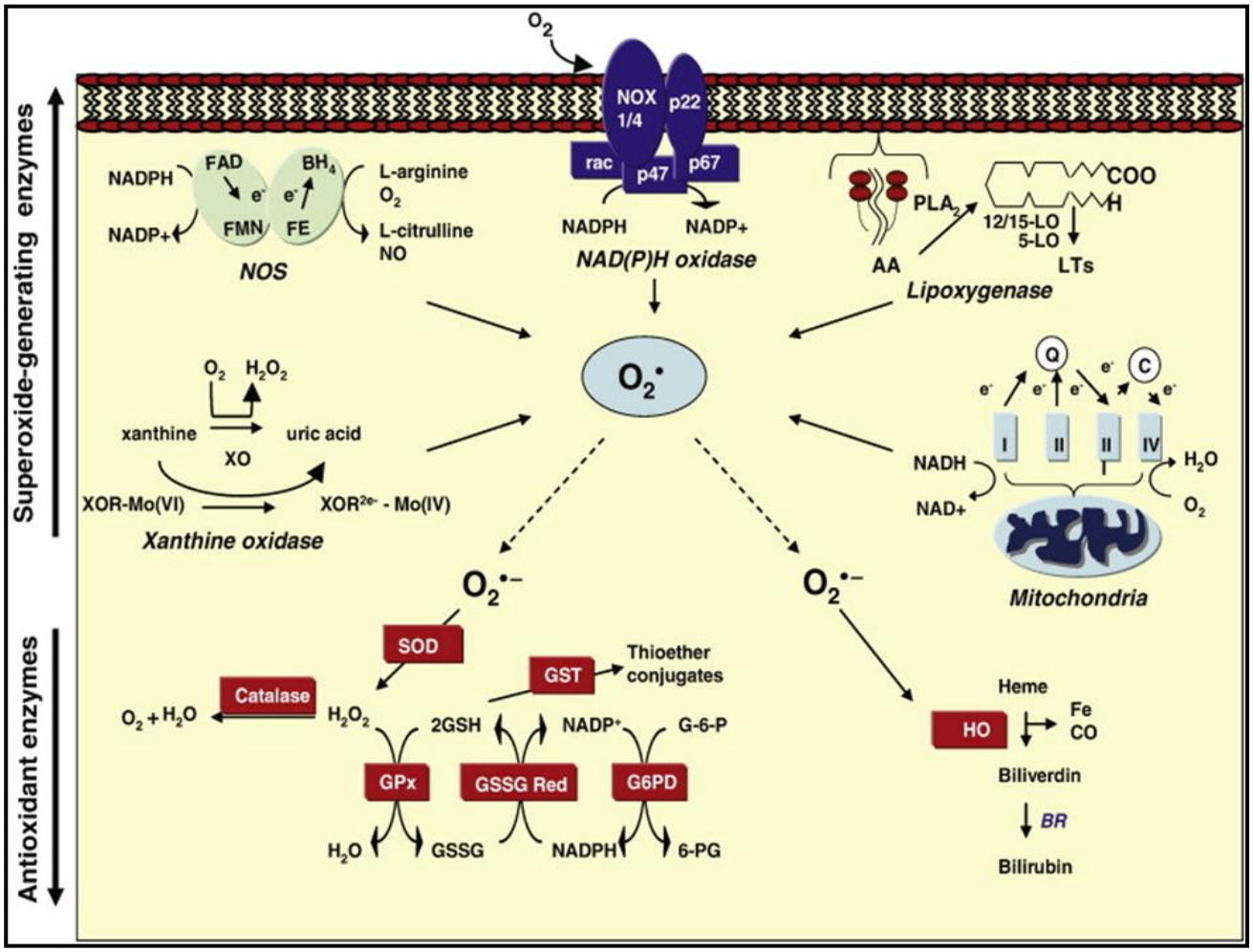

Fig.2.9.b. Important cellular ROS generating enzymes and their removal by antioxidants

b. Dietary anti-oxidants

Several compounds present in plants and vegetables have been suggested to have the ability of reacting with free radicals, without generating further radicals. Other compounds become oxidised after scavenging ROS,and thus need to be regenerated for further use (102).

Vitamins are considered to be antioxidants of major biological importance. Ascorbic acid (vitaminC) is a water-soluble antioxidant, commonly found in relatively high amounts in fruits and vegetables (116). It effectively scavenges several types of ROS/RNS *in vitro,* resulting in the formation of an ascorbyl radical,which can be further oxidised to dehydroascorbate. This molecule can then be regenerated, through the cellular reducing molecules of the cell, to ascorbate. In addition, ascorbic acid can regenerate other small antioxidant molecules from their respective radical species (such as α-tocopherol or GSH). Moreover, it can function as a cofactor for many enzymes, by maintaining the metal ions (such as iron and copper) present in the active centre of those enzymes, in a reduced state. However, the reduction of iron and copper by ascorbate can also result in a pro-oxidant effect, since these ions in the reduced form can be used to fuel the Fenton reaction (106,117).

Vitamin E is a lipophilic vitamin, synthesized only by plants, that exists in eight different forms,of which α-tocopherol is the most active. It is the major membrane-bound antioxidant employed by the cell, whose main function resides in protecting cells against lipid peroxidation (108,118). As mentioned above, during the antioxidant reaction, α-tocopherol is converted to an α-tocopheryl radical, which is then reduced to the original α-tocopherol form by ascorbic acid (164)

Vitamin A and its equivalent in animals, retinol, are also considered important antioxidants. It is present in many foods and can be formed from β-carotene transformation (119,120).

Vitamin B1 (thiamine), has been shown to offer protection in different situations where high levels of oxidative stress were involved (121). In the same way, high levels of vitamins B_2 (riboflavin) and B_{12}(cobalamin) have also been reported to protect against oxidative injury (122).

Carotenoids, of which β-carotene is probably the most studied, are pigments responsible for the colour of many fruits and vegetables. These substances have been recognised as the most potent quenchers of singlet oxygen (123) and have been described to help in the prevention of cancer, heart disease, and stroke (74,124). Other examples of carotenoids with protective effects on oxidative conditions are lycopene (a bright red carotenoid found in red fruits) and xanthophylls (e.g. lutein and zeaxanthin) (125,126).

(Poly) phenolic compounds are secondary plant metabolites possessing one or more aromatic rings with one or more hydroxyl groups within their structure (127). These comprise a wide variety of molecules,divided into several classes (like flavonoids, phenolic acids, stilbenes, and others), commonly found in fruits, vegetables, wine, tea, coffee, and some cocoa products like dark chocolate (128) (129). Many studies have reported a wide range of biological activities for these compounds, including anti-inflammatory (130), anti-carcinogenic, anti-allergic (131), and anti-hepatotoxic (132), which have been described to be mostly due to their antioxidant activity and also their ability to activate endogenous defence systems (102). (174, (133,134).

4. Oxidative stress

The term oxidative stress was first described by Seis in 1985 (135). Oxidative stress refers to the imbalance between the pro-oxidant and antioxidant levels in favor of prooxidants in cells and tissues. This scenario leads to modification of lipids, proteins, and DNA. Such modifications or

damage to these molecules are called oxidative damage. Prooxidant is a species that causes or promotes oxidation. Antioxidant is a molecule inhibits formation of prooxidants and inhibits oxidation. Antioxidants are usually present at a low concentration and yet inhibit oxidation of an oxidizable substrate. Oxidative stress can result from diminished antioxidant levels or antioxidant enzymes or defects in antioxidant machinery expressing the antioxidant gene. Depletions of dietary antioxidants (e.g., vitamins E, C, and D, flavonoids and carotenoids) and micronutrients (e.g., iron, copper, zinc, selenium) that are needed for proper functioning of antioxidant enzymes (catalase, copper, zinc SOD, or glutathione peroxidase) results in the accumulation of prooxidants (free radicals or reactive oxygen species), leading to oxidative stress.

Oxidative stress can also result from increased production of reactive oxygen species from exposure to toxins (e.g., paraquat or cigarette smoke) and activation of endogenous enzymes (e.g., NADPH oxidases) in chronic inflammatory conditions.

5. Oxidative damage

One of the consequences of oxidative stress is cell injury caused by oxidative damage. Targets of oxidative damage are DNA, lipid, and protein.

a. Oxidative damage of DNA

Nucleic acids are particularly sensitive to oxidative damage ROS can damage DNA by direct chemical attack of purine and pyrimidine bases and deoxyribose sugars and also by indirect mechanisms. There are more than 20 known product of oxidative damage of the nucleic acids, particularly hydroxyl radical is known to cause chemical modifications of DNA through the formation of one strand and two strands breaks and cross linkages with other molecules. Different saccharides radicals of DNA can arise by abstraction of a hydrogen atom from 2`deoxyribose

because all positions in saccharides are susceptible to oxidative damage. Hydroxyl radical reacts with aromatic rings. Therefore nitrogen bases of nucleic acids are modified. C5-C6 double bonds of pyrimidines and carbon atoms C4, C5, and C8 of purines are the most sensitive position for oxidative effect of hydroxyl radical, abstract electron and no hydrogen atom (136). In consequence of ROS attack on nuclear proteins generated protein radicals and radicals of base react under formation of DNA-protein crosslinking.

Mitochondrial DNA (mtDNA) is excessively sensitive to oxidative damage because mtDNA is situated near the inner mitochondrial membrane, where ROS are formed. Mitochondrial DNA is small and is not protected by histones like nuclear DNA. Mitochondria can repair an oxidative damage of mtDNA and this base excision repair pathway plays a dominant role in mtDNA repair (137). Damage of mtDNA can be potentially more important like damage of nuclear DNA because all mitochondrial genome code genes are expressed whereas nuclear DNA includes great number of untranscribed sequences (138). Linnane and coworkers (139) assume that accumulation of somatic mutations mtDNA is the main origin of human ageing and degenerative diseases.

b. Lipid peroxidation

Lipid peroxidation can cause damage of membrane proteins as well as lipids. Lipoproteins are also targets of oxidative damage. Lipid hydroperoxides are primary products of lipid peroxidation. Dissociation of hydroperoxides is important from a toxicological point of view for two reasons:

- new radicals are generated and ramify radical reactions,
- non-radical products are produced which can be also biologically active.

It was found, that lipid peroxidation produce unsaturated aldehydes, malondialdehyde, 4 hydroxy-2-nonenal (HNE) and other products that are cytotoxic and mutagenic and can damage other biomolecules (140). Malondialdehyde arises largely from peroxidation of polyunsaturated fatty acids with more than two double bonds and it can also arise enzymatically during eicosanoid

metabolism. 4-hydroxy-2-nonenal has toxic properties like cell growth inhibition, genotoxicity, chemotaxic activity and have the ability to modify lipoproteins and promote atherosclerosis (141). It can react with nucleophile components largely with metabolites and proteins containing thiol groups (142). The effect of HNE is dependent on its concentration. Lipid peroxidation can be overly destructive process in living system Aldehyde products of lipoperoxidation react with mitochondria membrane lipids and change physiochemical state of membrane (143). Peroxidation of membrane phospholipids is accompanied by change structural and functional characteristics of membranes. Lipid peroxidation also affects function of proteins that are component of biological membranes. Consequence of near physiological junction lipids and proteins can lead to oxidative damage of mitochondrial proteins to form proteins cross linkage, protein degradation or to lose of their function (138).

c. Protein oxidation

Protein modifications caused by ROS/RNS include formation of carbonyls, dityrosine, nitrated and chlorinated tyrosines. Nitrated, chlorinated, and brominated tyrosines have been detected in high levels in diseased tissues in patients with inflammatory diseases.

One of the important targets of oxidative damage can be proteins which play elementary roles such as biological accelerators, gene regulators, receptors, transport proteins and structural components of cells. Oxidative modification of proteins by reactive oxygen species or by other reactive molecules (e.g. products of lipid peroxidation) are implicated in the etiology or development of many diseases and it can also contribute to secondary damage of other molecules. Protein oxidation can lead to the breaking of peptide bonds (formation of products with lower molecular weight) and formation of protein-protein cross-links (formation of products with higher molecular weight) and protein netting. These changes can result in different secondary effects including protein

fragmentation, aggregation and unfolding. These processes are ordinarily associated with loss or change of protein activity and function (144,145). Increased oxidative damage of proteins result in:

- an increased production of reactive oxygen species (146),
- a decreased capacity to scavenge reactive oxygen species,
- an increased sensitivity of damaged proteins to become oxidized as a consequence of transcriptional and translational errors (147),
- a decreased levels or activities of the proteosome or proteases which degrade oxidized proteins (148).

d. Markers of oxidative damage

Proteins, lipids and DNA are main targets of reactive oxygen species (ROS). These molecules generate a spectrum of molecules in the condition of oxidative stress which may be estimated for example in plasma, serum, bronchoalveolar lavage fluid, tissues and in exhalated breath condensate and reflect a danger of ROS for a subject in consequence of origin and development of several diseases.

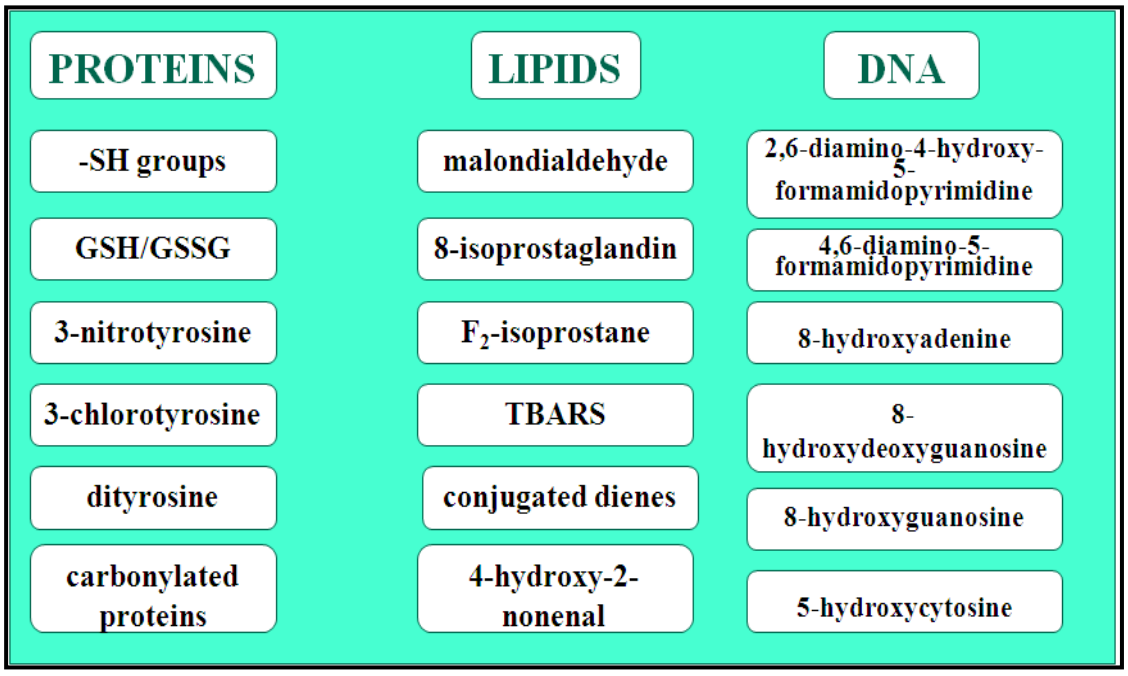

Figure: 2.10 Markers of Oxidative damage (149)

e. <u>Adaptive response in cells exposed to mild to moderate oxidative stress</u>

The cells cope with oxidants (O2•–, H_2O_2, LOOH) through several detoxification mechanisms afforded by endogenous antioxidant enzymes and small molecular-weight antioxidants. Paradoxically, this process (continued exposure to a mild dose of oxidants) has actually resulted in increased synthesis of antioxidant enzymes. This is an intrinsic mechanism by which cells restore the oxidant/antioxidant balance.

The three cellular components involved in this signaling mechanism at the transcriptional level are: Kelch-like ECH-associated protein 1 (Keap1), nuclear factor erythroid 2-related factor 2 (Nrf2), and antioxidant response elements (ARE). Research indicates that the Keap1-Nrf2-ARE signaling pathway is responsible for "turning on" the adaptive response against oxidant stress. The binding of Nrf2 to the DNA sequences present in ARE induce transcription of cytoprotective, antioxidant genes including SOD, GPx, CAT, gamma-GCS, GST. In addition, several other cytoprotective genes (heme oxygenase, NQO-1) are induced. Under normal conditions (reduced intracellular concentration), Nrf2 is stabilized through binding to Keap-1 in the cytoplasm. During enhanced ROS formation or exposure to electrophilic metabolites, the cysteine residues in Keap-1 are modified or oxidized causing the dissociation of Nrf2 and translocation to the nucleus and binding to the ARE. Depending upon the binding site present on the promoter region, the different antioxidant genes are induced (150).

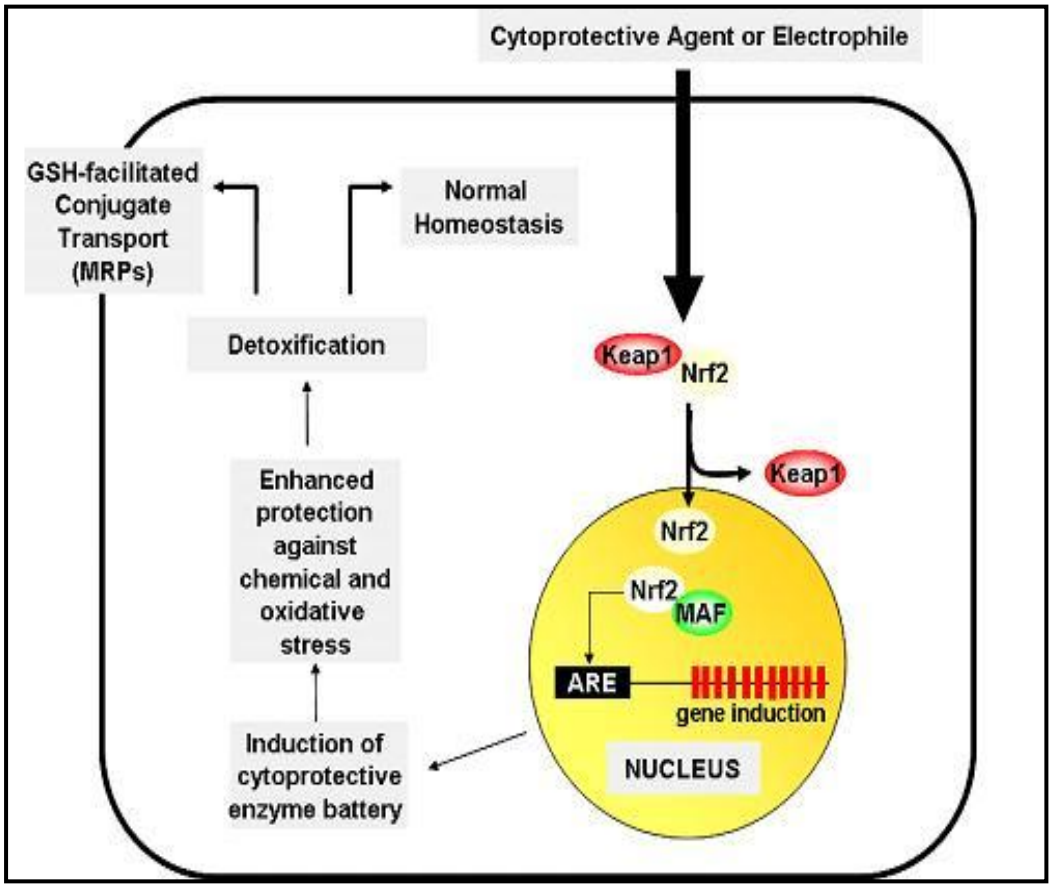

Figure: 2.11. Keap1-Nrf2-ARE signaling pathway

5. Nitrosative stress

Studies have shown that $NO^{\bullet}$ is produced from the metabolism of the amino acid, l-arginine. The enzyme(s) catalyzing this metabolic pathway are known as nitric oxide synthases ($^{\bullet}$NO synthases, or NOS). NOS converts l-arginine to l-citrulline and $^{\bullet}$NO via a 5-electron oxidation of one of the guanidine nitrogens of l-arginine. There are three isoforms of NOS that have been characterized, purified, and cloned in chronological order: neuronal nitric oxide synthase (nNOS) or NOS-1, inducible nitric oxide synthase (iNOS) or NOS-2, and endothelial nitric oxide synthase (eNOS) or NOS-3. The three isoforms are encoded by three different genes on different chromosomes and share nearly 50–60% homology with each other and with the cytochrome P-450 enzymes.

NOS isoforms located in different cellular compartments generate $^{\bullet}$NO for different reasons: nNOS in neurons makes $^{\bullet}$NO for communication between nerve cells; iNOS in macrophages and smooth-

muscle cells makes •NO in large quantities of •NO as part of its killing mechanism in response to lipopolysaccharide, cytokines, and glucocorticoids. Of course, if this form gets out of control, as occurs in septic shock and inflammatory disorders, severe consequences (death) follow; eNOS found in endothelium, brain, and heart makes •NO to relax blood vessels and maintain normal blood pressure.

It was shown that •NO and $O_2^{\bullet-}$ reacts at a nearly diffusion-controlled rate to form the peroxynitrite (151). This is significant because the higher the value of the rate constant, the greater is the likelihood of the two species reacting to form the product. Thus, when these two species are formed in cells, despite the presence of radical scavengers and antioxidant enzymes, they will react because of the higher rate constant. Potentially, there are two consequences and both of which are bad. The $^{\bullet}NO/O_2^{\bullet-}$ reaction forms a more cytotoxic species. Second, it removes •NO required for normal vasodilation.

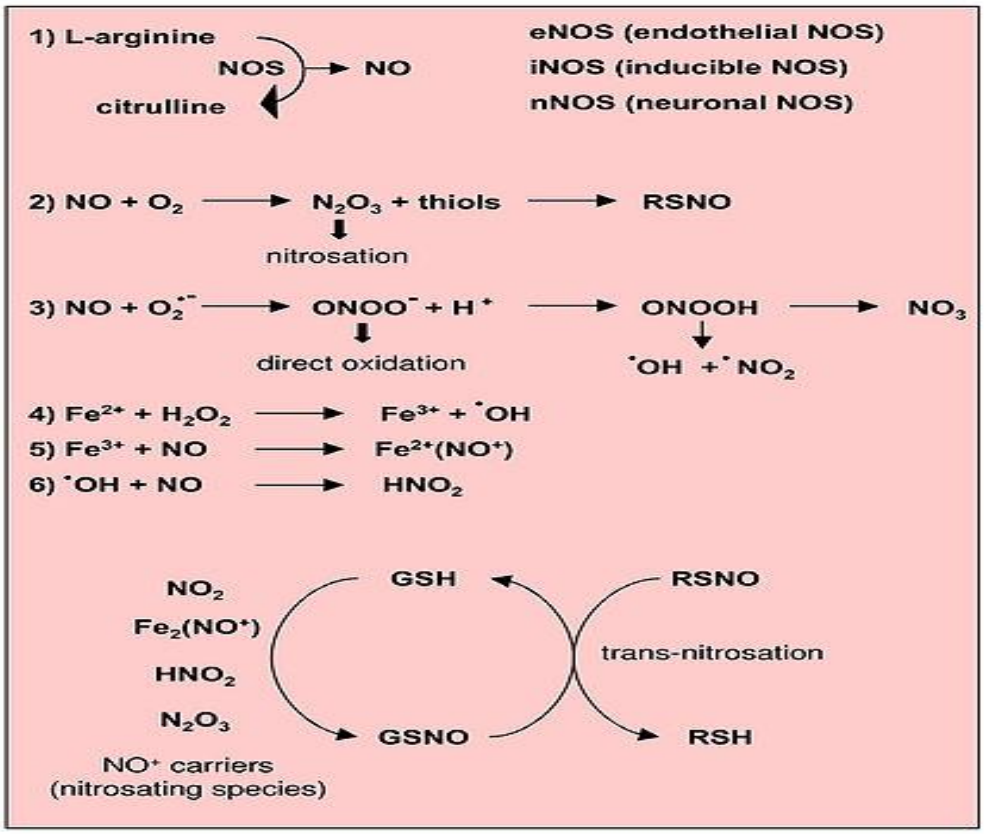

Figure: 2.12 Reactions leading to generation of NO and RNS (152)

a. Markers of nitrosative stress

Nitric oxide (NO), an important source of free radicals, is a diffusible gas that is spontaneously oxidized to form nitrite and then nitrate. The regulation of NO levels depends on the levels and expression of the different NOS. iNOS is not detectable in healthy tissue, it is upregulated by ROS and cytokines resulting in the overproduction of NO. In addition to macrophages and microglia, iNOS under pathological conditions can be expressed in most tissues. Toxicity occurs when excess NO rapidly combines with another free radical, superoxide, to form the powerful oxidizing and nitrating agent, peroxynitrite. The selective nitration of protein tyrosine residues by peroxynitrite causes cellular dysfunction, DNA damage, and cell death, as well as the formation of 3-nitrotyrosine (3-NT) (153–155). For this reason, 3-NT is considered a "footprint" of NO.

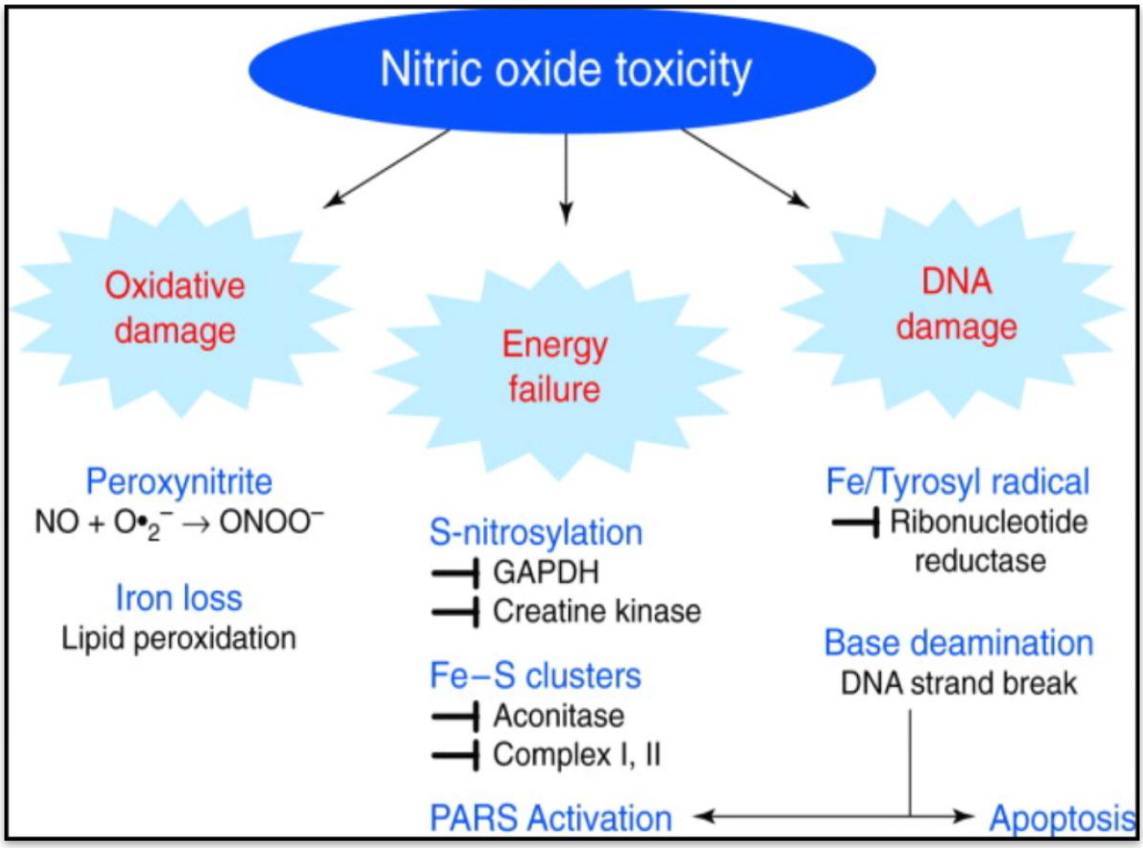

Figure: 2.13.Mechanisms of nitric oxide toxicity

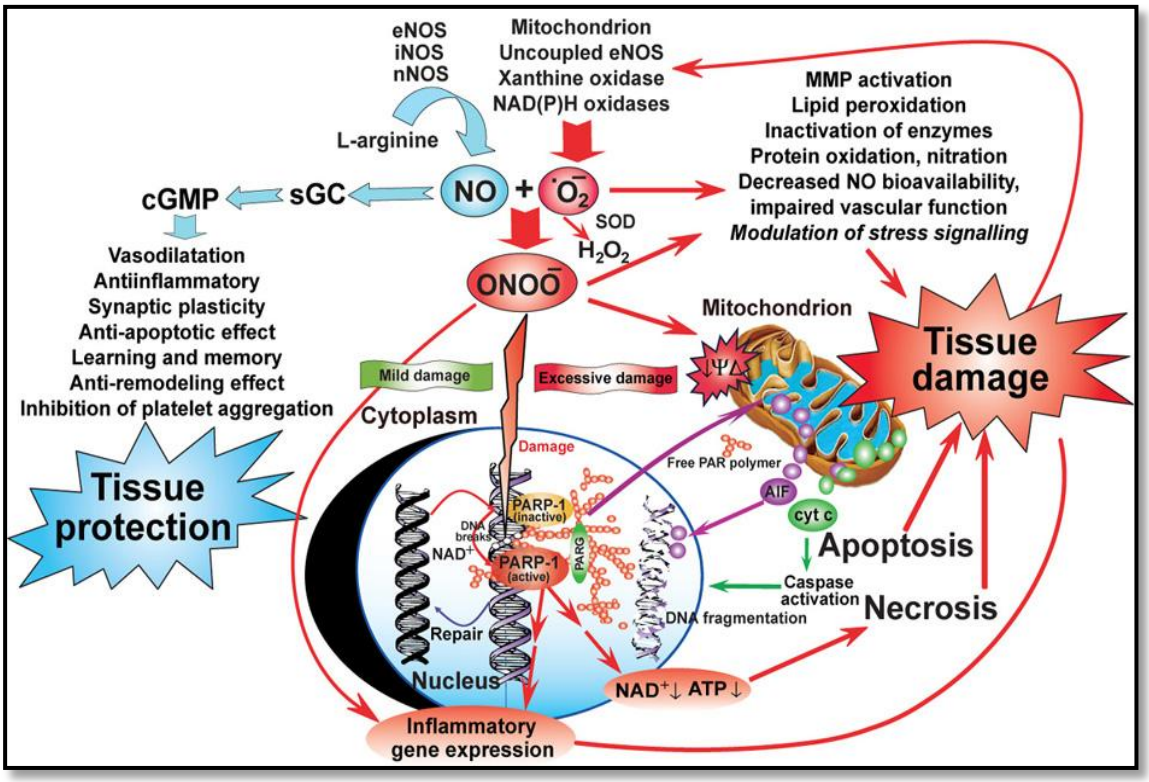

Figure: 2.14 Formation, chemical biology and major targets of peroxynitrite-induced cellular toxicity (156)**.**

b. Biological significance of protein tyrosine nitration

Peroxynitrite oxidizes protein thiols forming disulfide, nitrates tyrosyl groups in proteins forming nitrated proteins. One of the consequences of nitrating tyrosyl groups in protein is either a loss or gain of function in the activity (e.g., manganese superoxide dismutase; MnSOD). Addition of a –NO2 group to tyrosine lowers the pKa of its phenolic–OH by 2–3 units and adds a bulky substituted if placed in relevant tyrosines, nitration can alter protein function and conformation, impose steric restrictions, and also inhibit tyrosine phosphorylation. However, to have biological significance, a loss-of-function modification requires a large fraction of protein to become nitrated at specific critical tyrosines and result in 3-nitrotyrosine to tyrosine ratios in the range of 0.1–1.0; documentation of these large ratios for a given protein in vivo is scanty, and it is doubtful that many proteins will undergo such an extent of nitration. An alternative scenario is a gain-of-function modification, in which case a small fraction of nitrated protein can elicit a substantive biological signal. This attractive concept has been shown in a few proteins such as cytochrome c, which acquires a strong peroxidase activity after nitration (157), in nitrated fibrinogen, which accelerates clot formation and in protein kinase Cε, which becomes activated and translocates on nitration (158).

Nitration can interfere with signal transduction mechanism. Potentially, nitration decreases the pKa of the –OH group of the tyrosine from about 10 down to 7.5. As a result, the –OH group is ionized to –O−. This shift in the ionization of the –OH group present in the tyrosine group could impede phosphorylation and signaling mechanism. Peroxynitrite oxidizes unsaturated fatty acids in biological membranes to form nitrated fatty acids that show multiple and potent biological activities (159). Derivatives of oleic, linolenic, and arachidonic acids were detected and characterized in human body fluids (160). The reaction between peroxynitrite and DNA leads to multiple oxidized products from purine and pyrimidine bases. Some of the biomarkers of oxidative DNA damage (e.g., 8-hydroxy-2-deoxyguanosine (8-OHdG) and 8-nitroguanine) are formed from the reaction between peroxynitrite and DNA (161).

Figure: 2.15 a. Signalling and injury pathway of protein and lipid (162)

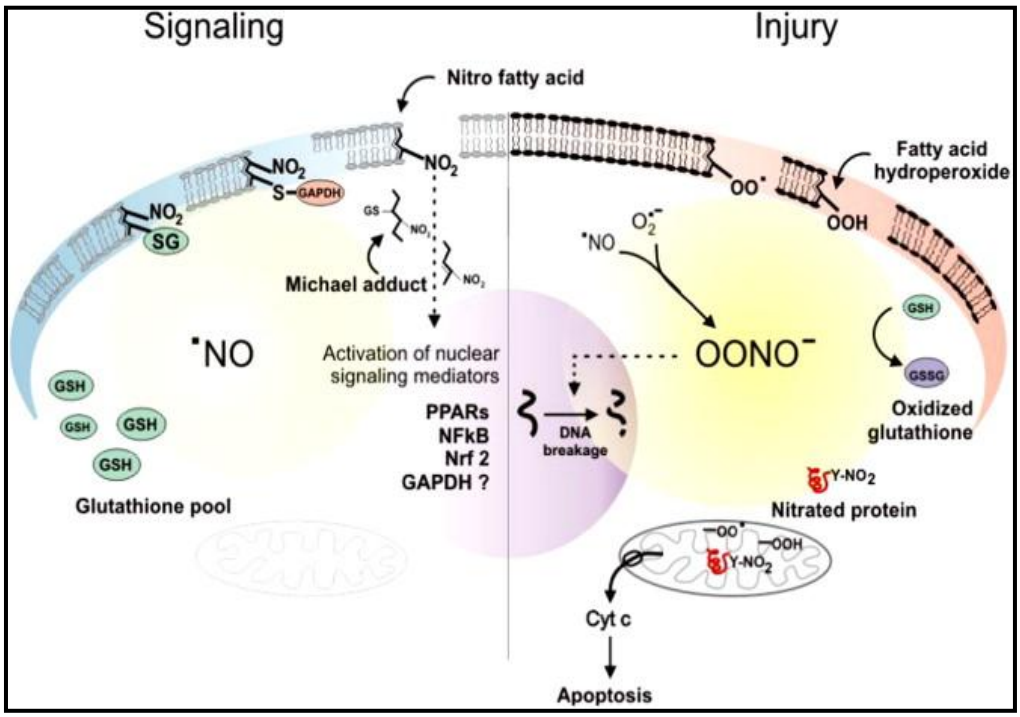

Figure: 2.15 b. Biomolecules of Peroxynitrite (163)

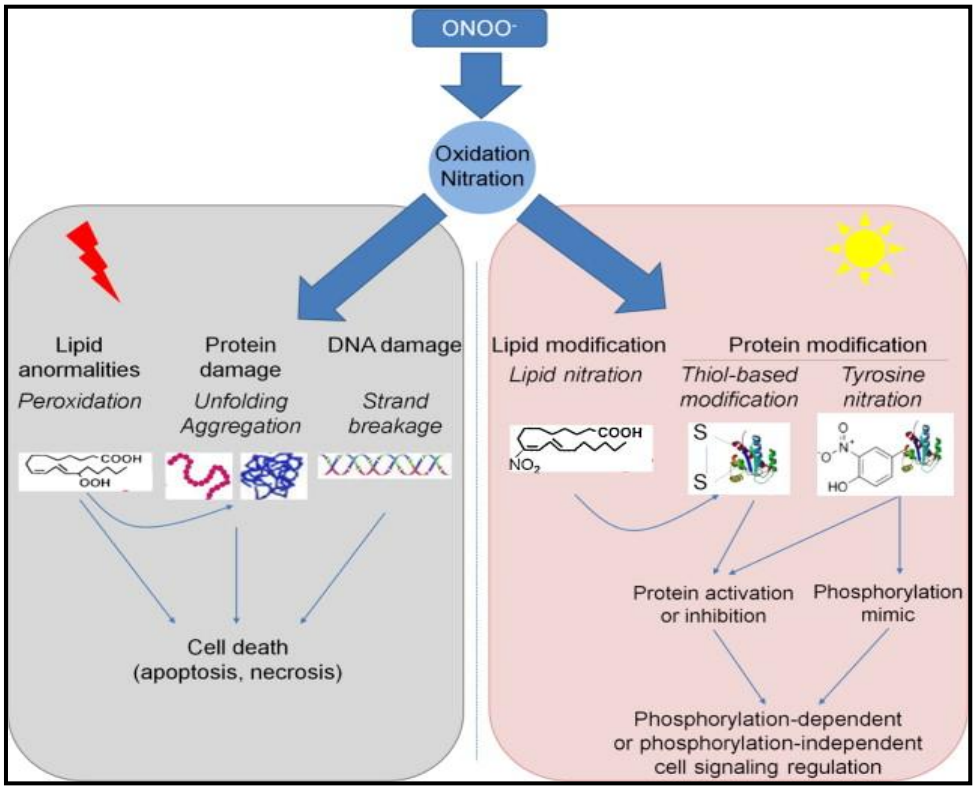

c. Biological significance of S nitrosylation

The modification of thiols can be regulated by redox-related signaling in the cell including ROS/RNS. In addition to S-nitrosylation and S-glutathionylation, free thiols can be oxidized to sulfenic acid (SOH), sulfinic acid (SO2H), disulfide bonds, or sulfonic acid (SO3H). With increasing oxidation states, the modifications become irreversible and this typically leads to irreversible modification of the activity of the protein . It has been suggested that S-nitrosylation and S-glutathionylation of thiol groups in proteins can protect these proteins against irreversible oxidative modifications (164–166).

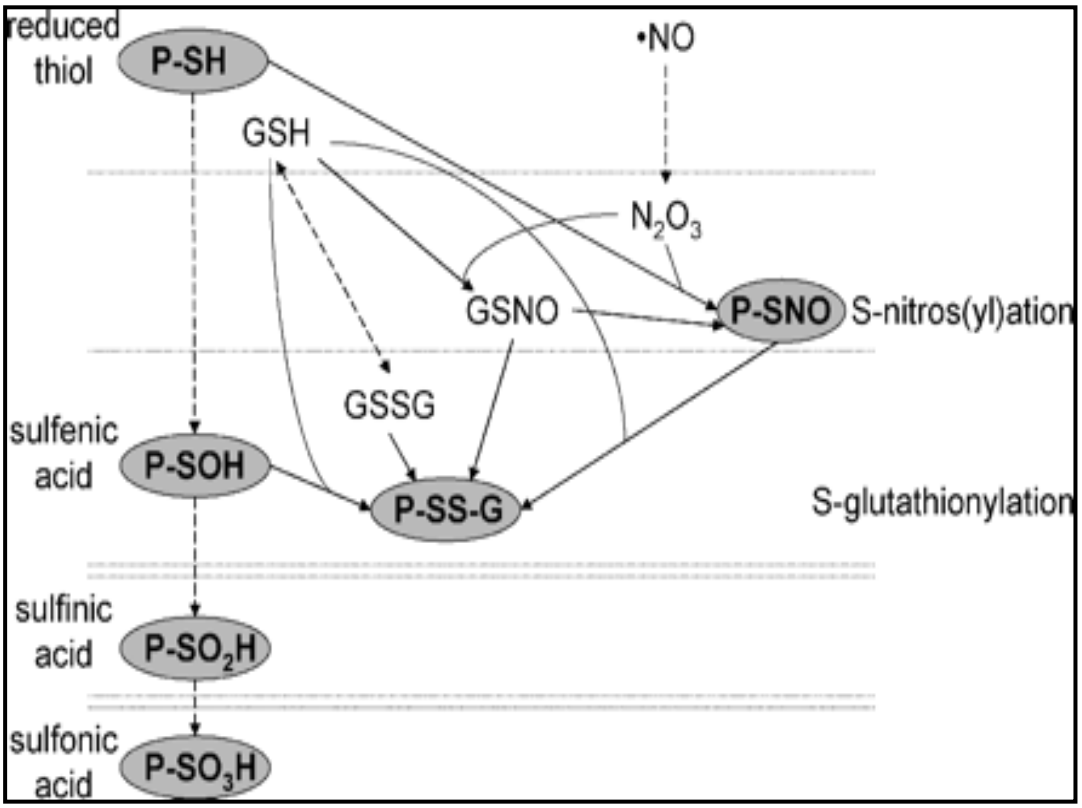

Figure: 2.16a. Scheme depicting several of the chemical pathways leading to the formation of protein S-nitrosylation and S-glutathionylation. Horizontal dotted lines separate one-electron oxidative states. Dashed lines represent oxidations by oxidative species not depicted, including molecular oxygen (O_2). For the sake of simplicity, lines representing a reaction of P-SH with GSSG or GSNO to yield P-SS-G have been omitted. GSH: reduced glutathione; GSNO; S-nitrosoglutathione; GSSG: oxidized glutathione

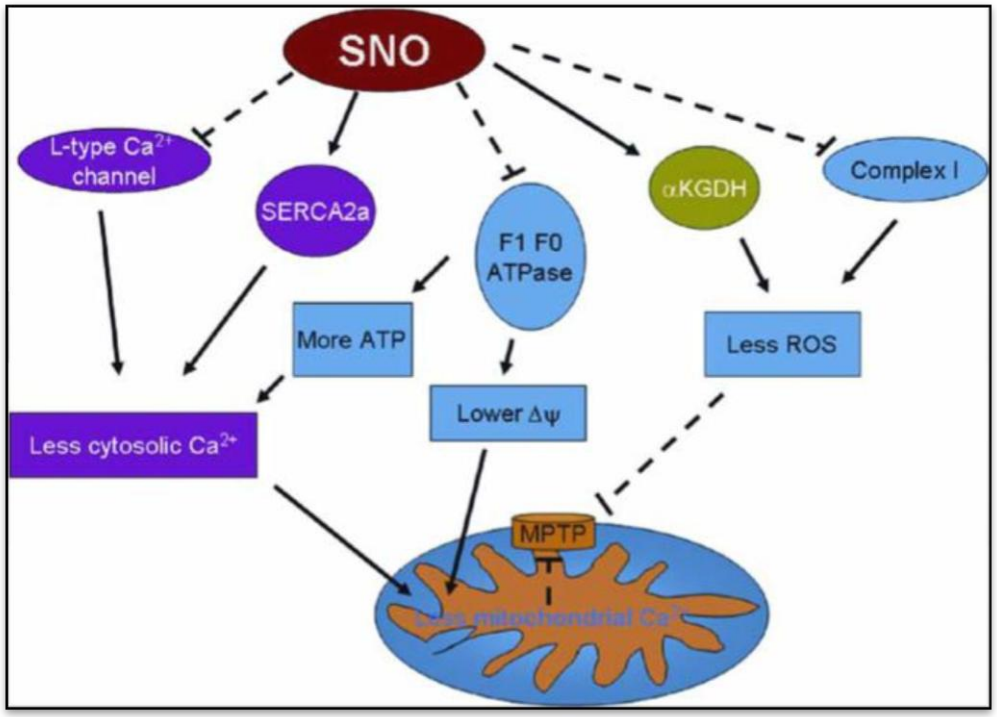

Figure: 12.16b. S-nitrosylation and inhibition of the L-type Ca^{2+} channel, would reduce Ca^{2+} entry into the myocyte during ischemia and early reperfusion. S-nitrosylation also results in activation of SERCA2a, thus further reducing cytosolic Ca^{2+} during ischemia and early reperfusion. S-nitrosylation causes inhibition of the F_1F_0ATPase which would reduce ATP consumption by reverse mode of the F_1F_0ATPase. S-nitrosylation and inhibition of complex I, which has been suggested to reduce ROS generation. Taken together, the increase of protein S-nitrosylation would be expected to lead to reduced Ca^{2+} overload and reduced ROS generation, therefore preventing cell death during I/R injury.

Furthermore, irreversible oxidation of thiols can block the physiological modification by S-nitrosylation or S-glutathionylation and thereby interfere with physiological signalling (167).

S-nitrosylation of the mitochondrial complex I (31,64), cytochrome c oxidase (120), complex V and creatine kinase (121) inhibit their activities, whereas S-nitrosylation of α-ketoglutarate dehydrogenase (α-KGDH) increases its activity (31). Protein S-nitrosylation has also shown to play an important cardioprotective role by modulating the activity of proteins involved in apoptosis and oxidative stress such as caspase 3 (125), cyclooxygenase-2 (COX-2) (86), hypoxia inducible factor 1α (HIF1α) (97), NADPH oxidase (168), and thioredoxin (128).

MITOCHONDRIA

Mitochondria are considered as “the power house of the cell” because they link the energy releasing activities of electrons and proton pump by oxidative phosphorylation with energy conservation in the form of ATP. The mitochondria structure consists of two membranes, an inner and outer membrane which is selectively permeable to thrown into a number of folds or cristae and permeable to most metabolites respectively. The inner membrane of mitochondria regulates mitochondrial enzyme movement, cations and substrates into cytosol. It contains specialized transport sites for small molecules, mitochondrial substrate and electron transport chain from the citric acid cycle which generates electrons and ATP synthase that carries out by oxidative phosphorylation and ATP synthesis. The matrix of mitochondria contains the enzymes of the TCA cycle, fatty acid oxidation, urea synthesis, substrates, nucleotide cofactors, inorganic ions, mitochondrial genetic machinery (DNA, RNA and ribosomes) that generates several mitochondrial proteins.

Figure: 2.17 Structural components of mitochondria (169)

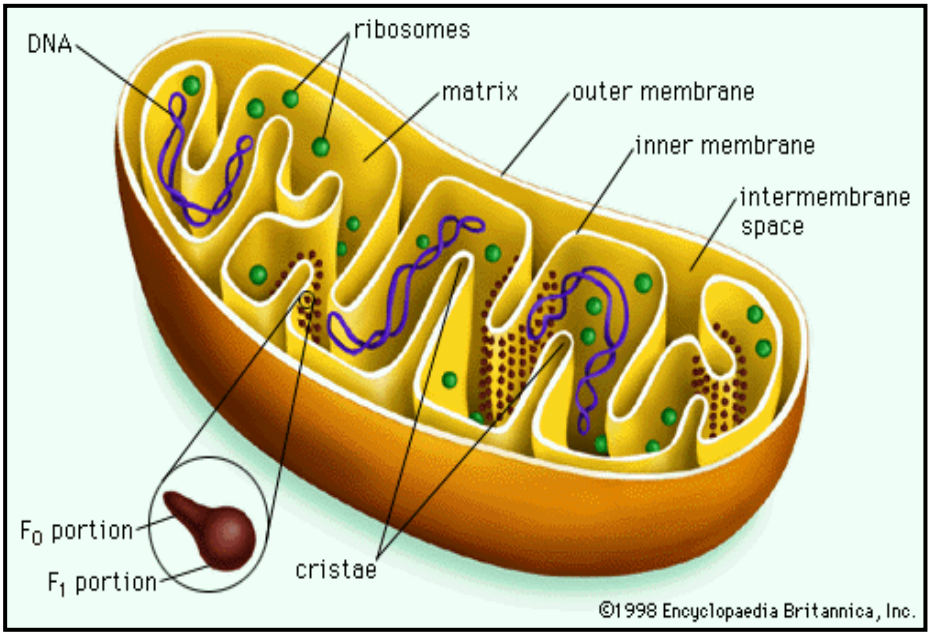

Figure: 2.17 b. Electron microscopic structure of mitochondria

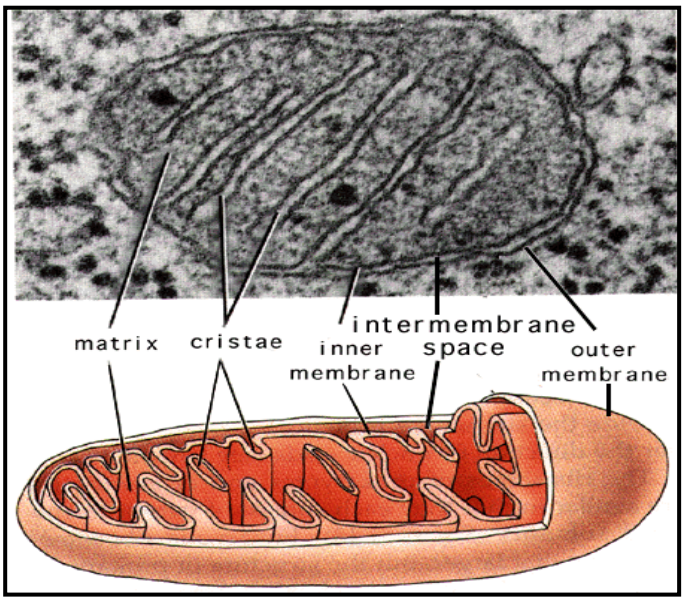

Table: 2.1 Overview Of Biochemical Pathway In Mitochondria (170)

Summary of the composition of the mitochondrial metabolic network
The abbreviations used are: C, cytosol; M, mitochondrial matrix; E, extracellular.

	Number of reactions	Compartment
Glycolysis	12	C
Citric acid cycle	10	M
Oxidative phosphorylation	6	M
ROS detoxification	9	C, M
Fatty acid oxidation	31	M
Phospholipid biosynthesis	16	M
Urea cycle	8	C, M
Porphyrin biosynthesis	12	C, M
Transport and others	85	C, M, E
Total network	189	C, M, E

Figure: 2.18 Some biochemical pathways that occur in the mitochondria (171)

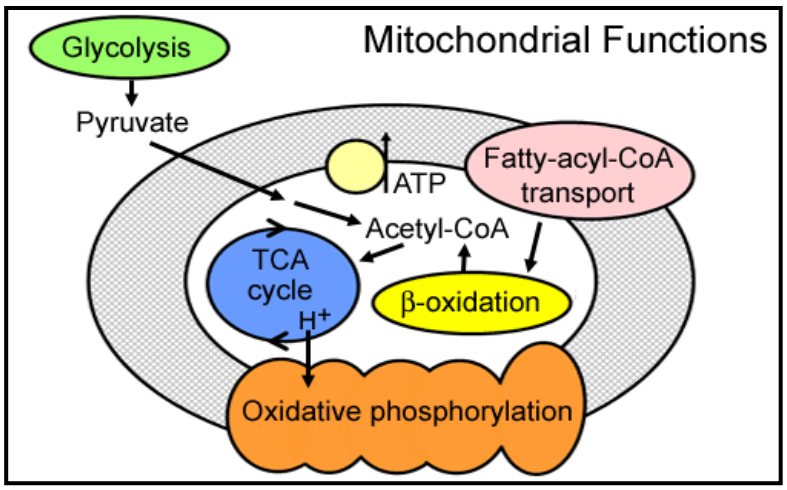

a. Overview of ATP synthesis

The final stage of cellular respiration occurs in the inner membranes of mitochondria. This stage has two parts: an electron transport chain and ATP production by ATP synthase. First, the carrier molecule NADH transfers electrons from the original glucose molecule to an electron transport chain. In this way the electrons move from carrier to carrier within the inner membrane of the mitochondria, eventually being "pulled" to oxygen at the end of the chain. Then the oxygen and electrons combine with hydrogen ions, forming water. Each transfer in the chain releases a small amount of energy. This energy is used to pump hydrogen ions across the membrane from where they are less concentrated to where they are more concentrated. This pumping action stores potential energy and is controlled by a protein structure called ATP synthases. Hydrogen ions pumped by electron transport rush back "downhill" through the ATP synthase. The ATP synthase uses the energy from the flow of H+ ions to convert ADP to ATP.

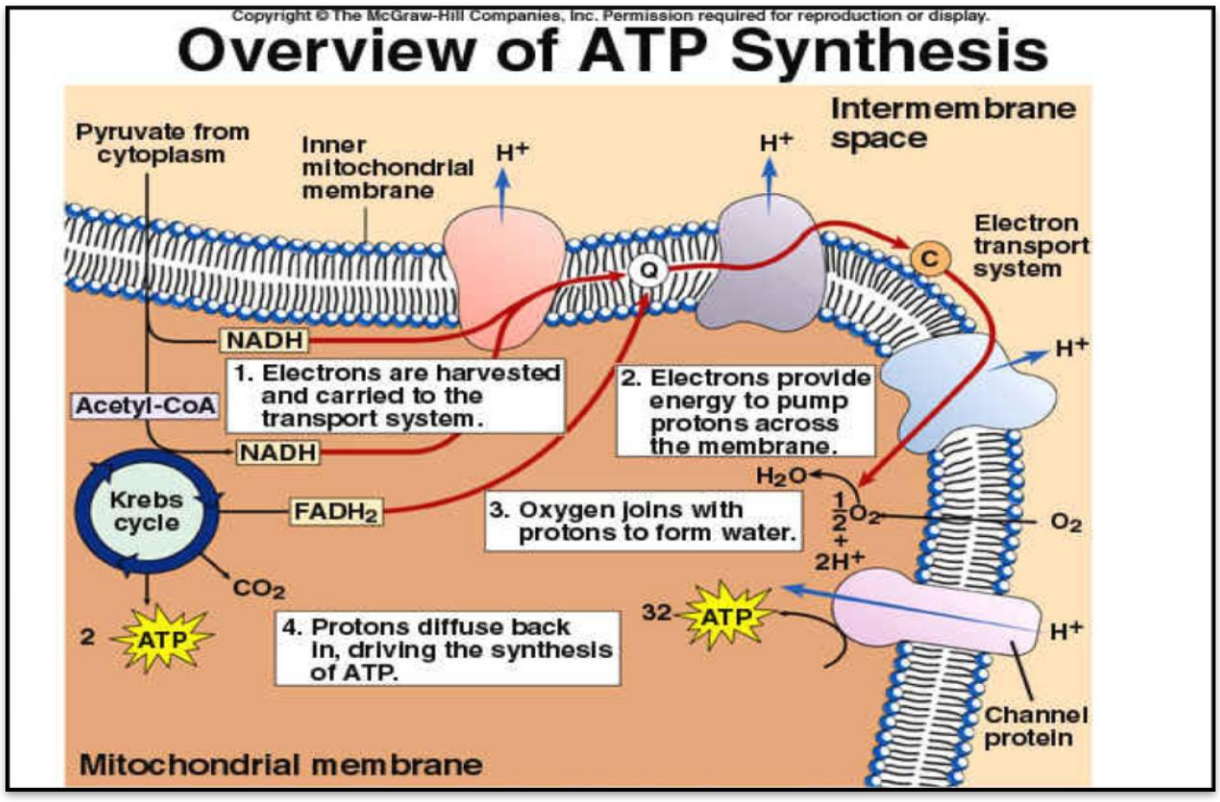

Figure: 2.19. Electron transport chain and oxidative phosphorylation

b. Mitochondria are sources and targets of ROS and RNS

Oxidative stress is inseparably linked to mitochondrial dysfunction, as mitochondria are both generators of and targets for reactive species (172). Mitochondria are rich in lipids and proteins, and have their own DNA and hence are readily susceptible to ROS mediated injury. Cardiolipin which is found almost entirely in the inner mitochondrial membrane is susceptible to peroxidation by ROS (173), as it contains PUFA. Mitochondria have a high content of proteins mainly in the form of enzymes and transporters as they are an important metabolic center of the cell. Therefore, the mitochondria have their own antioxidant system in order to protect itself .

Proteins may be oxidized by ROS resulting in the formation of carbonyls. Thus, carbonyl groups represent an irreversible protein modification, often leading to the inactivation of the proteins, (174). Lipid peroxidation and protein carbonyl content are two important parameters to assess the oxidative damage to lipids and proteins, respectively. Protein carbonyl content (Pco) is reported to be a sensitive and early marker of oxidative stress to tissues as compared with lipid peroxidation (175).

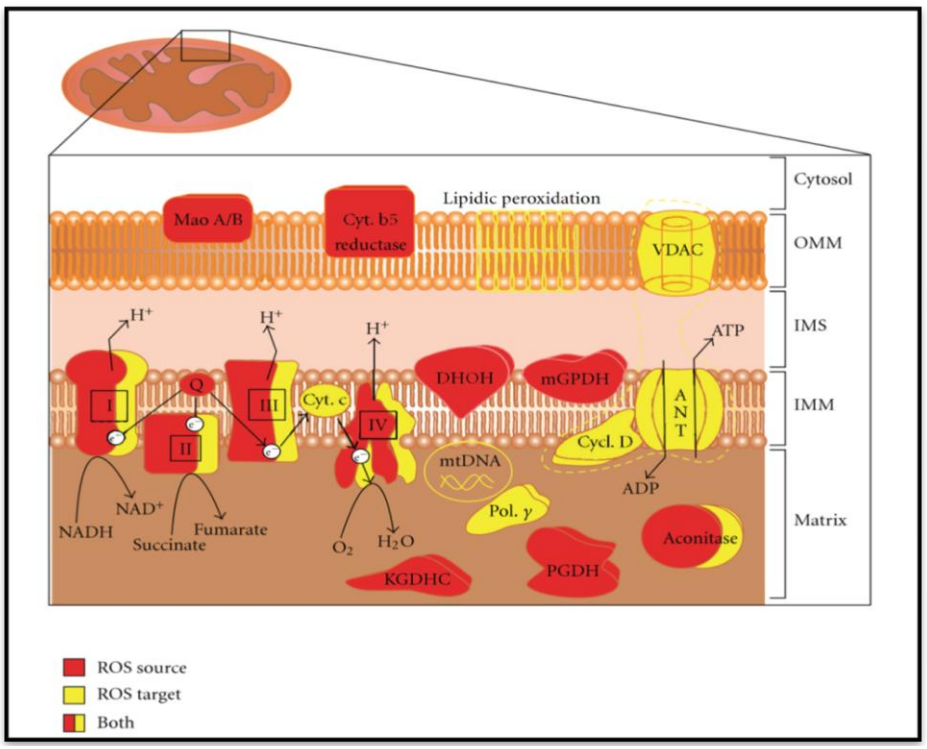

Figure: 2.20 Sources and targets of ROS in the mitochondria (176)

Recent studies have shown that the major site for the production of ROS is mitochondria known as (mtROS), which can directly stimulate the production of proinflammatory cytokines and pathological diseases.

The electrons (e^-) which are produced from NADH and $FADH_2$ pass through the ETC and ultimately leads to the production of reduced O_2 to form H_2O_2 at complex IV. In this leakage of e^- to form superoxide ($O_2^{\cdot-}$) at complex I and III to produce mitochondrial ROS. In this, complex I releases $O_2^{\cdot-}$ with the matrix, whereas complex III releases $O_2^{\cdot-}$ towards both the matrix and innermembrane space. Once free radicals are generated $O_2^{\cdot-}$ is dismutated to H_2O_2 by superoxide dismutase 1 in the inner mitochondrial space and SOD2 in the matrix region. Finally H_2O_2 is fully reduced to water by glutathione peroxidase. Both $O_2^{\cdot-}$ and H_2O_2 produced in this process are considered as mtROS. $O_2^{\cdot-}$ acts as a signalling molecule in the cell

Figure: 2.21. Mitochondrial ROS production and disposal (94)

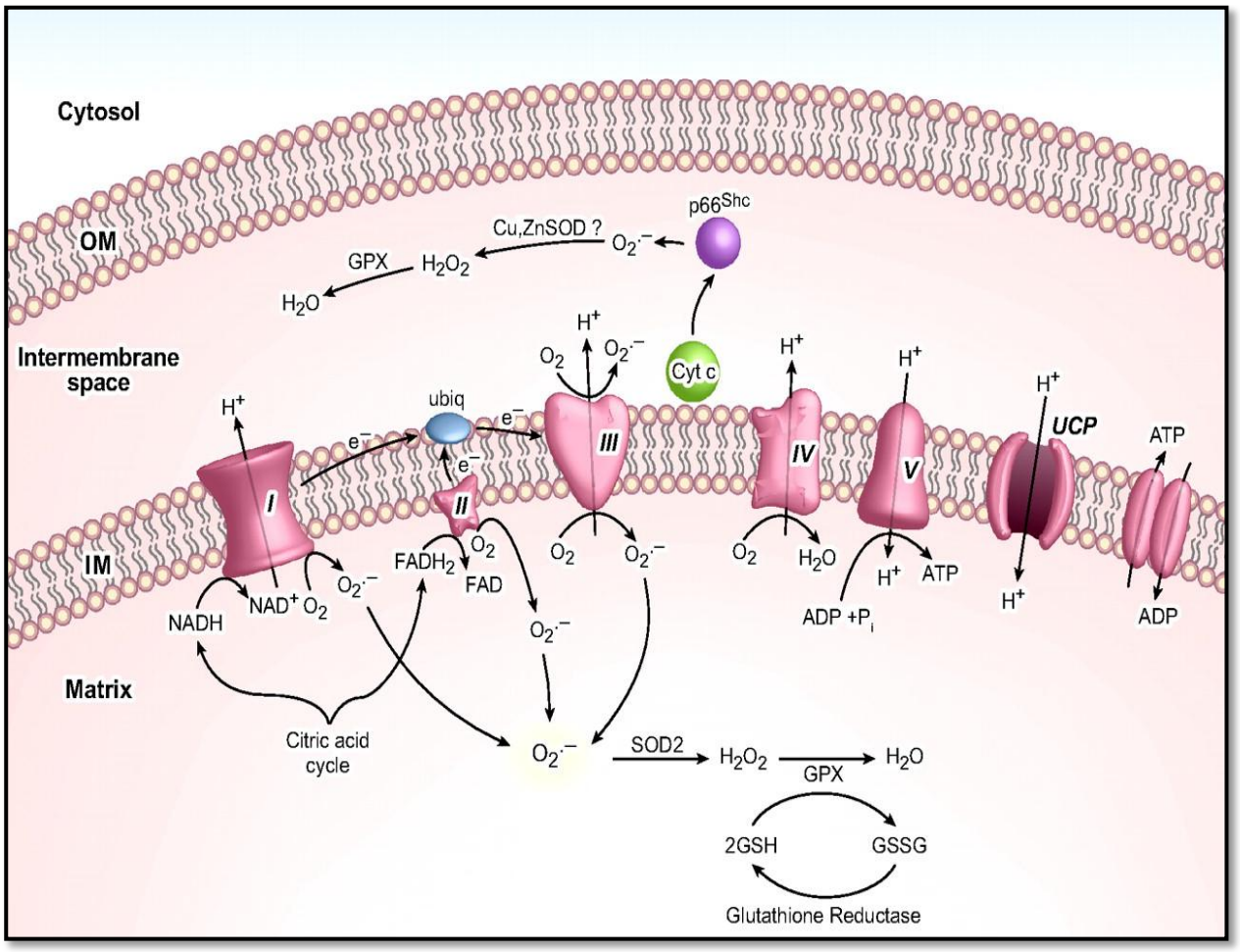

The mitochondrial production of nitric oxide is catalyzed by nitric-oxide synthase. This enzyme has the same cofactor and substrate requirements as other constitutive nitric-oxide synthases. Its occurrence was demonstrated in various mitochondrial preparations (intact, purified mitochondria, permeabilized mitochondria, mitoplasts, submitochondrial particles) from different organs (liver, heart) and species (rat, pig). Endogenous nitric oxide reversibly inhibits oxygen consumption and ATP synthesis by competitive inhibition of cytochrome oxidase (93).

c. Specific mitochondrial protein targets of ROS and RNS

The production of nitric oxide inhibits the oxygen consumption in mitochondria. It competes with oxygen to bind with cytochrome c oxidase in complex IV. NO inhibits complex IV which leads to reduced activity of electron transport chain, and ATP synthesis, as well as leakage of by electrons. Nitric oxide reacts with superoxide anion spontaneously to generate peroxynitrite ($ONOO^-$). Following this peroxynitrite-mediated amplication cycle could result in a progressive increase of mitrochondrial level of $ONOO^-$, can induce additional cytotoxic effects in mitochondria (177).

Mitochondrial proteins are nitrated in vitro and in vivo, including MnSOD, aconitase, cytochrome c, voltage-dependent anion channel, ATPase, and succinyl-CoA oxoacid-CoA transferase (178,179). The nitration/inactivation of MnSOD operates as a positive loop for enhanced intramitochondrial peroxynitrite formation, which in turn triggers apoptotic signaling of cell death, in part by the thiol oxidation-dependent assembly of the permeability transition pore (178). Detection of nitrated mitochondrial proteins and even nitrated cytochrome c in the cytosol may serve to reflect extents of mitochondrial $^{\bullet}NO$-dependent oxidative stress (157,178,179). Importantly, the enhanced peroxidatic activity of nitrated cytochrome c (157,178) may further contribute to oxidative damage.

Figure: 2.22. Protein targets of nitric oxide (177)

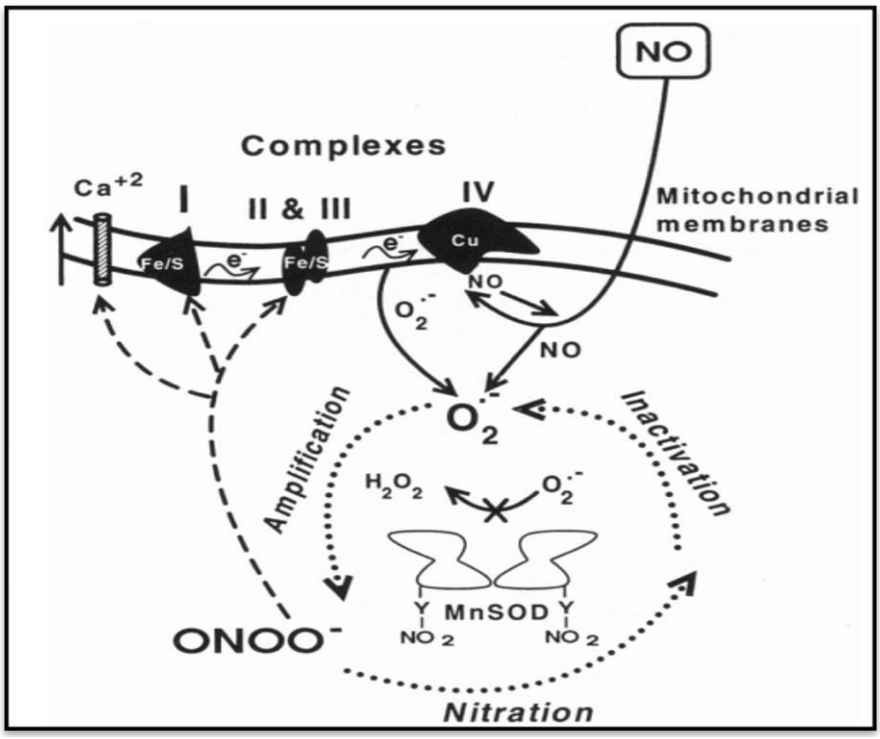

Figure: 2. 23 Deleterious Effects Of Mitochondrial Overproduction Of Reactive Oxygen Species (180)**.**

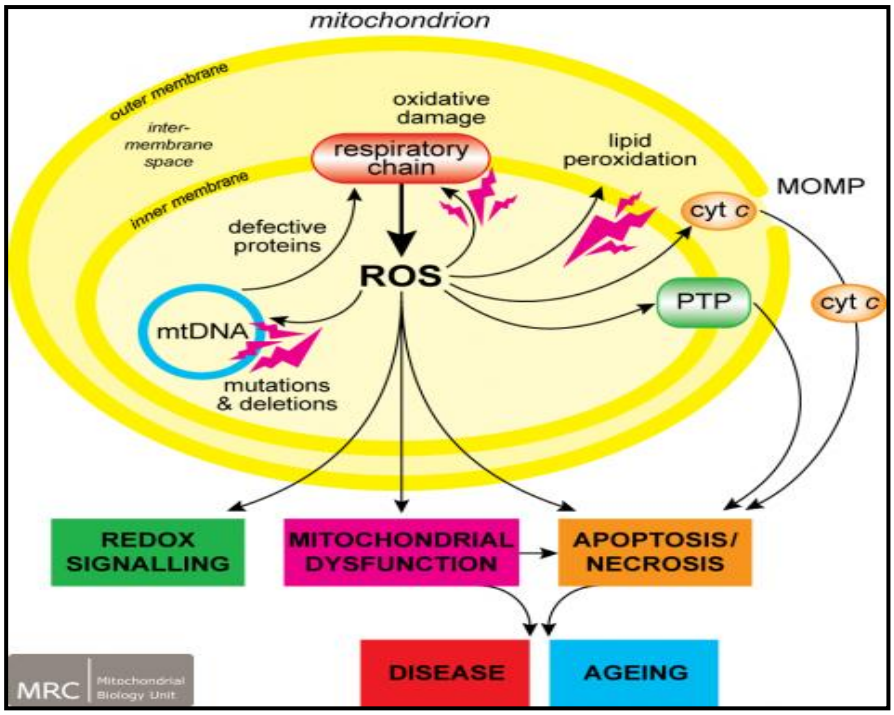

CELL DEATH PATHWAYS

The exposure to oxidative stress may ultimately result in cell death, as a consequence of severe damage caused to biomolecules by reactive oxygen and nitrogen species (92)

Necrosis is an uncontrolled form of cell death (181). During this process, rapid swelling of the cell, leading to the loss of membrane integrity and consequent release of the cells' contents, provoke an inflammatory response.

(a) Apoptosis is programed cell death. A variety of cell behaviours that may lead to active forms of cell death have been observed. These include apoptotic cell death, autophagic death, mitotic catastrophe, oncosis, anoikis, excitotoxicity, and paraptosis. In this way nuclear morphology as a distinction criterion, on programmed cell death has been divided into three possible classifications: classical apoptosis, autophagic cell death, and necrosis-like PCD (182,183).

Type I PCD or classical apoptosis is an active process by which dying cells are removed in a safe, non-inflammatory manner (184). It is a tightly regulated process, including tissue development, carcinogenesis, immune response, and balance control between proliferation and differentiation (88,185). At the morphological and biochemical levels, it is characterised by shrinkage of the cell,membrane surface blebbing, oligonucleosomal DNA fragmentation, and the breakdown of the cell into various membrane-bound fragments, called apoptotic bodies. Along with these events, occurs the activation of specific cysteine proteases, named caspases, as well as the loss of membrane phospholipid asymmetry, which results in the externalization of phosphatidylserine (186).). It is a complex process involving both pro and anti-apoptotic proteins, which can be initiated by two different signalling pathways: the **death receptor (extrinsic)** pathway and the stress- or **mitochondria mediated (intrinsic)** pathway (187).

Figure: 2.24 Overview Of Extrinsic And Intrinsic Apoptotic Pathways (188)

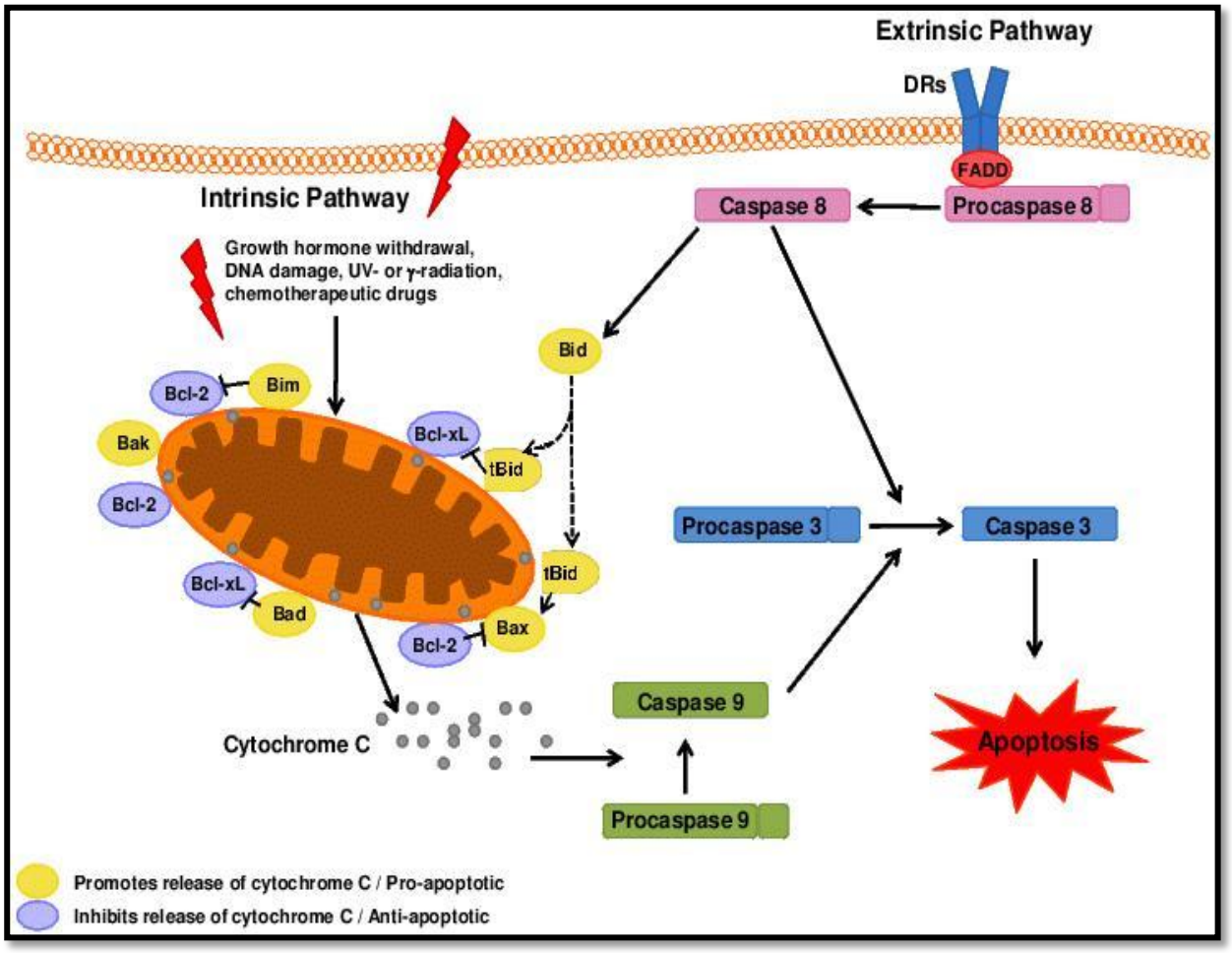

Type II PCD or autophagic cell death characterized by the presence of double- or multiple membrane vacuoles, mitochondrial dilation, enlargement of the endoplasmic reticulum (ER)and Golgi apparatus. The vacuoles formed during this process, which are also called autophagosomes, engulf portions of cytoplasm and organelles (like mitochondria and ER), then fuse with lysosomes, where the intravacuolar content is disintegrated by lysosomal enzymes. The mammalian protein kinase TOR (which stands for "target of rapamycin") plays a major role in the regulation of the autophagic process, by inhibiting this pathway

Recently, an active form of necrosis **(type III PCD)** was found to occur, not only under pathological conditions, also under normal physiological conditions (189). It lacks caspase and

lysosomal involvement and is mainly characterized by an early swelling of intracellular organelles, followed by loss of plasma membrane integrity (although nuclear disintegration is retarded). Programmed necrosis can occur by the induction of the tumor necrosis factor (TNF) or Fas ligand, via their respective death receptors, and gives an idea of the cell control in necrosis (190).

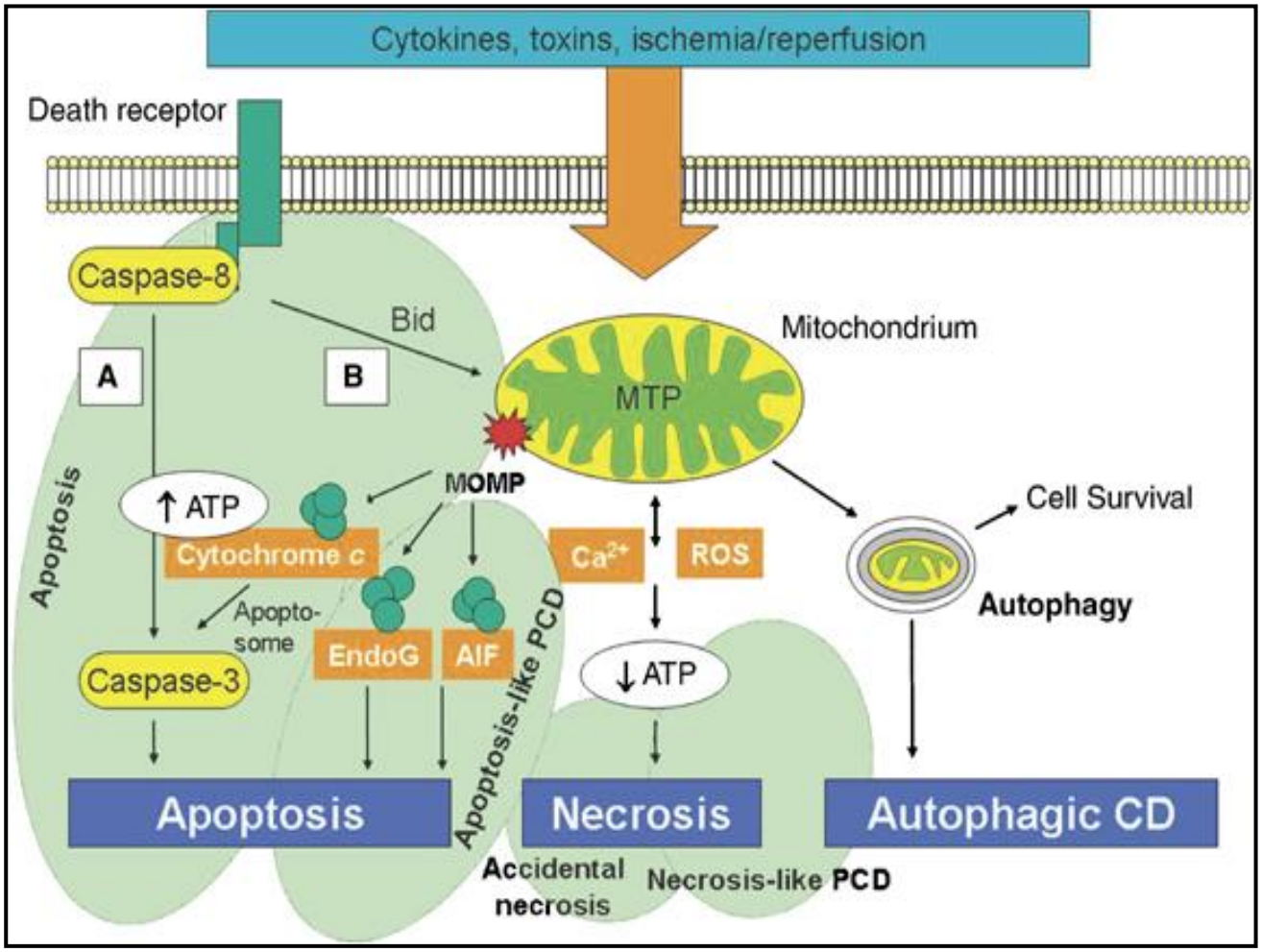

Figure:2.25 Signalling Of Mitochondrial Cell Death Pathway (191)**. AIF, apoptosis inducing factor; CD, cell death; EndoG, endonuclease G; MPT, mitochondrial permeability transition; MOMP, mitochondrial outer membrane permeabilization; ROS, reactive oxygen species.**

Figure:2.26 Apoptotic Cell Death Pathways (192)

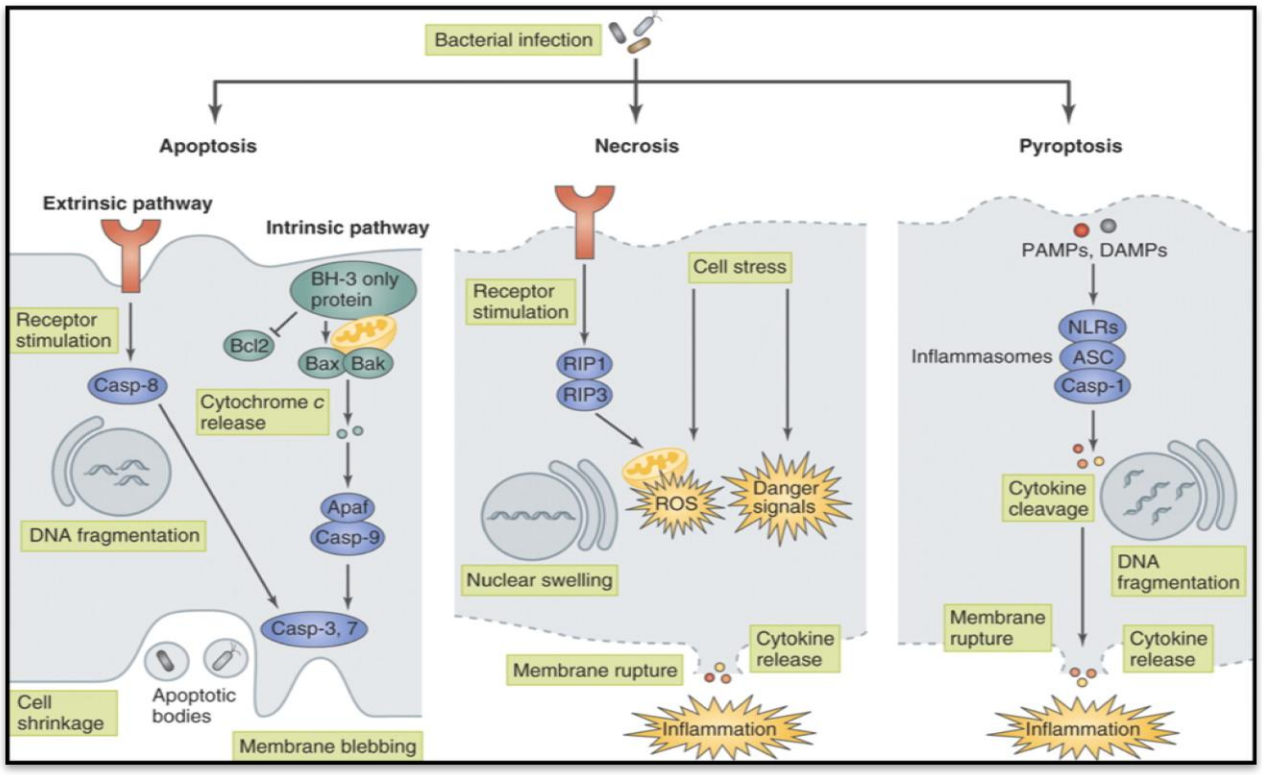

The role of ROS/RNS in the induction of cell death

The intracellular accumulation of reactive oxygen and nitrogen species also plays an important role in the initiation of cell death processes (100). In fact, the amount of reactive species accumulated in the cell, and the way the cell responds to that redox imbalance, can determine that same cell's fate. For example, mild oxidative stress may activate biological responses that can either lead to survival and proliferation, orcan induce apoptosis, while the accumulation of high levels of ROS may promote necrosis instead (193,194). Moreover, a sudden burst of ROS, resulting from the response to oxidative stress of cells already committed to apoptosis, can direct those cells towards a necrotic like death (100). The accumulation of reactive species has been described to precede changes in the mitochondrial membrane, nuclear condensation, and other typical apoptotic events (195). Indeed, some studies have reported that an increase in ROS induces cytochromec release from mitochondria (in a voltage-dependent anion channel (VDAC)-dependent way), and caspases activation (168,196).

Many studies have shown other evidences for the induction of apoptotic pathways by reactive species. Some mediators of apoptosis (e.g. JNK, ERK, PTEN) has been reported to lead to increased levels of ROS (197,198). Similarly, it has been shown that inhibition of the mitochondrial respiratory chain at complex I (199), or an impairment of the electron transfer chain by mutations in mitochondrial DNA, prevent the accumulation of ROS, and consequently protect cells against apoptosis (200). In addition, lipid peroxidation has also been reported to occur following an apoptotic signal (201,202). Moreover, inhibition of apoptosis by the addition of antioxidants has already been described (203,204). For example, the antioxidant enzyme MnSOD has been reported to inhibit apoptosis during ischemia/reperfusion injury (205), and "classical"antioxidants such as α-tocopherol and GSH have shown to prevent apoptosis induced by ascorbate-iron (201). Thus, these studies point towards a wide range of actions for ROS/RNS and add further importance to the use of antioxidants to prevent apoptosis and treat several disorders.

Figure: 2.27. Reactions of peroxynitrite leading to apoptotic or necrotic cell death. (206)

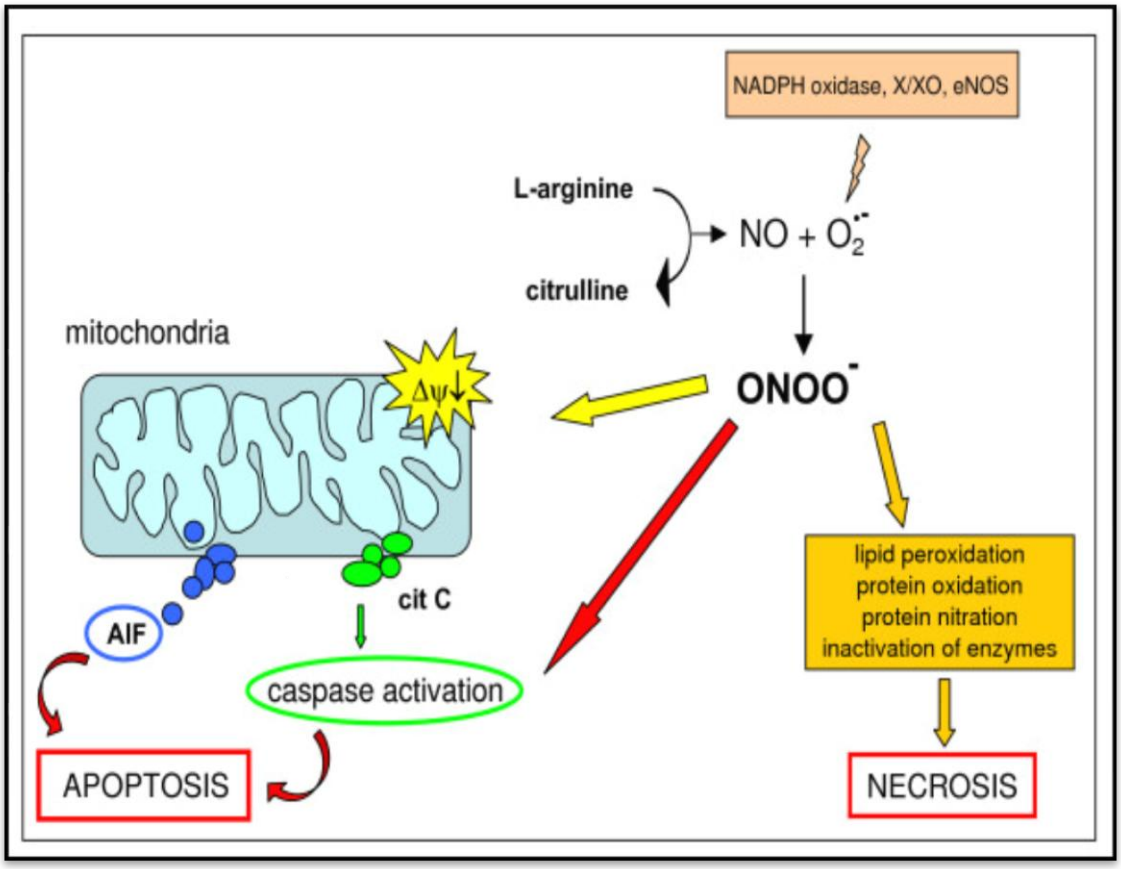

Oxidative stress, Nitrosative stress and disease

In normal conditions, cells can deal with mild levels of oxidative stress. They do so by upregulating the expression of genes responsible for the synthesis of antioxidant defense mechanisms. However, the intracellular accumulation of high levels of ROS/RNS can result in damage to all types of biomolecules, and ultimately leads to cell death, which has been associated with many pathological conditions (71). Oxidative stress plays a central role in a variety of pathological conditions ranging from inflammatory conditions of cancers. Oxidative stress also seems to be important in the etiology of several cardiovascular diseases, like atherosclerosis, ischemic heart disease, cardiomyopathies, and congestive heart failure, among others (72,79).

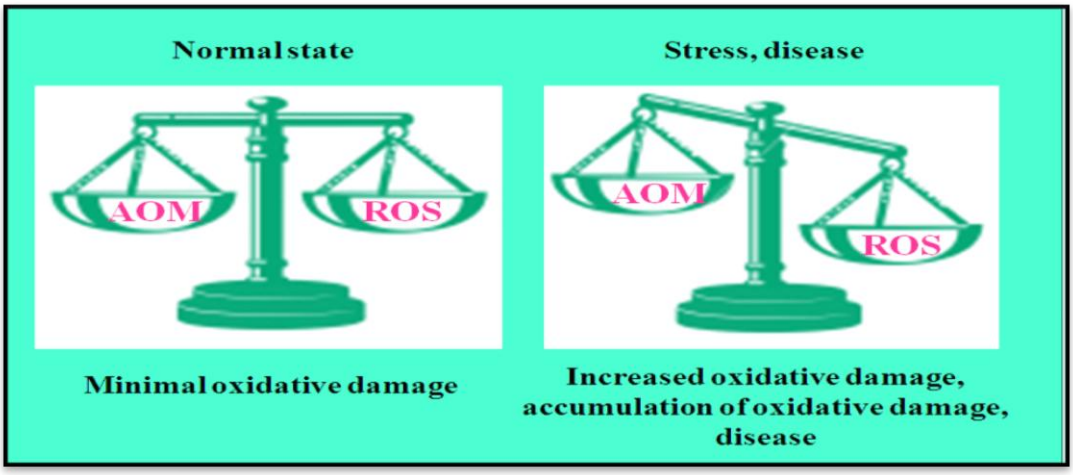

Figure:2.28 Reactive species in the development of disease. (149)**.**

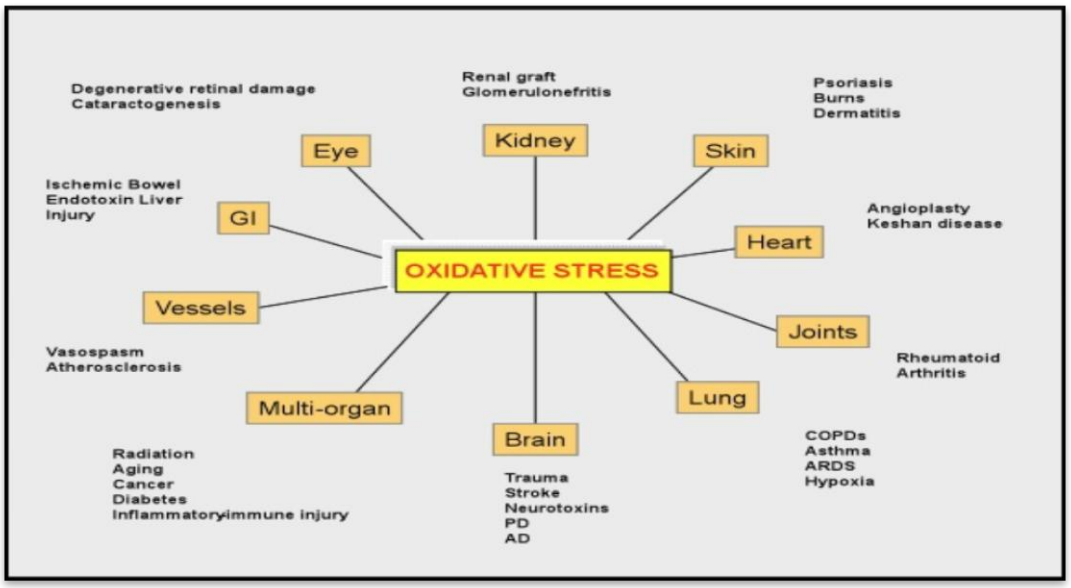

Figure: 2.29. Oxidative stress in Diseases (207)

NUCLEAR FACTOR KAPPA B (NF-κB)

Nuclear factor kappa B is a nuclear transcription factor was identified first by Sen and Baltimore in 1986, as a factor located in the nucleus of B cells that binds to the enhancer of the kappa light chain of immunoglobulins (208). It is a dimeric complex of the Rel protein family which composed of Rel (c-Rel), Rel A (p65), Rel B, NF-κB1 (p50 and its precursor p105) and NF-κB 2 (p52 and its precursor p100). It regulates the expression of various genes involved in the components of the immune system which include proinflammatory cytokines, chemokines, adhesion molecules, inducible enzymes (COX2 and iNOS) which regulate the innate immune response as well as proteins that regulate the specific immune response that control lymphocyte proliferation and differentiation.

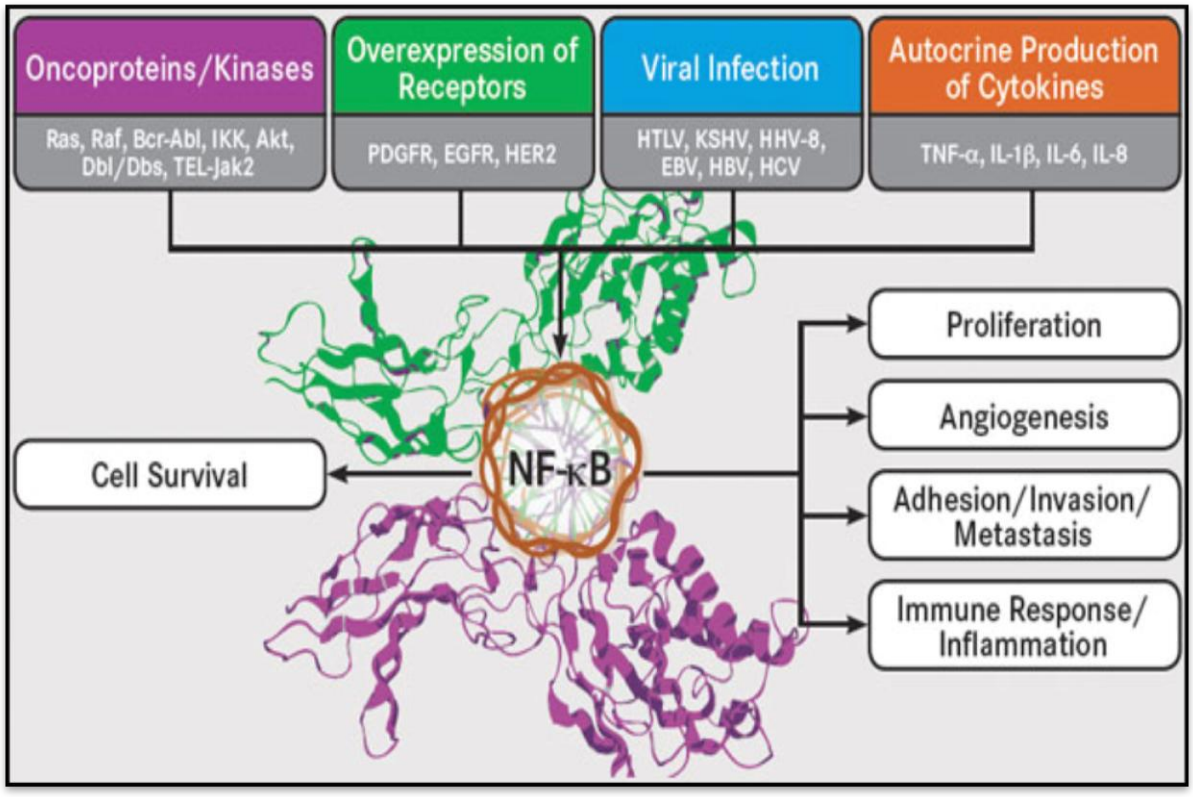

Figure:2.30 Different Roles of NF-κB (209)**.EBV, indicates Epstein-Barr virus; EGFR, epidermal growth factor receptor; HER2, human epidermal growth factor receptor 2; HBV, hepatitis B virus; HCV, hepatitis C virus; HHV-8, human herpesvirus 8; HTLV, human T-lymphotropic virus; IL, interleukin; PDGFR, platelet-derived growth factor receptor; TNF, tumor necrosis factor**

Oxidative stress is a primary activator of the heterodimeric NF-κB. Upon activation, release of cytoplasmic p-IκBα allows for translocation of NF-κB to the nucleus to enhance transcription of NF-κB-dependent genes and consequent release of proinflammatory cytokines in the pathogenesis of inflammation and fibrosis (210).

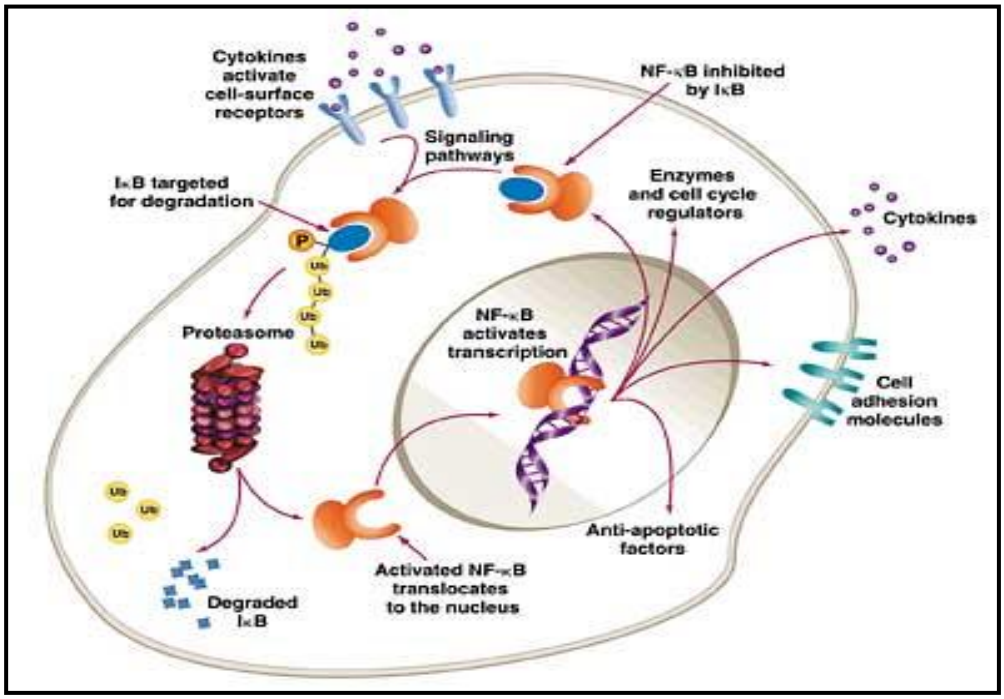

Figure: 2.31a. Activation of NF-κB Pathway (211)

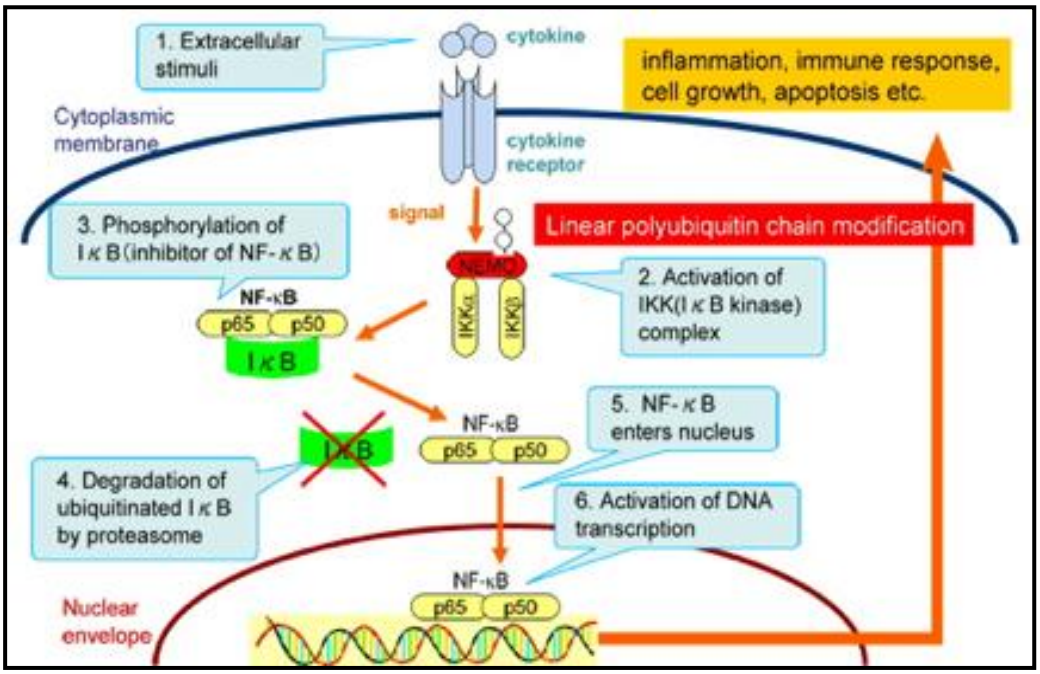

Figure: 2.31b. Signalling of NF-κB in response to immune response (212)

A model of ubiquitin signaling in the nuclear factor kappa-light-chain-enhancer of activated B cells (NF-kappa B). It was known that when ubiquitins bond to the NF-kappa B essential modifier (NEMO), the inhibitor kappa B kinases (I-kappa B) are released, activating the NF-kappa B. The NF-kappa B then penetrates deep inside the nucleus, and promotes transcription of DNA related to immune system response.

Two signalling pathways are involved in the activation of NF-κB known as the canonical or classical pathway and non-canonical or alternative pathway (213). The common regulatory component for this cascade is IκB kinase (IKK) complex which consists of alpha and beta subunit. The non-enzymatic regulatory scaffold protein is NEMO (NF-κB modulator known as IKKɤ). Activation of this NF-κB dimers are occurred by IKK mediated phosphorylation-induced proteasomal degradation of the inhibitor IκB , which enhance the active transcription factor NF-κB subunits to translocate into the nucleus and induce the expression of target genes.

In the canonical signalling pathway, binding of a ligand to a cell surface receptor such as Toll-like receptor recruits the adaptor TRAF to the cytosolic domain of the receptor which recruits IKK complex which cause phosphorylation and degradation of IκB inhibitor. This leads the activation of the NF-κB dimers (Rel A, Rel B and p50).

In the non-canonical pathway activation of p100/RelB complexes occurs during the lymphoid organ development for B and T lymphocytes generation. It utilises IKK complex which contains two IKK-α, but not NEMO. Instead this pathway induces the activation of NF-κB inducing kinase s and activates the IKKα complex which in turn activates the phosphorylation of p100 leading to the liberation of p52/RelB active heterodimer that alters the expression of target genes.

Figure: 2.32 Two signaling pathways of NF-κB (213)

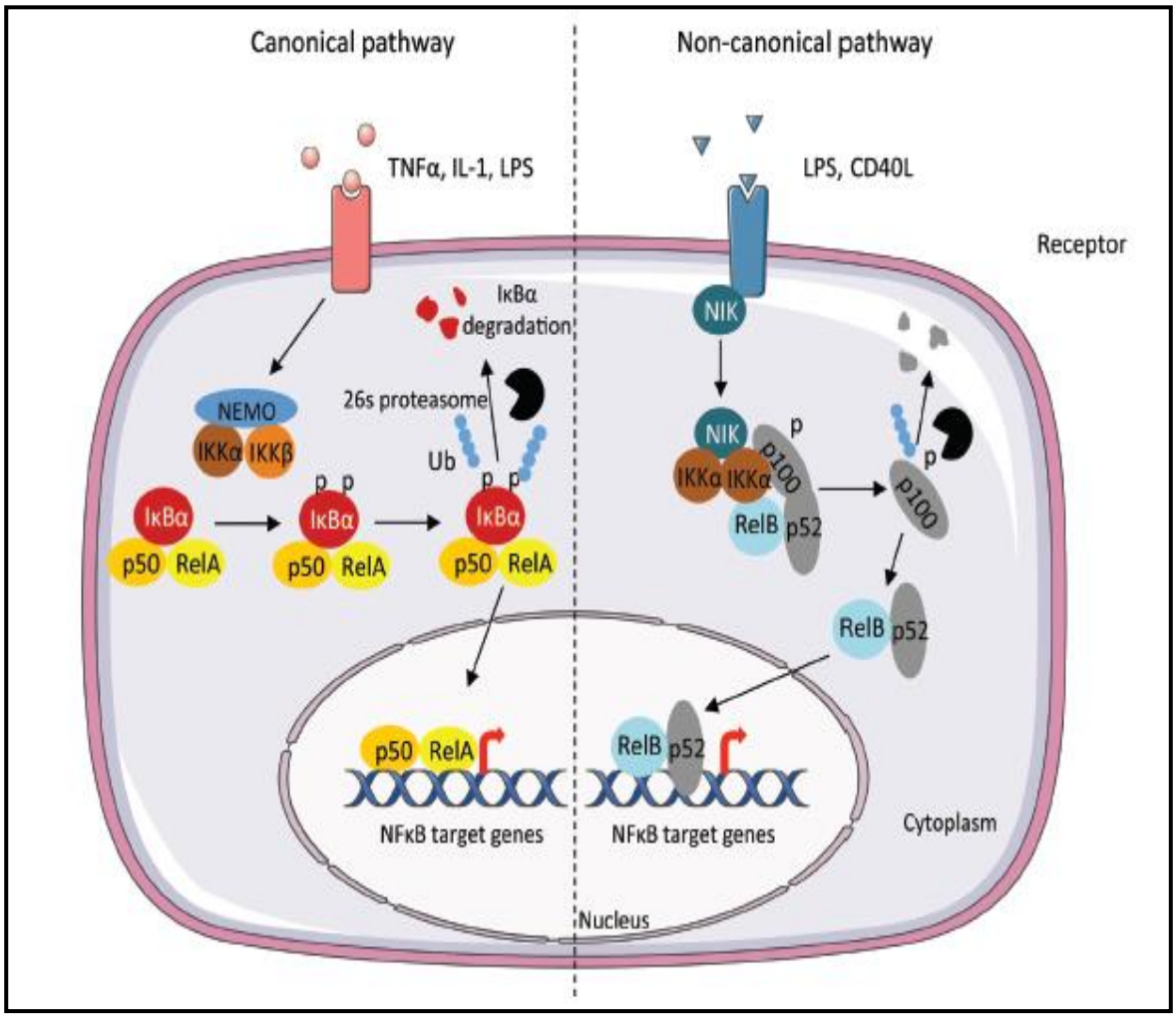

NF-κB Pathway and inflammation:

The NF-κB molecule is a transcription factor that controls the transcription of DNA for the perpetuation of the inflammatory immune response. It acts as a switch to turn inflammation on and off in the body. NF-κB has the ability to detect noxious stimuli, such as infectious agents, free radicals, and other cellular injuries, and then directs DNA to produce inflammatory cytokines. The NF-κB proteins are localized in the cytoplasm of the cell and are associated with a family of inhibitory proteins known as inhibitor of κB (IκB). The IκB proteins are normally bound to NF-κB and block their nuclear localization signal. A variety of provoking stimuli can degrade the IκB and

result in the nuclear translocation of NF-κB to be free to activate its target genes. It regulates the expression of various genes involved in the components of immune system which include proinflammatory cytokines, chemokines, adhesion molecules, inducible enzymes (COX-2 and iNOS) which regulate the innate immune response as well as proteins that regulate the specific immune response that control lymphocyte proliferation and differentiation (214,215).

Figure: 2.33. Role of NF-κB in inflammation (215)

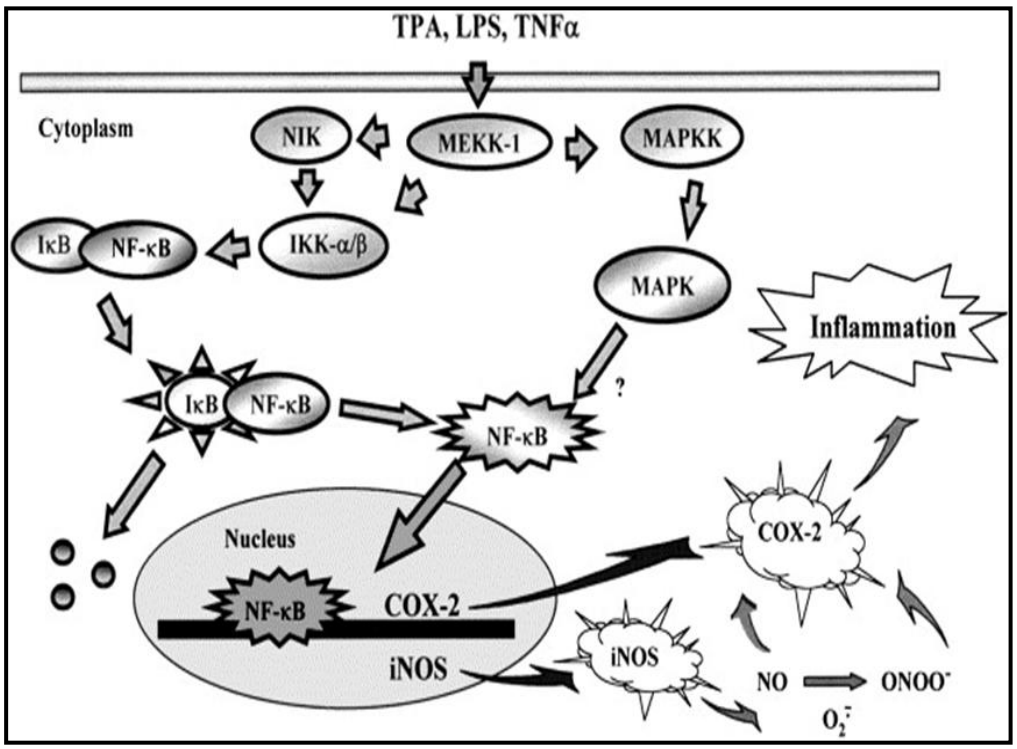

ROS is a known stimulus of NF-κB activation**.** Activation of nuclear factor-NF-κB has been observed in cells exposed to oxidative stress (216), and NF-κB is considered as potential biomarker for oxidative stress. NF-κB activates several genes resulting in cellular damage. The target genes of NF-κB include inducible nitric oxide synthase (iNOS), Tumor necrosis factor α, metalloproteinases, inducible cyclooxygenase and cytosolic phospholipase A_2 (217)

Figure: 2.34 Link between reactive species and NF-κB inflammation Pathway (218)

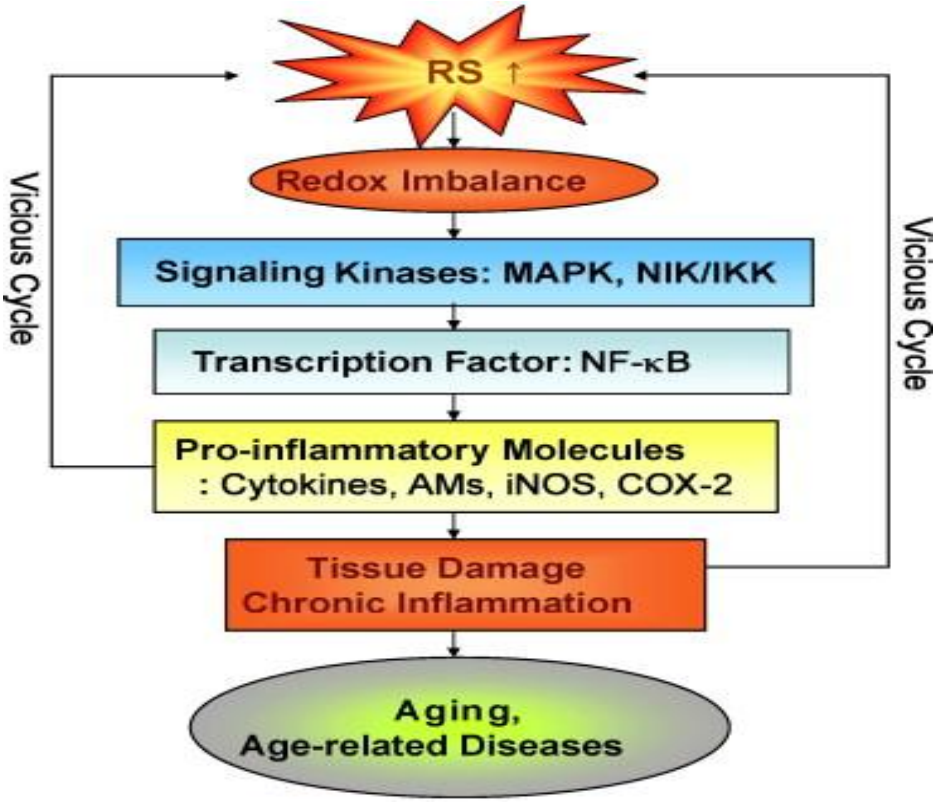

Figure: 2.35 Role of NF-κB in the pathogenesis of diseases (219)

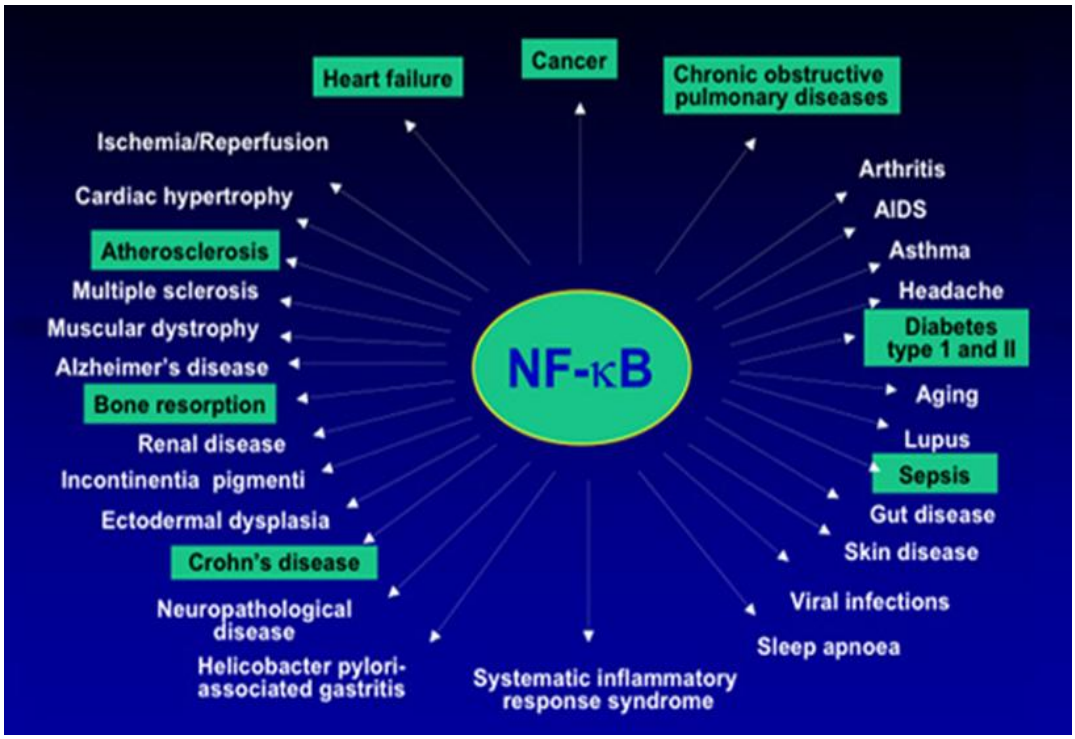

NFk B and PARP-1

PARP1 is an abundant nuclear chromatin-associated multifunctional enzyme found in most eukaryotes apart from yeast (220). It is a nuclear repair enzyme .The basal enzymatic activity of PARP1 is very low, but it is stimulated dramatically under conditions of cellular stress (220,221). Activation of PARP1 results in the synthesis of poly(ADP-ribose) (PAR) from nicotinamide adenine dinucleotide (NAD^+) and in the release of nicotinamide as reaction by-product (220,222).

In most tissues and cell types associated with high PARP1 expression, dysregulated NF-κB activity seems to contribute to cellular dysfunction and necrotic cell death during inflammatory disorders (223). The strongest indication for a direct role of PARP1 in NF-κB-dependent transcription was the impaired expression of NF-κB-dependent pro-inflammatory mediators in Parp1 knockout mice (224). Moreover, the upregulation of several inflammatory response genes after treatment with inflammatory stimuli was drastically reduced in Parp1 knockout mice (225–227). PARP1 is required and sufficient for specific transcriptional activation of NF-κB in response to pro-inflammatory stimuli and cellular stress. Furthermore, Tulin and Spradling found that Drosophila mutants lacking normal PARP levels display immune defects similar to mice lacking the NF-κB subunit p50. These results imply that the role of PARP1 in NF-κB-dependent gene expression during immune responses has been conserved during evolution. Together, several lines of evidence suggest a model in which PARP1 functions as a promoter-specific cofactor for NF-κB-dependent gene expression.

In response to inflammatory stress, the transcription factor complex nuclear factor (–PARP-1 (poly(ADP-ribose) polymerase-1) induces the transcription of pro-inflammatory genes (for example, the inducible nitric oxide synthase (iNOS) gene) in macrophages. The subsequent production of nitric oxide (NO) and reactive oxygen species triggers DNA-strand breaks that activate PARP-1. The over activation of PARP leads to NAD^+ and ATP depletion and, finally, cell death (228)

Figure: 2.36 Relationship between ROS, PARP-1, and NF-κB (229)

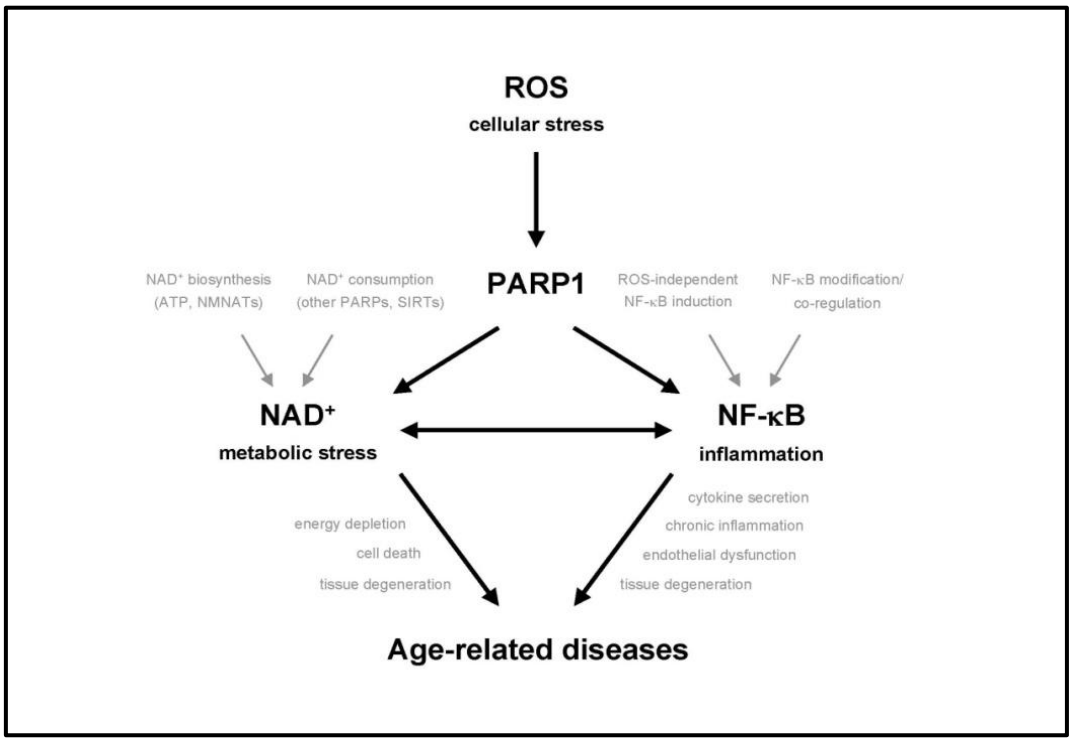

Light microscopic structure of normal rat kidney

The essential components of the nephron include the renal or malpighian corpuscle (glomerulus and Bowman's capsule), the proximal tubule, the thin limbs, the distal tubule, and the connecting tubule. It is composed of the straight portion of the proximal tubule (pars recta), the thin limb segments, and the straight portion of the distal tubule (thick ascending limb, or pars recta). The length of the loop of Henle is generally related to the position of its parent glomerulus in the cortex. Most nephrons originating from superficial and mid cortical locations have short loops of Henle that bend within the inner stripe of the outer medulla close to the inner medulla. A few species, including humans, also possess cortical nephrons with extremely short loops that never enter the medulla but turn back within the cortex. Nephrons originating from the juxtamedullary region near the corticomedullary boundary have long loops of Henle with long descending and ascending thin limb segments that enter the inner medulla. Many variations exist, however, between the two basic types of nephrons,depending on their relative position in the cortex.

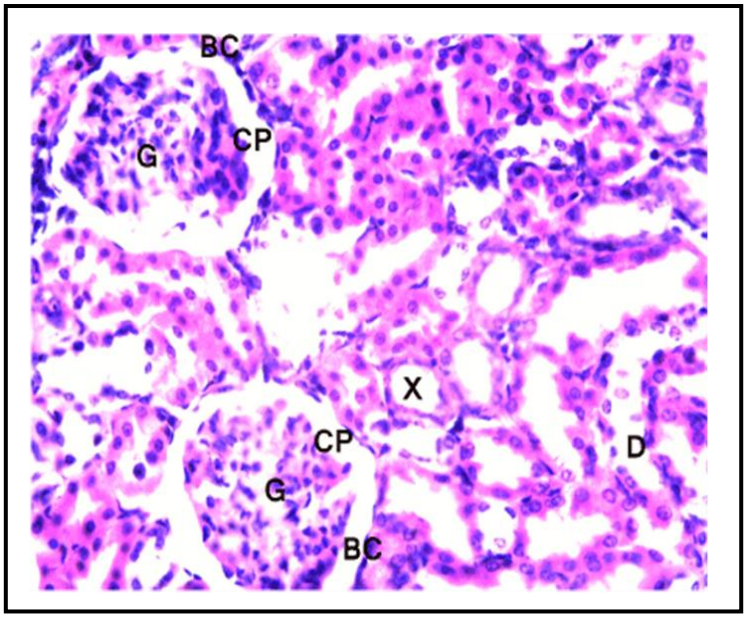

Figure: 2.37 a. Light photomicrography of kidney (cortical part) of a control rat. The renal glomeruli (G) show normal structure and the proximal (X) are lined with typical thick cubic epithelium and distal (D) convoluted tubules are lined with the relatively low simple cubic epithelium. Organization of the glomeruli and a flat epithelium lining the glomerular capsule (BC) with distinct capsular space (CP) can be seen (230) **. H &E, X200**

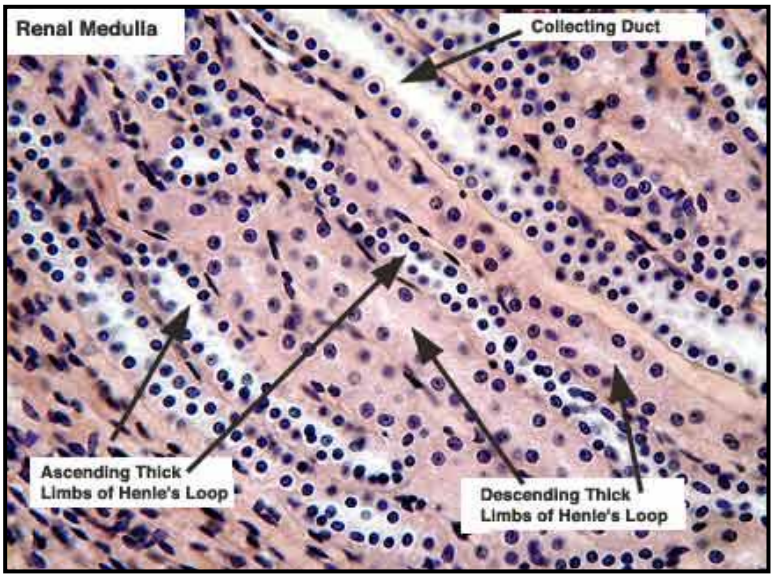

Figure: 2.37 b. This is a cross section of the Renal Medulla The medulla has no renal corpuscles and its tubules are generally thinner walled and straighter (thick and thin loops of Henle and collecting ducts), H &E, X200.

Electron microscopic structure of the proximal tubule

The proximal tubule begins abruptly at the urinary pole of the glomerulus. It consists of an initial convoluted portion, the pars convoluta, which is a direct continuation of the parietal epithelium of Bowman's capsule, and a straight portion, the pars recta, which is located in the medullary ray. The length of the proximal tubule is approximately 8 mm in the rat, and 4 nm to 5 mm in the mouse (231), compared with approximately 14 mm in the human. The outside diameter of the proximal tubule is about 40 mm. In the rat, three morphologically distinct segments—S1, S2, and S3—have been identified (232).

- The S1 segment is the initial portion of the proximal tubule; it begins at the glomerulus and constitutes approximately two thirds of the pars convoluta. It has a tall brush border and a well-developed vacuolar-lysosomal system. The basolateral plasma membrane forms extensive lateral invaginations, and lateral cell processes extending from the apical to the basal surface interdigitate with similar processes from adjacent cells. Elongated mitochondria are located in the lateral cell processes in proximity to the plasma membrane.
- The S2 segment consists of the remainder of the pars convoluta and the initial portion of the pars recta. The ultrastructure is a similar S1 segment; however, the brush border is shorter, the basolateral invaginations are less prominent, and the mitochondria are smaller. Numerous small lateral processes are located close to the base of the cell. The endocytic compartment is less prominent than in the S1 segment. However, the number and numerous large lysosomes are often observed in the S2 segment of the male rat (233).
- The S3 segment represents the remainder of the proximal tubule, located in the deep inner cortex and the outer stripe of the outer medulla. The lateral cell processes and invaginations are essentially absent, and mitochondria are small and randomly distributed within the cell. The brush border in the S3 segment is tall in the rat, intermediate length in the human kidney.

Peroxisomes are present throughout the proximal tubule. They increase in number along the length of the proximal tubule and are most prominent in the S3 segment.

The pars convoluted of the proximal tubule contains a well-developed endocytic-lysosomal apparatus that is involved in the reabsorption and degradation of macromolecules from the ultrafiltrate. It plays a major role in the reabsorption of Na, HCO_3^-, Cl^-, K^+, Ca^{2+}, PO_4^{3-}, water, and organic solutes such as glucose and amino acids. Approximately half of the ultrafiltrate is reabsorbed in the proximal tubule.

Electron micrograph of mitochondria from rat kidney shows many normal mitochondrial matrix granules as well as well-defined cristae, which are moderately dilated . The matrix is homogenous and the overall morphology is smooth and generally oblongated.

a. Normal rat kidney tubule viewed by TEM **b. EM of proximal tubular mitochondria**

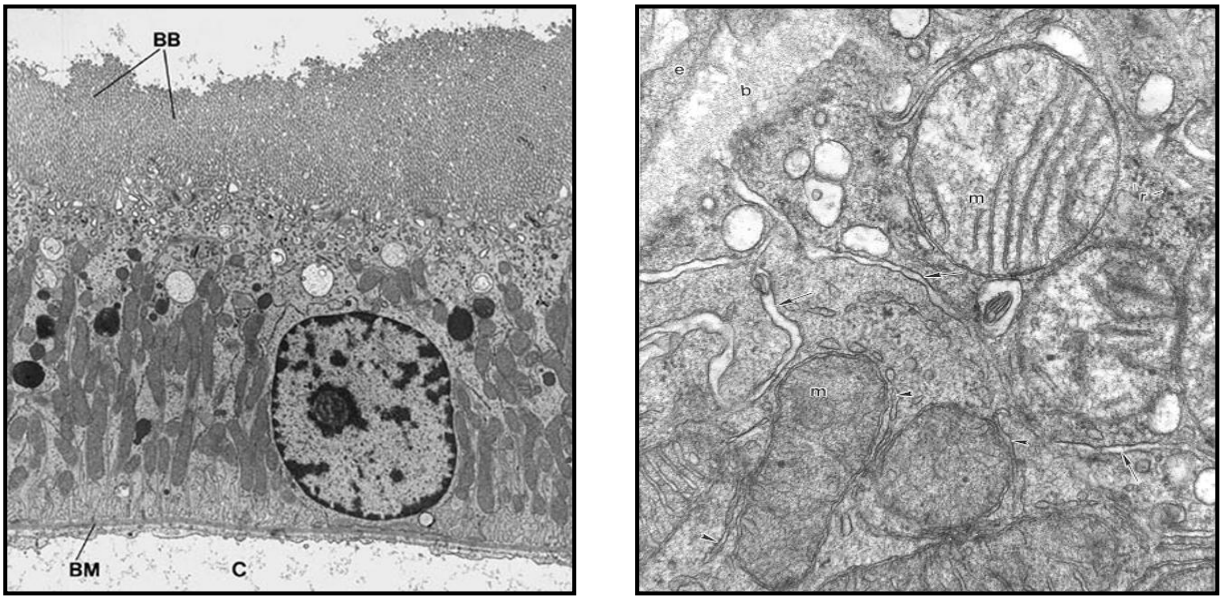

Figure: 2.38 a.Proximal tubule epithelium (S1) of rat kidney viewed by TEM. The apical cytoplasmic zone contains a vacuolar apparatus with many small vesicles and larger lysosomal elements ; the latter are also found in deeper parts of the epithelium. Beneath the apical zone, the epithelium is made up of interdigitating cell processes that contain large mitochondria. (Ã—4550.) BB, brush border; BM, basement membrane; C, peritubular capillary b. Proximal tubular mitochondria showing oval or elongated structure, with intact cristae and clear matrix (234)

Physiological roles of nitric oxide in the kidney

In kidney, NO mediates many physiologic functions and plays an important role in nephrotoxicity pathogenesis. The effect of NO depends on the production site, nitric oxide synthase (NOS), duration of action, and level of reactive oxygen intermediates present NO is generated by three isoforms of NOS (the neuronal, endothelial, and inducible). Immunostaining revealed that nNOS and eNOSwere localized mainly in renal tubules, collecting ducts, and glomeruli, whereas iNOS was found predominantly in renal tubules and collecting ducts Endothelial NOS (eNOS) is expressed in endothelial cells of renal and glomeruli and plays a role in intrarenal vascular tone by direct relaxation of afferent arteriole (235). Neuronal NO (nNOS) is expressed in macula densa and plays a role in regulation of tubule-glomerular response (235). The renal medulla is enriched in nitric oxide (NO) synthetic capacity, and the NO produced appears to participate in regulation of blood pressure (235).

Reactive oxygen/nitrogen species and renal side effects of drugs

Studies have shown that nephrotoxicity of many drugs is associated with overproduction of reactive species. These include indomethacin (236) [overproduction of ROS by mitochondrial damage], and cyclosporine (237) [induction of iNOS and peroxynitrite formation].

Cisplatin is a commonly used anti-tumour drug which is toxic to the renal proximal tubules (124,238). Gentamicin, an antibiotic is also toxic to the proximal tubules. Many studies have reported the role of oxidative stress in cisplatin and gentamicin induced proximal tubular damage Both these drugs are known to accumulate in mitochondria of renal tubular epithelial cells together with ROS leading to mitochondrial dysfunction. Many reports have suggested the depletion of intracellular GSH concentration and decreases the activities of antioxidant enzymes such as SOD, GSHPx, CAT and glutathione S-transferase in mitochondria (239). Reactive oxygen species are involved in pathogenic mechanism such as glomerulonephritis and tubulointerstitial fibrosis (240).

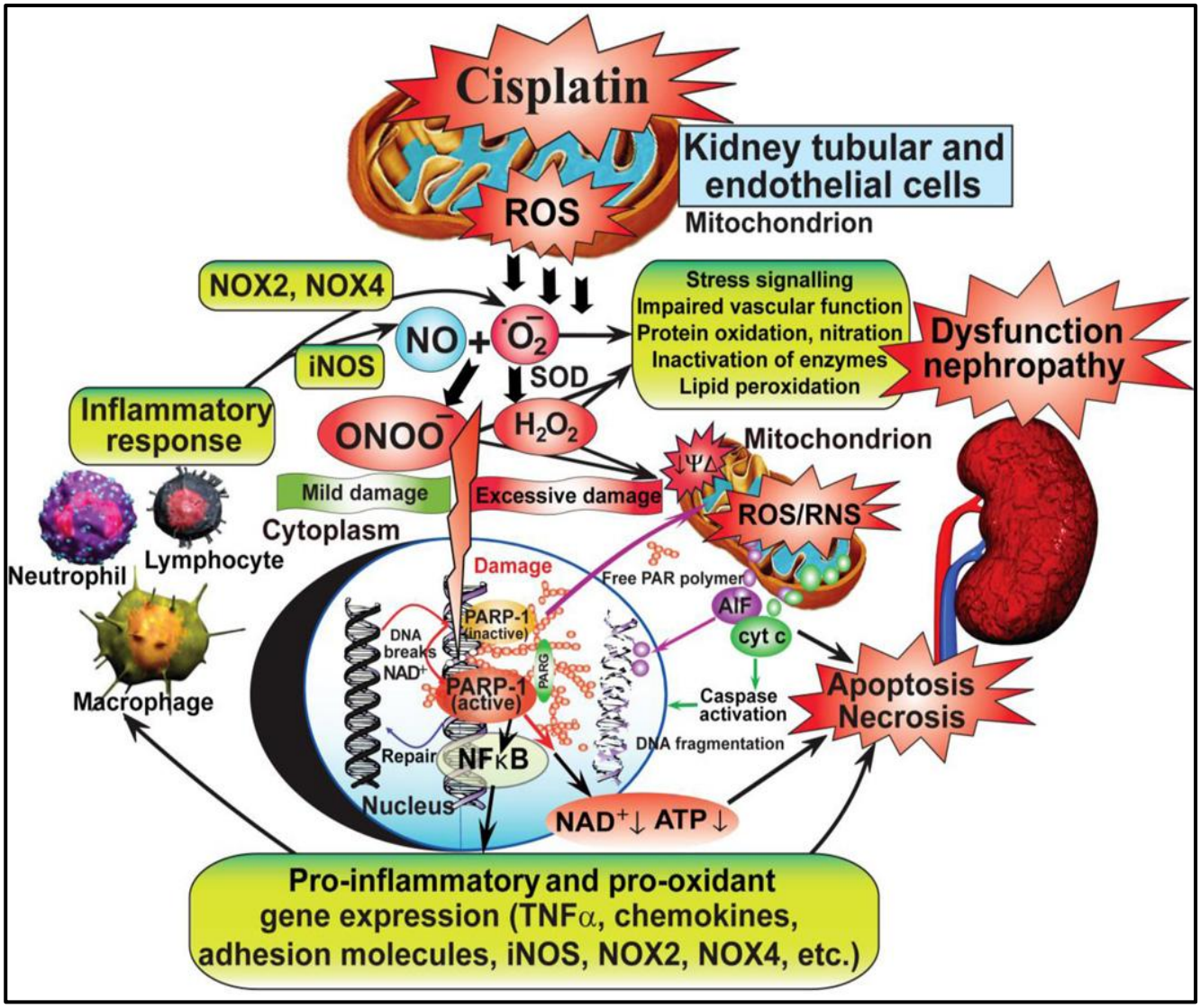

Figure: 2.39 Cisplatin nephrotoxicity: molecular mechanisms (241)**.Cisplatin initially triggers oxidative stress in the mitochondria of kidney proximal tubular and endothelial cells, which is followed by secondary wave of ROS/RNS generation and inflammatory response. The secondary ROS most likely also involves the phagocyte NAD(P)H oxidase isoform gp91phox/NOX2, as well as NOX4/renox (isoform considered to be an important source of ROS in the kidney under pathological conditions). The cisplatin-induced ROS/RNS generation also induces oxidative DNA injury and rapid activation of the nuclear enzyme poly(ADP)ribose polymerase-1 (PARP-1) with consequent tubular and/or endothelial cell death, activation of pro-inflammatory transcription factors such as NF-κB. Inflammation may further amplify oxidative/nitrative stress, and these interrelated processes eventually culminate in more concerted renal tubular and endothelial cell demise (both apoptotic and necrotic), secondary hypoxia, kidney dysfunction and failure.**

NF-κB inflammatory pathway in renal injury:

The activation of NF-κB has been implicated in various types of renal diseases including inflammation (242,243), Nephritis (244,245) and tubulointerstitial disorders (246,247).

Figure: 2.40 Role of NF-κB pathway in the pathogenesis of diabetic nephropathy (248)**.**

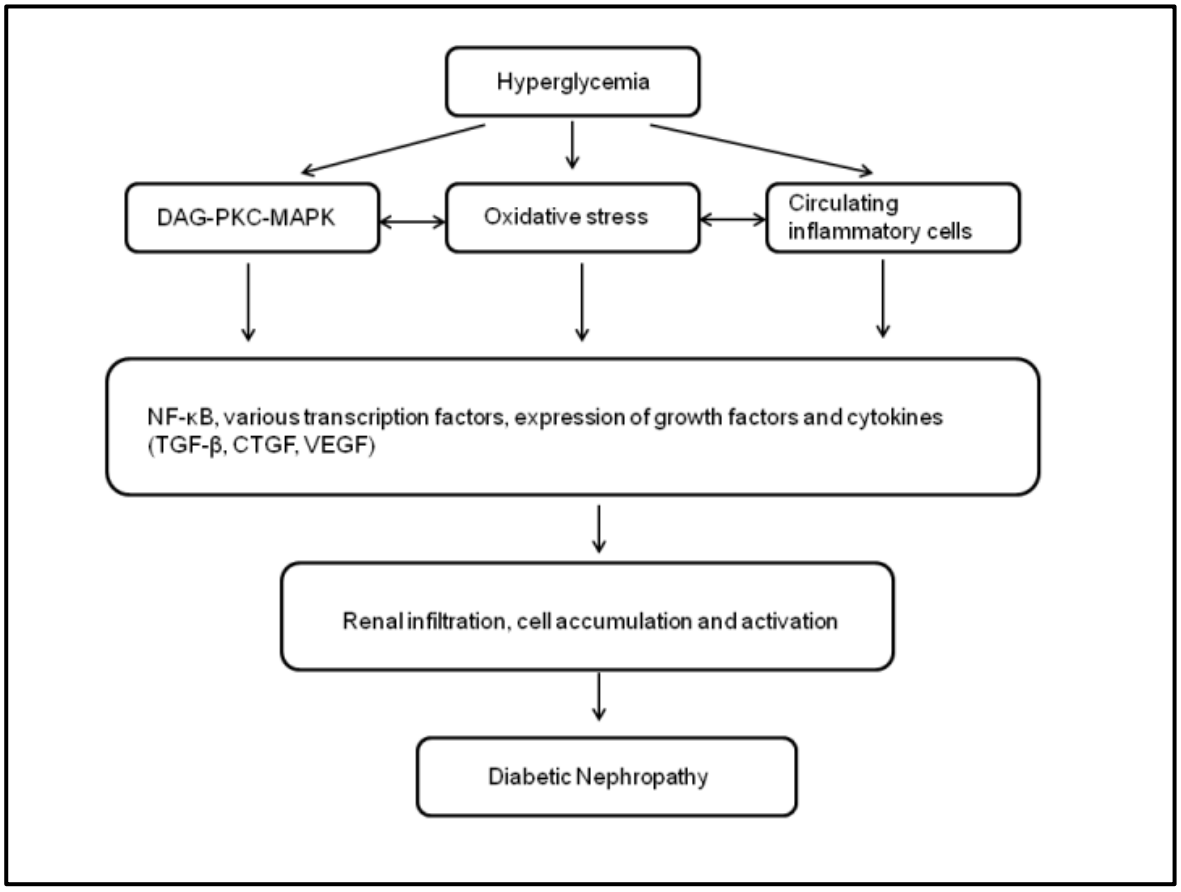

NO and NF-κB signaling pathways are intimately linked. NF-κB activation is essential for iNOS gene transcription (249), and NO-related molecules modulate NF-κB signal transduction in a cell and stimulus-specific manner In normal kidneys, iNOS is shown to be low and is induced by cytokines and its activity elevates NO level which is responsible for cell death (249). However, more recent studies suggest that iNOS is expressed in various segments of the nephron under normal physiological conditions (250) . Stimulation of iNOS has been shown to contribute to renal

cell injury . Over expression of iNOS has been implicated in toxin induced proximal tubular epithelial cell injury (251).

The other NF-κB response gene is cyclooxygenase (COX). COX- an enzyme that catalysis the formation of prostaglandins mainly that mediate inflammation and PGE2 is the major metabolite of COX activity is localized mainly to the outer and inner medullary parts of the nephron, including the PT (252). Cyclooxygenase (COX) has two iso forms, COX-1 and COX-2. COX-1 is a housekeeping enzyme, is constitutively expressed and is localized to arteries and arterioles, glomeruli, and collecting ducts. It is thought to be involved in regulation of renal blood flow, and control of platelet aggregation (252). In contrast, COX-2, the ‘‘inducible’’ isoform, is barely detectable in normal tissues but is responsible for the release of PGs during inflammatory conditions (253). Although COX-2 is considered to be the inducible form, it is constitutively expressed in the TALH and in the region of the macula densa, primarily a cortical structure (254), where it is involved in the stimulation of renin release from the juxtaglomerular cells (255). COX-2 is known to be activated by pro-inflammatory cytokines and ROS, and its transcription is regulated by several transcription factors including nuclear factor κB (256).

TNF-α is another NF-κB target gene. TNF-α genes contain functional NF-κB binding sites that are essential for their induction following injury. It is a proinflammatory cytokine capable of upregulating its own expression as well as the expression of other genes pivotal to the inflammatory response (257). Furthermore, exposure of renal tissue to TNF causes significant cellular damage and dysfunction (261). The TNF-α induced inflammatory cascade for renal injury involves immune cells and intrinsic renal cells, such as mesangial cells, glomerular and tubular epithelial cells, and endothelial cells (259). Tubular epithelial cells, the largest cell population in kidney parenchyma, are important players in renal inflammation after injury. TNF-α is shown to be induced and secreted by proximal tubular cells when subjected to either gentamicin (260) or cisplatin (261). TNF is

known to activate a wide array of cellular signaling pathways that result in divergent biological responses, including activation of NF-κB (262). This action has been supported by the latest finding that TNF-αR1 gene deletion prevented the increase of NF-κB translocation, iNOS and COX-2 expression, and MPO activity (263).

Renal epithelial cells possess surface receptors for TNF (TNFR) engagement of which by exogenous TNF triggers apoptosis. TNFR1 is present in normal glomeruli and is upregulated on infiltrating leukocytes in response to renal injury. TNFR2 is usually not expressed in normal kidney and is upregulated in tubular cells in response to renal injury (252).

Matrix metalloproteinases are a group of proteins that are collectively referred as martixins which participate in the degradation of the extracellular matrix (ECM). They are responsible for the metabolism of extracellular matrix (ECM) of the connective tissue. The expression profiles of MMPs and TIMPs in the kidney are complex and species dependent. MMP-2, -3, -9, -13, -14, -24, -25, -27, -28 and TIMP-1, -2, and -3 and are all expressed in the kidney (264). The profile of gelatinase expression in the kidney has been well characterized in both rats and humans. MMP-2 is the major gelatinase expressed in the glomerulus, proximal tubules and distal tubules in most species, including rats (80,265,266). The expression of MMP-9 is confined to the glomerulus and initial parts of the PCT (80,266,267). The role of MMPs in acute kidney injury in pathological processs related to oxidative stress such as ischemia-reperfusion, has been experimentally established previously (268). Studies with a single dose of 30 mg / kg BB-94, a broad spectrum MMP inhibitor, reduced proteinuria (269). MMP-2 and MMP-9 were shown to be increased in renal tubules, glomeruli and in the interstitium after ischemia / reperfusion injury (252,253).

Studies have demonstrated that superoxide, hydrogen peroxide or peroxy nitrite could enhance gelatinolytic activity of unpurified MMP-2 derived from smooth muscle cells (272). The

mechanism of activation of MMPs by reactive nitrogen and reactive oxygen species is thought to involve the oxidation of sulfhydryl groups located on cysteine residues that form the autoinhibitory peptide domain, thus influencing its interaction with the coordinated zinc atoms at the catalytic site (273).

MELATONIN

Melatonin is also known chemically as N-acetyl-5-methoxy tryptamine, was isolated first and characterized chemically from bovine pineal tissue in 1958 by Lerner et al (274). It is a naturally occurring compound in animals, plants (rice, barley, wheat, human milk, bananas, beets, cucumbers and tomatoes) and microbes. Melatonin is an amine with a molecular formula of $C_{13}H_{16}N_2O_2$ and molecular weight of 232. It is an indole neurohormone synthesized and secreted into the blood at night predominantly by the pineal gland. Usually the secretion of melatonin starts at 9.00AM and peaks between 2 to 4 AM at an approximate concentration of 200 pg/ml. It is therefore known as " hormone of darkness". It plays an important role in the regulation of circadian rhythm in both endocrine and non-endocrine tissue (275).

Melatonin is actually produced in the gastrointestinal tract (stomach, intestine), retina, testes, ovaries, spinal cord, lens, cochlea and skin. Apart from this it may also produce by peripheral cells such as bone marrow cells, lymphocytes and epithelial cells (276).

Figure: 2.41 Structure of Melatonin (276)

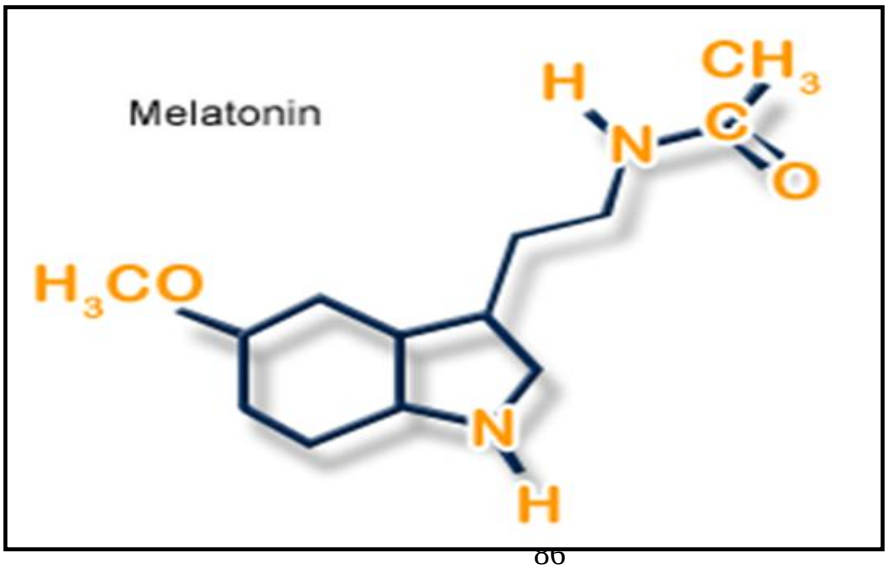

Physiological functions of MT

Melatonin induces the effect of synchronization of circadian rhythms i.e., sleep promoting effect (257).It affects various physiological functions like thermoregulation, enzyme metabolism and seasonal reproduction. It is also known to affect body mass, adiposity, energy intake and expenditure. It may vary from species to species.

Sites of action of melatonin

Melatonin can act on several tisuues including brain and retina, kidney cardiovascular system, liver gallbladder, intestine, immune cells, adipocytes, prostate and breast epithelial cells. MT has several effects based on the organs (277).

MT receptors

In addition to its antioxidative effects melatonin has been shown to act through specific nuclear and plasma membrane receptors. In humans and rodents, melatonin receptors (MT1, MT2, MT3) have been shown to be expressed in various extrapineal tisuues including brain and retina, kidney cardiovascular system, liver and gallbladder, intestine, immune cells, adipocytes, prostate and breast epithelial cells, ovary/granulosa cells, myometrium, and skin (278). Melatonin receptors have been found in the epithelial cells of the proximal tubule in the guinea pig kidney. These findings suggest that melatonin may influence renal function at the proximal tubular level.

Figure:2.42 Target tissue of Melatonin [Adapted from Dubocovich ML and Masana M (2003) Melatonin receptor signaling, in Encyclopedia of Hormones and Related Cell Regulators (Henry H and Norman A eds), pp 638–644, Academic Press, San Diego, CA. Copyright © 2003 Academic Press. Used with permission.]

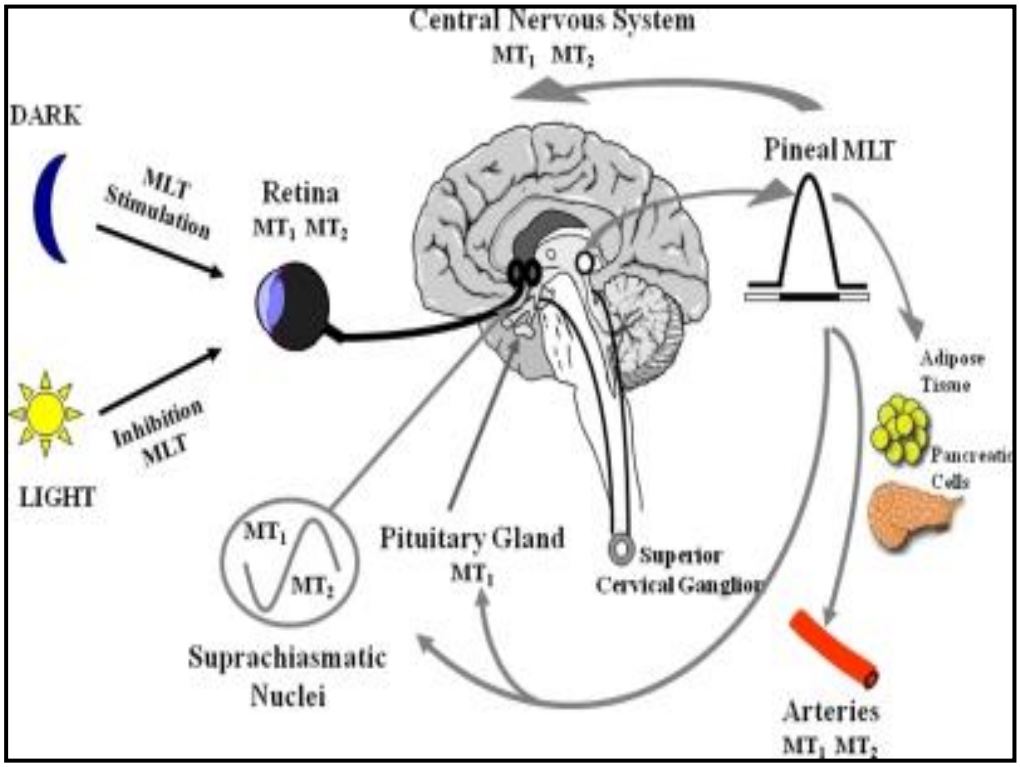

Figure: 2.43 . Pleiotropic effects of melatonin (279)

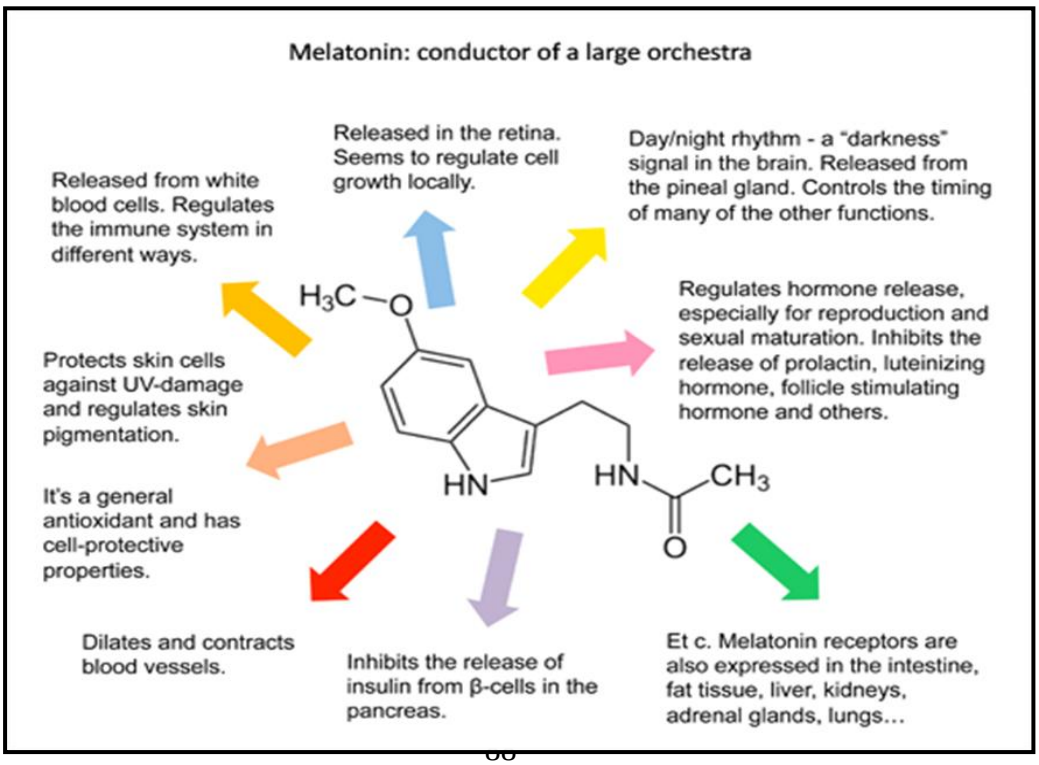

Melatonin receptor signalling:

MT_1 melatonin receptors can couple to both PTX-sensitive (G_i) and insensitive ($G_{q/11}$) G proteins. Activation of MT_1 melatonin receptors decreases forskolin-stimulated cAMP formation . Protein kinase A activity and phosphorylation of the cAMP responsive element-binding protein (CREB) are also inhibited. In addition, the MEK1/2-ERK1/2 pathway is stimulated by MT_1 receptors in non-neuronal cells

Activation of MT_2 melatonin receptors also can lead to inhibition of cGMP formation. In the SCN, melatonin increases PKC activity through activation of MT_2 melatonin receptors. MT_2 melatonin receptors interact with the phospholipase C/diacylglycerol signaling pathway (280).

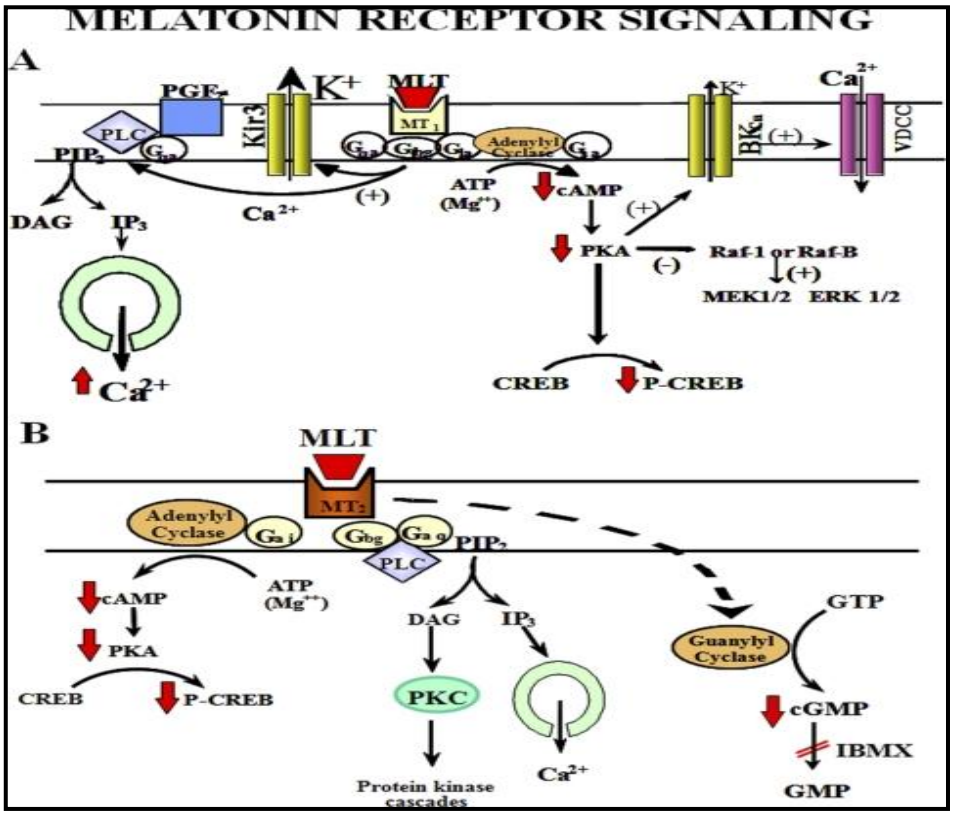

Figure: 2.44. MT_1 and MT_2 melatonin receptor signaling. A, melatonin (MLT) signals through activation of the MT_1 receptor via two parallel pathways mediated by the α-subunit (i.e., inhibition of cAMP formation) and the βγ-subunits [i.e., potentiation of phosphoinositide turnover stimulated by a G_q-coupled receptor (R)] of G_i. B, signaling pathways coupled to MT_2 melatonin receptor activation. Melatonin-mediated phase shifts of circadian rhythms through MT_2 receptors are mediated by PKC activation (the mechanism leading to PKC activation remains putative, however). DAG, diacylglycerol; PKA, protein kinase A; R, G_q-coupled receptor (i.e., prostaglandin $F_{2\alpha}$ receptor FP and purinergic receptor P2Y) (281).

Melatonin as an antioxidant

Melatonin has been shown to be effective in protecting against severe free radical-mediated nephrotoxicity in a variety of conditions, including, chemotherapy (282), ischemia-reperfusion injury (283), acute renal failure caused by mercuric chloride (284), and gentamicin (285) and cisplatin (286). Melatonin has many roles as an antioxidant. 1. MT acts a free radical scavenger. It has been reported to scavenge hydrogen peroxide, hydroxyl radical, nitric oxide, peroxynitrite anion, hypochlorous acid, superoxide anion and peroxyl radical. 2. Melatonin can stimulate some important antioxidative enzymes, i.e., superoxide dismutase, glutathione peroxidase and glutathione reductase (287). 3. Stimulation of GSH synthesis by melatonin (288).

Melatonin as an anti-inflammatory agent

Melatonin is reported to possess anti-inflammatory properties (289). Melatonin has been shown to be a potent inhibitor of MPO (290). Under normal physiological conditions, melatonin does not interact with myeloperoxidase because its concentration is too low (291). Galijasevic et al (290) showed that, at pharmacological concentrations, melatonin interferes with the catalytic activity of MPO by multiple pathways that includes switching the activity of MPO from peroxidation to catalase-like activity and transformation of MPO to an inactive form.

Figure: 2.45 Anti-inflammatory effects of melatonin (292)

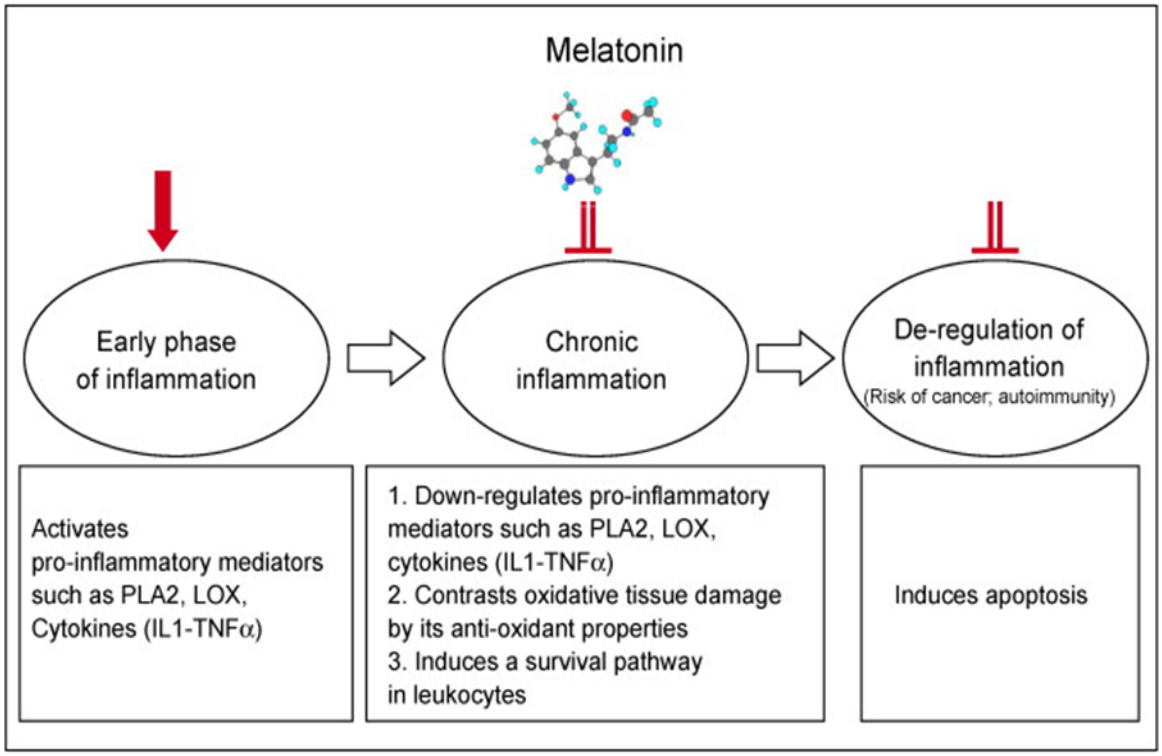

Melatonin as a mitochondrial protectant

During the last decade, a number of studies have demonstrated that melatonin plays an effective role in regulating mitochondrial homeostasis by multiple mechanisms. In addition to being a free radical scavenger, melatonin reduces nitric oxide (NO) generation within mitochondria. It maintains the electron flow, efficiency of oxidative phosphorylation, ATP production and bioenergetic function of the cell by regulating respiratory complex activities, Ca^{2+} influx, and mitochondrial permeability transition pore opening (293,294).

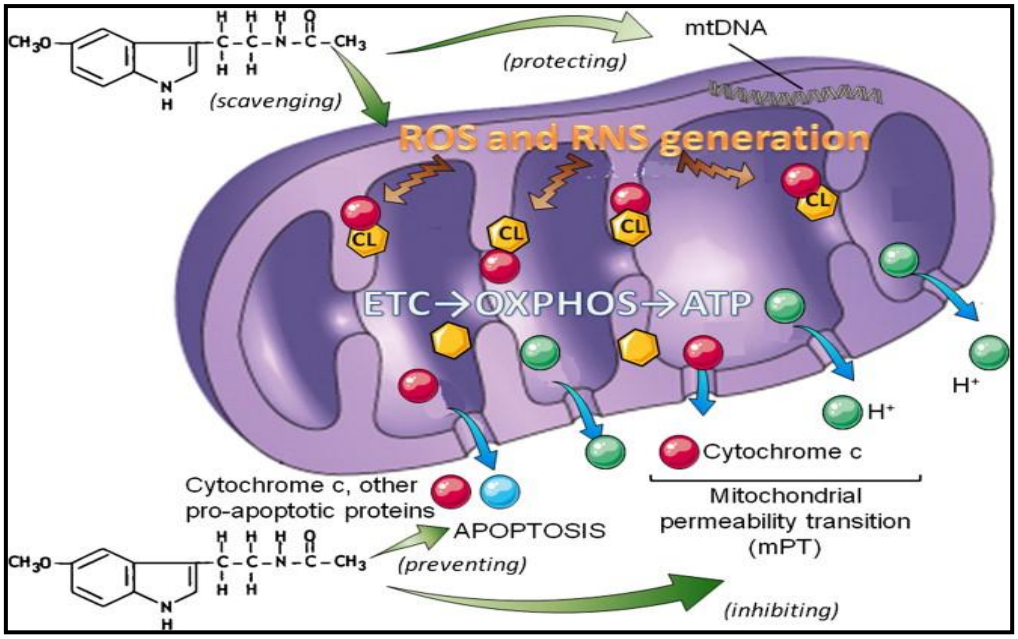

Figure: 2.46 Melatonin's protective effect on the mitochondria (295)

Melatonin as an inhibitor of NF-κB activation

Recently, many studies confirmed that melatonin exerts anti-inflammatory effect through inhibition of NF-κB. Some of these studies found that the expression level of NF-κB was suppressed by melatonin treatment (286,288), while others suggested that melatonin mainly disturbed the translocation of NF-κB .Generally, melatonin administration at pharmacological level suppresses the production of inflammatory cytokines and iNOS via inhibition of NF-κB. The underlying mechanisms may be through inhibition of NF-κB expression, reduction of IκB-α degradation and NF-κB translocation, or suppression of the DNA binding activity of NF-κB (296).

Melatonin as a nephroprotectant

Melatonin has been shown to be effective in protecting against severe free radical-mediated nephrotoxicity in a variety of conditions, including, chemotherapy (282), ischemia-reperfusion injury (283), acute renal failure caused by mercuric chloride (284), and gentamicin (285) and cisplatin (286).

Therapeutic applications of melatonin:

Melatonin is a major potential therapeutic tool for the treatment of neurodegenerative disorders like Parkinson's, Alzheimer's disease and to prevent lethal effects of septic shock. . Melatonin has been used for insomnia. Beneficial antioxidant effects of melatonin have been recently shown in clinical settings for several chronic diseases, including patients with rheumatoid arthritis (297), elderly patients with primary essential hypertension (298), and females with infertility (299). Melatonin is good for adjunctive therapy, as it is natural, inexpensive, widely available , and minimal side effects (except somnolence) (300–302).

Figure: 2.47 Effects of Melatonin on anti-inflammatory, anti-oxidant and anti-apoptotic (303)

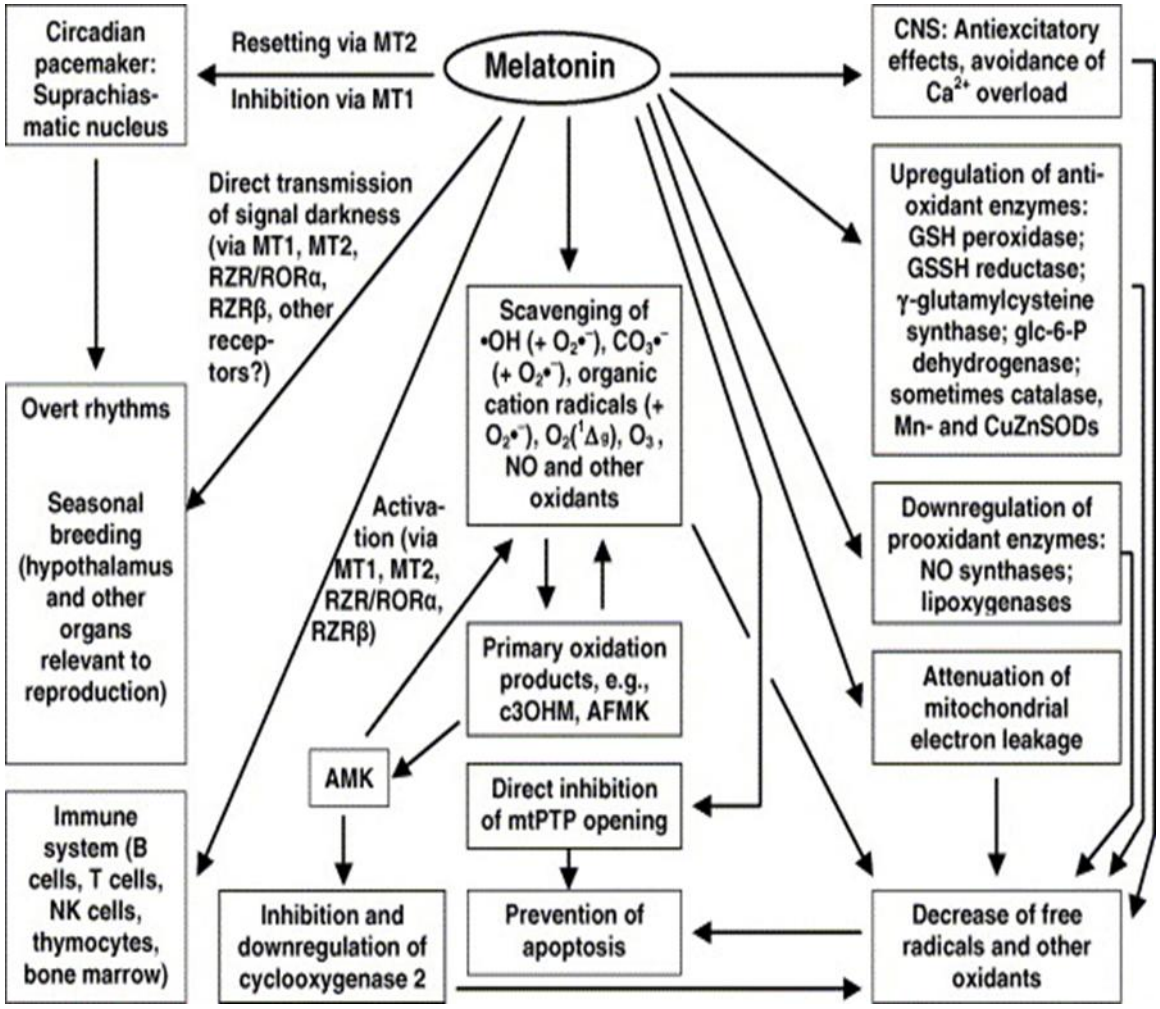

PREVIOUS STUDIES REPORTED ON MECHANISM OF TENOFOVIR NEPHROTOXICITY

Tenofovir is shown to be toxic specifically to proximal tubular cells, and it targets the mitochondria. The following studies have been reported regarding the mechanism of TDF nephrotoxicity

- Morphological evidence of mitochondrial toxicity such as swelling, disruption of cristae and amorphous deposits in the matrix (15)
- Depletion of mtDNA, and depression of cytochrome oxidase enzyme expression (304)
- Specific downregulation of proximal tubular sodium-phosphorus cotransporter, sodium/hydrogen exchanger 3, and aquaporin 2 (305).
- Presence of specific proximal tubular transporters that increase the intracellular tenofovir concentrations to toxic levels in proximal tubules (67,304).
- Inhibition of mtDNA polymerase γ encoded by POLG (306).
- Oxidative stress and reduced activities of renal catalase, glutathione-S-transferase, and superoxide dismutase.

The extent to which mitochondrial damage is responsible for proximal tubular cell injury and the mechanisms of such an effect remain unclear.

Plan of Work

Study-I was done to standardize a rat model of tenofovir nephrotoxicity induced renal damage and to characterize the morphological changes in the kidney cortex and medulla. Pilot studies were carried out by the administration of different oral doses of TDF; 5mg/ kg /day, 100 mg /kg body wt. /day, 300 mg/kg body wt./day and finally 600 mg/kg body wt./day for 5 weeks. Kidney tissue was fixed in 10% buffered formaldehyde and embedded in paraffin. Five micron serial sections were cut and stained with haematoxylin and eosin. The sections were examined by light microscopy.The kidney tissues were fixed in 3% glutaraldehyde and washed in buffer, post fixed by 1% osmium tetraoxide and processed for the observation of organelles by electron microscopy. Urine samples were collected in metabolic cages, samples were centrifuged and used for clinical chemistry parameters , and tubular proteinuria by SDS-PAGE.

Study-II was carried to investigate the effect of chronic administration of TDF on mitochondrial structure, function and the activities of electron transport complexes as well as mitochondrial antioxidants in the kidney. Mitochondria were isolated from kidney tissue and checked for its by the marker enzyme, succinate dehydrogenase. The isolated mitochondria were used for the measurement of tests of mitochondrial function such as RCR, MTT reduction and mitochondria swelling. The activities of the electron complexes and the antioxidant enzymes were measured in the mitochondrial homogenates. Ultrastructural changes of mitochondria were assessed by electron microscopy and graded by standard method. Finally, the level of cytochrome ‘c’ was determined by immunohistochemistry and western blot.

Study-III was designed to assess the effect of TDF on oxidative stress, nitrosative stress, antioxidant enzyme activities and oxidative stress related protein such as HSP 70, Heme oxygenase-1, and neutrophil

infiltration. One portion of the kidney was fixed in 10% formalin and used for the immunolocalisation of proteins using HRP as a secondary marker and DAB as a chromogen. Another portion of the kidney was homogenized and used for the following biochemical assays.

- Parameters of oxidative stress such as malondialdehyde, conjugated diene and protein carbonyl.
- Parameters of nitrosative stress by the measurement of nitrate levels and nitration of tyrosine protein by immunohistochemistry and western blot.
- Antioxidants and antioxidant enzymes such as reduced glutathione, protein thiol, glutathione peroxidase, glutathione reductase, glutathione S-transferases, superoxide dismutase and catalase.
- Protein expression of oxidative stress related protein - HSP 70 and Heme oxygenase-1 by immunohistochemical and immunoblot methods
- Myeloperoxidase activity, a sensitive and reliable marker of neutrophil infiltration

The other part of the kidney was snap frozen used for mRNA expression level by Real time PCR analysis.

- The RNA was isolated, integrity of RNA was assessed by Agarose gel electrophoresis, constructed cDNA and analysed mRNA gene expression- HSP 70 and HO-1

Study-IV was done to determine the effects of TDF on NF-κB, and its proinflammatory target genes and PARP activation on the kidneys. One portion of the kidney was fixed in 10% formalin, embedded in paraffin and 5µm section were used for immunohistochemistry, PARP expression by immunofluorscence. Another portion of the kidney was snap frozen in liquid nitrogen. The tissue was homogenized, centrifuged to isolate whole cell, cytosol and nuclear fraction, and used for western blot ,PCR assays, and assessment of enzyme activity as mentioned below..

- Immunolocalisation of proteins- NF-κB p65, PARP, nitrotyrosine, nitrocysteine, iNOS, COX 2, TNF-α, PLA_2 and caspase 3.
- Immunoblots of the whole cell lysates , cytosol and nuclear fraction for protein expression - NF-κB p65, IκB-α, PARP, nitrotyrosine, nitrocysteine, iNOS, TNF-α, PLA_2 and caspase3.
- Analysis of the expression of mRNA by RT PCR- NF-κB, iNOS, COX 2, TNF-α.
- Assessment of the activity of NF-κB p65 and caspase-3 in the nuclear fractions and cytosolic fractions by ELISA and fluorimetry respectively.
- Assessment of the activity of MMP-9 by gelatin zymography.

Study V was to done to investigate whether pretreatment with melatonin ameliorates TDF induced renal damage in rats. For this, rats were pretreated with 20 mg/kg and 40 mg/kg body weight of melatonin one hour prior to the administration of TDF for 35 days . The effect of pretreatment with melatonin on TDF induced oxidative stress, nitrosative stress, NF-κB pathway, and renal damage was studied. The following studies were done after melatonin pretreatment

- Light microscopy and electron microscopy of the kidneys
- Serum analysis – urea, creatinine, uric acid, phosphate, potassium and bicarbonate.
- Measurement of parameters of oxidative and nitrosative stress in the kidney- protein carbonyl, nitrate, nitrotyrosine and nitrocysteine by IHC.
- NF-κB signaling pathway PARP activation- Protein and mRNA expressions of NFp65, iNOS, COX-2, TNF-α and MMPs along with activity of NF-κB p65 by ELISA, PARP protein expression.
- The apoptosis level was assessed by TUNEL assay and the protein and activity assessment of caspase-3.

Materials And Methods

MATERIALS

EQUIPMENTS USED:

1. Elix and Milli-Q ultrapure water system (Millipore, USA)
2. pH meter (Systronics, India)
3. Refrigerated table top centrifuge (MPW R 350, MPW Poland)
4. Glass homogenizer and Teflon pestle (1ml capacity) (Kimble-Kontes, USA)
5. Mechanical homogenizer (REMI, Bombay, India)
6. Apparatus for SDS-PAGE amd Western Blottting (Bio-Rad, USA)
7. Gel Documentation System (Alpha Innotech, USA)
8. Real time thermocycler (Chromo4, Biorad, USA)
9. Elisa Plate reader (Bio-rad, USA)
10. Nanodrop 2000C UV/Visible spectrophotometer, Thermoscientific, USA.
11. Olympus Laser Scanning Confocal Microscopy, Japan.
12. Leica DM4000 B LED Flourscence Microscopy, Germany
13. Cobas 8000 Hitachi Automated Analyser, Roche Diagnostics, Switzerland.
14. Varian Cary Eclipse Fluorescence Spectrophotometer, Germany

CHEMICALS USED:

1. Acrylamide, Ammonium per sulphate, Adenosine diphosphate (ADP), Arsenazo – III, Beta-Actin antibody, β mercaptoethanol, bovine serum albumin (BSA), 1 – chloro – 2, 4 – dinitrobenzene (CDNB), Chloroform, Cetrimide, dimethyl sulfoxide (DMSO), diethyl pyrocarbonate (DEPC), dimethyl sulfoxide, D – mannose, 5,5' – dithiobis(2 – nitro benzoic acid) (DTNB), dithiothreitol (DTT), ethidium bromide, ethanol, ethylene diamine tetra acetic acid (EDTA), ethylene glycol tetra acetic acid (EGTA), formaldehyde, formamide, guanidine hydrochloride, glutathione (oxidized and reduced), glutathione reductase, Isopropanol, melatonin, 3-(4,5-dimethylthiazol-2-yll)-2,5-diphenyltetrazolium bromide (MTT), o–dianisidine dihydrochloride, phenylmethanesulfonylfluoride (PMSF), primary antibody against poly – ADP ribose polymerase (PARP) , sodium succinate, sodium dodecyl sulphate (SDS), sodium hydroxide, thiobarbituric acid (TBA), TRI reagent, Tris, xanthine oxidase were obtained from Sigma Aldrich, India.
2. Calcium chloride ($CaCl_2$), Coomassie brilliant blue, disodium hydrogen phosphate, dinitro phenyl hydrazine (DNPH), ethyl acetate, 4–(2–hydroxyethyl) piperazine (2–ethanesulfonic acid) (HEPES), hydrogen peroxide, 2–(p–iodophenyl)–3–(p–nitro phenyl)–5–phenyl tetrazolium (INT), magnesium chloride ($MgCl_2$), nicotinamide adenine dinucleotide (oxidized and reduced) (NAD and NADH), nicotinamide adenine dinucleotide phosphate (NADPH), p – nitro phenyl phosphate (PNPP), potassium chloride, potassium dihydrogen phosphate, sodium acetate, sodium bicarbonate, sodium carbonate, sodium chloride, sodium bisulfate, sodium di-hydrogen phosphate, sodium hydroxide, sodium sulphate, sodium sulphite, sucrose, Tris, trichloroacetic acid (TCA), Triton X–100, Tween-20, xanthine and zinc sulphate were obtained from Sisco Research Laboratories Pvt Ltd, Mumbai, India.

3. Glacial acetic acid, hydrochloric acid, sulphuric acid, methanol, hydrogen peroxide, perchloric acid, phenol and phosphoric acid were obtained from Qualigens Fine Chemicals, Mumbai, India.
4. Absolute alcholol (99.9%) (Hayman, England)
5. Agarose (Genei, Bangalore, India)
6. Bisacrylamide (Bio-Rad, USA)
7. Polyvinylidenedifluoride (PVDF) membrane (pore size 0.45µm) and MillicellR-ERS were obtained from Millipore, USA.
8. Skimmed milk powder (Sagar, India)
9. 96-well ELISA plates (nunc, USA)
10. 3-Morpholinopropane sulfonic acid (MOPS) (Fluka Biochemika, India
11. ELISA kit for NF-κB p65 activity from Imgenex, San Diego, USA.
12. Secondary antibodies (anti-rabbit and anti-mouse IgG conjugated with horse-radish peroxidase) and ECL West Dura substrate to develop the western blots were purchased from Thermo Scientific, USA.
13. Goat anti-mouse and anti-Rabbit peroxidase-conjugated antibodies and chemiluminescent substrate were purchased from Pierce International, USA.
14. Reverse transcription core kit, SYBR green PCR master mix kit and gene specific primers were obtained from Eurogentec, Belgium.
15. Micro centrifuge tubes and microtips were purchased from Tarsons products private limited, Kolkata, India.
16. Glasswares such as measuring cylinders, beakers, test tubes were purchased from Borosil, Chennai, India.
17. Filter tips were purchased from Molecular Bio Products, India.

18. Plates required for real-time PCR compatible for chromo4, PCR tubes with flat cap and optically clear caps were purchased from Axygen scientific private limited, India.
19. The primary monoclonal anti-nitrotyrosine antibody was obtained from Santa Cruz, USA.
20. Super Sensitive Polymer/HRP/DAB kit was obtained from BioGenex, Chennai, India. All chemicals used were of analytical grade.
21. Caspase-3 activity kit was obtained from Abcam, UK.

DIET USED FOR THE EXPERIMENTAL RAT

Standard rat chow

ANESTHETIC AGENT USED WHEN HANDLING THE RAT

Halothane (Nicholas Piramal India, Ltd.,)

METHODOLOGY

3.1. USAGE AND MAINTENANCE OF ANIMALS

Adult male Wistar rats weighing (180-200 gm) were used for the studies described. They were housed in standard rat cages (421 × 290 × 190 mm). All animals were exposed to 12 hour light-dark cycles and allowed access to food and water *ad libitum*. The experiments done were approved by Institutional Review Board (Approval No. 7050 dated 20.01.2010) and the Institutional Animal Ethics Committee (IAEC) and were in accordance with the guidelines of the Committee for the Purpose of Control and Supervision of Experimentation on Animals (CPCSEA), Government of India.

3.1.1 ANIMAL TREATMENT:

1. Tenofovir disoproxil fumurate was administered orally by gavage at the dose of 600mg/kg body weight /day for 35 consecutive days which is double the dose administered Biesecke et al (307). Control animals received sterile water alone. Animals were sacrificed on 36^{th} day, after withdrawal of blood by cardiac puncture, under light halothane anesthesia.
2. Rats were given Melatonin, an antioxidant used at a 2 different doses, 20mg/kg body weight and 40mg/kg body weight dissolved in ethanol and given intraperitoneally before 2 hours of Tenofovir treatment (308). Animals were sacrificed on the 36^{th} day, after withdrawal of blood by cardiac puncture, under light halothane anesthesia.

   Renal damage was assessed biochemically by the measurement of creatinine and urea in the blood and light microscopic examination of the kidney. The kidney was homogenized and used for various biochemical studies.

3.2 TISSUE PROCUREMENT

The treated rats were anesthetized with halothane and sacrificed by cervical dislocation. Both the kidneys were removed, washed with ice cold phosphate buffered saline (PBS) and used for analysis. In this one kidney was used for histology and biochemical analysis and other kidney was snap-frozen using liquid nitrogen and were stored at -70^{o} C until use.

3.3 HISTOLOGY

3.3.1 (a) Light microscopy

Kidney tissues of the animals treated with TDF was subjected to histopathological examination by light microscopic studies. This was obtained from animals sacrificed on the 36th day after TDF treatment. Kidney tissue was fixed in 10% buffered formaldehyde and embedded in paraffin. Four-micron serial sections were cut and stained with haematoxylin and eosin. The sections were examined in twenty high-power fields of 3 independent samples by light microscopy.

3.3.2 (b) Scanning electron microscopy of the kidneys:

For ultra structural study, the kidney tissue were fixed in 3% glutaraldehyde and washed in buffer, post-fixed by 1% osmium tetroxide and embedded in araldite (epoxy resin). Ultra-thin (below 100nm) sections were cut from selected blocks with a Leica ultracut UCT (Wien, Austria) and a diamond knife (Diatome, Switzerland). Sections were mounted on copper grids and stained with uranyl acetate and lead citrate and examined with a Philips EM 201C electron microscope (Eindhoven, Netherlands) and photographed.

3.3.3 (c) Immunohistochemistry

Immunohistochemistry was done as described by Cuzzocrea et al., (309,310) The kidney was fixed in 10% formalin and 4µm thick sections were obtained from paraffin-embedded tissues. After deparaffinization, the sections were permeabilized with 0.1% Triton X-100 in Tris- buffered saline for 15 minutes. Endogenous peroxidases were quenched by 3% hydrogen peroxide. After the buffer wash, the universal protein blocking agent was applied over the sections. Then, the respective primary antibody was applied over the sections and incubated overnight. The bound primary antibody was detected by the addition of secondary antibody conjugated with horseradish peroxidase polymer and DAB substrate. Later the slides were counterstained with Harris Haematoxylin and mounted**.**

Primary antibody dilution for IHC, iNOS (1:250), Cox 2 (1:200), HO-1 (1:200), NF-κB (1:100) Caspase 3 (1: 250), Caspase 9 (1:200), TNF alpha (1:500), Cytochrome C (1:100), AQP2 (1: 200), HSP 70 (1:100), PLA2 (1:250), IKB alpha (1:100), PARP (1:100), Nitrotyrosine (1:250) Nitrocysteine (1:100).

IHC Scoring Method

The whole section was scanned at low power in order to gauge the general level of intensity throughout, The strength of staining based on color and texture features. A strength score in the range 0-3 (311). The average intensity, corresponding to the presence of negative, weak, intermediate, and strong staining, was given a score from 0 to 3, respectively.

Qualitative scoring

Score	0	1	2	3
Intensity of Staining	no staining	weak (mild) staining	intermediate (moderate)	strong (intense)

3.3.4 (d) Immunofluorescence of PARP:

Immunostaining for PARP (poly (ADP-Ribose) were performed on Paraffin-embedded kidney tissues. The slides were deparaffinized, rehydrated and thoroughly washed. Antigen retrieval was carried out using Trypsin at 37^{o}C for 20mins. 3% BSA was used for protein blocking. The section was rinsed twice in PBS-T (PBS containing 0.1% Tween-20) prior to incubation with primary antibody. The primary monoclonal PARP antibody (1:200) was used to incubate for 2 h at 4°C. The sections were rinsed 3 times in PBS-T followed by a 45 min incubation at room temperature in the dark with Green Alexa Fluor 488-labelled anti-rabbit secondary antibody and then rinsed 4 × 5 min in PBS-T. Antibody was diluted in PBS containing 3% bovine serum albumin. Nuclear counterstaining with 4',6'-diamidino-2-phenylindole (DAPI) was performed after removal of excess secondary antibody. Slides were mounted in 90% glycerol in PBS, coverslipped and stored in the dark at 4°C. Immunofluorescence images were obtained for linear range of detection to avoid signal saturation using a Leica confocal microscope.

3.4 TISSUE HOMOGENATE

3.4.1 Preparation of kidney homogenate:

The kidney tissue obtained was washed in ice-cold saline, decapsulated and minced into small pieces using a pair of sharp scissors, and immediately homogenized (10% w/v) in the homogenization buffer containing 0.05M HEPES and 125mM KCL pH 7.4 using a Potter-Elvehjem homogenizer at 5000 rpm for 3 mins (10 to 15 strokes). The homogenates were centrifuged at 7500rpm for 10 mins. The supernatant was used for the assay of oxidative stress and for various enzymes.

3.4.2 Isolation of kidney mitochondria:

The kidney tissues were homogenized (5%) using homogenizing buffer consisting of 220 mM Mannitol / 70mM Sucrose / 5mM Tris / 1 mM EGTA; pH 7.4. The homogenates were centrifuged at 4000 x g for 10 minutes and the nuclear pellet was discarded. Crude mitochondrial fraction were obtained by centrifuging at 12000 x g for 20 minutes and the pellet was washed thrice with wash buffer containing 220mM Mannitol/ 70mM sucrose / 20mM HEPES; pH 7.4. The final pellet was suspended in the same buffer (312). The purity of the mitochondria was established by enrichment of marker enzyme, succinate dehydrogenase. The isolated mitochondria were used for assessing their function and also for measuring the activities of mitochondria

3.4.3 Assessment of the purity of the isolated mitochondria by the assay of the activity of succinate dehydrogenase, the mitochondrial marker enzyme:

Succinate dehydrogenase:

Activity of succinate dehydrogenase was assayed using 2-(p-iodophenyl)-3-(p-nitrophenyl)-5-phenyl tetrazolium (INT) as electron acceptor, which forms formazan crystals on reduction (313).

Reagents*:*

1. 0.5 M Potassium phosphate buffer pH 7.4
2. 1 % INT 2-(p-iodophenyl)-3-(p-nitrophenyl) 5-phenyltetrazolium in warm water
3. 0.5 M Sodium succinate
4. 10% Trichloroacetic acid (TCA)
5. Ethyl acetate

Assay: To 0.1ml of potassium phosphate buffer, 0.1ml of INT, 0.1ml of sodium succinate and enzyme solution were added and volume was made up to 1ml with water. The assay mixture was incubated in 37°C water bath for 15 minutes. After incubation, reaction was arrested with 10 %

TCA and the formazan formed was extracted into 4 ml of ethyl acetate and this was read at 490 nm. Molar extinction co–efficient of formazan in ethyl acetate is 20.1 x 10^3 at $A_{490\ nm}$. One unit of enzyme is defined as the amount required for converting 1 μmol of INT to its formazan per minute under standard assay conditions.

3.5 BIOCHEMICAL ANALYSIS:

3.5.1 Malondialdehyde: (314)

Reagents:

1. 8.1 % of SDS
2. 20 % of Glacial acetic acid pH-3.5
3. 0.8 % of Thiobarbituric acid (TBA)

Assay: The reaction mixture consisted of 0.8 ml of sample (1mg), 0.2 ml of 8.1 % SDS, 1.5 ml of 20 % glacial acetic acid adjusted to pH 3.5, and 1.5 ml of 0.8 % aqueous solution of TBA. The mixture was made up to 4ml with distilled water and heated at 95^{o}C for 60 minutes using a glass ball as condenser. After cooling with tap water, 1ml distilled water and 5ml n-butanol and pyridine mixture (15:1) were added and the solution was shaken vigorously. After centrifugation at 2000g for 10 minutes the absorbance of the organic layer was measured at 532nm. Amount of thiobarbituric reacting substances (TBARS) formed was calculated from a standard curve prepared using 1,1', 3,3' tetramethoxy propane and the values were expressed as nmoles per gram tissue.

3.5.2 Conjugated diene: (315)

Total lipids were extracted as described and evaporated to dryness under nitrogen. The extracted lipids were dissolved in 1 ml of heptane and the absorbance was measured at 233nm. The amount of

conjugated diene present in the sample was calculated using a molar absorption co-efficient of $2.52x10^{-4}$.

3.5.3 Protein carbonyl: (175)

Reagents:

1. 10 mM dinitro phenyl hydrazine (DNPH) in 2 N HCl
2. 100 % TCA
3. Ethanol: Ethyl acetate (1:1)
4. 6 M Guanidine HCl

Assay: To 0.5 ml of sample (1-2mg), an equal volume of 10 mM DNPH in 2 N HCl was added and incubated for 1 hour shaking intermittently at room temperature. Corresponding blank was carried out by adding 2N HCl to the sample. After incubation, the mixture was precipitated with 10 % TCA (final concentration) and centrifuged. The precipitate was washed twice with ethanol: ethyl acetate (1:1) and finally dissolved in 1 ml of 6 M guanidine HCl. The contents were centrifuged at low speed and the supernatant was read at 366nm. The difference in absorbance between the DNPH treated and HCl treated sample was determined and expressed as nmoles of carbonyl groups per mg of protein, using molar extinction co-efficient of 22 $mM^{-1}cm^{-1}$.

3.5.4 Thiol groups: (316)

Reagents

1. Solution I: 100 mM Tris-HCl buffer pH 7.4 containing 5mM EDTA & 0.5 % SDS.
2. Solution II: 200 mM Tris/HCl buffer pH 8.6 containing 2 mM EDTA.
3. 10 mM 5,5'-dithiobis (2-nitrobenzoic acid) (DTNB) in methanol.

Assay: To 1 ml of the sample suspension (1 mg protein /ml), 1 ml of 10 % TCA containing 1 mM EDTA was added. The protein precipitate was separated by high speed centrifugation for 10 minutes. For total thiol estimation the sample was taken directly without precipitation. To this, 1 ml of solution I and 0.5 % SDS were added followed by 2 ml of solution II and 30 µl of DTNB. The tubes were mixed well and kept in the dark for 15 min at room temperature. The intense yellow colour of the nitromercapto benzoate anion formed from the DTNB reaction with the thiol was read at 412 nm which has a molar absorption of 13,600 $m^{-1}cm^{-1}$.

3.5.5 Nonprotein thiol: (317)

Nonprotein thiol was determined by the method described by Sedlak and Lindsay. Briefly, proteins were removed by the addition of 21µl 50% trichloroacetic acid (TCA) to 400µl sample. Then, samples were centrifuged at 12000 rpm for 10 minutes. Then, 50µl of TCA extract and 100µl of 6mmol/l DTNB (Ellman's reagent) were added successively to 850µl 0.2mmol/l phosphate buffer, pH 8.2. After 1 hour the absorbance was measured at 412nm. The standard curve was prepared from 1mmol/L solution of reduced glutathione.

3.5.6 Estimation of Nitrate: (318)

Reagents:

1. 50mM Carbonate buffer; pH 9.0
2. 3N HCl
3. 120mM $ZnSO_4$
4. 0.35M NaOH
5. Copper – Cadmium alloy

Assay: To 100µl of homogenate, 400µl of Carbonate buffer and 0.15g of cadmium filings were added and incubated at room temperature for 1 hour with thorough shaking. The reaction was stopped by adding 100µl of 0.35M NaOH and 120mM $ZnSO_4$ and incubated at room temperature

for 10 minutes and centrifuged at 4000 g for 10 minutes. 100µl of clear supernatant was aliquoted into microtitre plate wells and 50µl of 1% sulfanilamide and 50µl of 0.1% N-naphthylethylene diamine were added. The contents were mixed well and the colour was read at 545nm after 10 minutes.

3.6 ASSAY OF ANTI-OXIDANT ENZYME ACTIVITIES

3.6.1 Superoxide dismutase (SOD):

Superoxide dismutase was measured as described by literature (319) .

Reagents*:*

1. 0.5M Sodium phosphate buffer pH 7.5.
2. 16% Triton X 100
3. 10mM EDTA
4. 1.2 mM MTT
5. 4 mM Xanthine
6. 1 IU of xanthine oxidase
7. 0.05 M Bathocuproine sulphonate di sodium salt (BCS)
8. Stop buffer: 1M Formate, 10% Triton X 100 and 40% HCHO pH 3.5.

Assay: The assay mixture consisted of 100µl of phosphate buffer, 10µl of BCS, 50µl of Triton X-100, 5µl of EDTA, 5µl of xanthine oxidase and 50µl of xanthine. To this finally 150 µl MTT and sample (50-150 µg protein) were added and the volume was made up to 1 ml with water. The mixture was incubated for 5 minutes at room temperature (37°C) and the reaction was terminated with the addition of 1ml of stop buffer. The colour developed was read at 540nm. Amount of superoxide formed was calculated using the molar extinction coefficient of MTT formazan E_{540} of

17,000 M^{-1} cm^{-1} at pH 7.4 - 10.5. The percentage of inhibition of MTT colour formation by the presence of SOD was calculated from the reduction of the MTT colour formation as compared to the MTT formazan formed in the absence of SOD, which is taken as 100 %. One unit of SOD was defined as the amount of protein required to inhibit MTT reduction by 50%.

3.6.2 Catalase:

Catalase activity was estimated by measuring the change in absorption at 240 nm using H_2O_2 as substrate (320).

Reagents*:*

1. 0.05 M Potassium phosphate buffer pH 7.0
2. 30 mM H_2O_2 in 0.05 M phosphate buffer pH 7.0

Assay: To 1 ml of 30 mM buffered H_2O_2, the enzyme (sample) was added to start the reaction. The final volume was made up to 2 ml with 0.05 M phosphate buffer pH 7.0. Change in absorbance was observed for 3 minutes at 240 nm. One unit is defined as the activity of the enzyme that disproportionates H_2O_2 at the rate of 10^{-3} absorbance/sec.

3.6.3. Glutathione-S-transferase (GSTase):

The activity of GSTase was measured spectrophotometrically using the substrate 1-chloro-2,4-dinitrobenzene (CDNB) (321).

Reagents:

1. 1 M Potassium phosphate buffer pH 6.5
2. 10 mM reduced glutathione (GSH)
3. 20 mM 1-chloro-2,4-dinitrobenzene (CDNB)

Assay: To 0.1 ml of 1M potassium phosphate buffer pH 6.5, 0.1 ml of 10 mM GSH, 0.05 ml 20 mM CDNB were added and the final volume was made upto 1 ml with distilled water. The reaction

was started by adding the enzyme and change in OD at 340 nm was measured for 3 minutes. One unit of enzyme is the amount required to conjugate 1 μmole of substrate with glutathione in one minute.

3.6.4 Glutathione reductase:

In the presence of enzyme, hydrogen is transferred from NADPH to GSSG and the reaction was measured at 340 nm (322).

Reagents:

1. 1 M Potassium phosphate buffer pH 7.6
2. 10 mM oxidized glutathione (GSSG)
3. 1 mM NADPH
4. 10 mM EDTA

Assay: To the reaction mixture containing 0.05 ml of 1 M phosphate buffer pH 7.6, 0.15 ml of 10 mM EDTA, 0.1 ml of 1 mM NADPH, and 0.1 ml 10 mM GSSG; the enzyme (sample) was added. The volume was made upto 1 ml and the decrease in OD at 340 nm was measured for 3 minutes. One unit is the amount of enzyme needed to oxidize 1 μmole of NADPH/min.

3.6.5 Glutathione peroxidase:

Glutathione peroxidase was determined by following the oxidation of NADPH at 340 nm using hydrogen peroxide (323) .

Reagents:

1. 0.4 M Sodium phosphate buffer pH 7.0
2. 4 mM EDTA
3. 10 mM Sodium azide (NaN_3)
4. 1.6 mM NADPH
5. 10M GSH
6. Glutathione reductase (~30 units/ml of 3.6 M $(NH_4)_2SO_4$ suspension)

7. 2.5 mM Hydrogen peroxide

Assay: To 0.25 ml of 0.4 M phosphate buffer, 0.2 ml of 4 mM EDTA, 0.2 ml of 10 mM GSH, 0.2 ml of NaN_3, 0.2 ml of 1.6 mM NADPH, 0.03 ml glutathione reductase (one unit) and the enzyme (sample) were added. The total volume was made upto 2 ml with distilled water. Reaction was started by adding 0.2 ml of H_2O_2 and change in OD at 340 nm was followed for 3 minutes. Extinction coefficient of enzyme 6.1 mm^{-1} is used for the calculation. One unit is the amount of enzyme needed to oxidize 1 nmole of NADPH/min.

3.6.6 Myeloperoxidase

Myeloperoxidase activity was measured with O-dianisidine-H_2O_2 assay. The rate of decomposition of H_2O_2 by myeloperoxidase was determined by measuring the rate of colour development at 460nm (324).

Reagents:

1. 50 mM Phosphate buffer; pH 6.0

2. O – dianisidine HCl

3. 0.1μM H_2O_2

Assay: To 10μl of sample, 11μl of H_2O_2, 17μl of O – dianisidine and 962μl of phosphate buffer were added and the colour was read at 460nm at an interval of 30 seconds for 4 minutes and the rate of change/minute was determined. Extinction coefficient of 1.13 X 10^4 cm^{-1} was used for the calculation. One unit is the amount of enzyme decomposing 1μmole of peroxide per minute.

3.7. ANALYTES IN SERUM AND URINE

3.7.1 Creatinine

Principle:

Colourimetric, Jaffe's alkaline picrate, without deproteinization. Creatinine in serum or urine forms a coloured complex with picrate in alkaline medium. The rate of absorbance change of the coloured complex is proportional to the creatinine concentration (325,326).

Creatinine +Picric acid $\xrightarrow[\text{NaOH}]{}$ creatinine picramate (red colour)

Reagents:

1. Sodium hydroxide 0.2mmol/l
2. Picric acid solution 25mmol/l

Assay: To 7.5µl of serum sample and 1:10 diluted urine sample, added 125µl of sodium hydroxide and 25µl of picric acid solution, mixed well. The intensity of the colour developed was measured at 520nm.

3.7.2 Urea

UV, enzymatic, rate, urease, glutamate dehydrogenase. Following an initial lag phase the rate of reaction is constant for 60secs, decrease in absorbance at 340nm is proportional to the concentration of urea in the sample (327) .

Principle:

$$\text{Urea} + H_2O \xrightarrow[\text{Urease}]{} 2NH_3 + CO_2$$

$$NH_4^+ + 2\ \text{Oxoglutarate} + \text{NADH} \xrightarrow[\text{GLDH}]{} \text{L-Glutamate} + NAD^+ + H_2O$$

Reagents:

Autozyme reagent 1:

1. Tris buffered pH 7.7	50mmol/l
2. 2-oxoglutarate	10mmol/l
3. Urease	10U/ml
4. GLDH	900U/l
5. NADH	0.25mmol/l

Assay:

To 2µl of serum sample, added 200ul of autozyme reagent and measured at 340nm.

3.7.3 Uric acid

Uric acid is the end product of nucleic acid metabolism and is excreted by the kidney.

Colourimetric, enzymatic, end point, uricase, peroxidase, hydrogen peroxide is formed from uric acid and reacts with 4-amino phenazone in a series of enzyme reaction to give a coloured product, the intensity of which is proportional to the concentration of uric acid (328).

Principle:

Uric acid in the sample is oxidised by uricase to allantoin. In this reaction one mole of hydrogen peroxide is formed for every mole of uric acid oxidised according to the following equation:

$$\text{Uric acid} + O_2 + 2H_2O \xrightarrow{\text{Uricase}} \text{Allantoin} + CO_2 + H_2O_2$$

$$2H_2O_2 + H^+ + \text{TOOS} + 4\text{AP} \xrightarrow{\text{HPOD}} \text{Quinoneimine dye} + 4H_20$$

(Red violet colour

This assay is carried out at 546 nm. This reaction is initiated by the addition of the sample to the reagent. The intensity of the colour of the solution of this dye is proportional to the concentration of uric acid in the sample.

Reagent required :

Reagent 1

Phosphate buffer pH 7.8	50mmol/l
TOOS	7mmol/l
Fatty alcohol polyglycol ether	4.8%
Ascorbate oxidase	>83.3µkat/l
Reagent 2	
Phosphate buffer pH 7.8	50mmol/l
Hexacyanoferrate (II)	0.30mmol/l
4-amino phenazone (4AP)	3mmol/l
Uricase	>8.3µkat/l
Peroxidase	>16.7µkat/l

Assay:

To 3.5 ml of diluted serum sample and 1:10 diluted urine sample , 125µl of reagent 1 and 25µl of reagent 2 were added, mixed and the colour developed was read at 540nm.

3.7.4 Phosphate

Phosphate is an essential precursor of high energy compounds and a component of nucleic acid, phospholipids, and bone. Phosphate is usually measured in conjuction with calcium and alkaline phosphatases as part of bone profile.

UV, end point , ammonium molybdate for serum and urine analysis. Inorganic phosphorous reacts with ammonium molybdate and sulphuric acid to give an unreduced phosphomolybdate complex. The absorbance of this complex at 340 nm is proportional to the inorganic phosphorous concentration in the specimen (329).

Principle:

$$7H_3PO_4 + 12\,(NH_4)_6\,Mo_7O_{24}.\,4H_2O \longrightarrow 7(NH_4)[PO_4(Mo_7O_3)_{12}] + 51NH^{4+} + 51OH^- + 33H_2O$$

Reagent preparation:

Reagent 1 (blank reagent): 800ml water, 40ml conc H2SO4, 17.6g Nacl, 2ml TritonX 100 in 2 litres deionised water.

Reagent 2 (Phosphate reagent): 400ml deionised water, 20ml conc sulphuric acid, 8.8g Nacl, 5.314g ammonium molybdte in 2 litres water.

Results to express urine result /24hr multiply X10 to give mg/l then Xurine volume in litres.

Assay: To 2.5µl of serum and 1:10 dilution of urine sample, added 125 µl of reagent 1 and 55 µl of reagent 2. The colour developed was measured at 340nm.

3.7.5 Total/Bicarbonate

Colorimetric, enzymatic, endpoint, for the measurement of total CO_2 in serum or plasma (Manufacturers instruction in the kit insert. Randox, UK) (330).

Principle:

$$\text{Phosphoenolpyruvate} + HCO^{3-} \xrightarrow[\textbf{PEPC}]{} \text{Oxaloacetate} + H_2PO^{4-}$$

$$OAA + NADH + H^{+} \xrightarrow[\textbf{MDH}]{} \text{Malate} + NAD^{+}$$

The reduction in absorbance at 340nm caused by the oxidation of NADH is proportional to the bicarbonate concentration in the sample.

Reagents :

Reagent 1

1. Tris buffer (25mmol/l), pH 6.5
2. CO_2 reagent (PEP 6.3mmol, NADH 0.45mmol, PEPC 200U, Malate dehase 600U and Mg_2^{+} 8mmol/ litre)

Reconstitute the vial of CO_2 reagent with 10ml of buffer. Allow the reagent to stand for 15 mins before use. Do not shake this reagent while reconstituting, as this may cause excessive CO_2 absorption. Gently invert the vial once.

Assay: To 2µl of serum and 1:10 diluted urine, added 200µl of reagent 1 and colour developed was measured at 380nm

3.7.6 Potasssium

The AVL 9180 electrode analyser is intended to be used for the measurement of potassium.

Principle: . It is based on the ion-selective electrode (ISE) measurement principle to precisely determine the measurement values of sodium, potassium and chloride.

3.7.7 Glucose (GOP-POD) method

Colorimetric, enzymatic glucose oxidase, peroxidase. Glucose in the specimen is oxidized with the liberation of hydrogen peroxide. The peroxidase enzyme catalyzes the reaction of this 4-amino phenazone to produce a dye, the colour of which is proportional to the concentration of glucose in the specimen (331).

Principle:

Glucose present in the given plasma sample is oxidised by glucose oxidase to gluconic acid with the liberation of hydrogen peroxide. The peroxidase present in the reagent convert hydrogen peroxide to water and nascent oxygen. The oxygen is accepted by 4-amino phenazone in presence of phenol to give a pink coloured chromogen which shows maximum absorbance at 510nm. The intensity of the test solution is compared with the colour given by a standard glucose similarly treated.

$$\text{Glucose} \xrightarrow[\text{GOD/ pH 7.0}]{} \text{Gluconic acid} + H_2O_2$$

$$H_2O_2 \xrightarrow[\text{POD}]{} H_2O + [O]$$

[O] + 4-amino phenazone + Phenol ⟶ Pink Chromogen

Reagents:

Reagent 1	Enzymes
Reagent 2	Phenol
Reagent 3	Standard glucose 100mg/dl
Reagent 4	Buffer

Assay:

To 2µl of serum sample, added 200µl of the reagent 1 and mixed well. The intensity of the pink colour formed was measured at a wavelength of 520nm.

3.8 MEASUREMENT OF PARAMETERS OF MITOCHONDRIAL FUNCTION

3.8.1 Measurement of oxygen uptake (RCR): (332,333)

Oxygen uptake was determined polarographically using a Clark type electrode in 2 ml of respiratory buffer (225 mM sucrose, 5 mM $MgCl_2$, 10 mM KH_2PO_4, 20 mM KCl, 10 mM Tris, and 5 mM Hepes pH 7.4), containing 5 mM succinate as respiratory substrate. 2 mg/ ml of mitochondrial protein was introduced into the oxygen electrode compartment (Rank oxygen electrode). The electrode output was connected to an appropriate recorder and the recorder was set such that 100% full range corresponded to total oxygen content of the mixture. Oxygen uptake was stimulated with 0.3 mM ADP and the rate of state 3 and state 4 respirations were measured. Oxygen uptake was calculated from the decrease in percent saturation of the mixture. The ratio of state 3 / state 4 respiratory rates was calculated for the respiratory control ratio (RCR).

3.8.2 MTT reduction assay: (334)

The MTT assay was done on the mitochondria using a microplate reader as described. Mitochondrial suspension (150 – 200 μgm protein) was added to the wells containing 6μl of 1.25 mM MTT and the volume was made up to 150 μl with 25 mM phosphate buffered saline, pH 7.4. MTT was dissolved in phosphate buffered saline (PBS) and filtered to remove small amount of insoluble residue. Plates were incubated at 30°C for 20 min followed by addition of 150 μl of dimethyl sulfoxide (DMSO) and mixed thoroughly to dissolve the formazan. The plates were shaken for a few minutes in an orbital shaker and then read on a multiwell scanning spectrophotometer (ELISA reader) using a test wavelength of 570 nm and reference wavelength of 630 nm. The amount of MTT formazan formed was calculated using the molar extinction coefficient of MTT formazan E_{570} of 17,000 $M^{-1}cm^{-1}$ at pH 7.4 to 8.0.

3.8.3 Mitochondrial swelling: (335,336)

Swelling of mitochondria was determined by following the decrease in absorbance at 540 nm for 10 minutes as described. Mitochondrial suspension was added to cuvette containing buffer (250 mM sucrose / 5 mM Hepes, pH 7.4). The combination was quickly mixed and the change in absorbance was measured at 540 nm for 10 minutes in a spectrophotometer.

3.9 Assay of the activities of the electron transport chain complexes

3.9.1 Complex I (NADH – Ubiquinone oxidoreductase) assay: (337)

Reagents:

1. 25 mM Potassium phosphate buffer containing 10mM $Mgcl_2$ (pH 7.2)
2. 1mM Rotenone
3. 5mM Coenzyme Q_2

4. 5% Bovine serum albumin (BSA)
5. 5mM NADH
6. 100mM KCN

Assay: The reaction mixture consists of 50µl of BSA, 10 µl of KCN and sample in appropriate volume of buffer to make the final volume to 1ml. The reaction was started by the addition of coenzyme Q_2 and the reaction rate was followed for 5 minutes. 10µl of rotenone was added and the reaction rate was followed for another 5 minutes. Molar extinction coefficient of NADH is 6.22.

3.9.2 Complex II (Succinate – Ubiquinone oxidoreductase) assay: (337)

Ubiquinone absorbs at 275nm but turbidity of mitochondrial and cell samples in UV range often causes problems. So, a secondary dye, Dichlorophenol indophenol (DCPIP) that absorbs at 600nm is used. Enzyme activity is that which is >90% inhibited by 2- theonyl trifluoroacetone (TTFA).

Reagents:

1. Potassium phosphate buffer (100mM; pH 7.4)
2. 0.5 M Sodium succinate
3. 2.5 mM EDTA
4. 3mM DCPIP
5. 100mM KCN
6. 1mM Rotenone
7. 5mM Ubiquinone – 2
8. 100mM TTFA

Assay: The assay mixture consisted of 500µl of buffer, 40 µl of succinate, 40 µl of EDTA, 40 µl of DCPIP, 10 µl of KCN, 10 µl of rotenone and the sample in a total volume of 1ml. The reaction mixture was incubated in the spectrophotometer for 10 minutes to minimize the succinate

dependent non – linear rate, and then the reaction was started by adding 10 µl of ubiquinone – 2 (or enough so that the final concentration is 50 µM). The reaction was monitored for 5minutes and then 10 µl of TTFA was added and monitored further for 5 minutes. The complex II activity was expressed as µmoles/min/mg protein using the molar extinction coefficient for DCPIP of 21 $mmol/L^{-1}$ cm^{-1}.

3.9.3 Complex IV (Cytochrome c oxidase) assay: (337)

The oxidation of reduced cytochrome c was followed at 550nm.

Reagents:

1. Potassium phosphate buffer (100mM; pH 7.0)
2. Potassium ferricyanide (100mM)
3. Reduced cytochrome c

Assay: In the reference cuvette 30 µl of reduced cytochrome c, 10 µl of ferricyanide were added and the volume was made to 1ml with buffer and set to zero. In the sample cuvette 30 µl of reduced cytochrome c and 10 µl of sample were added and the readings were monitored for 3 – 4 minutes. The enzyme activity is expressed as k/min/mg protein.

3.9.4 Complex V assay: (338)

The hydrolysis of ATP by the ATPase in the mitochondrial fraction liberates ADP which is converted back to ATP by pyruvate kinase utilizing the added phosphoenolpyruvate as a substrate and energy phosphate group donor. This maintains a constant concentration of ATP and a low steady state concentration of ADP (which is an inhibitor of ATP hydrolysis). The pyruvate produced in the pyruvate kinase reaction is then converted to lactate by lactate dehydrogenase and this is coupled to the oxidation of NADH to NAD. It is the decrease in NADH at 340nm which is measured.

Reagents:

1. Master mix: 100mM Tris buffer (pH 8.0), 250mM $MgCl_2$, 1M KCl, 100 mM KCN, 1mM rotenone, 5mg/ml BSA, pyruvate kinase (4 units), lactate dehydrogenase (4 units), 100 mM Phosphoenol pyruvate, 15 mM NADH.
2. 100 mM ATP
3. Oligomycin

Assay: 205 µl of master mix, 720 µl of distilled water; 5 µl of sample and 50 µl of 100mM ATP were added to the cuvette, mixed and incubated for 5 minutes. The readings were monitored for 5 minutes at 340nm and 30^0C. 20 µl of oligomycin was added and the readings were monitored for 5 min. The inhibitor sensitive rate was calculated by subtracting the rate before oligomycin addition from that observed after oligomycin addition and related this to the mitochondrial protein in the cuvette. The extinction coefficient for NADH is 6.22. The enzyme activity is expressed as moles/min/mg protein.

3.10 Carbonic anhydrase (CA) (Sigma protocol) (339)

Carbonic anhydrase activity is measured spectrophotometrically based on the action of enzyme on P-nitrophenyl acetate to form p-nitrophenol and acetate, the absorbance was measured at 348nm.

Reagents:

1. 15mM Tris Buffer)pH 7.6
2. 3mM p-Nitrophenyl acetate (PNPA) dissolved in acetone.

Assay: To 0.2ml of 3mM p-nitrophenyl acetate added 15mM tris buffer pH7.6 and made up to 1.0ml. The reaction started by adding 10µl sample immediately mixed and change in OD measured at 348nm for 3 min. One unit of enzyme is the amount required to form p-nitrophenol in one minute.

3.11 Aconitase (340)

Reagents:

1. 50mM Tris-HCl (pH7.4)
2. 0.6mM $MnCl_2$
3. 5mM Trisodium citrate
4. 200 µM $NADP^+$
5. Isocitrate dehydrogenase (1.5U/mg solid)

Assay: Prepared a reaction cocktail mixture which contains 750 µl of Tris-Hcl buffer, 100µl sodium citrate, 100ul of $MnCl_2$ and 20 µl of NADP. To this reaction cocktail added 20µl of enzyme Isocitrate dehydrogenase and started the reaction by adding 10µl of mitochondrial sample, mixed immediately and change in OD measured at 340nm for 5 mins.

3.12 Estimation of Protein Content (341)

Protein concentrations in all the extracts were determined.

Principle:

This method involves pre-treatment of protein with alkaline copper sulphate in the presence of tartrate, followed by addition of folin's phenol reagent (a mixture of phosphomolybdic tungstic acids). The peptide bonds reduce cupric ions to cuprous ions, in an alkaline medium, which then react with folin's phenol reagent . The phosphomolybdotungstate in folin's phenol reagent is reduced to heteropolymolybdenum blue by copper-catalysed oxidation of aromatic amino acids, to give rise to a blue coloured solution. The intensity of the colour depends on the tyrosine and tryptophan content of the protein. It is measured spectrophotometrically at 650nm.

Reagents

1. Lowry's Reagent
2. Folin's reagent (diluted 1:1 with deionised water)
3. BSA standards

Procedure: Protein solutions obtained were diluted 1:10. From each sample, 25 and 50 µl were each added to 2.5ml of freshly prepared lowry's reagent. The total volume in each tube was made upto 3ml with deionised water. The tubes were incubated at room temperature for 10mins. Folin's phenol reagent (0.25ml) was added to each tube. The reaction mixture was incubated at room temperature for 30mins. The blue colour produced was measured using a spectrophotometer, at a wavelength at 660nm.

3.13 Preparation of homogenates for western blots and gelatin zymogram

The snap frozen kidney tissue were used to prepare the homogenates were obtained from animals treated with TDF for 35 days. The tissues were homogenized on ice in 25 mmol/L Tris HCl pH7.5, 50mM KCl, 5mM EDTA, 4mM $Mgcl_2$, 2.5mM DTT, 0.125mM PMSF and protease inhibitor cocktail that contained leupeptin (2.5ug/ml), aprotinin (1µg/ml), and pepstatin (1µg/ml). The homogenates were centrifuged at 17,000g for 15 minutes at 4^oC (342). The supernatants obtained were used for zymogram. It was also used for carrying out western blots for all the proteins studied except PARP, NF-κB p65 and IκB-alpha. Cytosolic and nuclear fractions, prepared as described below, were used for western blots for p65. Cytosolic fractions were used for western blots for IκB-alpha.

3.14 Preparation of cytosolic and nuclear extracts

Cytosolic and nuclear extracts were prepared from kidney homogenate using a commercial kit (Imgenex, U.S.A) according to manufacturer's instructions. Snap-frozen tissue (300 mg) was

washed with 1X PBS-PMSF (0.5% phenylmethylsulfonyl fluoride) solution and homogenized in a Dounce tissue homogenizer (using 20 strokes) in 3 ml of Hypotonic buffer (150 mM sodium flouride, 10 mM HEPES (pH 7.9), 1 mM EDTA and molybdate solution, 1mM DTT, 10% Nonidet P-40). The homogenate was centrifuged at 2,000g for 30 seconds. The pellet obtained consisted of tissue debris and was discarded. The supernatant obtained was incubated on ice for 15-30 mins and then centrifuged at 5,000g for 10 min. The resulting supernatant containing the cytoplasmic extracts was collected and stored at -80°C till required for use. The pellet obtained was used as a nuclear extract. It was re-suspended in a small volume (100 µl) of Nuclear extraction buffer (Tris-Hcl (pH 8.0), NaCl, Triton-X 100, Sodium fluoride, Sodium phosphate, sodium pyrophosphate 0.5 mM dithiothreitol and 30 µl/ml of a protease inhibitor cocktail (AEBSF (500 µg /ml), aprotinin (1 µg /ml), E64 (5 µg /ml), leupeptin (0.5 µg /ml)) and incubated on ice for 30 mins. The lysed nuclei were then transferred to a microcentrifuge tube and centrifuged at 12,000g for 10 mins at 4°C. The supernatant obtained, containing the nuclear extract, was collected and stored at -80°C until use.

3.15 Sodium Dodecyl Sulphate - Polyacrylamide Gel Electrophoresis (SDS-PAGE)

The proteins extracts obtained as described above, were subjected to sodium dodecyl sulphate polyacrylamide gel electrophoresis (SDS-PAGE), using a 10% gel for iNOS, Caspase 3, Nitrotyrosine, Nitrocysteine, NF-κB p65, IκB α, HSp70, HO-1, MMP-9 and 8% gel for PARP, PLA2.

Reagents for preparation of separating gel

Solution A

SDS	0.4%
Tris	1.5M

TEMED 0.2%

The pH was adjusted to 8.8

Solution C

Acrylamide 40%

Bis-acrylamide 1.0656%

Ammonium per sulphate (APS) 10%

Separating gel of required percentage (depending on the protein of interest) was casted using the above mentioned reagents. The volume of reagents used to caste varying percentage of gels is shown in table: 3.1

Table : 3.1 Solution composition and gel percentage for separating gel

Gel percentage	Solution A (in ml)	Solution C (in ml)	Water (in ml)
For 10%	1.2	1.2	2.4
For 8%	0.96	0.96	2.88

Fifty microlitres of APS was added at the end to initiate polymerization.

Reagents for preparation of stacking gel

Solution B

SDS 0.4%

Tris 1.1M

TEMED 0.278%

The pH was adjusted to 6.8

Solution D

Acrylamide 20%

Bis-acrylamide 0.53%

Ammonium per sulphate(APS) 10%

A five percent stacking gel was casted using the above mentioned reagents. The volume of reagents used to prepare the stacking gel is shown in **table: 3.2**

Gel percentage	Solution B (in ml)	Solution D (in ml)	Water (in ml)
For 5%	1	1	2

Fifty microlitres of APS was added at the end to initiate polymerization.

Running Buffer

Tris base 25 mM

Glycine 190 mM

SDS 0.1%

The pH was adjusted to 8.6.

Protein Dissociation Buffer (10ml)

Tris (0.5M, pH 6.8) 2.5ml

SDS (10%) 4ml

Glycerol (100%) 2ml

B-mercaptoethanol 0.8ml

Bromophenol blue (0.1%) 300µl

Ultrapure water 400µl

Procedure

Step 1: Spacer plates and short plates were cleaned with ultrapure water before use.

Step 2: It was then placed in a casting frame and placed on a smooth glass surface so that the two plates were evenly aligned. The glass plates were clamped together with the spacers between them and placed on a gel casting rack.

Step 3: The solution containing the components of the running gel was prepared and poured into the space between the 2 glass plates.

Step 4: Butanol was layered on top to remove bubbles.

Step 5: The gel was then allowed to polymerize.

(Note: The time allowed for polymerization depended on the percentage of the gel prepared)

Step 6: Butanol was removed. The top of the gel was washed thoroughly with water.

Step 7: The stacking gel was prepared and poured on top of the running gel.

Step 8: The gel comb was inserted into the stacking gel; the solution was allowed to polymerize.

(Note: The comb used to correspond to the thickness of the spacer)

Step 9: The gel combs were removed after polymerization.

Step 10: The apparatus was set up in a cold room.

Step 11: Each sample (containing 100µg of protein) was mixed with a protein dissociation buffer in the ratio of 1:1 and kept in a boiling water bath for 5 mins.

Step 12: Samples were briefly centrifuged, they were then loaded into wells.

Step 13: Running gel buffer (pH 8.6) was added to electrophoresis tank. The apparatus was connected to the power pack and was run at 50V till the sample reached the separating gel. The voltage applied was increased to 80V at this point. Electrophoresis was stopped when the marker dye reached near the end of the gel.

3.16 WESTERN BLOTTING

Tris-buffered saline (TBS)

Trizma Hcl	2.423g
Sodium chloride	8.0g

The pH was adjusted to 7.6 and the volume was made up to 1 liter with ultrapure water.

Blocking Buffer

Tween-20	0.1%
Skimmed milk	5%

Blocking buffer was prepared in PBS, pH 7.4

Wash Buffer

Skimmed milk	5%

(in TBS, pH 7.4)

Stripping Buffer

β-mercaptoethanol	100mM
SDS	2%
Tris-HCL	62.5mM

Procedure

Step 1: Proteins separated by electrophoresis were electro-blotted onto polyvinylidene difluoride (PVDF) membranes at 90V for 3hrs.

Step 2: A commercially available protein molecular weight marker was also electrophoresed on the polyacrylamide gel and electroblotted onto the PVDF membrane along with the samples.

Step 3: The membranes were incubated with blocking buffer for 2hours at room temperature, followed by incubation with primary antibodies for 16 hours at $4^{o}C$. The primary antibodies were used at the following dilutions: anti-iNOS (1:500), anti-caspase 3 (1:1000), anti-caspase 9 (1:1000), anti-AQP2, (1:200), anti-HSP70 (1:2000), anti-HO 1(1:200) , anti-NF-κB p65 (1:200), anti-IκBα (1:200), anti-PLA2 (1:1000), anti-cytochrome c (1:000), anti-nitrotyrosine (1:250), anti-S-nitroso-cysteine (1:500), anti-TNF α (1:500), anti-PARP (1:1000), MMP-9 (1:500) and MMP-2 (1:500).

Step 4: The membrane was washed 3 times for 10 minutes each, using TBS with 0.02% Tween-20 at pH 7.4.

Step 5: Incubation with antibodies against the primary antibody and beta-actin was followed by incubation with peroxidase-labelled antibodies (1:1000). A commercially available S protein-HRP

(1 in 2500) conjugate (required for visualization of the molecular weight markers) was also incubated along with secondary antibody. The secondary antibody and the S protein were tagged with a peroxidase that acted on a chemiluminescent substrate.

Step 6: The bands obtained were visualized by use of ECL West Dura substrate and their intensity quantitated using a chemiluminescent imaging system (FluorChem ^{TM} SP, Alpha Innotech).

Step 7: The membrane was then treated with stripping buffer for 30 minutes at 55^{o}C to remove the primary and secondary antibodies.

Step 8: It was then washed thrice in ultrapure water for 10 minutes each time. Final washes were done twice with the wash buffer for 15 minutes each time.

Step 9: The membrane was then incubated with antibody against beta-actin (dilution of 1:5000) overnight at 4^{o}C.

Step 10: The membrane was then washed 3 times for 10 minutes each and incubated in goat anti-mouse secondary antibody (dilution 1 in 5000 in blocking buffer). The bands were visualized and quantified as described above.

Precautions taken during western blot assays

1. Touching the membrane with fingers was avoided. Gloves were used while handling membranes.
2. It was ensured that the paper and membrane were cut to the same size as the gel.
3. Care was taken to ensure that PVDF membranes were properly soaked in methanol for 15-20 seconds before use.
4. After placing the gel and membrane between sheets of filter paper, air bubbles between the gel and membrane were removed by rolling them out with a glass rod. Alternatively the layer was assembled in a dish of transfer buffer, to prevent formation of bubbles.
5. The apparatus was set up in a cold room to avoid heat generation during transfer.

3.16.1 Detection of cytochrome-c release by western blot

The fresh kidney tissue was homogenized using a mitochondrial isolation buffer (70 mM sucrose, 220 mM Mannitol, 1 mM EGTA and 5 mM Tris, pH 7.4). The homogenate was centrifuged at 4000g for 10 minutes at 4°C. The supernatant was collected and was then centrifuged at 12,000g for 20 minutes. The resultant supernatant was used as the cytosolic fraction, while the pellet obtained was used as the mitochondrial fraction (312). Cytosolic and mitochondrial samples, corresponding to 100 µg protein each, were denatured and separated by sodium dodecyl sulfate polyacrylamide gel electrophoresis (SDS-PAGE), using 10% gels and transferred to PVDF membrane. The membranes were blocked with 5% bovine serum albumin in TBS and 0.1% Tween-20 for 2 hours. Thereafter, the membranes were incubated with monoclonal antibodies to cytochrome c (1:1000 dilution) (Cell Signaling Technology, CA, USA). A detection system using a chemiluminescent substrate (Thermo Fisher Scientific Inc. U.S.A.) was used to visualize the protein bands. The bands were documented using an AlphaEase FC gel documentation system (Alpha Innotech Corporation, CA.) and normalized to those for beta-actin, which was used as a loading control.

3.17 NF-κB p65 activity by ELISA

For determining NF-κB , nuclear and cytoplasmic fractions were isolated from kidney homogenate using a commercial kit (Imgenex) according to manufacturer's instructions.

The NF-κB /p65 ELISA kit measures free p65 in the nucleus of tissues. This assay was done using a sandwich ELISA protocol. The anti-p65 antibody coated plate captures free p65 and the amount of bound p65 is detected by adding a second anti-p65 antibody followed by alkaline phosphatase-conjugated secondary antibody using colourimetric detection in an ELISA plate reader.

Procedure:

1. **Coating:** Diluted 100 µl of capture antibody in 10ml of coating buffer. Pippeted 100 µl of diluted antibody into each well for the standard, cytosolic and nuclear extracts of control, TDF, Melatonin+TDF and Melatonin alone groups. Then covered the 96 well plates and incubated the plate overnight for 12h at 4^{o}C. Washed the coated wells twice with 300 µl of 1X wash buffer.
2. **Blocking:** Added 200 µl of prepared blocking buffer to each well to block the remaining reactive surface. Incubated the plate for 1h at room temperature.
3. **Preparation of p65 Standard Curve:** The recombinant p65 standard was diluted with 420 µl of sterile deionised water. Standard setup was made in duplicates by serial dilution using the following concentrations (100, 50, 25, 12.5, 6.25, 3.125, 1.5625 and blank). The blocking buffer was removed from the wells and gently tapping the plate face-down on paper towels. 100 µl of fresh blocking buffer was replaced in the standard wells and test samples.
4. **Samples:** 100 µl of control, TDF, melatonin+TDF and melatonin protein samples were added and incubated the plate at 4^{o}C overnight at room temperature
5. **Washing:** Removed control and test lysates and washed 4 times with 300 µl of 1X wash buffer.
6. **Detecting Antibody:** Diluted 100 µl of Detecting antibody in 10ml of blocking buffer. 100 µl of diluted detecting antibody were added to each well and incubated for 1h at room temperature.
7. **Washing:** The antibody solution was removed and washed wells 4times with 300 µl of 1X wash buffer.
8. **Secondary Antibody:** Diluted 5 µl of AKP-conjugated secondary antibody in 10ml of blocking buffer. From this added 100 µl of diluted secondary antibody to each well and incubated for 1h at room temperature.
9. The secondary antibody was removed and washed thoroughly 5 times with 300 µl of 1X wash buffer. This ensures a thorough wash and lower background. During the last wash prepared

pNNP substrate. Tapped the plate upside down several times to remove any residual wash buffer.

10. **pNNP Substrate:** Dissolved 10mg pNPP into 10ml of pNPP substrate buffer and mixed. From this added 100 µl of pNPP substrate to each well and incubated the plate at room temperature for 30min. The colour developed was read at 405nm.

3.18 Estimation of activity of Caspase-3

The activity of caspase-3 was determined by isolation of tissue lysate from kidney using a commercial kit (Abcam) according to manufacturer's instruction. This assay is based on detection of cleavage of substrate DEVED-AFC (AFC: 7-amino4-trifluoromethyl coumarin). DEVD-AFC emits blue light (λmax =400nm); upon cleavage of the substrate by CPP32 or related caspases, free AFC emits a yellow-green fluorescence (λmax=505nm), which can be quantified using a fluorescence microplate reader.

Procedure:

The kidney tissues were homogenized in lysis buffer (1X volume of tissue, added 3X volume of lysis buffer) to generate tissue lysates. Incubated the tissue lysates on ice for 20 minutes and centrifuged at 5000 g for 10 minutes at 4°C. The supernatants obtained were used for the assay of Caspase-3 activity . Protein was estimated in the supernatants using bovine serum albumin as a standard (Lowry et al., 1951). An aliquot of the supernatant, corresponding to a protein concentration of 100 µg was made up to 45 µl using the assay buffer. To this, 50 µl of reaction buffer (added 10 µl of 1M DTT for 1ml of stock 2X reaction buffer) and 5µl of the specific substrate were added to the enzyme concerned and the mixture was incubated at 37°C for 2 hours. The samples were read in a fluorescence spectrophotometer with a 400nm excitation filter and 505

nm emission filter. The fold increase in Caspase activity can be determined by comparing these results with the level of control values.

3.19 Detection of MMP-9 by Zymogram: (Gelatin Zymography)

Supernatant from renal homogenates were loaded, at a standard concentration of 100µg protein per well, into 10% polyacrylamide gel containing 0.1% gelatin (270) and electrophoresed at 4^{o}C. The gel was removed from the cassette and washed three times (30minutes) with the wash buffer (2.5% Triton X 100) at 4^{o}C. The gel was then washed twice with water and incubated in a development buffer (50mM Tris, pH 7.5, 0.15M NaCl, 10mM $CaCl_2$ and 0.2% Brij-35) for 16-18hours at 37^{o}C. Each gel was stained with 0.05% Coomassie blue G-250 in 30% methanol/10% acetic acid for 40minutes and destined for 15minutes in 30% methanol/10% acetic acid. MMP activity was detected as areas of clearing in the gel, where gelatin had been cleaved by MMPs. The gels were digitized using a CCD frame digitizer system (Alpha Innotech) and densitometric analysis of the cleared zones was done using AlphaEase FC (Alpha Innotech).

3.20 Sodium Dodecyl Sulphate-Polyacrylamide Gel Electrophoresis (SDS-PAGE) for detection of urinary proteins:

Urine proteins were measured by Lowry's method and fractionated by SDS-PAGE using 8% resolving gel and 5% stacking gel. Each sample containing 100µg of urinary protein was mixed with a protein dissociation buffer in the ratio of 1:1 and kept in a boiling water bath for 5 mins. Samples were briefly centrifuged, they were then loaded into wells. Running gel buffer (pH 8.6) was added to electrophoresis tank. The apparatus was connected to the power pack and was run at 70V till the sample reached the separating gel. The voltage applied was increased to 90V at this point. Electrophoresis was stopped when the marker dye reached near the end of the gel. After electrophoretic separation, the gel was stained with Coomassie blue solution (0.01% Coomassie

brilliant blue R250, 50% (v/v) methanol and10% (v/v) glacial acetic acid) for 3hrs at room temperature and subsequently detained in the destaining solution (50% (v/v) methanol and 10% (v/v) acetic acid) for 2h. The gel image was captured and analyzed by a gel documentation system (Alpha Innotech) , using Alpha Ease software.

3.21 Terminal deoxynucleotidyl transferase biotin-dUTP nick end labeling (TUNEL)

Transferase biotin-dUTP nick end labeling assay was done by an in-situ cell death kit conjugated with TMR red (Roche Diagnostics, Germany) according to the manufacturer's instructions.

Principle: TUNEL (Terminal deoxynucleotidyl Transferase Biotin-dUTP Nick End Labelling) method identifies apoptotic cells in-situ by using terminal deoxynucleotidyl transferase (TdT) to transfer biotin-dUTP to the free 3'-OH of cleaved DNA. The biotin-labelled cleavage sites are then visualized by reaction with fluorescein conjugated avidin (avidin-FITC).

Procedure: The Tunel assay was performed on paraffin-embedded kidney tissues. The slides were deparaffinized with xylene 3 times for 3 mins followed by 100% ethanol, 90% ethanol and 80% ethanol , rehydrated with water 4 times for 2 mins and thoroughly washed sections with PBS for 30 minutes at 37°C. Prepared proteinase K solution by diluting an aliquot of proteinase K with PBS and covered sections with diluted proteinase K and incubated for 30 minutes at 37° C, this helps to expose the DNA for end-labelling with TdT. Then stopped the proteinase K digestion by washing the sections with PBS 4times for 2 minutes each. Simultaneously, for positive control the proteinase K treated slide was incubated with 1mg/ml of DNase I for 60 minutes at 37°C which cleaves the DNA to create substrate for the end-labelling reaction and stopped the DNase I reaction by washing the slides for 15 minutes with PBS. Then sections were equilibrated with TdT buffer. TdT end-labelling cocktail was prepared by mixing TdT buffer, Biotin-dUTP and TdT at a ratio of 90:5:5

respectively and incubated all sections with TdT end-labelling cocktail for 60 minutes at 37°C. Then stop the reaction by immersing the section in TB buffer (1X) for 5minutes at room temperature. Sections were washed with PBS for 4X2 minutes. The Blocking buffer was prepared by diluting Blocking Solution at 1:3 ratio with PBS , applied to the sections and incubated at room temperature for 20 minutes. The avidin-FITC was prepared by diluting with blocking buffer at 1:9 ratio and applied to the sample sections, incubated in the dark for 30 minutes. Then sections were washed with PBS for 2X15 minutes in the dark and counterstained with Propidium Iodide. Slides were mounted in 90% glycerol in PBS, coverslipped and stored in the dark at 4°C. Fluorescence images were obtained linear range of detection to avoid signal saturation using an Olympus Laser Scanning Confocal Microscope.

3.22 RNA ISOLATION, QUANTITATION AND STORAGE

3.22.1 Isolation of RNA:

Principle:

RNA in cells or tissue is separated from the DNA after extraction with an acidic solution containing guanidium thiocynate, sodium acetate, phenol and chloroform. This step is followed by centrifugation. Under acidic conditions, total RNA remains in the upper aqueous phase obtained at the end of centrifugation, while most of the DNA and protein remain either in the interface or in the lower organic phase. Total RNA is then recovered from the upper aqueous phase by precipitation with isoproponal.

Reagents

1. **Diethyl pyrocarbonate (DEPC)-treated water:**

   The use of DEPC-treated water is required in the isolation of RNA in order to inactivate any RNase that may be present in water and laboratory glassware. The use of such water reduces the

risk of RNA being degraded during the process of isolation. DEPC should be not be used with Tris or HEPES, since they react with DEPC and inactivate it.

Added 0.1 ml of DEPC to 100 ml water and mixed vigorously to get the DEPC into solution completely, Kept overnight at room temperature. It was then autoclaved for 15 minutes to inactivate the DEPC.

2. **75% ethanol:**

   75 ml absolute ethanol was added to 25 ml DEPC-treated water and mixed.

3. **1% sodium dodecyl sulfate (SDS):**

   1 gm of SDS (of DNase- and RNase-free grade) was weighed and made upto 100ml using DEPC-treated water. The solution was stored at room temperature.

Procedure:

Total RNA was extracted from the kidney of control and experimental rats, using TRI reagent (Sigma) as described below (as per manufacturer's instructions).

Step 1: To each 50-100mg of tissue, 1ml of TRI reagent was added. The samples were then homogenised in a glass homogenizer, using a mechanical homogenizer (25 to 30 strokes).

Step 2: Each homogenized sample was kept on ice for 10 minutes. To this, 200 µl of chloroform was added. The mixture was shaken vigorously for 30 seconds. It was then placed on ice for a further period of 15minutes.

Step 3: The mixture was centrifuged at 12000g for 15mins at 4°C. At the end of the centrifugation, three layers had formed: an upper aqueous layer, an interpahase and a lower organic layer. The upper aqueous layer contained RNA while the inter-phase contained genomic DNA. The lower organic (phenol) layer was composed of cellular protein and debris.

Step 4: About 500 µl of the upper aqueous layer was transferred to a fresh 1.5ml microtube. Care was taken not to disturb the interface in order to avoid DNA contamination.

Step 5: To the aqueous portion that was removed, 500 µl of pure isoproponal was added. The mixture was allowed to stand on ice for 10 mins.

Step 6: The mixture was then centrifuged at 12000 g for 10 min at 4°C.

Step 7: The supernatant obtained was discarded and 1ml of 75% ethanol in water was added to the tube. The contents of the tube were gently mixed, using a vortex mixer.

Step 8: The mixture was then centrifuged at 12000 g for 5 min at 4°C.

Step 9: The supernatant was discarded and the RNA pellet obtained was air dried.

Step 10: The dried pellet was disssolved in 30-50µl of DEPC water, by placing the tube in a heated water bath (55-65°C)

Precautions taken during RNA isolation:

1. All materials used during the process of isolation (such as micro-tubes, water, and reagents) were autoclaved prior to use. Commercially available sterile hand gloves were used throughout the procedures.
2. All pipetting procedures were carried out in a specially designated clean hood.
3. The tissues obtained after sacrifice of the animals were immediately snap frozen, to prevent RNA degradation and stored at -70°C. Care was taken to see that the tissue was completely homogenized.
4. The aqueous phase obtained was removed carefully without disturbing the intermediate layer containing DNA and the lower phase containing protein.
5. Care was taken to see that the final RNA pellet was completely dissolved in sterile DEPC water.

3.22.2 Assessment of integrity of RNA by Formaldehyde Agarose Gel Electrophoresis

The integrity of the RNA isolated was assessed by electrophoresing an aliquot of the sample in a 1.2% formaldehyde-agarose gel.

Principle

The most common method used to assess the integrity of total RNA is to electrophores an aliquot of the RNA sample obtained on a denaturing agarose gel stained with ethidium bromide (EtBr). RNA has the tendency to form both secondary and tertiary structures that can impede its separation by electrophoresis. Consequently, the electrophoresis of RNA needs to be performed under denaturing conditions. Heat-denaturing the RNA sample prior to electrophoresis is insufficient, as secondary structures will reform unless a denaturing system is used. Formaldehyde and formamide are used as denaturants. The presence of 2 distinct bands, representing the 28s and 18s ribosomal subunits of RNA, in an approximate band density ratio of 2:1 was considered evidence of intact RNA.

Reagents

1. **DEPC-treated water:**

   0.1 ml DEPC was added to 100 ml water. DEPC water was shaken vigorously to get the DEPC into solution completely. This was kept overnight at room temperature. The solution was then autoclaved for 15 minutes to inactivate the DEPC.

2. **10X MOPS Buffer: (100ml)**

   - 0.2M MOPS
   - 10mM EDTA
   - 50mM sodium acetate

   Dissolved MOPS in DEPC-treated water and adjusted pH to 7, using NaOH. Then added sodium acetate and EDTA. The solution was autoclaved.

3. Agarose gel :

- 1.2%

4. RNA sample mix

- RNA (containing up to 20µg) : 8µl
- MOPS (10X) : 2µl
- Formaldehyde (37%): 3.5µl
- Formamide(99.5%): 10µl

5. Sample loading buffer:

- 50% glycerol
- 0.4% bromophenol blue
- 1mM EDTA

6. Running Buffer:

1X MOPS

Procedure:

1. Gel casting:

Step 1: The open sides of the casting tray were sealed using autoclavable adhesive tape. Care was taken to ensure that the sealing was leak-proof..

Step 2: The comb was fitted in the casting tray.

Step 3: 0.48g of agarose was weighed and sprinkled into 32.5ml DEPC-treated water.

Step 4: The above mixture was heated on a hot plate for the agarose to melt and dissolve.

Step 5: The molten agarose was removed and cooled to around 60°C.

Step 6: 4ml of 10X MOPS buffer and 2.150ml of 37% formaldehyde were added to give a final concentration of 1.99% formaldehyde.

Step 7: 2 µl of ethidium bromide was added to the mixture and mixed well.

Note: Ethidium bromide is a carcinogen and was handled with care.

Step 8: The agarose solution was poured and allowed to polymerize into the casting tray.

Step 9: Allowed to set for 30 min.

Step 10: Then the comb was removed carefully

2. Sample loading and electrophoresis:

Step 1: The tank for the electrophoresis was rinsed with DEPC-treated water before use.

Step 2: 1X MOPS buffer was added to the tank.

Step 3: The gel was removed from the casting tray and placed in the buffer tank, with the gel being totally immersed.

Step 4: 2 µl of sample loading buffer was mixed with each sample and mixed well. Each sample was loaded into a well in the gel.

Step 5: The apparatus was connected to the power pack. The samples were run at 150V till the marker dye reaches the end of the gel.

Step 6: The gel was taken out of the buffer and placed on a viewing tray. The bands in the gel were visualized under UV light (in a gel documentation system).

3.22.3 Quantitation Of Isolated RNA

Isolated RNA was quantified by spectrophotometry.

Principle: Nucleic acids strongly absorb ultraviolet light at wavelength of 260nm. An optical density reading of 1.0 at 260nm is taken to indicate an RNA concentration of 40ug/ml.

Procedure: Each RNA sample was quantitated against DEPC water blank using a Nanodrop spectrophotometer. 1 µl of DEPC water was used as a blank and then 1 µl each of the samples was loaded on the pedestal of the spectrophotometer set at a measuring wavelength of 260nm. The pedestal was carefully cleaned with a tissue paper before the succeeding sample was loaded. The

spectrophotometer software automatically calculated the RNA values using the formula mentioned below:

Calculations:

1O.D = 40µg/ml

Concentration of RNA = OD 260 x 40µg/ml x dilution factor

Storage of isolated RNA:

The final solution containing RNA in DEPC water was divided into aliquots and stored at -70^{o} C until further analysis.

3.23 Reverse Transcription And Quantitative Polymerase Chain Reaction (RT-qPCR):

Real time PCR is the technique to quantitate the amount of mRNA present in a sample by collecting data at the end of each cycle throughout the PCR process. Several fluorescent chemistries are employed for this purpose. The intensity of the fluorescence emitted corresponds to the concentration of the PCR product. Fluorescent dyes bind to double-stranded DNA and emits fluorescence (eg. SYBR green I). As the concentration of double-stranded DNA increases at the end of each cycle, more dye can bind and emit fluorescence. Thus, the intensity of fluorescence emitted is proportional to the concentration of the PCR product present. The cycle at which the flurescence intensity exceeds the background levels is called the cycle threshold (Ct) or Crossing point (CP).

RT-qPCR is a combination of 3 steps. First, the conversion of mRNA into cDNA. Second, amplification of the converted cDNA using specific primers. Third, detection and quantitation of the amplified products.

3.23.1 cDNA construction:

Procedure

cDNA was synthesized using the reverse transcriptase care kit purchased from Eurogentec, according to the manufacturer's instructions. For this, 1µg of total RNA was used for reverse transcription to cDNA. The components of a single (10 µl) reverse transcription reaction were as follows:

a) 10X reaction buffer - 1 µl (final concentration -1X)

b) 25 mM Mgcl2 - 2 µl (final concentration -5mM)

c) 2.5mM dNTP -2 µl (final concentration -500µM)

d) Random nonamers -0.5 µl (final concentration -2.5µM)

e) RNase inhibitors - 0.2 µl (0.4U/µl)

f) Reverse transcriptase -0.25µl (1.25U/µl)

g) RNase free water - to make a final volume up to 10µl after addition of the template

h) Template (1µg of total RNA)

A master mix was prepared using all the components of the reaction mixture except RNase free water and the RNA template. Appropriate volumes of the master mix were then added to each PCR tube. The template was added next to each tube. Finally, RNase free water was added to make the final volume of the reaction mixture to 10 µl. Negative control tubes were also used for the reactions. These consisted of a tube which contained all the above reagents except reverse transcriptase and another which had all the reagents except the RNA template. The latter control was to eliminate the possibility of the RNA sample being contaminated with genomic DNA. The tubes were subjected to centrifugation briefly in a microfuge. They were then placed in the real-time thermocycler. (chromo4, Bio-Rad). The reverse transcription reaction was programmed as follows,

Initial step : 10min at 25°C

Reverse Transcription step : 30 min at 48 °C

Inactivation of Reverse transcriptase : 5 min at 95°C

At the end of the run, the sample was stored at -20°C until further analysis.

Precautions taken during cDNA construction

1. All materials used during the process of isolation (such as micro-tubes, water and reagents) were autoclaved prior to use. Commercially available sterile hand gloves were used throughout the procedures.
2. All pipetting procedures were carried out in a clean hood.
3. The components of the reverse transcriptase core kit were opened and added inside a clean hood.
4. The reverse transcriptase enzyme was transferred from -70degree to -20°C prior to the preparation of cDNA construction and was brought to the hood only at the time of requirement of this component.
5. Quantitation of RNA was done on the same day that cDNA construction was done to ensure accuracy.
6. The same amount of total RNA (1 µg) was added into each reaction tube.
7. The maximum number of samples that could be processed in a day was done, to avoid batch-to-batch variation.
8. NRT controls were always included to rule out contamination of the RNA samples with genomic DNA.

3.23.2 Real-Time Polymerase Chain Reaction Assays:

Procedure

The cDNA that was obtained by reverse transcription was subject to amplification by the Polymerase Chain Reaction (PCR). The components for performing a single 20 µl real time PCR reaction were as follows:

1) cDNA template- 2 µl of the reaction mixture obtained at the end of reverse transcription
2) SYBER green Mastermix 2X- 10 µl
3) Gene specific primers - 4 µl
4) Autoclaved ultrapure water -4 µl

The reactions were set up in a 96-well plate format and all samples were analyzed in triplicate to ensure reproducibility.

Step 1: A master mix was prepared using all the components of the reaction mixture, excluding the template.

Step 2: 2 µl of the cDNA was then added to the real-time PCR tubes/plates.

Step 3: 18 µl of the master mix were then added to the PCR tubes.

Step 4: The caps were closed tightly and the tubes were briefly subjected to centrifugation in a microfuge.

The reactions were performed in a real-time thermocycler, programmed using Opticon Monitor software as follows.

1) Incubation at 50°C for 2 min
2) Incubation at 95°C for 10 min
3) Denaturation step at 95°C for 1 min
4) Annealing step was done at the temperature and time optimized for each gene as shown in table-3.3
5) Extension step 72°C for 1 min
6) Readings were taken
7) Step 3 onwards was repeated for 39 more cycles.
8) Melting curve analysis was done from 60 to 95°C, read at every 1°C
9) Samples were then cooled and maintained at 4°C for 10 minutes within the cycler.
10) End

11) The products obtained were stored at -20°C

Gene- specific primers used for the PCR assays for the genes of interest are shown below:

1. Rat Beta Actin (343)

Forward primer - 5'-GGACTTCGAGCAGGAGA-TGG-3'

Reverse primer - 5'-GCACCGTGTTGGCGTAGAGG-3'

2. Rat GAPDH (344)

Forward primer - 5'-ACCACAGTCCATGCCATCAC-3'

Reverse primer - 5'-TCCACCACCCTGTTGCTGTA-3'

3. Rat iNOS (345)

Forward primer - 5' GACCAAACTGTGTGCCTGGA 3'

Reverse primer - 5' TACTCTGAGGGCTGACACAAGG 3'

4. Rat TNF alpha α (346)

Forward primer - 5' TAC TGA ACT TCG GGG TGA TTG GTC C 3'

Reverse primer - 5' CAG CCT TGT CCC TTG AAG AGA ACC 3'

5. Rat COX-2 (343)

Forward primer 5 '-ATGACTTCCCTGGGTTTGGT-3'

Reverse primer 5'-GTCCCCCATTGTGGTATCTG-3'

6. Rat NF-κB (Gene ID 309165)

Forward primer 5 '- TGTCCATGCAGCTTCGGCGG-3'

Reverse primer 5'-GGCCGGGGTTCAGTTGGTCC-3'

7. Rat IκB (345)

Forward primer 5’- CAGCGTCTGAAGATTTTCCA-3’

Reverse primer 5’- AGTAACCTACCAGGGCTACTCC-3’

8. Rat HO-1 (347)

Forward primer 5′-AGAGTCCCTCACAGACAGAGTTT-3′

Reverse primer 5′-CCTGCAGAGAGAAGGCTACATGA-3′

9. Rat Hsp70 (348)

Forward primer 5´-CCGCCTACTTCAACGACTC-3´

Reverse primer 5´-TCTTGAACTCCTCCACGAAG-3´

10. Caspase-3 (349)

Forward primer 5´-AATTCAAGGGACGGGTCATG-3´

Reverse primer 5´-GCTTGTGCGCGTACAGTTTC-3´

11. Rat MMP-9 (350)

Forward primer 5’-TCGAAGGCGACCTCAAGTG-3’

Reverse primer 5’-TTCGGTGTAGCTTTGGATCCA-3’

The annealing and extension temperatures and times for each gene of interest and the concentrations of primers used were optimized for all the five genes studied (Table-2). The optimal salt (MgCl2) concentration for each reaction was determined to be 5 mmol/L.

Validations of the reaction conditions were done using a standard curve, generated with serial dilutions of the cDNA template for each gene. (Figure-3.20.2)

Table 3.3 Annealing temperature and time, extension temperature and time and the concentration of forward and reverse primers for each gene.

GENE PRIMER	ANNEALING TEMP. AND TIME	EXTENSION TEMP. AND TIME	CONC. OF FORWARD(FP) AND REVERSE (RP)
Beta-actin	60 °C X 1min	72 °C X 40secs	FP= 0.2 µmol/L RP=0.2 µmol/L
GAPDH	60 °C X 1 min	72 °C X 40secs	FP= 0.2 µmol/L RP=0.2 µmol/L
iNOS	60 °C X 20 secs	72 °C X 40secs	FP=100 nm/L RP=100 nm/L
TNF-α	51 °C X 20 secs	72 °C X 40secs	FP=100 nm/L RP=100 nm/L
COX2	59.5 °C X 20 secs	72 °C X 40secs	FP=100 nm/L RP=100 nm /L
NF-κB	65 °C X 20 secs	72 °C X 40secs	FP=100 nm/L RP=100 nm/L
IκBα	60 °C X 1min	72 °C X 40secs	FP= 0.2 µmol/L RP=0.2 µmol/L
HO-1	60 °C X 20secs	72 °C X 40secs	FP= 0.2 µmol/L RP=0.2 µmol/L
HSP 70	60 °C X 1min	72 °C X 40secs	FP= 0.2 µmol/L RP=0.2 µmol/L
Caspase-3	60 °C X 1min	72 °C X 40secs	FP= 0.2 µmol/L RP=0. 2µmol/L
MMP9	60 °C X 1min	72 °C X 40secs	FP= 0.2 µmol/L RP=0.2 µmol/L

3.23.3 Construction of a standard curve

Serial dilutions of cDNA were used to construct a standard curve for a PCR assay. This is done as depicted in the figure below.

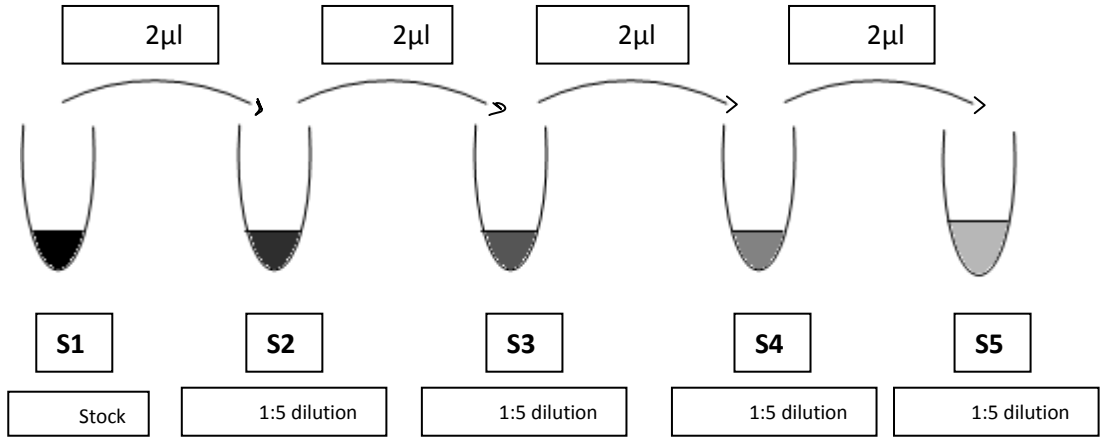

3.23.4 Analysis of data obtained from the PCR assays

Background fluorescence was normalized by setting the baseline at zero. The outcome parameter generated at the end of the PCR was the cycle threshold value. The term Ct or cycle threshold is defined as the PCR cycle at which the fluorescent signal of the reporter dye crosses an arbitrarily placed threshold (312). The threshold was determined by examining the amplification plot on a log-linear scale. The point where the cycles are parallel for all samples was considered to be an appropriate setting point for the threshold.

The efficiency of the PCR for each gene was determined by the following equation:

$$m = -(1/\log E)$$

where m is the slope of the standard curve and E is the efficiency.

3.23.5 Expression levels of genes of interest

Expression levels of the genes of interest were expressed relative to those of an internal reference gene. This is a procedure that is done commonly in qRT-PCR for controlling for errors by using an internal reference. The internal reference gene is presumed not to change under the experimental conditions used in the system and hence can control for errors while performing qPCR and hence minimizes variability between samples.

Data for each gene of interest was normalized relative to beta-actin. This was done by substracting the Ct values of beta-actin in each sample from that of the gene of interest eg. TNF α or NF-κB 65. The value obtained was referred to as the ΔCt value. The relative fold-change in the gene of interest was determined according to the comparative Ct method using the following formula: Relative fold change = $2^{\wedge -(\Delta Ct)}$ (351)

Precautions taken during real-time PCR assays

1. DNase/RNase-free consumables were used.
2. A dedicated set of micropipettes were used for all qPCR reactions.
3. cDNA templates were diluted, if required, so that between 3µl and 10 µl are added to each qPCR reaction. This reduces inaccuracies due to pipetting very low volumes.
4. All reaction components were stored in aliquots. If amplification was found to occur in the "no template control (NTC)" tube, it was assumed that contamination with DNA had occurred. Fresh aliquots were used.
5. An NTC tube was included in every batch of assays to detect any potential contamination or reagents.
6. All reagents were thawed on ice and mixed well prior to making up reaction mixes.

7. Care was taken to avoid exposing fluorescent probes and fluorescent nucleic acid binding dyes to light.
8. When preparing master mixes, care was taken to ensure that all samples and controls were accounted for. The quantity of master mix prepared each time was that for n+1 samples, where n was the number of samples that were to be assayed. This ensured that there was an adequate amount of master mix for all the reaction tubes in each batch.
9. The reaction tubes/plates were centrifuged briefly to remove any air bubbles in the mixture.

Results, Analysis and Discussion

STUDY- I

Standardization of Rat model of TDF induced renal damage

Abstract

Tenofovir is the drug of choice for HIV infected patients as it has several advantages such as efficacy, convenience, low resistance and tolerability over other anti-retrovirals. However, recent studies show that renal tubular dysfunction develops in nearly 15% of patients treated with tenofovir for 2-9 years. As the main target of TDF toxicity is the proximal tubule, patients can develop Fanconi syndrome , which may persist even after discontinuation of the drug. Several human and animal studies have shown damage to specifically renal proximal tubular mitochondria However, the mechanism of toxicity of tenofovir is not known. A reliable animal model is therefore necessary to elucidate the mechanism of tenofovir nephrotoxicity and also to carry out intervention studies.

In order to establish a rat model of tenofovir nephrotoxicity, different oral doses of tenofovir were administered to adult rats for 5 weeks. Based on our studies, the optimal dose required to produce nephrotoxicity that resembled human renal biopsies is 600 mg/kg body wt. At this dose the tenofovir- treated rat kidneys showed structural and functional alterations in the proximal tubule that closely resembled renal biopsies taken from HIV patients on long term tenofovir therapy. Thus, this rat model is a good model for the study of tenofovir nephrotoxicity.

The model will be useful not only for the study of the mechanism of nephrotoxicity of tenofovir but also for carrying out intervention studies. This model will also permit to study drug interactions by overcoming the limitations of cell culture and the difficulties of obtaining human kidney samples. It may also be employed to develop markers for the early diagnosis of the mitochondrial tubulopathy.

Introduction

Tenofovir disoproxil fumarate (TDF) is an oral prodrug of tenofovir, a reverse transcriptase inhibitor of human immunodeficiency virus type 1 (HIV-1) (1). It is currently the only NRTI approved by the US Food and Drug administration (FDA) for the treatment of HIV infection (5). In HIV-infected patients, treatment with TDF has been associated with excellent virological suppression and favorable clinical outcomes (13,352). Recently, however, renal dysfunction has been reported in patients with human immunodeficiency virus (HIV) infection treated with tenofovir for several years (2-9 years)(53). Numerous case reports and case series have described severe cases of renal tubular toxicity associated with TDF exposure. Several case reports, observational studies, and animal models, support the idea that tenofovir is a proximal tubular toxin (16,55,57,58,66) .As the main place of TDF toxicity is the proximal tubule, patients can develop Fanconi syndrome (characterized by phosphaturia, glycosuria, bicarbonate wasting, tubular proteinuria, and aminoaciduria) (54,353), which may persist even after discontinuation of the drug (63,354). It has been suggested that TDF causes direct proximal tubular damage, which may lead to renal failure. Proximal tubular cells are particularly sensitive to the toxic effects of tenofovir due to their unique set of cell membrane transporters that favor entry of the drug (10).

Current evidence suggests that mitochondria are the target organelles of tenofovir cytotoxicity (14,15,304,305). Morphological evidence of mitochondrial toxicity was found in human biopsies of tenofovir nephrotoxicity (14,15). In the TDF treated HIV patients who underwent kidney biopsy, the main abnormality on light microscopy was acute proximal tubule damage, and eosinophilic intracytoplasmic inclusions formed of giant mitochondria. Electron microscopy showed widespread morphologic abnormalities in proximal tubule mitochondria, with marked variations in size and shape and disruption of cristae, mitochondrial swelling, and intramitochondrial paracrystals (14,15).

Although it is well established that proximal tubular mitochondria are targets of tenofovir cytotoxicity, the extent to which mitochondrial damage contributes to proximal tubular damage and the mechanisms of such an effect remain unclear. In order to investigate the mechanism of TDF nephrotoxicity a reliable animal model is necessary. To date no standard animal model is available for the study of mechanism of TDF nephrotoxicity. In the present study we describe a reliable and reproducible model of TDF nephrotoxicity using rats. This model can be useful to investigate the mechanism of TDF nephrotoxicity as well as to carry out intervention studies.

Brief Experimental setup:

Adult male Wistar rats weighing 200-250 g were used for the studies. Rats were treated with different doses of TDF for 5 weeks (35 days), and the kidneys were removed and used for light microscopic and electron microscopic examination. On the basis of a number of NRTI treatment protocols used by other workers treatment duration of 35 days was used in these initial studies as the duration of TDF treatment for 35 days is suggested to model chronic human treatment (355).

Histological Examination

Kidney samples were processed routinely. Sections (4 μm) were stained with hematoxylin and eosin (H& E) and examined microscopically in a blinded fashion. Photomicrographs of glass slides were obtained using a Leica photomicroscope.

Fine Structure of Kidney Tissues Using Electron Microscopy (EM)

Sections (0.5 μm) were cut with glass knives and stained with Toluidine Blue for orientation. Ultrathin (900 Å) sections were cut with a diamond knife, stained with uranyl acetate and lead citrate and examined by EM, evaluated and photographed. Each EM photomicrograph was reviewed independently by two investigators. Parameters included the presence of structurally

abnormal mitochondria, increased numbers of mitochondrial profiles per field, intra-mitochondrial lamellar bodies, abnormal cristae density, mitochondrial swelling, disrupted cristae and intra-mitochondrial paracrystals (356).

Pilot study 1

The daily oral dose of tenofovir disoproxil fumarate (TDF) in humans is 300 mg/60 kg. Therefore to remain clinically relevant, we administered TDF daily by gavage (morning) at doses that resembled human therapy on a mg/kg/day basis i.e. 5mg/kg; ~250 g rat =1.25 mg/day). Control rats were given sterile water alone for 35days. The rats were sacrificed 24 hrs. after the final dose of TDF.

Histological Analysis of Kidney Tissues

Glomeruli and tubules appeared to be intact in both TDF-treated rats and in vehicle-treated rats (figure not shown)

Electron microscopic features of tubular epithelium in rats treated with Tenofovir

Vehicle-treated rats showed normal renal proximal tubular epithelial cells with characteristic, oval mitochondria having densely packed cristae. Renal tubule electron microscopic profiles from TDF treated rats also appeared normal (figure not shown).

Pilot study 2

Rats were treated orally once a day for 5weeks with 100mg/kg/d of tenofovir DF dissolved in water as described by Lebrecht et al., (304) Based on body surface, an equivalent dose of oral tenofovir DF in a 60-kg human would be 16.2 mg/ kg/d (357). Based on area under the curve exposure, the tenofovir DF dose used in the present model was about twice the clinical dose used in patients

(358). Control animals were treated with water on the same schedule as the drug treatment .At this dose also we could not observe any histological changes between TDF treated and control rat kidneys when examined under light microscope (Figure:4.1) and electron microscope (Figure: 4.2)

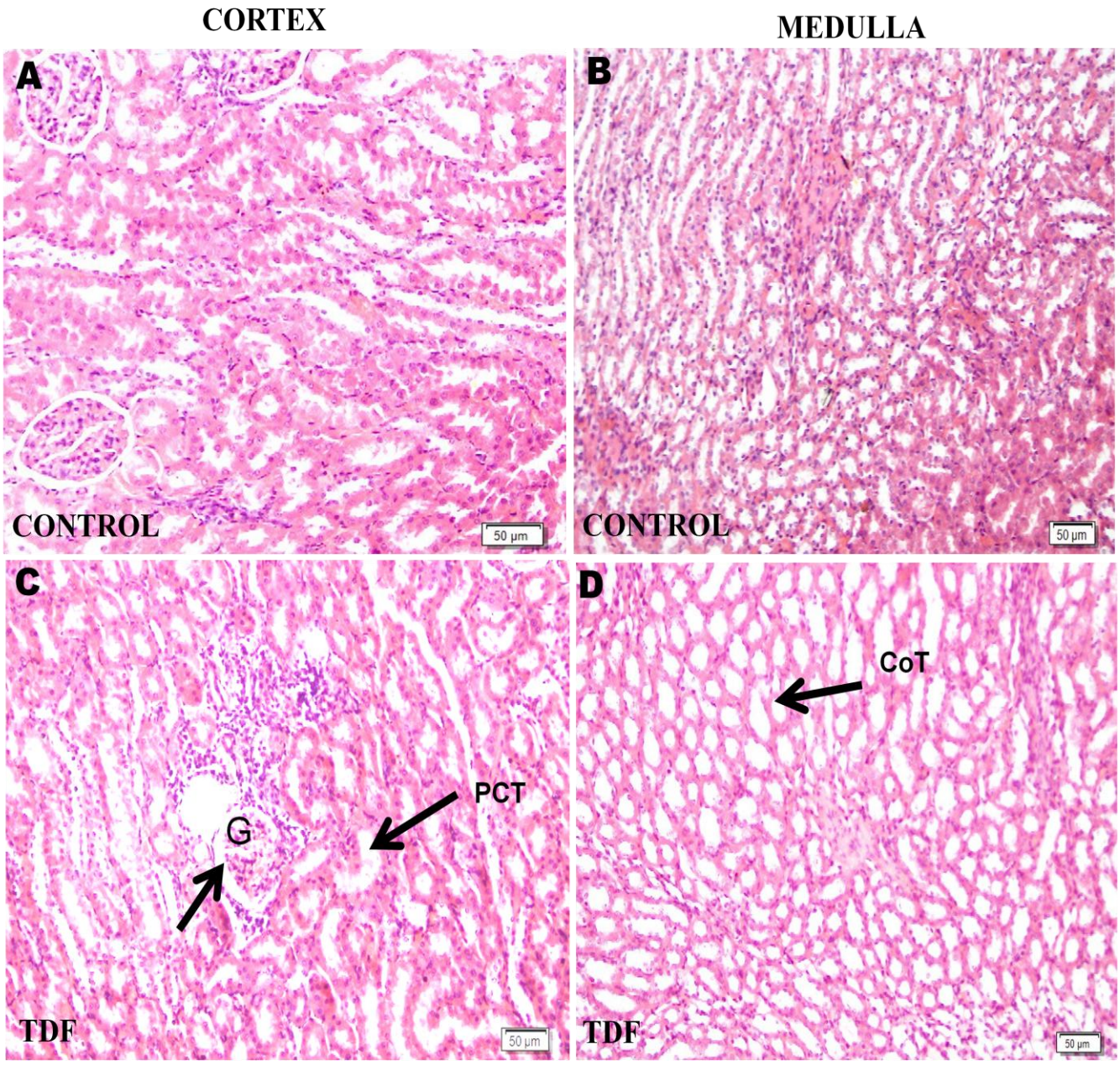

Fig.4.1 Representative light microphotographs of (A) renal cortex of a control rat showing normal architecture [H& E X 200] (B) Renal medulla of a control rat showing normal architecture [H & E X 200] (C) Renal cortex of a 100 mg/kg/d TDF treated rat showing almost normal structure (black arrow), (H &E, X 200). (D) Renal medulla of a 100 mg kg/d TDF treated rat showing normal architecture (H & E, X 200).

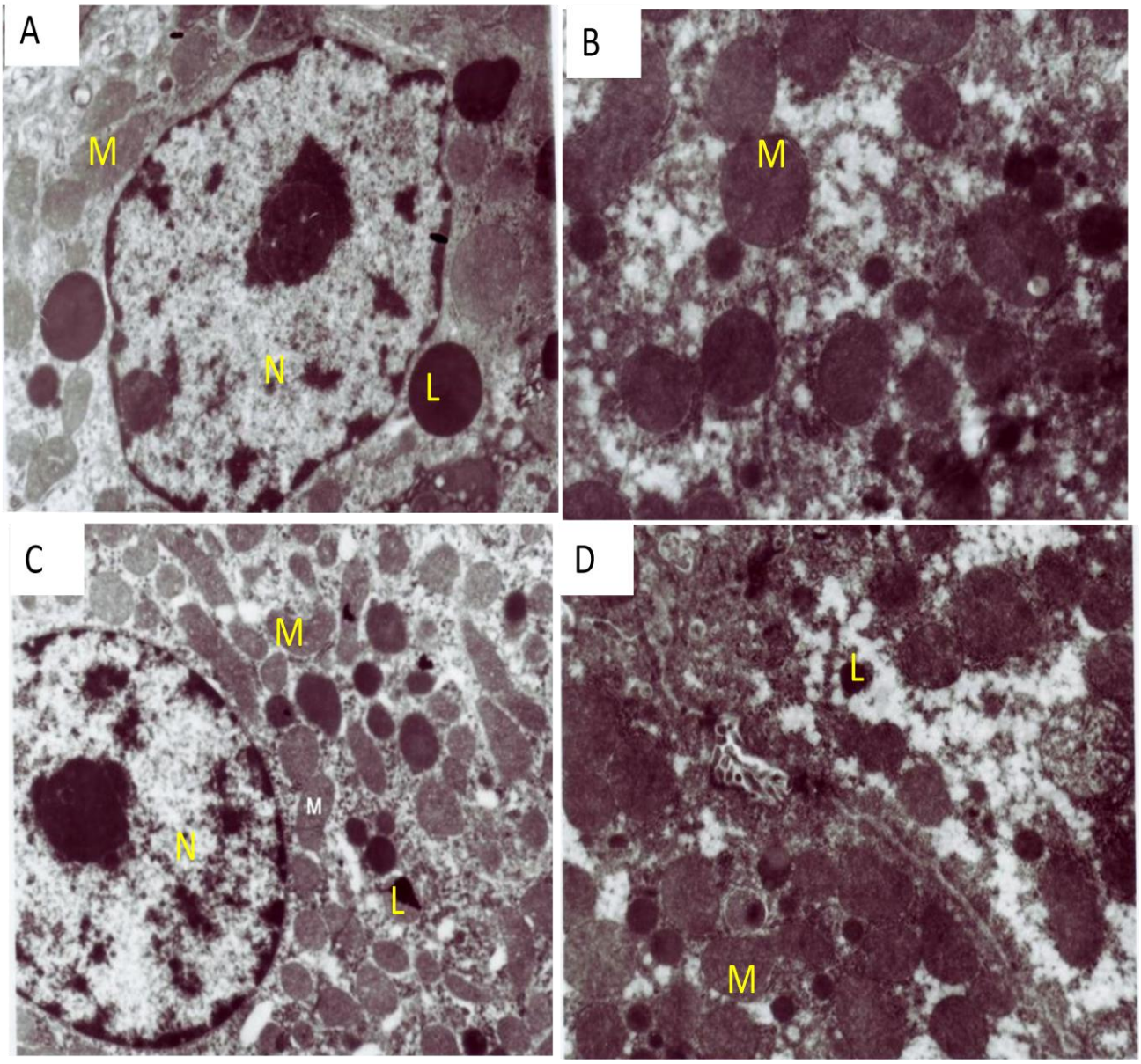

Fig. 4.2. Representative electron micrographs of (A) control kidney tubule (original magnification × 15000). (B) Control proximal tubular mitochondria (original magnification × 22000). (C) 100 mg/kg body wt. TDF treated kidney tubule showing normal morphology (original magnification × 15000). (D) 100 mg/kg body wt. TDF treated kidney proximal tubular mitochondria showing normal morphology (x 15000).M-mitochondria, L- lysosome, and N-nucleus.

Pilot study 3

Rats were administered by gavage once daily 300 mg/kg TDF for 35 days. This dose corresponds to 5–6 times the human dose, based on blood levels (AUC). Despite this high dose, no appreciable tubular damage was detectable by light microscopy, except for tubular dilation (Figure: 4.3). Electron microscopy revealed the presence of swollen mitochondria (Figure: 4.4). However proximal tubular dysfunction was not observed biochemically i.e., Fanconi Syndrome was not observed (data not shown).

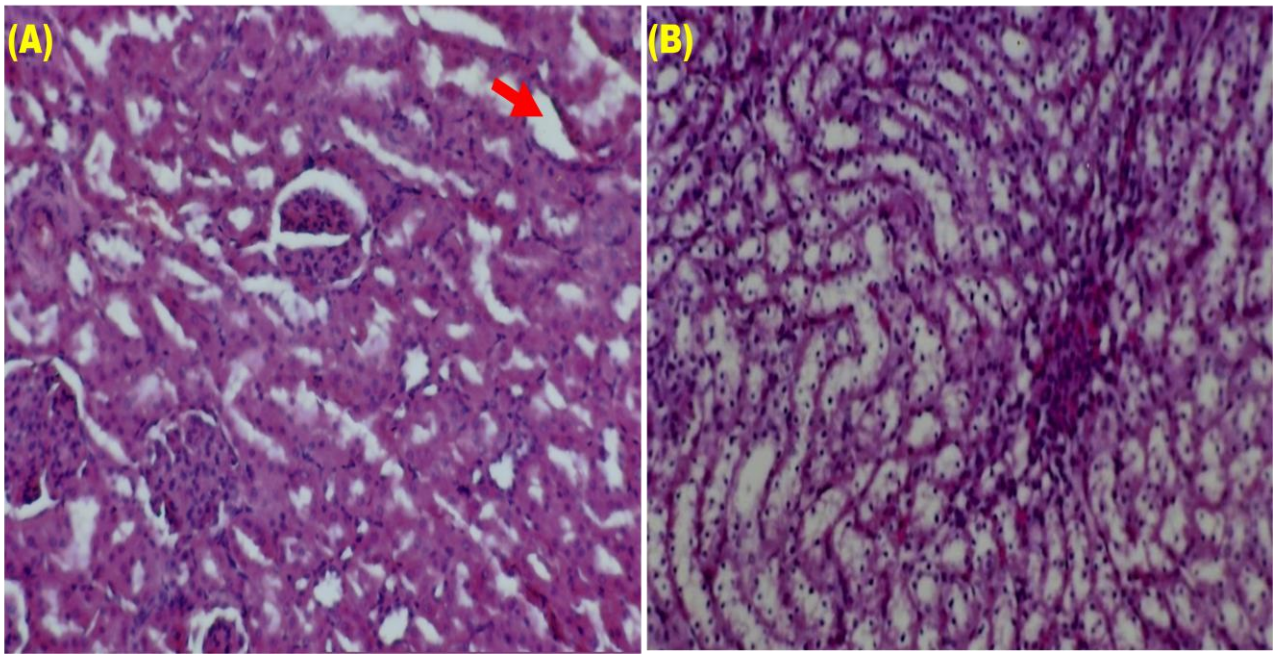

Fig.4.3. Representative light microscopic photographs of 300 mg kg body wt. TDF treated rat (H &E, X 200]. (A) Cortex showing mild dilatation of the tubules (Red arrow). (B) Medulla showing normal architecture.

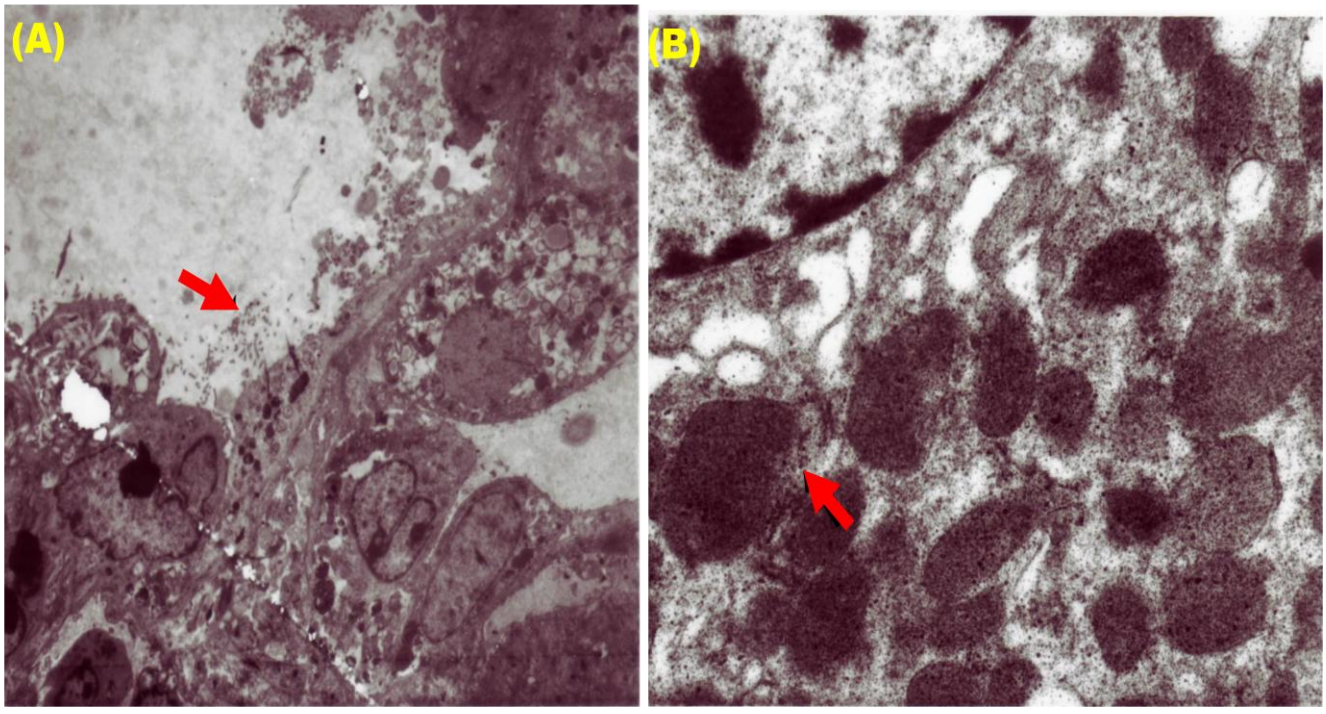

Fig. 4.4. Representative electron micrographs of 300 mg kg body wt. TDF treated rat (A) kidney tubule original magnification × 22000, showing the destruction of proximal tubular microvilli (arrow). (B) Proximal tubular mitochondria (x 15000), showing swelling.

Pilot study 4

Tenofovir has been shown to cause bone toxicity in animal models when given at 6–12 times higher dose than recommended for humans (64). This corresponds to 600 mg/kg/day.

The morphological changes seen in this model were similar to that seen in human renal biopsies taken from HIV patients on long term TDF therapy. In addition Fanconi syndrome, characteristic of proximal tubular dysfunction was also observed. Therefore, the dose was fixed at 600 mg/kg/d and the duration of treatment as 35 days.

Standardised protocol

Adult male Wistar rats weighing 200-250g were used for the study. The rats were housed in individual cages and treated as follows.

Group I (control) -The rats in this group (n = 6) received sterile water.

Group II- The rats (n = 6) in this group received 600 mg/ kg body weight TDF divided into 2 doses (one in the morning and another in the evening) by gavage for 5 weeks (35 days).

All the rats survived the treatment period. They were sacrificed 24 hours after the final dose of TDF /sterile water, after withdrawal of blood under light halothane anesthesia. The kidneys were removed and used for histological examination. Urine and serum samples were collected for clinical chemistry. The kidneys were processed and examined under a light microscope and electron microscope as described previously. Urine samples were centrifuged in aliquots to remove s uspended material, and the supernatants were analyzed. Serum was used for the estimation of phosphate, potassium, uric acid, glucose, urea and creatinine. Urine was used for the estimation of bicarbonate, phosphate, potassium, and uric acid .Glucose and protein were semi quantified by dipstick. Proteins in urine were detected by SDS PAGE as described in methodology 3.17.

Statistical analysis:

Statistical analysis of data obtained was carried out using the Statistics Package for the Social Sciences (SPSS) software package, version 16. Data represents mean ± SD, the difference between two groups were analyzed by the Mann-Whitney test. A p-value of less than 0.05 was taken as statistically significant.

RESULTS

1. Effect of TDF on body weight, kidney weight and gross appearance of the kidneys:

The body weight and kidney weight were decreased by 5% and 9% respectively in the TDF- treated rats as compared with control (Figure: 4.5) and (Figure: 4.6) respectively. The gross appearance of kidney of TDF groups showed pale appearance as compared with controls (Figure: 4.7).

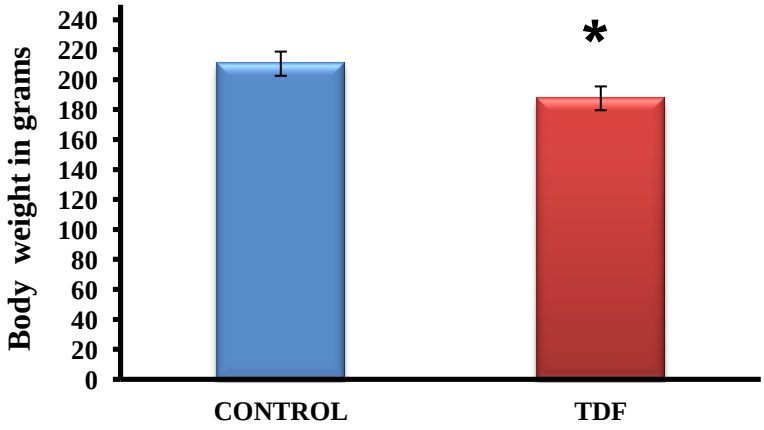

Figure: 4.5 Effect of TDF on changes in body weight in control and test rats N=6 in each group. Data shown are mean ±SD in each group. * p value < 0.05 as compared with controls.

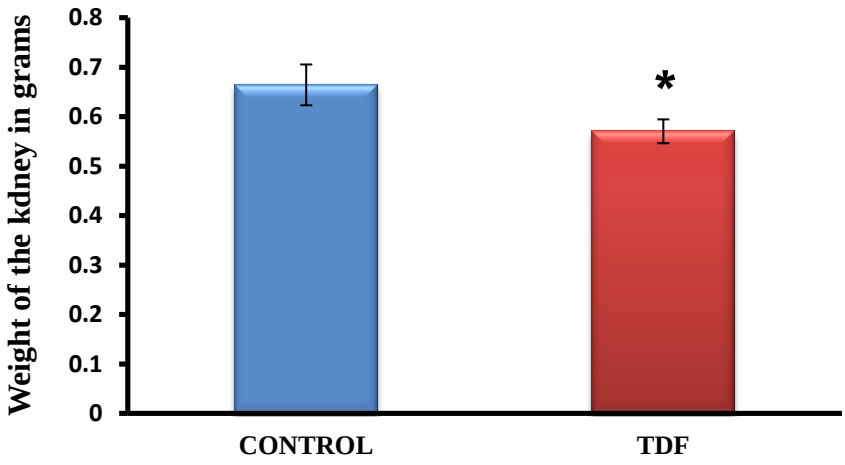

Figure: 4.6 Effect of TDF on changes in kidney weight in control and TDF treated rats. N=6 in each group. Data shown are mean ±SD in each group. *p value < 0.05 as compared with controls.

(A) **(B)**

Figure: 4.7 (A) Gross appearance of normal kidney of control rat (B) Pale appearance of rat kidney treated with TDF.

1. **Effect of TDF on the histology of the rat kidney**

The kidneys of control rats showed normal morphology. In the cortex normal glomerular and tubular components were seen and in the medulla normal renal tubular elements were seen. TDF induced renal damage involved mainly the renal tubules. Severe necrosis of cortex involving tubules were observed .The proximal convoluted tubules were distorted and their lining epithelium was destroyed. Some glomeruli were shrunken. In the medulla there was destruction of the lining epithelium of the loops of Henle and the collecting duct. Edema of tubules, diffuse epithelial cell shrinkage, epithelial desquamation and mild necrotic changes were also observed (Figure: 4.8 A-B) and (Figure: 4.8 C-D) respectively.

Histological scoring of light microscopy in the kidney of control and TDF rat is tabulated in Table:4.1

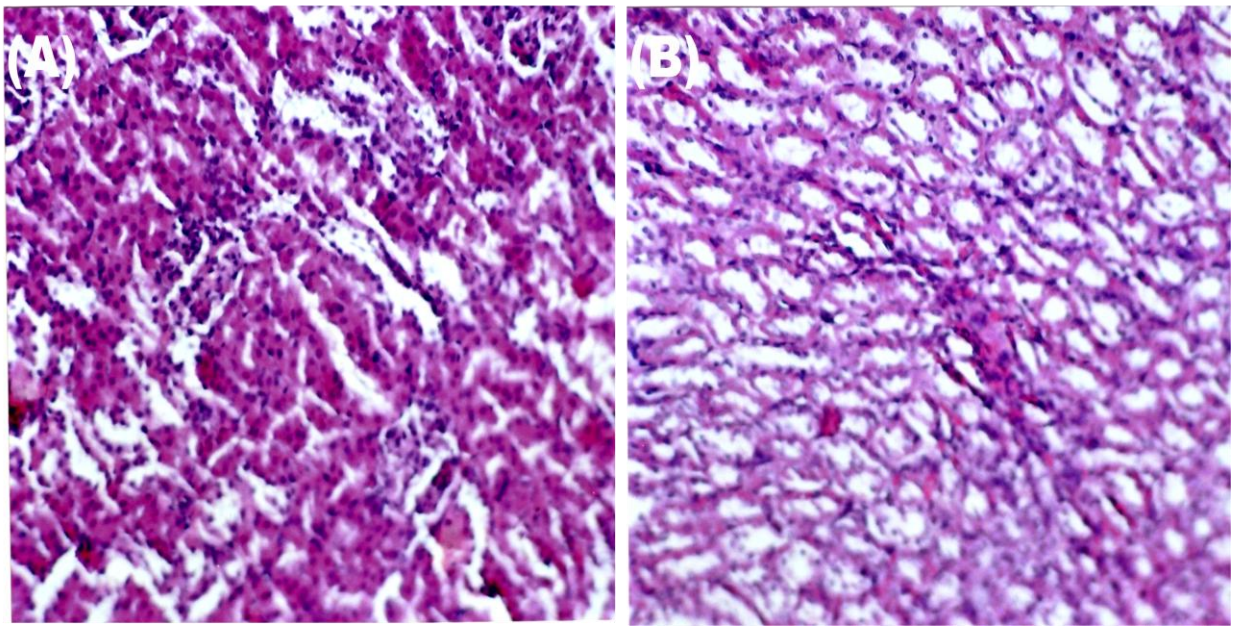

Figure: 4.8 (A)&(B) Representative light micrographs of the kidney of control rat (A), cortex and (B) medulla, showing normal architecture, (H &E) magnification X100. (n = 3).

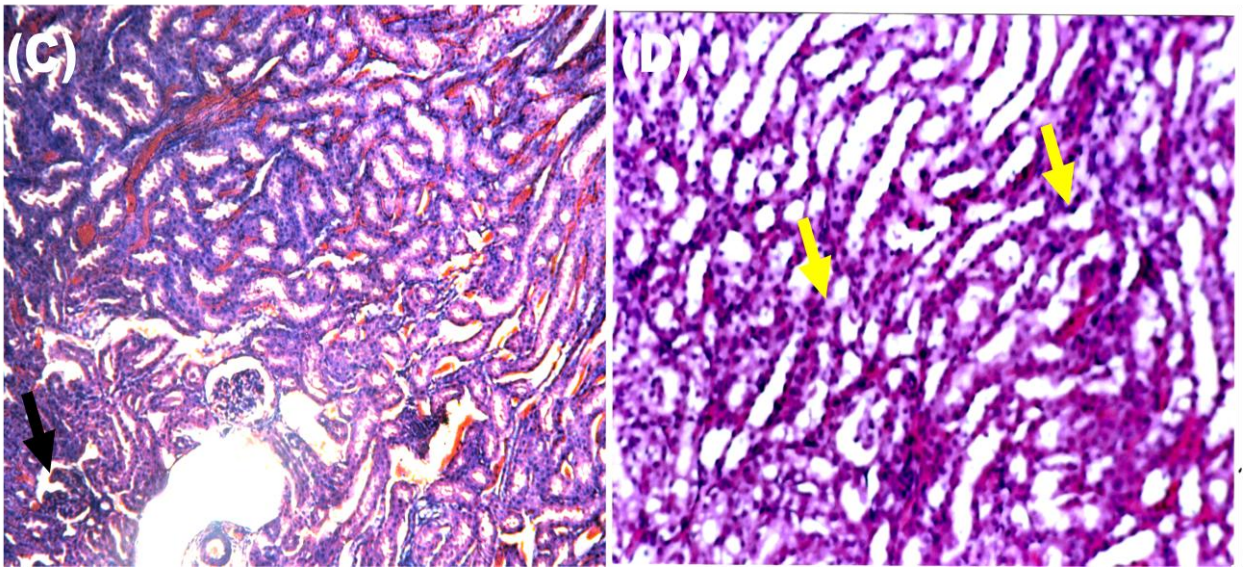

Figure: 4.8 (C) & (D). Representative light micrographs of the kidney of the TDF (600 mg/kg body weight) treated rat kidney (C) cortex and (D) medulla showing distortion and degeneration of the tubular epithelium, distorted shape of the glomeruli and some shrunken glomeruli (black arrow).There is distortion of Henle and the collecting tubules (yellow arrow) in medulla, (H& E) magnification X100

Table: 4.1 HISTOLOGICAL CHANGES IN THE CORTEX AND MEDULLA KIDNEY OF RATS TREATED WITH TDF FOR 35 DAYS (359)

S.NO	MORPHOLOGY (35 DAYS)	CONTROL CORTEX	CONTROL MEDULLA	TDF CORTEX	TDF MEDULLA
1.	Degeneration of Tubular Epithelium	-	-	+++	+++
2.	Distortion of Brush Border	-	-	+++	-
3.	Tubular Dilatation	-	-	++	++
4.	Tubular Cell Swelling	-	-	++	-
5.	Distortion of Basement Membrane	-	-	++	-
6.	Cytoplasmic Vacuoles	-	-	-	+++
7.	Interstitial Inflammation	-	-	+	+

- **indicates no changes in the morphology**
+ **indicates mild changes**
++ **indicates moderate changes**
+++ **indicates severe damage**

2. Ultra structural changes in the rat kidney after TDF treatment

Proximal tubular epithelia of water-treated rats had characteristic, oval mitochondria with densely packed cristae. Proximal tubular epithelia of TDF-treated rats showed moderate to severe mitochondrial damage. The mitochondria showed marked variations in size and shape. Many were swollen (giant mitochondria), cristae were disrupted, and amorphous deposits were observed in the matrix. In some epithelial cells, the mitochondria were reduced in number. An increase in mitochondria with irregular shape was observed in the cytoplasm of basal part of tubule cell. Numerous vacuoles were seen in the cytoplasm of the kidney tubule and lysosomes were reduced in number. Nucleus appeared shrunken. Figure: 4.9.1 A-D (Control), Figure:4.9.2 A-H (TDF treated rats).

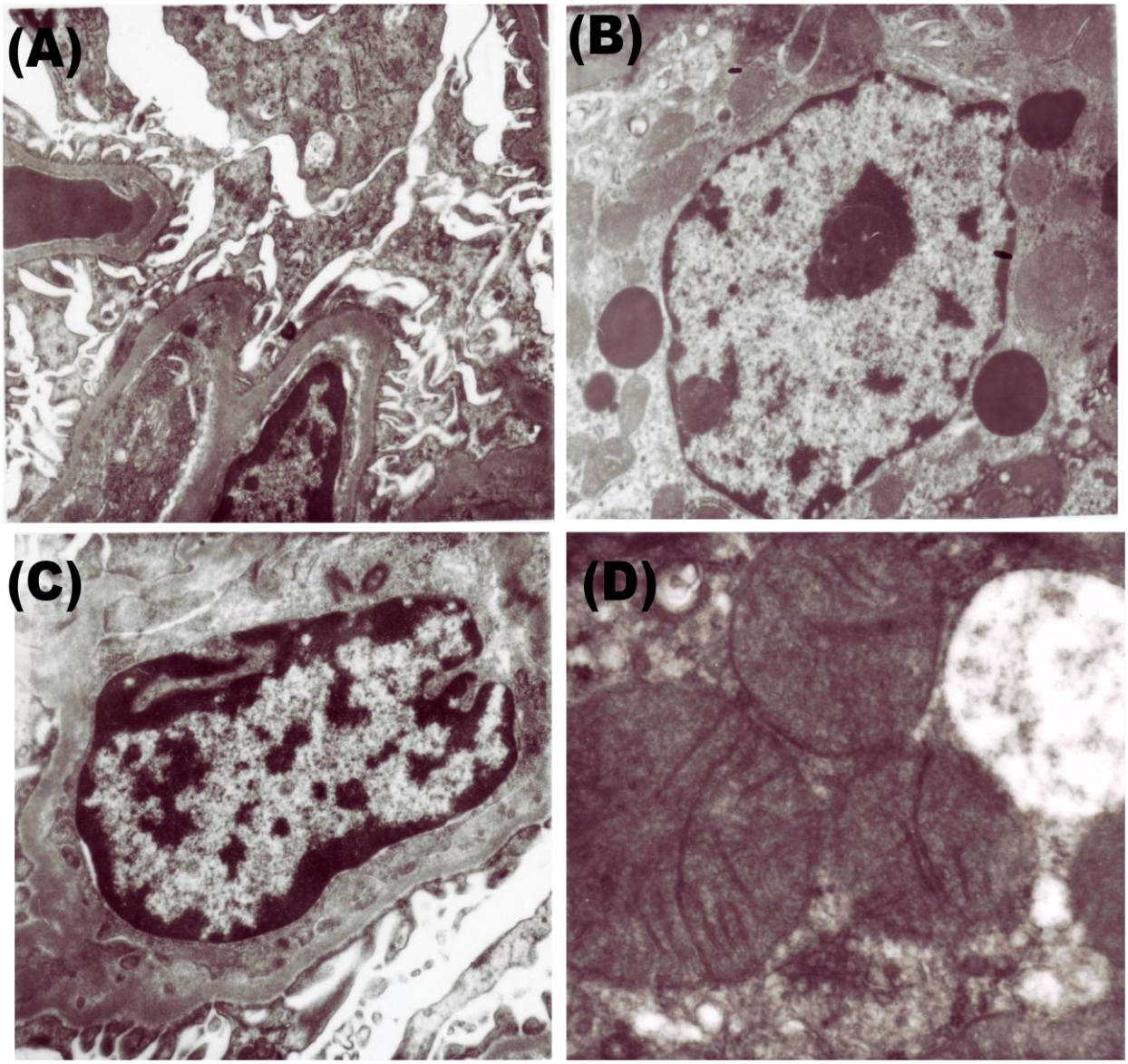

Figure: 4.9.1 (A)-(D)

(A) Normal kidney glomerulus (B) Normal Kidney tubules (original magnification × 22000) (C) Normal renal mesengial cells (D) Normal mitochondrial structure in the renal tubules of control rats (original magnification × 22000)

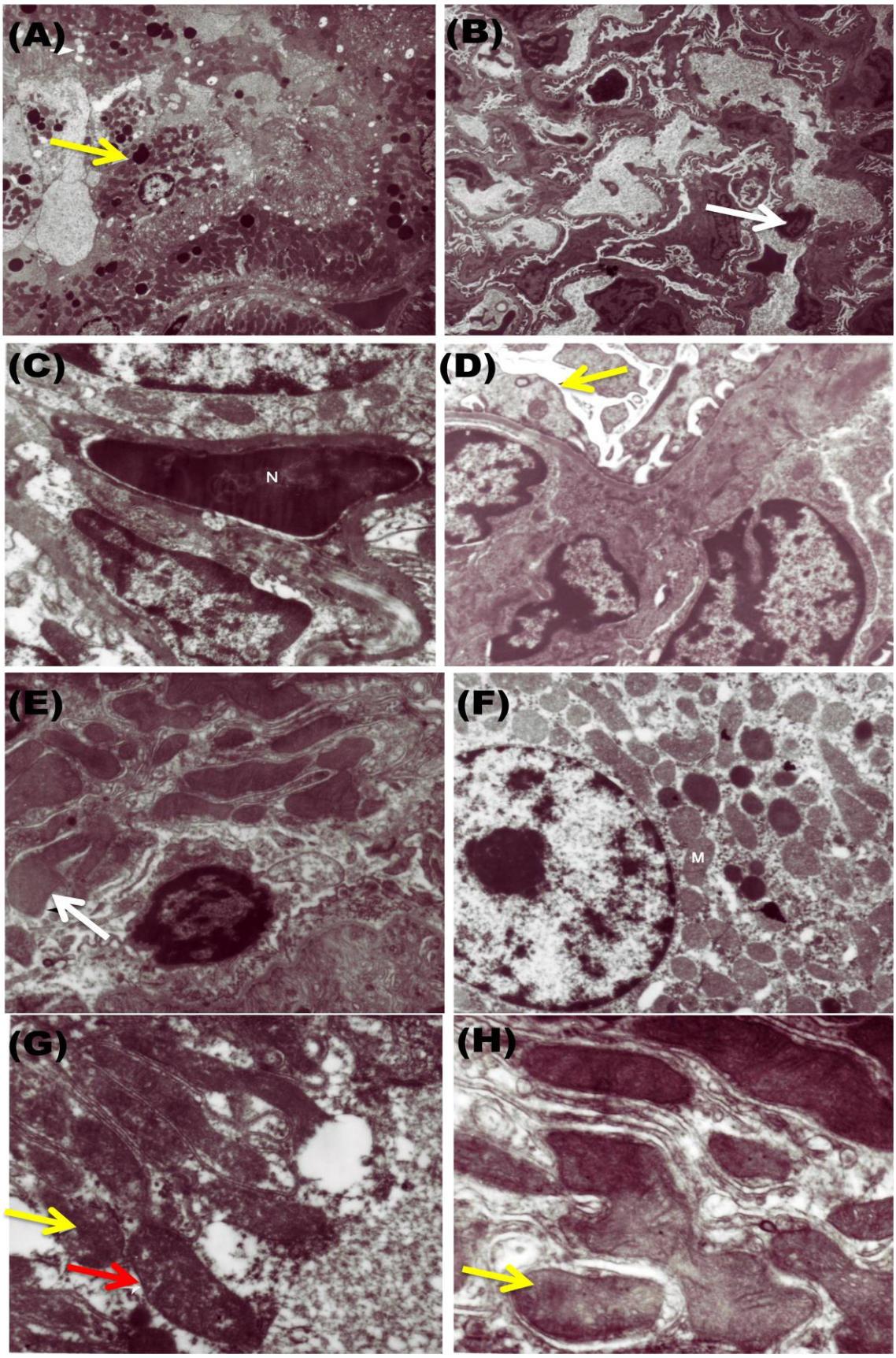

(Please see next page for legends for the figures)

Figure: 4.9.2 (A) Vacuoles seen in the cytoplasm of the kidney tubule (yellow arrow) Less number of lysosomes (white arrowhead) (B) Nucleus shrunken. Chromatin deposits are less in the nucleus of the endothelial cell (white arrow) (C) Nucleus of mesangial cell (N) distorted (D) Yellow Arrow indicates the fusion of foot processes (E) Mitochondria swollen (white arrow). Cristae disrupted. (F) Increased number of mitochondria (M) in basal part of tubule cytoplasm (G) Mitochondria swelling (red arrow), disruption of mitochondrial cristae . Amorphous deposits in the matrix of mitochondria (yellow arrow) in the renal tubules of TDF treated rats (H) Mitochondria swollen (original magnification × 22000).

Effect of TDF on proximal tubular functions

1. Serum and urine levels of electrolytes

Proximal tubular function was impaired in TDF-treated rats, as evidenced by increased urinary phosphate, potassium and bicarbonate excretion and a considerable reduction in serum phosphate and potassium **(Table: 4.2).**

Table:4.2 Serum and Urine levels of potassium, phosphate, bicarbonate, uric acid and glucose in the TDF treated rats compared with control rats.

Parameter	Control (n = 6)	TDF treated (n = 6)
Serum		
Phosphate (mmol/L)	5.88 ± 0.78	4.10 ± 0.36*
Potassium (mmol/L)	6.31 ± 0.47	5.58 ± 0.51*
Uric Acid (mg%)	1.53 ± 0.35	2.9 ± 1.3*
Glucose (mg%)	94.33 ± 12.6	90.8 ± 15.4
Urine		
Bicarbonate (mmol/L)	0.25 ± 0.058	2.56 ± 1.21**
Uric acid (mg/100 mL)	5.1 ± 1.69	12.9 ± 5.0 **
Potassium (mmol/L)	2.68 ± 1.3	10.38 ± 2.9**
Phosphate (mmol/L)	0.27 ± 0.1	4.68 ± 1.52*

Values are represented as Mean ± S.D., number of rats (n = 6) in Control and TDF.

*** denotes p < 0.05, ** P < 0.01 vs. control.**

2. Tubular proteinuria

Tubular proteinuria is characterized by the dominant excretion of low-molecular-weight proteins such as alpha 1-microglobulin or retinol-binding protein (RBP), which correlate better with the extent of tubulo-interstitial damage than does determination of total 24-h protein concentrations. The urinary protein pattern revealed two protein bands in the alpha 2 region (alpha 2 microglobulin, retinol binding protein), and one band in the beta 2 region (beta 2 microglobulin) (Figure: 4.10), suggesting proximal tubular injury.

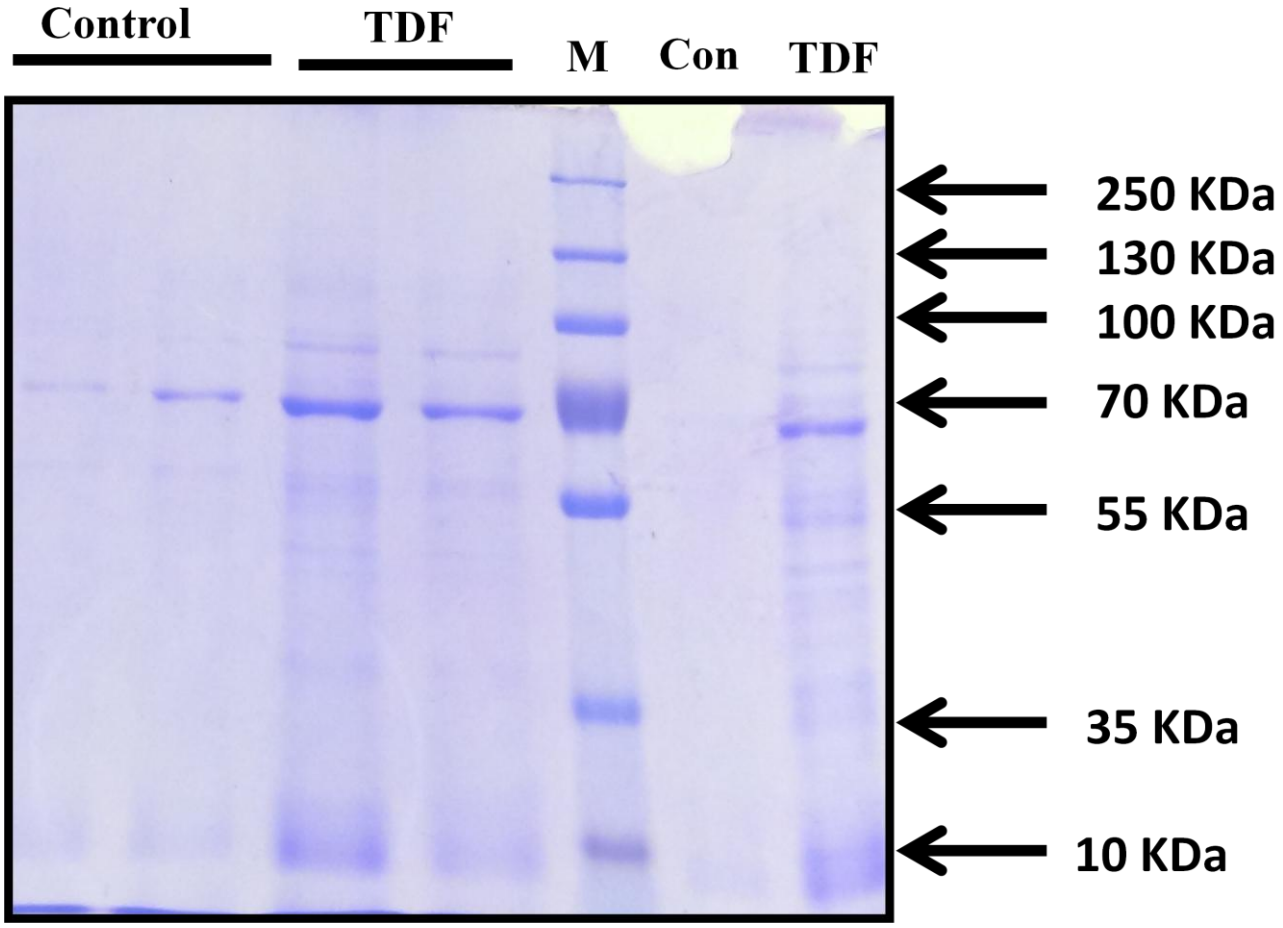

Figure: 4.10 SDS-PAGE analyses of urinary proteins showing multiple bands of low molecular weight proteins 50–70 kDa in the TDF treated rats as compared with control group, and additional faint bands with MW of over 70 kDa, suggesting a complete tubular proteinuria with progressive disruption of filtration barrier.

DISCUSSION:

For treatment -naıve patients, as well as for treatment experienced patients, TDF has become a favored nucleoside component of antiretroviral regimens. However, TDF has serious side effects, especially with long-term use. Numerous case reports and case series have described severe cases of renal tubular toxicity associated with TDF exposure (16,53,55,58). The main site of toxicity seems to be the proximal tubule, and in more severe cases, patients can develop Fanconi syndrome (which is characterized by tubular proteinuria, aminoaciduria, phosphaturia, glycosuria, and bicarbonate wasting (54,353) or acute kidney injury (354).

It is well established that proximal tubular mitochondria are targets of tenofovir cytotoxicity. However, the extent to which mitochondrial damage is responsible for proximal tubular cell loss and the mechanisms of such an effect remain unclear. In order to investigate the mechanism of TDF nephrotoxicity a reliable animal model is necessary. Therefore, our aim was to standardize a rat model of TDF nephrotoxicity.

To this end, our first trial was based on clinically relevant dose of TDF 5 mg/ kg body wt. /day for 5 weeks. However at this dose no damage to the tubules as well as glomerulus was observed. In an earlier study Kohler et al. (31) have used this clinically relevant dose on a mouse model and these authors also could not find any changes in the tubules. Next we tried twice the dose that is used for humans (100 mg/kg/d) as described by Lebrecht et al. (304). We could not find any tubular damage. No adverse effects related to mitochondrial injury were observed in animals treated with TDF at doses 6× the human dose, i.e., 300 mg/kg/d for 5 weeks. In accordance with our study, Biesicker et al has shown that treatment of rats with TDF at doses 6× the human dose over a period of 28, 56 or 90 days had no toxic effect on the kidneys (307).

When we administered dose of TDF that corresponds to 12 x human doses to rats for 5 weeks, we were able to demonstrate proximal tubular damage by light microscopy and severe damage to the proximal tubular mitochondria by electron microscopy. The main abnormality on light microscopy was acute proximal tubule damage, and eosinophilic intracytoplasmic inclusions formed of giant mitochondria. Similarly in our study we were able to demonstrate damage to the proximal tubules. Mild destruction of the lining epithelium of the loops of Henle and the collecting duct and some glomeruli were shrunken, suggesting that tubular toxicity induced by TDF is not restricted to proximal tubular cells. Similar findings have been reported by Libo´ Rio et al in rats (305).

Electron microscopy of renal biopsies showed widespread morphological abnormalities in proximal tubule mitochondria, with marked variations in size and shape and loss of the normal cristae, mitochondrial swelling, and intramitochondrial paracrystals. In some proximal tubule cells mitochondrial number was decreased. Varying degrees of chronic tubulointerstitial scarring (i.e., tubular atrophy and interstitial fibrosis) have also been reported (15). Similarly in our study many mitochondria were swollen (giant mitochondria), cristae were disrupted, and amorphous deposits were observed in the matrix. In some epithelial cells, the mitochondria were reduced in number. An increase in mitochondria with irregular shape was observed in the cytoplasm of basal part of tubule cell. Thus our animal model of TDF nephrotoxicity bears close resemblance to that of TDF nephrotoxicity in humans when examined histologically.

Next, we investigated whether this model of TDF nephrotoxicity mimics that of humans functionally. Proximal tubular cells account for most of the tubular transport of molecules, reabsorbing over 200 g NaCl, 1 kg glucose, and other molecules from the tubular lumen every day. Energy for this transport is provided by a high number of mitochondria. This is needed to satisfy the

high-energy requirement for driving sodium-potassium pumps in order to reabsorb the filtered nutrients such as glucose and amino acids as well as ions such as sodium, chloride, phosphate and bicarbonate. Proximal tubular cells are therefore rich in mitochondria and cell membrane transporters (360). Thus, proximal tubular mitochondrial injury will impair molecular transport, and urinary acidification resulting in Fanconi Syndroma and bicarbonate wasting.

It has been demonstrated that the TDF use in humans provokes proximal tubular dysfunction, including glycosuria, tubular proteinuria, hypophosphatemia, hyperphosphaturia, hypokalemia and renal tubular acidosis. Kinai and Hanbusa (361) reported that 12 out of 17 patients on TDF presented with high levels of urinary β-2 microglobulin accompanied by significant decreases in tubular reabsorption of phosphate. In the present study, we were able to demonstrate hypophosphatemia, hypokalemia, phosphaturia, and loss of HCO_3^- in urine in the TDF treated rats. Thus, it is possible that, in rats, prolonged exposure to TDF would cause generalized proximal tubular dysfunction such as that described in humans. One of the most consistent findings in patients suffering from TDF nephrotoxicity is hypophosphatemia (354). The TDF treated rats in our study presented with hyperphosphaturia, which is the most likely cause of the hypophosphatemia seen in those same rats. Tubular reabsorption of phosphorus is largely performed in the proximal tubules via NaPi-IIa. A significant decrease in NaPi-IIa protein expression has been reported in TDF-treated rats (355). This may be the cause of hyperphosphaturia that is observed in humans and animal models of TDF nephrotoxicity.

The main target of TDF toxicity is the proximal tubule, and the presence of tubular proteinuria is considered to be the most sensitive test for proximal tubule dysfunction (362). Proteins with low molecular weights pass freely through the glomerulus but are then almost completely reabsorbed in the proximal tubules. However, protein reabsorption is a highly energy-consuming process. In

addition, its transport capacity is limited. Tubular proteinuria occurs when the renal tubules cannot reabsorb low molecular weight proteins. Tubular proteinuria is associated with drug toxicity including aminoglycosides, cephalosporins, and cyclosporine. Conventional brands of the dipsticks are not suited for the exclusion of renal tubular disease. Their detection limit far exceeds the upper normal reference range and lies somewhere between 150 and 300 mg/l. Furthermore, they measure mostly albumin. Smaller molecules, as seen in mainly tubular are detected to a much lesser extent or not at all. SDS electrophoresis identifies proteins above their detection limits with a molecular weight marker protein, glomerular proteins with Mr 66 000 and tubular marker proteins with Mr. 66 000) (363,364). Tubular proteinuria is characterized by the dominant excretion of proteins such as 1-microglobulin or retinol-binding protein (RBP), which correlate better with the extent of tubule-interstitial damage than does determination of total 24-h protein concentrations (33). Increased β-2 microglobulinuria in human immunodeficiency virus-1-infected children and adolescents treated with tenofovir has been reported, and urinary β2-microglobulin is considered as a sensitive marker for renal injury caused by tenofovir disoproxil fumarate (365,366). We were able to detect tubular proteinuria by SDS-PAGE electrophoresis of urine sample of TDF treated rats thereby confirming that TDF causes proximal tubular dysfunction.

In conclusion, this rat model is a good model for the study of TDF nephrotoxicity as it resembles that of TDF nephrotoxicity in humans both structurally and biochemically. The model will be useful not only for the study of the mechanism of nephrotoxicity of TDF but also for carrying out intervention studies. This model will also permit to study drug interactions by overcoming the limitations of cell culture and the difficulties of obtaining human kidney samples. It may also be employed to develop markers for the early diagnosis of the mitochondrial tubulopathy.

For all our studies the TDF dose was fixed at 600 mg/kg body wt./day, administered orally by gavage , for 5 weeks.

.

STUDY II

Chronic TDF administration altered renal mitochondrial structure and function and reduced the activities of the ETC complexes and mitochondrial antioxidant enzymes

ABSTRACT

TDF targets proximal tubular mitochondria. However, its effects on mitochondrial functions has not been explored in detail, to the best of our knowledge. Mitochondria were isolated from the kidneys of TDF treated rats and control rats, and were used for the assessment of mitochondrial functions, and assay of ETC complexes and antioxidant enzymes. Impaired mitochondrial function such as respiratory control ratio (RCR), MTT reduction, and mitochondrial swelling were observed in the TDF treated rat kidney mitochondria. The activities of the electron chain complexes I, IV and V were decreased by 46%, 20 % and 21 % respectively in the TDF treated rat kidneys. The activity of complex II, a marker enzyme of mitochondrial inner membrane integrity was decreased by 26%. A 50 % increase in protein carbonyl content was observed in the kidneys of TDF treated rats as compared with the control. The activity of catalase was increased by 28% in the TDF treated rat kidneys. The activities of superoxide dismutase, GST, carbonic anhydrase and aconitase were decreased by 61% , 57% , 45 % and 45 % respectively. It is suggested that TDF induced proximal tubular mitochondrial dysfunction and ETC defects may impair ATP production, resulting in proximal tubular damage and dysfunction.

INTRODUCTION

Current evidence suggests that mitochondria are the subcellular target organelles of tenofovir cytotoxicity. Several human and animal studies have shown that TDF damages renal proximal tubular mitochondria (14,67,367) . Human kidney biopsies and kidneys obtained after chronic TDF treatment showed severe morphologic abnormalities in proximal tubule mitochondria, with marked variations in size, shape, disruption of cristae, mitochondrial swelling, and intra-mitochondrial paracrystals and sometimes decreased number of mitochondria (14). The mechanism by which TDF causes mitochondrial injury is not clear.

Mitochondrial swelling is considered to be a characteristic feature of deteriorated function of this organelle (34). Mitochondria are the energy source of the cell, and the components in the electron transport chain, which play a central role in ATP synthesis, are found in the cristae. Thus, damage to the cristae can result in the disruption of electron transport chain, decreased activity of the electron chain complexes and hence decrease ATP production by the mitochondria.

We hypothesized that TDF induced proximal tubular damage and dysfunction may be due to the impairment of mitochondrial function and lowering of the activities of the electron chain complexes that are required for ATP synthesis. Mitochondrial respiratory control indicates the ability of mitochondria to function at a low rate yet respond to ADP by making ATP at a high rate (368) Decreased RCR indicates uncoupling of oxidative phosphorylation, high proton leak, and is diagnostic of extensive mitochondrial damage (368)

MTT reduction assay requires intact mitochondrial membrane. Mitochondrial damage will result in loss of the ability to provide energy for metabolic function and so the extent of reduction of MTT

will be decreased. Thus, MTT reduction assay is a useful measure of mitochondrial activity as well as cell viability (369).

Mitochondrial swelling is considered as an indicator of altered membrane permeability transition (MPT) (370). MPT is a physiopathological event that results in increased permeability of the inner mitochondrial membrane to solutes resulting in mitochondrial swelling.

ATP synthesis by the mitochondria requires functional electron chain complexes (ETC) in addition to the intact inner mitochondrial membrane. Inhibition of the electron transport chain complexes and oxidative phosphorylation have been shown to decrease ATP synthesis and increase superoxide anion production (371), thereby propagating the generation and toxicity of ROS i.e. ROS INDUCED ROS RELEASE-coined by Sollott and colleagues (372).

It is well known that mitochondrial damage can result in the overproduction of reactive oxygen species (ROS) and reactive nitrogen species (RNS), which upon accumulation can cause oxidative and nitrosative damage to the lipids, proteins and DNA (35,373). Proximal tubular cells have a requirement for ATP for the active reabsorption of filtered nutrients and ions. Thus, damage to the proximal tubular mitochondria can have two consequences, proximal tubular dysfunction resulting in Fanconi Syndrome and increased production of ROS thereby resulting in increased oxidant stress.

Manganese superoxide dismutase (MnSOD) is the first line of defense against ROS (superoxide) generated by the mitochondria and it catalyze the dismutation of highly reactive superoxide radicals to hydrogen peroxide and molecular oxygen (374). Altered function or expression of MnSOD can result in the accumulation of superoxide anion to toxic levels and can have remarkable

consequences on mitochondrial function and the overall health of cells due to oxidative damage to various mitochondria-localized metabolic pathways (374).

The antioxidants within the mitochondria include reduced glutathione, glutathione reductase, and carbonic anhydrase. Mitochondrial glutathione is considered as the key survival antioxidant (173). Overproduction of superoxide anion or deficiency of SOD can result in the mitochondrial accumulation of highly reactive superoxide radicals, which when present in excess can react with mitochondrial nitric oxide to produce peroxynitrite, a reactive nitrogen species (RNS) (375) and a potent oxidant that can modify proteins to form 3-nitrotyrosine (3 NT) (376). 3NT content is considered to be an indicator of oxidative modification of proteins along with protein carbonyl content (376).

Therefore, in the present study we studied the effect of chronic administration of TDF to rats on the renal mitochondrial functions such as respiratory control ratio (RCR), MTT reduction and mitochondrial swelling and the activities of electron transport chain complexes, and parameters of oxido-nitrosative stress, and antioxidant systems, MnSOD, GST, and carbonic anhydrase.

BRIEF EXPERIMENTAL SETUP

Adult Male Wistar rats (200–250 g) were used for the experiments.

The rats were divided into 2 groups and were treated as follows.

Group I : The control rats in this group (n = 6) received sterile water alone for 35 days.

Group II : The rats (n = 6) in this group received 600 mg/ kg body weight TDF by gavage for 35 days.

All the rats were sacrificed 24 hours after the final dose of TDF / sterile water, after withdrawal of blood under light halothane anesthesia.

Morphological examination of the kidney

Electron microscopy was used to visualize the extent of mitochondrial ultrastructural injury in the proximal tubular cells, which was then quantitatively assessed (Scale of 0–5) based upon the cell injury staging system described by Trump and colleagues (377).

TABLE 5. 1: MITOCHONDRIAL INJURY SCORING SYSTEM BASED UPON THE STAGES OF CELLULAR INJURY*

Cellular Injury Stage†	Mitochondrial Injury Score†	Mitochondrial characteristics
Stage I	0.0	Normal appearance
Stage II/III	1.0	Swelling of endoplasmic reticulum, minimal mitochondrial swelling
Stage IV‡	2.0	Mild mitochondrial swelling
	3.0‡	Moderate or focal high-amplitude swelling
	4.0	Diffuse high-amplitude swelling, disruption of cristal membrane integrity.
Stage V/VI	5.0	High-amplitude swelling with mitochondrial flocculent densities and/or calcifications.

† Stages and scores do not directly correlate because indices of cell injury other than mitochondrial changes were not taken into consideration during determinations of mitochondrial injury. ‡Irreversible cell damage is noted to occur during this stage, and mitochondrial injury scores greater than 3.0 are predictive of ultimate cell death .

Measurement of parameters of mitochondrial function

Left kidney was removed, weighed and were homogenized with 5% homogenizing buffer, centrifuged at 4000g for 10 minutes to obtain crude mitochondrial fraction, followed by centrifugation at 12000g for 20minutes, washed pellet with buffer and resuspended with the same buffer to obtained pure isolated mitochondria. The purity of mitochondria was assessed by the marker enzyme succinate dehydrogenase and used for assessing mitochondrial damage by measuring various parameters of mitochondrial functions such as Respiratory control ratio by clark type electrode, MTT reduction by ELISA reader, mitochondrial swelling, and antioxidant enzyme activity by using Nanodrop spectrophotometer as described above in the methodology.

Assay of protein carbonyl and antioxidants

The level of protein carbonyl and activity of antioxidant enzymes (SOD, GST, catalase, carbonic anhydrase and aconitase) in isolated mitochondria was done by using Nanodrop spectrophotometer as described above in the methodology.

Assay of the activities of the electron transport chain complexes

The activities of the ETC complexes Complex I (NADH – Ubiquinone oxidoreductase), Complex II (Succinate – Ubiquinone oxidoreductase), Complex III (Ubiquinol cytochrome c reductase), Complex IV (Cytochrome c oxidase) and Complex V (ATP synthase) were assayed spectrophotometrically. The enzyme activity is expressed as k/min/mg protein.

Protein Expression of cytochrome 'c' levels by immunohistochemistry and western blot

RESULTS

a. TDF treatment caused severe damage to the proximal tubular mitochondria

Vehicle-treated rats showed **(Figure: 5.1)** normal tubular structure with numerous mitochondria and lysosomes (black arrows) (A). Oval mitochondria with densely packed cristae were observed (B). Proximal tubular epithelia of TDF-treated rats showed moderate to severe damage to the mitochondria. The mitochondria showed marked variations in size and shape. Mitochondrial toxicity included swelling (giant) mitochondria, disruption of an accumulation of amorphous deposits in the matrix. (C). An increase in the number of mitochondria with irregular shape and fragmented cristae was observed in the cytoplasm of basal part of tubule cell. In some epithelial cells, the mitochondria were reduced in number. The cytoplasm showed an increased number of vacuoles and reduced number of lysosomes. Nucleus appeared shrunken (D), and accumulation of amorphous deposits in the mitochondrial matrix (E) Increased number of mitochondria (M) was observed in the tubule cytoplasm (F), especially in the basal part of tubule cell (arrow) (G). Many mitochondria were swollen and irregularly shaped (H).

Mitochondrial injury score which was quantitatively assessed (Scale of 0–5) Table:5.1, based upon the cell injury staging system described by Trump and colleagues showed a score of 4 or 5 suggesting severe mitochondrial injury. These findings suggest that TDF targets mainly the proximal tubular mitochondria and to a lesser extent the lysosomes and nucleus.

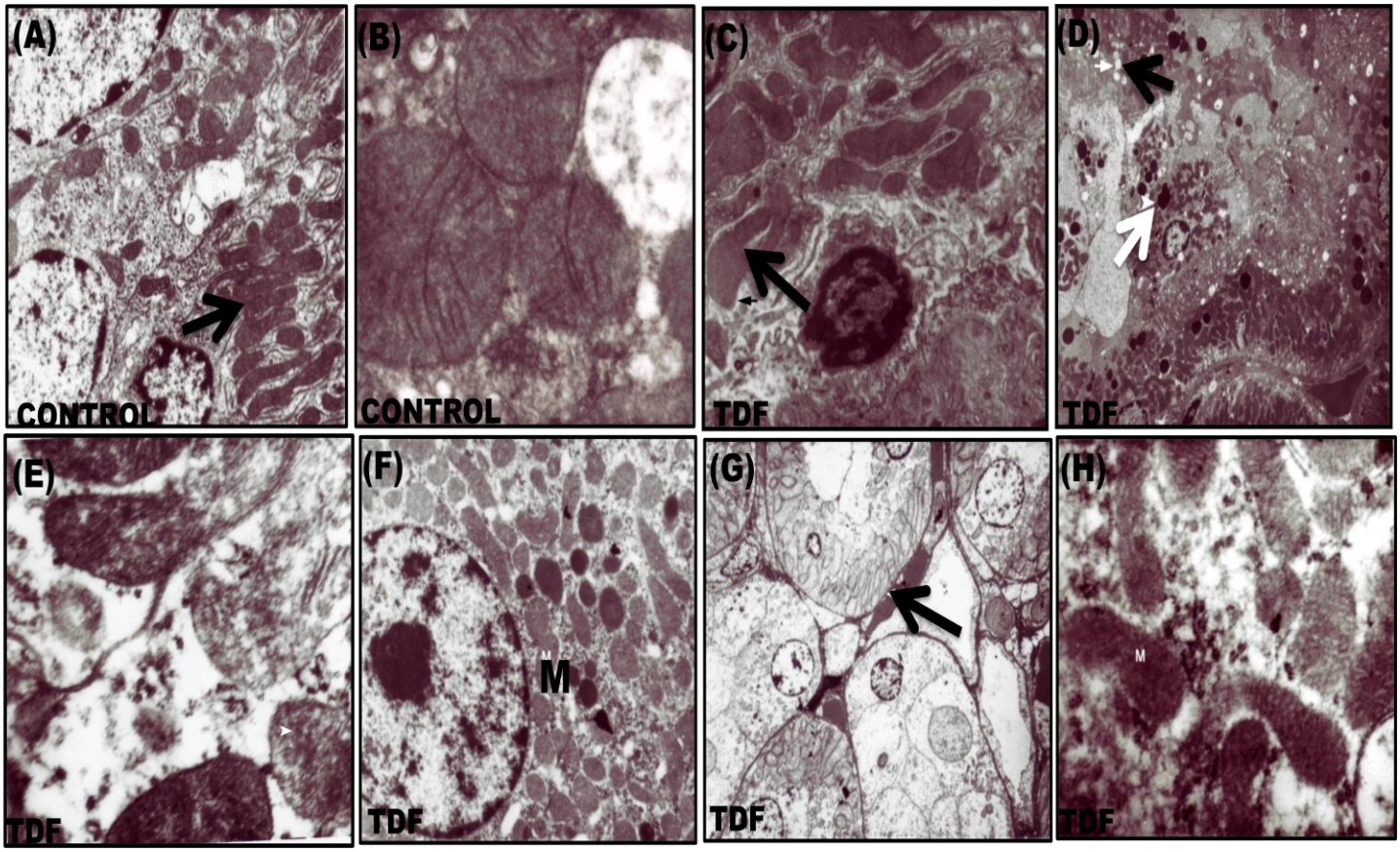

Figure: 5.1 Representative electron micrographs of control and TDF treated kidney tubules. A) Normal Kidney tubules (original magnification × 22000) (B) Normal mitochondrial structure in the renal tubules of control rats (original magnification × 22000) (C) Disruption of mitochondrial cristae (black arrow), mitochondrial swelling (black arrow) in the renal tubules of TDF treated rats (D) Vacuoles seen in the cytoplasm of the kidney tubule (black arrow) Less number of lysosomes (white arrow) (E) Amorphous deposits in the mitochondrial matrix (white arrow) (F) Increased number of mitochondria (M) in tubule cytoplasm (G) Increased mitochondria in basal part of tubule cell (arrow) (H) Swollen mitochondria (M) (original magnification ×22 000).

b. Chronic TDF administration impaired mitochondrial function (fig.5.2):

Chronic TDF administration resulted in decreased RCR and MTT reduction and caused mitochondrial swelling, suggesting impaired mitochondrial function.

RCR : RCR was reduced by 44 % in the kidneys of TDF treated rats suggesting mitochondrial dysfunction. Decreased RCR indicates uncoupling of oxidative phosphorylation and suggests extensive mitochondrial damage. (Figure: 5.2.1)

Mitochondrial swelling: Change in absorbance of mitochondria isolated from kidney tissue of control and TDF – dosed rats was significantly decreased compared to control suggesting swelling. Mitochondrial swelling is considered as an indicator of altered membrane permeability transition (MPT). (Figure: 5.2.2)

MTT reduction assay : MTT reduction was decreased by 22 % in the TDF treated rat kidneys ($p<0.05$). This suggests decreased mitochondrial membrane integrity, mitochondrial function and cell viability. (Figure: 5.2.3)

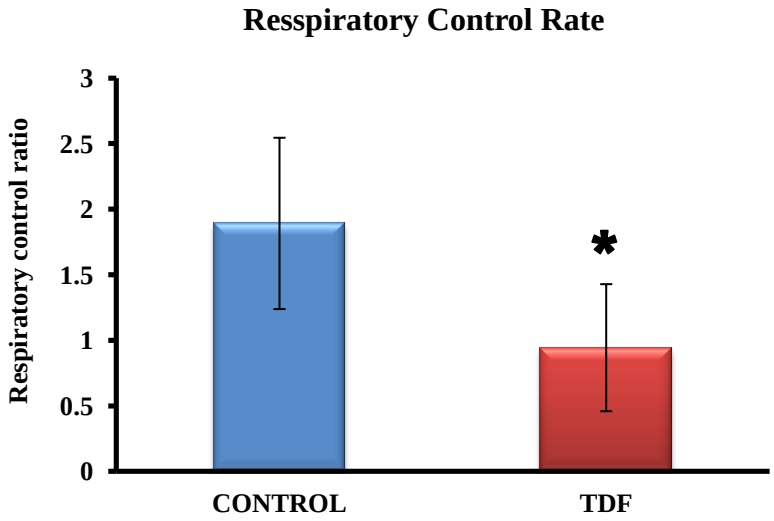

Figure: 5.2.1 Respiratory control ratio (RCR) of mitochondria isolated from kidney tissue of control and TDF treated rats. Data represent mean ± SD, n=6 in each group, * p-value <0.05 vs control.

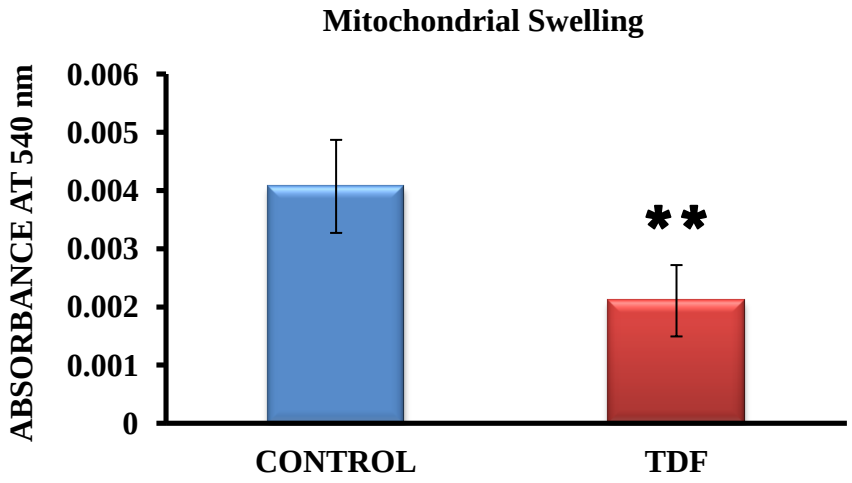

Figure: 5.2.2 The degree of change in absorbance of mitochondria isolated from the kidney tissue of control and TDF treated rats. The data represent mean ±SD, n=6 each group, ** p-value <0.01.

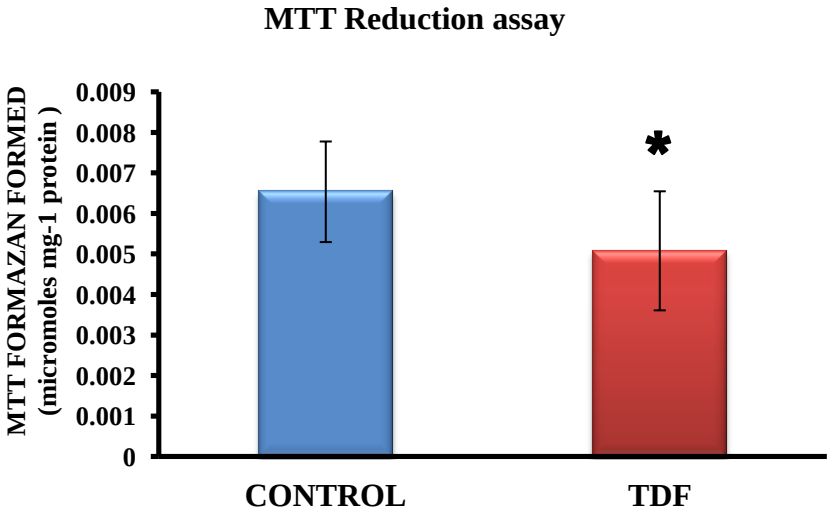

Figure: 5.2.3 MTT reduction of mitochondria isolated from the kidney tissue of control and TDF treated rats. Data represent mean ±SD, n=6 each group , * p-value <0.05.

c. **Effect of TDF on mitochondrial protein oxidation and activities of antioxidant enzymes**

A 50 % increase in protein carbonyl content was observed in the kidneys of TDF treated rats as compared with the control, a marker of oxidative stress (Figure:5.3.1). The activities of all the mitochondrial antioxidant enzymes estimated except catalase were significantly decreased in the kidneys of TDF treated rats as compared with the control. The activity of superoxide dismutase (SOD) was decreased by 57% (Figure:5.3.2), GST 50% (Figure:5.3.3) as compared with control. The activity of catalase was increased by 28% (Figure:5.3.4) in the TDF treated rat kidneys. The activities of both carbonic anhydrase and aconitase were decreased by 45% (Fig. 5.3.5) & (Fig.5.3.6) in TDF treated rat kidneys as compared with control respectively.

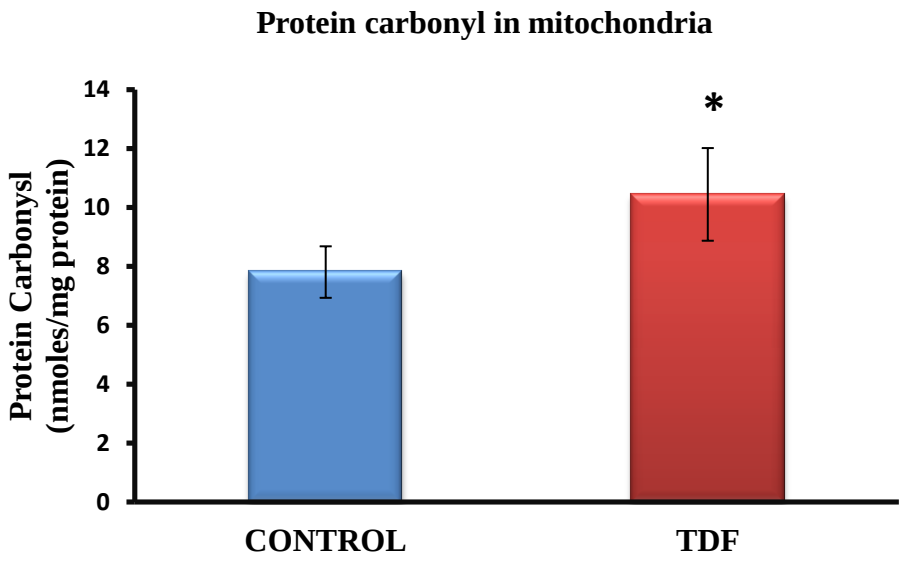

Figure: 5.3.1 Protein carbonyl (PC) levels in the kidney mitochondria of control and TDF treated rats. Data represent means ± SD, n=6 in each group. * p < 0.05 compared with controls.

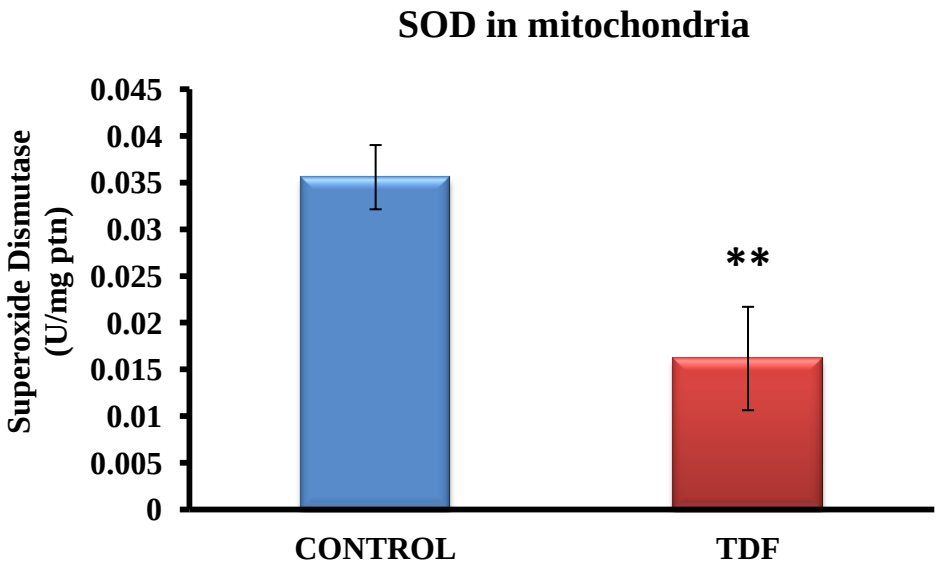

Figure: 5.3.2 Superoxide dismutase activity in the kidney mitochondria of control and TDF treated rats. Data represent means ± SD, n=6 in each group. ** p < 0.01 compared with controls.

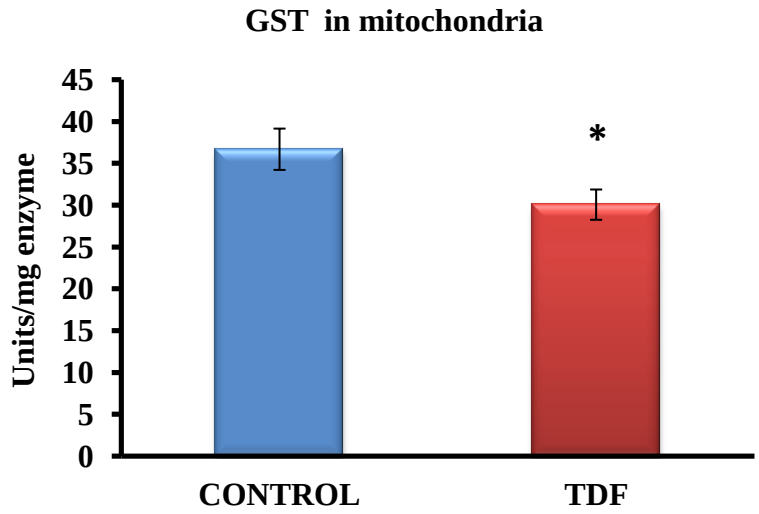

Figure: 5.3.3 Glutathione S-transferase activity in the kidney mitochondria of control and TDF treated rats. Data represent means ± SD, n=6 in each group. * p value < 0.05 as compared with controls.

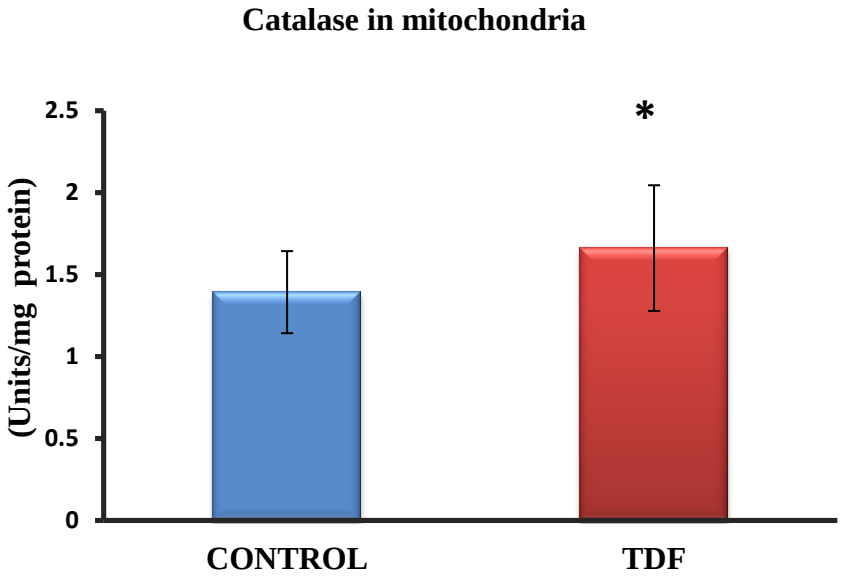

Figure: 5.3.4 Catalase levels in the kidney mitochondria of control and TDF treated rats. Data represent means ± SD, n=6 in each group. * p < 0.05 compared with controls.

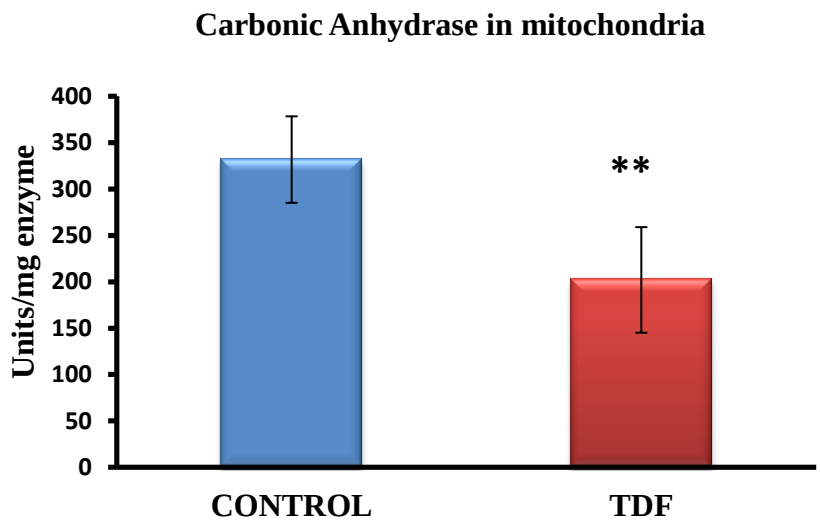

Figure: 5.3.5 Carbonic anhydrase activity in the kidney mitochondria of control and TDF treated rats. Data represent means ± SD, n=6 in each group. ** p < 0.01 compared with controls.

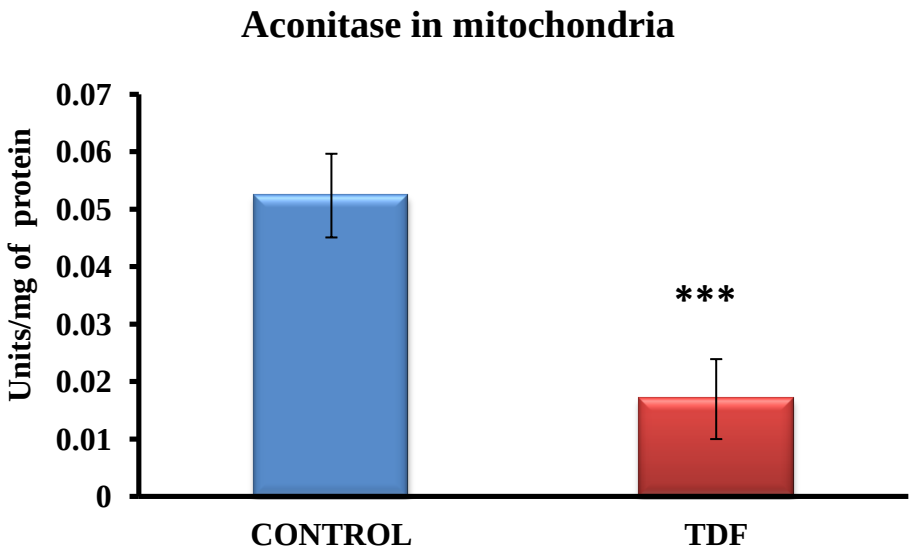

Figure: 5.3.6 Aconitase activity in the kidney mitochondria of control and TDF treated rats. Data represent means ± SD, n=6 in each group. *** p < 0.001 compared with controls.

d. Effect of TDF on the activities of mitochondrial respiratory chain complexes

TDF administration decreased the activities of the mitochondrial electron chain complexes I, II,IV and V. A marked decrease (56 %) in the activity of complex I (Figure: 5.4.1) was observed in the TDF treated rat kidney mitochondria. The activity of complexes II was decreased by 26 % as compared with control (Figure: 5.4.2). Complex IV activity was reduced by 21 % (Figure: 5.4.3) and complex V activity by 18 % (Figure: 5.4.4) in the TDF treated rat kidney mitochondria.

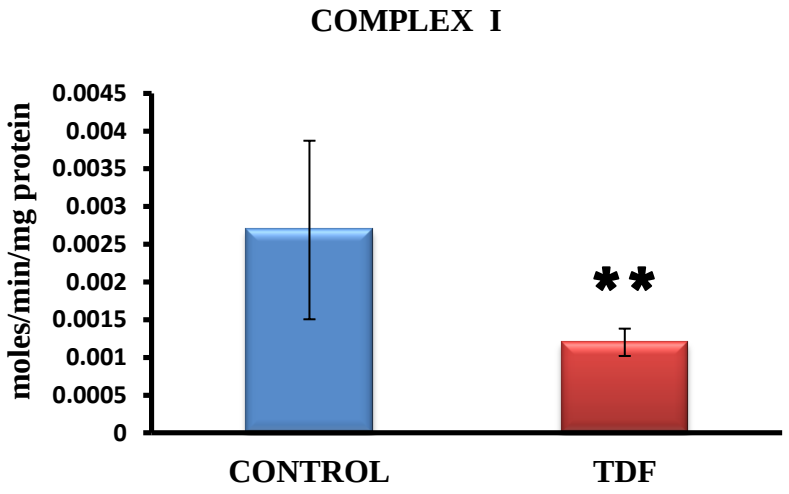

Figure: 5.4.1 Complex-I activity of mitochondria isolated from the kidney tissue of control and TDF dosed rats. Data represent mean ± SD, n= 6 in each group, ** P value < 0.01 as compared with control.

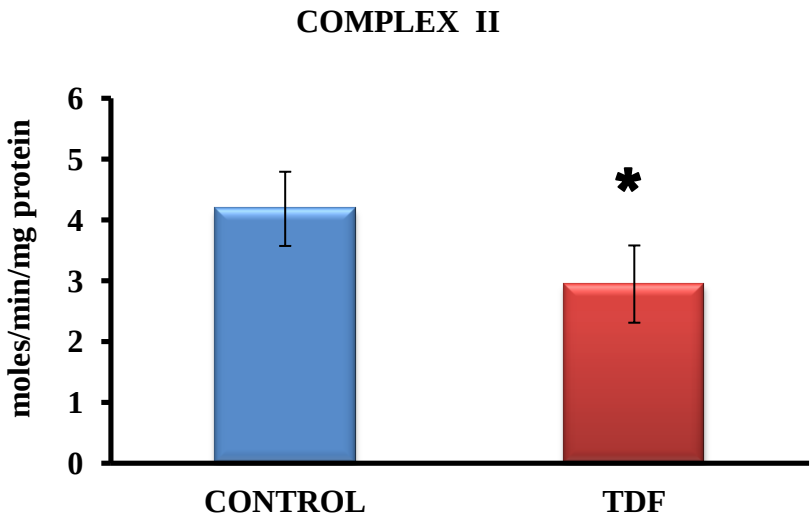

Figure: 5.4.2 Complex-II activity of mitochondria isolated from the kidney tissue of control and TDF – dosed rats. Data represent mean ± SD, n= 6 in each group, p-value < 0.05 as compared with control.

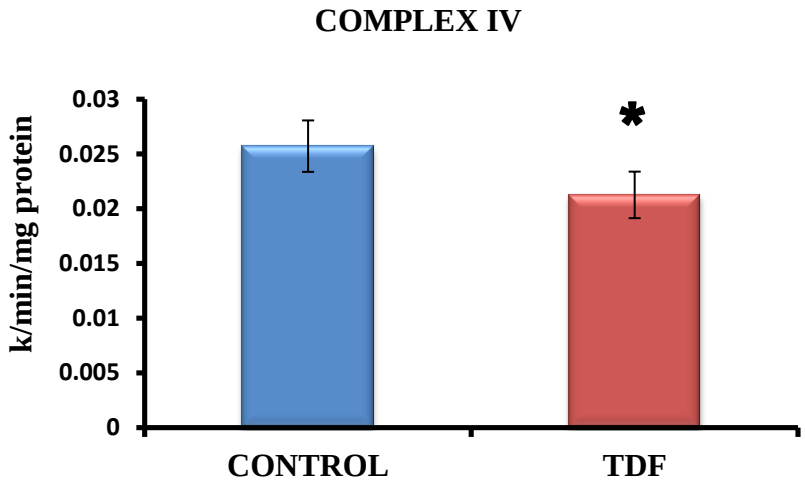

Figure:5.4.3 Complex-IV activity of mitochondria isolated from kidney tissue of control and TDF – dosed rats. Data represent mean ± SD, n= 6 in each group, * P-value <0.05 as compared with control.

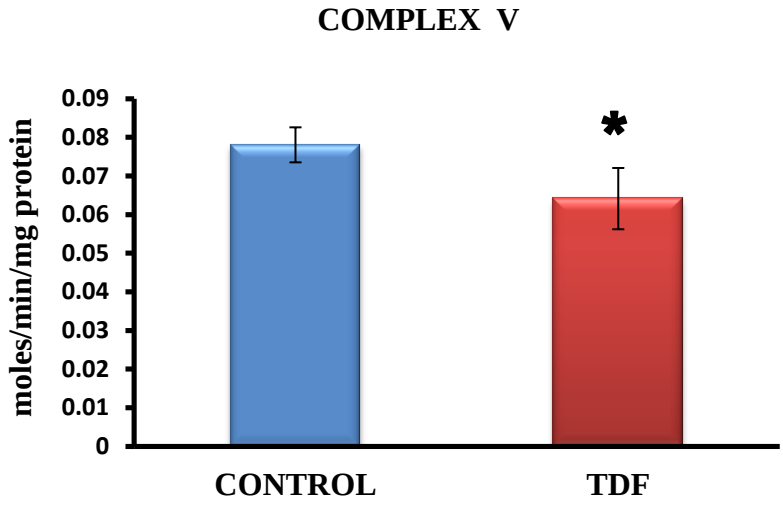

Figure: 5.4.4 Complex-V activity of mitochondria isolated from kidney tissue of control and TDF – dosed rats. Data represent mean ± SD, n= 6 in each group, * P-vaue <0.05 as compared with control.

e. Protein Expression of cytochrome 'c' levels by immunohistochemistry and western blot (Figure: 5.5 and 5.6)

Immunostaining for cytochrome c in the control rat kidneys showed minimal staining in cortex as well as medulla. Immunolocalization of the protein cytochrome 'c' shows increase in the glomerulus. In the TDF treated rat kidneys, the glomerulus stained intensely and the proximal and distal tubules showed mild staining. In the medulla, the collecting ducts, and loop of Henle showed moderate staining for cytochrome c **(Figure: 5.5)**.

Immunoblot analysis of cytochrome c in the mitochondrial fractions showed a significant decrease, which may be due to release of cytochrome 'c' from mitochondria to the cytosol **(Figure: 5.6 A & B).**

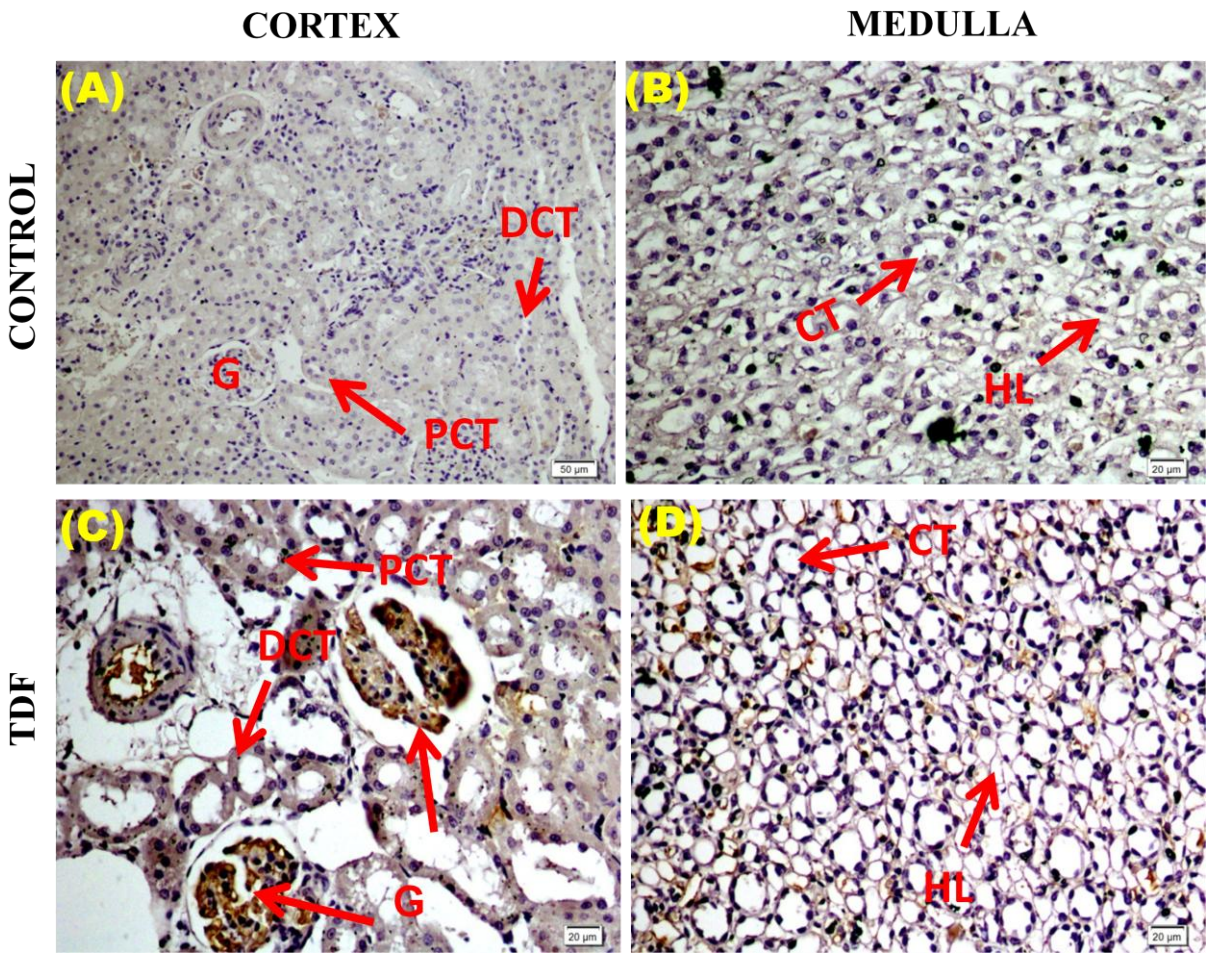

Figure: 5.5. Representative immunohistographs of cytochrome-c expressions in the kidneys of control rats and TDF treated rats. Scale Bars = 20µm

(A&B) - Control rats treated with sterile water for 35 days showing negligible staining for cyt.c in the cortex (A) and medulla (B).

(C&D)- TDF treated rats showing intense staining in the glomeruls and mild staining in the PCT, and DCT of the cortex. In the medulla, the loop of Henle (HL) and collecting tubule (CT) show moderate staining for cyt.c.

(A)

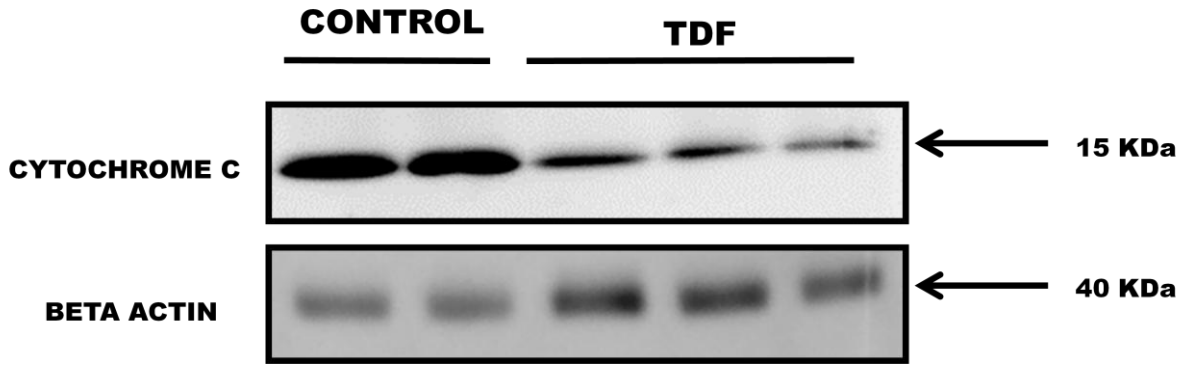

(B)

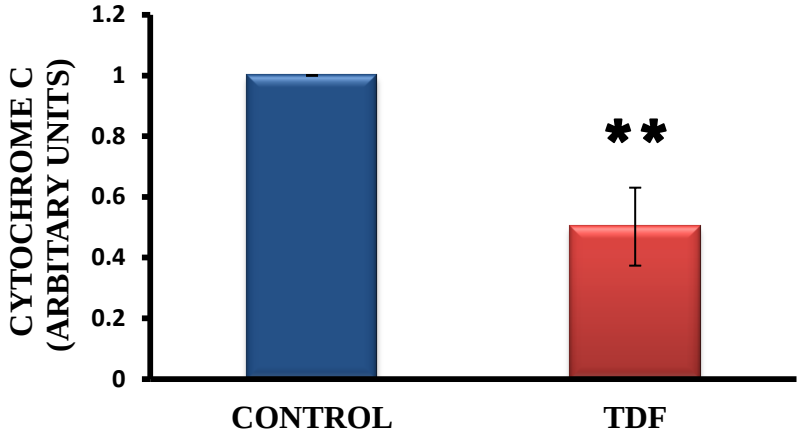

Figure: 5.6 A : This is a representative blot of cytochrome-c with (15kD) bands in mitochondrial fraction of control and TDF-treated rats (n=5 in each group), as assessed by using a 10% polyacrylamide gel, loading 100µg protein per lane. β-actin was used as the loading control.

Figure 5.6 B: Relative concentration of cytochrome-c in mitochondrial fractions of renal homogenates as analysed by densitometric quantification of bands of western blots in control and TDF-treated rats (n=5 in each group) , obtained by image analysis of western blots with the concentration of the controls set at one. Data represents mean ± SD. ** $p<0.01$ when compared with control.

DISCUSSION

Although it is well established that TDF targets the proximal tubular mitochondria the effect of TDF on the mitochondrial function and activities of ETC have not been studied in detail. Gross changes seen in the proximal tubular mitochondria of TDF treated might indicate altered function and mitochondrial swelling is considered to be a characteristic feature of its deteriorated function (34). Therefore, we assayed the parameters of mitochondrial function including RCR, MTT reduction and mitochondrial swelling.

Proximal tubular cells have a high- requirement for ATP (and mitochondria) for driving sodium-potassium pumps in order to reabsorb the filtered nutrients such as glucose and amino acids as well as ions such as sodium, chloride, phosphate and bicarbonate (378). Damage to proximal tubular mitochondria can limit the availability of ATP for proximal tubular function resulting in the loss of the nutrients and ions in urine (Fanconi syndrome). We observed Fanconi Syndrome in the TDF treated rats, suggesting the involvement of mitochondrial damage in TDF nephrotoxicity.

Proximal tubular cells have numerous mitochondria and are the most reliant on oxidative phosphorylation for ATP and they are intrinsically vulnerable to mitochondrial dysfunction because of limited anaerobic ATP-generating capacity (379). Mitochondrial respiratory control indicates the ability of mitochondria to function at a low rate yet respond to ADP by making ATP at a high rate (368). Decreased RCR indicates uncoupling of oxidative phosphorylation, high proton leak, and is diagnostic of extensive mitochondrial damage (368). RCR was reduced significantly in the renal mitochondria of TDF treated rats suggesting mitochondrial dysfunction.

MTT reduction assay requires intact mitochondrial membrane. Mitochondrial damage will result in loss of the ability to provide energy for metabolic function and so the extent of reduction of MTT will be decreased. Thus, MTT reduction assay is a useful measure of mitochondrial activity as well as cell viability (369). MTT reduction was significantly decreased in the renal mitochondria after TDF treatment suggesting a decreased mitochondrial function and cell viability upon TDF

treatment. Mitochondrial swelling was observed in the TDF treated rat kidneys both histologically and biochemically, suggesting increased mitochondrial permeability. Mitochondrial swelling is considered as an indicator of altered membrane permeability transition (MPT) (370). MPT is a physiopathological event that results in increased permeability of the inner mitochondrial membrane to solutes resulting in mitochondrial swelling and causes the release of cytochrome 'c' from mitochondria to cytosol. Mitochondrial swelling is considered to be a characteristic feature of the deteriorated function of this organelle.

ATP synthesis by the mitochondria requires intact inner mitochondrial membrane .SDH, a key enzyme in the Krebs cycle is the marker enzyme of mitochondrial inner membrane integrity and its activity level shows the degree of mitochondrial activity (380). It is an important enzyme of the citric acid cycle and reduction in SDH activity has been reported to decrease the rates of mitochondrial respiration, & ATP production (381). In the present study, SDH activity was decreased by 26 % ($P < 0.01$) in TDF treated rat kidney as compared with control .Decrease in SDH activity demonstrates that the kidney mitochondria of TDF treated rats were damaged, which may in turn affect ATP production. It also gives an additional support of the harmful effect of TDF intoxication on mitochondrial membrane integrity.

ATP synthesis by the mitochondria requires functional ETC complexes in addition to intact inner mitochondrial membrane. Therefore, we next assayed the activities of the mitochondrial ETC complexes, complexes I-IV. We found a marked decrease (56 %) in the activity of complex I in the TDF treated rat kidney mitochondria. The activity of complex II was decreased by 26% in the TDF treated rat kidneys as compared with controls .We found a significant decrease in the activity of complex IV in TDF treated rat kidneys. Complex IV is the primary site of cellular oxygen consumption and is thus central to oxidative phosphorylation and the generation of ATP (382). Its

inhibition can result in decreased synthesis of ATP. Inhibition of the electron transport chain complexes (complexes I and IV in this case) and oxidative phosphorylation have been shown to increase superoxide anion production (371), thereby propagating the generation and toxicity of ROS i.e. ROS INDUCED ROS RELEASE-coined by Sollott and colleagues (372).

Having documented that TDF causes mitochondrial dysfunction and inhibition of complexes I and IV, we next investigated whether the disruption affected ATP generation. The generation of ATP is through complex-V in the mitochondria. To determine the levels of ATP, we evaluated complex-V ATP synthase activity in the mitochondria isolated from control and TDF treated rats. A significant decrease in the activity of complex V was observed in the TDF treated rat renal mitochondria suggesting low ATP production.

Thus far only one study has been reported showing the effect of TDF administration on the activities of ETC complexes, to the best of our knowledge. Lebrecht et al (55) has shown that the histochemical activities of cytochrome oxidase (COX) and NADH-DH were decreased in the kidney cortex of tenofovir DF–treated rats, while the activity of succinate dehydrogenase (SDH), marker of integrity of mitochondrial inner membrane was not affected. However these authors have not studied the effect of chronic administration of TDF on mitochondrial functions such as RCR, MTT reduction and mitochondrial swelling, proximal tubular function, and the activity complex V which synthesizes ATP.

Defects in electron transport chain complexes results in the generation of large amounts of ROS (mainly as superoxide anion). Manganese superoxide dismutase (MnSOD) is the first line of defense against ROS (superoxide) generated by the mitochondria and it catalyze the dismutation of highly reactive superoxide radicals to hydrogen peroxide and molecular oxygen (374). Altered

function or expression of MnSOD can result in the accumulation of superoxide anion to toxic levels and can have remarkable consequences on mitochondrial function and the overall health of cells due to oxidative damage to various mitochondria-localized metabolic pathways (374). In the present study chronic TDF administration resulted in a drastic decrease (61 %) in renal SOD activity suggesting that reduced activity of SOD may contribute to proximal tubular mitochondrial damage and dysfunction.

In order to determine whether oxidative stress plays a role in TDF nephrotoxicity of mitochondria, we determined content protein carbonyl (Pco) level, the indicators of oxidative damage to proteins in TDF treated rat kidneys. We observed an increase in mitochondrial protein carbonyl content, suggesting that oxidative stress may play a role in TDF induced damage to the proximal tubular mitochondria. ROS-induced oxidative stress alters many cellular processes leading to apoptotic cell death. Therefore, the cells are equipped with antioxidant defense systems to combat with the ROS. The cellular defense mechanism include antioxidant enzymes such as superoxide dismutase, glutathione s-transferase , catalase, carbonic anhydrase and aconitase.

Mitochondrial glutathione is considered as the key survival antioxidant and its depletion in tissues has been shown to promote oxidative stress and tissue injury (383). In the present study, we observed a 50 % decrease in the mitochondrial GSH content in the TDF treated rat kidneys. Lowering of the mitochondrial GSH (mtGSH) by substances such as alcohol has been shown to make these organelles more susceptible to oxidative damage, and precedes the development of mitochondrial dysfunctions, such as lipid peroxidation and the impairment of ATP synthesis (383).

Carbonic anhydrase is reported to be involved in glutathione-mediated anti-oxidant activity (384). In the present study, TDF treatment resulted in significant loss of CA activity in the kidneys. Thus

significant decrease in reduced glutathione levels induced by TDF, leads to a reduction of effectiveness of the antioxidant enzyme defense system, thereby sensitizing the cells to reactive oxygen species. The activity of aconitase is essential for mitochondrial function (385). A decrease in the activity of aconitase observed in our study suggests loss of physiological function of mitochondria.

Studies have reported decreased oxidative phosphorylation releases mitochondrial cytochrome c into the cytosol, thereby altering the mitochondrial structure and function which may lead to cell death (386). Consistently, our data shows decreased cytochrome 'c' content in the isolated mitochondria in TDF treated animals. The cytochrome c decreases significantly and contributes to the decreased consumption of oxygen rate by cytochrome c oxidase in the mitochondria. The decline in mitochondria cytochrome c can result in a global decrease in oxidative phosphorylation capacity as well as substrates require electron flux through cytochrome c and cytochrome oxidase.

In summary, the results of the present study show that chronic tenofovir treatment causes proximal tubular mitochondrial dysfunction and decreased activities of the ETC complexes I, II, IV, and V. How tenofovir inhibits the enzymatic complexes of the respiratory chain remains to be elucidated. It may be a direct toxic effect of tenofovir on the ETC complexes or it may be an indirect effect of increased mitochondrial production of ROS/RNS that may damage the mitochondrial lipids, proteins, and DNA resulting in enhanced lipid peroxidation, protein oxidation and mtDNA depletion. Studies of the site and type of interaction of tenofovir with the different enzymatic complexes will give more clues about the mechanism of inhibition that may lead to proximal tubular damage. Studies using mitochondrial targeted antioxidants such as, Mito Q or Mito-CP (387) can help confirm the contribution of proximal tubular mitochondrial damage in TDF nephrotoxicity.

STUDY III

Oxidative stress, Nitrosative stress and Neutrophil infiltration contribute to Tenofovir induced renal damage

Abstract

Oxygen free radicals and nitric oxide have been implicated in the pathophysiology of kidney injury. This study examined plausible role of oxidative and nitrosative stress in mediating TDF induced renal damage. Rats were treated with 600 mg/ kg body weight of TDF for 35 days, sacrificed 24 hrs. after the final dose of TDF, and the kidneys were removed and used for biochemical assays. A significant increase in the protein carbonyl levels and a significant decrease in protein thiol content was observed in TDF treated rats . The level of TBARS and conjugated diene were not altered significantly. Reduced glutathione, an important intracellular antioxidant was decreased by 61 % in the kidneys of TDF treated rats as compared with the control. The activities of all the antioxidant enzymes estimated were significantly decreased in the kidneys of TDF treated rats as compared with the control. The activity of superoxide dismutase (SOD) was decreased by 61 %, glutathione S transferase by 47 %, and glutathione reductase by 43 % as compared with control. A 2 fold decrease in the activity of glutathione peroxidase was observed in the TDF treated rats. The western blot analysis of Heme oxygenase (HO-1) and HSP 70 showed a significant reduction in the TDF treated groups as compared with control (p-value 0.001 and 0.029) respectively. The mRNA expression of HO-1 and HSP 70 was significantly decreased in the TDF treated rat kidneys. Renal nitrate content was increased more than 2.5 fold. Nitrotyrosine content, the footprint of peroxynitrite was significantly increased in the TDF treated rat kidneys as compared with control. A nine fold increase in myeloperoxidase activity, a marker of neutrophil infiltration was observed in the kidneys of TDF treated rats. Results from this study demonstrate that oxidative stress, nitrosative stress, and neutrophil infiltration may play important roles in TDF tubulopathy

Introduction

In the previous study we have shown that mitochondrial injury plays an important role in TDF induced renal damage. It is well proven that mitochondria are the major sources of reactive species (ROS and RNS) (35,36,373). ROS generated by the mitochondrial damage are superoxide anion, hydrogen peroxide, hydroxyl radical. Increased generation of ROS exerts its toxic effect on biomolecules such as proteins, lipids and DNA leading to the accumulation of oxidative damaged products within the cells. Cells are well equipped with antioxidant defense system such as antioxidant glutathione and antioxidants enzymes include superoxide dismutases, catalase, glutathione peroxidase, glutathione reductase and glutathione S transferase to minimize the toxic effects (173,388). The decrease in the antioxidant systems in the cell can increase susceptibility of the cells to the toxicity of ROS resulting in oxidative stress. Thus oxidative stress can result from overproduction of ROS and decrease in the antioxidant system in the cell (389)

In general, besides their direct damaging effects on the tissues, ROS trigger the accumulation of leukocytes in the tissues involved, and thus aggravate tissue injury indirectly through activated neutrophils which secretes myeloperoxidase (MPO) and other proteases (390). The production of MPO acts as a marker for neutrophil infiltration (391). Thus, MPO plays a major important role in the oxidant production by neutrophils.

Renal cells are exposed to variety of stresses. These cells have an intrinsic ability to increase resistance to injury by producing cytoprotective proteins in response to stress (392). Heat shock proteins (HSP) are one such group of proteins. These proteins are classified into different types, according to the molecular weights. Among them, a 70-kilodalton protein, appears to be most preserved evolutionary. This protein is induced in experimental animals under condition of stress (393,394) . Studies have shown that induction of HSP results in the inhibiton of NF-κB activation and thereby brings about inhibition of expression of proinflammatory genes (395).

HO-1 and HSP 70 are inducible proteins, sensitive to various stimuli and agents that cause oxidative stress and many pathological conditions such as heat shock ischemia, hypoxia, radiation and cellular transformation (353,354). HO-1 increases the resistance to tissue injury by cytoprotective pathway in kidney and other tissues (397).

We hypothesized that the oxidative stress, nitrosative stress and neutrophil activation may play a important role in the pathogenesis of TDF induced renal damage

Brief experimental setup

Adult male Wistar rats weighing 200-250 g were used for the experimental study. The rats were housed in individual cages and treated as follows.

Group I (control) - The rats in this group (n = 6) received sterile water.

Group II- The rats (n = 6) in this group received 600 mg/ kg bodyweight Tenofovir disoproxil fumarate by gavage for 35 days.

All the rats were sacrificed 24 hours after the final dose of TDF / sterile water, after withdrawal of blood under light halothane anesthesia.

- **One portion of the kidney was removed and used for biochemical analysis, and immunohistochemical analysis.**

  (a) **The biochemical parameters** were carried out by preparing 10% (w/v) of fresh kidney homogenates using ice-cold HEPES and KCl buffer in a Potter-Elvehjem homogenizer. The homogenate was centrifuged at 4°C at 11,000g for 30min to remove unlysed particles and the supernatant was used for the following assays as described under the section materials and methods.

  Protein carbonyl content, TBARS, conjugated dine, glutathione, protein thiol, activities of SOD, GST, glutathione reductase, catalase, and myeloperoxidase, nitrate level, and NT content

(b) For immunohistochemistry, the kidney tissue was fixed in 10% formalin, 5µm thick sections were obtained from paraffin-embedded tissues and followed the procedure as described above in the methodology section.

Nitrotyrosine, HSP 70, HO-1 were localized using specific antibodies

- The other portion of kidney was snap frozen in liquid nitrogen and stored in -70^{o}C until use for protein and mRNA expression of HO-1, HSP70 by western blot and RT PCR respectively, nitrotyrosine by western blot

Statistical analysis:

Statistical analysis of data obtained was carried out using the Statistics Package for the Social Sciences (SPSS) software package, version 16. Data represents mean ± SD, the difference between two groups were analysed by Mann-Whitney test. A p-value of less than 0.05 was taken as statististically significant.

Results

(A) <u>Studies on the effect of TDF on oxidative stress parameters</u>

A 2 fold increase in protein carbonyl content was observed in the kidneys of TDF treated rats as compared with the control (Figure:6.1.1). TBARS, an indicator of lipid peroxidation was increased in the kidneys of TDF treated rats as compared with the control (Figure:6.1.3), but the increase was not statistically significant and there was no change in the level of conjugated diene (Figure:6.1.4). Reduced glutathione, an important intracellular antioxidant was decreased by 61 % (Figure:6.1.5) and protein thiol by 33 % (Figure:6.1.2) in the kidneys of TDF treated rats as compared with the control. A nine fold increase in myeloperoxidase activity, a marker of neutrophil infiltration was observed in the kidneys of TDF treated rats (Figure:6.1.6). The activities of all the antioxidant enzymes estimated were significantly decreased in the kidneys of TDF treated rats as compared with the control. The activity of

superoxide dismutase (SOD) was decreased by 61 % (Figure:6.1.7), glutathione S transferase by 47 %, (Figure:6.1.8) and glutathione reductase by 43 % as (Figure:6.1.10) compared with control. A 2 fold decrease in the activity of glutathione peroxidase (Figure:6.1.9) was observed in the TDF treated rats.

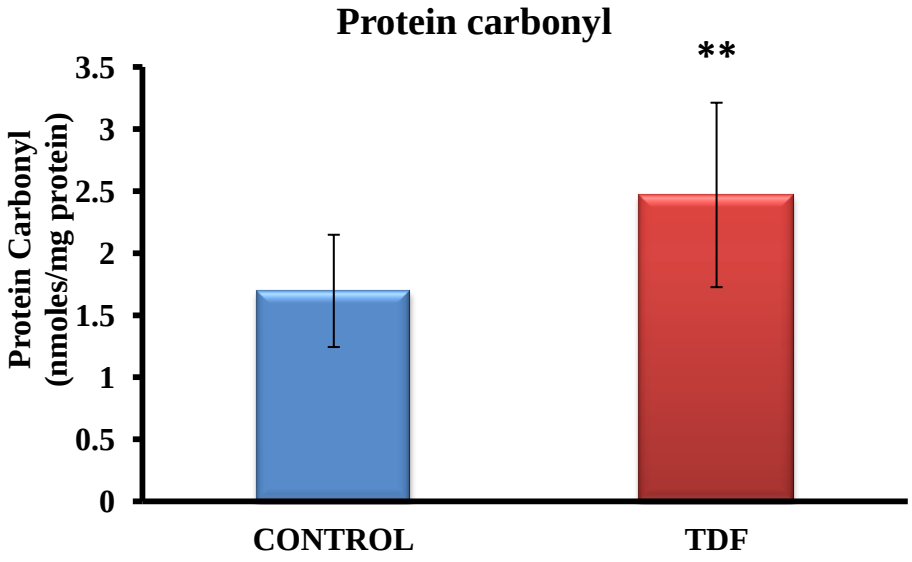

Figure: 6.1.1 Effect of TDF on Protein Carbonyl (PC) levels in the kidney of control and TDF treated rats. Data represent mean ± SD, n=6 animals in each group. ** p < 0.01 compared with controls.

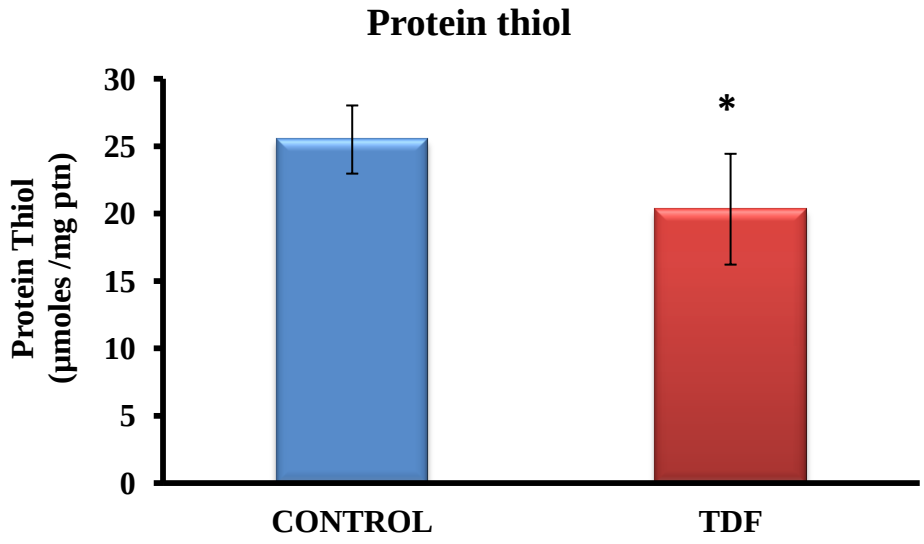

Figure: 6.1.2 Effect of TDF on Protein Thiol levels in the kidney of rats and TDF treated rats. Data represent mean ± SD, n=6 animals in each group. * p < 0.05 compared with controls.

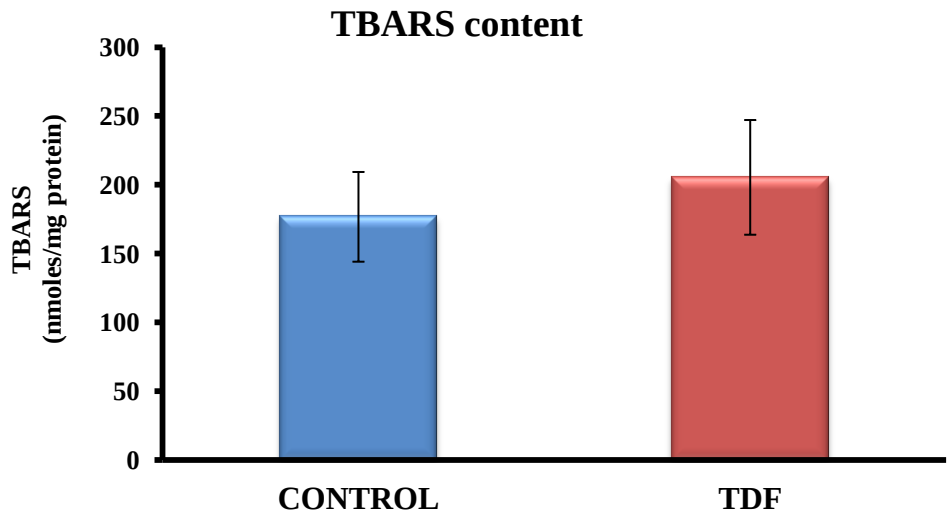

Figure: 6.1.3 Effect of TDF on TBARS levels in the kidneys of control rats and TDF treated rats. Data represent mean ± SD, n=6 animals in each group.

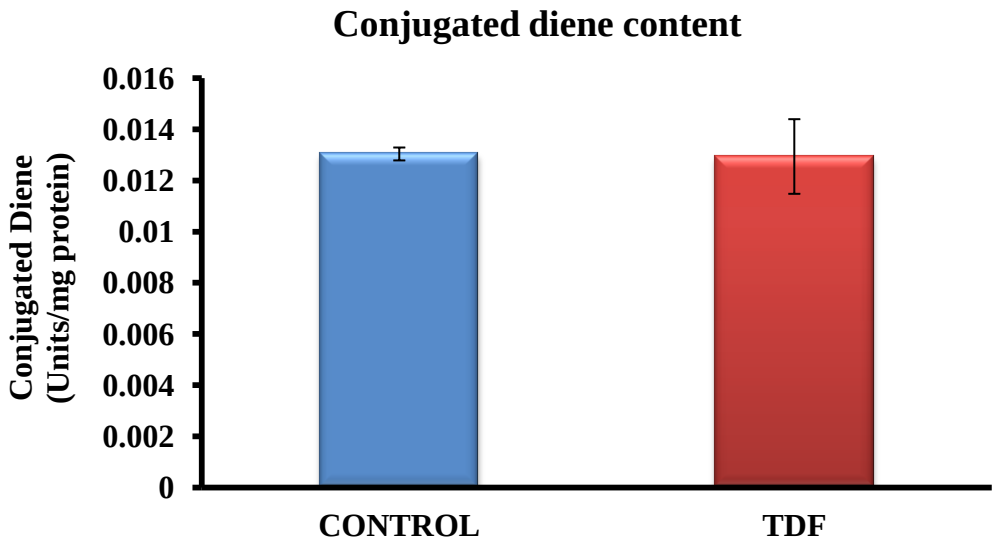

Figure: 6.1.4 Effect of TDF on conjugated diene levels in the kidneys of control rats and TDF treated rats. Data represent mean ± SD, n=6 animals in each group.

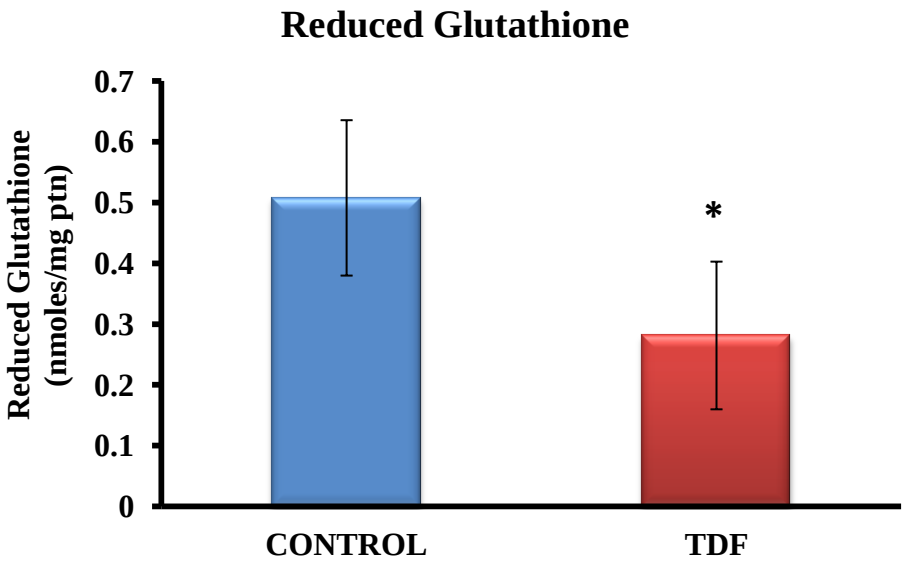

Figure: 6.1.5 Effect of TDF on reduced glutathione levels in the kidneys of control rats and TDF treated rats . Data represent mean ± SD, n=6 animals in each group. * p < 0.05 compared with controls.

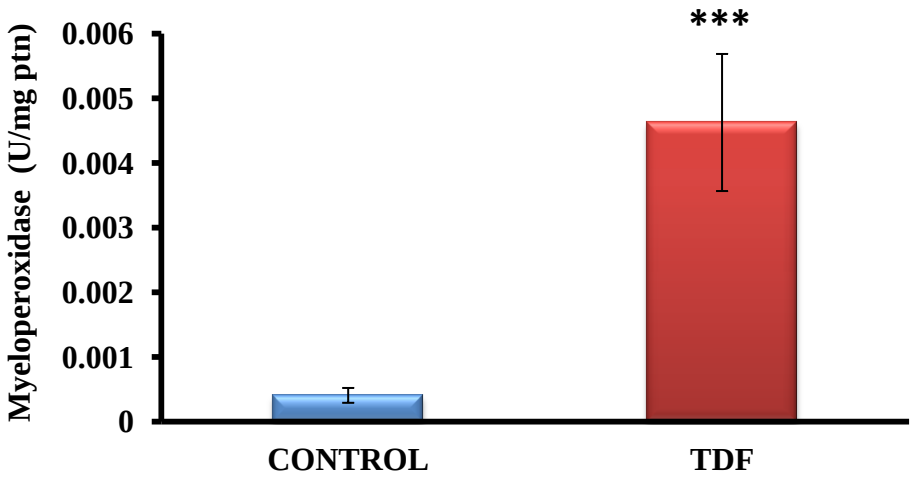

Figure: 6.1.6 Effect of TDF on myeloperoxidase activity in the kidneys of control rats and TDF treated rats. Data represent mean ± SD, n=6 animals in each group. *** p < 0.001 compared with controls.

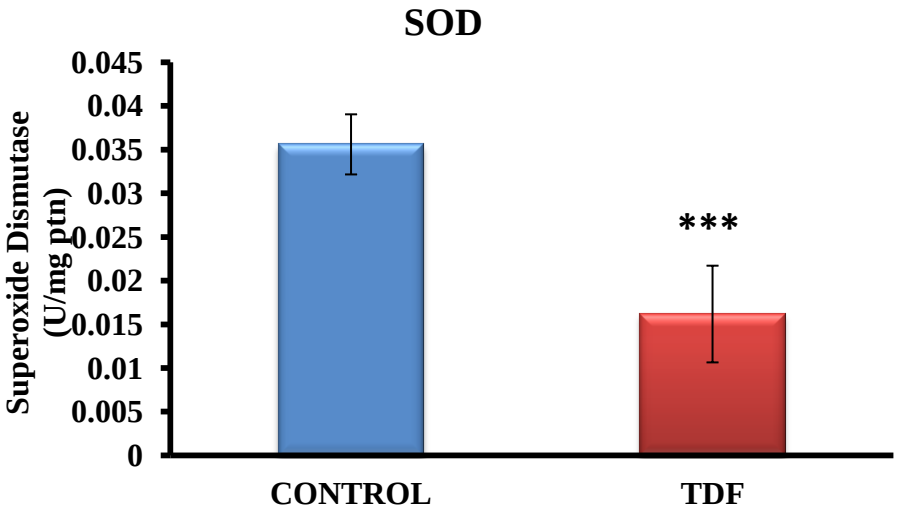

Figure: 6.1.7 Effect of TDF on SOD activity in the kidneys of control rats and TDF treated rats. Data represent mean ± SD, n=6 animals in each group. *** p < 0.001 compared with controls.

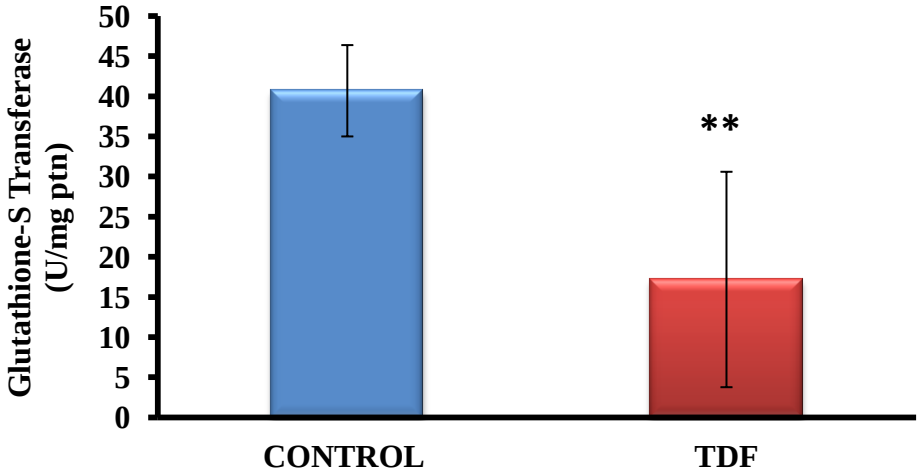

Figure: 6.1.8 Effect of TDF on Glutathione S-transferase activity in the kidneys of control rats and TDF treated rats. Data represent mean ± SD, n=6 animals in each group. ** p < 0.01 compared with controls.

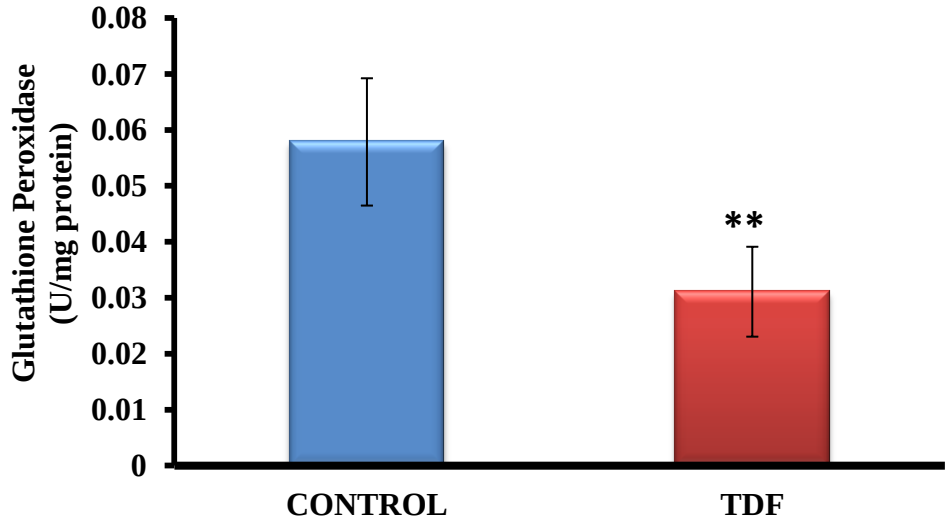

Figure: 6.1.9 Effect of TDF on glutathione peroxidase activity in the kidneys of control rats and TDF treated rats. Data represent mean ± SD, n=6 animals in each group. ** p < 0.01 compared with controls.

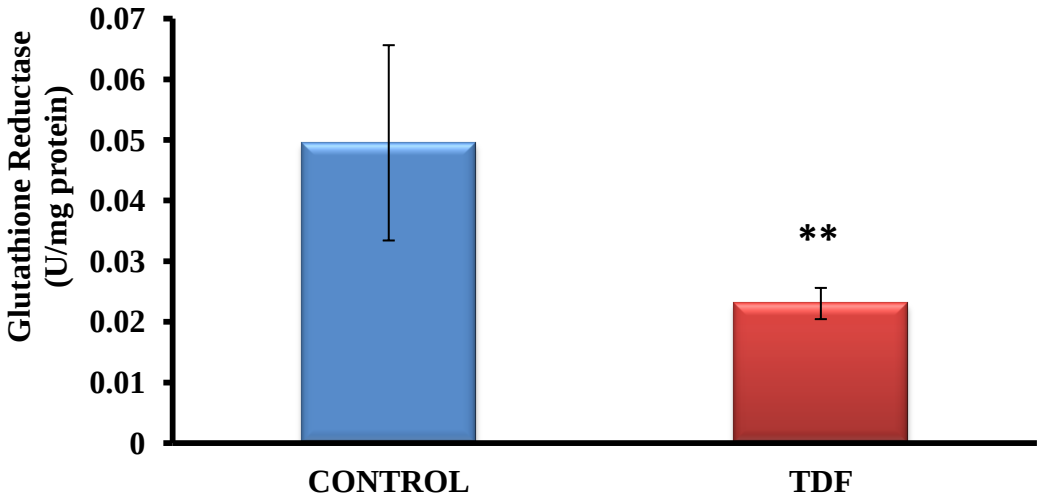

Figure: 6.1.10 Effect of TDF on glutathione reductase activity in the kidneys of control rats and TDF treated rats. Data represent mean ± SD, n=6 animals in each group. ** p < 0.01 compared with controls.

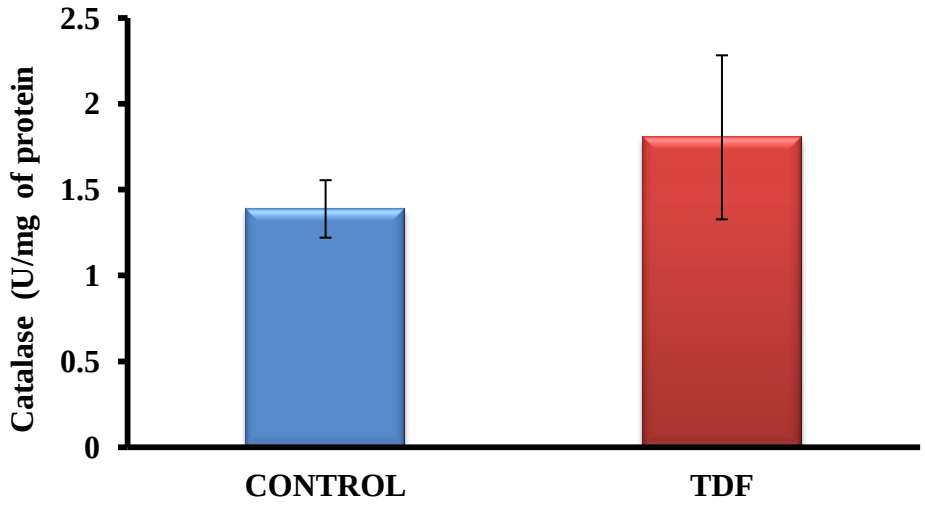

Figure: 6.1.11 Effect of TDF on catalase activity in the kidneys of control rats and TDF treated rats. Data represent mean ± SD, n=6 animals in each group.

(b) Expression level of HSP 70 and HO-1 by immunohistochemistry, western blot and Real-time PCR :

- In the control rat kidneys, immunohistochemical localisation of HSP 70 protein showed moderate staining in the glomerulus, whereas proximal and distal convoluted tubules showed high intensity of stain in the cortex. In the medulla the loop of Henle, and collecting ducts stained intensly for HSP70. In the TDF treated rat kidneys, only mild staining in the glomerulus, proximal and distal convoluted tubules of the cortex, mild stain in the loop of Henle and collecting ducts of medulla were observed (Figure:6.2.1).

  Regarding HO-1 immunostaining, mild staining was observed in the glomerulus and negligible staining in kidney tubules of control rats. Negligible staining for HO-1 was observed in the cortex and medulla of TDF treated rats as compared with control (Figure:6.2.2).

- Immunoblots of Heme oxygenase (HO-1) (Figure:6.3.2 A&B) and HSP 70 (Figure:6.3.1 A&B) revealed siginificant reduction in the protein expression in both oxidative stress related proteins.

- PCR of mRNA gene expression of HSP 70 and HO-1:

Figure: 6.4.3 shows representative image of the gel confirming the integrity of RNA isolated.

To determine whether mRNA gene expression level of HSP 70 and HO-1 was regulated by TDF, we examined the effect of TDF on HSP70 and HO-1 mRNA expression level by qPCR and normalized by β-actin. As shown in (Figure:6.4.1), (Figure:6.4.2) TDF treatment significantly downregulated the gene expressions of HSP70 and HO-1.

Figure: 6.2.1 Immunohistochemistry of HSP 70

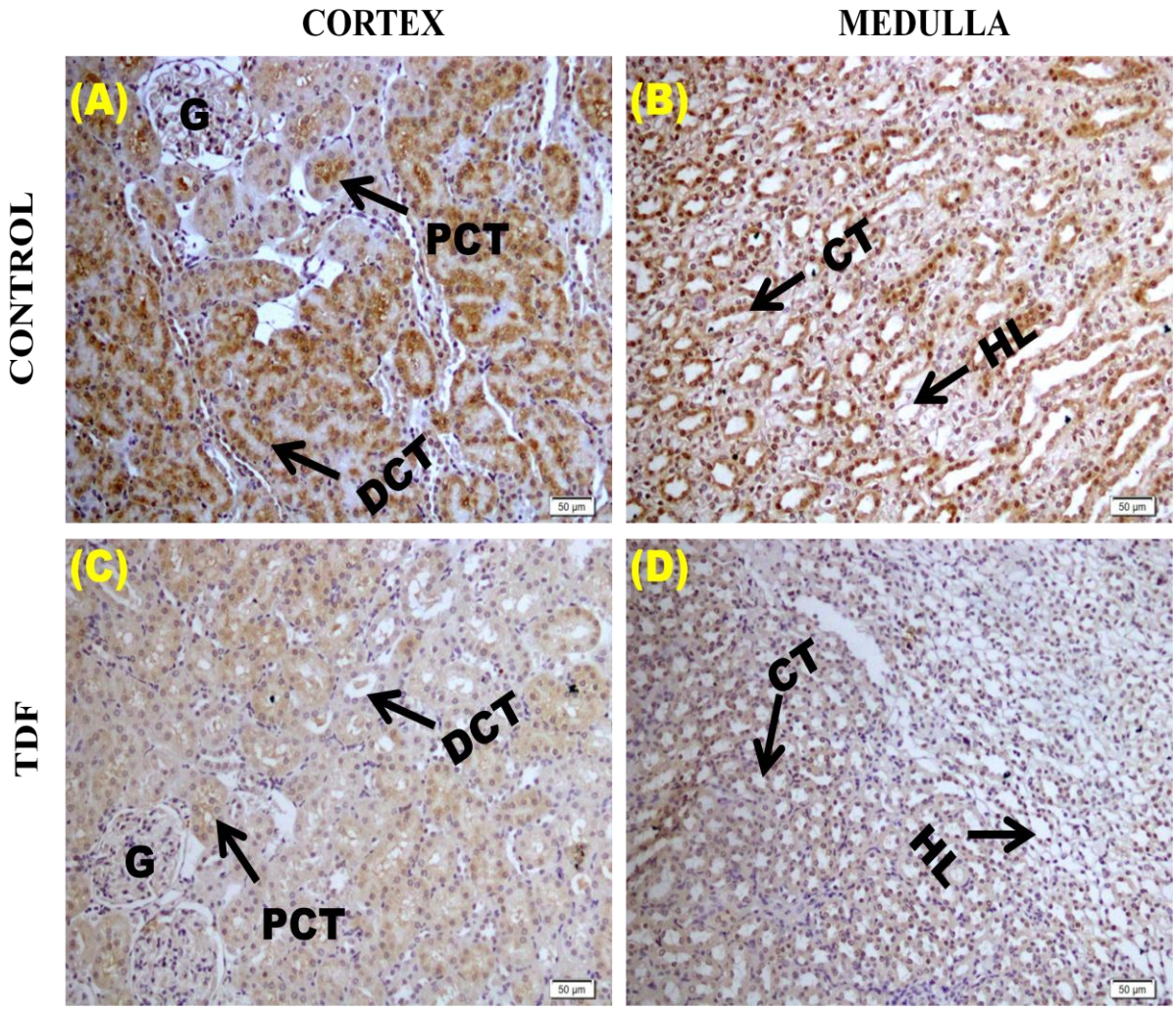

Figure: 6.2.1 Representative immunohistomicrographs of HSP 70 protein expression in the kidneys of control rats (A & B) and TDF treated rats (C &D). Scale Bars = 50µm

(A) & (B) Moderate expression of HSP 70 in glomeruls, increased expression in the proximal convoluted tubules (PCT) and distal convoluted tubules (DCT) of cortex region, diffused expression in the region of Henle's loop (HL) and collecting tubules (CT) of control rats.

(C) & (D) Decreased expression of HSP70 in the glomerulus (G), focal positivity in the proximal convoluted tubules (PCT) and distal convoluted tubules, (DCT) of the cortex region, low intensity of stain in the loop of Henle, collecting tubule (HL, CT) of the medulla of TDF treated rat.

Figure: 6.2.2

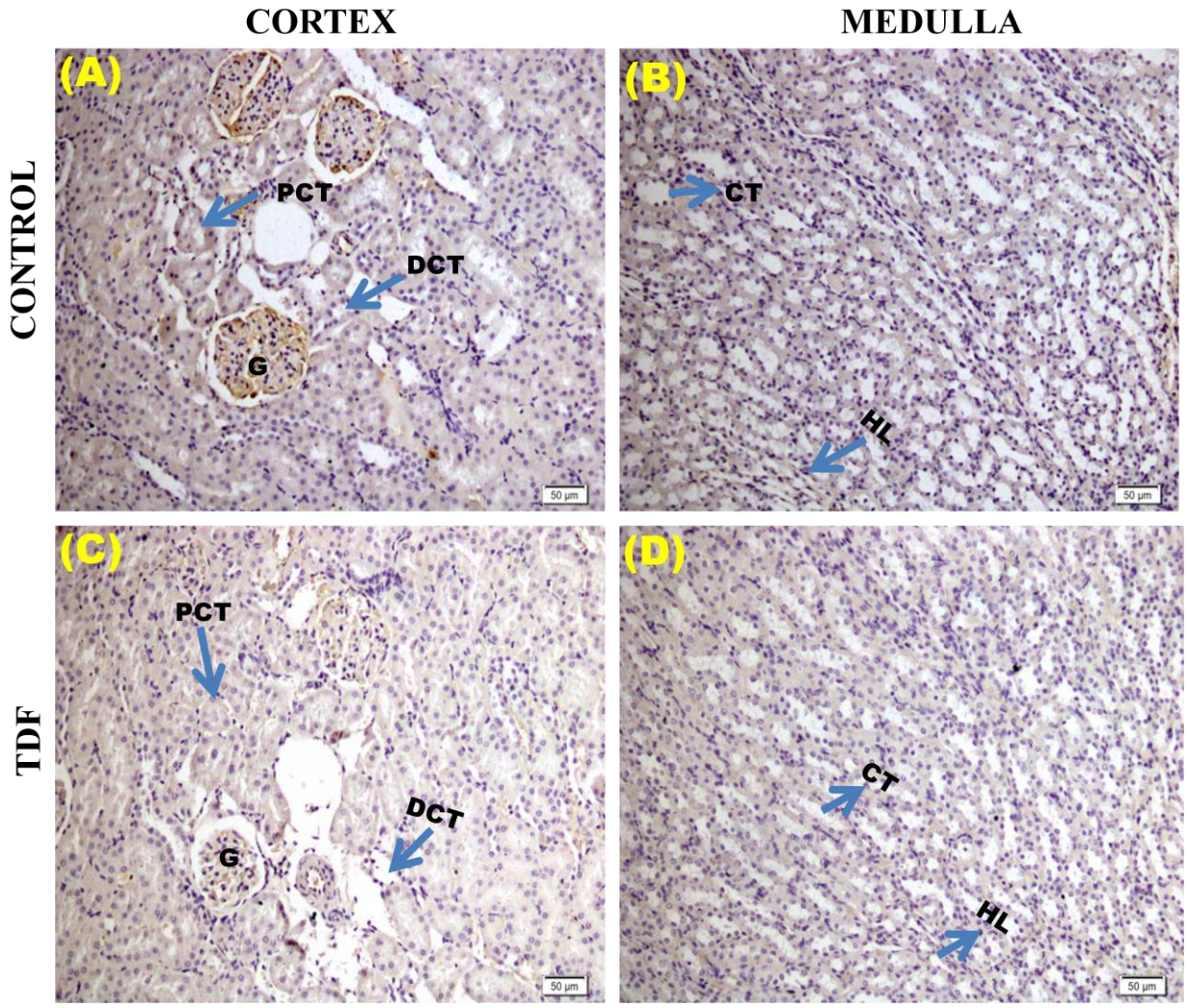

Figure: 6.2.2 Representative immunohistomicrographs of HO-1 protein expression in the kidneys of control rats (A & B) and TDF treated rats (C &D). Scale Bars = 20µm

(A) & (B) **Mild expression of HO-1 in the Glomerulus (G), negative expresssion in proximal convoluted tubule (PCT), distal convoluted tubules (DCT) of cortex and loop of Henle (HL) and collecting tubules (CT) in control rats.**

(C) & (D) **Negative expression of HO-1 in the glomerulus (G),proximal convoluted tubules (PCT), distal convoluted tubules (DCT) of the cortex, and in the loop of Henle (HL) and collecting tubule (CT) of the medulla of TDF treated rats.**

Figure: 6.3.1 Immunohistochemistry Heme oxygenase-1

Figure: 6.3.1

(A)

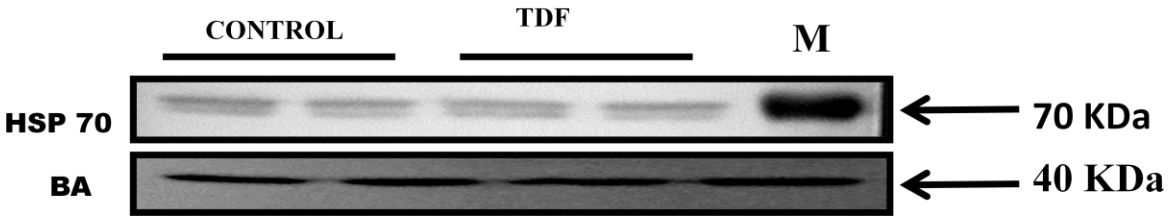

(B)

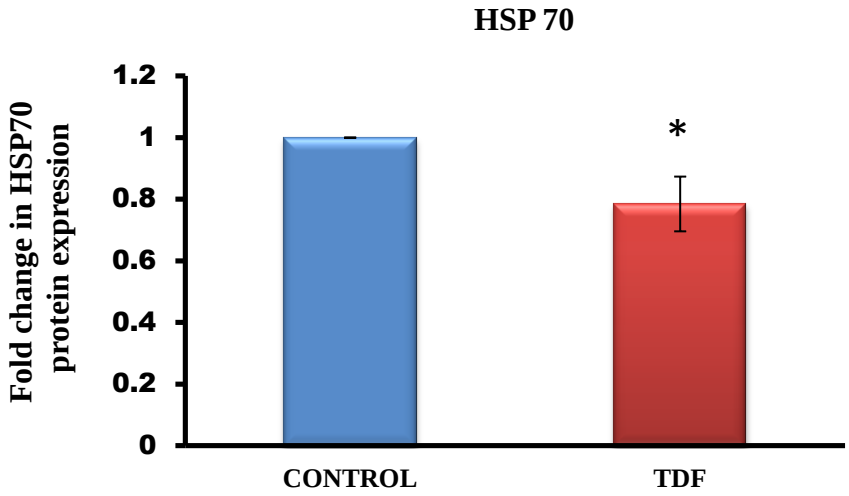

Figure: 6.3.1 A: Representative western blots of HSP 70 protein (70 kD) bands levels in the kidneys of control rats and TDF-treated rats (n=5 in each group), as assessed by using a 10% polyacrylamide gel, loading 100µg protein per lane. β-actin was used as the loading control.

Figure: 6.3.1 B: Relative concentration of HSP 70 in renal homogenates as analysed by densitometric quantification of bands in the control rats and TDF-treated rats (n=5 in each group). Data represents mean ± SD, obtained by image analysis of western blots with the concentration of the controls set at one. * indicates $p<0.05$ when compared with control values.

Figure:6.3.2

(A)

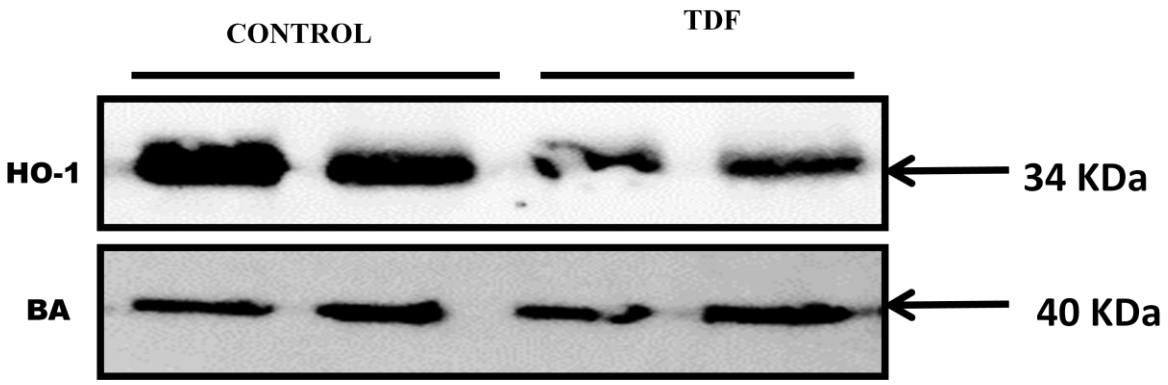

(B)

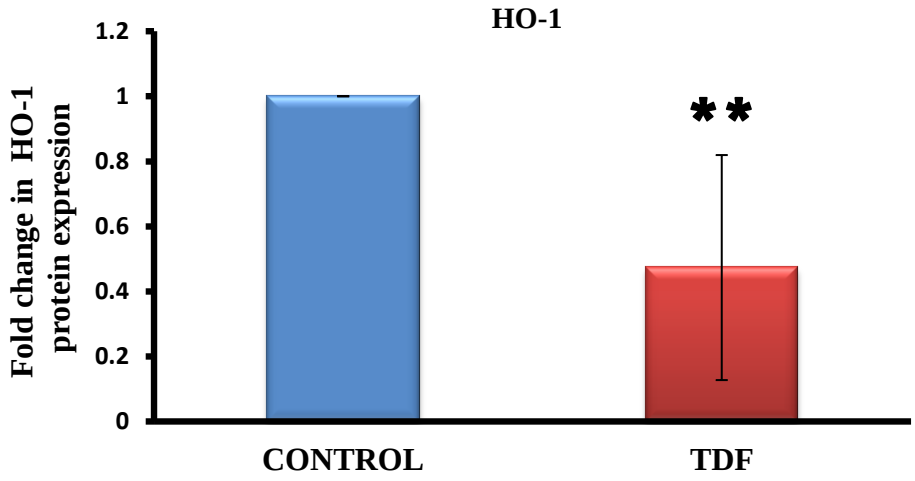

Figure: 6.3.2 A: Representative western blots of Heme oxygenase-1 protein levels (34kD) bands in renal homogenates of control rats and TDF-treated rats (n= 5 in each group), as assessed by using a 10% polyacrylamide gel, loading 100µg protein per lane. β-actin was used as the loading control.

Figure: 6.3.2 B: Relative concentration of Heme oxygenase-1 in renal homogenates as analysed by densitometric quantification of bands of western blots in control rats and TDF-treated rats (n=5 in each group). Data represents mean ± SD, obtained by image analysis of western blots with the concentration of the controls set at one. ** indicates $p<0.01$ when compared with corresponding control values.

Figure: 6.4.1 mRNA gene expression of HSP 70

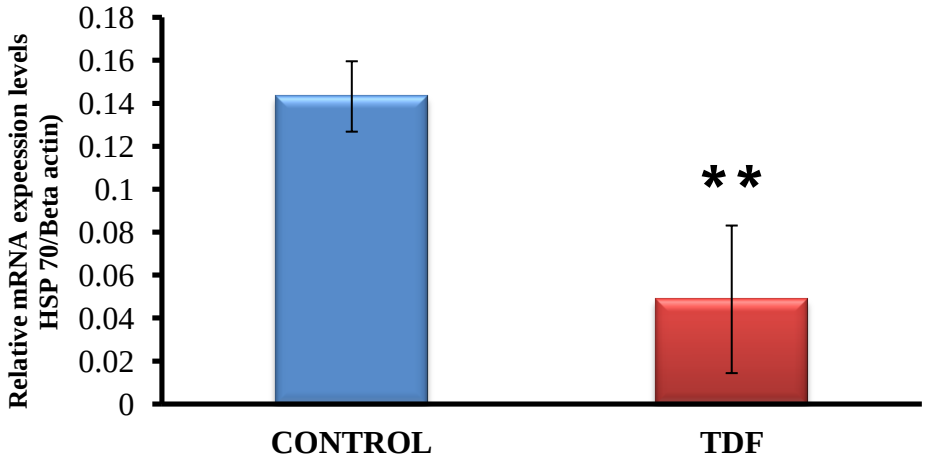

Figure: 6.4.1 Relative expression of HSP 70 mRNA in kidneys of control rats and TDF treated rats. Data represent mean ± SD of 5 rats in each group . **indicates p<0.01 when compared with control values.

Figure: 6.4.2 mRNA gene expression of HO-1

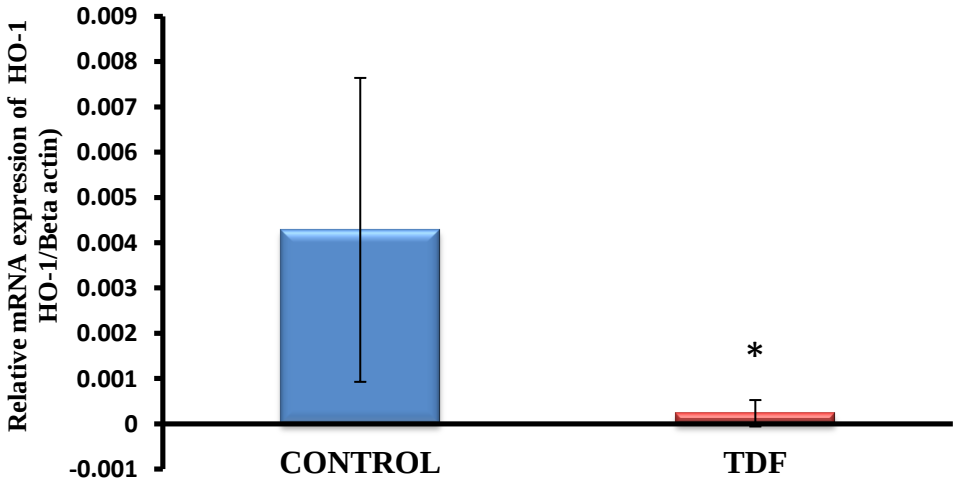

Figure: 6.4.2 Relative mRNA expression of Heme oxygenase-1 gene in the kidneys of control rats and TDF treated rats. Data represent mean ± SD of 5 rats in each gruop. * p<0.05 when compared with control values.

Figure: 6.4.3 RNA AGAROSE GEL ELECTROPHORESIS

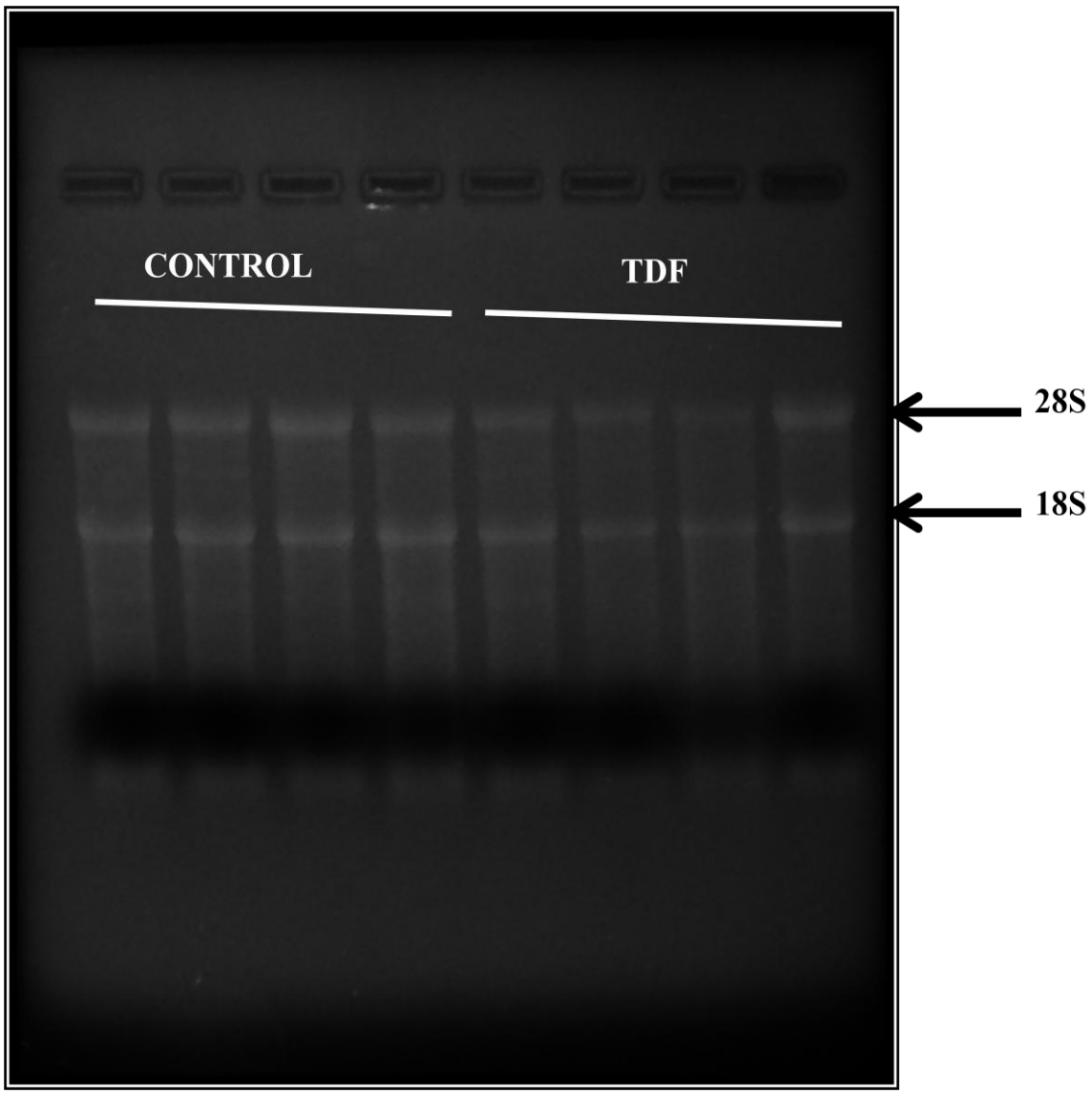

Figure: 6.4.3 Representative Agarose gel electrophoresis image of RNA isolated from the kidneys of control rats and TDF treated rats indicating integrity of RNA

(B) Studies on the effect of TDF on nitrosative stress parameters in the kidney tissues

a. **Tissue Nitrate levels**-Nitrate levels were significantly increased in the kidneys of TDF treated rats as compared with control (Figure:6.5.1).

b. Immunohistochemical localization of Nitrotyrosine in the control rats, basal nitrotyrosine immunoreactivity was found in the cortex and medulla, with proximal tubular cells showing least staining for NT. Nitrotyrosine expression was up-regulated in the cortex and medulla of TDF treated rats (Figure:6.5.2). The staining for NT was more intense in the medulla as compared with cortex. In the cortex, nitrotyrosine was localized to the apical region of proximal tubular cells, glomerulus, and distal convoluted tubules. In the medulla, the collecting duct and LH stained intensly for NT.

- 3NT levels as measured by Western blot analysis showed a significant increase in the TDF treated rat kidneys as compared with control groups (Figure:6.5.3)

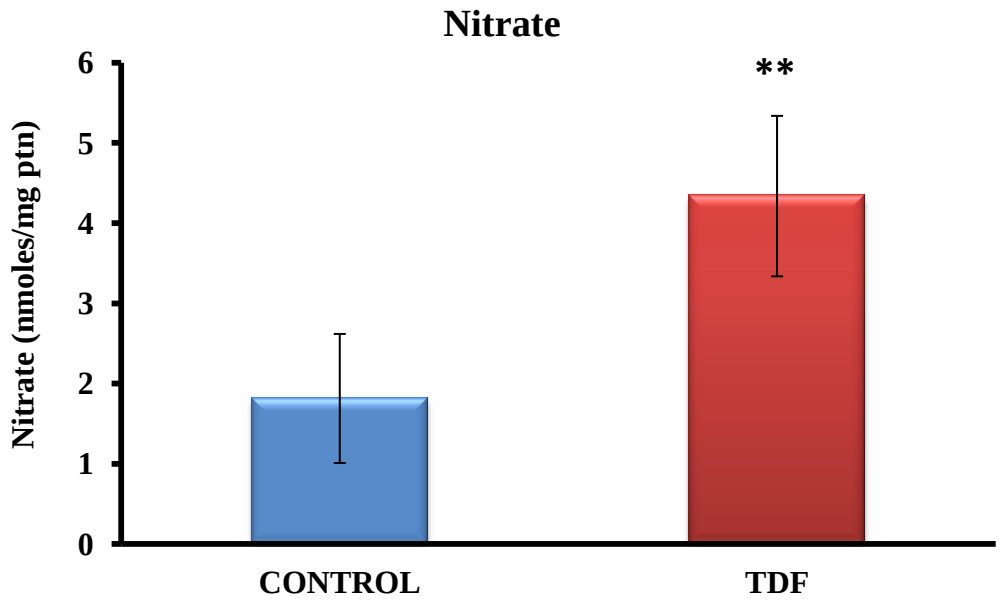

Figure: 6.5.1 Effect of TDF on nitrate levels in the kidneys of control rats and TDF treated rats. Data represent mean ± SD, n=6 animals in each group. ** $p < 0.01$ compared with controls.

Figure: 6.5.2 Immunohistochemical staining for nitrotyrosine

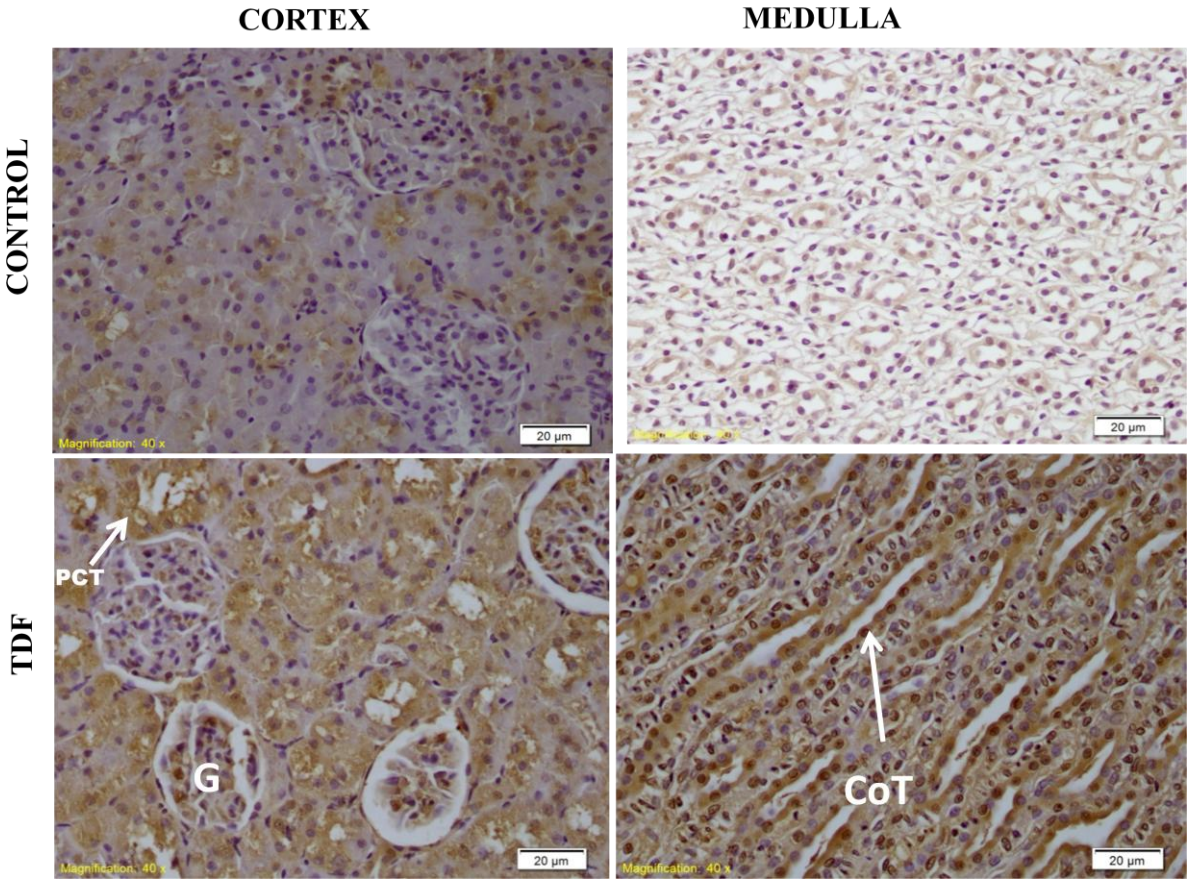

Figure: 6.5.2 Representative images of immunohistochemical detection of 3 NT control (A) & (B) and TDF treated (C) & (D). Scale Bars = 20µm

(A) & (B) In control rats, basal nitrotyrosine immunoreactivity was found in the cortex and medulla, with proximal tubular cells showing least staining for NT.

(C) & (D) Nitrotyrosine expression was up-regulated in the cortex and medulla of TDF treated rats. The staining for NT was more intense in the medulla as compared with cortex. In the cortex, nitrotyrosine was localized to the apical region of proximal tubular cells, glomerulus, and distal convoluted tubules. In the medulla, the collecting duct and LH stained intensely for NT. Scale bar 20µm. G -glomerulus, PCT-proximal convoluted tubule, DCT- distal convoluted tubule , HL-Henles loop. CoT- collecting tubule.

Figure: 6.5.3

(A)

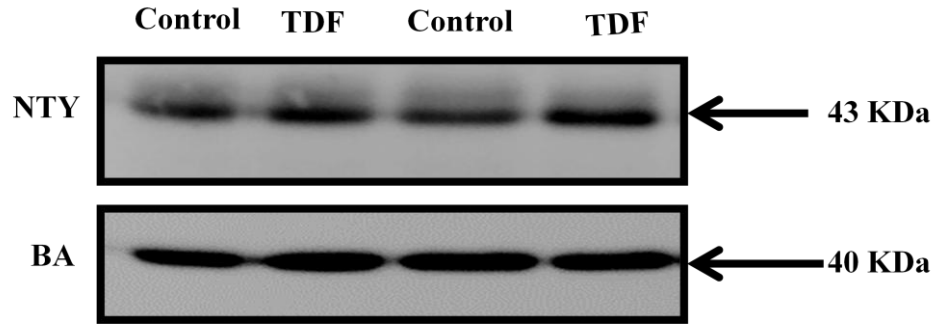

(B)

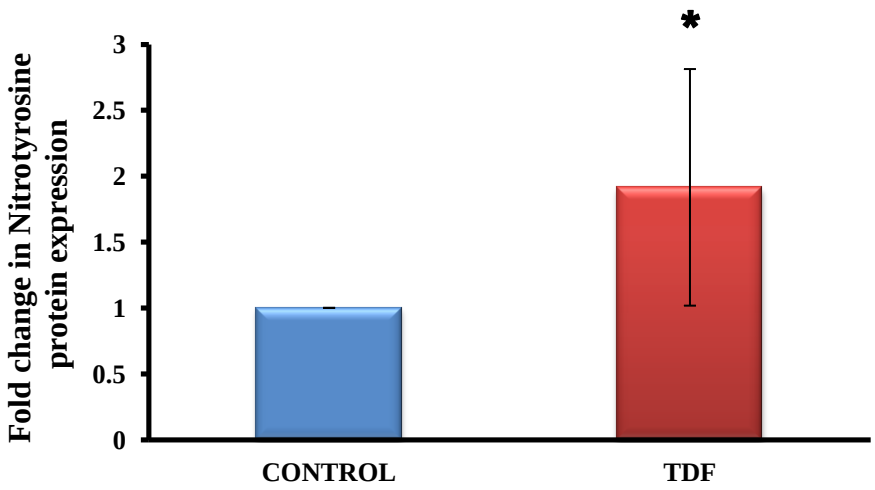

Figure: 6.5.3 A Representative Western blots of nitrotyrosine protein levels in renal homogenates of control rats and TDF-treated rats (n=5 in each group), as assessed using a 10% polyacrylamide gel, loading 100µg protein per lane. β-actin was used as the loading control.

Figure: 6.5.3 B Relative concentration of nitrotyrosine in renal homogenates as analysed by densitometric quantification of bands of western blots in control and TDF-treated rats (n=5 in each group). Data represents mean ± SD, obtained by image analysis of western blots with the concentration of the controls set at one. * $p<0.05$ when compared with control values.

DISCUSSION:

It is well known that damaged mitochondria are the main sources of reactive oxygen species. To overcome ROS induced damage to the lipids and proteins, cells are equipped with antioxidant defense systems that minimize the susceptibility to ROS. These defense mechanisms include antioxidants such as reduced glutathione and protein thiol, and antioxidant enzymes such as superoxide dismutase, catalase, glutathione peroxidase, glutathione reductase and glutathione S transferase. In the present study, we observed increase in protein carbonyl content, a sensitive indicator of oxidative damage to proteins, decrease in the level of the major intracellular antioxidant glutathione and decrease in the activities of glutathione related enzymes namely glutathione peroxidase, glutathione reductase and glutathione S transferase. Besides, the activity of SOD, an important antioxidant enzyme was decreased in the kidneys of TDF treated rats as compared with control.

Protein carbonyl content (Pco) is reported to be a sensitive and early marker of oxidative stress to tissues as compared with lipid peroxidation (175). The present study shows for the first time an increase in Pco content in the kidneys following treatment with TDF. It is well documented that protein oxidation marks the protein for degradation (398). Proteins (enzymes) regulate various metabolic pathways and damage to proteins may result in the alteration of normal metabolic pathway resulting in cell death and tissue damage. In general, besides their direct damaging effects on the tissues, reactive oxygen species trigger the accumulation of leukocytes in the tissues involved, and thus aggravates tissue injury indirectly through activated neutrophils. The activated neutrophils secrete myeloperoxidase (MPO) and other proteases (390). In turn, MPO plays important role in oxidant production by neutrophils. In the present study a marked elevation (9 fold) in MPO activity was observed after TDF treatment of rats, indicating that neutrophil accumulation contributes to TDF induced small renal damage. The generation of oxidants by neutrophils is critical to host defenses against microbial pathogens (399,400). Oxidant production begins with a

cytoplasmic membrane associated NADPH oxidase, which reduces molecular oxygen to superoxide. Dismutation of superoxide then yields hydrogen peroxide (H_2O_2), but both superoxide and H_2O_2 are relatively nontoxic to bacteria. However, activated neutrophils also secrete the heme protein MPO (16). MPO plays a fundamental role in oxidant production by neutrophils and has been used as an effective quantitative index of inflammation due to correlation between MPO activities and histological analysis of neutrophil infiltration (401). A unique activity of MPO is its ability to use chloride as a co-substrate with hydrogen peroxide to generate chlorinating oxidants such as hypochlorous acid, a potent antimicrobial agent. However, evidence has emerged that MPO-derived oxidants contribute to tissue damage and the initiation and propagation of acute and chronic vascular inflammatory disease. The MPO-hydrogen peroxide-chloride system leads to a variety of chlorinated protein and lipid adducts that in turn may cause dysfunction of cells in different compartments of the kidney. Hypochlorous acid reacts readily with amino acids, proteins, carbohydrates, lipids, nucleobases and antioxidants (402). Proteins are the major molecular target for hypochlorous acid. Of primary importance among the hypochlorous acid-mediated protein modifications are tyrosine chlorination, formation of chloramines and carbonyls (403), and in some cases cross-linking (404). Protein carbonyl is a biomarker of oxidative hypochlorous acid attacks on proteins, and in the inflamed lung, for instance, a high correlation between protein carbonyl concentration and MPO activity was observed (405). Thus, carbonyl groups represent an irreversible protein modification, often leading to the inactivation of the proteins (376,406,407)]. It is noteworthy to mention that in the present study, a significant increase in MPO activity (9 fold) and protein carbonyl content (2 fold) was observed in the kidneys of TDF-treated rats. This finding suggests that activated neutrophils contribute to increased ROS generation and oxidative stress observed in TDF treated rat kidneys.

In the present study, a significant decrease in the levels of reduced glutathione in the kidneys was observed following treatment with TDF. It is well established that depletion of reduced glutathione in tissues promotes oxidative stress and tissue injury (406). The decrease in the activities of the free radical detoxifying enzymes, GPO and GSTase in the kidneys of TDF treated rats observed in the present study may be due to lack of availability of sufficient amounts of reduced glutathione as a coenzyme for these enzymes. The activity of glutathione reductase, the enzyme crucial for the regeneration of reduced glutathione from oxidized glutathione was significantly less in the kidneys of TDF treated as compared with that of control. The reduced activity of this enzyme may account for the decreased availability of reduced glutathione for scavenging reactive oxygen species, thereby rendering the cells to increased oxidative stress and tissue injury. Thus, a significant decrease in reduced glutathione levels promoted by TDF, leads to a reduction of effectiveness of the antioxidant enzyme defense system, thereby sensitizing the cells to reactive oxygen species (408).

With respect to the activities of other antioxidant enzymes, superoxide dismutase and catalase, a significant decrease in the activity was observed with respect to SOD only. SOD provides the first line of defense against superoxide generated in mitochondria. SOD competes with nitric oxide for reaction with superoxide and prevents generation of peroxynitrite, a potent oxidant that can modify proteins to form 3-nitrotyrosine (376). Thus, sufficient amounts of catalytically competent SOD are required to prevent tissue damage. Inactivation of SOD could lead to self-amplification of oxidative stress in the tissues progressively enhancing peroxynitrite production and secondary damage.

Next, we investigated the role of the antioxidant proteins HSP70 and HO-1 in TDF induced renal damage. For this, we studied the protein expression and mRNA expression of these two proteins by immunostaining and qPCR respectively. The immunoexpressions of HSP 70 and HO-1 were decreased in the kidneys of TDF treated rats as compared with control. Consistent with this, the protein and mRNA expression revealed the downregulation of the HSP 70 and Heme oxygenase-

1. Significant down regulation of renal expression of HSP 70 and Heme oxygenase-1 has been reported in pathological conditions such as ischemia, nephrotoxins, nephritides and in experimental diabetes (393,396).

The cytotoxic potential of NO is a consequence of its to form peroxy nitrite (409),which is a potent nitrating and oxidizing agent. Peroxynitrite readily reacts with proteins to form 3-nitrotyrosine (409), or oxidation of thiol groups to form nitrosothiols (410), which can either lead to inactivation or activation of the proteins (410,411). 3-NT, is considered as the footprint of ONOO, and its appearance in tissue samples is taken as a diagnostic tool for exposure to peroxynitrite (77). In healthy rats, minimal staining for nitrotyrosine was seen in the epithelial cells of proximal tubules in agreement with the findings of Bian et al (412). TDF treatment resulted in increased 3 NT lervel both immunohistochemical method and immunoblot thereby providing evidence for peroxynitrite formation.

Based on these observations it is concluded that oxidative stress, nitrosative stress, glutathione depletion, decrease in the activities of antioxidant enzymes , down regulation of antioxidant proteins HSP 70 and HO-1 ,and neutrophil infiltration contribute to TDF induced renal damage in rats. The sources of ROS in TDF induced kidney injury may be the damaged mitochondria and activated neutrophils. However, other sources of ROS such as xanthine oxidase, NADPH oxidase, etc. can contribute to increased ROS production in the kidneys of TDF treated rats.The source of RNS may be the mitochondrial NOS.

STUDY IV

Tenofovir induced renal damage is associated with activation of NF-κB inflammatory Signaling Pathway and PARP overactivation

ABSTRACT

Reactive oxygen species is a potent stimulus for the activation of , a key transcription factor, which is known to mediate inflammation by regulating the expression of cytokines and chemokines. In normal resting state, NF-κB is silenced by its specific inhibitor, IκB in the cytosol. Upon activation, after phosphorylation and degradation of IκB, NF-κB is released and translocated in to nucleus where it promotes the expression of inflammatory gene products such as TNF-α, inducible nitric oxide synthase (iNOS), cyclooxygenase (COX)-2, intercellular adhesion molecule and induces inflammatory activation of lymphocytes, monocyte/macrophages and endothelial cells.

In the present study, we investigated the effect of chronic TDF administration on (a). protein expression by western blot and immunostaining methods, gene mRNA expression by PCR, and activity by ELISA ,and IκB-α protein expression by western blot and mRNA expression by PCR, (b) iNOS protein expression by western blot and immunostaining methods, gene mRNA expression by PCR, (c) Protein tyrosine nitration and nitrosocysteine formation by Western blot and immunostaining (d) COX-2 gene mRNA expression and protein expression, (e) TNF α protein expression by western blot, and immunostaining, and mRNA expression by PCR, and (f) PLA_2 protein expression by western blot and immunostaining methods ,(g) MMP-9 activity by gelatin zymogram. In addition, we also determined the PARP-1 protein expression by immunofluroscence and western blot , and caspase 3 protein expression by western blot, mRNA expression by RT PCR , and activity by fluorimetry.

The results of the present study show that NF-κB signaling, a principal signaling pathway mediating pro-inflammatory response in various conditions, was activated in the kidneys of TDF treated rats , as shown by an increase in the mRNA and protein expressions of , and its target proinflammatory genes, iNOS, COX-2, TNF α and PLA_2. Consistently, decrease in IκB-α protein expression was observed; however, no change in mRNA expression was observed. The results also show PARP

overactivation and increased caspase-3 protein and activity in the kidneys of TDF treated rats as compared with control.

It is concluded that the activation of and its downstream proinflammatory target genes iNOS, COX-2, TNF-α, PLA_2 and MMP-9 contribute to the pathophysiology of TDF induced renal damage. It is also suggested that PARP overactivation, and increased caspase 3 activity may contribute to proximal tubular necrosis and apoptosis respectively in the TDF treated rats.

INTRODUCTION

Reactive oxygen species, inflammatory cytokines (eg, tumour necrosis factor-α (TNF α), activate the , a key transcription factor, which is known to mediate inflammation by regulating the expression of cytokines and chemokines (413). The present study is an attempt to verify whether NF-κB signaling pathway plays a role TDF in nephrotoxicity.

In normal resting state, NF-κB is silenced by its specific inhibitor, IκB in the cytosol. Classical IκBs, like the prototypical protein IκBα, sequester NF-κB transcription factors in the cytoplasm by masking of their nuclear localization signals (NLS),thereby binding of NF-κB to the DNA is inhibited. Upon activation, after phosphorylation and degradation of IκB, NF-κB is released and translocated into nucleus where it promotes the expression of inflammatory gene products such as TNF-α , inducible nitric oxide synthase (iNOS), cyclo-oxygenase (COX-2), intercellular adhesion molecule and induces inflammatory activation of lymphocytes, monocyte/macrophages and endothelial cells (413). Recent studies have shown a role of the NF-κB in some organ injuries such as kidney and liver (414,415).

NO (product of iNOS) (416) and PGs (product of COX-2) (417) play key roles in defense mechanisms against xenobiotic stimuli, it has been perceived that the proteins (i.e., NOS or COX) are main regulators having harmful role in the pathological process of inflammation. In case of eicosanoids, it has been shown that production of a large amount of PGs have detrimental effects in

inflammation-related diseases, which were mainly dependent on the COX-2 (418). The cytotoxic potential of NO is a consequence of its ability to form peroxy nitrite (409), which is a potent nitrating and oxidizing agent. Peroxynitrite readily reacts with proteins to form 3-nitrotyrosine (410) or oxidation of thiol groups to form nitrosothiols (410) which can either lead to inactivation or activation (411) of the proteins. 3- Nitrotyrosine can be used as a marker for endogenous production of peroxynitrite (77).

TNF α is a proinflammatory cytokine released by immune cells, intrinsic renal cells, epithelial and mesangial cells capable of inducing renal tubular cell apoptosis and renal dysfunction by multiple ways (40,419).

The expression profile of MMPs in the kidney are complex and species dependent. MMP-2,3,9,13,14,24 are all expressed in the kidney (264). The profile of gelatinase expression in the kidney has been well charactrised in both rats and humans. The expression of MMP-9 is confined to the glomerulus and initial parts of the PCT (266,267). The role of MMPs in acute kidney injury in pathology related to oxidative stress such as ischemia-perfusion has been established experimentally (268). The mechanism of activation of MMPs by reactive oxygen and nitrogen species is thought to involve the oxidation of sulphydryl groups located on cysteine residues that form the auto inhibitory peptide domain, thus influencing its interaction with zinc at the catalytic site. This could result in changes that may induce, modulate or inhibit the enzyme activity in response to redox state within the cell (273). Studies have reported on the MMP-9 show an increase in enzyme activity coinciding with evidence of S-nitrosylation of the pro-peptide domain on mass spectroscopy (420). In addition to activation of the enzyme, exposure to $ONOO^-$ may also alter the structural binding characteristics, thus favouring an increase in MMP activity (421).

Therefore, the aim of our study was to evaluate the role of NF-κB signaling pathway in TDF induced renal injury. The specific objectives were to study the effect of chronic TDF administration

on (a) NF-κB protein expression by western blot and immunostaining methods, NF-κB mRNA expression by PCR, and activity by ELISA.(b) iNOS protein expression by western blot and immunostaing methods, gene mRNA expression by PCR . (c) Protein tyrosine nitration and nitrosocysteine formation by Western blot and immunostaining (d) COX-2 gene and protein expression (e) TNF α protein expression by western blot, imunostaining, and mRNA expression by PCR. (f) MMP-9 protein and mRNA expression,and activity in the kidney.

BRIEF EXPERIMENTAL SETUP

Adult male Wistar rats (200–250gm) were used for the studies. They were housed in standard rat cages (421 × 290 × 190 mm). All animals were exposed to 12 hour light–dark cycles and allowed access *ad libitum* to water and standard rat chow.

Animal treatment

The rats were assigned randomly into 2 groups and were treated as follows.Group I (control): The rats in this group (n = 6) received sterile water by gavage.

Group II-The rats (n = 6) in this group received 600 mg/ kg body weight Tenofovir disoproxil fumarate daily by gavage for 35days.

Control animals were administered sterile water by gavage on the same schedule as TDF treatment and were killed at the same time point as that of TDF treated rats. The animals were weighed and sacrificed 24hrs after the final dose of the drug by light halothane. Both the kidneys were harvested, one kidney was fixed in neutral buffered formalin and paraffin embedded used for IHC and IF with 0.5µm section, another kidney was snap frozen in liquid nitrogen and used for the B protein and mRNA expressions of NF-κB gene and its target genes by western blot and RT PCR respectively .

- **Immunohistochemical localization of NF-κB p65, NTY, NCY, iNOS, COX-2, TNF-α, PLA2, PARP and caspase-3 in kidney**

- **Western blot analysis to determine the protein levels of iNOS, TNF-α, PLA2, Nitrotyrosine, nitrocysteine, NF-κB p65, IκB-α, PARP and Caspase-3 :**

  Whole cell lysate, nuclear and cytosolic extract were prepared from snap frozen kidney tissue as previously described in methodology section. The whole cell extract was used for the determination of nitrotyrosine (NT) and nitrocysteine (Ncy), iNOS , TNF-α and MMP-9. Nuclear fractions were used for the determination of NF-κB p65 and PARP, cytosolic fractions were used for IKB-α, and caspase 3. The concentration of protein in all tissue extract were determined (341). From this 100µg of protein extracts were subjected to SDS-PAGE followed by Western blotting using specific antibodies as described in methodology.

- **RT PCR quantification of NF-κB, IκB-α, iNOS, COX-2, TNF-α, Caspase 3 and MMP-9.**

  The obtained values were expressed as relative gene expression levels by normalizing with values of housekeeping genes (Beta-actin and GAPDH).

- **Quantification of Nuclear Factor kappaB p65 unit by ELISA**

  The nuclear levels of p65 may correlate positively with the activation of NF-κB pathway. The NF-κB/p65 ActivELISA (Imgenex, San Diego, USA) kit was used to measure NF-κB free p65 in the nuclear fraction and cytosolic fraction. The analysis was done according to the manufacturer's instructions. The results were expressed as ng/mg protein.

- **Quantification of caspase-3 activity by Flourimetry assay as described in the methodology section.**

Statistical analysis:

Statistical analysis of data obtained was carried out using the Statistics Package for the Social Sciences (SPSS) software package, version 16. Data represents mean ± SD, the difference between two groups were analysed by Mann-Whitney test. A p-value of less than 0.05 was taken as statistically significant.

RESULTS

A. Chronic TDF administration resulted in the upregulation of NF-κB protein expression, nuclear translocation of NF-κBp65 , NF-κB mRNA expression, and NF-κBp65 activity

(a) Effect of TDF on NF-κB p65 by immunohistochemistry:

The immunohistochemical studies revealed that negligible NF-κB expression(Figure:7.1.1), both in cortical and medullar structures of control rat kidneys. Immunohistochemical evaluation of kidneys of TDF treated rats showed increased expression of NF-κB both in the cortex as well as medulla.The medulla stained more intensely than cortex. In the renal cortex , diffuse and moderate NF-κB staining was seen in the glomerulus, and very minimal staining in the proximal and distal tubules. In the medulla, the Henle loops and collecting ducts showed intense staining for NF-κB.

(b) Effect of TDF on NF-κB protein levels in nuclear and cytoplasmic fractions:

NF-κB protein expression was markedly higher in the TDF treated rat kidneys as compared with control. Since p65 is a major component in the NF-κB complex activation, we examined p65 translocation to the nucleus by immunoblotting (examined nuclear and cytosolic protein levels) by Western blotting using p65- polyclonal antibodies. The results shown in (Figure:7.1.2 A), clearly reveal that the nuclear translocation of NF-κB was significantly greater in TDF treated rats. In control rats, p65 was detectable both in the cytosol and nuclear fractions, but predominantly

cytoplasm. In the TDF treated rats, p65 was higher than in controls and was present both in the nucleus and the cytoplasm. Fig.7.1.2B shows increased NF-κBp65 protein level in the nuclear fractions of TDF treated rat kidneys as compared with control. Fig. 7.2.1C is densitometric quantitification of NF-κBp65 , showing increased NF-κBp65 protein expression in the TDF treated rat kidneys.

(c) Effect of TDF on NF-κB p65 activity in the nuclear and cytoplasmic fractions:

The nuclear levels of p65 may correlate positively with the activation of the NF-κB pathway . Therefore, we determinded p65 level by ELISA . In the controls, p65 was very low both in the cytosolic fraction and nuclear fraction. In the TDF treated rat kidneys, nuclear activity of NF-κBp65 was much higher as compared with cytosolic activity. p65 activity increased by 18 fold in the cytosolic fraction and by 28 fold in the nuclear fraction as compared with control (Figure:7.1.3)

(d) Effect of TDF on NF-κB gene expression

The above observations were further supported by results of mRNA expression of NF-κB normalized with GAPDH by quantitative real-time RT-PCR . The control kidneys had moderate transcription of NF-κB gene. In the TDF treated rat kidneys, mRNA expression of NF-κB was significantly increased (75 %) as compared with control (Figure:7.1.4).

(A) Figure: 7.1.1 Immunohistochemistry of NF-κB p65

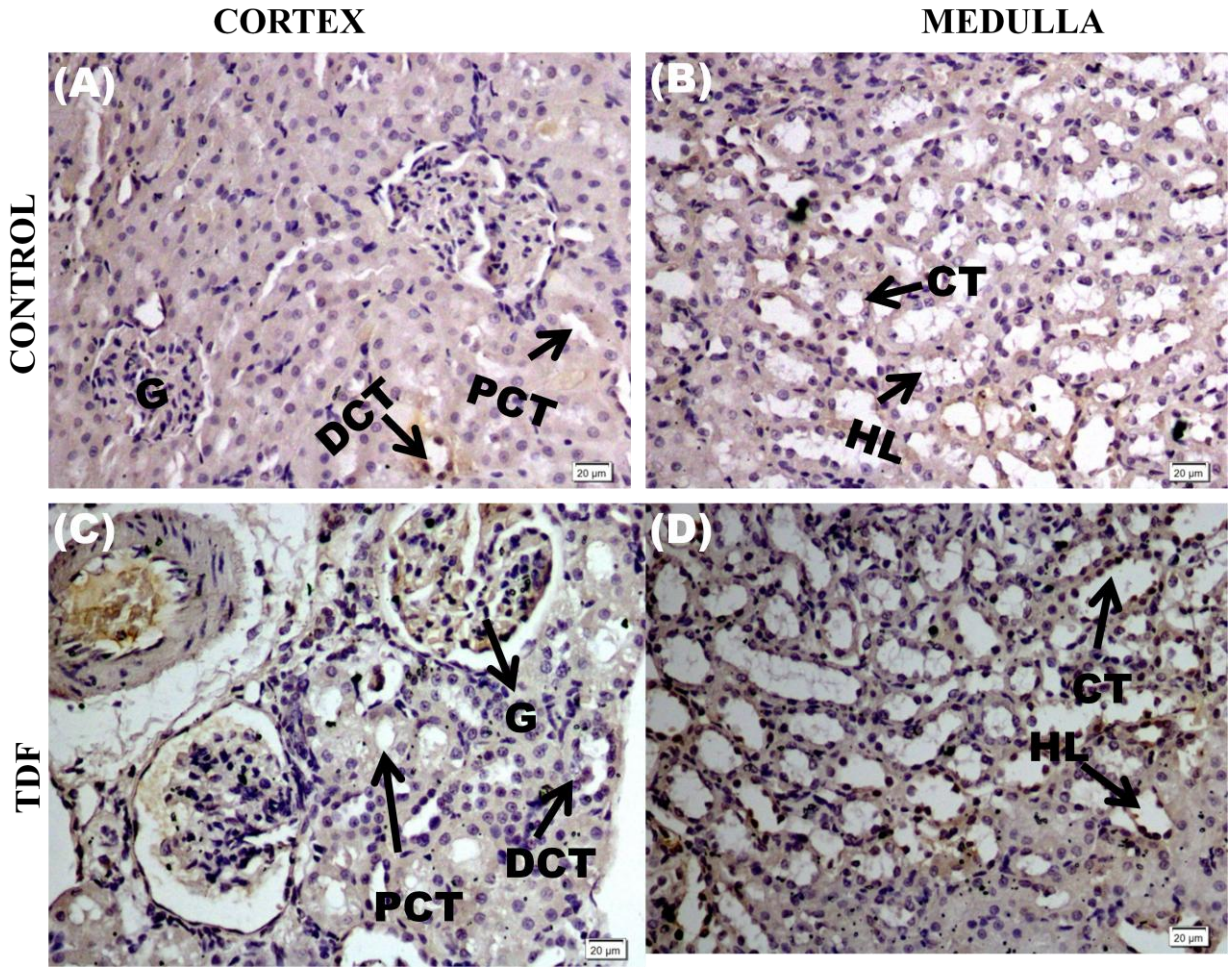

Figure: 7.1.1 Representative images of immunohistochemical detection of NF-κB p65 in control (A) & (B), TDF treated (C) & (D) rat kidneys. Scale Bars =20µm

A & B. Negligible staining for NF-κB was observed both in cortical and medullar structures of kidney taken from control rats.

C & D. However, in the renal cortex of TDF treated rats diffuse and moderate NF-κB staining was seen in the glomerulus, and almost no staining in the proximal and distal tubules. In the medulla, the Henle loops and collecting ducts showed visible increase in the immunostaining for NF-κB. Brown color indicates immunopositivity, n=5 rats for each group. Black arrows indicate G-glomerulus, PCT-proximal convoluted tubule, DCT- distal convoluted tubule ,HL-Henles loop. CT- collecting tubule.

Figure: 7.1.2 Western blot for NF-κB p65 protein

(A)

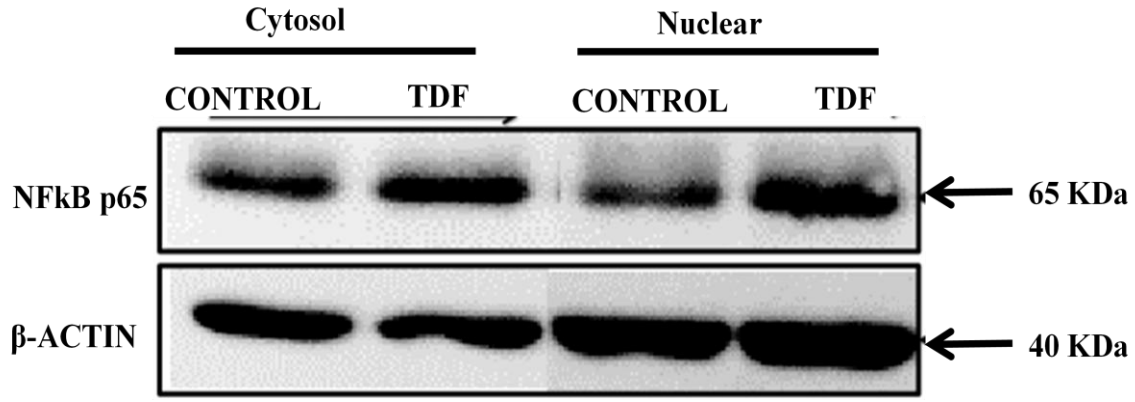

(B)

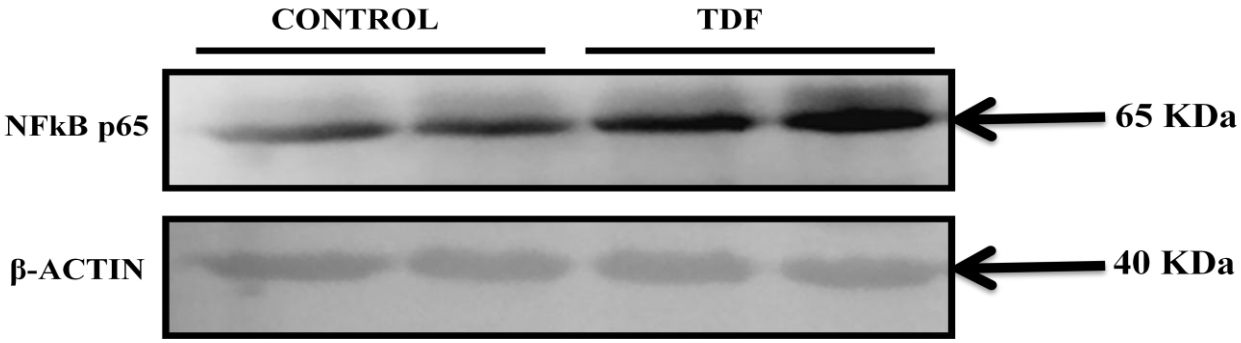

(C)

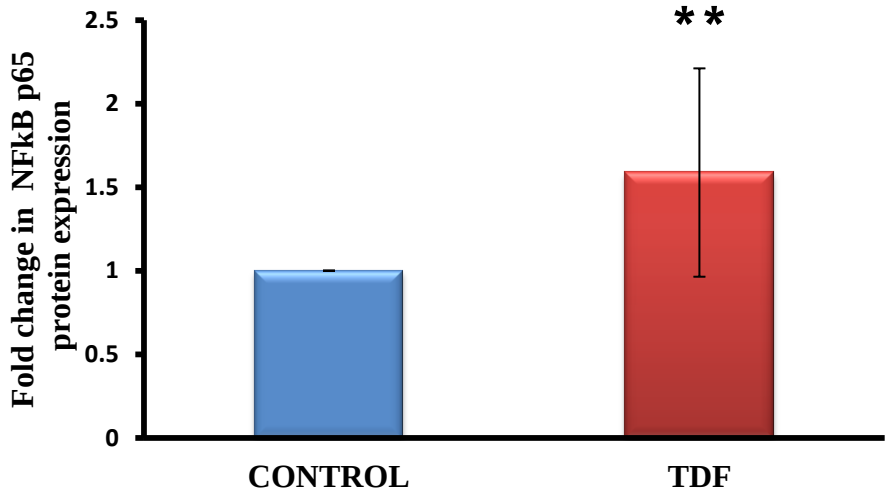

Figure:7.1.2 A: Representative western blots of nuclear and cytosolic NFκB p65 protein 65kD) bands levels in renal homogenates of control rats and TDF-treated rats (n=5 in each group, as assessed by using a 10% polyacrylamide gel, loading 100µg protein per lane. β-actin was used as the loading control.

Figure 7.1.2.B. Representative western blots of nuclear NFκB p65 protein levels in renal homogenates of control rats and TDF-treated rats (n=5 in each group) , as assessed by using a 10% polyacrylamide gel, loading 100µg protein per lane. β-actin was used as the loading control.

Figure:7.1.2 C: Relative concentration of nuclear NFκB p65 in renal homogenates as analyzed by densitometric quantification of bands of western blots in control and TDF-treated rats (n=5 in each group). Data represents mean ± SD, obtained by image analysis of western blots with the concentration of the controls set at one. ** indicates p<0.01 when compared with control values.

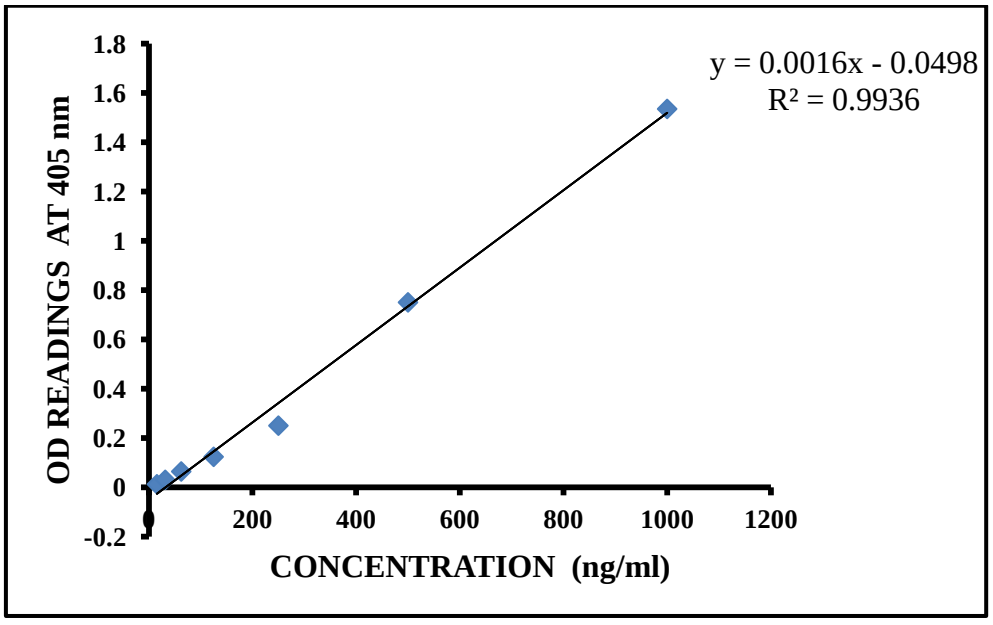

Figure:7.1.3 A. Standard curve for NF-κB p65. The graph depicts the log of the concentration of recombinant NF-κB p65 on the x-axis and log of the absorbance value for each of the standard samples used (s1-S7) on the y axis.

(A) NF-κBp65 activity in the cytosolic fractions of renal homogenates

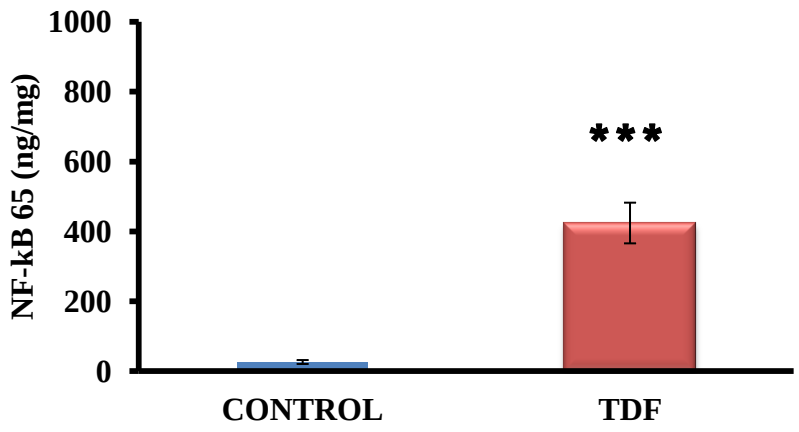

(B) NF-κBp65 activity in the nuclear fractions of renal homogenates

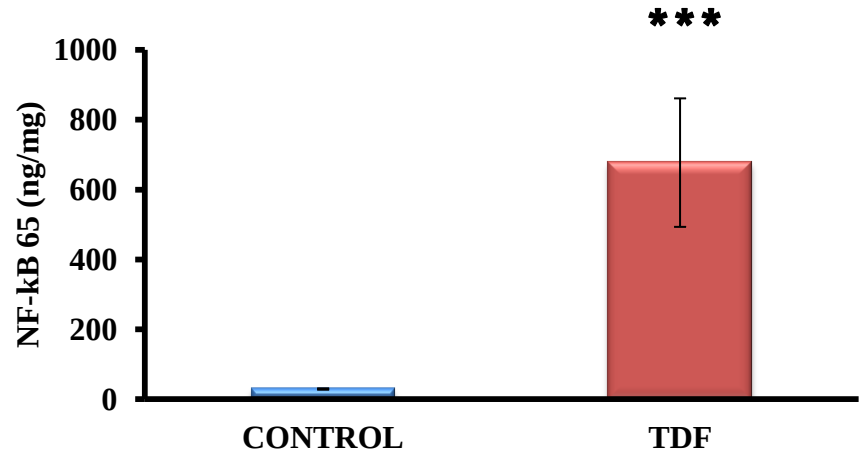

Figure : 7.1.3 NF-κBp65 activity in the (B) cytosolic and (C) nuclear fractions of control rat and TDF treated rat kidneys. In the controls, p65 activity was very low both in the cytosolic fraction and nuclear fraction. In the TDF treated rats, both the cytosolic fraction and nuclear fractions showed massive increase as compared with control. p65 activity was increased by 18 fold in the cytosolic fraction and by 28 fold in the nuclear fraction as compared with control. Values are mean ± SD, n =5 rats in each group. ***P < 0.001

Figure: 7.1 .4 mRNA expression of NF-κB p65

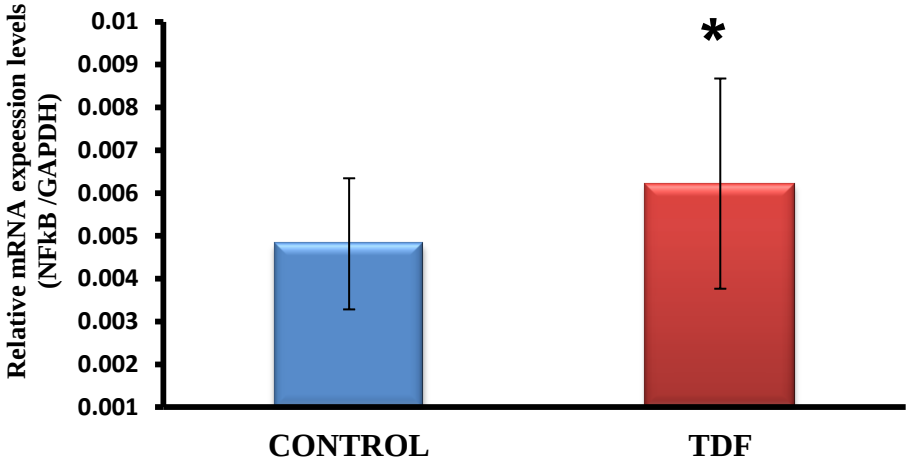

Figure: 7.1 .4 Relative gene expression of NF-κB mRNA in kidneys of control rats and TDF treated rats , (n=5). Data is shown as mean ± SD. *indicates p<0.05 when compared with control values.

(e) **Effect of TDF on IκB-α protein and mRNA gene expression**

IκBα protein level is a representative of activation in cytosol because IκB-α after phosphorylation is subsequently ubiquitinated and degraded via the proteasome pathway (422). Therefore, we investigated the IκB-α protein level and mRNA level in the control rat kidneys and TDF treated rat kidneys. We examined nuclear protein levels by Western blotting using anti IκB- polyclonal antibodies. Our data showed that the protein levels of IκB-α was higher in the control rats and was significantly decreased in the TDF treated rat kidneys (Figure: 7.2.1 A &B) .However, the mRNA levels of IκB-α in TDF treated rat kidneys was not significantly different from controls. These results imply that TDF treatment reduces IκB-α protein level, but has no effect on its mRNA expression (Figure:7.2.2).

Figure: 7.2.1 Western blot for IκB-α protein

(A)

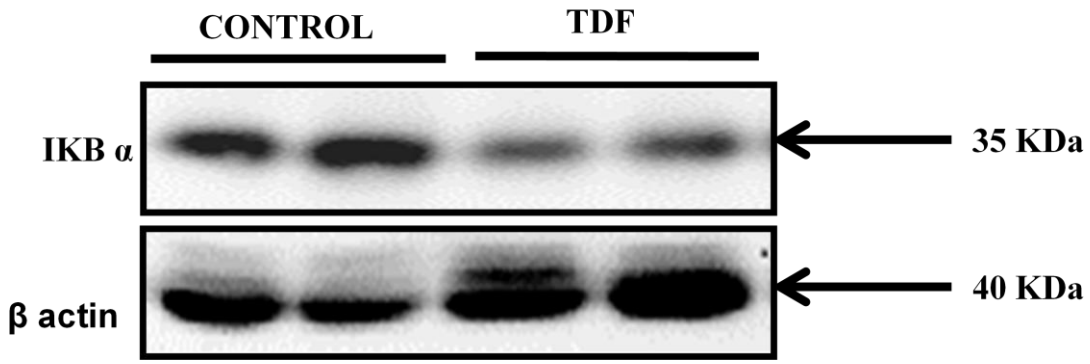

(B)

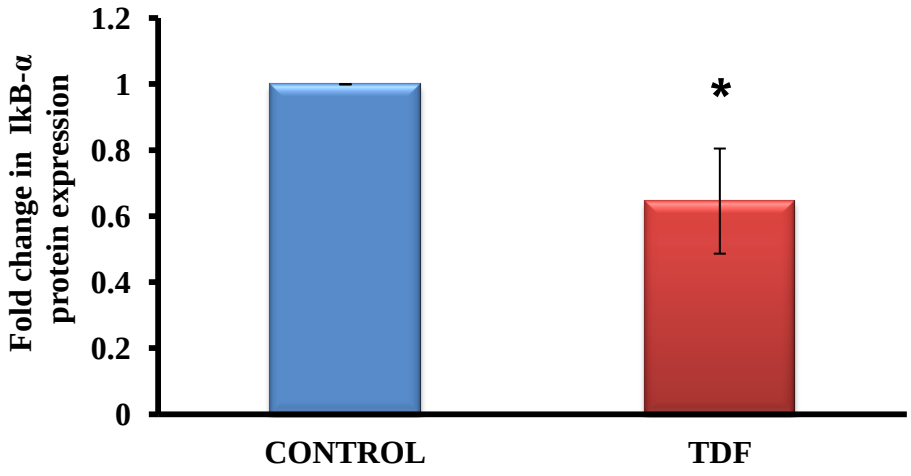

Figure: 7.2.1 A: Representative western blots of cytosol of IκB-α protein levels in renal homogenates of control and TDF-treated rats (n=5 in each group), as assessed by using a 10% polyacrylamide gel, loading 100µg protein per lane. β-actin was used as the loading control.

Figure: 7.2.1 B: Relative concentration of cytosol of IκB-α in renal homogenates as analysed by densitometric quantification of bands of western blots in control and TDF-treated rats (n=5 in each group). Data represents mean ± SD, obtained by image analysis of western blots with the concentration of the controls set at one.

Figure: 7.2.2. mRNA expression of IκB-α

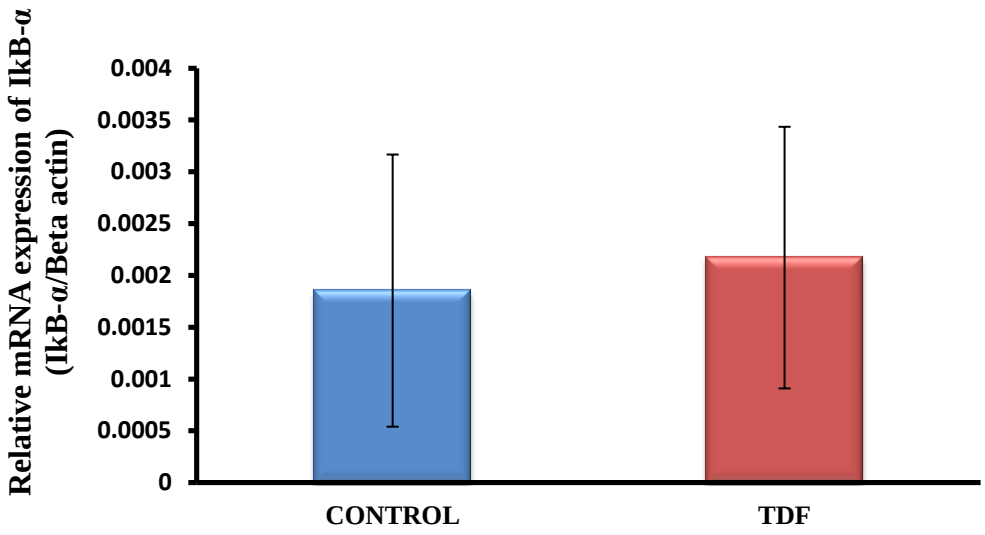

Figure: 7.2.2. Relative gene expression of IKB-α mRNA in kidney of control rats and TDF treated rats (n=5) in each group. Data reprsent mean ± SD.

B. TDF increases the protein and mRNA expressions of NF-κB target proinflammatory genes

1. Effect of TDF on the expression of iNOS protein, its products nitrotyrosine (NTY), and nitrocysteine (NCY), and mRNA expression of iNOS:

The immunohistochemical studies revealed basal iNOS (Figure:7.3.1),immunostaining both in cortical and medullar structures of kidney taken from control rats. The expression of iNOS in the medulla was more intense than in the cortex. The basal iNOS expression in the medulla, particularly in the MTAL and medullary collecting duct.

In TDF-treated rats, extensive and prominent iNOS immunoreactivity was noted in the medulla, whereas iNOS immunostaining in the cortex was sparse. In the cortex, iNOS immunoreactivity was seen in the vascular endothelium and the macula densa segment (MDS, few DCT and PCT). In the medulla, strong and uniform iNOS immunostaining was seen in the MTAL and collecting duct cells as well as in the endothelium of the vasa recta.

Our findings were corroborated by immunoblotting technique,. The iNOS protein blots and scanned band densitometry of the renal specimens from control rats and examined after TDF treatment are depicted in (Figure:7.3.2), wherein a 2 fold increase in iNOS proteins was observed in the TDF treated rat kidneys as compared with control.

These observations were further supported by results of mRNA expression which noticed basal transcription of iNOS (Figure:7.3.3), in the control rat kidneys. There was also significantly higher transcriptional upregulation of iNOS, as compared to controls. NO, the product of NOS was increased—more than 2 fold in the kidneys of TDF treated rats as compared with control.

Figure:7.3.1 Immunohistochemistry of iNOS

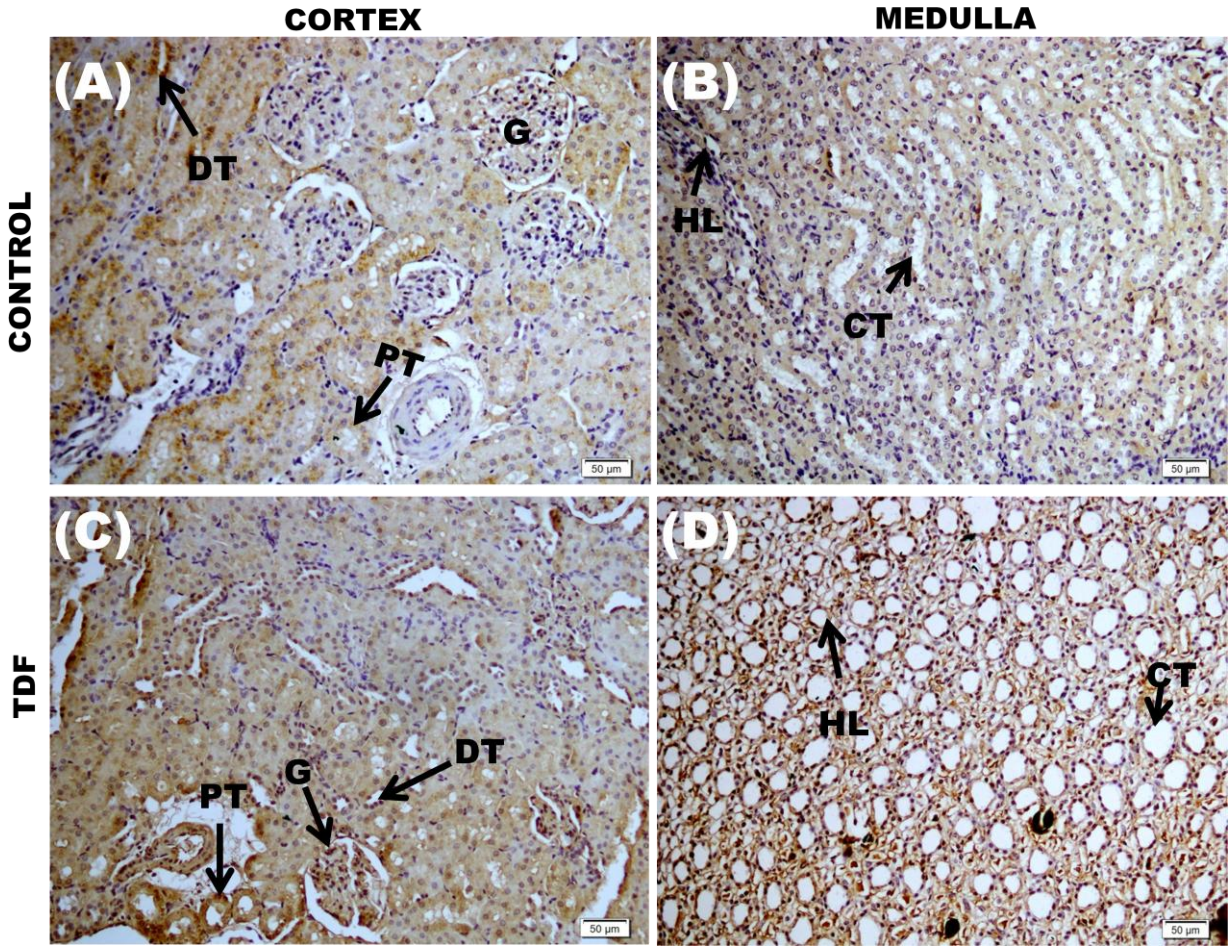

Figure: 7.3.1 Representative images of immunohistochemical detection of iNOS in control , and TDF treated (TDF), treated rat kidneys. Scale Bars = 20µm. Basal iNOS immunostaining was seen both in cortical and medullar structures of kidney taken from control rats. The expression of iNOS was prominent in the proximal tubules and distal tubules, as well as in the MTAL and medullary collecting ducts. In TDF-treated rats, extensive and prominent iNOS immunoreactivity was noted in the medulla, whereas iNOS immunostaining in the cortex was sparse. In the cortex, iNOS immunoreactivity was seen in the glomerulus, and few DT and PT. In the medulla, strong and uniform iNOS immunostaining was seen in the MTAL and collecting duct cells as well as in the endothelium of the vasa recta. Brown color indicates immunopositivity . N=5 rats for each group. Scale bar 50µm. Black arrows indicate G-glomerulus, PT-proximal convoluted tubule, DT- distal convoluted tubule , HL-Henle's loop. CT- collecting tubule.

Figure:7.3.2 Western blot for iNOS protein

(A)

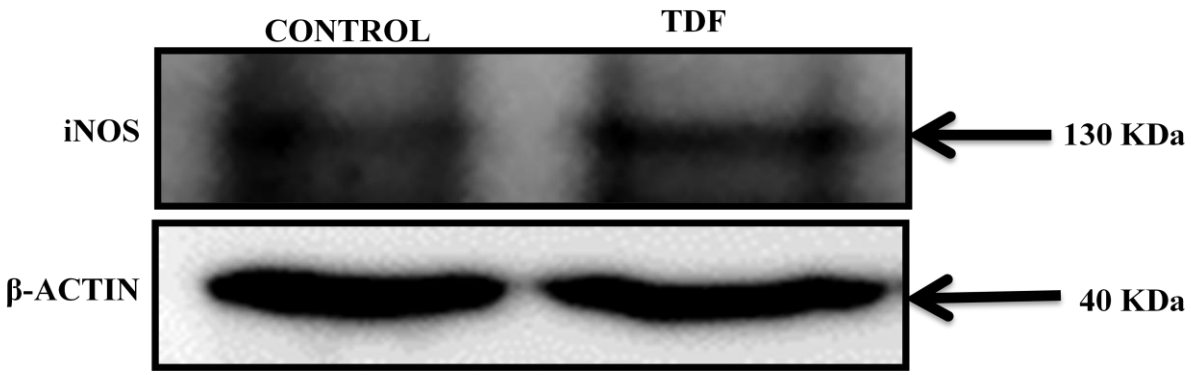

(B)

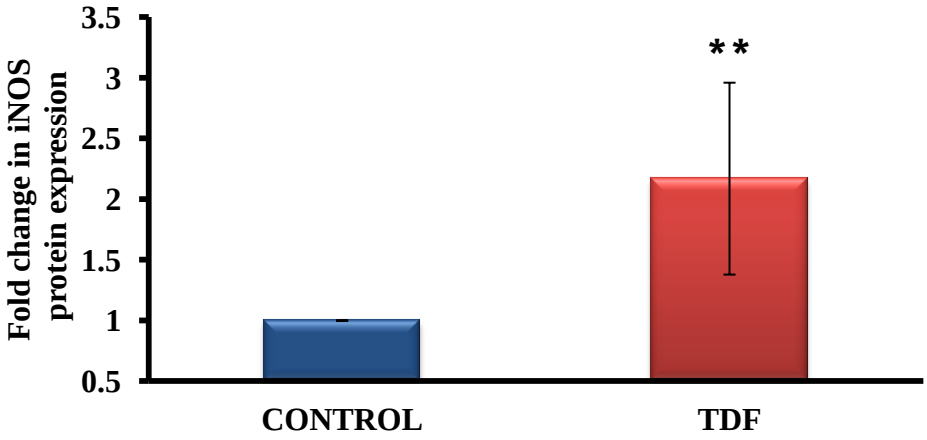

Figure:7.3.2 A Representative western blots of iNOS protein in renal homogenates of control and TDF-treated rats (n=5) in each group), as assessed using a 10% polyacrylamide gel, loading 100µg protein per lane. β-actin was used as the loading control.

Figure:7.3.2 B Relative concentration of iNOS protein in renal homogenates as analysed by densitometric quantification of bands of western blots (n=5) in each group. Data represents mean ± SD, obtained by image analysis of western blots with the concentration of the controls set at one. ** indicates $p<0.01$ when compared with control .

Figure:7.3.3 mRNA expression of iNOS

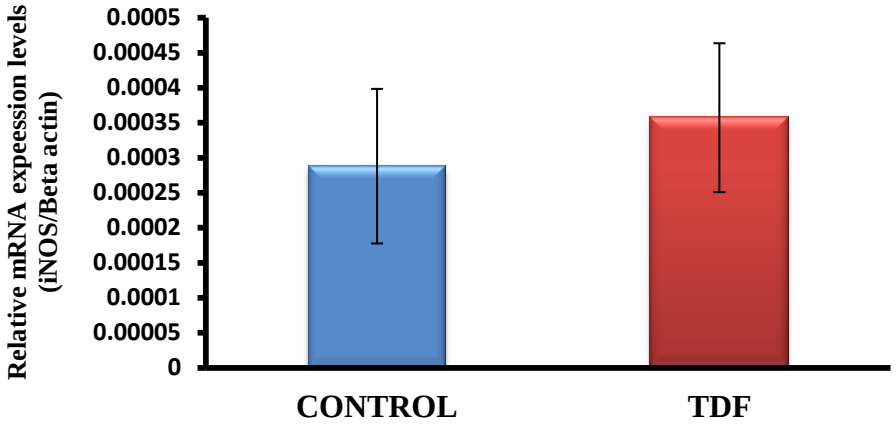

Figure: 7.3.3 Relative gene expression iNOS mRNA in kidney of control rats and TDF treated rats (n=5) in each group. Data represent mean ± SD.

The cytotoxic potential of NO is a consequence of its to form peroxynitrite ,which is a potent nitrating and oxidizing agent. 3 nitrotyrosine is considered as the footprint of peroxynitrite formation. Therefore, we determined 3 NT in the kidneys by IHC and immunoblot. In control rats, basal nitrotyrosine immunoreactivity was found in the cortex and medulla, with proximal tubular cells showing least staining for NT. Nitrotyrosine expression was up-regulated in the cortex and medulla of TDF treated rats (Figure:7.4.1), The staining for NT was more intense in the medulla as compared with cortex . In the cortex, nitrotyrosine was localized to the apical region of proximal tubular cells , glomerulus, and distal convoluted tubules. In the medulla, the collecting duct and LH stained intensly for NT.

3NT levels as measured by Western blot analysis showed a significant increase in the TDF treated rat kidneys as compared with control (Figure:7.4.2A &B).

In addition to nitration of tyrosine residues damage the cells, PON can damage the cells by the oxidation of free thiols-cysteine residues to nitrosothiols (409). Protein S nitrosylation can either activate or inhibit an enzyme. Therefore we determined nitrosocysteine levels of proteins by immunostaining and immunoblotting techniques using nitrocysteine antibody. In control rats, basal immunoreactivity for nitrosocysteine found in the cortex and medulla. In the TDF treated rats, staining for nitroscysteine was intense and was uniformly distributed through all the regions of the cortex and medula. Nitrocysteine staining was more intense in the medulla as compared with control (Figure:7.5.1), Nitrocysteine levels as measured by Western blot analysis showed a significant increase in the TDF treated rat kidneys as compared with control. (Figure:7.5.2).

The distribution pattern of nitrotyrosine and nitocysteine immunoreactivity were similar in the TDF treated rat kidney suggesting that PON is the source of NO for their formation.

Figure:7.4.1 Immunohistochemistry of Nitrotyrosine

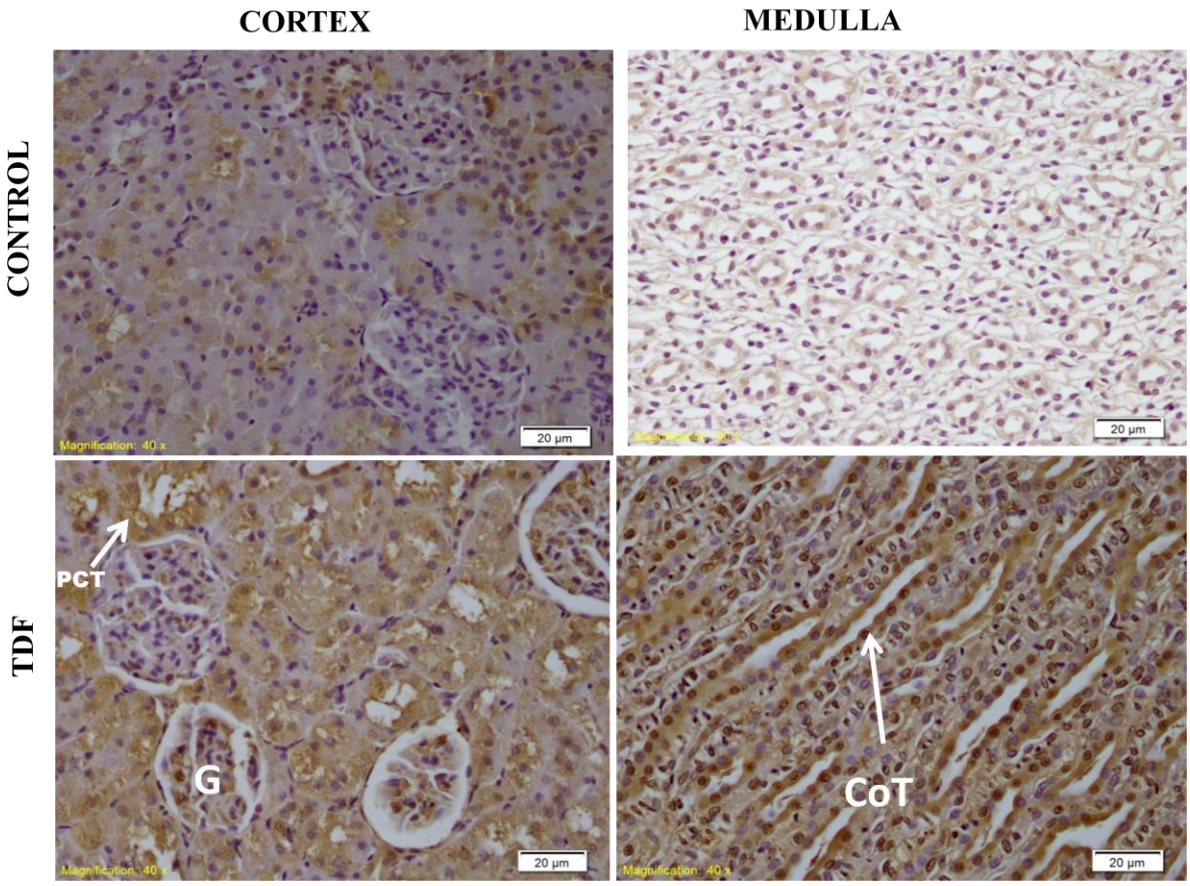

Figure: 7.4.1 Representative images of immunohistochemical detection of 3 NT in control (A) & (B) and TDF treated (C) & (D) rat kidneys. Scale Bars = 20µm.

A & B **In control rats, basal nitrotyrosine immunoreactivity was found in the cortex and medulla, with proximal tubular cells showing least staining for NT.**

C & D **Nitrotyrosine expression was up-regulated in the cortex and medulla of TDF treated rats .The staining for NT was more intense in the medulla as compared with cortex. In the cortex, nitrotyrosine was localized to the apical region of proximal tubular cells , glomerulus, and distal convoluted tubules. In the medulla ,the collecting duct and LH stained intensly for NT. Scale bar 20µm. G-glomerulus, PCT-proximal convoluted tubule, DCT- distal convoluted tubule , HL-Henles loop. CoT- collecting tubule.**

Figure: 7.4.2 Western blot for Nitrotyrosine protein

(A)

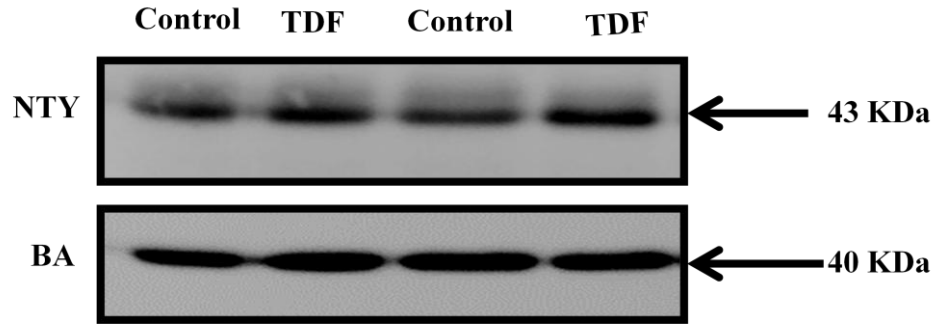

(B)

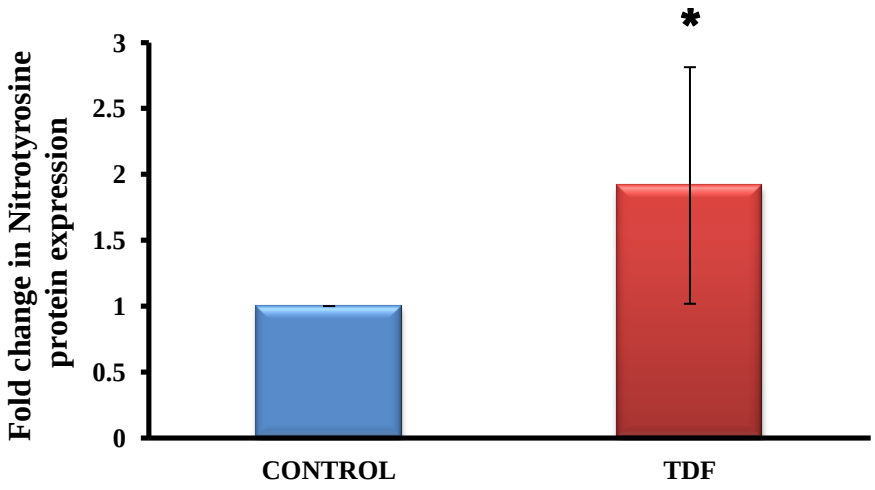

Figure 7.4.2 A : Representative western blots of Nitrotyrosine protein levels in control and TDF-treated rats (n=5 in each group), as assessed by using a 10% polyacrylamide gel, loading 100µg protein per lane. β-actin was used as the loading control.

Figure 7.4.2 B: Relative concentration of nitrotyrosine in renal homogenates as analysed by densitometric quantification of bands of western blots in control and TDF-treated rats (n=5 in each group). Data represents mean ± SD, obtained by image analysis of western blots with the concentration of the controls set at one. * indicates $p<0.05$ when compared with control values.

Figure:7.5.1 Immunohistochemistry of Nitrocysteine

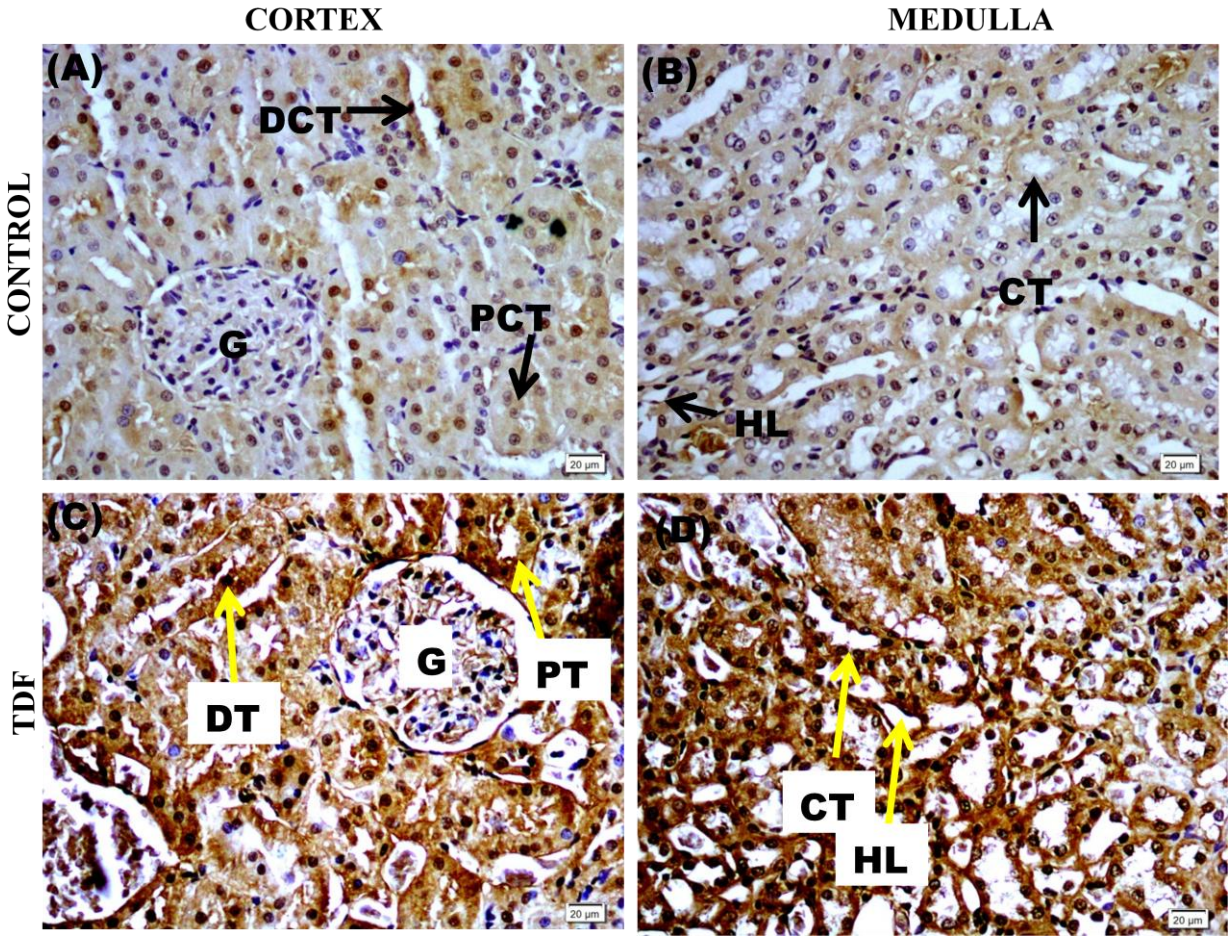

Figure: 7.5.1 Representative images of immunohistochemical detection of nitrocysteine in control (A) & (B), and TDF treated (C) & (D) rat kidneys. Scale Bars = 20µm.

A & B. In control rats, basal nitrocysteine immunoreactivity was found in the cortex and medulla.

C &D Nitrocysteine expression was up-regulated in the cortex and medulla of TDF treated rats. The staining for nitrocysteine was more intense in the medulla as compared with cortex . In the cortex, nitrocysteine was localized to the apical region of proximal tubular cells , glomerulus, and distal convoluted tubules. In the medulla ,the collecting duct and LH stained intensly for nitroocysteine . Scale bar 20µm. G -glomerulus, PT-proximal convoluted tubule, DT- distal convoluted tubule , HL-Henles loop. CT- collecting tubule.

Figure: 7.5.2 Western Blot for Nitrocysteine protein

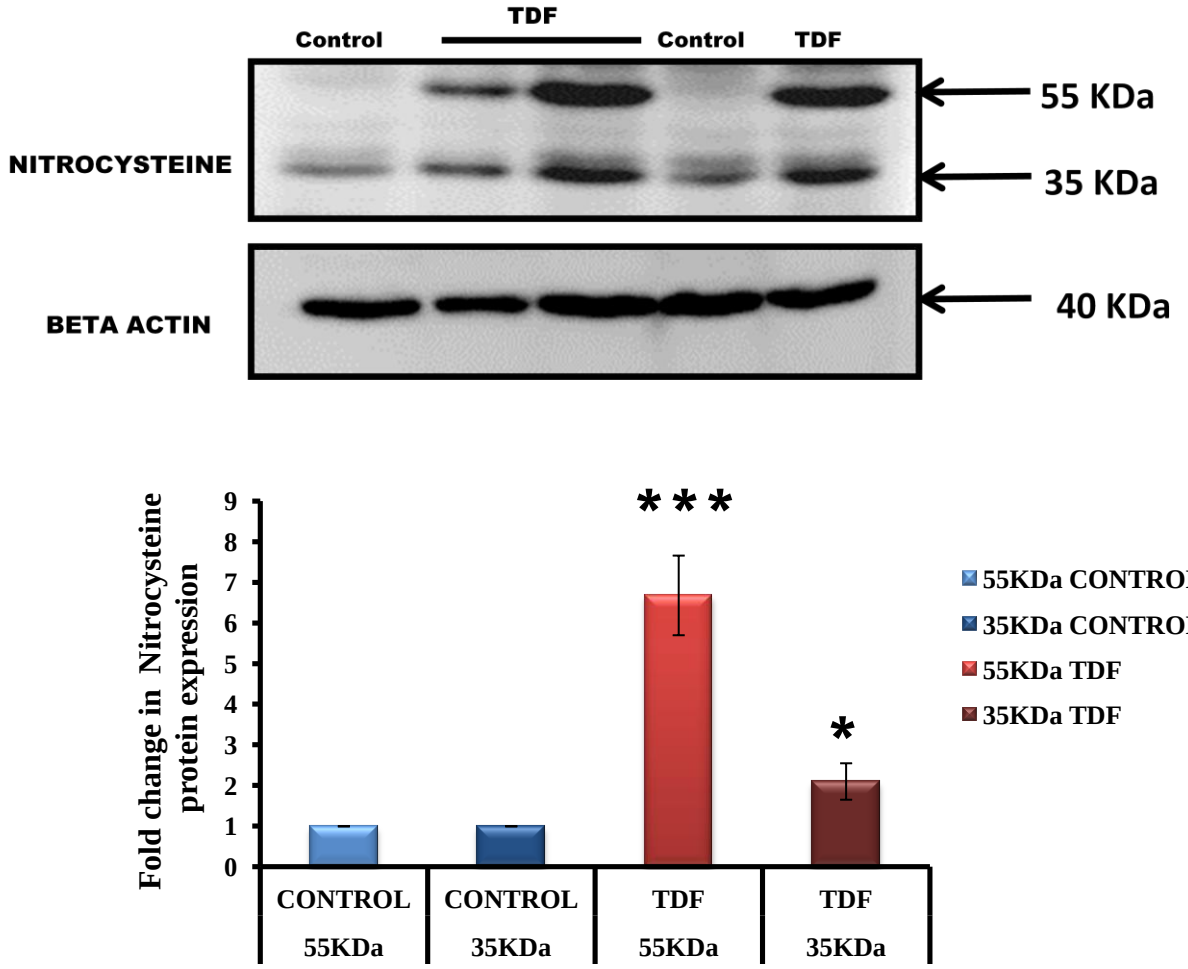

Figure:7.5.2 A Representative western blots of nitrocysteine protein levels in control and TDF-treated rats (n=5 in each group), as assessed by using a 10% polyacrylamide gel, loading 100µg protein per lane. β-actin was used as the loading control.

Figure:7.5.2 B Relative concentration of nitrocysteine in renal homogenates as analyzed by densitometric quantification of bands of western blots in control and TDF-treated rats (n=5 in each group) Data represents mean ± SD, obtained by image analysis of western blots with the concentration of the controls set at one. * p<0.05 , *** p < 0.001 when compared with ccontrol values.

2. Effect of TDF treatment on COX-2 protein expression and mRNA expression :

Representative photomicrographs of COX2 protein determined by immunohistochemistry is shown in (Figure:7.6.1). In the control rat kidneys, immunostaining revealed no constitutive expression of COX-2 in the renal cortex and medulla . In the TDF treated rat kidneys, the glomerulus , the HL and collecting ducts showed intense staining for COX-2, as a representative marker of the pathway. Diffuse staining was observed in the DCT and PCT. To determine whether the COX-2 regulation by TDF can also be demonstrated at the mRNA level, we examined the effects of TDF on COX-2 mRNA expression determined by real-time RT-PCR and normalized by β-actin. As shown in Figure:7.6.2. TDF treatment induced more than 2.5 fold increase in COX-2 mRNA expression.

3. Effect of TDF on TNF protein and mRNA expression :

Sections of each renal sample were stained for TNF-α using immunohistochemical techniques. While no TNF-α staining was present in the control rats, a significant immunostaining for TNFα was detected after TDF treatment (Figure:7.7.1). TNF-α immunostaining was seen both in the cortex as well as medulla. The glomerulus, PCT, DCT, Loop of henle, collecting ducts stained for TNF, supporting previous observations that source of TNF may be intrinsic renal cells including endothelial, glomerular and tubular epithelial cells, mesangial cell in addition to the infiltrating inflammatory cells.

To corroborate our findings,we investigated TNF-α protein expression by immunoblot in renal homogenates. Control rats demonstrated low levels of TNF-α expression and in TDF treated rats more than 2 fold increase in TNF-α levels was observed (Figure:7.7.2).

Next we quantified the TNF-α mRNA expression in renal samples as shown in Figure:7.7.3. Control rats had basal expression of TNF-α mRNA. TDF administration resulted in nearly 4 fold increase in TNF-α mRNA expression.

Figure: 7.6.1 Immunohistochemistry of COX-2

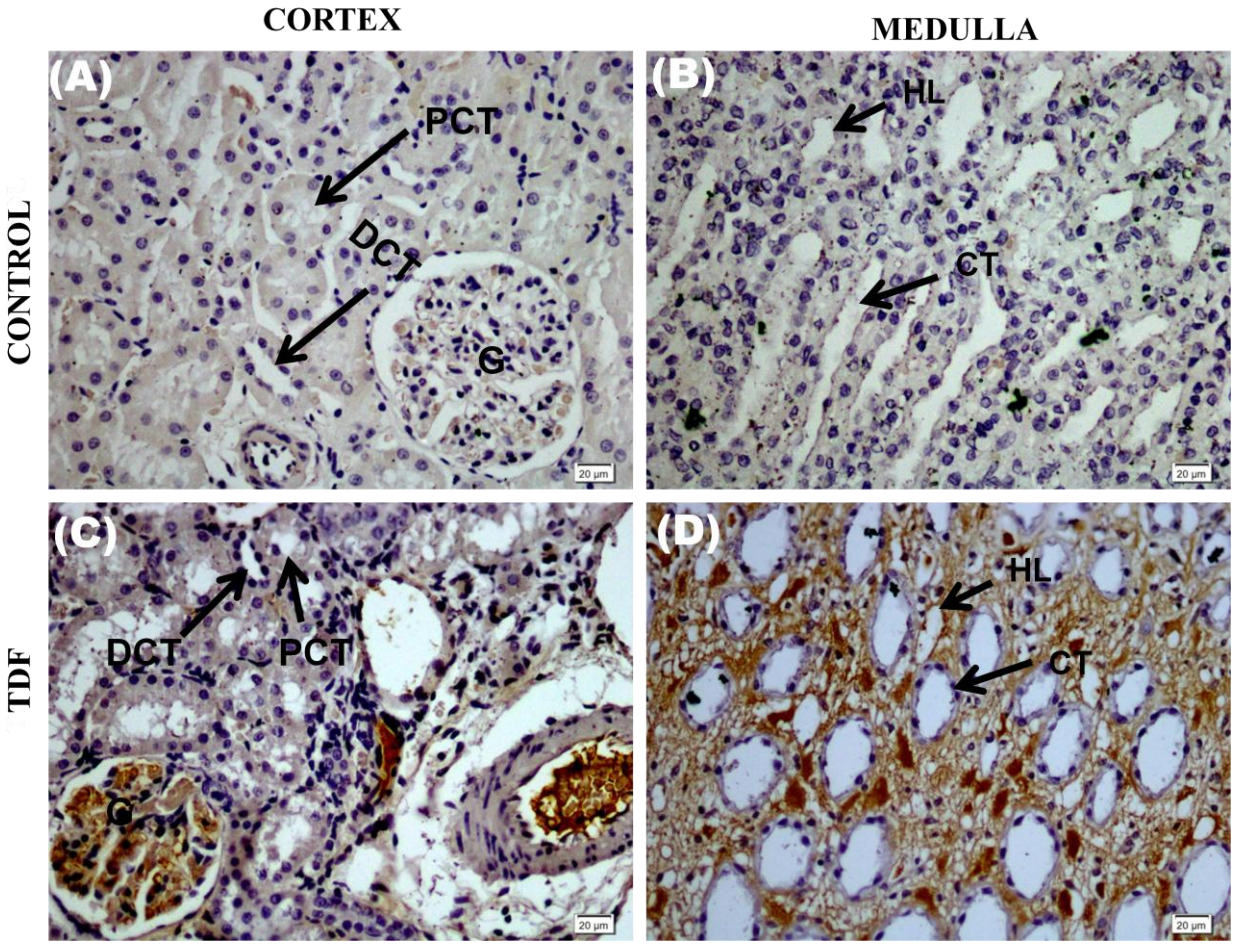

Figure: 7.6.1 Representative images of immunohistochemical detection of COX-2 in control , and TDF treated (TDF), treated rat kidneys. Scale Bars = 20µm.

A &B. The cortex and medulla of control rats showed no staining.

C & D. In the TDF-treated rats, extensive and prominent COX-2 immunoreactivity was noted in the glomerulus, whereas in the tubules it was sparse. In the medulla, strong COX-2 immunostaining was seen in the MTAL and collecting duct cells . Brown color indicates immunopositivity. N=5 rats for each group. Scale bar 20µm. Black arrows indicate G-glomerulus, PCT-proximal convoluted tubule, DCT- distal convoluted tubule , HL-Henles loop. CT- collecting tubule.

Figure: 7.6.2 mRNA expression of COX-2

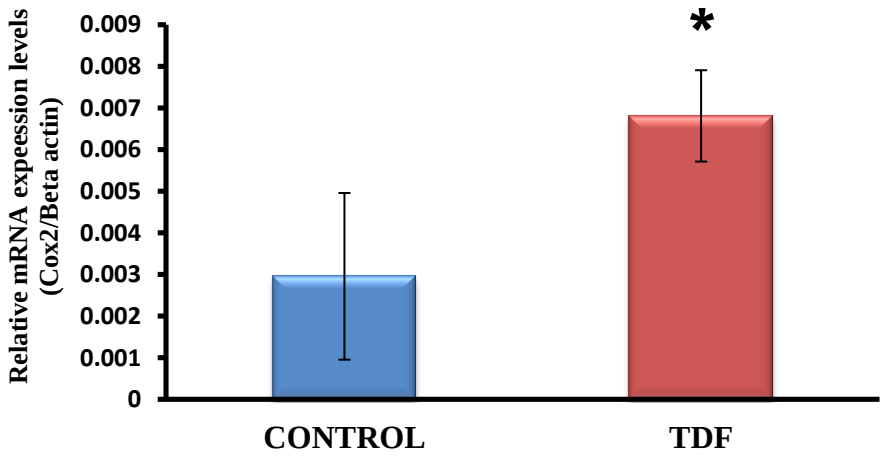

Figure: 7.6.2 Relative expression of COX-2 mRNA in kidney of control and TDF treated rats (n=4-6). Data represent mean ± SD. *p<0.05 when compared with control values.

Figure: 7.7.1 Immunohistochemistry of TNF α

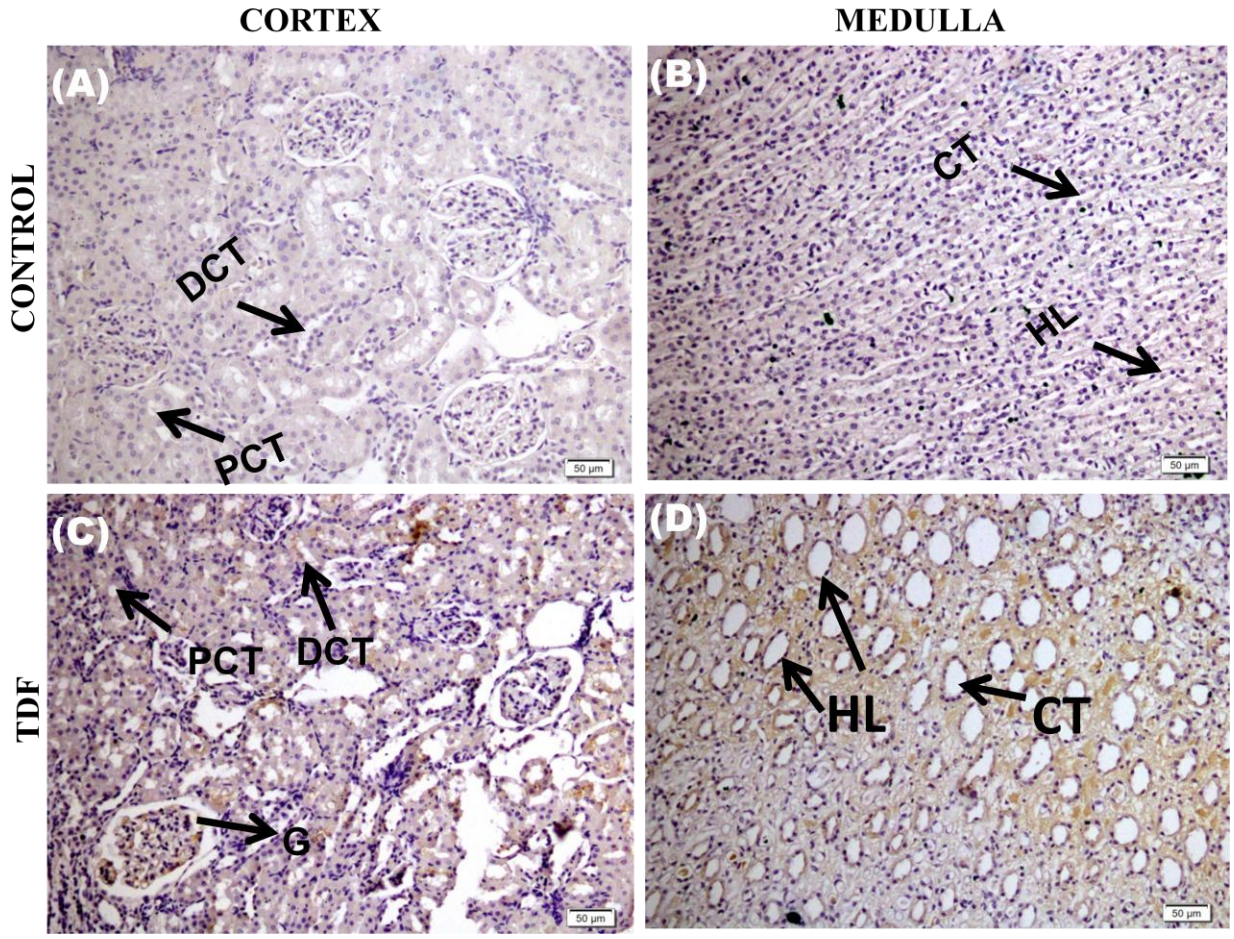

Figure: 7.7.1 Representative images of immunohistochemical detection of TNF α in control , and TDF treated rat kidneys. Scale Bars = 20µm.

A & B. The cortex and medulla of control rats showed no staining.

C & D. In TDF-treated rats, mild TNF α immunoreactivity was noted in the glomerulus and in few tubules. In the medulla, moderate TNF α immunostaining was seen in the MTAL and collecting duct cells. Brown color indicates immunopositivity. N=4 rats for each group. Scale bar 50µm. Black arrows indicate G-glomerulus, PCT-proximal convoluted tubule, DCT-distal convoluted tubule , HL-Henles loop. CT- collecting tubule.

Figure: 7.7.2 Western blot for TNF-α protein

(A)

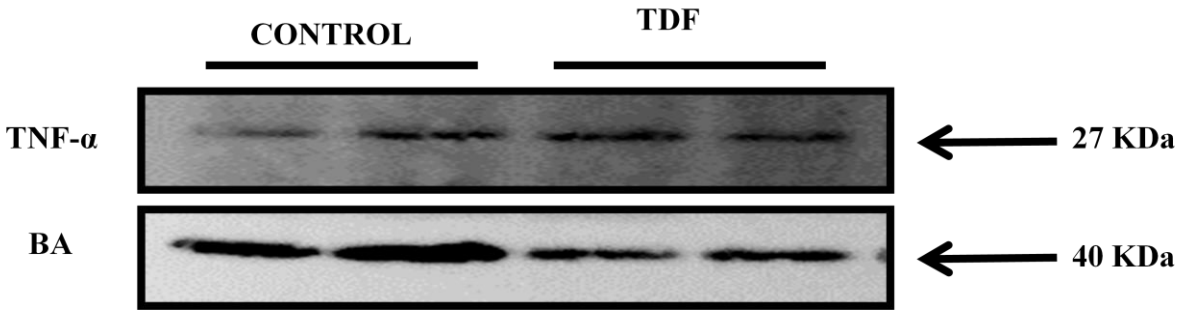

(B)

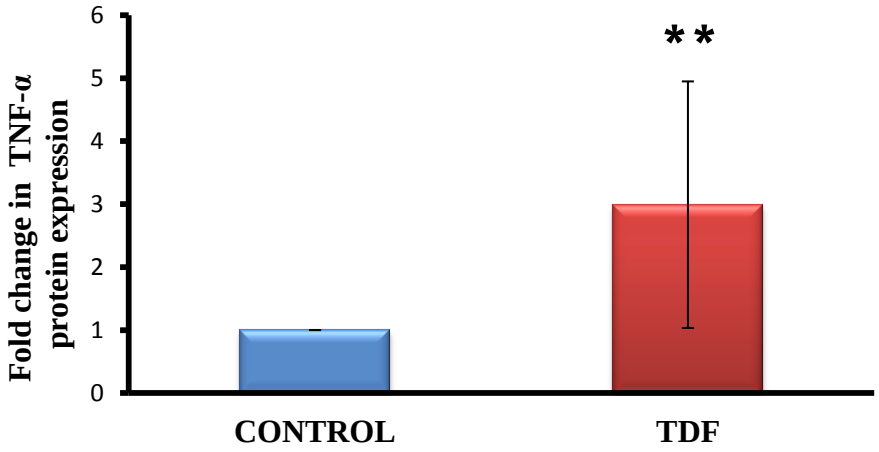

Figure: 7.7.2 A. Representative western blots of TNF-α protein levels in control and TDF-treated rats (n=5 in each group), as assessed by using a 10% polyacrylamide gel, loading 100μg protein per lane. β-actin was used as the loading control.

Figure: 7.7.2 B. Relative concentration of TNF-α in renal homogenates as analysed by densitometric quantification of bands of western blots in control and TDF-treated rats (n=5 in each group). Data represents mean ± SD, obtained by image analysis of western blots with the concentration of the controls set at one. ** $p<0.01$ when compared with control values.

Figure: 7.7.3 mRNA expression of TNF-α

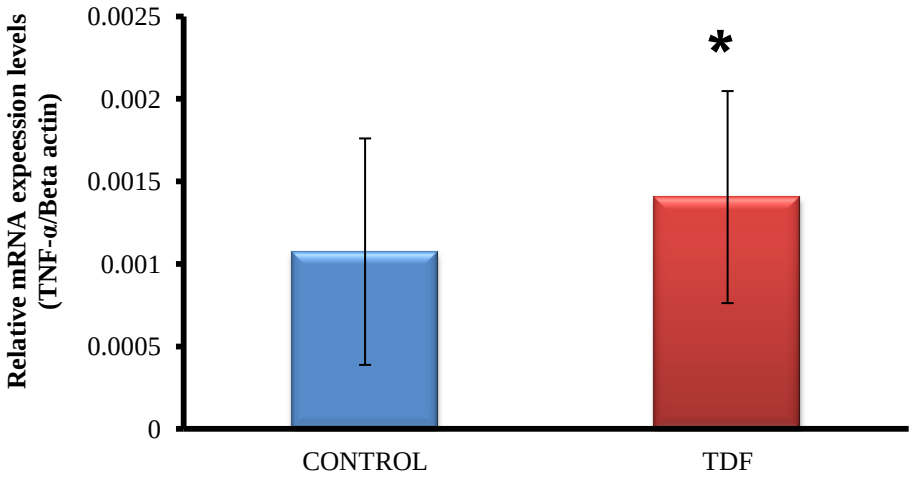

Figure: 7.7.3 Relative gene expression TNF-α mRNA in kidney of control and TDF treated rats (n=5). Data represent mean ± SD. * p<0.05 when compared with control values.

4. Effect of TDF on PLA_2 protein :

Representative images of PLA_2 immunostaining is show in Figure:7.8.1.In the control rats almost no staining was observed in the cortex as well as in medulla. However, in the TDF treated rats, moderate staining for PLA_2 was observed both in the cortex as well as in medulla. Similarly, western blot analysis shows an increase in the TDF treated rats, though not significant statistically (Figure:7.8.2).

Figure: 7.8.1 Immunohistochemistry of PLA 2

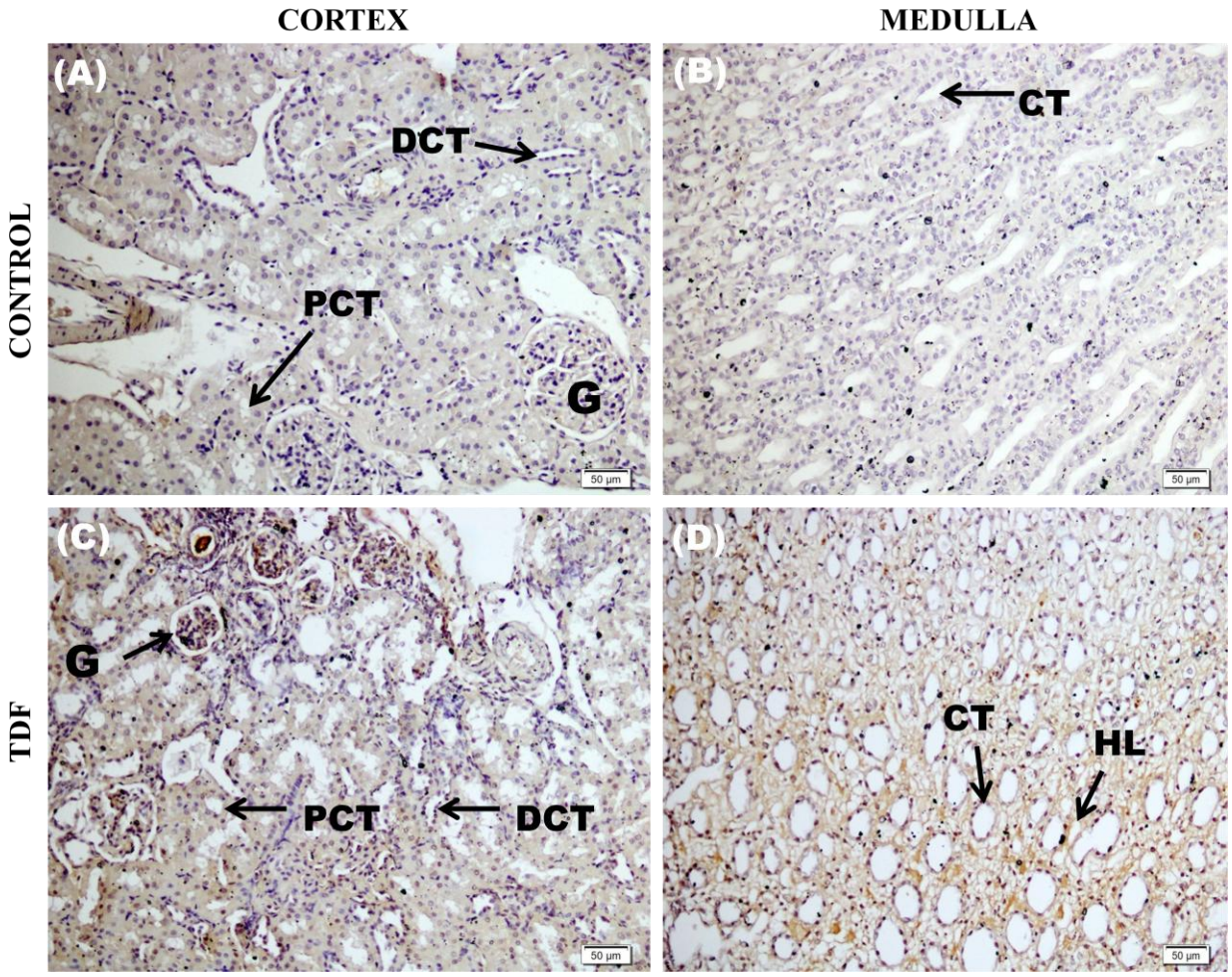

Figure: 7.8.1 Representative immunohistomicrographs Phospholipase A_2 in the kidney of rat. (Scale Bars = 20µm)

(A&B) Control rats show basal mild staining for PLA_2 in cortex and medulla

(C&D) TDF treated rats show moderate staining for PLA_2 in the cortex. Glomerulus (G), and PCT and DCT . Mild staining was seen in the connective tissue, convoluated tubules (CT), loop of Henle (HL) of the medulla. Brown color indicates immunopositivity. N=4 rats for each group. Black arrows indicate G-glomerulus, PCT-proximal convoluted tubule, DCT- distal convoluted tubule , HL-Henles loop. CT- collecting tubule.

Figure:7.8.2 Western blot for PLA 2 protein

(A)

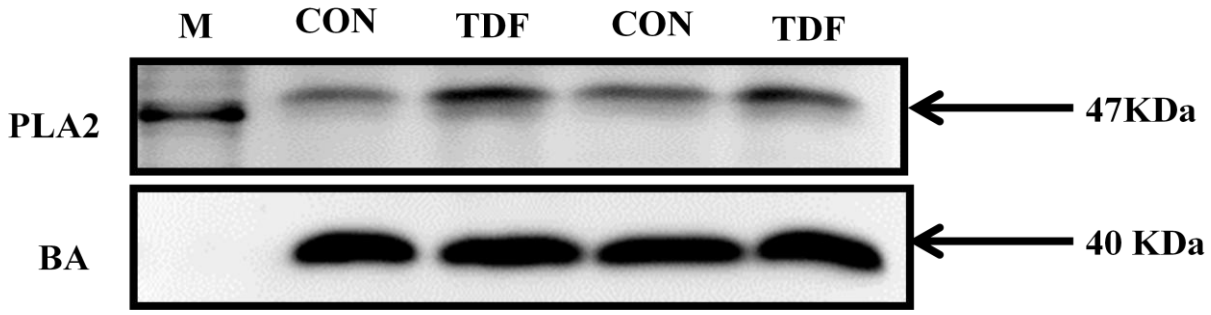

(B)

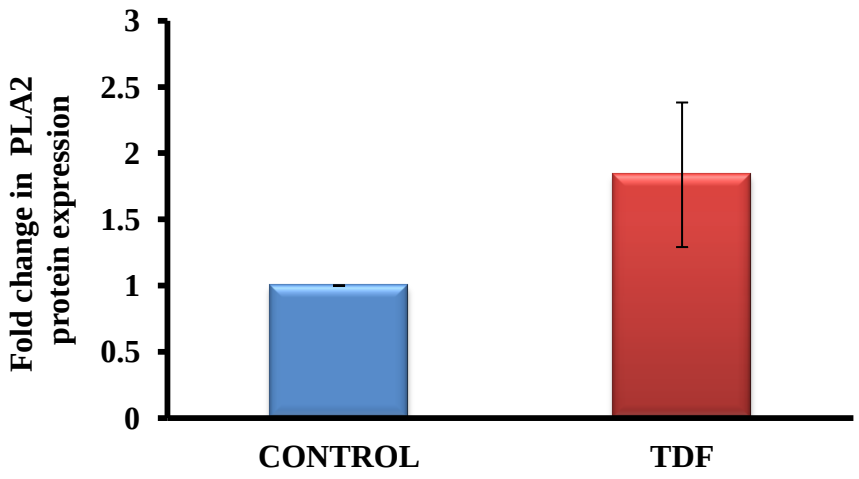

Figure:7.8.2 A. Representative western blots of PLA2 protein levels in control and TDF-treated rats (n=5 in each group), as assessed by using a 8% polyacrylamide gel, loading 100µg protein per lane. β-actin was used as the loading control.

Figure: 7.8.2 B. Relative concentration of PLA2 in renal homogenates as analysed by densitometric quantification of bands of western blots in control and TDF-treated rats (n=5 in each group). Data represents mean ± SD, obtained by image analysis of western blots with the concentration of the controls set at one. 'M' denotes molecular weight.

D. Effect of TDF treatment on PARP expression by immunohistochemistry and western blot

(i) PARP expression by immunohistochemistry:

Immunohistochemical appearance of the kidney-control .Glomerulus showed negligible staining for PARP. In TDF treated rat kidney cortex, the glomerulus and convoluted tubules stained for PARP. In the medulla, the collecting tubules and Henles loop (HL) were positive to PARP stain. Representative images are shown in (Figure:7.9.1 A-D).

(ii**) PARP expression by Immunoflourescence**: The glomeruli and tubules of TDF treated rats showed increased number of PARP nuclei positive cells (Figure:7.9.2 A & B).

(**iii) PARP expression by western blot**

PARP protein in the nuclear fraction of kidney homogenate from TDF treated rats showed significant increase as compared with control (Figure:7.9.3 A & B)

E. Effect of TDF treatment on Caspase-3 protein and mRNA expression, and activity:

a) Caspase -3 protein expression by Immunohistochemistry

The protein level of caspase-3 showed a significant increase in the kidneys of TDF treated rats as compared to control. (Figure:7.10.1 A-D)

b) Caspase 3 protein expression by Western Blot:

The protein level of caspase-3 showed a significant increase in the kidneys of TDF treated rats as compared to control in Immunblot (Figure:7.10.2 A&B). Consistently, the acitivity of caspase-3 was increased significantly in response to TDF as compared to control group. (Figure:7.10.4).

c. mRNA gene expression level of caspase-3

To determine whether mRNA gene expression level of caspase-3 was up regulated by TDF, we examined the effect of TDF on caspase-3 mRNA expression level by qPCR and normalized by β-actin. As shown in (Figure:7.10.3). TDF treatment were significantly upregulated expression of caspase-3 gene.

Figure: 7.9.1 Immunohistochemistry of PARP

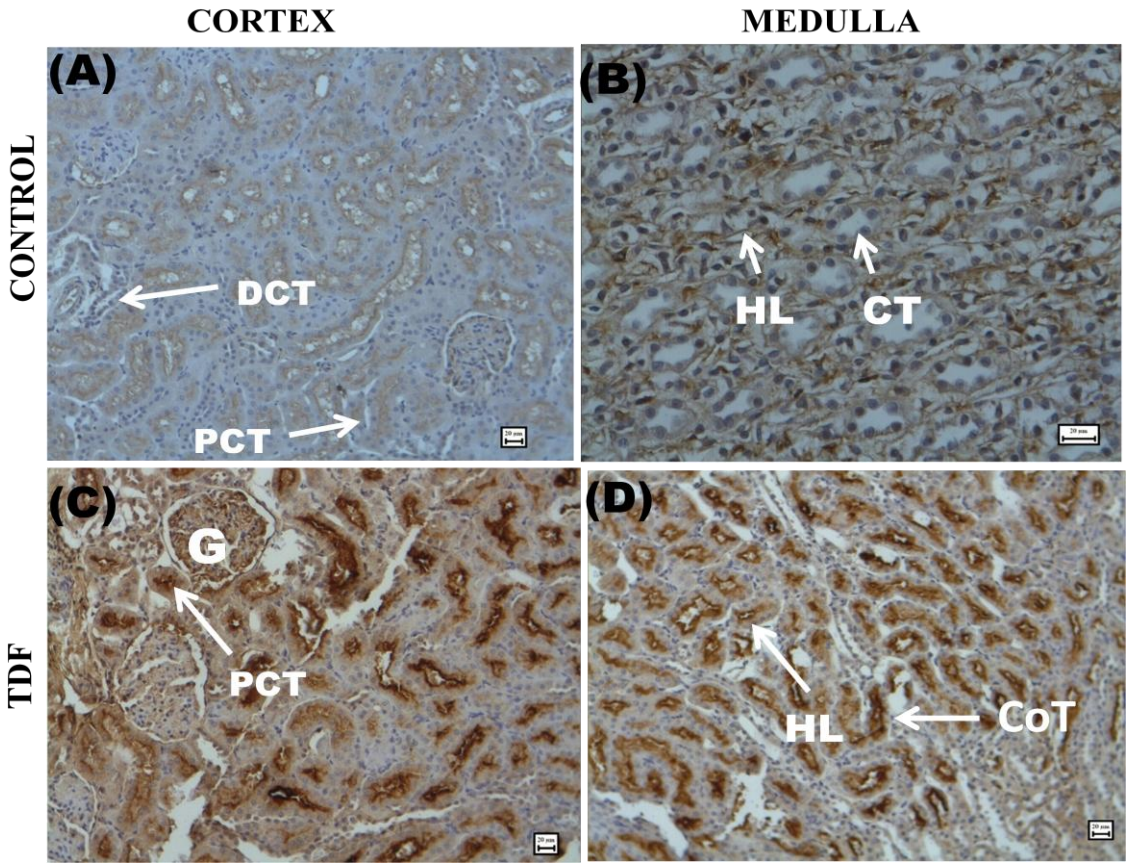

Figure: 7.9.1 Representative immunohistomicrographs of PARP expression in the kidneys of control rats and TDF treated rats, (Scale Bars = 20µm)

(A&B) Uniform mild PARP staining in the cortex and medulla of control rats.

(C &D) TDF treated rats show very intense staining for PARP in all the elements of the cortex as well as medulla. Glomerulus (G) , the convoluted tubules (PCT and DCT), the collecting tubules (CoT) and Henle's loop (HL).

Figure: 7.9.2A IMMUNOFLUORESCENCE OF PARP IN RENAL CORTEX

(A)

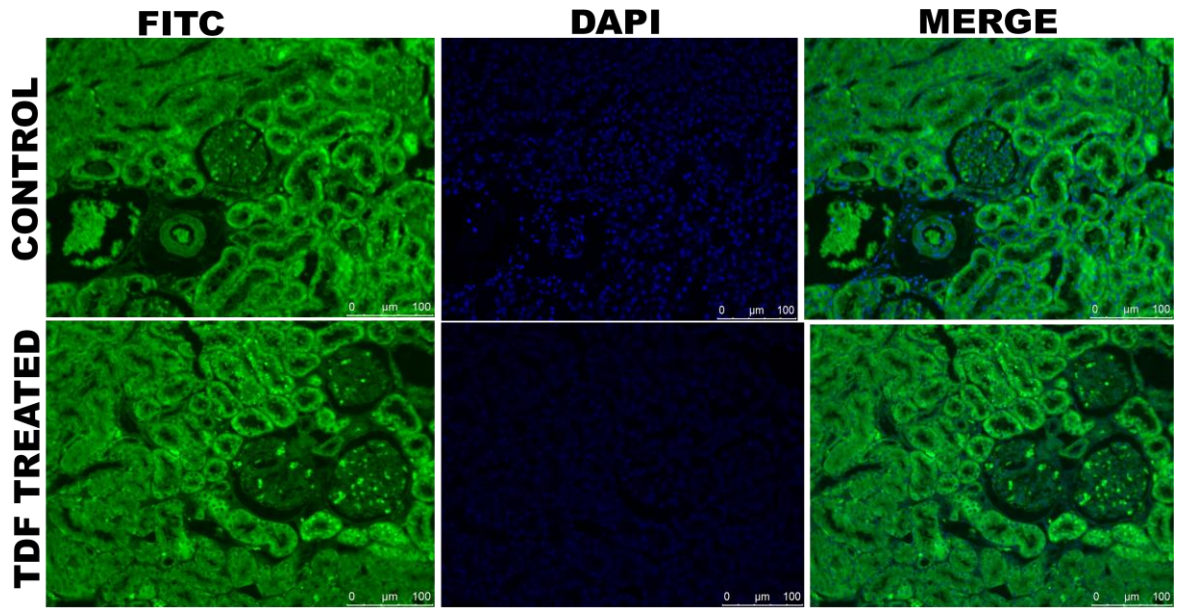

Figure: 7.9.2A. Representative immunofluorescence images of cortex of control rats and TDF treated rats. Nuclei were counter stained with DAPI. Blue indicates DAPI stained nuclei, green indicates FITC (morphology of the cortex).

B. IMMUNOFLUORESCENCE OF PARP IN RENAL MEDULLA

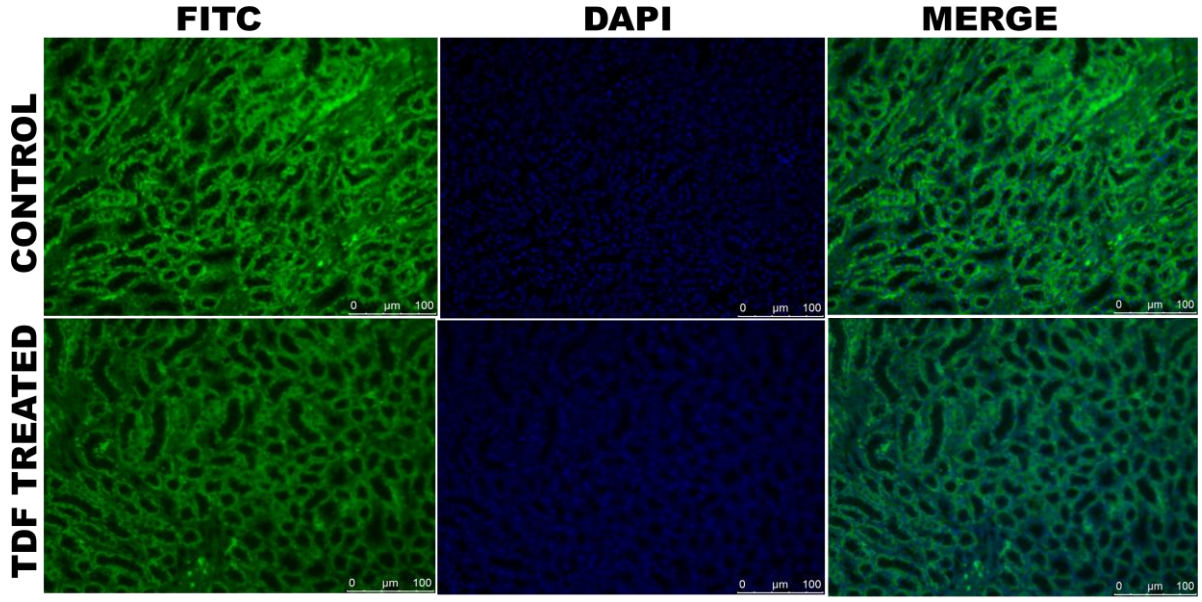

Figure: 7.9.2B. Representative immunofluorescence images of medulla of control rats and TDF treated rats. Nuclei were counter stained with DAPI. Blue indicates DAPI stained nuclei, green indicates FITC (morphology of the medulla).

Figure: 7.9.3 Western blot for nuclear PARP protein

(A)

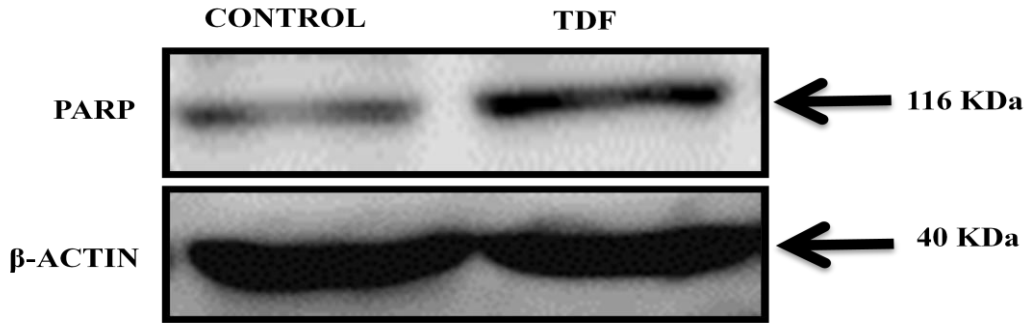

(B)

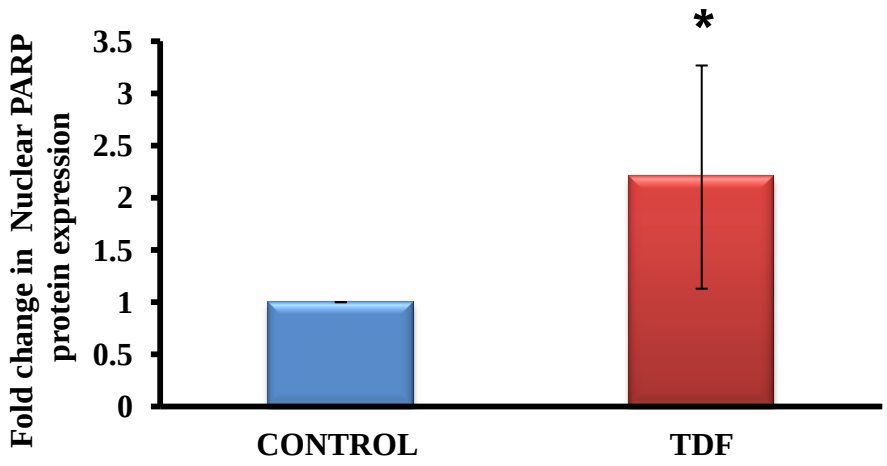

Figure: 7.9.3 A: Representative immunoblots of nuclear PARP protein expression in the renal homogenates of control rats and TDF-treated rats (n=5 in each group), as assessed by using a 8% polyacrylamide gel, loading 100µg protein per lane. β-actin was used as the loading control.

Figure: 7.9.3 B: Relative concentration of nuclear PARP in renal homogenates as analysed by densitometric quantification of bands of western blots in control and TDF-treated rats (n=5 in each group). Data represents mean ± SD, obtained by image analysis of western blots with the concentration of the controls set at one. * indicates $p<0.05$ when compared with corresponding control values.

Figure: 7.10.1 Immunohistochemistry of caspase 3

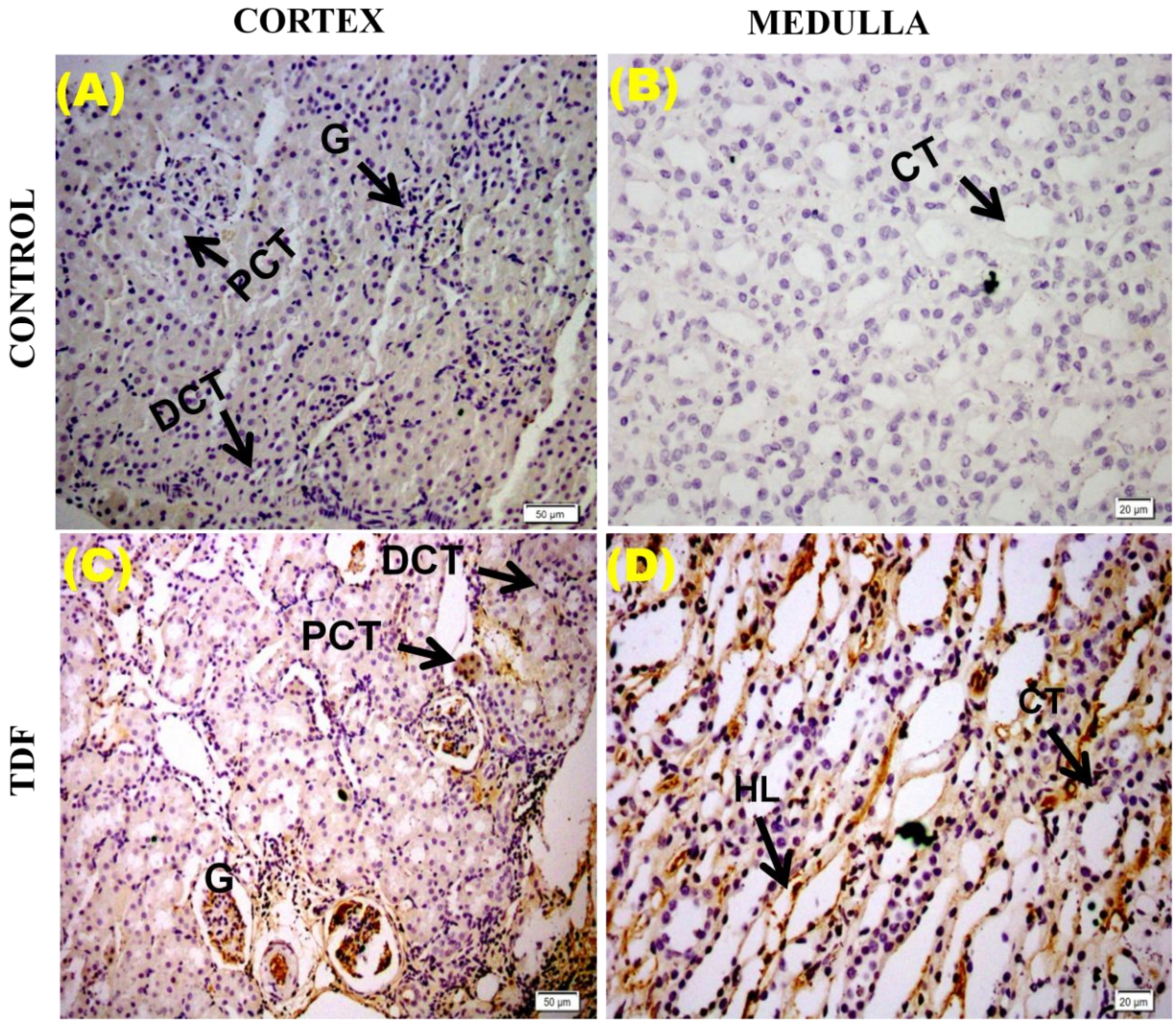

Figure: 7.10.1 Representative immunohistomicrographs of caspase-3 in the kidneys of control rats and TDF treated rats. Scale Bars = 20µm.

(A& B) Control rats showing negligible staining for caspase 3 in the cortex and medulla.

(C &D) TDF treated rats show intense staining for caspase 3 in all the regions of cortex and medulla. In the cortex the glomeruli showed intense staining when compared with the tubule cells (PCT). In the medulla, the collecting tubules (CT) and Henle's loop (HL) show the increased intensity of the stain

Figure: 7.10.2 Western blot for Caspase 3 protein

(A)

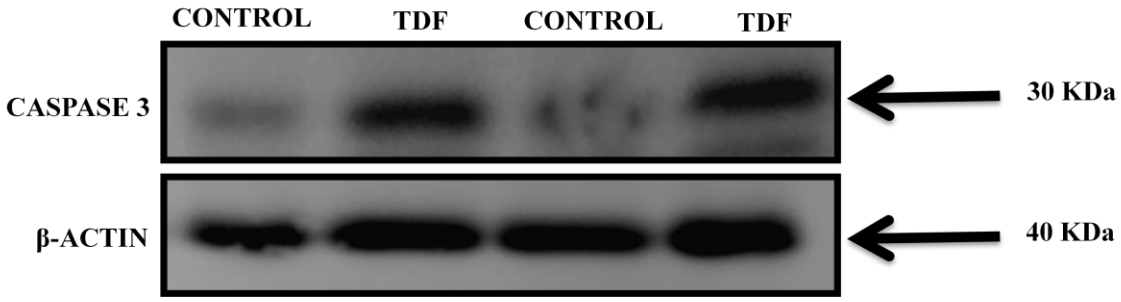

(B)

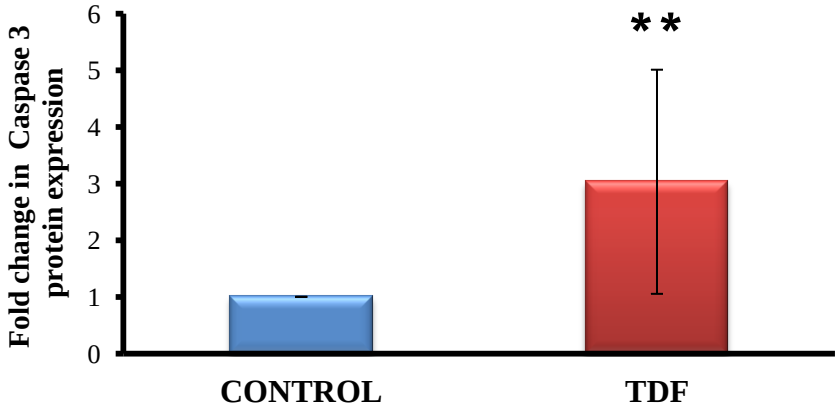

Figure: 7.10.2 A : Representative western blots for caspase 3 protein levels (30kD) bands in the control and TDF-treated rats, (n=5 in each group), as assessed by using a 10% polyacrylamide gel, loading 100µg protein per lane. β-actin was used as the loading control.

Figure: 7.10.2 B : Relative concentration of Caspase 3 in renal homogenates as analysed by densitometric quantification of bands of western blots in control and TDF-treated rats (n=5 in each group), obtained by image analysis of western blots with the concentration of the controls set at one. Data represents mean ± SD ** indicates $p<0.01$ when compared with corresponding control values.

Figure: 7.10.3 mRNA expression of Caspase 3

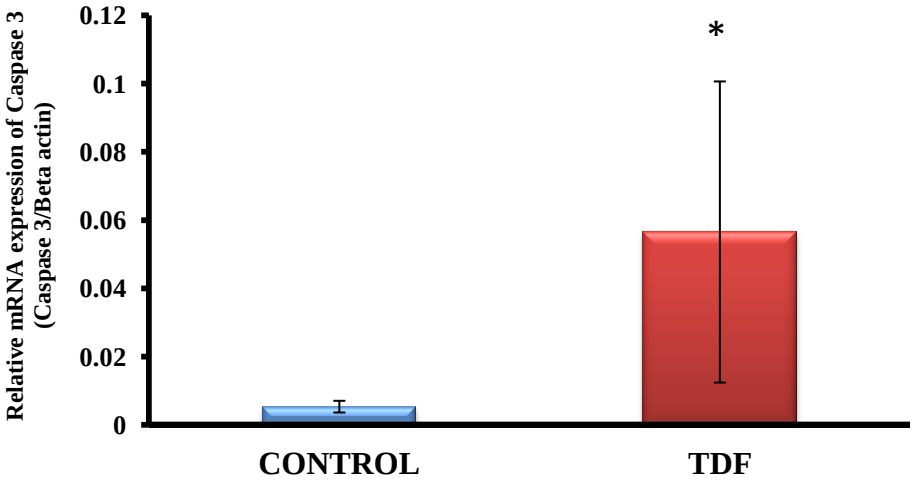

Figure: 7.10.3. Relative gene expression of Caspase 3 mRNA in kidneys of control rats and TDF treated rats, (n=5). Data represent mean ± SD. * p<0.05 when compared with control values.

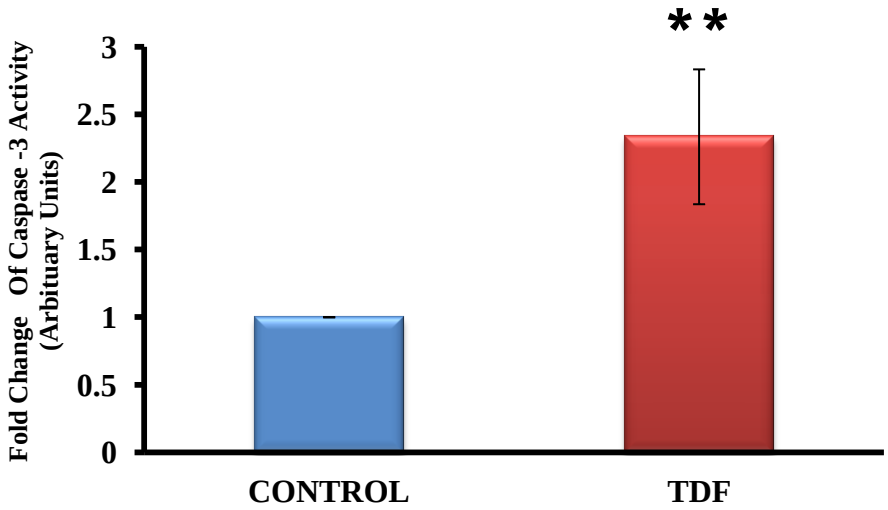

Figure : 7.10.4 Activity of caspase-3 in kidneys of control rats and TDF treated rats , (n=6) in each group. Data represent mean ± SD. ** p<0.01 when compared with control values.

Effect of TDF on MMP-9 activity , protein and mRNA gene expression

Preliminary zymogram studies showed a significant increase in the activity of MMP-9 in TDF rats (Figure: 7.11.1). The protein and mRNA expresssion of MMP 9 was also assessed by western blotting and real time PCR (Figure: 7.11.2 and Figure: 7.113) respectively. This result was consistent with the gelatinase zymogram, a significant increase was found in the protein and mRNA level of MMP-9.

Figure:7.11.1 MMP-9 activity by Zymogram

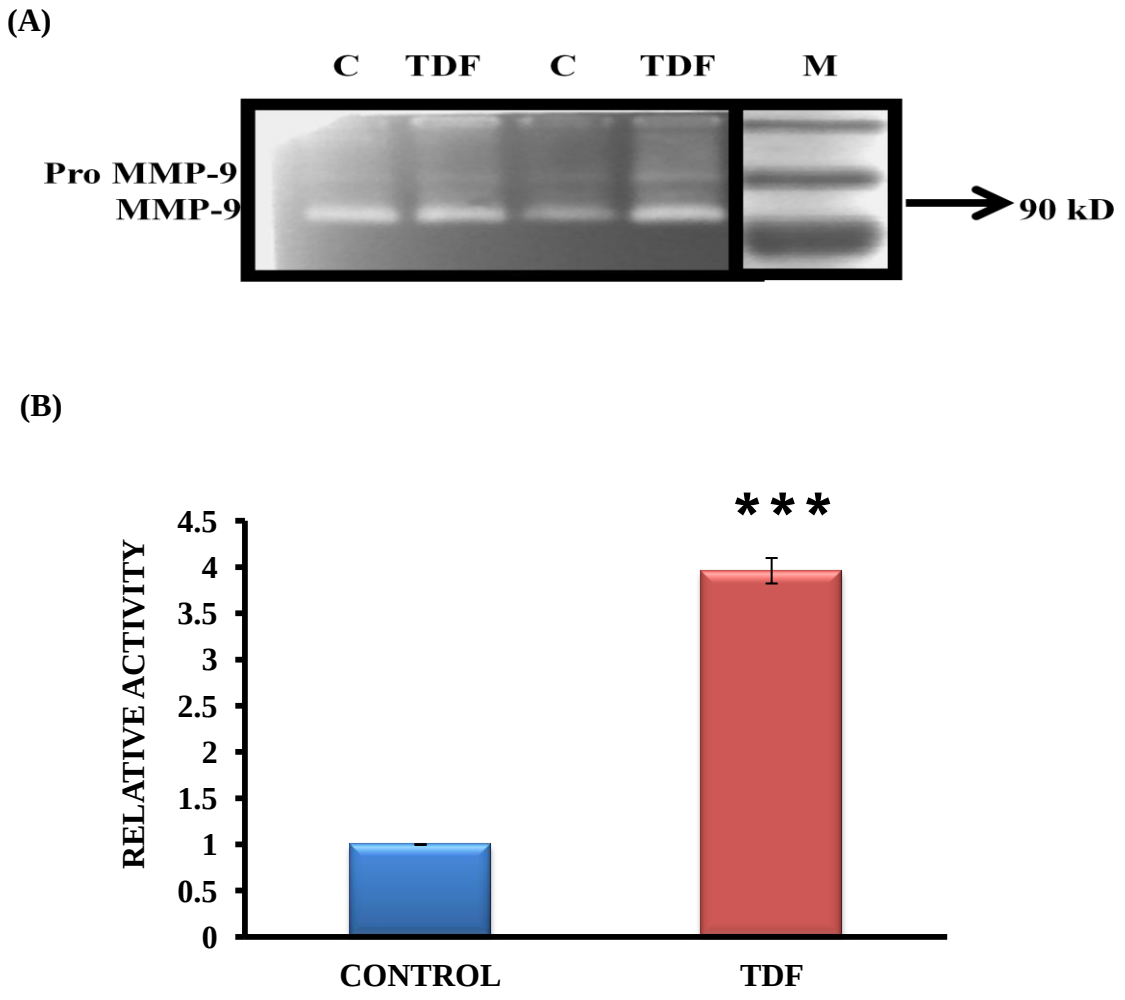

Figure: 7.11.1 A. Zymogram for MMP9 activity in the renal homogenate of control rats and TDF treated rats. B. Relative activity expressed as mean ± SD, (n=6), obtained by image analysis of zymogram, with the activity of the controls set at one. ***p < 0.001 vs control.

Figure: 7.11.2 Western Blot for MMP9

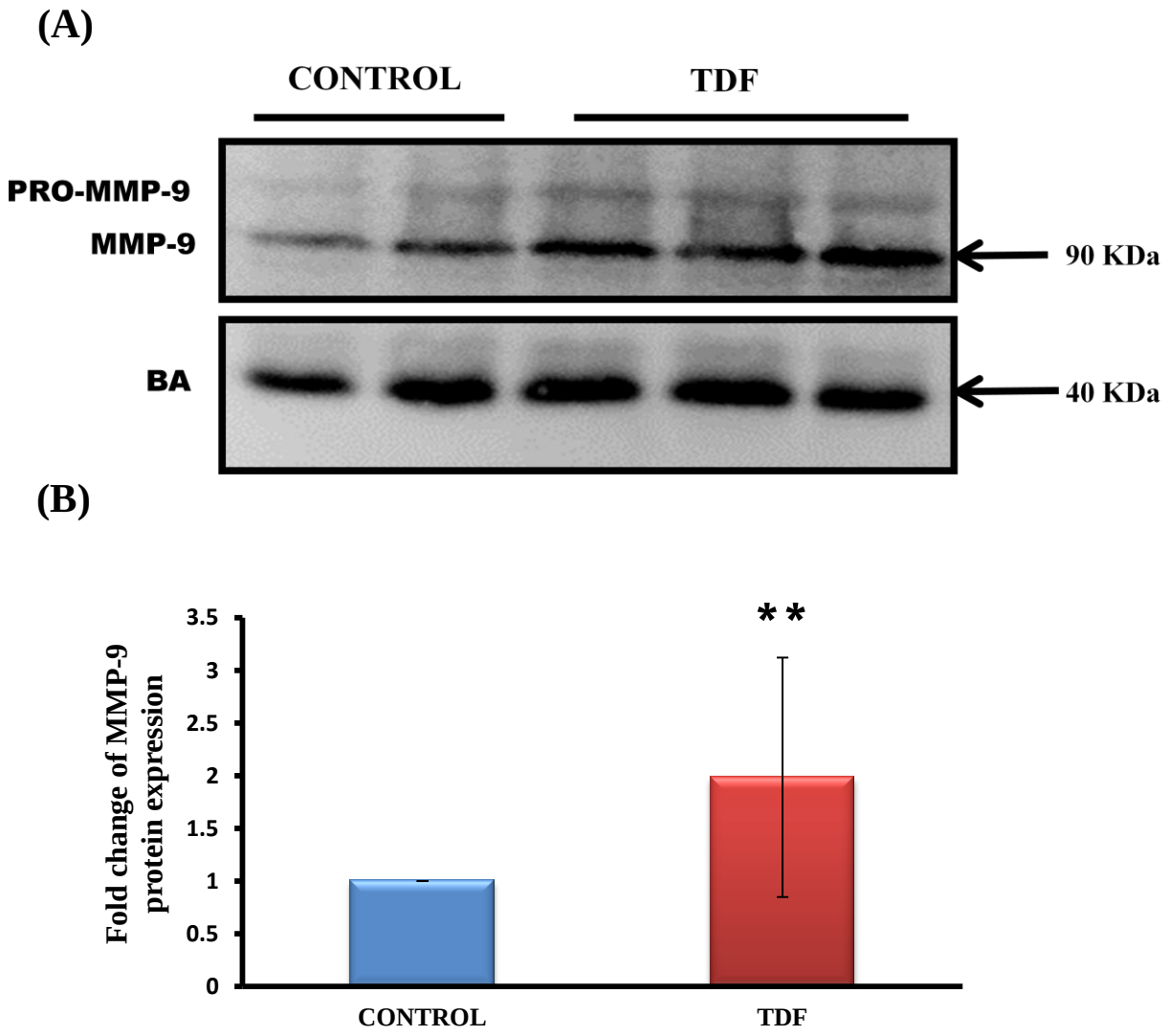

Figure: 7.11.2 A : Representative western blots of MMP-9 protein levels (90kD) bands in the control rats and TDF-treated rats, (n=5 in each group), as assessed by using a 10% polyacrylamide gel, loading 100µg protein per lane. β-actin was used as the loading control.

Figure: 7.11.2 B : Relative concentration of MMP-9 in renal homogenates as analysed by densitometric quantification of bands of western blots in control and TDF-treated rats (n=5 in each group). Data represents mean ± SD, obtained by image analysis of western blots with the concentration of the controls set at one. ** indicates $p<0.01$ when compared with control values.

Figure: 7.11.3. mRNA expression of MMP-9

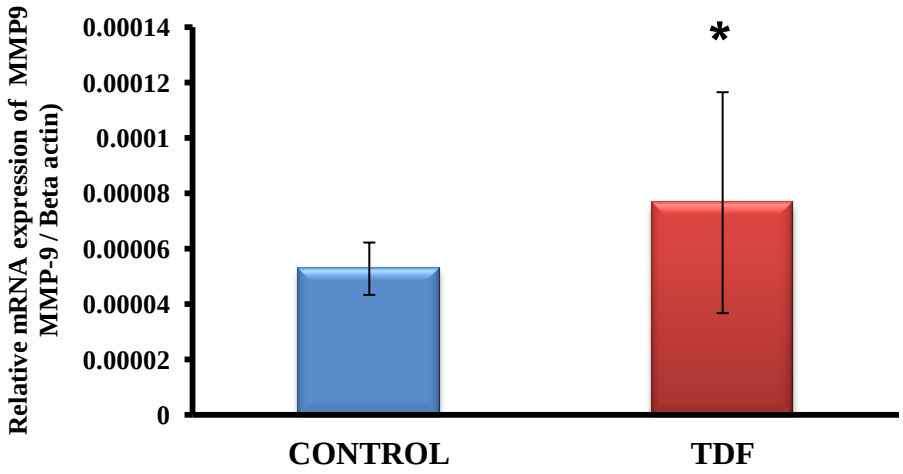

Figure: 7.11.3. Relative expression of MMP-9 mRNA in kidney of control, and TDF treated rats, (n=5). Data represent mean ± SD. *indicates p<0.05 when compared with corresponding control values.

DISCUSSION

Continuous inflammation triggers tubular cell damage, fibrosis and eventually progression to the final stage of kidney disease (423), NF-κB is an important proinflammatory transcription factor that plays a pivotal role in the cellular signaling mechanism for oxidative stress-induced inflammation in various conditions (424). NF-κB signaling pathway is shown to play a role in the pathogenesis of renal injury caused by various agents (425). ROS-dependent activation of the NF-κB pathway promotes apoptosis in proximal tubular cells (39). Cisplatin and gentamicin, both of which are predominantly proximal tubular toxins, cause apoptosis and inflammation of epithelial cells lining the tubular structures via induction of NF-κB signaling (41,419). Therefore, we hypothesized that tenofovir may act through similar mechanism.

In normal resting state, NF-κB is silenced by its complexing with specific inhibitor, IκB in the cytosol. Reactive oxygen species , inflammatory cytokines (eg, tumour necrosis factor-a (TNF-α), activate the NF-κB signaling pathway (425).After phosphorylation and degradation of IκB (422), NF-κB is released and translocated in to nucleus where it promotes the expression of NF-κB responsive proinflammatory genes TNF-α, inducible nitric oxide synthase (iNOS), cyclo-oxygenase(COX)-2, intercellular adhesion molecule and induces inflammatory activation of lymphocytes, monocyte/macrophages and endothelial cells.

.

We first investigated whether NKκB is activated in the kidneys of rats that are treated with TDF. For this, we studied the protein and mRNA expression and activity of NF-κBp65 by immunostaining, immunoblotting, RT PCR and ELISA respectively. Basal NF-κB protein expression was observed in the cytosol of control rats and TDF treated rats. The functional significance of this protein in the cytoplasm is not known and needs to be explored. However, the hypothesis of Nakayama et al (42) that the presence of NF-κB in the cytoplasm may easily result in

the instant activation of NF-κB, even by faint stimulation, seems quite reasonable. Evaluation of NF-κB protein expression, mRNA expression and activity revealed increased activation of NF-κB in the TDF treated rats as compared with control. This suggest that TDF affects NF-κB activation at the mRNA level and protein level.

IκBα is a critical regulator of the transcription factor (43). In unstimulated cells, IκBα continuously shuttles between the nucleus and the cytoplasm (426). However, in most cells, the nuclear export of IκBα is dominant over its import, resulting in the cytoplasmic localization of IκBα. Even though IκBα has been originally discovered as a cytoplasmic inhibitor of , it is now clear that it has important nuclear functions as well. The IκBα can enter the nucleus, remove from gene promoters, and transport proteins back to the cytoplasm (426). This feedback regulation by post-induction repression represents a crucial regulatory mechanism terminating activation during persistent stimulation, and limiting the response. Loss of this negative feedback regulation as well as increased degradation of IκBα have been associated with increased activation in inflammatory diseases as well as in numerous types of cancer and leukemia (427).

In the present study we found that the cytosolic IκB-α protein expression was significantly lesser in the TDF treated rat kidneys as compared with control. But we found no difference in IκB mRNA levels between control rats and TDF treated rats. This suggest that TDF affects the expression of IκB at the protein level and not at the gene level. The low levels of IκB protein in the TDF treated rats can can lead to sustained activation of NF-κB. The consequence of low level of IκB may be decreased association between IκB alpha and NF-κBp65 in the cystosol, there by increasing the availability of free (active) p65 to translocate into the nucleus, and decreased dissociation of from DNA. In fact, in the absence of NF-κB inhibitor (IκBa−/−) there is an aberrant regulatory activity of NF-κB that leads to its persistent nuclear activity driving an inflammatory response that fails to restore homeostasis (428). The cause of lower IκB protein levels in the TDF treated rat kidneys is

not clear. We speculate that the low IκB protein levels may be due to its proteosomal degradation. Our speculation is based on the report that ROS such as hydroxyl radicals and superoxide anions act as mediators of NF-κB activation by stimulating IκB degradation (429).

NF-κB is redox-responsive (430) and the regulation of the nuclear translocation of NF-κB is also redox sensitive (431). Elevated ROS levels deplete intracellular thiol groups, thereby modulating redox potential. The effects of redox imbalance caused by oxidative stress is capable of greatly affecting redox sensitive gene regulation, including the upregulation of genes whose expressions are positively associated with pro-inflammatory NF-κB (nuclear factor-κB) (432,433). When the redox system is disrupted, IκBa is phosphorylated at serine residues, ubiquitinated at lysine residues, and degraded through the proteosomal pathway, which exposes the nuclear localization signals on p50-p65 heterodimer. p65 then undergoes phosphorylation, leading to the nuclear translocation of NF-κB and its binding to a specific DNA sequence, which in turn results in the transcriptions of genes, such as, TNF-α, interleukins, ICAM-1,VCAM-1, iNOS, and COX-2 (433).

Studies have shown that in the cytosol, mitochondrial ROS may mediate the changes in cytoplasmic redox state that signal NF-κB activation. In fact, specific blocking production of oxygen radicals from the electron transport chain prevents the activation of NF-κB in cytokine-stimulated cells (434). Interestingly, in our previous study we have demonstrated chronic TDF administration invokes renal tubular mitochondrial damage, oxidative stress and depletion of cellular antioxidants (389), suggesting that NF-κB plays a role in TDF induced renal inflammation, and that it may be upregulated in response to mitochondrial damage induced altered redox state.

In kidney, NO mediates many physiological functions and plays an important role in nephrotoxicity pathogenesis. The effect of NO depends on the production site, nitric oxide synthase (NOS), duration of action, and level of reactive oxygen intermediates present. NO is generated by three

isoforms of NOS (the neuronal, endothelial, and inducible). Immunostaining revealed that nNOS and eNOS were localized mainly in renal tubules, collecting ducts, and glomeruli,whereas iNOS was found predominantly in renal tubules and collecting ducts. Endothelial NOS (eNOS) is expressed in endothelial cells of renal and glomeruli and plays a role in intrarenal vascular tone by direct relaxation of afferent arteriole (435). Neuronal NO (nNOS) is expressed in macula densa and plays a role in regulation of tubule-glomerular response (435). The renal medulla is enriched in nitric oxide (NO) synthetic capacity and the NO produced appears to participate in regulation of blood pressure (435).

NO and NF-κB signaling pathways are intimately linked. NF-κB activation is essential for NOS2 gene transcription (436), and NO-related molecules modulate NF-κB signal transduction in a cell- and stimulus-specific manner. In normal kidneys, iNOS is shown to be low and is induced by cytokines and its activity elevates NO level which is responsible for cell death. However, more recent studies suggest that iNOS is expressed in various segments of the nephron under normal physiological conditions. Bachmann et al. observed iNOS mRNA primarily in the inner medulla of the normal rat kidney and in the glomerulus. The iNOS mRNA was located in the medullary thick ascending limb (MTAL) with smaller amounts in the medullary collecting duct and vasa recta bundle.

In our study, the immunostaining of iNOS protein in all regions of the kidney and was more intense in the outer medulla in the control rat lends support to the notion that iNOS is‘constitutively’ and differentially expressed in various regions of the kidney. Prominent expression of iNOS was detected in the thick ascending limb of LH, and inner medullary CD, whereas much less expression of iNOS was noted in the thin limbs of LH, PCT, and the outer medullary CD, in agreement with the findings of Bachman (250). The basal iNOS expression in the medulla, particularly in the

MTAL and medullary collecting duct may be related to the hypoxic milieu in which these segments normally function (437).

Inducible NOS iNOS) has been shown to be stimulated by proinflammatory cytokines (TNF), NF-κB and oxidative stress (40,436). In our study we found increased iNOS protein expression by immunostaining and immunoblotting in the TDF treated rats as compared with controls. iNOS mRNA was increased in the TDF treated rat kidneys but was not significantly different from the control. All these findings suggest that iNOS plays a role in TDF nephrotoxicity. Stimulation of iNOS has been shown to contribute to renal cell injury. Over expression of iNOS has been implicated in toxin induced proximal tubular epithelial cell injury (39,41,436).

The cytotoxic potential of NO is a consequence of its ability to form peroxy nitrite (409),which is a potent nitrating and oxidizing agent. Peroxynitrite readily reacts with proteins to form 3-nitrotyrosine (409), or oxidises thiol groups to form nitrosothiols (410), which can either lead to inactivation or activation (410,411) of the proteins. 3-NT, is considered as the footprint of $ONOO^-$, and its appearance in tissue samples is taken as a diagnostic tool for exposure to peroxynitrite (77). In healthy rats, minimal staining for nitrotyrosine was seen in the epithelial cells of proximal tubules in agreement with the findings of Bian et al (412). TDF treatment resulted in increased 3-NT level both immunohistochemical method and immunoblot, providing evidence for peroxynitrite formation.

Peroxynitrite can damage the cells by the oxidation of free thiols-cysteine residues (410). Accumulating evidence indicates that dysregulated, diminished, or excessive S-nitrosylation may be implicated in a wide range of pathophysiological conditions (410). In the present study, we observed a massive increase in nitrocysteine staining (assessed by immunostaining and

immunoblotting methods) in kidneys of TDF treated rat. This suggest that S-nitrosylation may play a role in TDF nephrotoxicity. S-nitrosylation is modulated by the cellular redox status; its formation is dependent on the state of redox equilibrium and is prevented by high levels of antioxidants (438). NO has been found to block cell death after GSH depletion by preserving the redox status of mitochondrial protein thiols, probably by a mechanism that involves S-nitrosylation of mitochondrial protein thiols (439). This may represent an endogenous protective mechanism for the mammalian cell against nitrosative/oxidative stress when intracellular thiols or other redox constituents have decreased below a critical concentration. We have previously shown that TDF treatment results in the depletion of renal reduced GSH and protein thiol (389). This may explain the massive increase in nitrocysteine levels in the TDF treated rat kidneys.

Many redox-related enzymes contain active cysteine (s), which are capable of undergoing NO-mediated S-nitrosylation. Among these are catalase, glutathione peroxidase, glutathione reductase , glutathione transferase P1, and thioredoxin (410). These enzymes have been shown to be inactivated by S nitrosylation. It is worthwhile to mention here that in our earlier study (study III) TDF administration results in the loss of activity of GPO, GR, GST (389), suggesting that TDF induced loss of activity of these enzymes may due to their nitrosylation.

.

The other NF-κB response gene is cyclooxygenase (COX). COX-2 an enzyme that catalysis the formation of prostaglandins mainly that mediate inflammation and PGE2 is the major metabolite of COX activity is localized mainly to the outer and inner medullary parts of the nephron, including the PT (252). Cyclooxygenase (COX) has two isoforms, COX-1 and COX-2. COX-1 is a housekeeping enzyme, is constitutively expressed and is localized to arteries and arterioles, glomeruli, and collecting ducts. It is thought to be involved in the regulation of renal blood flow, and control of platelet aggregation (252). In contrast, COX-2, the ‘‘inducible’’ isoform, is barely

detectable in normal tissues but it is responsible for the release of PGs during inflammatory conditions (253). Although COX-2 is considered to be the inducible form, it is constitutively expressed in the TALH and in the region of the macula densa, primarily a cortical structure (254), where it is involved in the stimulation of renin release from the juxtaglomerular cells (255). COX-2 is known to be activated by pro-inflammatory cytokines and ROS, and its transcription is regulated by several transcription factors including nuclear factor κB (256).

In the present study, expression of COX-2 was barely detectable in the kidneys of control rats. On the other hand, COX-2 protein expression as well as mRNA expression was significantly increased in the TDF treated rat kidneys. The increase in COX-2 mRNA and protein level may be due to its upregulation by NF-κB. Although we did not measure COX-2 activity, we speculate that it must be higher in the TDF treated rats. Our speculation is based on reports that iNOS binds directly to and activates COX-2 by S-nitrosylation of a single cysteine (C526), resulting in an increased Vmax and enhanced prostaglandin E2 production (221). In addition, COX-2 S-nitrosylation and prostaglandin E2 formation were attenuated by blocking iNOS–COX-2 interaction. Recently Snyder and colleagues demonstrated by coimmunoprecipitation that iNOS and COX-2 exhibit a direct and exclusive interaction (440).

TNF-α is another NF-κB target gene. TNF-α genes contain functional NF-κB binding sites that are essential for their induction following injury (419) . It is a proinflammatory cytokine capable of upregulating its own expression as well as the expression of other genes pivotal to the inflammatory response (257). Furthermore, exposure of renal tissue to TNF-α causes significant cellular damage and dysfunction (40,258). The TNF-α induced inflammatory cascade for renal injury involves immune cells and intrinsic renal cells, such as mesangial cells, glomerular and tubular epithelial cells, and endothelial cells (439)

.

Tubular epithelial cells, the largest cell population in kidney parenchyma, are important players in renal inflammation after injury. TNF-α is shown to be induced and secreted by proximal tubular cells when subjected to either gentamicin (260) or cisplatin (261). This provides direct support for the concept that damaged proximal tubules contribute to, the enhanced renal cytokine/chemokine production state. In the present study, TDF administration resulted increased TNF-α protein expression in as well as its mRNA expression, suggesting that TDF nephrotoxicity may be mediated by increasing the transcription of TNF-α gene via NF-κB activation. TNF is known to activate a wide array of cellular signaling pathways that result in divergent biological responses, including activation of NF-κB (262). This action has been supported by the latest finding that TNF-αR1 gene deletion prevented the increase of NF-κB translocation, iNOS and COX-2 expression, and MPO activity (441).

Renal epithelial cells possess surface receptors for TNF (TNFR) engagement of which by exogenous TNF-α triggers apoptosis. TNFR1 is present in normal glomeruli and is upregulated on infiltrating leukocytes in response to renal injury. TNFR2 is usually not expressed in normal kidney and is upregulated in tubular cells in response to renal injury (442).

The mechanisms of TNF-α-induced renal injury are multiple. TNF-α it is a proinflammatory cytokine capable of inducing glomerular, endothelial damage, neutrophil infiltration, fibrin deposition and renal failure (443–446). TNF- induces renal cellular apoptosis and reduces glomerular blood flow and glomerular filtration rate by stimulating the production of a variety of vasoactive mediators (i.e. platelet-activating factor, endothelin-1, prostaglandins, nitric oxide (443,444). TNF-α also stimulates the production of other inflammatory mediators, including

reactive oxygen species and IL-1, which generate an increase in glomerular permeability and contribute to further cellular and organ dysfunction (445,446).

We also attempted to determine whether matrix metalloproteinases-9 , another NF-κB response gene, is involved in the pathogenesis of TDF induced renal damage. In this study we have shown that chronic administration of TDF increases the protein expression, and the activity of MMP-9 in rat kidney. Oxidative stress has been reported as a critical initiator in drug induced damage. The sources of oxidants resulting in such stress may be both in the intracellular and extracellular compartments. Apart from cellular and mitochondrial oxidative stress, it is also induced in other forms of acute renal injury , is a modulator of extra cellular matrix remodeling in the kidney (418). Thus the drug-induced effects seen in the kidney suggest the possibility that extracellular matrix remodeling may be an important factor in both the pathogenesis and recovery of TDF induced renal damage. Moderate elevations in the levels of ROS have been reported to increase the activity of MMP-9 (254). The process of S-glutathiolation of pro-MMP 9 has been described as a regulator of this increase in activity (419). Studies have been reported increase in MMP-9 results in tubular dysfunction and increased vascular permeability (246). Higher concentration (500 µM-5 µM) of peroxy nitrite cause protein fragmentation (380). The present results suggest a renal environment with high levels of matrix metalloproteinase-9 could be involved in the pathogenesis of renal damage.

Inflammatory infiltrate is associated with or preceeds tubular atrophy. Inflammation may further amplify oxidative/nitrative stress, and these interrelated processes eventually culminate in more concerted renal tubular and endothelial cell demise (both apoptotic and necrotic), secondary hypoxia, kidney dysfunction, and failure (423). Thus persistent tubular injury and neutrophil infiltration induced by TDF may lead to interstitial fibrosis, and renal failure.

In summary , the activation of NF-κB and its downstream proinflammatory target genes iNOS, and COX-2, TNF-α and MMP 9 play a critical role in the pathophysiology of TDF induced PT cell death resulting in PT tubular dysfunction (which manifests as Fanconi Syndrome). The cellular sources of ROS in TDF mediated renal damage are most probably the damaged mitochondria and neutrophil derived MPO. However, other sources such as xanthine oxidase and NADPH oxidase cannot be excluded. The cellular sources of peroxynitrite may be the nitric oxide derived from the overexpression of iNOS, and mtNOS as well as increased MPO activity of the infiltrated neutrophils.

STUDY-V

Melatonin Pretreatment ameliorates TDF induced Renal damage by attenuating oxido-nitrosative stress, neutrophil infiltration, and NF-κB inflammatory signaling pathway

ABSTRACT

Prevention of TDF tubulotoxicity is vital to avoid irreversible tubulointerstitial damage in HIV infected patients. Identifying an agent that prevents TDF induced renal injury can lead to better tolerance to TDF and therefore a more effective treatment can be achieved in HIV infected patients. Our previous studies have demonstrated that TDF induced renal damage is associated with increased oxido-nitrosative stress, neutrophil infiltration, and activation of NFκB inflammatory signaling pathway. Melatonin is a well-established natural antioxidant and anti-inflammatory agent. The aim of this study was to determine whether melatonin pretreatment protects against TDF induced renal damage. Rats were pretreated with melatonin in 2 different doses as 20 mg/kg body weight and 40 mg/kg body weight 1 hour before administration of 600 mg/kg body weight TDF. The animals were sacrificed 24 hrs after the final dose of the TDF. Kidney tissues were used for assessment of injury using light microscopy and electron microscopy. Serum sample was used for the measurement of bicarbonate, phosphate etc. The kidney homogenates were used to analyse oxido-nitrosative stress parameters, NFκB signaling pathway, and apoptosis. The results show that melatonin pretreatment attenuates TDF nephrotoxicity in a dose dependent manner. Melatonin's protective effect appears to be mediated by attenuation of oxidative stress and nitrosative stress, inhibition of nuclear translocation and activity of NFκB, decreased mRNA expression of NFκB responsive proinflammatory genes , iNOS, COX-2, TNF-α, and MMP-9. Melatonin pretreatment attenuated TDF induced apoptosis as measured by TUNEL assay and caspase 3 activity.

INTRODUCTION

Numerous case reports and case series have described severe cases of renal tubular toxicity associated with TDF exposure. It has been shown that continuous tubular damage may promote tubular cell death (atrophy), and interstitial fibrosis and subsequent decreased glomerular filtration and renal failure. Melatonin is a well-established natural antioxidant and anti-inflammatory agent. It is not only a strong scavenger of free radicals, reactive oxygen species (ROS) and RNS (nitric oxide) (447). It is also a stimulator of the cellular antioxidant systems (448) and has the ability to reduce free radical production at the mitochondrial level (449).

As TDF induced mitochondrial tubulopathy is associated with overproduction of ROS and RNS and depletion of antioxidant system, and MT has been shown to protect against tubular damage caused by different nephrotoxins, primarily by its antioxidant property and anti-inflammatory effect, we tested the hypothesis that melatonin supplementation may prevent TDF nephrotoxicity by attenuating oxidative stress and inflammation. To this end, we assessed the protective effects of melatonin by studying the markers of renal oxidative stress, nitrosative stress, NFκB inflammatory pathway and inflammation, along with histopathological changes in the kidney.

Animals and treatments:

Adult male Wistar rats (200–250 gm.) were used for the studies. They were housed in standard rat cages (421 × 290 × 190 mm). All animals were exposed to 12 hour light–dark cycles and allowed access ad libitum to water and standard rat chow. The dose of melatonin (20 mg/kg body wt. /day) was decided based on a recent study reported by Xu et al., (450) which showed that intraperitoneal administration of 20 mg/kg body wt. /day of melatonin protects against diquat induced renal damage (389).

Experimental design:

The rats were randomly assigned to 4 groups and were treated as follows.

Group I (control): The rats in this group (n = 6) received sterile water only by gavage for 35 days

Group II: The rats (n = 6) in this group received 600 mg/ kg body weight TDF in sterile water by gavage for 35 days.

Group III: The rats (n = 6) in this group received once daily 20 mg/kg body wt. melatonin i.p. one hour before the administration of 600 mg/ kg body weight TDF in sterile water by gavage for 35 days.

Group IV: The rats were pre-treated daily with 20 mg/kg body wt. melatonin i.p. one hour. before the administration of sterile water by gavage

Control animals were treated with sterile water on the same schedule as TDF treatment and were killed at the same time point for TDF treated and control rats.

Mortality checks, clinical observations, and body weights:

All animals were observed daily for any clinical signs of toxicity, morbidity, and mortality throughout the experimental period. The body weight of each rat was also monitored on a weekly basis till the end of treatment.

Necropsy and blood and urine collection for biochemistry:

All the rats were sacrificed 24 hours after the final dose of TDF / sterile water. Twenty-four hours before sacrifice, the rats were placed individually in metabolic cages, and urine was collected for biochemical analysis. On the 36th day, blood samples were collected from the rats under halothane

anesthesia, by cardiac puncture into tubes and allowed to clot at room temperature. Thereafter, serum was separated by centrifugation at 1200 g for 15 min at 4 °C for clinical chemistry.

Both the kidneys were removed and weighed. Half of the left kidney was cut in cross-section and fixed at 10 % buffered formalin for light microscopy, and the remaining half was fixed in 3% glutaraldehyde for electron microscopy. Half of right kidney was used for biochemical assay, remaining half kidney was snap-frozen in liquid nitrogen and stored at - 70º C for western blot and PCR assays.

Morphological examination of the kidney:

After fixation of kidney tissues in 10 % buffered formalin for 24 h at room temperature, the slices were embedded in paraffin and then sectioned. Four micrometer-thick paraffin sections were stained with hematoxylin and eosin for light microscope examination using established protocol.

Examination of the ultrastructural changes in the kidney tissues by electron microscope

Electron microscopy was done based on the methods employed routinely in the Lewis lab (355). The extent of mitochondrial ultrastructural injury in the proximal tubular cells was then quantitatively assessed (Scale of 0–5) based upon the cell injury staging system described by Trump and colleagues (377).

Serum clinical chemistry:

Serum was separated out and used for the estimation of phosphate, potassium, bicarbonate, uric acid, glucose, urea and creatinine by conventional methods.

TUNEL ASSAY (Terminal deoxynucleotidyl transferase dUTP nick-end labeling assay):

The terminal deoxynucleotidyl transferase dUTP nick-end labeling (TUNEL) assay was conducted in accordance with the manufacturer's protocols. Briefly, kidney tissues were fixed in 10 % paraformaldehyde and permeabilized in sodium citrate, pH 6.0. The sections were observed under an Olympus Fluoview (FV1000) confocal microscope , Japan. Images were collected with a digital camera (Carl Zeiss)

Biochemical assays carried out

- Oxidative stress and nitrosative stress markers and antioxidant enzymes:
- Immunohistochemical staining for NT, NCY, COX 2, PARP and caspase 3
- Western blots for NFκB p65, NT, iNOS, TNF alpha, MMP-9, PARP & caspase-3
- RTqPCR for mRNA expression of NFκB p65, iNOS, TNF alpha, COX 2, MMP-9 and caspase 3 genes
- The activity of NFκB p65 and caspase-3 by ELISA and Fluorimetry respectively

The detailed procedures were followed as described in the methodology section

Statistical analysis

All data were analyzed by one-way analysis of variance (ANOVA) using a Bonferroni correction for the multiple t-test as a post-hoc test. A value of $P < 0.05$ was taken to indicate statistical significance. Data analysis was carried out using Statistical Package for the Social Sciences (SPPS), version 16.

RESULTS:

1. Melatonin pretreatment ameliorated TDF induced decrease in body weight and kidney weight

There were significant differences in body weight and kidney weights between control and TDF treated rats. Pretreatment with melatonin partially but significantly prevented TDF induced reduction in kidney weight and body weight (Figure: 8.1.1) & (Figure: 81.2)

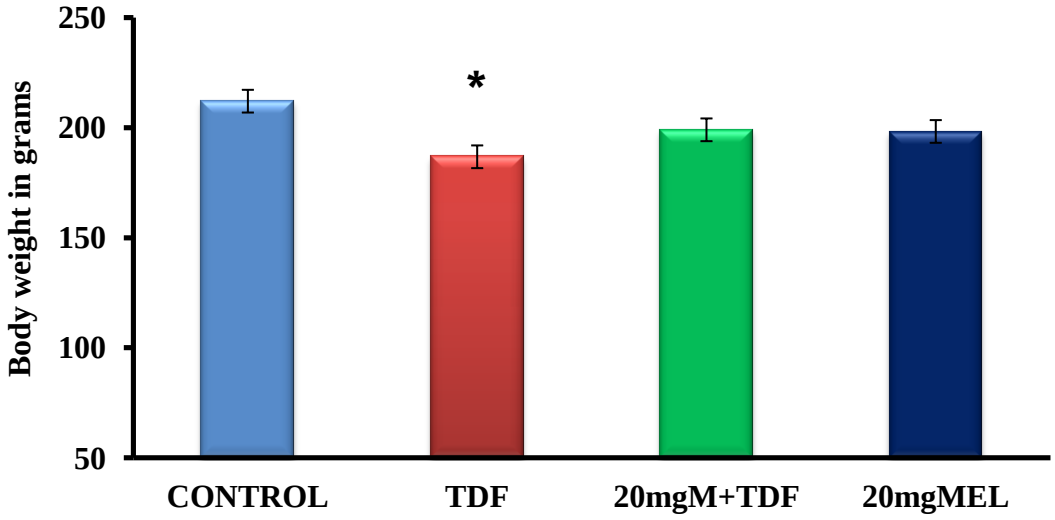

Figure: 8.1.1 Effect of melatonin pretreatment on changes in body weight in control and TDF treated rats, n=6 in each group. Data represent mean ±SD. * p value < 0.05 as compared with controls.

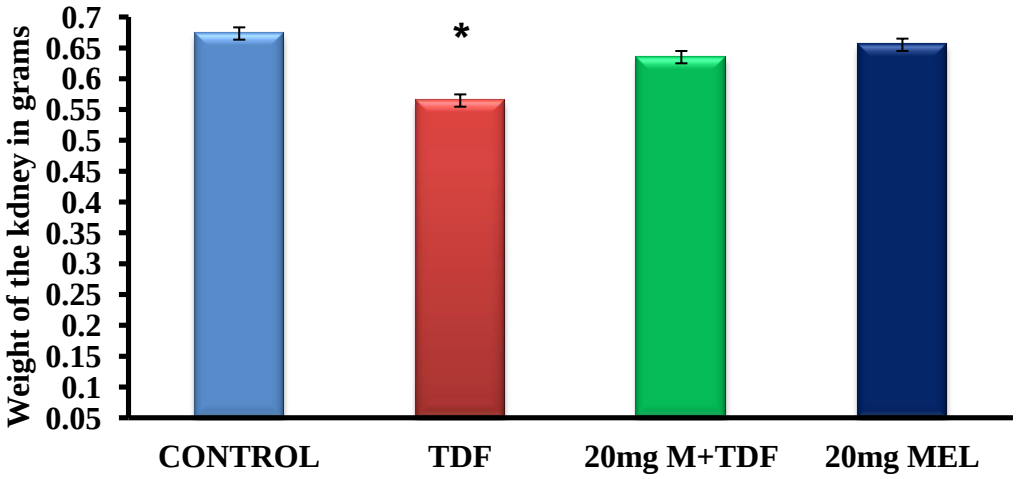

Figure: 8.1.2 Effect of melatonin pretreatment on changes in kidney weight in control and TDF treated rats , n=6 in each group. Data represent mean ± SD. * p value < 0.05 as compared with controls.

2. Melatonin pretreatment ameliorated TDF induced renal damage

The H &E staining results of kidneys of control rats and TDF treated rats is shown in Figure: 8.2.1. The kidneys of control rats showed normal morphology. Sections of the kidneys from the control group showed normal histological structure of the glomeruli and renal tubules in the cortex and normal tubules in the medulla. The proximal tubule epithelial cells exhibited no spaces or gaps between the cells. Treatment with 20 mg/kg body wt. melatonin alone had no significant toxic effect on the renal histology and the features were comparable with that of control rats.

In the TDF treated rat kidney (TDF) cortex, the proximal convoluted tubules were distorted and their lining epithelium was destroyed. Interstitial edema and cytoplasmic vacuolations were also observed. Isolated proximal tubules showed some detachment of cells and congestion. Analysis of similar tissue sections from 6 animals from each treatment group indicated that these changes were remarkably consistent from one animal to another. Some glomeruli showed atrophy. In the medulla, there was destruction of the lining epithelium of the loops of Henle and the collecting duct. Pretreatment with melatonin (MT+TDF) attenuated TDF induced renal damage. There was comparatively less damage to the tubules and glomerulus in the melatonin pretreated rats as compared with rats treated with TDF alone. The cortex of MT pretreated rats showed near normal morphology although some tubules showed mild epithelial desquamation and edema. However, there was no vacuolization or necrosis. The glomeruli appeared normal. Pretreatment with MT reduced TDF induced damage to the medulla. Most of the tubules appeared normal. Few tubules showed dilatation.

Figure: 8.2.1

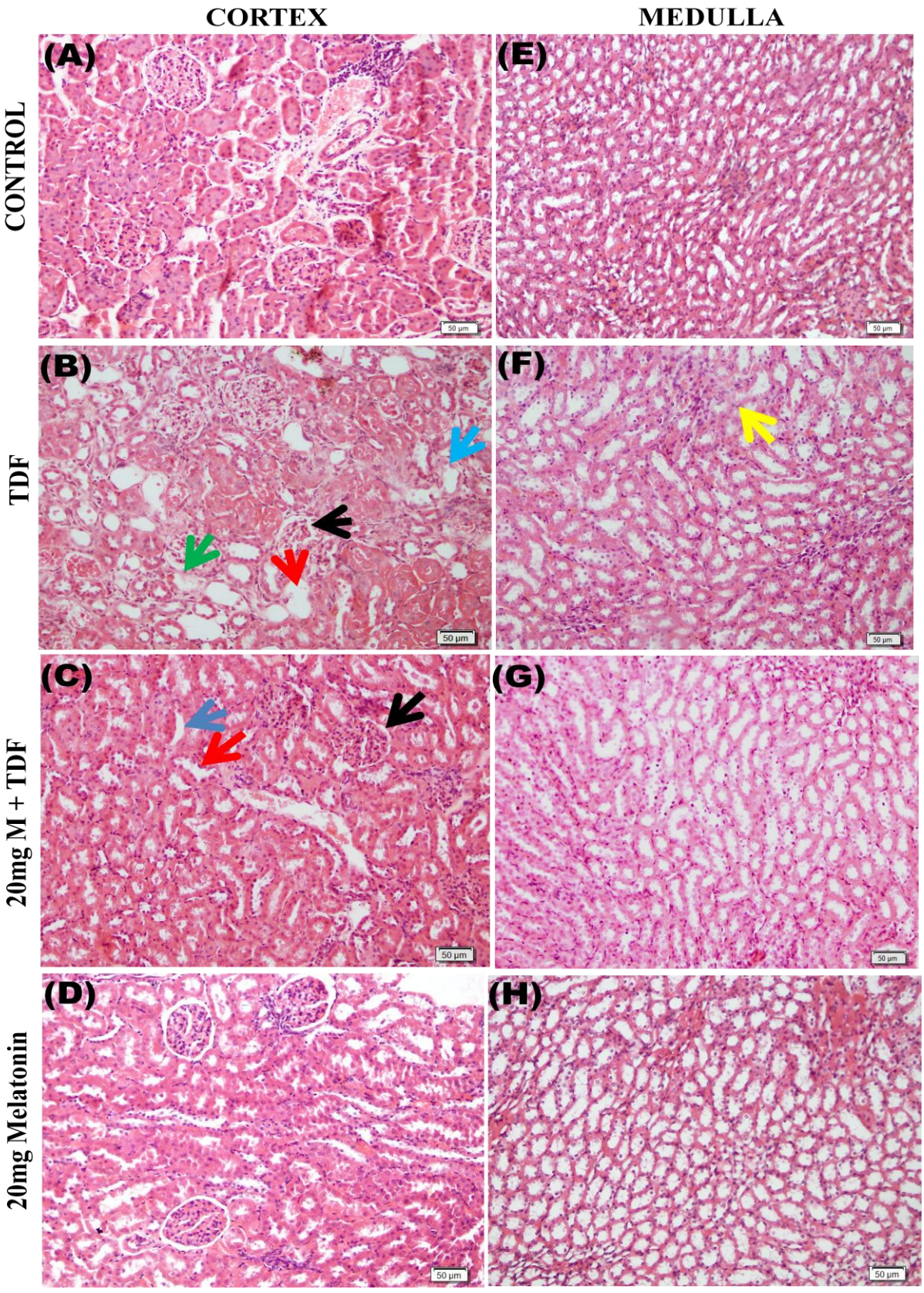

(Please see next page for figure legends)

Figure: 8.2.1 Representative images of the effect of melatonin pretreatment on renal histology

(A). Cortex and (E) medulla of control rats showing normal architecture, (Hematoxylin and Eosin) magnification X100.

(B) In the cortex of TDF treated rats, the convoluted tubules are distorted and their lining epithelium is destroyed in proximal tubules (green arrow), destruction of the epithelial cells of distal convoluted tubules (blue arrow), dilation of proximal convoluted tubules (red arrow) and some glomeruli are shrunken (Black arrow). (F) Medulla of TDF treated rat showing destruction of the lining epithelium of the loops of Henle and the convoluted tubules (yellow arrow) in medulla, (Hematoxylin and Eosin) magnification X100.

(C) Cortex of 20 mg Melatonin + TDF treated rat. Black arrow indicates the normal glomerulus [G]. The damage was very much less as compared with the group treated with TDF alone. There was mild dilation of the proximal tubules (Blue arrow) , and distal convoluted tubules (Red arrow). (G) Medulla of 20 mg melatonin + TDF treated rat -Normal architecture, Hematoxylin and Eosin, magnification X100.

(D) Cortex of 20mg Melatonin treated rat - Normal architecture. (H) Medulla of kidney 20mg Melatonin treated rat-Normal architecture, Hematoxylin and Eosin, magnification X100.

3. Melatonin pretreatment prevented TDF induced ultrastructural abnormalities in the kidney tubule:

Figure: 8.2.2 shows the effect of melatonin pretreatment on the subcellular organelles of the kidney tubules.

In the control (C) and melatonin treated (MT) rat kidneys the tubular organization was well preserved with normal tubular cells cuboidal in shape, containing well-defined nuclei, and a uniform cytoplasm, undilated intercellular spaces, normal tight junctions, and numerous spherical and elongated mitochondria. The PT cytoplasm also contained a prominent Golgi apparatus, abundant smooth (SER) and rough (RER) endoplasmic reticulum, numerous free ribosomes and primary lysosomes. Numerous peroxisomes were also present.

Proximal tubular epithelia of TDF-treated rats (TDF) showed moderate to severe damage to the mitochondria. Mitochondrial degeneration, reduction in number, and inner membrane separation from outer membrane, dissolution of cristae ,and amorphous deposit in mitochondrial matrix were the characteristic findings. Based on the scale defined by Trumph, the mitochondrial injury score was between 4 and 5. Nuclei of tubular epithelial cells, endothelial cells, and mesangial cells were shrunken. Fusion of foot processes was also observed.

Pretreatment with melatonin (MT +TDF) reduced TDF induced ultrastructural abnormalities in the proximal tubules. The microvilli were normal in height and density. Vacuoles were decreased in number. Lysosomes were increased in number . Less number of mitochondria of varying shapes and size was observed. Many mitochondria appeared normal with distinct cristae and matrix. Based on the scale defined by Trumph, the mitochondrial injury was mild or absent and the mitochondrial score was 0 or/ 1. The nucleus appeared normal with prominent nucleolus.

Figure: 8.2.2

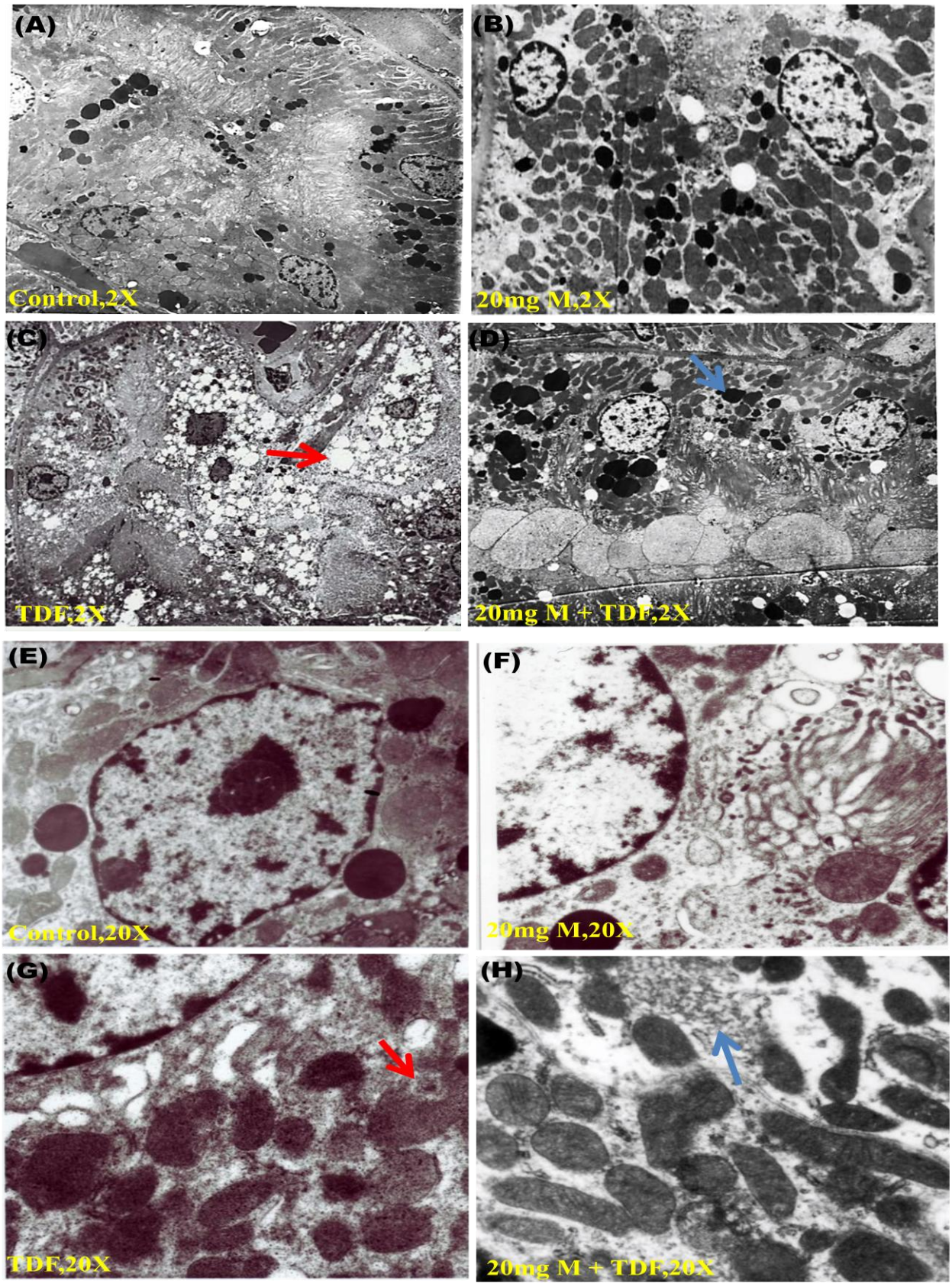

(Please see next page for figure legends)

Figure : 8.2.2 Representative electron micrographs of melatonin pretreated control rat kidney and TDF treated rat kidney.

Lower magnification (x 2000) (A-D)

A. Control .Normal appearance of tubules showing numerous mitochondria, lysosomes and distinct nucleus.

B. M-. Melatonin treated-Presence of numerous mitochondria and lysosomes in the kidney tubule.

C. TDF- TDF treated showing numerous vacuoles seen in the cytoplasm of the kidney tubule (Red arrow). There was less number of lysosomes (blue arrow).

D. M +TDF. Melatonin pretreated .The tubules of the melatonin pretreated rats showed near normal structure .There was less number of vacuoles, the lysosomes were increased in number, and there was less number of abnormal mitochondria

Higher magnification (x 22,000) (E-H)

E. Control rat tubule showing normal mitochondrial structure.

F –M- melatonin treated. Presence of numerous elongated mitochondria with regular cristae and clear matrix

G. TDF- Many mitochondria were swollen. There was a disruption of mitochondrial cristae (Red) and amorphous deposits were present in the mitochondrial matrix (M) (Blue arrow)

H. MT +TDF. There was minimal damage to the mitochondria. Many mitochondria appeared normal, with regular cristae and clear matrix (Blue arrow).

4. Effect of melatonin pretreatment on serum urea and creatinine

TDF treatment resulted in a slight increase in serum urea levels (Figure: 8.3.1), but had no effect on serum creatinine levels (Figure:8.3.2). Melatonin pretreatment prevented TDF induced increase in serum urea levels.

5.Melatonin pretreatment partially attenuated TDF induced tubular dysfunction

Proximal tubular function was impaired in TDF-treated rats (Figure: 8.3.3 to 8.3.6), as evidenced by increased urinary phosphate, potassium and bicarbonate excretion and a substantial reduction in serum phosphate, bicarbonate, and potassium.

MT pretreatment completely restored the serum bicarbonate levels pretreatment with MT returned serum uric acid level to normal values . MT pretreatment had no significant effect on TDF induced hypokalemia and hypophosphatemia, although it showed a trend towards restoration .

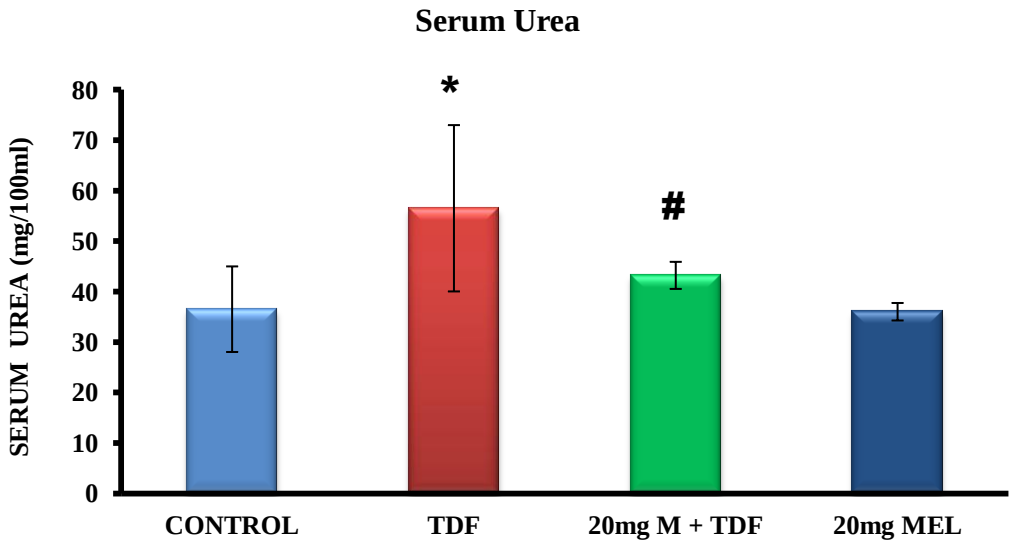

Figure: 8.3.1 Effect of melatonin pretreatment on serum urea level in control and TDF treated rats, n=6 in each group. Data represent mean ±SD. * p value < 0.05 as compared with controls, # p value < 0.05 as compared with TDF.

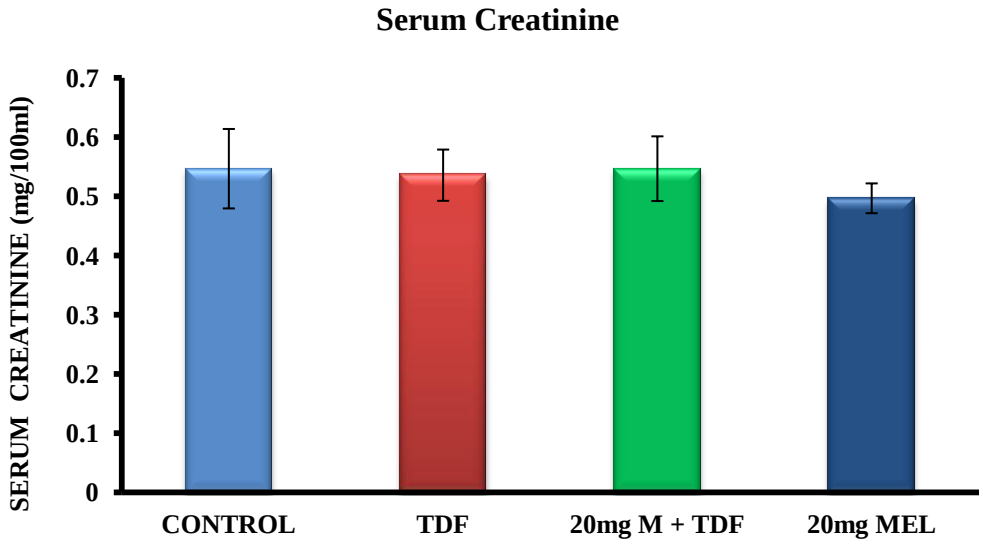

Figure: 8.3.2 Effect of melatonin pretreatment on serum creatinine in control and TDF treated rats , n=6 in each group. Data represent mean ± SD.

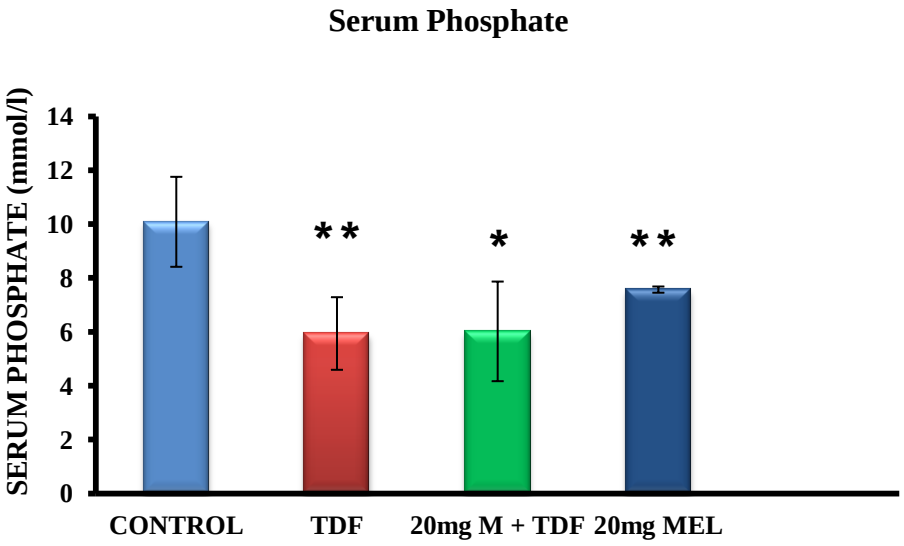

Figure: 8.3.3 Effect of melatonin pretreatment on TDF induced hypophosphatemia. Values represent mean ± S.D., n= 6. ** P < 0.01, * P < 0.05 vs. control.

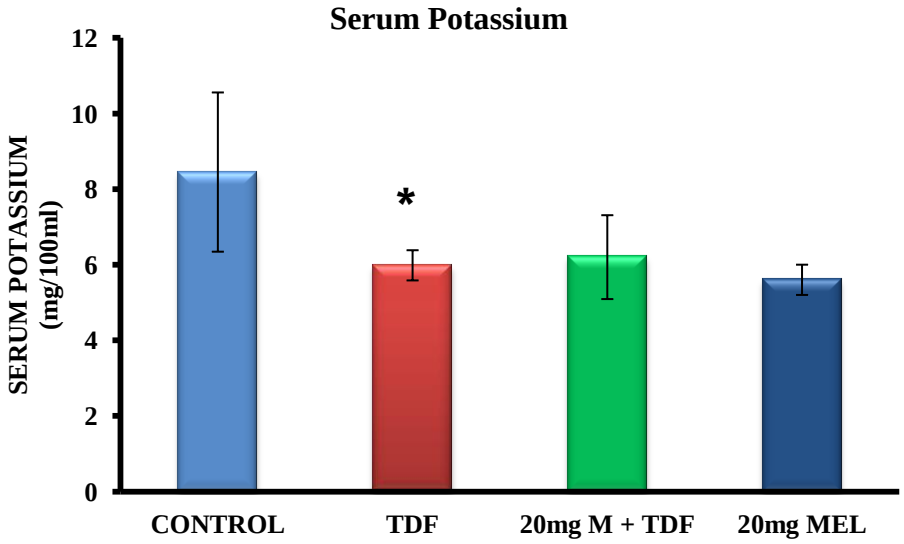

Figure: 8.3.4 Effect of melatonin pretreatment on TDF induced hypokalemia. Values represent mean ± S.D., n= 6. *P < 0.05 vs. control.

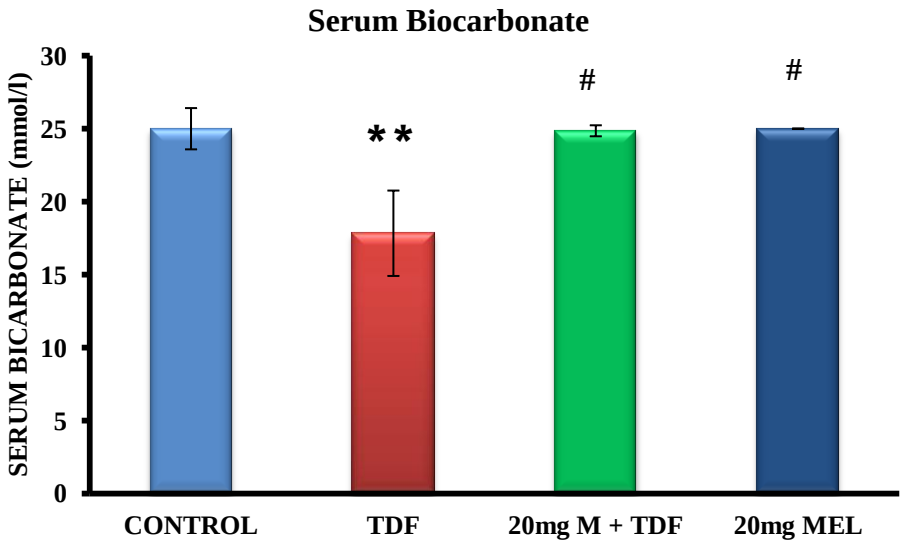

Figure: 8.3.5 Effect of melatonin pretreatment on TDF induced decrease in serum bicarbonate levels. Values represent mean ± S.D., n= 6. ** P < 0.01 vs. control, # P < 0.01 vs. TDF.

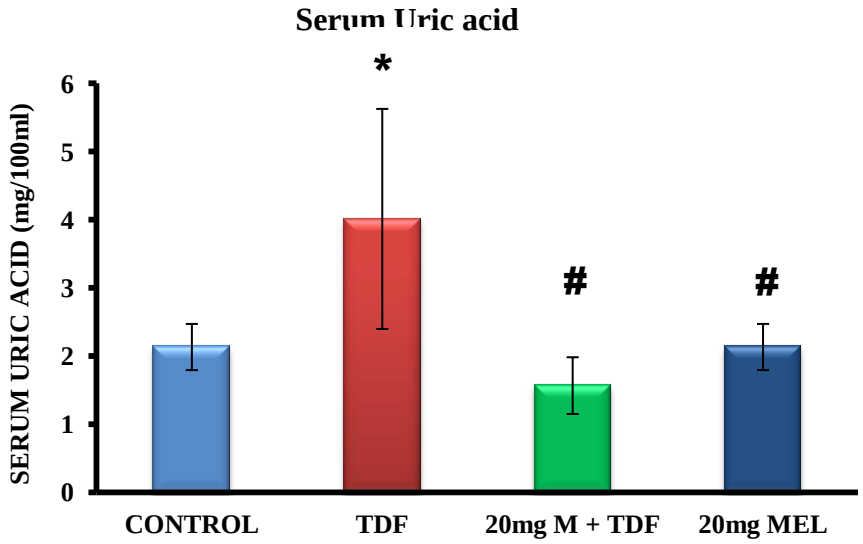

Figure: 8.3.6 Effect of melatonin pretreatment on TDF induced increase in serum uric acid levels. Values represent mean ± S.D., n= 6. *P < 0.05 vs. control, # P < 0.05 vs. TDF.

6. Melatonin pretreatment attenuated TDF induced renal oxidative stress

A 2 fold increase in protein carbonyl content was observed in the kidneys of TDF treated rats. Pretreatment with melatonin completely prevented TDF induced increase in renal PCo content (Figure: 8.4.1). However, it had no effect on protein thiol (Figure: 8.4.2), TBARS (Figure: 8.4.3). and conjugated diene (Figure: 8.4.4) .

7. Melatonin pretreatment prevented TDF induced renal inflammation:

A 2 fold increase in myeloperoxidase activity, a marker of neutrophil infiltration was observed in the kidneys of TDF treated rats. MT pretreatment completely prevented TDF induced kidney inflammation as evidenced by its ability to completely inhibit MPO activity (Figure: 8.4.5).

8. Melatonin pretreatment partially restored renal antioxidant system

The activities of all the antioxidant enzymes estimated were significantly decreased in the kidneys of TDF treated rats as compared with the control. With regard to the glutathione antioxidant system, MT pretreatment restored the activity of GST almost completely (Figure: 8.4.6) and that of GR partially but significantly (Figure: 8.4.7) and GPO activity (Figure: 8.4.8). Reduced glutathione, was not restored to control values upon melatonin pretreatment (Figure: 8.4.9). MT pretreatment had no significant effect on TDF induced reduction in SOD activity (Figure: 8.4.10) and increase in catalase activity (Figure: 8.4.11).

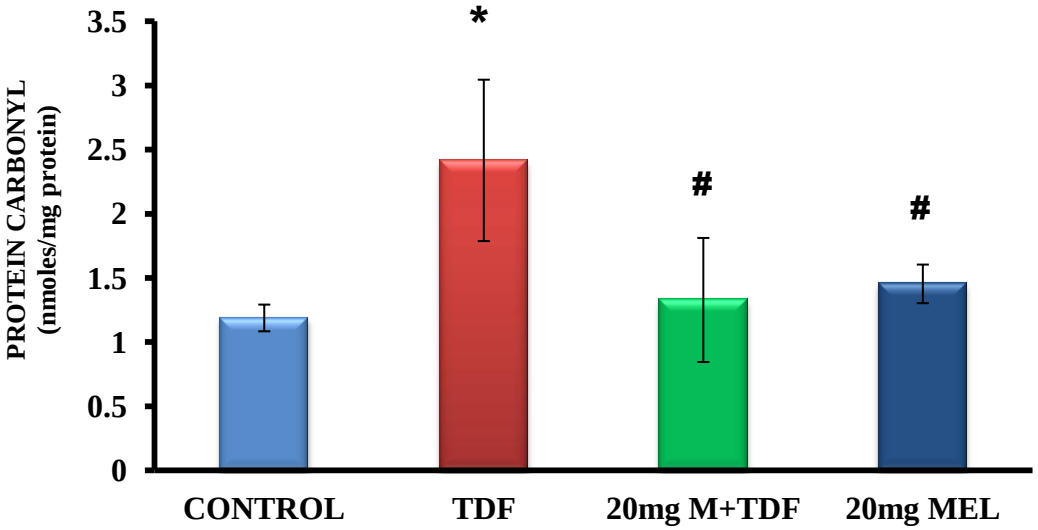

Figure: 8.4.1 Effect of melatonin pretreatment on protein carbonyl levels in the kidneys of rats. Data represent mean ± SD, n=6 in each group. *p<0.05 compared with controls, # p <0.05 Vs. TDF.

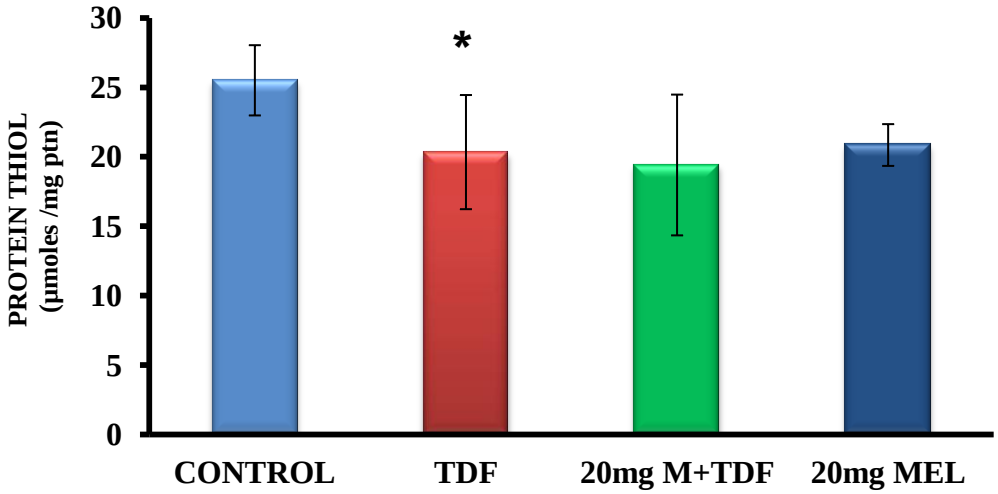

Figure: 8.4.2 Effect of melatonin pretreatment on protein thiol level in the kidneys of rats. Data represent mean ± SD, n=6 in each group. *p<0.05 compared with controls.

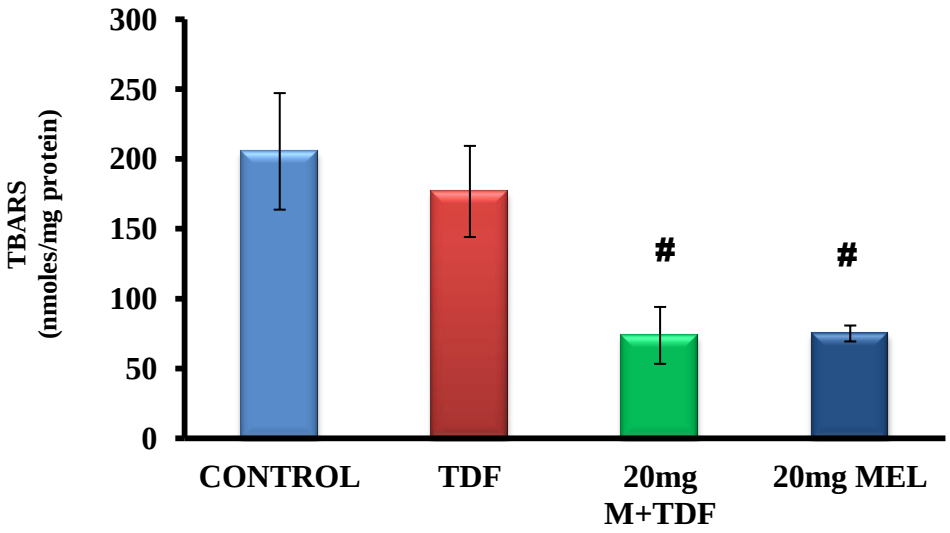

Figure: 8.4.3 Effect of melatonin pretreatment on TBARS levels in the kidneys of rats. Data represent mean ± SD, n=6 in each group. # p < 0.05 compared with TDF.

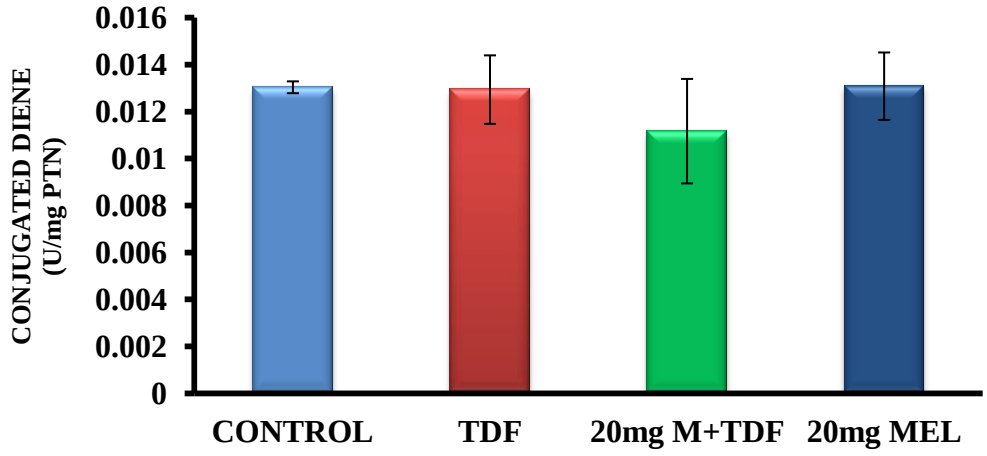

Figure: 8.4.4 Effect of melatonin pretreatment on Conjugated diene levels in the kidneys of rats. Data represent mean ± SD, n=6 in each group.

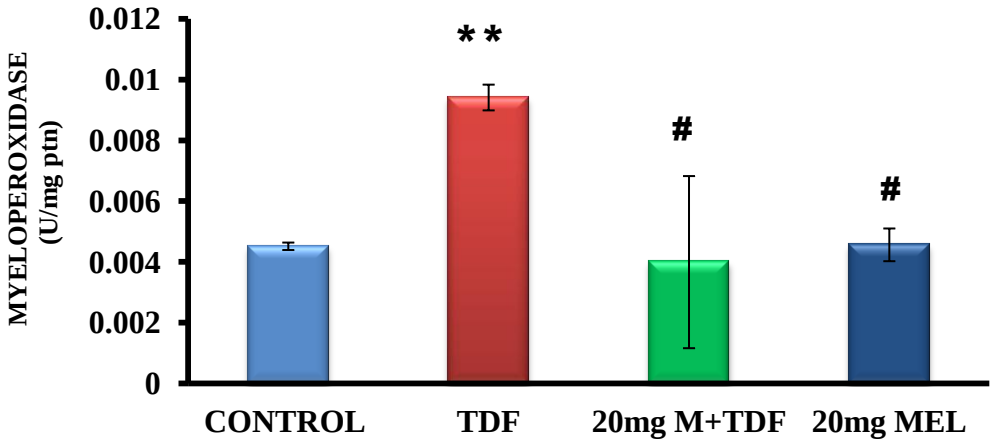

Figure: 8.4.5 Effect of melatonin pretreatment on myeloperoxidase activity in the kidneys of rats . Data represent mean ± SD, n=6 in each group. **p< 0.01 compared with controls, # p < 0.05 vs. TDF.

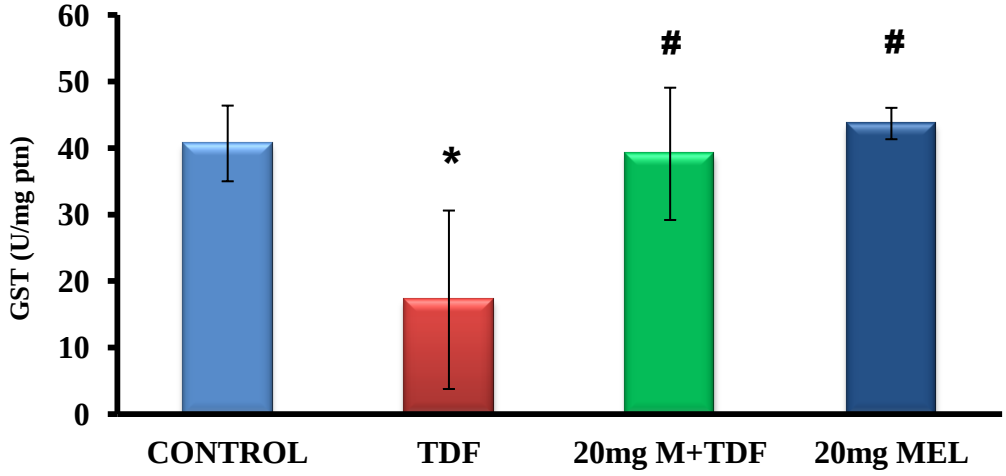

Figure: 8.4.6 Effect of melatonin pretreatment on GST activity in the kidneys of rats .Data represent mean ± SD, n=6 in each group.* p < 0.05 vs. control, # p < 0.05 compared with TDF.

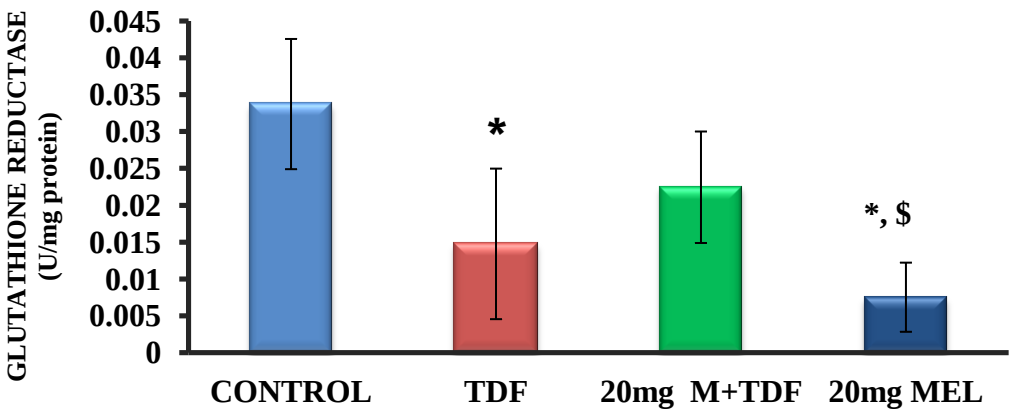

Figure: 8.4.7 Effect of melatonin pretreatment on glutathione reductase activity in the kidneys of rats. Data represent mean ± SD, n=6 in each group. * p < 0.05 vs. control, $ p < 0.05 vs. M+TDF.

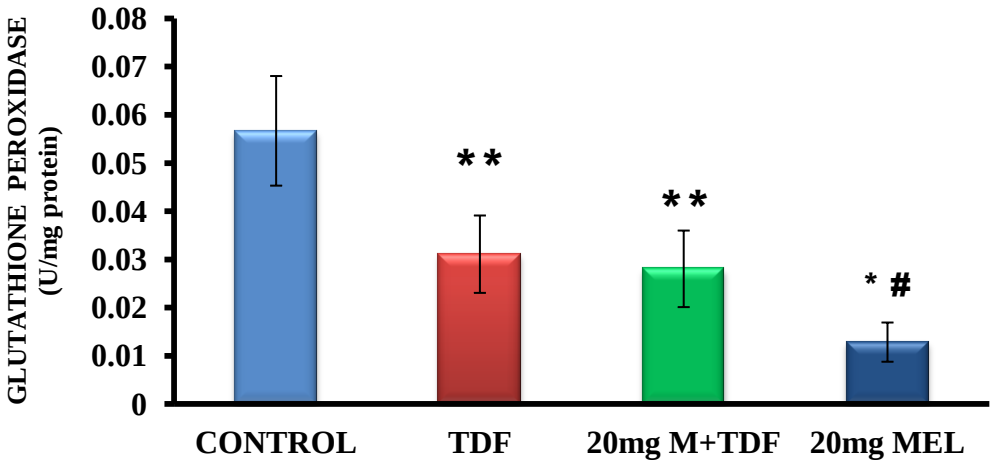

Figure: 8.4.8 Effect of melatonin pretreatment on glutathione peroxidase activity in the kidneys of rats. Data represent mean ± SD, n=6 in each group. * p < 0.05, ** p < 0.01 vs. control, # p < 0.05 vs. TDF.

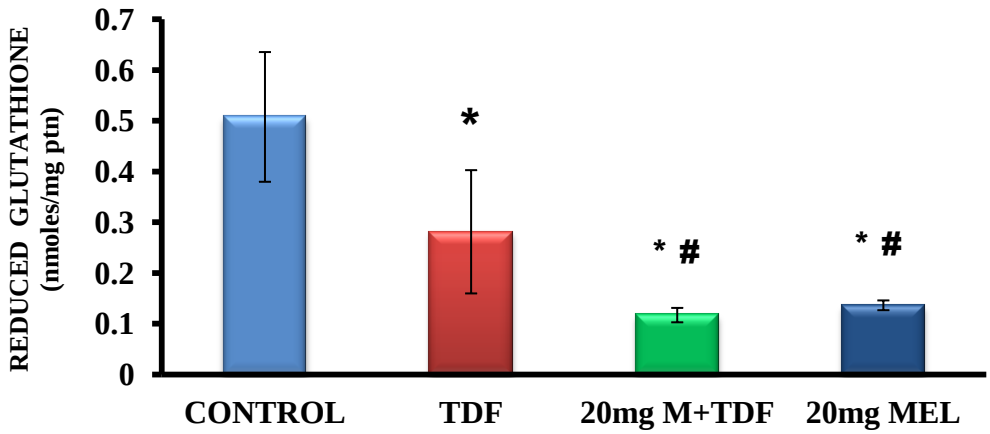

Figure: 8.4.9 Effect of melatonin pretreatment on Reduced Glutathione in the kidneys of rats. Data represent mean ± SD, n=6 in each group. * p < 0.05 vs. control, # p < 0.05 vs. TDF.

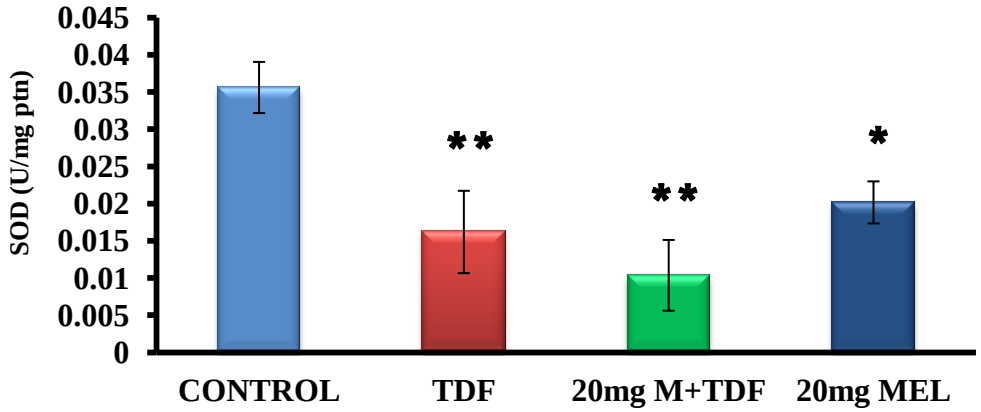

Figure: 8.4.10 Effect of melatonin pretreatment on SOD activity in the kidneys of rats. Data represent mean ± SD, n=6 in each group. * p < 0.05 , p < 0.01 vs. control.**

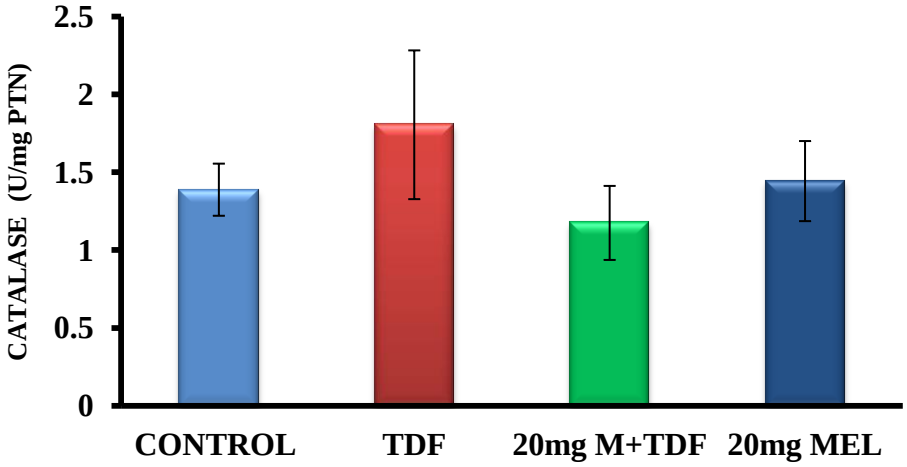

Figure: 8.4.11 Effect of melatonin pretreatment on catalase activity in the kidneys of rats. Data represent mean ± SD, n=6 in each group.

9. Melatonin pretreatment attenuated TDF induced renal nitrosative stress

a) Melatonin pretreatment attenuated TDF induced increased renal nitrate level

A 50% increase in nitrate level was observed in the TDF treated rat kidneys as compared with control. Pretreatment with melatonin completely prevented TDF induced elevation in nitrate levels (Figure: 8.5.1)

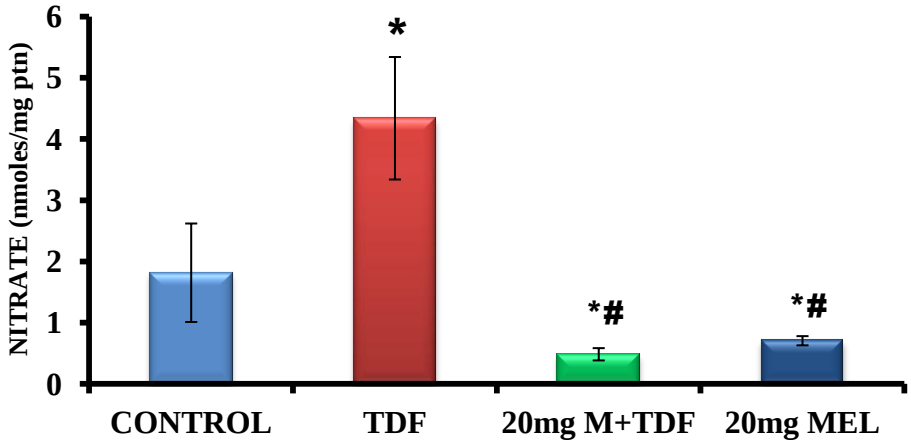

Figure: 8.5.1 Effect of melatonin pretreatment on nitrate levels in renal homogenate of rats. Data represent mean ± SD, n=6 in each group, *p< 0.01 vs. control, # p< 0.001 vs. TDF.

10. Melatonin pretreatment prevented TDF induced increased nitrotyrosine and nitrosocysteine contents in the kidney

NT immunoreactivities were increased in glomeruli and tubuli of the renal cortex of TDF treated rats compared with controls, and this increase in both compartments was markedly reduced by melatonin pretreatment (Figure: 8.5.2). Western Blot analysis is shown in Figure:8.5.3. NT protein level was significantly higher in the TDF treated rats as compared with control. Pretreatment with melatonin significantly reduced the NT levels.

Immunolocalisation of nitrocysteine showed negligible expression in control, whereas the the stain was intense in glomeruli and proximal and distal convoluted tubules of the TDF treated rats. Melatonin pretreatment minimized TDF induced increased NT expression (Figure: 8.5.4).

Figure: 8.5.2 1 Immunohistochemistry of Nitrotyrosine

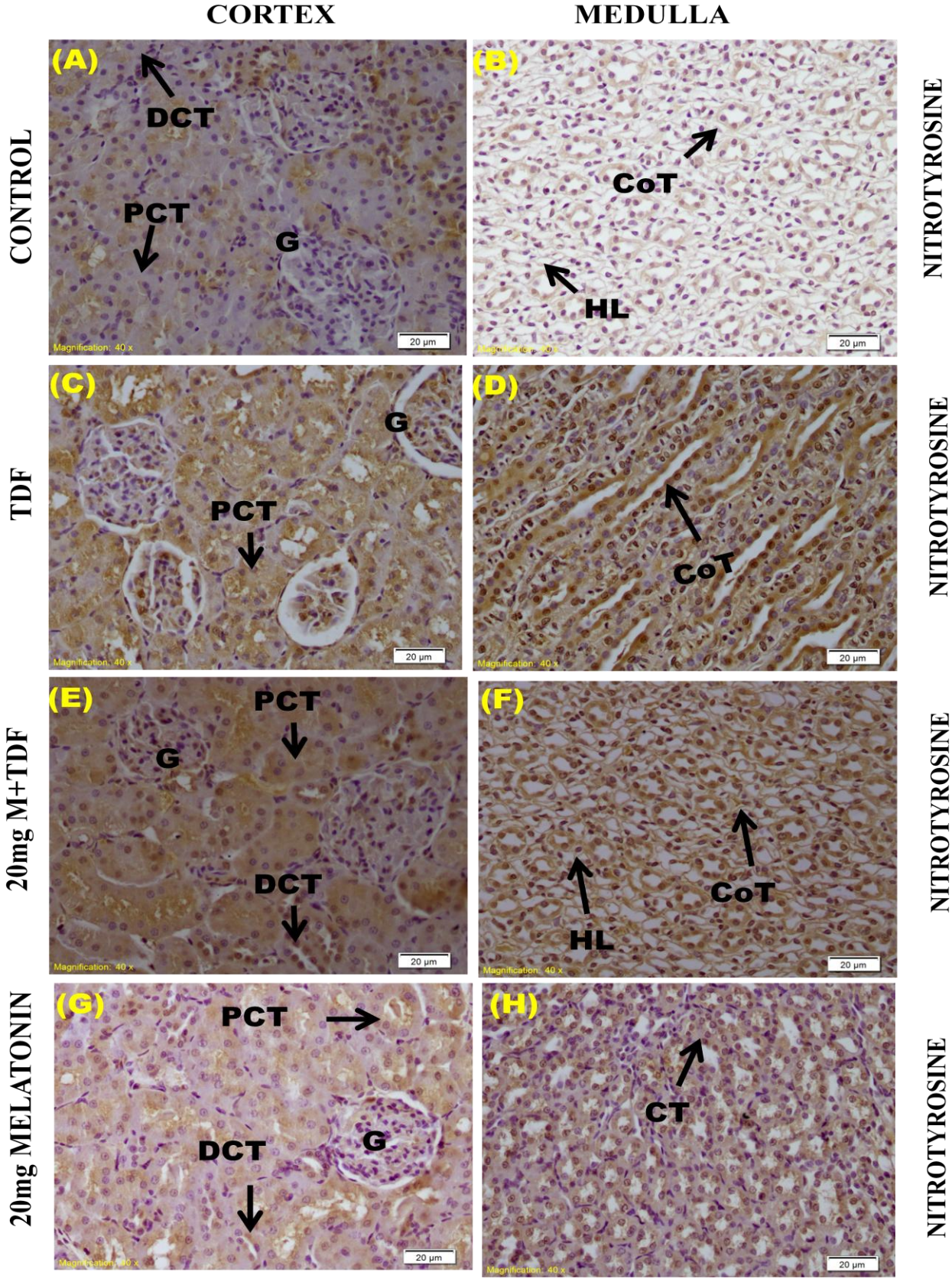

(Please see next page for legends of the figures)

Figure: 8.5.2 Immunohistochemical localization of Nitrotyrosine in kidney tissue (Scale Bar 20µm)

(A)&(B) Control- Negligible expression of NTY in glomerulus (G), proximal convoluted tubules (PCT) and distal convoluted tubules (DCT) of the cortex and negative expression of NTY in the loop of Henle (HL) and collecting tubules (CT)

(C)&(D) TDF- Focal increased levels of NTY stain in the glomerulus (G), proximal convoluted tubules (PCT) and distal convoluted tubules (DCT) of the cortex and intense stain in the loop of Henle (HL) and collecting tubule (CT) of the medulla

(E)&(F) M +TDF- Moderate expression of NTY in glomerulus (G), proximal convolutes tubules (PCT) and distal convoluted tubules (DCT) of the cortex, Henle's loop (HL) and collecting tubules (CT) of the medulla

(G)&(H) M-Mild expression of NTY in the glomerulus, proximal and distal tubules of cortex, and in the medulla of 20mg Melatonin treated rats. .

Figure: 8.5.3 Western blot for Nitrotyrosine protein

(A)

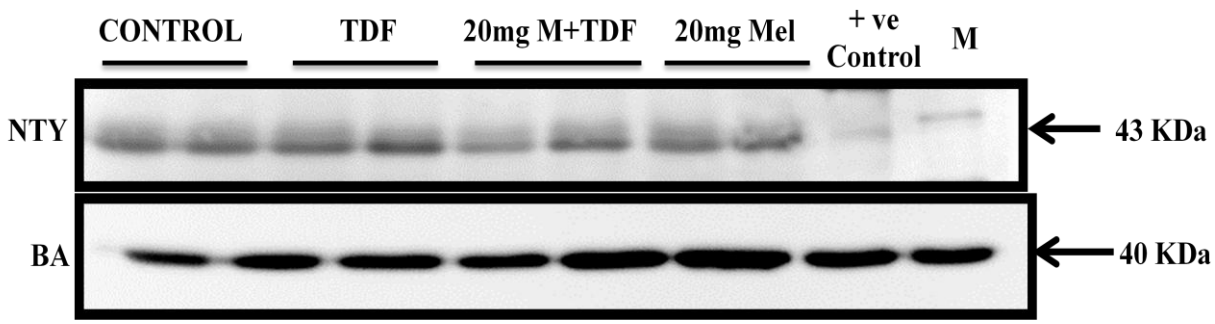

(B)

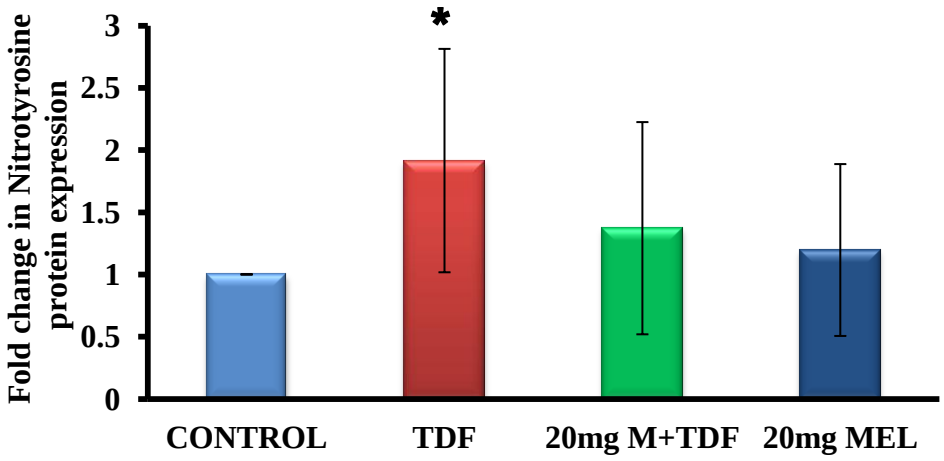

Figure: 8.5.3 A : The upper panel shows representative Western blots of the effect of melatonin pretreatment on nitrotyrosine protein levels in the kidneys of rats., as assessed by using a 10% polyacrylamide gel, loading 100µg protein per lane. β-actin was used as the loading control.

Figure: 8.5.3 B: The lower panel represents blot densitometry (fold change of protein expression) of the Nitrotyrosine bands in renal homogenates as analysed by densitometric quantification of bands of western blots , (n=5) in each group. Data represents mean ± SD, obtained by image analysis of western blots with the concentration of the controls set at one. * indicates $p<0.05$ when compared with corresponding control values.

Fig. 8.5.4. 1 Immunohistochemistry of Nitrocysteine

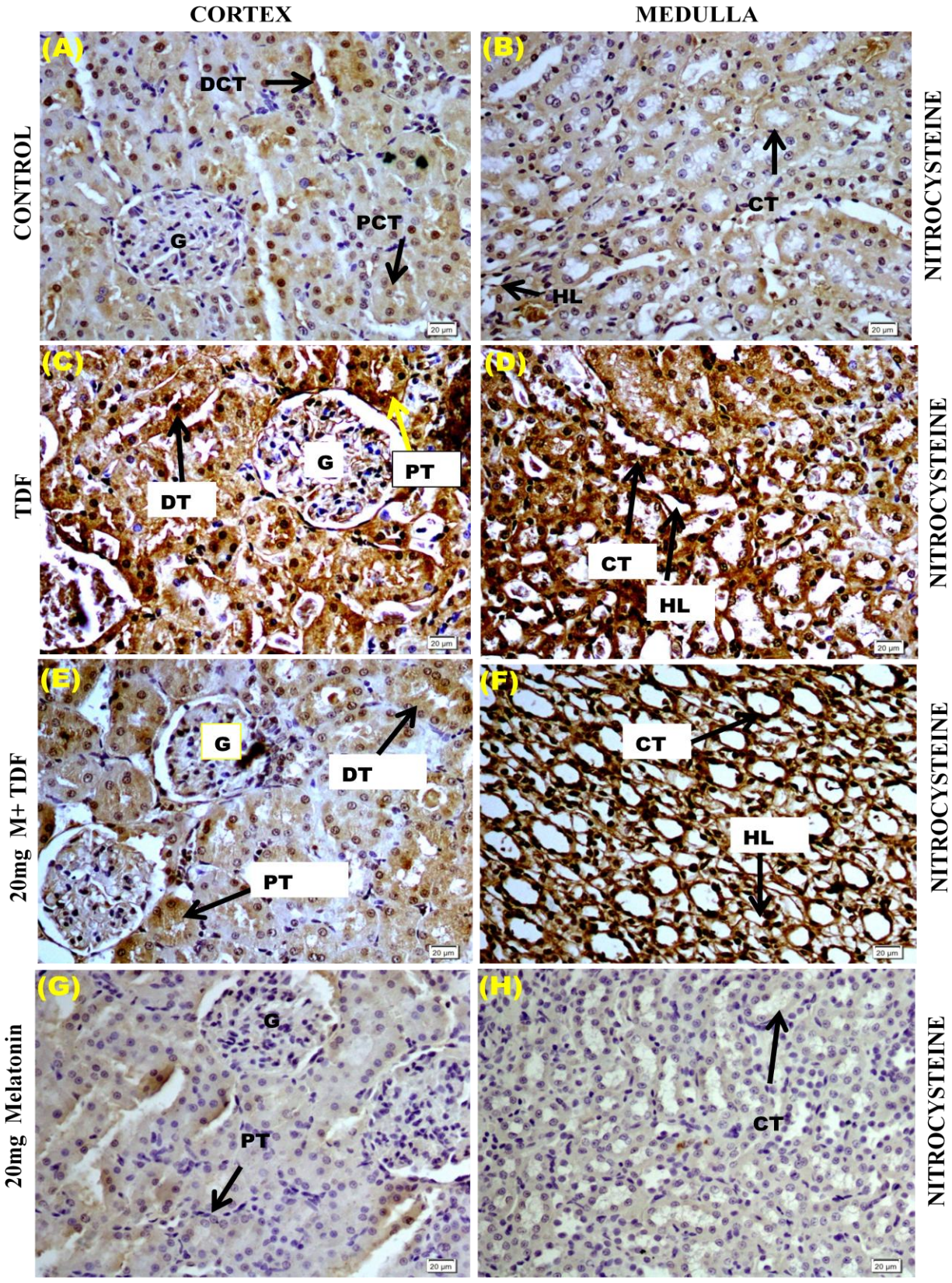

(Please see next page for legends of the figures)

Figure: 8.5.4 Immunohistochemical localization of Nitrocysteine (NCY) in kidney tissue (Scale Bar 20µm)

(A)&(B) Control- Negligible expression of NCY in glomerulus (G), and distal convoluted tubules (DCT) of cortex, and mild expression in proximal convoluted tubules (PCT), and in loop of Henle (HL) and collecting tubules (CT) in control rats treated with sterile water.

(C)&(D) TDF- Intense staining of NCY in the glomerulus (G), proximal convoluted tubules, (PT) and distal convoluted tubules (DT) of the cortex region, in the loop of Henle (HL) and collecting tubule (CT) of the medulla in rats treated with TDF.

(E)&(F) M+TDF- Mild expression of NCY in glomerulus (G), and increased expression of proximal convoluted tubules (PT) and distal convoluted tubule (DT) of the cortex, but intense expression in Henle's loop (HL) and collecting tubules (CT) of the medulla in 20mg melatonin + TDF treated rats.

(G)&(H) M- Negligible staining for NCY in the glomerulus (G), proximal tubules (PT) and distal tubules (DT) in cortex region, negative expression of NCY in the medulla of 20mg Melatonin treated rats.

11. Melatonin pretreatment attenuated TDF induced NFκBp65 protein expression, mRNA expression as well as activity

Immunoblot analysis (Figure: 8.6.1) of NFκB p65 protein expression revealed basal expression in the cytosolic and nuclear fractions of kidney homogenate. TDF treated rats showed significant increase in both cytosolic and nuclear content of NFκB p65 as compared with control. Melatonin pretreatment completely prevented TDF induced NFκB protein expression both in the cytosol as well as the nucleus. These results suggest that MT pretreatment attenuates NFκB protein expression.

NFκB activity (Figure: 8.6.2 A & B)- Basal NFκB p65 activity was seen in the control rats. TDF treatment resulted in massive increase (170 fold) in activity as compared with control. Melatonin pretreatment reduced the NFκBp65 activity to lesser than control values.

NFκB mRNA expression determined by RT PCR revealed basal expression in control rat kidneys, and was significantly induced after TDF treatment. Pretreatment with melatonin almost completely prevented TDF induced NFκB gene expression (Figure: 8.6.3).This suggests that melatonin MT pretreatment attenuates NFκB gene expression.

Figure: 8.6.1 Western blot for NFκB p65 Protein Expression

(A)

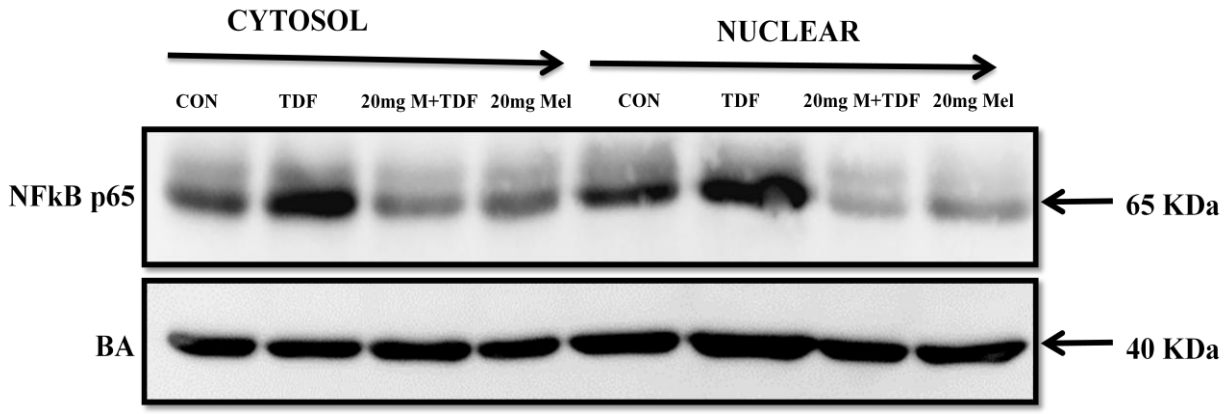

(B)

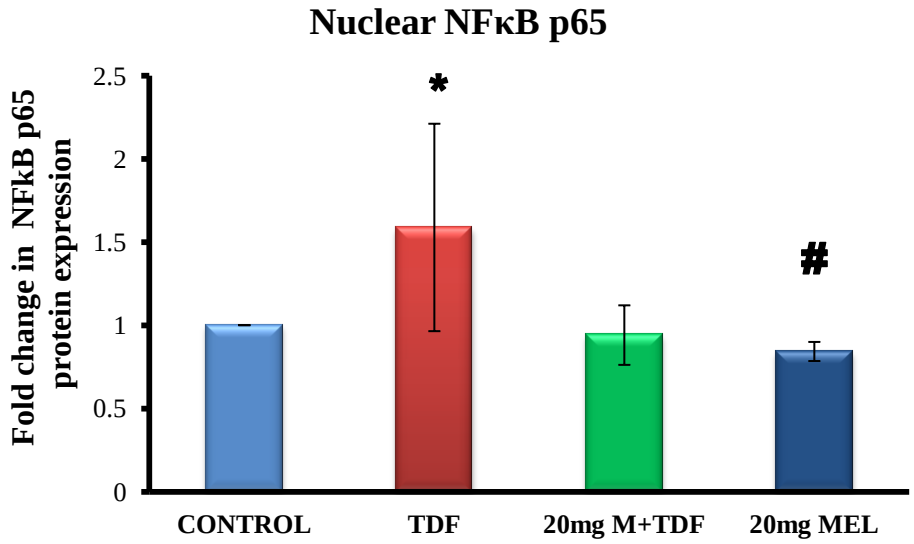

Figure: 8.6.1 (A) The upper panel shows representative Western blots of the effect of melatonin pretreatment on NFκB p65 protein levels in the kidneys of rats, as assessed by using a 10% polyacrylamide gel, loading 100µg protein per lane. β-actin was used as the loading control.

Figure: 8.6.1 (B) The lower panel represents blot densitometry (fold change of protein expression) of the NFκBp65 in renal homogenates as analysed by densitometric quantification of bands of western blots , (n=5) in each group. Data represents mean ± SD, obtained by image analysis of western blots with the concentration of the controls set at one. * p<0.05 vs. control , # p<0.05 vs. TDF.

Figure: 8.6.2 NFκ B p65 activity

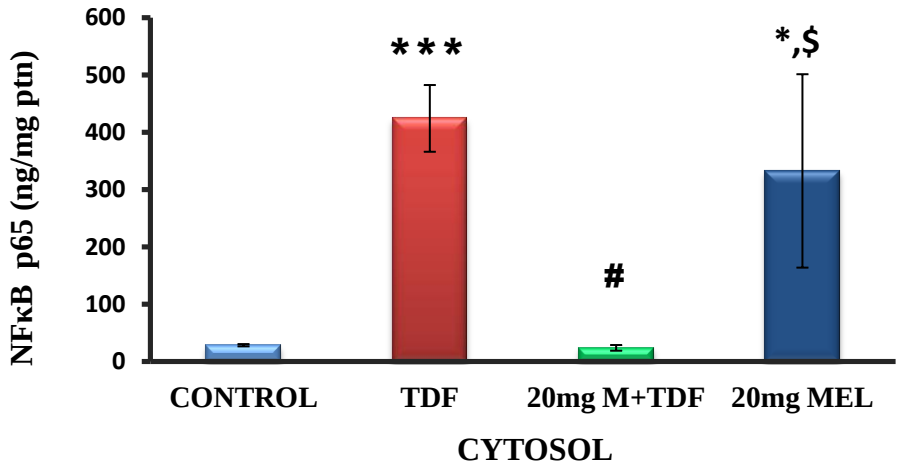

Figure: 8.6.2A Effect of melatonin pretreatment on NFκB p65 activity by ELISA in cytosol fraction of rats (n=6 in each group). Data represent mean ±SD , * p< 0.01, *** p < 0.001 vs. control, # p < 0.01 vs. TDF, $ p < 0.01 vs. M +TDF.

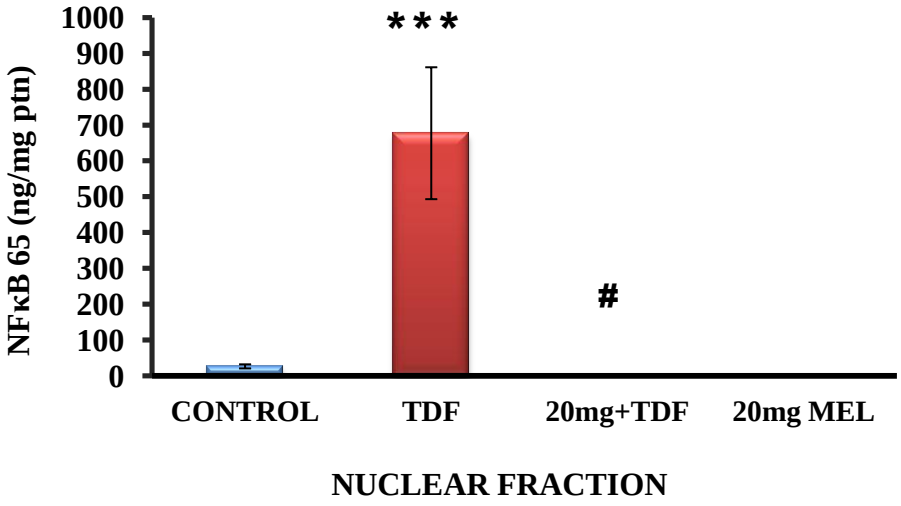

Figure: 8.6.2B Effect of melatonin pretreatment on NFκB p65 activity by ELISA in nuclear fraction of rats, n=6 in each group. Data represent mean ±SD . *** p < 0.001 compared with control, # p < 0.01 compared with TDF group.

Figure: 8.6.3 mRNA expression of NFκB

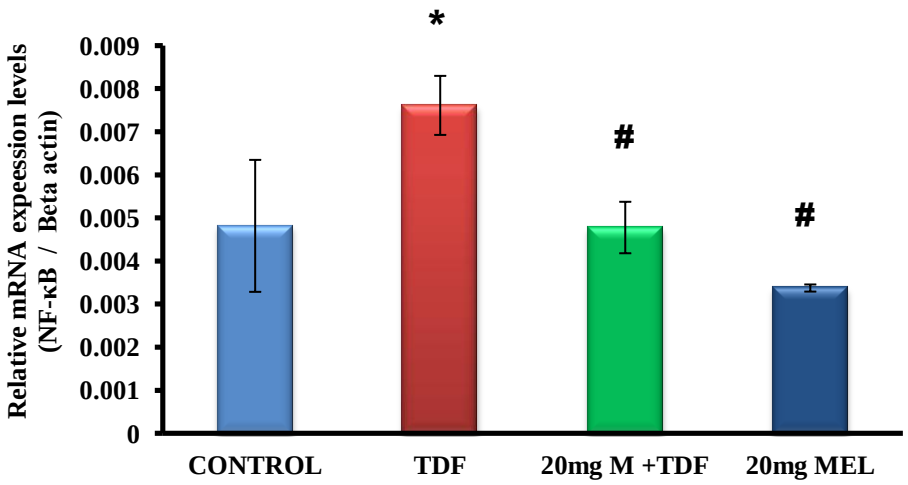

Figure: 8.6.3. Relative expression of NFκB mRNA in kidneys of rats, (n=5). Data represent mean ± SD. * p<0.05 vs.control, # p<0.05 vs.TDF

12. Melatonin pretreatment decreased iNOS, COX-2 , TNF , and MMP-9 protein expression and gene expression

a. Melatonin pretreatment on iNOS protein expression and mRNA expression

Immunoblot on TDF treatment depicted in Figure: 8.7.1 shows a 2 fold increase in iNOS protein as compared with control. Decrease expression was observed in pretreated melatonin groups, but was not statistically not significant.

These observations were further supported by results of mRNA expression which noticed basal transcription of iNOS (Figure: 8.7.2) in the control rat kidneys. There was also significantly higher transcriptional upregulation of iNOS,) as compared to controls.

b. Melatonin pretreatment on COX-2 protein expression and mRNA expression

In the control rat kidneys, immunostaining revealed no constitutive expression of COX-2 in the renal cortex and medulla . In the TDF treated rat kidneys, the glomerulus , the LH and collecting ducts showed intense staining for COX-2, as a representative marker of the -pathway. Diffuse staining was observed in the DCT and PCT. (Figure: 8.8.1)

To determine whether the COX-2 regulation by TDF. Further, the gene expression demonstrated at the mRNA level of TDF was determined by real-time RT-PCR and normalized by β-actin. As shown in Figure:8.8.2, TDF treatment induced more than 2.5 fold increase in COX-2 mRNA expression. Melatonin pretreatment completely attenuated the effect of TDF.

Figure: 8.7.1 Western blot for iNOS protein

(A)

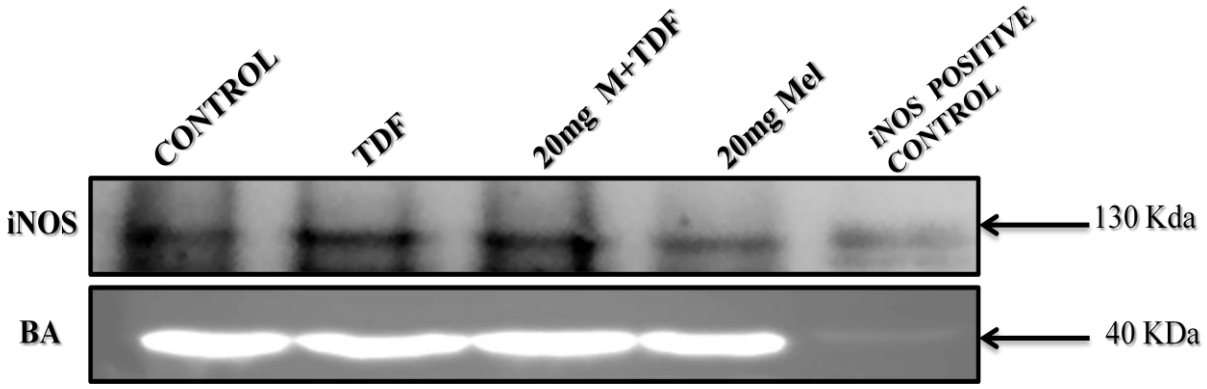

(B)

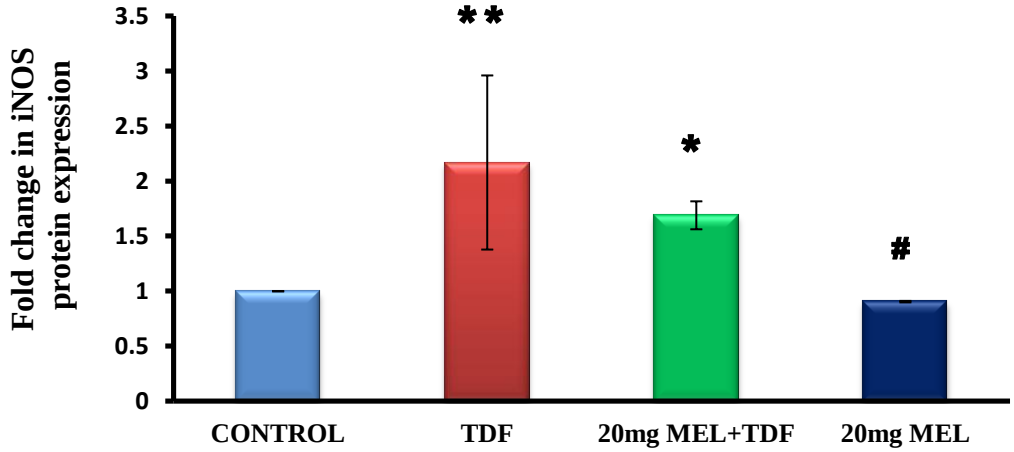

Figure :8.7.1 A : Representative western blots of iNOS protein levels (130 kD) bands in control and TDF-treated rats (n=5 in each group) of renal homogenates, as assessed by using a 10% polyacrylamide gel, loading 100µg protein per lane. The lane labeled "+ve "represents positive control that consists of lysate of LPS treated RAW 264.7 cells. β-actin was used as the loading control.

Figure:8.7.1B: Relative concentration of iNOS in renal homogenates as analysed by densitometric quantification of bands of western blots in control and TDF-treated rats (n=5 in each group). Data represents mean ± SD, obtained by image analysis of western blots with the concentration of the controls set at one. ** p<0.01, * p<0.05 vs. control, # p < 0.0 vs. TDF.

Figure:8.7.2 mRNA expression of iNOS

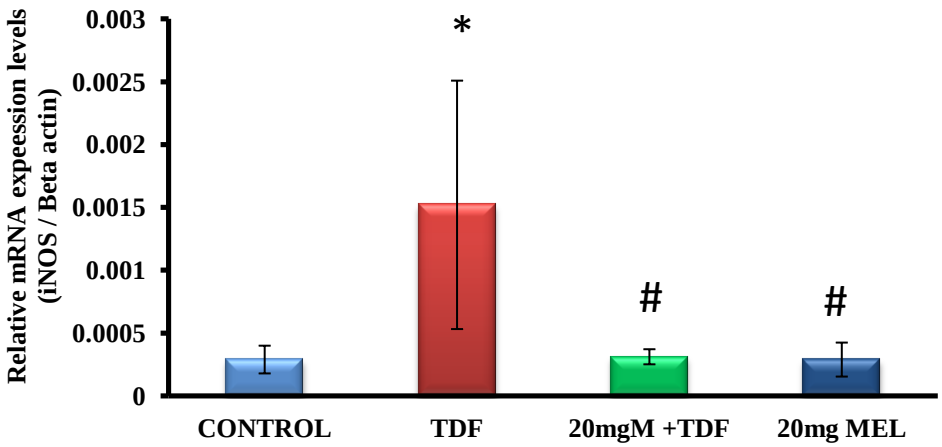

Figure:8.7.2 Relative expression of iNOS mRNA in kidneys of rats, (n=5). Data represents mean ± SD. * p<0.05 vs.control values, # p<0.05 vs. TDF

Figure: 8.8.1 Immunohistochemistry of COX-2

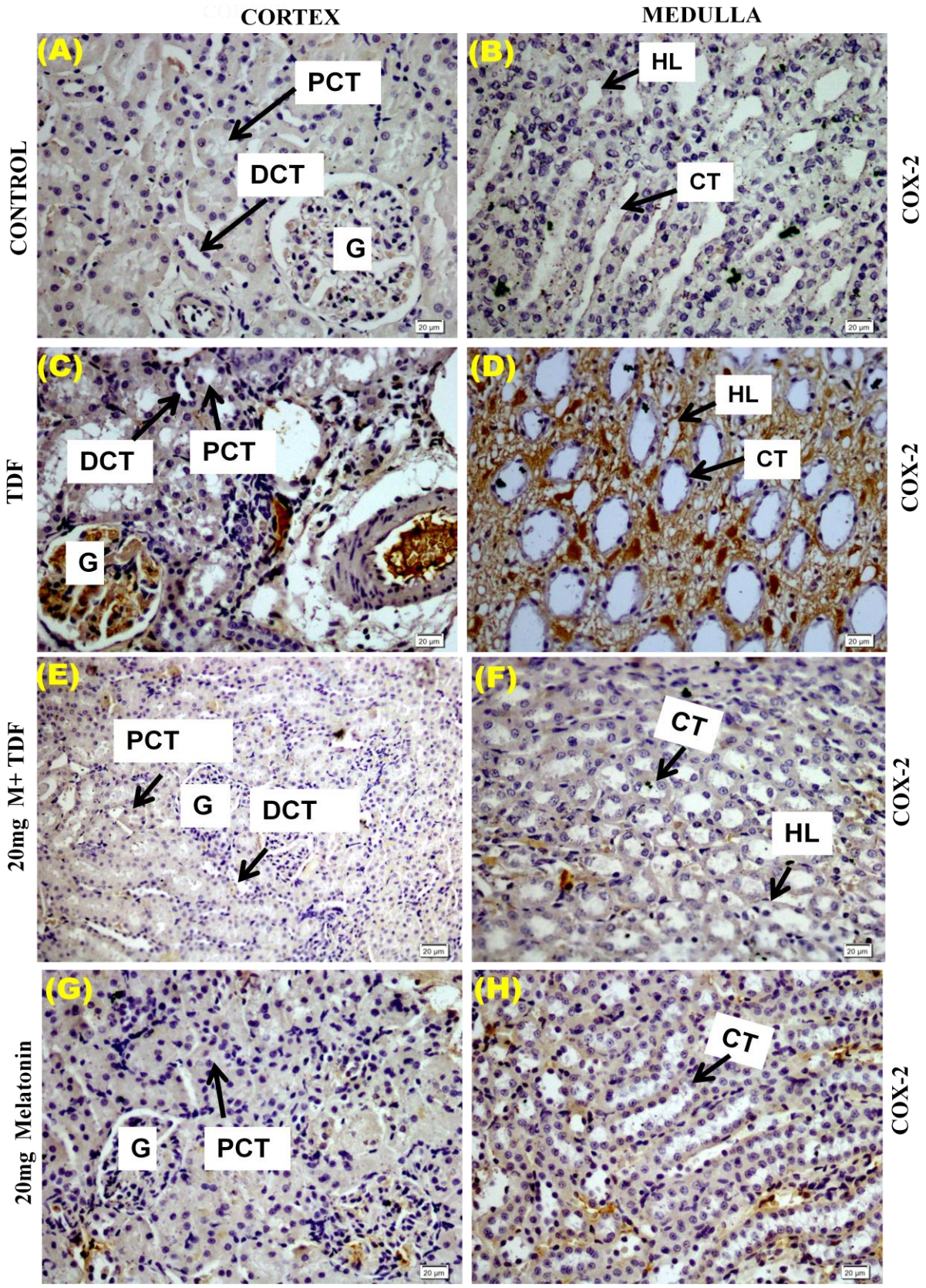

(Please see next page for legends of the figures)

Figure: 8.8.1 Immunohistochemical localization of Cyclooxygenase-2 (COX-2) in kidney tissue. Scale Bar = 20µm.

(A)&(B) Control- Negligible expression of COX-2 in glomerulus (G), proximal convoluted tubules (PCT) and disatal convoluted tubules and (DCT) in cortex, Henle's loop (HL) and collecting tubules (CT) in control groups (40X).

(C)&(D) TDF-Intense staining of COX-2 in the glomerulus (G), negligble expression in the proximal (PCT) and distal convoluted tubules (DCT) of the cortex, intense staining of the intestitium around the loop of Henle (HL) and collecting tubule, (CT) in the medulla of TDF groups.

(E)&(F) M+ TDF- Negligible staining for COX-2 in the proximal convoluted tubules (PCT) and distal convoluted tubules (DCT) of the cortex, negative expression of COX-2 in the glomerulus region (G), and negative expression the Henle's loop (HL) and collecting tubules (CT) of the medulla in 20mg melatonin + TDF treated rats.

(G)&(H) M-Negligible expression of COX-2 in the glomerulus (G), proximal convoluted tubules (PCT) and distal convoluted tubules (DCT) in cortex, negative expression in the medulla of 20mg Melatonin treated rats.

Figure: 8.8.2 mRNA expression of COX-2

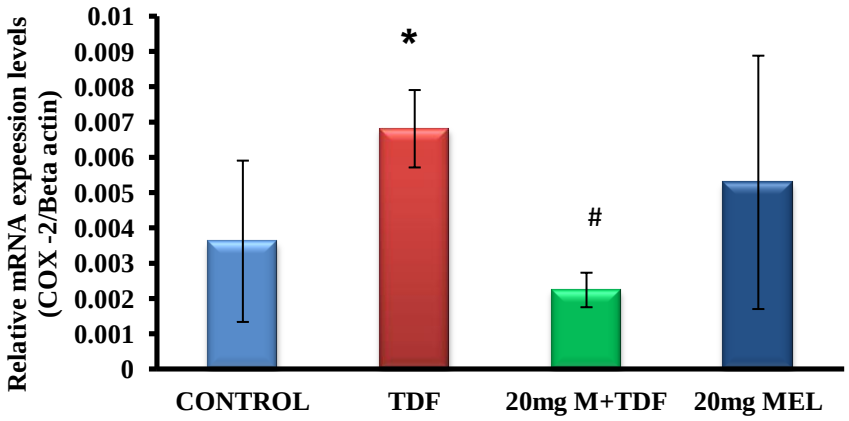

Figure: 8.8.2 Relative expression of COX 2 mRNA in kidneys of rats ,(n=5). Data represents mean ± SD. *indicates p<0.05 vs. control , # p<0.01 vs. TDF.

c. Melatonin pretreatment on TNF protein expression and mRNA expression

Control rats demonstrated low levels of TNF-α expression and in TDF treated rats more than 2 fold increase in TNF-α levels was observed in Figure: 8.9.1A. Melatonin pretreatment completely attenuated TDF induced increase in TNF protein level. Densitometric analysis of TNF protein expressed as percent of β actin is Figure: 8.9.1 B. Next we quantified the TNF mRNA exression in renal samples. Control rats had basal expression of TNF-α mRNA. No significant effect was observed in the TDF treated rats. Figure: 8.9.2.

d. Melatonin pretreatment on MMP 9 protein expression, mRNA expression, and activity

Basal MMP-9 activity was seen in the control rats. TDF treatment resulted in more then 2 fold increase in activity as compared with control. Melatonin pretreatment reduced the MMP-9 activity. (8.10.1)

Immunoblot analysis (Figure:8.10.2 A& B) of MMP-9 protein expression revealed increase expression in TDF treated rat kidneys. Melatonin pretreatment did not have any significant effect on MMP-9 protein expression. mRNA expression determined by RT PCR revealed basal expression in control rat kidneys, and was not significantly induced after TDF treatment. Pretreatment with melatonin had no effect on MMP-9 (Figure:8.10.3).

Figure: 8.9.1 Western blot for TNF-α protein

(A)

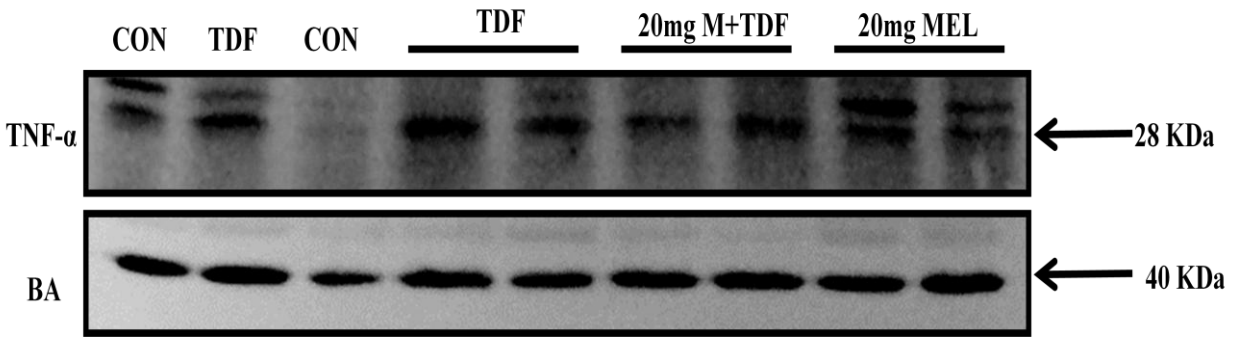

(B)

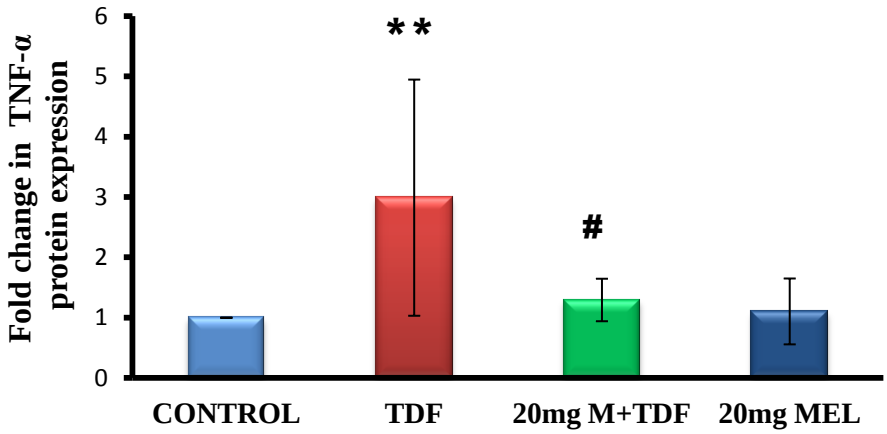

Figure:8.9.1 A :Western blots of TNF-α protein levels, as assessed by using a 10% polyacrylamide gel, loading 100µg protein per lane. The upper panel shows a representative blot images of TNF-α protein level with (28 kD) bands. β-actin was used as the loading control.

Figure:8.9.1 B: The lower panel represents blot densitometry (fold change of protein expression) of the TNF-α bands in renal homogenates was analysed by densitometric quantification of bands of western blots , n=5. Data represents mean ± SD, obtained by image analysis of western blots with the concentration of the controls set at one. ** $p<0.01$ vs. control , # $p < 0.05$ vs. TDF.

Figure: 8.9.2 mRNA expression of TNF-α

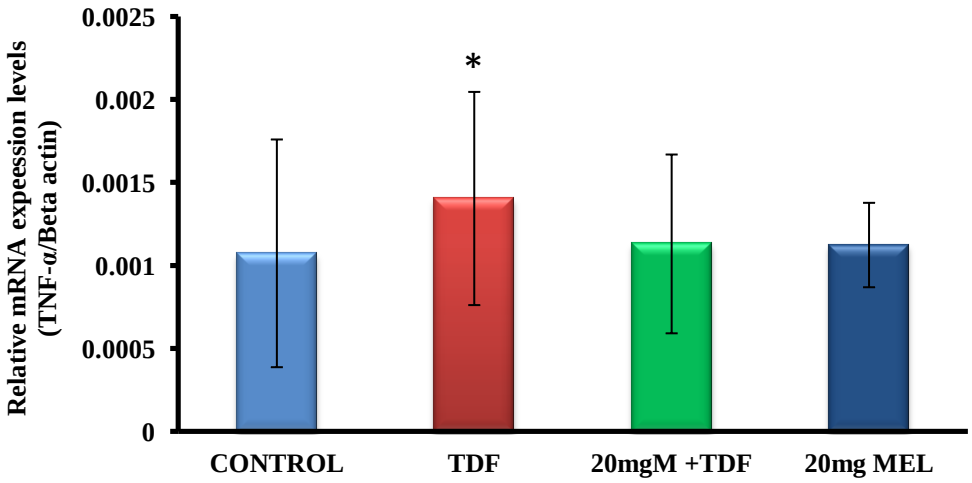

Figure:8.9.2. Relative expression of TNF-α mRNA in kidneys of rats, n=5. Data represent mean ± SD. *indicates p<0.05 when compared with corresponding control values.

Figure: 8.10.1 MMP-9 activity by Zymogram

(A)

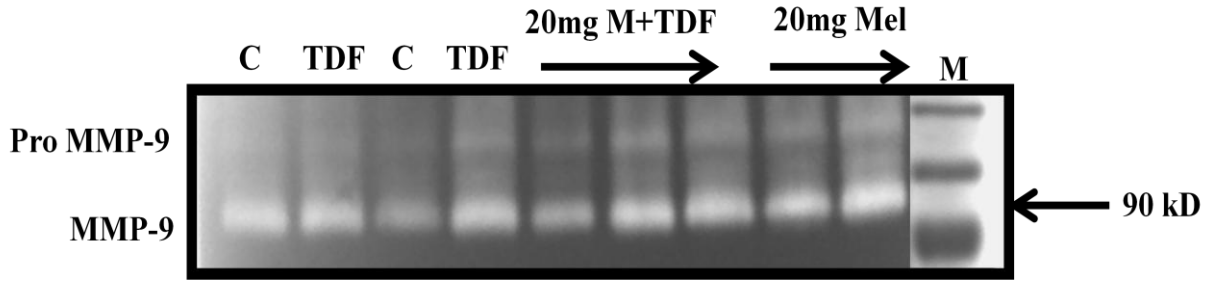

(B)

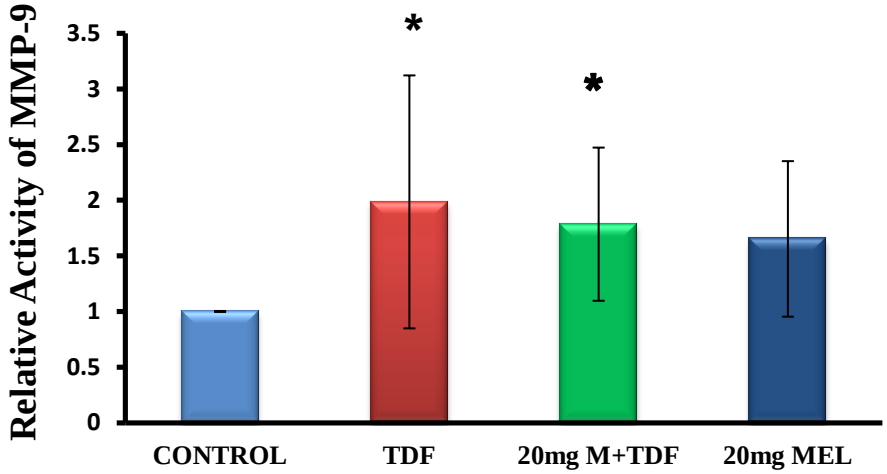

Figure: 8.10.1 MMP-9 activity in renal homogenate in response to melatonin pretreatment. n=5. Data mean ± SD obtained by image analysis of zymograms, with the activity of the controls set at one. C- Control, TDF, 20mg M+TDF and 20mg Melatonin. * indicates $p<0.05$ when compared with corresponding control values

Figure: 8.10.2 Western blot for MMP-9 protein

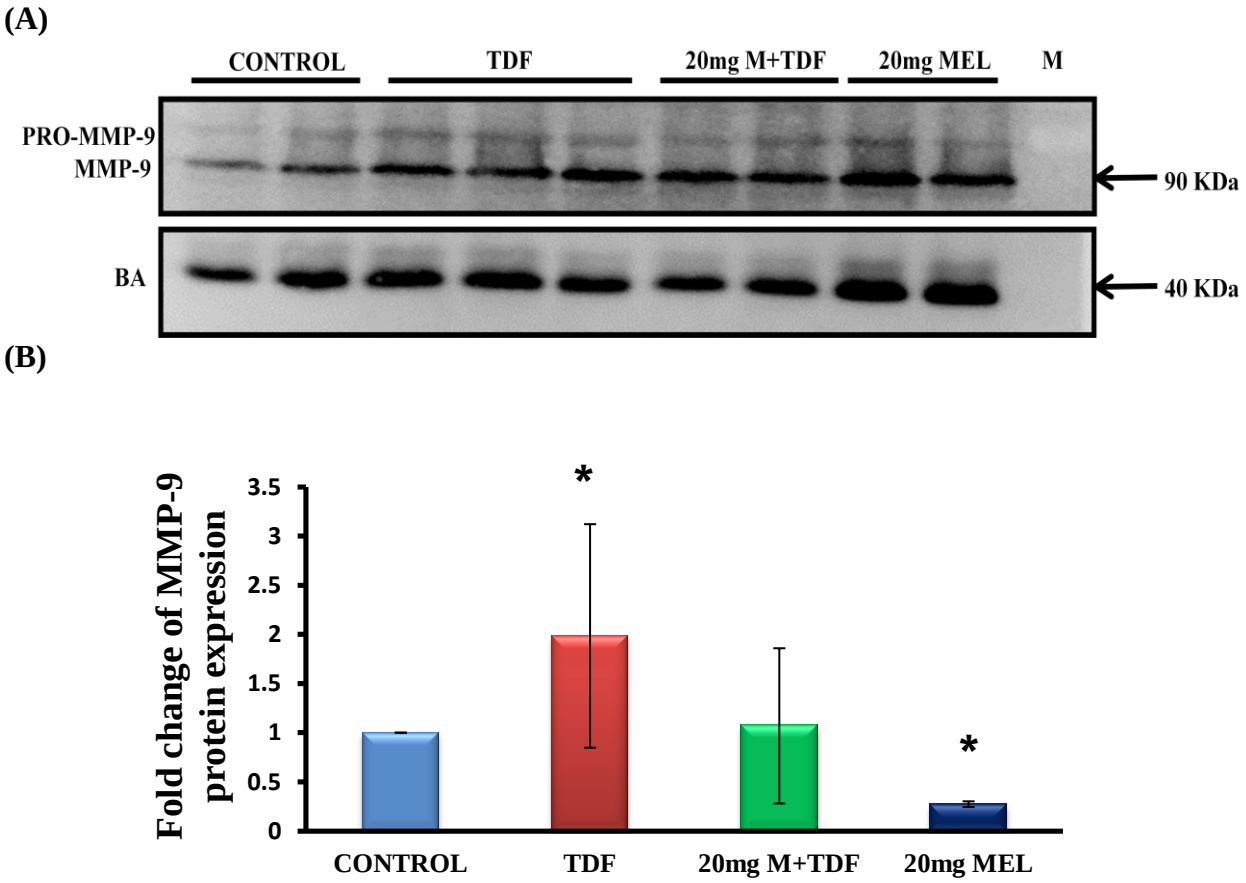

Figure: 8.10.2 A: Western blots of MMP-9 protein levels, as assessed by using a 10% polyacrylamide gel, loading 100µg protein per lane. The upper panel shows a representative blot images of MMP-9 protein level with (90 kD) bands. β-actin was used as the loading control.

Figure: 8.10.2 B: The lower panel represents blot densitometry (fold change of protein expression). Values represents mean ± SD, obtained by image analysis of western blots with the concentration of the controls set at one. * indicates $p<0.05$ when compared with corresponding control values.

Figure:8.10.3 mRNA expression of MMP-9

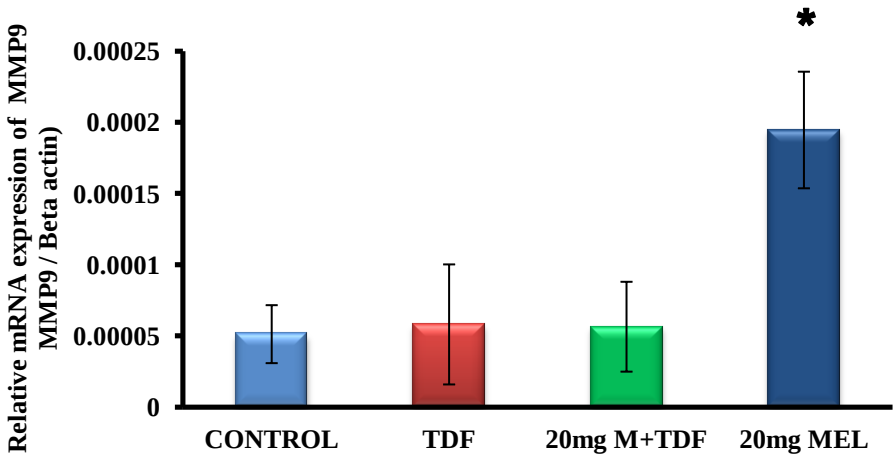

Figure: 8.10.3 Relative expression of MMP-9 mRNA in kidneys of rats, n = 5 in each group. Data represent mean ±SD. *p<0.05 vs. control.

13. Melatonin pretreatment on TDF induced PARP overactivation

Control kidney cortex and medulla showed basal staining for PARP. In TDF treated rat cortex, the glomerulus showed moderate staining for PARP and the convoluted tubules showed intense satining. In the medulla, the collecting tubules and Henle's loop were positive to PARP stain. Melatonin pretreatment decreased the intensity of the stain, it was less as compared with TDF groups, melatonin alone treated group showed negligible expression (Figure:8.11.1).

Western blot shown in Figure: 8.11.2 Significant increase in the expression of PARP protein as observed with control,and this effect was not reduced in pre-treatment with melatonin.

Figure: 8.11.1 Immunohistochemistry of PARP

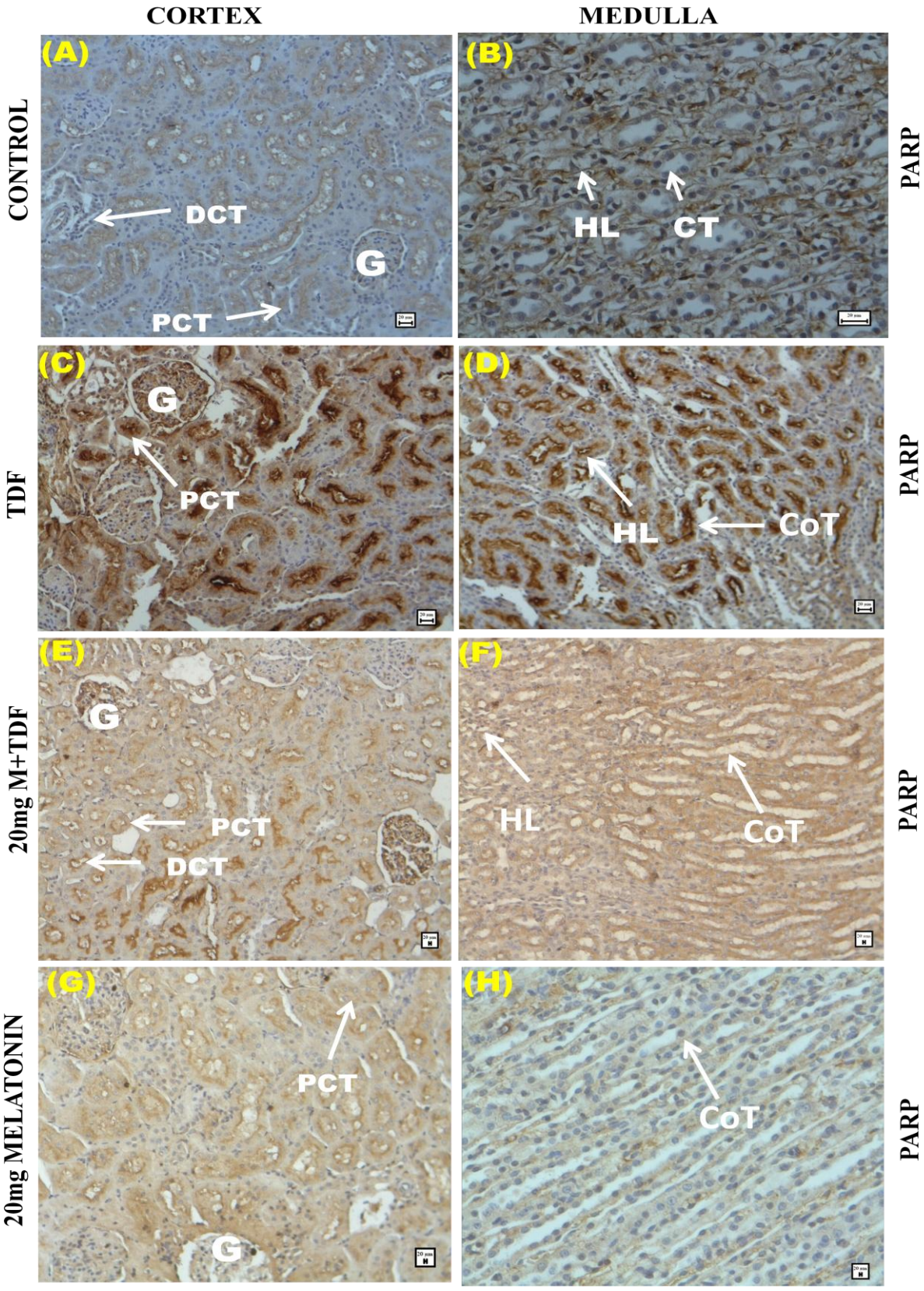

(Please see next page for legends of the figures)

Figure: 8.11.1 Immunohistochemical localization of PARP in kidney tissue.

(A) & (B) Control-Negligible expression of PARP in Glomerulus (G), mild expression of proximal convoluted tubule (PCT) and distal convoluted tubules (DCT) of cortex, loop of Henle (HL) and collecting tubules (CT) in control groups

(C) & (D) TDF-Focal increased expression of PARP stain in the glomerulus (G) and strong positivity in proximal convoluted tubules (PCT), distal convoluted tubules (DCT) of the cortex, and in the loop of Henle (HL) and collecting tubule (CT) of the medulla in TDF group.

(E)&(F) M +TDF-Moderate expression of PARP in glomerulus (G), in the proximal (PCT) and distal convoluted tubules (DCT) of the cortex, Henle's loop (HL) and collecting tubules (CT) of the medulla in 20mg melatonin + TDF treated rats.

(G)&(H) M-Negligible expression of PARP in glomerulus (G), mild expression in proximal convoluted tubules (PCT) and distal convoluted tubules (DCT) of cortex, negligible expression in loop of Henle (HL) and in collecting tubules (CT) of the medulla when pretreated with 20mg Melatonin. Scale Bars = 20µm

Figure: 8.11.2 Western blot for PARP protein

(A)

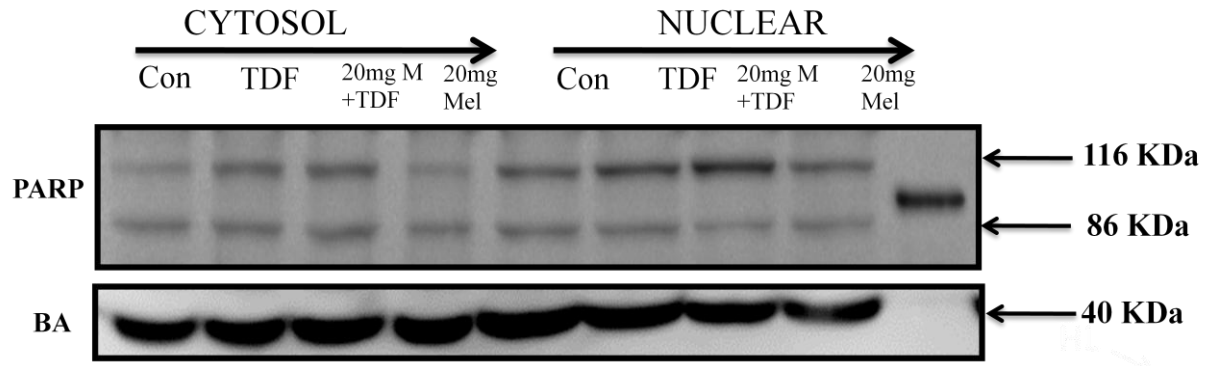

(B)

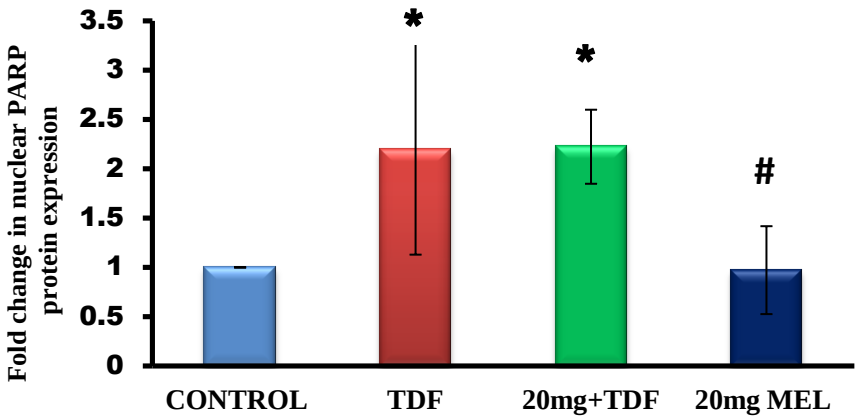

Figure: 8.11.2 A: Western blots of PARP protein levels showing the effect of melatonin pretreatment. The upper panel shows (116 kDa, 86 kDa) bands in cytosol and nuclear fraction. β-actin was used as the loading control.

Figure: 8.11.2 B: The lower panel represents blot densitometry (fold change of protein expression) of the PARP bands at 116 kDa in renal homogenates as analysed in the nuclear fraction by densitometric quantification of bands , n= 5 in each group. Each data represents mean ± SD, obtained by image analysis of western blots with the concentration of the controls set at one. * indicates p<0.05 when compared with control, # indicates p<0.05 when compared with TDF.

14. Melatonin pretreatment prevented TDF induced caspase 3 protein expression, gene expression, and activity:

Immunohistochemistry showed that caspase 3 expression was virtually absent in the glomerulus and tubuli of control rats (Figure: 8.12.1). In the TDF treated rats, cell nuclei of both glomerular and tubular cells stained intensely for caspase 3. Pretreatment with melatonin completely prevented TDF induced increase in caspase 3 proteins. Western blot analysis also revealed massive increase in caspase 3 protein levels, which was significantly decreased upon melatonin pretreatment (Figure: 8.12.2).

Melatonin pretreatment had no significant effect on TDF induced increase in caspase 3 mRNA expression (Figure: 8.12.3). As a biochemical marker of apoptosis, we measured caspase activity (Figure: 8.12.4). With respect to caspase 3 activity more than 2 fold increase was observed in TDF treated rats as compared with control. Melatonin pretreatment partially but significantly reduced TDF induced increased caspase 3 activity.

Figure: 8.12.1 Immunohistochemistry of Caspase-3

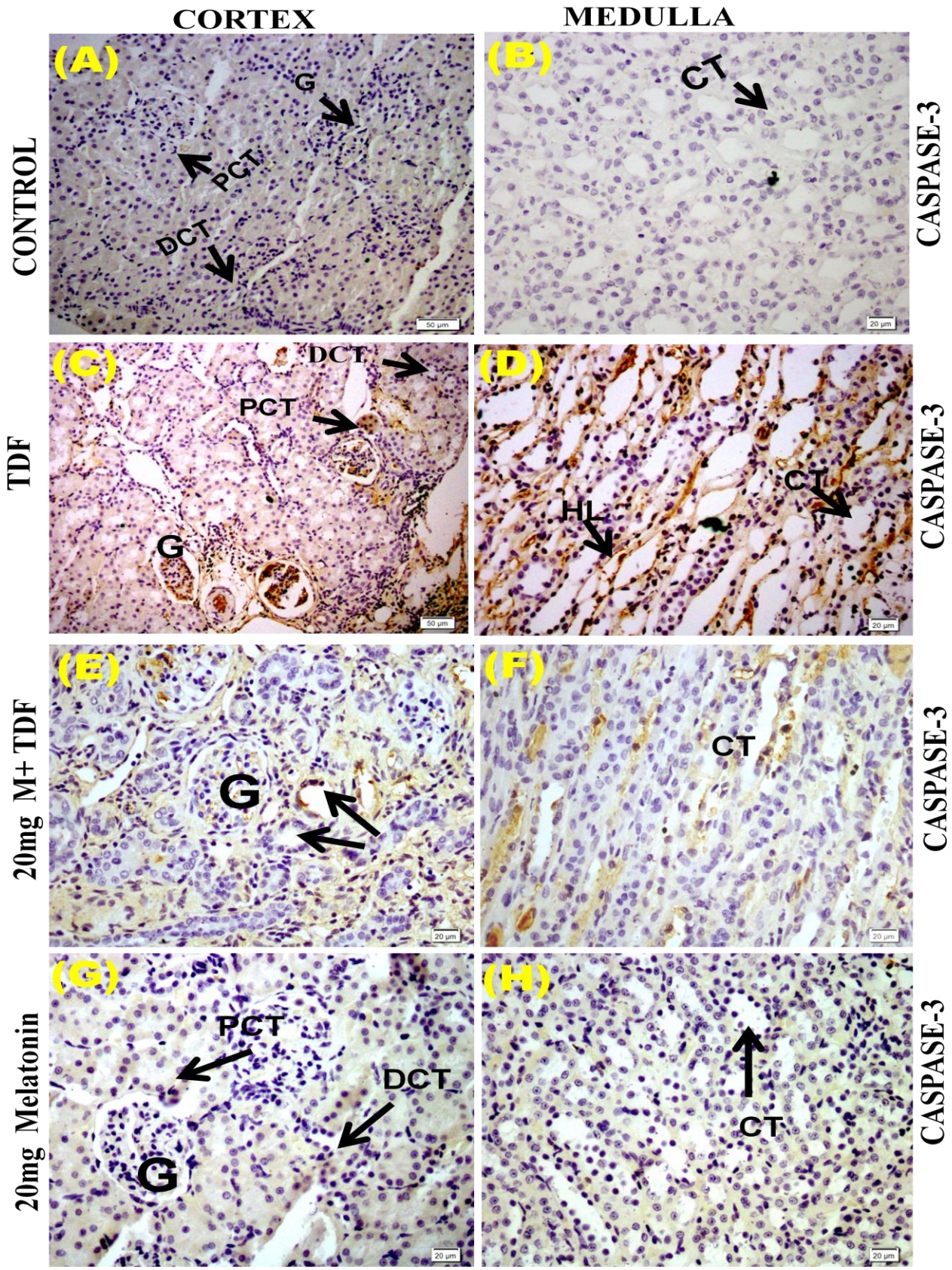

(Please see next page for legends of the figures)

Figure: 8.12.1 Representative images of Immunohistochemical localization of caspase-3 in kidney tissue.

(A)&(B) Control-Negative expression of caspase-3 in Glomerulus (G), in the proximal convoluted tubule (PCT) and distal convoluted tubules (DCT) of cortex, loop of Henle (HL) and collecting tubules (CT) in control groups

(C)&(D) TDF-Increased expression of caspase-3 in the glomerulus (G), mild expression in the proximal tubular cells (PCT), distal tubules (DCT) of the cortex region, intense staining in the loop of Henle (HL) and moderate expression in the collecting tubule (CT) of the medulla in TDF group.

(E)&(F) M +TDF- Negligible expression of Caspase-3 in glomerulus (G), moderate expression in the proximal (PCT) and distal tubules (DCT) of the cortex, Henle's loop (HL) and collecting tubules (CT) of the medulla in 20mg melatonin + TDF treated rats.

(G)&(H) M-Negative expression of PARP in glomerulus (G), proximal convoluted tubules (PCT), distal convoluted tubules (DCT) of cortex and in the loop of Henle (HL), collecting tubules (CT) of the medulla when treated with 20mg Melatonin.

Figure: 8.12.2 Western blot for Caspase-3 protein

(A)

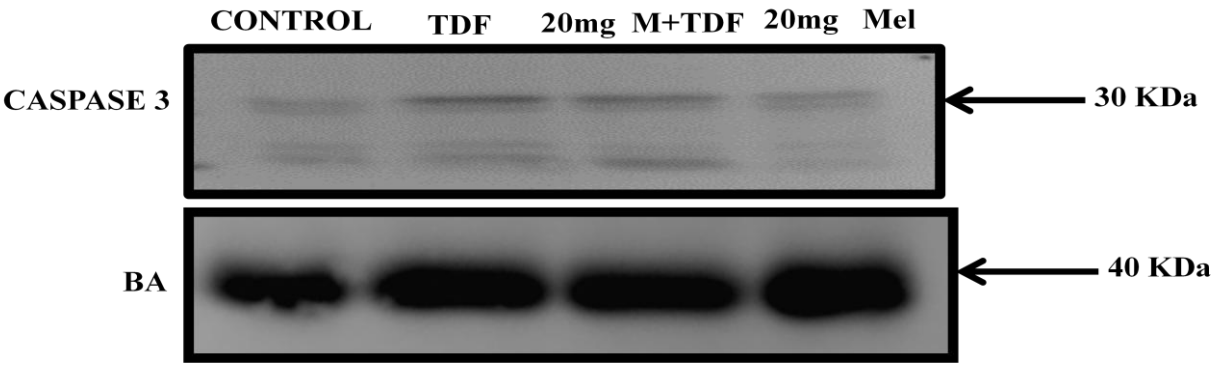

(B)

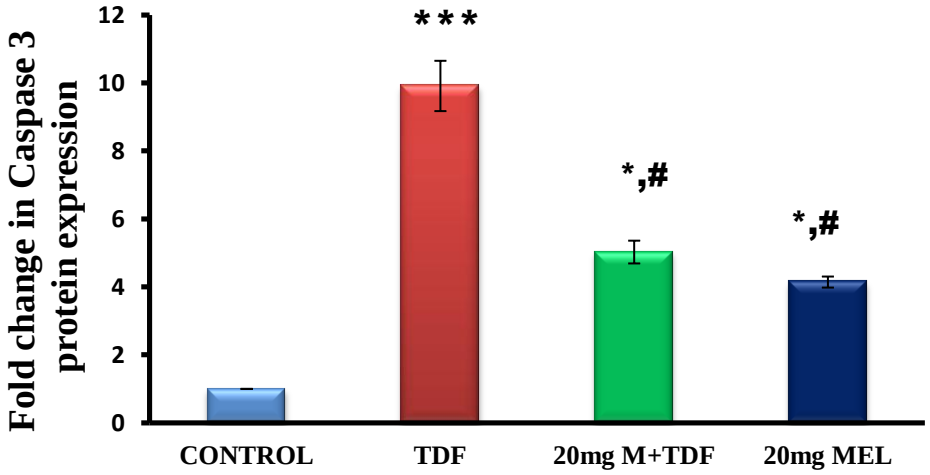

Figure: 8.12.2A Western blots of Caspase 3 protein levels showing the effects of melatonin pretreatment, as assessed by using a 10% polyacrylamide gel, loading 100µg protein per lane. The upper panel shows a representative blot images of caspase-3 protein level with (30 kD) bands. β-actin was used as the loading control.

Figure: 8.12.2B. The lower panel represents blot densitometry (fold change of protein expression) of the caspase 3 bands in renal homogenates (n= 5 in each group). Each data values represents mean ± SD, obtained by image analysis of western blots with the concentration of the controls set at one. * p<0.05, *** P < 0.001vs. control, # p < 0.01 vs. control values.

Figure: 8.12.3 mRNA expression of Caspase-3

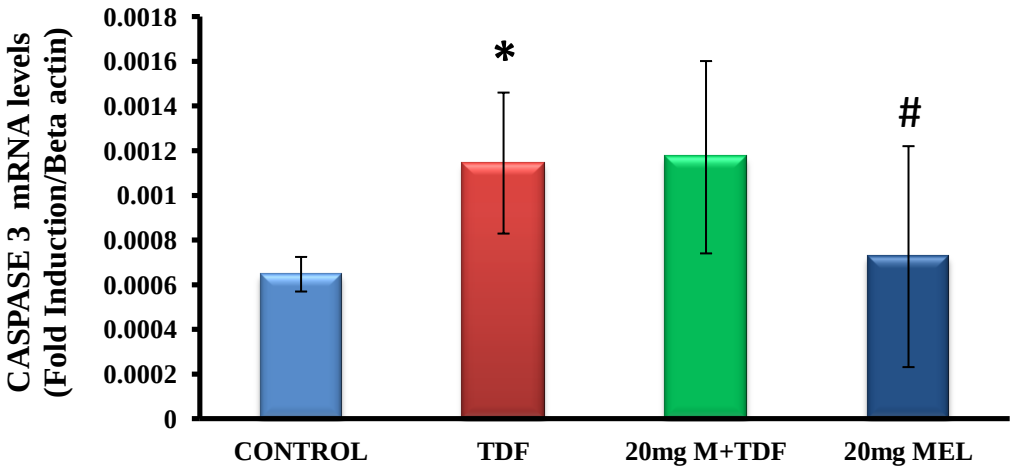

Figure: 8.12.3 Relative expression of Caspase 3 mRNA in kidneys of rats, n=5 in each group. Data represents mean ±SD. *indicates p<0.05 vs. control values, # p < 0.05 vs.TDF group.

Figure: 8.12.4 Activity of Caspase-3

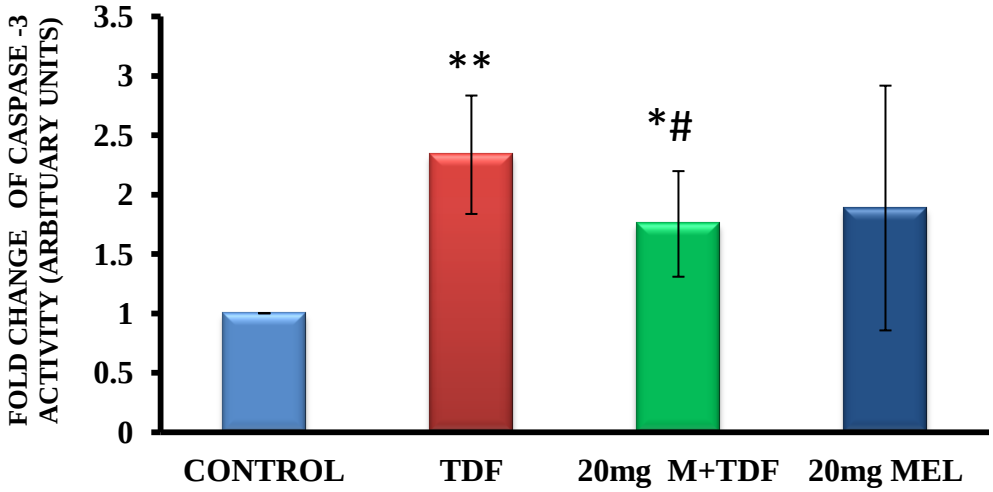

Figure: 8.12.4 Effect of melatonin pretreatment on caspase-3, n=6 in each group. Data represents mean ±SD . * p < 0.05 , ** p < 0.01 vs. control, # p < 0.05 vs. TDF

15. Melatonin pretreatment reduced TDF induced renal cell apoptosis (TUNEL assay)

Kidneys of control rats showed few apoptotic cells in both glomeruli and tubuli. Kidneys from the rats with TDF treatment showed an increase in the number of TUNEL-positive nuclei in both tubular cells as well as glomerular cells, indicating extensive apoptosis in both cell types. Melatonin pretreatment reduced the number of apoptotic cells (Figure: 8.13.1A & B)

Pretreatment with a higher dose of melatonin 40 mg /kg body wt. /day offered more protection against TDF induced renal damage (data not shown).

Figure: 8.13.1 A **Figure: 8.13.1 A TUNEL assay – Kidney Cortex**

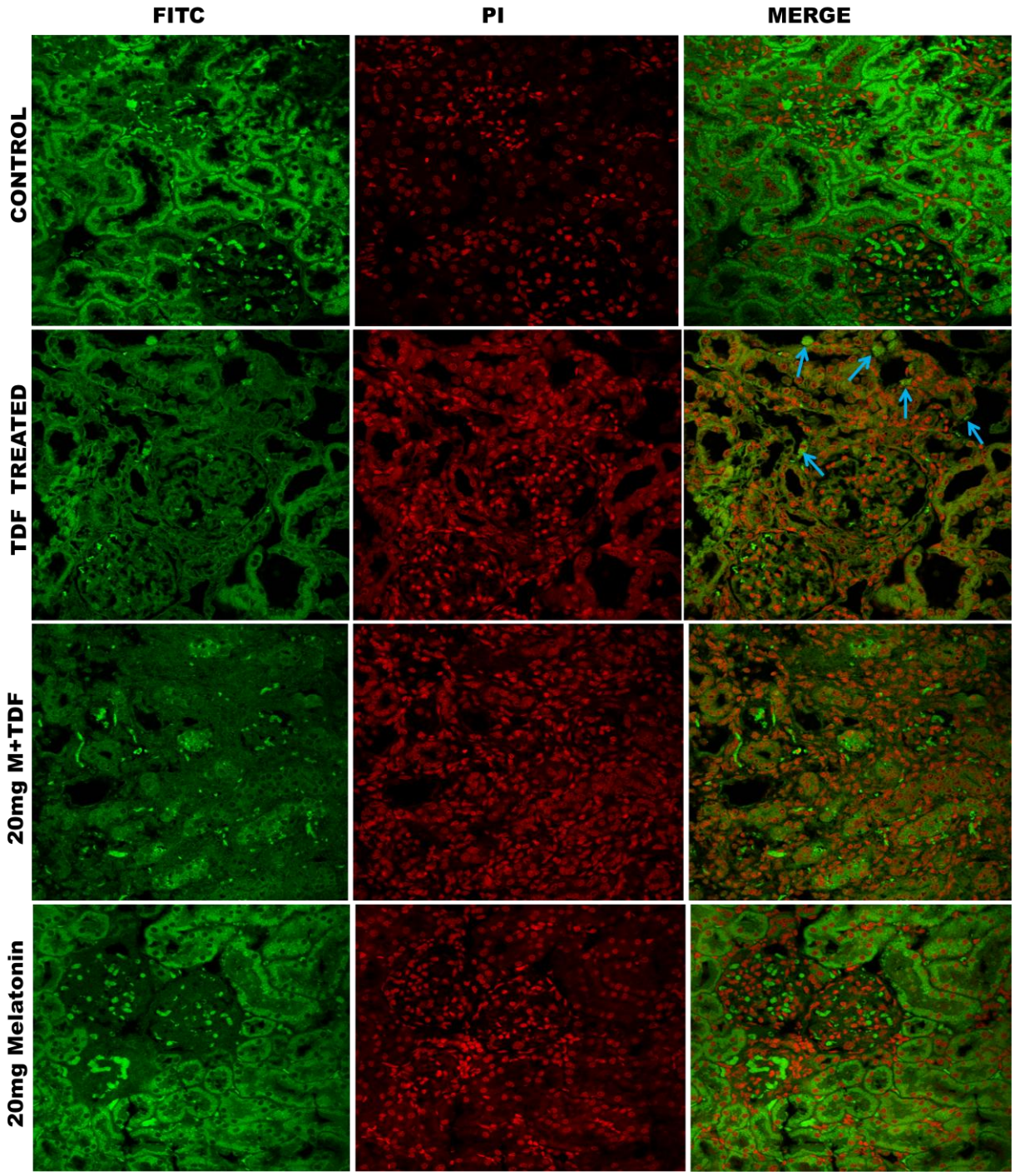

Figure: 8.13.1(A) Effect of melatonin pretreatment on apoptosis induced by TDF in kidney cortex. Apoptosis was evaluated by TUNEL staining using terminal deoxynucleotidyl transferase-mediated deoxyuridine triphosphate (TdT) nick-end labeling (A-D). Nuclei were counter stained with Propidium Iodide (PI) (E-H). Thus, red indicates propidium Iodide (PI) stained nuclei, TUNEL-positive nuclei stain green and when red and green nuclei overlap they appear yellow. Arrows indicate TUNEL-positive cells. Scale bars = 60 µm.

Fig.8.13.1 B TUNEL assay – Kidney Medulla

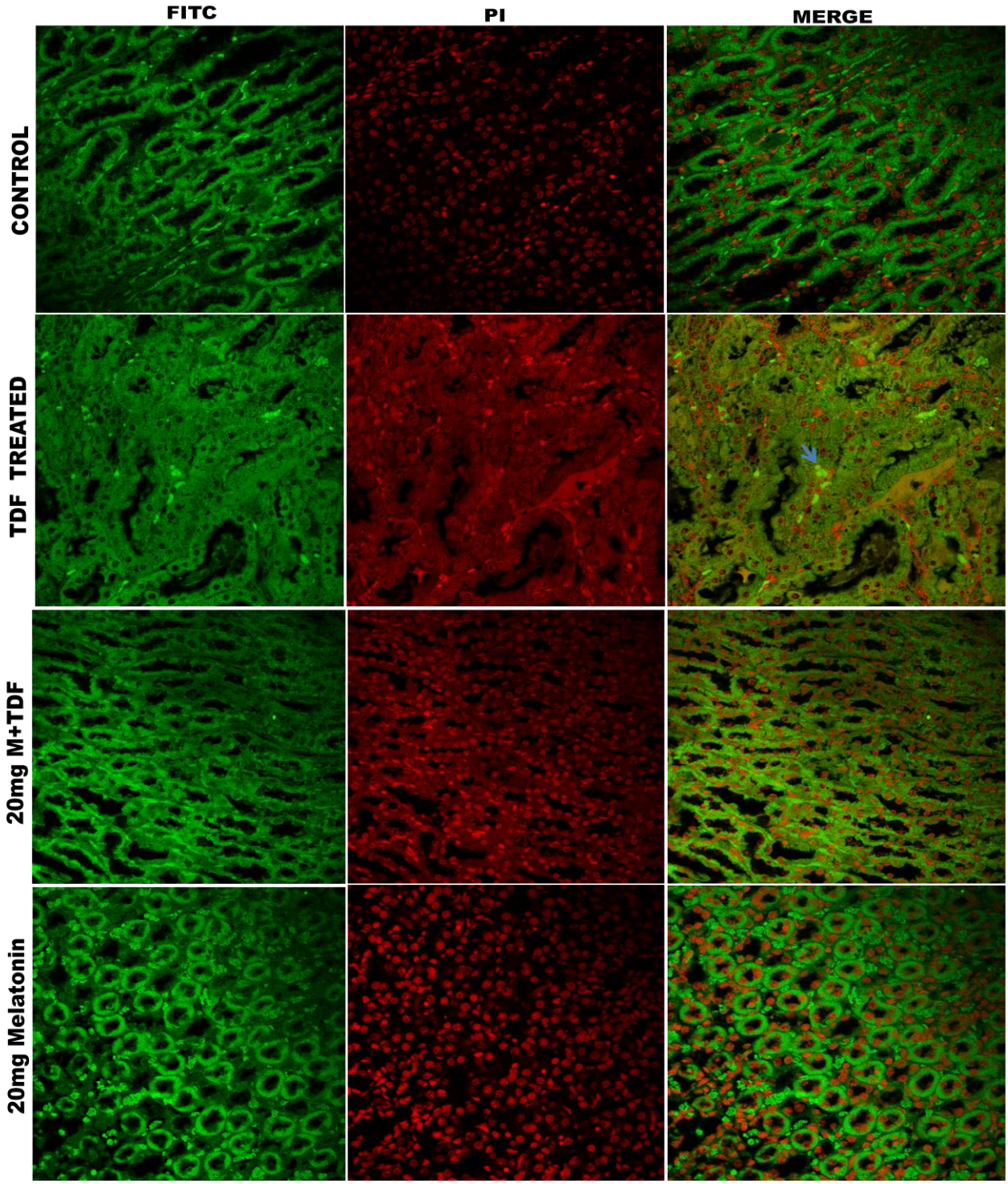

Fig.8.13.1 (B) Effect of melatonin pretreatment on apoptosis induced by TDF on kidney medulla. Apoptosis was evaluated by TUNEL staining using terminal deoxynucleotidyl transferase-mediated deoxyuridine triphosphate (TdT) nick-end labeling (A-D). Nuclei were counter stained with Propidium Iodide (PI) (E-H). Thus, red indicates propidium Iodide (PI) stained nuclei, TUNEL-positive nuclei stain green and when red and green nuclei overlap they appear yellow. Arrows indicate TUNEL-positive cells. Scale bars = 60 µm.

Discussion

During the last decade, a number of studies have demonstrated that melatonin plays an effective role in regulating mitochondrial homeostasis by multiple mechanisms. In addition to being a free radical scavenger, melatonin reduces nitric oxide (NO) generation within mitochondria. It maintains the electron flow, efficiency of oxidative phosphorylation, ATP production and bioenergetic function of the cell by regulating respiratory complex activities, Ca2+ influx, and mitochondrial permeability transition pore opening (23–26,451). In the present study, we have shown that MT pretreatment minimizes TDF induced mitochondrial damage by preserving mitochondrial structure as evidenced by electron microscopy. In addition MT pretreatment also decreased nitrate level, NT expression as well as iNOS mRNA expression. These findings suggest MT protects against TDF induced renal damage by protecting the mitochondria, which may be due to its direct effect on the mitochondria or due to its free radical scavenging capacity

As TDF induced mitochondrial tubulopathy is associated with overproduction of ROS and RNS and depletion of antioxidant system , and MT has been shown to protect against tubular damage caused by different nephrotoxins, primarily by its antioxidant property and anti-inflammatory effect, we tested the hypothesis that melatonin supplementation may prevent TDF nephrotoxicity by attenuating oxidative stress and inflammation. Protective effects of melatonin were assessed by studying markers of renal oxidative stress, nitrosative stress, and inflammation, along with biochemical and histopathological changes in the kidney.

Melatonin pretreatment attenuated TDF induced oxidative stress (measured as protein carbonyl content) and restored the activities of certain antioxidant enzymes (GR and GST).These biochemical observations were supplemented by histopathological examination of kidney sections, which revealed that MLT also reduced the severity of TDF-induced histological alterations in the kidney. These results suggest that administration of TDF causes oxidative stress to renal tissue and that MLT protects against the oxidative damage associated with TDF. Melatonin has many roles as

an antioxidant. 1. MT acts as a free radical scavenger .It has been reported to scavenge hydrogen peroxide, hydroxyl radical , nitric oxide , peroxynitrite anion , hypochlorous acid ,superoxide anion and peroxyl radical (447). 2. Melatonin can stimulate some important antioxidative enzymes, i.e., superoxide dismutase, glutathione peroxidase and glutathione reductase (448). 3. Stimulation of GSH synthesis by melatonin (288).

Melatonin pretreatment has been shown to protect the rats against the nephrotoxicity of gentamicin (285) and cisplatin (286), both of which are tubular toxins , by attenuating oxidative stress and restoration of the antioxidant system (glutathione and anti-oxidant enzymes). Unexpectedly, in our study MT pretreatment protected against TDF nephrotoxicity although it did not attenuate TDF induced glutathione depletion and loss of anti-oxidant enzyme activity, although TDF is also a proximal tubular toxin. This was somewhat surprising because evidence has accumulated that melatonin is both a direct free radical scavenger and an indirect antioxidant because of its ability to promote the activities of a variety of antioxidative enzymes including SOD and glutathione peroxidase (447).

Two conclusions maybe drawn from these observations

1. Renoprotective effect of MT may be due to its direct free radical scavenging effect rather than on GSH or AO system

2. The ability of melatonin to ameliorate TDF-induced renal damage may involve other mechanisms other its antioxidant effect.

Interestingly, GSH independent protective effects of MT have been shown in few studies. MT has been shown to protect against free radical induced organ injury such as glycerol induced acute renal failure (452) and acetaminophen induced liver injury without restoration of GSH levels (453). In addition, it has been shown that, melatonin is effective in protecting mouse hearts that are completely deficient in Gpx1, suggesting that the action of melatonin is independent of its effect on this antioxidant enzyme (289).

Melatonin pretreatment attenuated TDF induced increased renal nitrate level, thereby reducing the availability of nitric oxide to form potent oxidant peroxynitrite which has potent inflammatory effect (454). Neutrophils are the first leukocytes to arrive within the injured cell. Neutrophils, recruited into the tissue (455), can contribute to tissue destruction by the production of reactive oxygen metabolites (456), granule enzymes (MPO), and cytokines that further amplify the inflammatory response (457). MPO has the ability to amplify oxidative stress, by using hydrogen peroxide to produce reactive oxidant species with a higher oxidative capacity thus increasing and propagating the damage (458).

Melatonin is reported to possess anti-inflammatory properties (289). In the present study, it was shown that pretreatment with melatonin attenuated the inflammatory cell infiltration as assessed by the specific granulocyte enzyme MPO. ,increased oxidative stress (as shown by increased protein carbonyl content) as well as renal damage The reduction of PMN infiltration elicited by melatonin treatment may be by a direct effect of melatonin on the inflammatory process induced by TDF or secondary MT-induced decrease in proximal tubular damage or both. Both the mechanisms may be possible because melatonin has been shown to be a potent inhibitor of MPO (290) and in addition to its antioxidative effects melatonin has been shown to act through specific nuclear and plasma membrane receptors. In humans and rodents, melatonin receptors (MT1,MT2, MT3) have been shown to be expressed in various extrapineal tissues including brain and retina, kidney tubules, cardiovascular system, liver and gallbladder, intestine, immune cells, adipocytes, prostate and breast epithelial cells, ovary/granulosa cells, myometrium, and skin (291,459).

.

As we demonstrated the activation of inflammatory pathway in TDF treated rat kidneys, we examined whether MT pretreatment exerts its protective effect by inhibiting the NFκB inflammatory pathway. Melatonin pretreatment attenuated TDF induced increased nuclear p65 protein expression, activity as well as mRNA expression. Besides, MT pretreatment significantly

inhibited TDF induced iNOS gene expression. All these findings suggest that the protective effect of MT may mediate via its inhibitory effect on inflammatory pathway.

Recently, many studies confirmed that melatonin exerts anti-inflammatory effect through inhibition of NF-κB. Some of these studies found that the expression level of NF-κB was suppressed by melatonin treatment (215,460–462), while others suggested that melatonin mainly disturbed the translocation of NF-κB. Generally, melatonin administration at pharmacological level suppresses the production of inflammatory cytokines and iNOS via inhibition of NF-κB. The underlying mechanisms may be through inhibition of NF-κB expression, reduction of IκB-α degradation and NF-κB translocation, or suppression of the DNA binding activity of NF-κB (285,462). In the present study, MTs protective effect appears to be mediated via inhibition of p65 mRNA expression and, nuclear translocation.

Nitric oxide has been found to be an important mediator in inflammatory response (463). Melatonin also plays a role in the regulation of nitric oxide synthesis (464). Jung et al. also observed that melatonin intraperitoneal (i.p.) administration (50 mg/kg) in rats suppresses the mRNA expression of proinflammatory genes including iNOS, TNF-α, and COX-2 (465). In the present study we have demonstrated that MT pretreatment inhibits the mRNA expression of iNOS, suggesting that MT protective effect is mediated via downregulation of the NFκB signaling pathway.

It is not clear whether melatonin's protective effect on the kidney is receptor mediated or not. There is some evidence suggesting that melatonin may act through signal transduction pathways to influence cellular activity (280). Several lines of evidence suggest that melatonin regulates renal physiology (466–468). The hypothesis that melatonin plays a significant role in renal physiology is supported by the expression of specific, high-affinity melatonin receptors in the kidney of several mammalian species, including humans (275,278). By immunofluorescence, MT1 receptors are predominantly localized in the proximal tubular segments (275). This localization suggests that melatonin probably influences renal function through regulation of proximal tubular function.

However, it is unclear whether activation of melatonin receptors may participate in the prevention of TDF induced renal injury by melatonin. The results of the present study show that melatonin pretreatment ameliorated TDF induced kidney damage by attenuating mitochondrial damage, oxido-nitrative stress, and signaling pathway .

Summary and Conclusions

Tenofovir disoproxil fumarate is a commonly used drug for the treatment of AIDS. However, the usage of the drug is often limited by its nephrotoxicity after long time usage (2-9 years). Tenofovir and related nucleotide analogs have primarily been associated with proximal tubular dysfunction and acute kidney injury. Tenofovir targets the proximal tubular mitochondria. However, the mechanism of TDF induced mitochondrial damage and consequence of mitochondrial damage is not known.

The objectives of the study were to

1. Standardize a rat model of Tenofovir induced renal damage
2. Assess the effect of tenofovir on mitochondrial structure and function in the kidney.
3. Investigate the role of oxidative stress and nitrosative stress in the tenofovir induced renal damage using rat as a model.
4. Investigate the role of NFκB activation and its target genes, PARP activation in the tenofovir induced renal damage.
5. Study the effect of melatonin, a potent anti-oxidant, anti-inflammatory agent and NFκB inhibitor on tenofovir - induced renal damage.

Study I

The first study was designed to standardize the rat model of TDF induced renal damage. The TDF dose was standardized at oral administration of 600 mg/kg body weight/day for 5 weeks. Light microscopy revealed damage mainly to the cortex. The proximal tubules and distal convoluted tubules were distorted and dilated. Degeneration of the proximal tubular epithelium was also observed. Some glomeruli were shrunken. In the medulla, and the lining epithelium of loop of Henle and the collecting duct was destroyed. Electron microscopy of the proximal tubular epithelial cells revealed damage mainly to the mitochondria. The ultra structural changes in the mitochondria include swollen mitochondria, disrupted cristae, and amorphous deposits in the matrix. The mitochondrial injury was graded as severe (4/5). Other ultrastructural changes include shrunken nuclei, increased number of vacuoles, and decrease in the lysosomal number.

Proximal tubular function was impaired in TDF-treated rats, as evidenced by increased urinary phosphate, bicarbonate, uric acid and potassium, and hypophosphatemia and hypokalemia. In addition, low molecular weight proteinuria which is a sensitive indicator of tubular damage was also observed. As the tenofovir-treated rats showed proximal tubular structural (mitochondrial damage) and functional alterations (Fanconi Syndrome) that closely resembled HIV patients on long term tenofovir therapy, this model appears to be a suitable model for the study of tenofovir nephrotoxicity.

We followed this model for our further studies.

Study II

Mitochondrial swelling and disruption of cristae are considered to be characteristic features of the deteriorated function of this organelle. The components in the electron transport chain, which play the central role in ATP synthesis, are found in the cristae. Thus, damage to the cristae can result in the disruption of ETC and hence decrease ATP production by the mitochondria. Therefore, we next investigated the effect of TDF treatment on mitochondrial function, the activities of the ETC complexes and the mitochondrial antioxidants.

Impaired mitochondrial function such as respiratory control ratio (RCR), MTT reduction, and mitochondrial swelling was observed. The activities of the electron chain complexes I, II, IV and V were decreased by 46%, 26%, 20% and 21% respectively in the TDF treated rat kidneys. The activities of the mitochondrial antioxidant enzymes were decreased significantly. Superoxide dismutase activity was decreased by 61%, aconitase and carbonic anhydrase by 45%. It is concluded that TDF induced renal tubular damage is associated with mitochondrial dysfunction and loss of the activities of ETC complex and mitochondrial antioxidant system.

Study III

Damaged mitochondria are major sources of reactive oxygen species and reactive nitrogen species. Therefore, we next examined whether oxidative and nitrosative stress contributes to TDF nephrotoxicity. We assayed the parameters of oxidative stress- TBARS and protein carbonyl content, glutathione level, protein thiol, activities of antioxidant enzymes, glutathione reductase, glutathione peroxidase, glutathione-S-transferase, catalase, and superoxide dismutase, as well as MPO, marker of neutrophil infiltration. In addition, we examined the expression of oxidant stress proteins HSP and HO-1 in the rat kidneys by immunohistochemical method and Western blot method , in addition to mRNA expression by RT PCR. Levels of nitrate, nitrotyrosine and nitrosocysteine were also analyzed .

A 2 fold increase in protein carbonyl content was observed in the kidneys of TDF treated rats as compared with the control. Reduced glutathione, an important intracellular antioxidant was decreased by 61% and protein thiol by 33% in the kidneys of TDF treated rats as compared with the control. A nine fold increase in myeloperoxidase activity, a marker of neutrophil infiltration was observed in the kidneys of TDF treated rats. The activities of all the antioxidant enzymes estimated were significantly decreased in the kidneys of TDF treated rats as compared with the control. The activity of superoxide dismutase (SOD) was decreased by 61%, glutathione S transferase by 47 %, and glutathione reductase by 43 % as compared with control. A 4 fold decrease in the activity of glutathione peroxidase was observed in the TDF treated rats. The western blot analysis of Heme oxygenase (HO-1) and HSP 70 showed siginificant reduction in the treated groups as compared with control (p-value 0.001 and 0.05) respectively. The mRNA expression of HO-1 and HSP 70 was significantly decreased in the TDF treated rat kidneys. These results clearly demonstrate that oxidative stress, nitrosative stress, and neutrophil infiltration contribute to TDF nephrotoxicity.

Study IV

Reactive oxygen species are a potent stimulus for the activation of , a key transcription factor, which is known to mediate inflammation by regulating the expression of cytokines and chemokines. Upon activation, after phosphorylation and degradation of IkB, NF-κB is released and translocated into nucleus where it promotes the expression of inflammatory gene products such as TNF-α, inducible nitric oxide synthase (iNOS), cyclooxygenase (COX)-2, intercellular adhesion molecule and induces inflammatory activation of lymphocytes, monocyte/macrophages and endothelial cells . Therefore, we investigated the effect of chronic TDF administration on (a) protein expression by western blot and immunostaining methods, gene mRNA expression by PCR, and activity by ELISA, (b) iNOS protein expression by western blot and immunostaing methods, gene mRNA expression by PCR, (c) Protein tyrosine nitration and nitrosocysteine formation by Western blot and immunostaining (d) COX-2 gene and protein expression, (e) TNF α protein expression by western blot, and immunostaining, and mRNA expression by PCR and (f) MMP expression by zymography, western blot and RT-PCR.

The results of the present study clearly show that the NF-κB signaling, a principal signaling pathway mediating pro-inflammatory response is activated in the kidneys of TDF treated rats, as shown by an increase in the mRNA and protein expressions of NFκB, and its target proinflammatory genes, iNOS, COX-2, TNF-α and MMP. The activation of NFκB and its downstream proinflammatory target genes iNOS, and COX-2, and TNF-α may play a critical role in the pathophysiology of TDF induced proximal tubular damage and death.

Study V

Prevention of the TDF tubular toxicity is vital to avoid irreversible tubulointerstitial damage. Identifying an agent that prevents TDF induced renal injury can lead to better tolerance to TDF and therefore a more effective treatment can be achieved in HIV infected patients. Melatonin is a well-established natural antioxidant and anti-inflammatory agent. It is not only a strong scavenger of free radicals, reactive oxygen species (ROS) and RNS (nitric oxide). It is also a stimulator of the cellular antioxidant systems and has the ability to reduce free radical production at the mitochondrial level . Therefore, we investigated whether melatonin pretreatment protects against TDF nephrotoxicity.

Melatonin pretreatment protected the rats against TDF nephrotoxicity both histologically and biochemically. Histologically, melatonin pretreatment prevented TDF induced proximal tubular injury and mitochondrial injury such as swelling, disruption of cristae and deposition of amorphous material in the matrix. It restored the lysosomal and mitochondrial numbers in the proximal tubules. Biochemically, melatonin pretreatment attenuated TDF induced renal oxidative stress, nitrosative stress, NFκB activation and expression of proinflammatory genes, iNOS,COX-2, TNF-α, MMP and reduced proximal tubular dysfunction. This study shows that melatonin pretreatment protects rats from tenofovir induced damage to proximal tubular mitochondria by attenuating oxidative stress, nitrosative stress, and inflammation.

Beneficial antioxidant effects of melatonin have been recently shown in clinical settings for several chronic diseases, including patients with rheumatoid arthritis, elderly patients with primary essential hypertension, and females with infertility. Clinical studies are needed to determine the effectiveness of melatonin against TDF induced nephrotoxicity. If proven effective, melatonin would be an excellent adjunctive therapy as it is natural, inexpensive, widely available, and has minimal side effects (somnolence) .

Scope for Future Studies

Nephrotoxicity is one of the most common side effects of chronic tenofovir therapy in HIV infected patients and may necessitate discontinuation of chemotherapy. Agents that can reduce the incidence or severity of tenofovir related nephrotoxicity are urgently needed . Melatonin has been shown to reduce the toxicity of many drugs and in some cases improve their efficacy (287). The results of our study provide evidence for melatonin as an agent that can protect against TDF nephrotoxicity. Melatonin is safe, nontoxic, inexpensive, and available in pure form for human use as a drug . **Execution of clinical trials using melatonin as a renoprotective agent in HIV infected patients on tenofovir therapy is our primary goal.**

Natural plant products have shown tremendous potential to serve as the alternative therapeutic agents so as to counter the side effects of various drugs. These include flavonoids such as quercitin, apigenin, rutin, and hesperidin , that are present in apples, apricots, black tea and green tea etc.) and Resveratrol that is present in red wine, red and purple grapes etc.,). **Conducting preclinical studies to evaluate the effectiveness of resveratrol /hesperidin in the attenuation of tenofovir nephrotoxicity is our next objective.**

How tenofovir inhibits the enzymatic complexes of the respiratory chain remains to be elucidated. Studies of the site and type of interaction of tenofovir at the different enzymatic complexes will give more clues about the mechanism of inhibition that may lead to proximal tubular damage. Studies using mitochondrially targeted antioxidants such as, MitoQ or Mito-CP can help confirm the contribution of proximal tubular mitochondrial damage in TDF nephrotoxicity. **Investigating whether the administration of MitoQ protects against TDF induced proximal tubular mitochondrial injury and dysfunction, and nephropathy in rats is another objective.**

Bibliography

1. Gallant JE, Deresinski S. Tenofovir disoproxil fumarate. Clin. Infect. Dis. 2003 Oct 1;37(7):944–50.

2. Cohen MH, Johnson JR, Pazdur R. U.S. Food and Drug Administration Drug Approval Summary: conversion of imatinib mesylate (STI571; Gleevec) tablets from accelerated approval to full approval. Clin. Cancer Res. 2005 Jan 1;11(1):12–9.

3. Hostetler KY. Alkoxyalkyl prodrugs of acyclic nucleoside phosphonates enhance oral antiviral activity and reduce toxicity: current state of the art. Antiviral Res. 2009 May;82(2):A84–98.

4. Birkus G, Hitchcock MJM, Cihlar T. Assessment of mitochondrial toxicity in human cells treated with tenofovir: comparison with other nucleoside reverse transcriptase inhibitors. Antimicrob. Agents Chemother. 2002 Mar;46(3):716–23.

5. Belongia EA, Costa J, Gareen IF, Grem JL, Inadomi JM, Kern ER, et al. NIH consensus development statement on management of hepatitis B. NIH Consens State Sci Statements. 2008 Oct 22;25(2):1–29.

6. Panel on Antiretroviral Guidelines for Adults and Adolescents. Guidelines for the Use of Antiretroviral Agents in HIV-1- Infected Adults and Adolescents, 2011,.

7. Rodriguez-Nóvoa S, Alvarez E, Labarga P, Soriano V. Renal toxicity associated with tenofovir use. Expert Opin Drug Saf. 2010 Jul;9(4):545–59.

8. Nelson MR, Katlama C, Montaner JS, Cooper DA, Gazzard B, Clotet B, et al. The safety of tenofovir disoproxil fumarate for the treatment of HIV infection in adults: the first 4 years. AIDS. 2007 Jun 19;21(10):1273–81.

9. Goicoechea M, Liu S, Best B, Sun S, Jain S, Kemper C, et al. Greater tenofovir-associated renal function decline with protease inhibitor-based versus nonnucleoside reverse-transcriptase inhibitor-based therapy. J. Infect. Dis. 2008 Jan 1;197(1):102–8.

10. Cihlar T, Ho ES, Lin DC, Mulato AS. Human renal organic anion transporter 1 (hOAT1) and its role in the nephrotoxicity of antiviral nucleotide analogs. Nucleosides Nucleotides Nucleic Acids. 2001 Jul;20(4-7):641–8.

11. Ray AS, Cihlar T, Robinson KL, Tong L, Vela JE, Fuller MD, et al. Mechanism of active renal tubular efflux of tenofovir. Antimicrob. Agents Chemother. 2006 Oct;50(10):3297–304.

12. Gallant JE, Parish MA, Keruly JC, Moore RD. Changes in renal function associated with tenofovir disoproxil fumarate treatment, compared with nucleoside reverse-transcriptase inhibitor treatment. Clin. Infect. Dis. 2005 Apr 15;40(8):1194–8.

13. Gallant JE, Staszewski S, Pozniak AL, DeJesus E, Suleiman JMAH, Miller MD, et al. Efficacy and safety of tenofovir DF vs stavudine in combination therapy in antiretroviral-naive patients: a 3-year randomized trial. JAMA. 2004 Jul 14;292(2):191–201.

14. Maggiolo F, Roat E, Pinti M, Nasi M, Gibellini L, De Biasi S, et al. Mitochondrial changes during D-drug-containing once-daily therapy in HIV-positive treatment-naive patients. Antivir. Ther. (Lond.). 2010;15(1):51–9.

15. Herlitz LC, Mohan S, Stokes MB, Radhakrishnan J, D'Agati VD, Markowitz GS. Tenofovir nephrotoxicity: acute tubular necrosis with distinctive clinical, pathological, and mitochondrial abnormalities. Kidney Int. 2010 Dec;78(11):1171–7.

16. Karras A, Lafaurie M, Furco A, Bourgarit A, Droz D, Sereni D, et al. Tenofovir-related nephrotoxicity in human immunodeficiency virus-infected patients: three cases of renal failure, Fanconi syndrome, and nephrogenic diabetes insipidus. Clin. Infect. Dis. 2003 Apr 15;36(8):1070–3.

17. James CW, Steinhaus MC, Szabo S, Dressier RM. Tenofovir-related nephrotoxicity: case report and review of the literature. Pharmacotherapy. 2004 Mar;24(3):415–8.

18. Izzedine H, Baumelou A, Deray G. Acute renal failure in HIV patients. Nephrol. Dial. Transplant. 2007 Oct;22(10):2757–62.

19. Nordberg J, Arnér ES. Reactive oxygen species, antioxidants, and the mammalian thioredoxin system. Free Radic. Biol. Med. 2001 Dec 1;31(11):1287–312.

20. Spiteller G. Lipid peroxidation in aging and age-dependent diseases. Exp. Gerontol. 2001 Sep;36(9):1425–57.

21. European Medicines Agency. 'Circadin, melatonin'. European Public Assessment Report (EPAR). European Medicines Agency. Retrieved 5 June 2013.

22. Malhotra S, Sawhney G, Pandhi P. The Therapeutic Potential of Melatonin: A Review of the Science. MedGenMed [Internet]. 2004 Apr 14 [cited 2013 Aug 4];6(2). Available from: http://www.ncbi.nlm.nih.gov/pmc/articles/PMC1395802/

23. Martín M, Macías M, Escames G, León J, Acuña-Castroviejo D. Melatonin but not vitamins C and E maintains glutathione homeostasis in t-butyl hydroperoxide-induced mitochondrial oxidative stress. FASEB J. 2000 Sep;14(12):1677–9.

24. Martín M, Macías M, Escames G, Reiter RJ, Agapito MT, Ortiz GG, et al. Melatonin-induced increased activity of the respiratory chain complexes I and IV can prevent mitochondrial damage induced by ruthenium red in vivo. J. Pineal Res. 2000 May;28(4):242–8.

25. Leon J, Acuña-Castroviejo D, Sainz RM, Mayo JC, Tan D-X, Reiter RJ. Melatonin and mitochondrial function. Life Sci. 2004 Jul 2;75(7):765–90.

26. López A, García JA, Escames G, Venegas C, Ortiz F, López LC, et al. Melatonin protects the mitochondria from oxidative damage reducing oxygen consumption, membrane potential, and superoxide anion production. J. Pineal Res. 2009 Mar;46(2):188–98.

27. Cui K, Luo X, Xu K, Ven Murthy MR. Role of oxidative stress in neurodegeneration: recent developments in assay methods for oxidative stress and nutraceutical antioxidants. Prog. Neuropsychopharmacol. Biol. Psychiatry. 2004 Aug;28(5):771–99.

28. Mwanjewe J, Hui BK, Coughlin MD, Grover AK. Treatment of PC12 cells with nerve growth factor increases iron uptake. Biochem. J. 2001 Aug 1;357(Pt 3):881–6.

29. Levi S, Santambrogio P, Corsi B, Cozzi A, Arosio P. Evidence that residues exposed on the three-fold channels have active roles in the mechanism of ferritin iron incorporation. Biochem. J. 1996 Jul 15;317 (Pt 2):467–73.

30. Beal MF. Oxidatively modified proteins in aging and disease. Free Radic. Biol. Med. 2002 May 1;32(9):797–803.

31. Kohler JJ, Hosseini SH, Hoying-Brandt A, Green E, Johnson DM, Russ R, et al. Tenofovir renal toxicity targets mitochondria of renal proximal tubules. Lab. Invest. 2009 May;89(5):513–9.

32. Lieberthal W, Menza SA, Levine JS. Graded ATP depletion can cause necrosis or apoptosis of cultured mouse proximal tubular cells. Am. J. Physiol. 1998 Feb;274(2 Pt 2):F315–327.

33. Perazella MA. Tenofovir-induced kidney disease: an acquired renal tubular mitochondriopathy. Kidney Int. 2010 Dec;78(11):1060–3.

34. Lim MS, Lim PLK, Gupta R, Boelsterli UA. Critical role of free cytosolic calcium, but not uncoupling, in mitochondrial permeability transition and cell death induced by diclofenac oxidative metabolites in immortalized human hepatocytes. Toxicol. Appl. Pharmacol. 2006 Dec 15;217(3):322–31.

35. Radak Z, Zhao Z, Goto S, Koltai E. Age-associated neurodegeneration and oxidative damage to lipids, proteins and DNA. Mol. Aspects Med. 2011 Aug;32(4-6):305–15.

36. Murphy MP. How mitochondria produce reactive oxygen species. Biochem. J. 2009 Jan 1;417(1):1–13.

37. Andreyev AY, Kushnareva YE, Starkov AA. Mitochondrial metabolism of reactive oxygen species. Biochemistry Mosc. 2005 Feb;70(2):200–14.

38. Koehler CM, Beverly KN, Leverich EP. Redox pathways of the mitochondrion. Antioxid. Redox Signal. 2006 Jun;8(5-6):813–22.

39. Samikkannu T, Thomas JJ, Bhat GJ, Wittman V, Thekkumkara TJ. Acute effect of high glucose on long-term cell growth: a role for transient glucose increase in proximal tubule cell injury. Am. J. Physiol. Renal Physiol. 2006 Jul;291(1):F162–175.

40. Luster MI, Simeonova PP, Gallucci R, Matheson J. Tumor necrosis factor alpha and toxicology. Crit. Rev. Toxicol. 1999 Sep;29(5):491–511.

41. Jung YJ, Lee JE, Lee AS, Kang KP, Lee S, Park SK, et al. SIRT1 overexpression decreases cisplatin-induced acetylation of NF-κB p65 subunit and cytotoxicity in renal proximal tubule cells. Biochem. Biophys. Res. Commun. 2012 Mar 9;419(2):206–10.

42. Nakayama H, Ikebe T, Beppu M, Shirasuna K. High expression levels of nuclear factor kappaB, IkappaB kinase alpha and Akt kinase in squamous cell carcinoma of the oral cavity. Cancer. 2001 Dec 15;92(12):3037–44.

43. Mercurio F, Zhu H, Murray BW, Shevchenko A, Bennett BL, Li J, et al. IKK-1 and IKK-2: cytokine-activated IkappaB kinases essential for NF-kappaB activation. Science. 1997 Oct 31;278(5339):860–6.

44. 13 th June 2005 Topic of the day: HIV Soothsayer.

45. Izzedine H, Launay-Vacher V, Deray G. Antiviral drug-induced nephrotoxicity. Am. J. Kidney Dis. 2005 May;45(5):804–17.

46. Valdivielso JM, Blantz RC. Acute renal failure: is nitric oxide the bad guy? Antioxid. Redox Signal. 2002 Dec;4(6):925–34.

47. Evans Branch III, PharmD, Melony Floyd, PharmD, and Marlon Honeywell, PharmD. Tenofovir: The First Nucleotide Analog for HIV-1. (P&T® • July 2002 • Vol. 27 No. 7).

48. Gilead Sciences, Inc. Foster City, California, USA. Application for Inclusion of Tenofovir Disoproxil Fumarate (TDF) On WHO Model List of Essential Medic. 2006.

49. Rodriguez-Nóvoa S, Alvarez E, Labarga P, Soriano V. Renal toxicity associated with tenofovir use. Expert Opin Drug Saf. 2010 Jul;9(4):545–59.

50. Tenofovir Drug Information.Pdf.

51. De Clercq E. Antiviral drugs in current clinical use. J. Clin. Virol. 2004 Jun;30(2):115–33.

52. Izzedine H, Harris M, Perazella MA. The nephrotoxic effects of HAART. Nat Rev Nephrol. 2009 Oct;5(10):563–73.

53. Fux CA, Christen A, Zgraggen S, Mohaupt MG, Furrer H. Effect of tenofovir on renal glomerular and tubular function. AIDS. 2007 Jul 11;21(11):1483–5.

54. Malik A, Abraham P, Malik N. Acute renal failure and Fanconi syndrome in an AIDS patient on tenofovir treatment--case report and review of literature. J. Infect. 2005 Aug;51(2):E61–65.

55. Peyrière H, Reynes J, Rouanet I, Daniel N, De Boever CM, Mauboussin J-M, et al. Renal tubular dysfunction associated with tenofovir therapy: report of 7 cases. J. Acquir. Immune Defic. Syndr. 2004 Mar 1;35(3):269–73.

56. Quimby D, Brito MO. Fanconi syndrome associated with use of tenofovir in HIV-infected patients: a case report and review of the literature. AIDS Read. 2005 Jul;15(7):357–64.

57. Antoniou T, Raboud J, Chirhin S, Yoong D, Govan V, Gough K, et al. Incidence of and risk factors for tenofovir-induced nephrotoxicity: a retrospective cohort study. HIV Med. 2005 Jul;6(4):284–90.

58. Hall AM, Hendry BM, Nitsch D, Connolly JO. Tenofovir-associated kidney toxicity in HIV-infected patients: a review of the evidence. Am. J. Kidney Dis. 2011 May;57(5):773–80.

59. Young B, Buchacz K, Moorman A, Wood KC, Brooks JT, HIV Outpatient Study (HOPS) Investigators. Renal function in patients with preexisting renal disease receiving tenofovir-containing highly active antiretroviral therapy in the HIV outpatient study. AIDS Patient Care STDS. 2009 Aug;23(8):589–92.

60. Breton G, Alexandre M, Duval X, Prie D, Peytavin G, Leport C, et al. Tubulopathy consecutive to tenofovir-containing antiretroviral therapy in two patients infected with human immunodeficiency virus-1. Scand. J. Infect. Dis. 2004;36(6-7):527–8.

61. Karras A, Lafaurie M, Furco A, Bourgarit A, Droz D, Sereni D, et al. Tenofovir-related nephrotoxicity in human immunodeficiency virus-infected patients: three cases of renal failure, Fanconi syndrome, and nephrogenic diabetes insipidus. Clin. Infect. Dis. 2003 Apr 15;36(8):1070–3.

62. Badiou S, De Boever CM, Terrier N, Baillat V, Cristol J-P, Reynes J. Is tenofovir involved in hypophosphatemia and decrease of tubular phosphate reabsorption in HIV-positive adults? J. Infect. 2006 May;52(5):335–8.

63. Rifkin BS, Perazella MA. Tenofovir-associated nephrotoxicity: Fanconi syndrome and renal failure. Am. J. Med. 2004 Aug 15;117(4):282–4.

64. Woodward CLN, Hall AM, Williams IG, Madge S, Copas A, Nair D, et al. Tenofovir-associated renal and bone toxicity. HIV Med. 2009 Sep;10(8):482–7.

65. Herlitz LC, Mohan S, Stokes MB, Radhakrishnan J, D'Agati VD, Markowitz GS. Tenofovir nephrotoxicity: acute tubular necrosis with distinctive clinical, pathological, and mitochondrial abnormalities. Kidney Int. 2010 Dec;78(11):1171–7.

66. Labarga P, Barreiro P, Martin-Carbonero L, Rodriguez-Novoa S, Solera C, Medrano J, et al. Kidney tubular abnormalities in the absence of impaired glomerular function in HIV patients treated with tenofovir. AIDS. 2009 Mar 27;23(6):689–96.

67. Kohler JJ, Hosseini SH, Hoying-Brandt A, Green E, Johnson DM, Russ R, et al. Tenofovir renal toxicity targets mitochondria of renal proximal tubules. Lab. Invest. 2009 May;89(5):513–9.

68. Mujais S, Batlle DC. Functional correlates of tubulo-interstitial damage. Semin. Nephrol. 1988 Mar;8(1):94–9.

69. Butterfield DA, Howard B, Yatin S, Koppal T, Drake J, Hensley K, et al. Elevated oxidative stress in models of normal brain aging and Alzheimer's disease. Life Sci. 1999;65(18-19):1883–92.

70. Halliwell,B.;Gutteridge,J.M.C. Free RadicalsinBiologyandMedicine. 4thed. Oxford: OxfordUniversityPress;2007.

71. Valko M, Rhodes CJ, Moncol J, Izakovic M, Mazur M. Free radicals, metals and antioxidants in oxidative stress-induced cancer. Chem. Biol. Interact. 2006 Mar 10;160(1):1–40.

72. Willcox JK, Ash SL, Catignani GL. Antioxidants and prevention of chronic disease. Crit Rev Food Sci Nutr. 2004;44(4):275–95.

73. Halliwell B. Role of free radicals in the neurodegenerative diseases: therapeutic implications for antioxidant treatment. Drugs Aging. 2001;18(9):685–716.

74. Valko M, Izakovic M, Mazur M, Rhodes CJ, Telser J. Role of oxygen radicals in DNA damage and cancer incidence. Mol. Cell. Biochem. 2004 Nov;266(1-2):37–56.

75. Rubbo H, Radi R, Anselmi D, Kirk M, Barnes S, Butler J, et al. Nitric oxide reaction with lipid peroxyl radicals spares alpha-tocopherol during lipid peroxidation. Greater oxidant protection from the pair nitric oxide/alpha-tocopherol than alpha-tocopherol/ascorbate. J. Biol. Chem. 2000 Apr 14;275(15):10812–8.

76. Antunes F, Nunes C, Laranjinha J, Cadenas E. Redox interactions of nitric oxide with dopamine and its derivatives. Toxicology. 2005 Mar 15;208(2):207–12.

77. Radi R, Peluffo G, Alvarez MN, Naviliat M, Cayota A. Unraveling peroxynitrite formation in biological systems. Free Radic. Biol. Med. 2001 Mar 1;30(5):463–88.

78. Zhang J, Veasey S. Making sense of oxidative stress in obstructive sleep apnea: mediator or distracter? Front Neurol. 2012;3:179.

79. Valko M, Leibfritz D, Moncol J, Cronin MTD, Mazur M, Telser J. Free radicals and antioxidants in normal physiological functions and human disease. Int. J. Biochem. Cell Biol. 2007;39(1):44–84.

80. Schafer FQ, Buettner GR. Redox environment of the cell as viewed through the redox state of the glutathione disulfide/glutathione couple. Free Radic. Biol. Med. 2001 Jun 1;30(11):1191–212.

81. Babior BM, Takeuchi C, Ruedi J, Gutierrez A, Wentworth P Jr. Investigating antibody-catalyzed ozone generation by human neutrophils. Proc. Natl. Acad. Sci. U.S.A. 2003 Mar 18;100(6):3031–4.

82. Griendling KK, Sorescu D, Lassègue B, Ushio-Fukai M. Modulation of protein kinase activity and gene expression by reactive oxygen species and their role in vascular physiology and pathophysiology. Arterioscler. Thromb. Vasc. Biol. 2000 Oct;20(10):2175–83.

83. Martínez-Ruiz A, Lamas S. S-nitrosylation: a potential new paradigm in signal transduction. Cardiovasc. Res. 2004 Apr 1;62(1):43–52.

84. Zhu H, Bunn HF. Oxygen sensing and signaling: impact on the regulation of physiologically important genes. Respir Physiol. 1999 Apr 1;115(2):239–47.

85. Semenza GL. HIF-1: mediator of physiological and pathophysiological responses to hypoxia. J. Appl. Physiol. 2000 Apr;88(4):1474–80.

86. Sellak H, Franzini E, Hakim J, Pasquier C. Reactive oxygen species rapidly increase endothelial ICAM-1 ability to bind neutrophils without detectable upregulation. Blood. 1994 May 1;83(9):2669–77.

87. Dalton TP, Shertzer HG, Puga A. Regulation of gene expression by reactive oxygen. Annu. Rev. Pharmacol. Toxicol. 1999;39:67–101.

88. Cai J, Jones DP. Mitochondrial redox signaling during apoptosis. J. Bioenerg. Biomembr. 1999 Aug;31(4):327–34.

89. Fleury C, Mignotte B, Vayssière J-L. Mitochondrial reactive oxygen species in cell death signaling. Biochimie. 2002 Mar;84(2-3):131–41.

90. Nunes C, Almeida L, Laranjinha J. 3,4-Dihydroxyphenylacetic acid (DOPAC) modulates the toxicity induced by nitric oxide in PC-12 cells via mitochondrial dysfunctioning. Neurotoxicology. 2008 Nov;29(6):998–1007.

91. Gracy RW, Talent JM, Kong Y, Conrad CC. Reactive oxygen species: the unavoidable environmental insult? Mutat. Res. 1999 Jul 16;428(1-2):17–22.

92. Silva JP, Coutinho OP. Free radicals in the regulation of damage and cell death - basic mechanisms and prevention. Drug Discov Ther. 2010 Jun;4(3):144–67.

93. Giulivi C. Characterization and function of mitochondrial nitric-oxide synthase. Free Radic. Biol. Med. 2003 Feb 15;34(4):397–408.

94. Li X, Fang P, Mai J, Choi ET, Wang H, Yang X. Targeting mitochondrial reactive oxygen species as novel therapy for inflammatory diseases and cancers. J Hematol Oncol. 2013;6:19.

95. Moon YJ, Wang X, Morris ME. Dietary flavonoids: effects on xenobiotic and carcinogen metabolism. Toxicol In Vitro. 2006 Mar;20(2):187–210.

96. Gupta M, Dobashi K, Greene EL, Orak JK, Singh I. Studies on hepatic injury and antioxidant enzyme activities in rat subcellular organelles following in vivo ischemia and reperfusion. Mol. Cell. Biochem. 1997 Nov;176(1-2):337–47.

97. Behl C, Moosmann B. Antioxidant neuroprotection in Alzheimer's disease as preventive and therapeutic approach. Free Radic. Biol. Med. 2002 Jul 15;33(2):182–91.

98. Bitto A, Minutoli L, Squadrito F, Polito F, Altavilla D. Raxofelast, (+/-)5-(acetyloxy)-2,3-dihydro-4,6,7-trimethyl-2-benzofuranacetic acid: a new antioxidant to modulate the inflammatory response during ischemia-reperfusion injury and impaired wound healing. Mini Rev Med Chem. 2007 Mar;7(3):339–43.

99. Buettner GR, Ng CF, Wang M, Rodgers VGJ, Schafer FQ. A new paradigm: manganese superoxide dismutase influences the production of H2O2 in cells and thereby their biological state. Free Radic. Biol. Med. 2006 Oct 15;41(8):1338–50.

100. Matés JM. Effects of antioxidant enzymes in the molecular control of reactive oxygen species toxicology. Toxicology. 2000 Nov 16;153(1-3):83–104.

101. Drake J, Sultana R, Aksenova M, Calabrese V, Butterfield DA. Elevation of mitochondrial glutathione by gamma-glutamylcysteine ethyl ester protects mitochondria against peroxynitrite-induced oxidative stress. J. Neurosci. Res. 2003 Dec 15;74(6):917–27.

102. Masella R, Di Benedetto R, Varì R, Filesi C, Giovannini C. Novel mechanisms of natural antioxidant compounds in biological systems: involvement of glutathione and glutathione-related enzymes. J. Nutr. Biochem. 2005 Oct;16(10):577–86.

103. Lillig CH, Lönn ME, Enoksson M, Fernandes AP, Holmgren A. Short interfering RNA-mediated silencing of glutaredoxin 2 increases the sensitivity of HeLa cells toward doxorubicin and phenylarsine oxide. Proc. Natl. Acad. Sci. U.S.A. 2004 Sep 7;101(36):13227–32.

104. Baty JW, Hampton MB, Winterbourn CC. Proteomic detection of hydrogen peroxide-sensitive thiol proteins in Jurkat cells. Biochem. J. 2005 Aug 1;389(Pt 3):785–95.

105. Dobra K, Hjerpe A. Targeted therapy--possible new therapeutic option for malignant mesothelioma? Connect. Tissue Res. 2008;49(3):270–2.

106. Shapiro SS, Saliou C. Role of vitamins in skin care. Nutrition. 2001 Oct;17(10):839–44.

107. Barañano DE, Snyder SH. Neural roles for heme oxygenase: contrasts to nitric oxide synthase. Proc. Natl. Acad. Sci. U.S.A. 2001 Sep 25;98(20):10996–1002.

108. Vanasco V, Cimolai MC, Evelson P, Alvarez S. The oxidative stress and the mitochondrial dysfunction caused by endotoxemia are prevented by alpha-lipoic acid. Free Radic. Res. 2008 Sep;42(9):815–23.

109. Korkmaz A, Reiter RJ, Topal T, Manchester LC, Oter S, Tan D-X. Melatonin: an established antioxidant worthy of use in clinical trials. Mol. Med. 2009 Feb;15(1-2):43–50.

110. Cherubini A, Ruggiero C, Polidori MC, Mecocci P. Potential markers of oxidative stress in stroke. Free Radic. Biol. Med. 2005 Oct 1;39(7):841–52.

111. Niki E. Oxidative stress and aging. Intern. Med. 2000 Apr;39(4):324–6.

112. Paredi P, Leckie MJ, Horvath I, Allegra L, Kharitonov SA, Barnes PJ. Changes in exhaled carbon monoxide and nitric oxide levels following allergen challenge in patients with asthma. Eur. Respir. J. 1999 Jan;13(1):48–52.

113. Otterbein LE, Choi AM. Heme oxygenase: colors of defense against cellular stress. Am. J. Physiol. Lung Cell Mol. Physiol. 2000 Dec;279(6):L1029–1037.

114. Nath KA, Grande JP, Haggard JJ, Croatt AJ, Katusic ZS, Solovey A, et al. Oxidative stress and induction of heme oxygenase-1 in the kidney in sickle cell disease. Am. J. Pathol. 2001 Mar;158(3):893–903.

115. Sardana MK, Drummond GS, Sassa S, Kappas A. The potent heme oxygenase inducing action of arsenic and parasiticidal arsenicals. Pharmacology. 1981;23(5):247–53.

116. Arrigoni O, De Tullio MC. Ascorbic acid: much more than just an antioxidant. Biochim. Biophys. Acta. 2002 Jan 15;1569(1-3):1–9.

117. Carr A, Frei B. Does vitamin C act as a pro-oxidant under physiological conditions? FASEB J. 1999 Jun;13(9):1007–24.

118. Munteanu A, Zingg J-M, Ogru E, Libinaki R, Gianello R, West S, et al. Modulation of cell proliferation and gene expression by alpha-tocopheryl phosphates: relevance to atherosclerosis and inflammation. Biochem. Biophys. Res. Commun. 2004 May 21;318(1):311–6.

119. Robichová S, Slamenová D, Chalupa I, Sebová L. DNA lesions and cytogenetic changes induced by N-nitrosomorpholine in HepG2, V79 and VH10 cells: the protective effects of Vitamins A, C and E. Mutat. Res. 2004 Jun 13;560(2):91–9.

120. Romieu I. Nutrition and lung health. Int. J. Tuberc. Lung Dis. 2005 Apr;9(4):362–74.

121. Mehta R, Shangari N, O'Brien PJ. Preventing cell death induced by carbonyl stress, oxidative stress or mitochondrial toxins with vitamin B anti-AGE agents. Mol Nutr Food Res. 2008 Mar;52(3):379–85.

122. Depeint F, Bruce WR, Shangari N, Mehta R, O'Brien PJ. Mitochondrial function and toxicity: role of the B vitamin family on mitochondrial energy metabolism. Chem. Biol. Interact. 2006 Oct 27;163(1-2):94–112.

123. Cemeli E, Baumgartner A, Anderson D. Antioxidants and the Comet assay. Mutat. Res. 2009 Feb;681(1):51–67.

124. Tamimi RM, Hankinson SE, Campos H, Spiegelman D, Zhang S, Colditz GA, et al. Plasma carotenoids, retinol, and tocopherols and risk of breast cancer. Am. J. Epidemiol. 2005 Jan 15;161(2):153–60.

125. Santocono M, Zurria M, Berrettini M, Fedeli D, Falcioni G. Lutein, zeaxanthin and astaxanthin protect against DNA damage in SK-N-SH human neuroblastoma cells induced by reactive nitrogen species. J. Photochem. Photobiol. B, Biol. 2007 Jul 27;88(1):1–10.

126. Rao AV, Rao LG. Carotenoids and human health. Pharmacol. Res. 2007 Mar;55(3):207–16.

127. Ferguson LR. Role of plant polyphenols in genomic stability. Mutat. Res. 2001 Apr 18;475(1-2):89–111.

128. Manach C, Scalbert A, Morand C, Rémésy C, Jiménez L. Polyphenols: food sources and bioavailability. Am. J. Clin. Nutr. 2004 May;79(5):727–47.

129. Mozaffarieh M, Grieshaber MC, Orgül S, Flammer J. The potential value of natural antioxidative treatment in glaucoma. Surv Ophthalmol. 2008 Oct;53(5):479–505.

130. Ruiz PA, Haller D. Functional diversity of flavonoids in the inhibition of the proinflammatory NF-kappaB, IRF, and Akt signaling pathways in murine intestinal epithelial cells. J. Nutr. 2006 Mar;136(3):664–71.

131. Hendriks JJA, Alblas J, Van der Pol SMA, Van Tol EAF, Dijkstra CD, De Vries HE. Flavonoids influence monocytic GTPase activity and are protective in experimental allergic encephalitis. J. Exp. Med. 2004 Dec 20;200(12):1667–72.

132. Lima CF, Fernandes-Ferreira M, Pereira-Wilson C. Phenolic compounds protect HepG2 cells from oxidative damage: relevance of glutathione levels. Life Sci. 2006 Oct 19;79(21):2056–68.

133. Serafini, Laranjinha, Almeida, Maiani. Inhibition of human LDL lipid peroxidation by phenol-rich beverages and their impact on plasma total antioxidant capacity in humans. J. Nutr. Biochem. 2000 Nov;11(11-12):585–90.

134. Di Carlo G, Mascolo N, Izzo AA, Capasso F. Flavonoids: old and new aspects of a class of natural therapeutic drugs. Life Sci. 1999;65(4):337–53.

135. Sies, H. (1985). Oxidative stress:Introductory remarks, In: Oxidative stress, Helmut Sies, pp. 1-8. Academic Press, London.

136. Von Sonntag C, Schuchmann HP. Suppression of hydroxyl radical reactions in biological systems: considerations based on competition kinetics. Meth. Enzymol. 1994;233:47–56.

137. Croteau DL, Bohr VA. Repair of oxidative damage to nuclear and mitochondrial DNA in mammalian cells. J. Biol. Chem. 1997 Oct 10;272(41):25409–12.

138. Van Remmen H, Richardson A. Oxidative damage to mitochondria and aging. Exp. Gerontol. 2001 Jul;36(7):957–68.

139. Linnane AW, Marzuki S, Ozawa T, Tanaka M. Mitochondrial DNA mutations as an important contributor to ageing and degenerative diseases. Lancet. 1989 Mar 25;1(8639):642–5.

140. Keller JN, Mark RJ, Bruce AJ, Blanc E, Rothstein JD, Uchida K, et al. 4-Hydroxynonenal, an aldehydic product of membrane lipid peroxidation, impairs glutamate transport and mitochondrial function in synaptosomes. Neuroscience. 1997 Oct;80(3):685–96.

141. Esterbauer H, Schaur RJ, Zollner H. Chemistry and biochemistry of 4-hydroxynonenal, malonaldehyde and related aldehydes. Free Radic. Biol. Med. 1991;11(1):81–128.

142. Eaton P, Li JM, Hearse DJ, Shattock MJ. Formation of 4-hydroxy-2-nonenal-modified proteins in ischemic rat heart. Am. J. Physiol. 1999 Mar;276(3 Pt 2):H935–943.

143. Chen JJ, Bertrand H, Yu BP. Inhibition of adenine nucleotide translocator by lipid peroxidation products. Free Radic. Biol. Med. 1995 Nov;19(5):583–90.

144. Liu C-Y, Lee C-F, Wei Y-H. Role of reactive oxygen species-elicited apoptosis in the pathophysiology of mitochondrial and neurodegenerative diseases associated with mitochondrial DNA mutations. J. Formos. Med. Assoc. 2009 Aug;108(8):599–611.

145. Beal MF. Mitochondria take center stage in aging and neurodegeneration. Ann. Neurol. 2005 Oct;58(4):495–505.

146. Hengartner MO. The biochemistry of apoptosis. Nature. 2000 Oct 12;407(6805):770–6.

147. Agarwal S, Sohal RS. Relationship between susceptibility to protein oxidation, aging, and maximum life span potential of different species. Exp. Gerontol. 1996 Jun;31(3):365–72.

148. Cakatay U, Telci A, Kayalì R, Tekeli F, Akçay T, Sivas A. Relation of oxidative protein damage and nitrotyrosine levels in the aging rat brain. Exp. Gerontol. 2001 Feb;36(2):221–9.

149. Oxidative Changes and Possible Effects of Polymorphism of Antioxidant Enzymes in Neurodegenerative Disease.InTECH chap 18; pp421-447.

150. Miyata T, Takizawa S, Van Ypersele de Strihou C. Hypoxia. 1. Intracellular sensors for oxygen and oxidative stress: novel therapeutic targets. Am. J. Physiol., Cell Physiol. 2011 Feb;300(2):C226–231.

151. Beckman JS, Beckman TW, Chen J, Marshall PA, Freeman BA. Apparent hydroxyl radical production by peroxynitrite: implications for endothelial injury from nitric oxide and superoxide. Proc. Natl. Acad. Sci. U.S.A. 1990 Feb;87(4):1620–4.

152. Novo E, Parola M. Redox mechanisms in hepatic chronic wound healing and fibrogenesis. Fibrogenesis Tissue Repair. 2008;1(1):5.

153. Burney S, Caulfield JL, Niles JC, Wishnok JS, Tannenbaum SR. The chemistry of DNA damage from nitric oxide and peroxynitrite. Mutat. Res. 1999 Mar 8;424(1-2):37–49.

154. Calcerrada P, Peluffo G, Radi R. Nitric oxide-derived oxidants with a focus on peroxynitrite: molecular targets, cellular responses and therapeutic implications. Curr. Pharm. Des. 2011 Dec;17(35):3905–32.

155. Beckman JS. Oxidative damage and tyrosine nitration from peroxynitrite. Chem. Res. Toxicol. 1996 Aug;9(5):836–44.

156. Liaudet L, Vassalli G, Pacher P. Role of peroxynitrite in the redox regulation of cell signal transduction pathways. Front Biosci (Landmark Ed). 2009;14:4809–14.

157. Cassina AM, Hodara R, Souza JM, Thomson L, Castro L, Ischiropoulos H, et al. Cytochrome c nitration by peroxynitrite. J. Biol. Chem. 2000 Jul 14;275(28):21409–15.

158. Balafanova Z, Bolli R, Zhang J, Zheng Y, Pass JM, Bhatnagar A, et al. Nitric oxide (NO) induces nitration of protein kinase Cepsilon (PKCepsilon), facilitating PKCepsilon translocation via enhanced PKCepsilon -RACK2 interactions: a novel mechanism of no-triggered activation of PKCepsilon. J. Biol. Chem. 2002 Apr 26;277(17):15021–7.

159. Trostchansky A, Bonilla L, González-Perilli L, Rubbo H. Nitro-Fatty acids: formation, redox signaling, and therapeutic potential. Antioxid. Redox Signal. 2013 Oct 10;19(11):1257–65.

160. Schopfer FJ, Cipollina C, Freeman BA. Formation and signaling actions of electrophilic lipids. Chem. Rev. 2011 Oct 12;111(10):5997–6021.

161. Ohshima H, Sawa T, Akaike T. 8-nitroguanine, a product of nitrative DNA damage caused by reactive nitrogen species: formation, occurrence, and implications in inflammation and carcinogenesis. Antioxid. Redox Signal. 2006 Jun;8(5-6):1033–45.

162. Rubbo H, Radi R. Protein and lipid nitration: role in redox signaling and injury. Biochim. Biophys. Acta. 2008 Nov;1780(11):1318–24.

163. Vandelle E, Delledonne M. Peroxynitrite formation and function in plants. Plant Sci. 2011 Nov;181(5):534–9.

164. Sun J, Steenbergen C, Murphy E. S-nitrosylation: NO-related redox signaling to protect against oxidative stress. Antioxid. Redox Signal. 2006 Oct;8(9-10):1693–705.

165. Martínez-Ruiz A, Lamas S. Signalling by NO-induced protein S-nitrosylation and S-glutathionylation: convergences and divergences. Cardiovasc. Res. 2007 Jul 15;75(2):220–8.

166. Whiteman M, Chua YL, Zhang D, Duan W, Liou Y-C, Armstrong JS. Nitric oxide protects against mitochondrial permeabilization induced by glutathione depletion: role of S-nitrosylation? Biochem. Biophys. Res. Commun. 2006 Jan 6;339(1):255–62.

167. Adachi T, Weisbrod RM, Pimentel DR, Ying J, Sharov VS, Schöneich C, et al. S-Glutathiolation by peroxynitrite activates SERCA during arterial relaxation by nitric oxide. Nat. Med. 2004 Nov;10(11):1200–7.

168. Pias EK, Aw TY. Early redox imbalance mediates hydroperoxide-induced apoptosis in mitotic competent undifferentiated PC-12 cells. Cell Death Differ. 2002 Sep;9(9):1007–16.

169. Nelson DL, Cox MM. Oxidative Phosphorylation and Photophosphorylation. Lehninger Principles of Biochemistry. Fourth edition ed. New York: W.H. Freeman and company 2005:690-721.

170. Vo TD, Greenberg HJ, Palsson BO. Reconstruction and functional characterization of the human mitochondrial metabolic network based on proteomic and biochemical data. J. Biol. Chem. 2004 Sep 17;279(38):39532–40.

171. Neuromuscular Disease Center Washington University, St. Louis, Mo Usa.

172. Wiswedel I, Gardemann A, Storch A, Peter D, Schild L. Degradation of phospholipids by oxidative stress--exceptional significance of cardiolipin. Free Radic. Res. 2010 Feb;44(2):135–45.

173. Marí M, Morales A, Colell A, García-Ruiz C, Fernández-Checa JC. Mitochondrial glutathione, a key survival antioxidant. Antioxid. Redox Signal. 2009 Nov;11(11):2685–700.

174. Dalle-Donne I, Aldini G, Carini M, Colombo R, Rossi R, Milzani A. Protein carbonylation, cellular dysfunction, and disease progression. J. Cell. Mol. Med. 2006 Jun;10(2):389–406.

175. Levine RL, Garland D, Oliver CN, Amici A, Climent I, Lenz AG, et al. Determination of carbonyl content in oxidatively modified proteins. Meth. Enzymol. 1990;186:464–78.

176. Marchi S, Giorgi C, Suski JM, Agnoletto C, Bononi A, Bonora M, et al. Mitochondria-ros crosstalk in the control of cell death and aging. J Signal Transduct. 2012;2012:329635.

177. MacMillan-Crow LA, Crow JP, Kerby JD, Beckman JS, Thompson JA. Nitration and inactivation of manganese superoxide dismutase in chronic rejection of human renal allografts. Proc. Natl. Acad. Sci. U.S.A. 1996 Oct 15;93(21):11853–8.

178. Radi R, Cassina A, Hodara R, Quijano C, Castro L. Peroxynitrite reactions and formation in mitochondria. Free Radic. Biol. Med. 2002 Dec 1;33(11):1451–64.

179. Turko IV, Li L, Aulak KS, Stuehr DJ, Chang J-Y, Murad F. Protein tyrosine nitration in the mitochondria from diabetic mouse heart. Implications to dysfunctional mitochondria in diabetes. J. Biol. Chem. 2003 Sep 5;278(36):33972–7.

180. Galley HF. Bench-to-bedside review: Targeting antioxidants to mitochondria in sepsis. Critical Care. 2010 Aug 20;14(4):230.

181. Elmore S. Apoptosis: A Review of Programmed Cell Death. Toxicol Pathol. 2007;35(4):495–516.

182. Lorenzo HK, Susin SA. Therapeutic potential of AIF-mediated caspase-independent programmed cell death. Drug Resist. Updat. 2007 Dec;10(6):235–55.

183. Kroemer G, Galluzzi L, Vandenabeele P, Abrams J, Alnemri ES, Baehrecke EH, et al. Classification of cell death: recommendations of the Nomenclature Committee on Cell Death 2009. Cell Death Differ. 2009 Jan;16(1):3–11.

184. Leist M, Jäättelä M. Four deaths and a funeral: from caspases to alternative mechanisms. Nat. Rev. Mol. Cell Biol. 2001 Aug;2(8):589–98.

185. Gil J, Almeida S, Oliveira CR, Rego AC. Cytosolic and mitochondrial ROS in staurosporine-induced retinal cell apoptosis. Free Radic. Biol. Med. 2003 Dec 1;35(11):1500–14.

186. Matés JM, Pérez-Gómez C, Núñez de Castro I. Antioxidant enzymes and human diseases. Clin. Biochem. 1999 Nov;32(8):595–603.

187. Cui H, Schroering A, Ding H-F. p53 mediates DNA damaging drug-induced apoptosis through a caspase-9-dependent pathway in SH-SY5Y neuroblastoma cells. Mol. Cancer Ther. 2002 Jul;1(9):679–86.

188. Lamkanfi M, Dixit VM. Manipulation of host cell death pathways during microbial infections. Cell Host Microbe. 2010 Jul 22;8(1):44–54.

189. Leon LJ, Pasupuleti N, Gorin F, Carraway KL. A Cell-Permeant Amiloride Derivative Induces Caspase-Independent, AIF-Mediated Programmed Necrotic Death of Breast Cancer Cells. PLoS ONE. 2013 Apr 30;8(4):e63038.

190. Ugolini G, Raoul C, Ferri A, Haenggeli C, Yamamoto Y, Salaün D, et al. Fas/tumor necrosis factor receptor death signaling is required for axotomy-induced death of motoneurons in vivo. J. Neurosci. 2003 Sep 17;23(24):8526–31.

191. Houwerzijl EJ, Blom NR, Van der Want JJL, Vellenga E, De Wolf JTM. Megakaryocytic dysfunction in myelodysplastic syndromes and idiopathic thrombocytopenic purpura is in part due to different forms of cell death. Leukemia. 2006 Nov;20(11):1937–42.

192. Ashida H, Mimuro H, Ogawa M, Kobayashi T, Sanada T, Kim M, et al. Cell death and infection: a double-edged sword for host and pathogen survival. J. Cell Biol. 2011 Dec 12;195(6):931–42.

193. López-Sánchez N, Rodríguez J-R, Frade JM. Mitochondrial c-Jun NH2-terminal kinase prevents the accumulation of reactive oxygen species and reduces necrotic damage in neural tumor cells that lack trophic support. Mol. Cancer Res. 2007 Jan;5(1):47–60.

194. Lin Y, Choksi S, Shen H-M, Yang Q-F, Hur GM, Kim YS, et al. Tumor necrosis factor-induced nonapoptotic cell death requires receptor-interacting protein-mediated cellular reactive oxygen species accumulation. J. Biol. Chem. 2004 Mar 12;279(11):10822–8.

195. Aquilano K, Filomeni G, Di Renzo L, Vito M di, Stefano C di, Salimei PS, et al. Reactive oxygen and nitrogen species are involved in sorbitol-induced apoptosis of human erithroleukaemia cells K562. Free Radic. Res. 2007 Apr;41(4):452–60.

196. Petrosillo G, Ruggiero FM, Paradies G. Role of reactive oxygen species and cardiolipin in the release of cytochrome c from mitochondria. FASEB J. 2003 Dec;17(15):2202–8.

197. Kim D-S, Kim H-R, Woo E-R, Hong S-T, Chae H-J, Chae S-W. Inhibitory effects of rosmarinic acid on adriamycin-induced apoptosis in H9c2 cardiac muscle cells by inhibiting reactive oxygen species and the activations of c-Jun N-terminal kinase and extracellular signal-regulated kinase. Biochem. Pharmacol. 2005 Oct 1;70(7):1066–78.

198. Zhu Y, Hoell P, Ahlemeyer B, Krieglstein J. PTEN: a crucial mediator of mitochondria-dependent apoptosis. Apoptosis. 2006 Feb;11(2):197–207.

199. Deshpande SS, Angkeow P, Huang J, Ozaki M, Irani K. Rac1 inhibits TNF-alpha-induced endothelial cell apoptosis: dual regulation by reactive oxygen species. FASEB J. 2000 Sep;14(12):1705–14.

200. Hiona A, Leeuwenburgh C. The role of mitochondrial DNA mutations in aging and sarcopenia: implications for the mitochondrial vicious cycle theory of aging. Exp. Gerontol. 2008 Jan;43(1):24–33.

201. Hiroi M, Ogihara T, Hirano K, Hasegawa M, Morinobu T, Tamai H, et al. Regulation of apoptosis by glutathione redox state in PC12 cells exposed simultaneously to iron and ascorbic acid. Free Radic. Biol. Med. 2005 Apr 15;38(8):1057–72.

202. Matés JM, Sánchez-Jiménez FM. Role of reactive oxygen species in apoptosis: implications for cancer therapy. Int. J. Biochem. Cell Biol. 2000 Feb;32(2):157–70.

203. Jung JY, Han CR, Jeong YJ, Kim HJ, Lim HS, Lee KH, et al. Epigallocatechin gallate inhibits nitric oxide-induced apoptosis in rat PC12 cells. Neurosci. Lett. 2007 Jan 16;411(3):222–7.

204. Choi M-M, Kim E-A, Hahn H-G, Nam KD, Yang S-J, Choi SY, et al. Protective effect of benzothiazole derivative KHG21834 on amyloid beta-induced neurotoxicity in PC12 cells and cortical and mesencephalic neurons. Toxicology. 2007 Oct 8;239(3):156–66.

205. Marczin N, El-Habashi N, Hoare GS, Bundy RE, Yacoub M. Antioxidants in myocardial ischemia-reperfusion injury: therapeutic potential and basic mechanisms. Arch. Biochem. Biophys. 2003 Dec 15;420(2):222–36.

206. Avery SV. Molecular targets of oxidative stress. Biochem. J. 2011 Mar 1;434(2):201–10.

207. Okezie I. Aruoma1, L. Stephen Coles2, Bernie Landes3, and John E. Repine4. Characteristics and Bioefficacy of Ergothioneine—A Unique Natural Dietary Antioxidant. e-Journal of Age Management Medicine | May 2011.

208. Sen R, Baltimore D. Inducibility of kappa immunoglobulin enhancer-binding protein Nf-kappa B by a posttranslational mechanism. Cell. 1986 Dec 26;47(6):921–8.

209. Sethi G, Sung B, Aggarwal BB. Nuclear factor-kappaB activation: from bench to bedside. Exp. Biol. Med. (Maywood). 2008 Jan;233(1):21–31.

210. Barnes PJ, Karin M. Nuclear factor-kappaB: a pivotal transcription factor in chronic inflammatory diseases. N. Engl. J. Med. 1997 Apr 10;336(15):1066–71.

211. Bortezomib, a proteasome inhibitor, in cancer therapy: From concept to clinic Albanell, J., Adams, J. (Drugs Fut 2002, 27(11): 1079).

212. Understanding the immune response mechanism with protein crystallography [Ubiquitin, NEMO, Ectodermal Dysplasia, Drug Design] Scientists at KEK Photon Factory are exploring pr. 2010 Jun 30;

213. Viennois E, Chen F, Merlin D. NF-κB pathway in colitis-associated cancers. Transl Gastrointest Cancer. 2013 Jan 1;2(1):21–9.

214. Shishodia S, Amin HM, Lai R, Aggarwal BB. Curcumin (diferuloylmethane) inhibits constitutive NF-kappaB activation, induces G1/S arrest, suppresses proliferation, and induces apoptosis in mantle cell lymphoma. Biochem. Pharmacol. 2005 Sep 1;70(5):700–13.

215. Ozbek E, Ilbey YO, Ozbek M, Simsek A, Cekmen M, Somay A. Melatonin attenuates unilateral ureteral obstruction-induced renal injury by reducing oxidative stress, iNOS, MAPK, and NF-κB expression. J. Endourol. 2009 Jul;23(7):1165–73.

216. Van den Berg R, Haenen GR, Van den Berg H, Bast A. Transcription factor NF-kappaB as a potential biomarker for oxidative stress. Br. J. Nutr. 2001 Aug;86 Suppl 1:S121–127.

217. De Plaen IG, Qu X-W, Wang H, Tan X-D, Wang L, Han X-B, et al. Endotoxin, but not platelet-activating factor, activates nuclear factor-kappaB and increases IkappaBalpha and IkappaBbeta turnover in enterocytes. Immunology. 2002 Aug;106(4):577–83.

218. Chung HY, Cesari M, Anton S, Marzetti E, Giovannini S, Seo AY, et al. Molecular inflammation: underpinnings of aging and age-related diseases. Ageing Res. Rev. 2009 Jan;8(1):18–30.

219. The Curcumin Story [Internet]. Available from: http://www.curcumin.co.nz/curcumin-story.htm

220. Hassa PO, Haenni SS, Elser M, Hottiger MO. Nuclear ADP-ribosylation reactions in mammalian cells: where are we today and where are we going? Microbiol. Mol. Biol. Rev. 2006 Sep;70(3):789–829.

221. Kim MY, Zhang T, Kraus WL. Poly(ADP-ribosyl)ation by PARP-1: 'PAR-laying' NAD+ into a nuclear signal. Genes Dev. 2005 Sep 1;19(17):1951–67.

222. Hassa PO, Hottiger MO. The diverse biological roles of mammalian PARPS, a small but powerful family of poly-ADP-ribose polymerases. Front. Biosci. 2008;13:3046–82.

223. Hassa PO, Hottiger MO. The functional role of poly(ADP-ribose)polymerase 1 as novel coactivator of NF-kappaB in inflammatory disorders. Cell. Mol. Life Sci. 2002 Sep;59(9):1534–53.

224. Shall S, De Murcia G. Poly(ADP-ribose) polymerase-1: what have we learned from the deficient mouse model? Mutat. Res. 2000 Jun 30;460(1):1–15.

225. Wang ZQ, Auer B, Stingl L, Berghammer H, Haidacher D, Schweiger M, et al. Mice lacking ADPRT and poly(ADP-ribosyl)ation develop normally but are susceptible to skin disease. Genes Dev. 1995 Mar 1;9(5):509–20.

226. Burkart V, Wang ZQ, Radons J, Heller B, Herceg Z, Stingl L, et al. Mice lacking the poly(ADP-ribose) polymerase gene are resistant to pancreatic beta-cell destruction and diabetes development induced by streptozocin. Nat. Med. 1999 Mar;5(3):314–9.

227. Oliver FJ, Ménissier-de Murcia J, Nacci C, Decker P, Andriantsitohaina R, Muller S, et al. Resistance to endotoxic shock as a consequence of defective NF-kappaB activation in poly (ADP-ribose) polymerase-1 deficient mice. EMBO J. 1999 Aug 16;18(16):4446–54.

228. Schreiber V, Dantzer F, Ame J-C, De Murcia G. Poly(ADP-ribose): novel functions for an old molecule. Nat. Rev. Mol. Cell Biol. 2006 Jul;7(7):517–28.

229. Altmeyer M, Messner S, Hassa PO, Fey M, Hottiger MO. Molecular mechanism of poly(ADP-ribosyl)ation by PARP1 and identification of lysine residues as ADP-ribose acceptor sites. Nucleic Acids Research. 2009 Apr 16;37(11):3723–38.

230. Alsayed Ali Mahran1, Husam Eldien H. Osman1, Ahmed M. A. Abd El-Mawla2,3* and Adel M. Attia4. Mahran AA, Husam Eldien HO, Abd El-Mawla AMA, Attia AM (2011) Protective Effect of Zinc (Zn) on the Histology and Histochemistry of Liver and Kidney of Albino Rat Treated with Cadmium. J Cytol Histol.

231. Bailey MA, Imbert-Teboul M, Turner C, Srai SK, Burnstock G, Unwin RJ. Evidence for basolateral P2Y(6) receptors along the rat proximal tubule: functional and molecular characterization. J. Am. Soc. Nephrol. 2001 Aug;12(8):1640–7.

232. Zhai XY, Birn H, Jensen KB, Thomsen JS, Andreasen A, Christensen EI. Digital Three-Dimensional Reconstruction and Ultrastructure of the Mouse Proximal Tubule. JASN. 2003 Jan 3;14(3):611–9.

233. Dees JH, Heatfield BM, Reuber MD, Trump BF. Adenocarcinoma of the kidney. III. Histogenesis of renal adenocarcinomas induced in rats by N-(4'-fluoro-4-biphenylyl)acetamide. J. Natl. Cancer Inst. 1980 Jun;64(6):1537–45.

234. Christensen EI, Willnow TE. Essential role of megalin in renal proximal tubule for vitamin homeostasis. J. Am. Soc. Nephrol. 1999 Oct;10(10):2224–36.

235. Dautzenberg M, Keilhoff G, Just A. Modulation of the myogenic response in renal blood flow autoregulation by NO depends on endothelial nitric oxide synthase (eNOS), but not neuronal or inducible NOS. J. Physiol. (Lond.). 2011 Oct 1;589(Pt 19):4731–44.

236. Basivireddy J, Jacob M, Pulimood AB, Balasubramanian KA. Indomethacin-induced renal damage: role of oxygen free radicals. Biochem. Pharmacol. 2004 Feb 1;67(3):587–99.

237. Gossmann J, Radounikli A, Bernemann A, Schellinski O, Raab HP, Bickeböller R, et al. Pathophysiology of cyclosporine-induced nephrotoxicity in humans: a role for nitric oxide? Kidney Blood Press. Res. 2001;24(2):111–5.

238. Townsend DM, Deng M, Zhang L, Lapus MG, Hanigan MH. Metabolism of Cisplatin to a Nephrotoxin in Proximal Tubule Cells. JASN. 2003 Jan 1;14(1):1–10.

239. Matsushima H, Yonemura K, Ohishi K, Hishida A. The role of oxygen free radicals in cisplatin-induced acute renal failure in rats. J. Lab. Clin. Med. 1998 Jun;131(6):518–26.

240. Basnakian AG, Kaushal GP, Shah SV. Apoptotic pathways of oxidative damage to renal tubular epithelial cells. Antioxid. Redox Signal. 2002 Dec;4(6):915–24.

241. Hanigan MH, Devarajan P. Cisplatin nephrotoxicity: molecular mechanisms. Cancer Ther. 2003;1:47–61.

242. Böhrer H, Qiu F, Zimmermann T, Zhang Y, Jllmer T, Männel D, et al. Role of NFkappaB in the mortality of sepsis. J. Clin. Invest. 1997 Sep 1;100(5):972–85.

243. Khachigian LM, Collins T, Fries JW. N-acetyl cysteine blocks mesangial VCAM-1 and NF-kappa B expression in vivo. Am. J. Pathol. 1997 Nov;151(5):1225–9.

244. Sakurai H, Shigemori N, Hisada Y, Ishizuka T, Kawashima K, Sugita T. Suppression of NF-kappa B and AP-1 activation by glucocorticoids in experimental glomerulonephritis in rats: molecular mechanisms of anti-nephritic action. Biochim. Biophys. Acta. 1997 Dec 31;1362(2-3):252–62.

245. Seto M, Kim S, Yoshifusa H, Nakamura Y, Masuda T, Hamaguchi A, et al. Effects of prednisolone on glomerular signal transduction cascades in experimental glomerulonephritis. J. Am. Soc. Nephrol. 1998 Aug;9(8):1367–76.

246. Guo G, Morrissey J, McCracken R, Tolley T, Klahr S. Role of TNFR1 and TNFR2 receptors in tubulointerstitial fibrosis of obstructive nephropathy. Am. J. Physiol. 1999 Nov;277(5 Pt 2):F766–772.

247. Morrissey JJ, Klahr S. Differential effects of ACE and AT1 receptor inhibition on chemoattractant and adhesion molecule synthesis. Am. J. Physiol. 1998 Mar;274(3 Pt 2):F580–586.

248. Soetikno V, nabe KW. Role of Protein Kinase C-MAPK, Oxidative Stress and Inflammation Pathways in Diabetic Nephropathy. Journal of Nephrology & Therapeutics [Internet]. 2012 [cited 2013 Oct 6];02(S1). Available from: http://www.omicsgroup.org/citations/export-citations.php?doi=10.4172/2161-0959.S2-001&pdate=2012-01-14

249. Tak PP, Firestein GS. NF-kappaB: a key role in inflammatory diseases. J. Clin. Invest. 2001 Jan;107(1):7–11.

250. Distribution of NOS in the kidney. In: Goligorsky, MS.; Gross, SS., editors. Nitric Oxide and the Kidney: Physiology and Pathophysiology. Chapman and Hall; New York: 1997. p. 133-57.

251. Chen M, Bao W, Aizman R, Huang P, Aspevall O, Gustafsson LE, et al. Activation of Extracellular Signal-Regulated Kinase Mediates Apoptosis Induced by Uropathogenic

Escherichia coli Toxins via Nitric Oxide Synthase: Protective Role of Heme Oxygenase-1. J Infect Dis. 2004 Jan 7;190(1):127–35.

252. Smith WL, Bell TG. Immunohistochemical localization of the prostaglandin-forming cyclooxygenase in renal cortex. Am. J. Physiol. 1978 Nov;235(5):F451–457.

253. Vio CP, Cespedes C, Gallardo P, Masferrer JL. Renal identification of cyclooxygenase-2 in a subset of thick ascending limb cells. Hypertension. 1997 Sep;30(3 Pt 2):687–92.

254. Harris RC, McKanna JA, Akai Y, Jacobson HR, Dubois RN, Breyer MD. Cyclooxygenase-2 is associated with the macula densa of rat kidney and increases with salt restriction. J. Clin. Invest. 1994 Dec;94(6):2504–10.

255. Traynor TR, Smart A, Briggs JP, Schnermann J. Inhibition of macula densa-stimulated renin secretion by pharmacological blockade of cyclooxygenase-2. Am. J. Physiol. 1999 Nov;277(5 Pt 2):F706–710.

256. Surh YJ, Chun KS, Cha HH, Han SS, Keum YS, Park KK, et al. Molecular mechanisms underlying chemopreventive activities of anti-inflammatory phytochemicals: down-regulation of COX-2 and iNOS through suppression of NF-kappa B activation. Mutat. Res. 2001 Sep 1;480-481:243–68.

257. Giroir BP, Johnson JH, Brown T, Allen GL, Beutler B. The tissue distribution of tumor necrosis factor biosynthesis during endotoxemia. J. Clin. Invest. 1992 Sep;90(3):693–8.

258. Lieberthal W, Koh JS, Levine JS. Necrosis and apoptosis in acute renal failure. Semin. Nephrol. 1998 Sep;18(5):505–18.

259. Sheridan AM, Bonventre JV. Cell biology and molecular mechanisms of injury in ischemic acute renal failure. Curr. Opin. Nephrol. Hypertens. 2000 Jul;9(4):427–34.

260. Zager RA. 'Subclinical' gentamicin nephrotoxicity: a potential risk factor for exaggerated endotoxin-driven TNF-alpha production. Am. J. Physiol. Renal Physiol. 2007 Jul;293(1):F43–49.

261. Ramesh G, Reeves WB. Salicylate reduces cisplatin nephrotoxicity by inhibition of tumor necrosis factor-alpha. Kidney Int. 2004 Feb;65(2):490–9.

262. Nakao S, Ogtata Y, Shimizu E, Yamazaki M, Furuyama S, Sugiya H. Tumor necrosis factor alpha (TNF-alpha)-induced prostaglandin E2 release is mediated by the activation of cyclooxygenase-2 (COX-2) transcription via NFkappaB in human gingival fibroblasts. Mol. Cell. Biochem. 2002 Sep;238(1-2):11–8.

263. Di Paola R, Genovese T, Impellizzeri D, Ahmad A, Cuzzocrea S, Esposito E. The renal injury and inflammation caused by ischemia-reperfusion are reduced by genetic inhibition of TNF-αR1: a comparison with infliximab treatment. Eur. J. Pharmacol. 2013 Jan 30;700(1-3):134–46.

264. Catania JM, Chen G, Parrish AR. Role of matrix metalloproteinases in renal pathophysiologies. Am. J. Physiol. Renal Physiol. 2007 Mar;292(3):F905–911.

265. Tomita M, Koike H, Han GD, Shimizu F, Kawachi H. Decreased collagen-degrading activity could be a marker of prolonged mesangial matrix expansion. Clin. Exp. Nephrol. 2004 Mar;8(1):17–26.

266. Inkinen KA, Soots AP, Krogerus LA, Lautenschlager IT, Ahonen JP. Fibrosis and matrix metalloproteinases in rat renal allografts. Transpl. Int. 2005 May;18(5):506–12.

267. McMillan JI, Riordan JW, Couser WG, Pollock AS, Lovett DH. Characterization of a glomerular epithelial cell metalloproteinase as matrix metalloproteinase-9 with enhanced expression in a model of membranous nephropathy. J. Clin. Invest. 1996 Feb 15;97(4):1094–101.

268. Ziswiler R, Daniel C, Franz E, Marti HP. Renal matrix metalloproteinase activity is unaffected by experimental ischemia-reperfusion injury and matrix metalloproteinase inhibition does not alter outcome of renal function. Exp. Nephrol. 2001 Apr;9(2):118–24.

269. Ermolli M, Schumacher M, Lods N, Hammoud M, Marti HP. Differential expression of MMP-2/MMP-9 and potential benefit of an MMP inhibitor in experimental acute kidney allograft rejection. Transpl. Immunol. 2003 Jun;11(2):137–45.

270. Basile DP, Fredrich K, Weihrauch D, Hattan N, Chilian WM. Angiostatin and matrix metalloprotease expression following ischemic acute renal failure. Am. J. Physiol. Renal Physiol. 2004 May;286(5):F893–902.

271. Caron A, Desrosiers RR, Langlois S, Béliveau R. Ischemia-reperfusion injury stimulates gelatinase expression and activity in kidney glomeruli. Can. J. Physiol. Pharmacol. 2005 Mar;83(3):287–300.

272. Rajagopalan S, Meng XP, Ramasamy S, Harrison DG, Galis ZS. Reactive oxygen species produced by macrophage-derived foam cells regulate the activity of vascular matrix metalloproteinases in vitro. Implications for atherosclerotic plaque stability. J. Clin. Invest. 1996 Dec 1;98(11):2572–9.

273. Owens MW, Milligan SA, Jourd'heuil D, Grisham MB. Effects of reactive metabolites of oxygen and nitrogen on gelatinase A activity. Am. J. Physiol. 1997 Aug;273(2 Pt 1):L445–450.

274. Lerner, A. B., Case, J. D., Takahashi, Y., Lee, T. H. & Mori, W. (1958). Isolation Of Melatonin, The Pineal Gland Factor That Lightens Melanocytes. J. Amer. Chem. Soc., 80, 25.

275. Song Y, Chan CW, Brown GM, Pang SF, Silverman M. Studies of the renal action of melatonin: evidence that the effects are mediated by 37 kDa receptors of the Mel1a subtype localized primarily to the basolateral membrane of the proximal tubule. FASEB J. 1997 Jan;11(1):93–100.

276. JetKonnect™ Official Site. Melatonin: Hormone That Tells You When to Sleep. 2010 Jul 9;

277. Kostoglou-Athanassiou I. Therapeutic applications of melatonin. Ther Adv Endocrinol Metab. 2013 Feb;4(1):13–24.

278. Ekmekcioglu C. Melatonin receptors in humans: biological role and clinical relevance. Biomed. Pharmacother. 2006 Apr;60(3):97–108.

279. V Saxena. Melatonin HQ [Internet]. Available from: http://melatoninhq.com/

280. Kilic U, Yilmaz B, Ugur M, Yüksel A, Reiter RJ, Hermann DM, et al. Evidence that membrane-bound G protein-coupled melatonin receptors MT1 and MT2 are not involved in the neuroprotective effects of melatonin in focal cerebral ischemia. J. Pineal Res. 2012 Mar;52(2):228–35.

281. Dubocovich ML, Delagrange P, Krause DN, Sugden D, Cardinali DP, Olcese J. International Union of Basic and Clinical Pharmacology. LXXV. Nomenclature, classification, and

pharmacology of G protein-coupled melatonin receptors. Pharmacol. Rev. 2010 Sep;62(3):343–80.

282. Gultekin F, Hicyilmaz H. Renal deterioration caused by carcinogens as a consequence of free radical mediated tissue damage: a review of the protective action of melatonin. Arch. Toxicol. 2007 Oct;81(10):675–81.

283. Aktoz T, Aydogdu N, Alagol B, Yalcin O, Huseyinova G, Atakan IH. The protective effects of melatonin and vitamin E against renal ischemia-reperfusion injury in rats. Ren Fail. 2007;29(5):535–42.

284. Nava M, Romero F, Quiroz Y, Parra G, Bonet L, Rodríguez-Iturbe B. Melatonin attenuates acute renal failure and oxidative stress induced by mercuric chloride in rats. Am. J. Physiol. Renal Physiol. 2000 Nov;279(5):F910–918.

285. Sener G, Sehirli AO, Altunbas HZ, Ersoy Y, Paskaloglu K, Arbak S, et al. Melatonin protects against gentamicin-induced nephrotoxicity in rats. J. Pineal Res. 2002 May;32(4):231–6.

286. Hara M, Yoshida M, Nishijima H, Yokosuka M, Iigo M, Ohtani-Kaneko R, et al. Melatonin, a pineal secretory product with antioxidant properties, protects against cisplatin-induced nephrotoxicity in rats. J. Pineal Res. 2001 Apr;30(3):129–38.

287. Reiter RJ, Carneiro RC, Oh CS. Melatonin in relation to cellular antioxidative defense mechanisms. Horm. Metab. Res. 1997 Aug;29(8):363–72.

288. Winiarska K, Fraczyk T, Malinska D, Drozak J, Bryla J. Melatonin attenuates diabetes-induced oxidative stress in rabbits. J. Pineal Res. 2006 Mar;40(2):168–76.

289. Chen Z, Chua CC, Gao J, Chua K-W, Ho Y-S, Hamdy RC, et al. Prevention of ischemia/reperfusion-induced cardiac apoptosis and injury by melatonin is independent of glutathione peroxdiase 1. J. Pineal Res. 2009 Mar;46(2):235–41.

290. Galijasevic S, Abdulhamid I, Abu-Soud HM. Melatonin is a potent inhibitor for myeloperoxidase. Biochemistry. 2008 Feb 26;47(8):2668–77.

291. Brzezinski A. Melatonin in humans. N. Engl. J. Med. 1997 Jan 16;336(3):186–95.

292. Radogna F, Diederich M, Ghibelli L. Melatonin: a pleiotropic molecule regulating inflammation. Biochem. Pharmacol. 2010 Dec 15;80(12):1844–52.

293. Srinivasan V, Spence DW, Pandi-Perumal SR, Brown GM, Cardinali DP. Melatonin in mitochondrial dysfunction and related disorders. Int J Alzheimers Dis. 2011;2011:326320.

294. Kristián T. Metabolic stages, mitochondria and calcium in hypoxic/ischemic brain damage. Cell Calcium. 2004 Oct;36(3-4):221–33.

295. Yuji Okatani, Akihiko Wakatsuki and Russel J. Reiter. Melatonin and Mitochondrial Respiration. Melatonin: Biological Basis of its Function in Health and Disease. 2005.

296. Lin G-J, Huang S-H, Chen S-J, Wang C-H, Chang D-M, Sytwu H-K. Modulation by Melatonin of the Pathogenesis of Inflammatory Autoimmune Diseases. Int J Mol Sci. 2013 May 31;14(6):11742–66.

297. Hsu C, Han B, Liu M, Yeh C, Casida JE. Phosphine-induced oxidative damage in rats: attenuation by melatonin. Free Radic. Biol. Med. 2000 Feb 15;28(4):636–42.

298. Gultekin F, Delibas N, Yasar S, Kilinc I. In vivo changes in antioxidant systems and protective role of melatonin and a combination of vitamin C and vitamin E on oxidative damage in erythrocytes induced by chlorpyrifos-ethyl in rats. Arch. Toxicol. 2001 Apr;75(2):88–96.

299. Rosales-Corral S, Tan D-X, Reiter RJ, Valdivia-Velázquez M, Martínez-Barboza G, Acosta-Martínez JP, et al. Orally administered melatonin reduces oxidative stress and proinflammatory cytokines induced by amyloid-beta peptide in rat brain: a comparative, in vivo study versus vitamin C and E. J. Pineal Res. 2003 Sep;35(2):80–4.

300. Anwar MM, Meki A-RMA. Oxidative stress in streptozotocin-induced diabetic rats: effects of garlic oil and melatonin. Comp. Biochem. Physiol., Part A Mol. Integr. Physiol. 2003 Aug;135(4):539–47.

301. Forrest CM, Mackay GM, Stoy N, Stone TW, Darlington LG. Inflammatory status and kynurenine metabolism in rheumatoid arthritis treated with melatonin. Br J Clin Pharmacol. 2007 Oct;64(4):517–26.

302. Kedziora-Kornatowska K, Szewczyk-Golec K, Czuczejko J, Pawluk H, Van Marke de Lumen K, Kozakiewicz M, et al. Antioxidative effects of melatonin administration in elderly primary essential hypertension patients. J. Pineal Res. 2008 Oct;45(3):312–7.

303. Hardeland R, Pandi-Perumal SR, Cardinali DP. Melatonin. Int. J. Biochem. Cell Biol. 2006 Mar;38(3):313–6.

304. Lebrecht D, Venhoff AC, Kirschner J, Wiech T, Venhoff N, Walker UA. Mitochondrial tubulopathy in tenofovir disoproxil fumarate-treated rats. J. Acquir. Immune Defic. Syndr. 2009 Jul 1;51(3):258–63.

305. Libório AB, Andrade L, Pereira LVB, Sanches TRC, Shimizu MH, Seguro AC. Rosiglitazone reverses tenofovir-induced nephrotoxicity. Kidney Int. 2008 Oct;74(7):910–8.

306. Lewis W, Day BJ, Copeland WC. Mitochondrial toxicity of NRTI antiviral drugs: an integrated cellular perspective. Nat Rev Drug Discov. 2003 Oct;2(10):812–22.

307. Biesecker G, Karimi S, Desjardins J, Meyer D, Abbott B, Bendele R, et al. Evaluation of mitochondrial DNA content and enzyme levels in tenofovir DF-treated rats, rhesus monkeys and woodchucks. Antiviral Res. 2003 May;58(3):217–25.

308. Kolli VK, Kanakasabapathy I, Faith M, Ramamoorthy H, Isaac B, Natarajan K, et al. A preclinical study on the protective effect of melatonin against methotrexate-induced small intestinal damage: effect mediated by attenuation of nitrosative stress, protein tyrosine nitration, and PARP activation. Cancer Chemotherapy and Pharmacology. 2013 Feb 19;71(5):1209–18.

309. Cuzzocrea S, Zingarelli B, Costantino G, Szabó A, Salzman AL, Caputi AP, et al. Beneficial effects of 3-aminobenzamide, an inhibitor of poly (ADP-ribose) synthetase in a rat model of splanchnic artery occlusion and reperfusion. Br. J. Pharmacol. 1997 Jul;121(6):1065–74.

310. Küpper JH, Van Gool L, Müller M, Bürkle A. Detection of poly(ADP-ribose) polymerase and its reaction product poly(ADP-ribose) by immunocytochemistry. Histochem. J. 1996 May;28(5):391–5.

311. Detre S, Saclani Jotti G, Dowsett M. A ‘quickscore’ method for immunohistochemical semiquantitation: validation for oestrogen receptor in breast carcinomas. J. Clin. Pathol. 1995 Sep;48(9):876–8.

312. González-Flecha B, Boveris A. Mitochondrial sites of hydrogen peroxide production in reperfused rat kidney cortex. Biochim. Biophys. Acta. 1995 Apr 13;1243(3):361–6.

313. Rice Me, Shelton E. Comparison Of The Reduction Of Two Tetrazolium Salts With Succinoxidase Activity Of Tissue Homogenates. J. Natl. Cancer Inst. 1957 Jan;18(1):117–25.

314. Ohkawa H, Ohishi N, Yagi K. Assay for lipid peroxides in animal tissues by thiobarbituric acid reaction. Anal. Biochem. 1979 Jun;95(2):351–8.

315. Chan HW, Levett G. Autoxidation of methyl linoleate. Separation and analysis of isomeric mixtures of methyl linoleate hydroperoxides and methyl hydroxylinoleates. Lipids. 1977 Jan;12(1):99–104.

316. Habeeb AF. [37] Reaction of protein sulfhydryl groups with Ellman's reagent. Meth. Enzymol. 1972;25:457–64.

317. Sedlak J, Lindsay RH. Estimation of total, protein-bound, and nonprotein sulfhydryl groups in tissue with Ellman's reagent. Anal. Biochem. 1968 Oct 24;25(1):192–205.

318. Sastry KVH, Moudgal RP, Mohan J, Tyagi JS, Rao GS. Spectrophotometric determination of serum nitrite and nitrate by copper-cadmium alloy. Anal. Biochem. 2002 Jul 1;306(1):79–82.

319. Ohkuma N, Matsuo S, Tsutsui M, Ohkawara A. [Superoxide dismutase in the epidermis (author's transl)]. Nihon Hifuka Gakkai Zasshi. 1982 Apr;92(5):583–90.

320. Aebi H. Catalase in vitro. Meth. Enzymol. 1984;105:121–6.

321. Awasthi YC, Dao DD, Saneto RP. Interrelationship between anionic and cationic forms of glutathione S-transferases of human liver. Biochem. J. 1980 Oct 1;191(1):1–10.

322. Racker E. Glutathione Reductase From Bakers' Yeast And Beef Liver. J. Biol. Chem. 1955 Dec;217(2):855–65.

323. Zakowski JJ, Tappel AL. Purification and properties of rat liver mitochondrial glutathione peroxidase. Biochim. Biophys. Acta. 1978 Sep 11;526(1):65–76.

324. Wallace JL, MacNaughton WK, Morris GP, Beck PL. Inhibition of leukotriene synthesis markedly accelerates healing in a rat model of inflammatory bowel disease. Gastroenterology. 1989 Jan;96(1):29–36.

325. Slot C. Plasma creatinine determination. A new and specific Jaffe reaction method. Scand. J. Clin. Lab. Invest. 1965;17(4):381–7.

326. Seaton B, Ali A. Simplified manual high performance clinical chemistry methods for developing countries. Med Lab Sci. 1984 Oct;41(4):327–36.

327. Talke H, Schubert Ge. [Enzymatic Urea Determination In The Blood And Serum In The Warburg Optical Test]. Klin. Wochenschr. 1965 Feb 1;43:174–5.

328. Thefeld W, Hoffmeister H, Busche EW, Koller PU, Vollmar J. [Normal values of serum uric acid levels in relation to age and sex as determined using a new enzymatic uric acid color test]. Dtsch. Med. Wochenschr. 1973 Feb 23;98(8):380–4.

329. Atkinson A, Gatenby AD, Lowe AG. The determination of inorganic orthophosphate in biological systems. Biochim. Biophys. Acta. 1973 Aug 17;320(1):195–204.

330. Forrester RL, Wataji LJ, Silverman DA, Pierre KJ. Enzymatic method for determination of CO2 in serum. Clin. Chem. 1976 Feb;22(2):243–5.

331. Barham D, Trinder P. An improved colour reagent for the determination of blood glucose by the oxidase system. Analyst. 1972 Feb;97(151):142–5.

332. CHANCE B, BALTSCHEFFSKY M. Spectroscopic effects of adenosine diphosphate upon the respiratory pigments of rat-heart-muscle sarcosomes. Biochem. J. 1958 Feb;68(2):283–95.

333. Madesh M, Anup R, Benard O, Balasubramanian KA. Apoptosis in the monkey small intestinal epithelium: structural and functional alterations in the mitochondria. Free Radic. Biol. Med. 1999 Apr;26(7-8):836–43.

334. Madesh M, Balasubramanian KA. A microtiter plate assay for superoxide using MTT reduction method. Indian J. Biochem. Biophys. 1997 Dec;34(6):535–9.

335. Takeyama N, Matsuo N, Tanaka T. Oxidative damage to mitochondria is mediated by the Ca(2+)-dependent inner-membrane permeability transition. Biochem. J. 1993 Sep 15;294 (Pt 3):719–25.

336. TEDESCHI H, HARRIS DL. The osmotic behavior and permeability to non-electrolytes of mitochondria. Arch. Biochem. Biophys. 1955 Sep;58(1):52–67.

337. Darley-Usmar VM. The molecular aetiology of human mitochondrial myopathies. Biochem. Soc. Trans. 1987 Feb;15(1):102–3.

338. Soper JW, Pedersen PL. Isolation of an oligomycin-sensitive ATPase complex from rat liver mitochondria. Meth. Enzymol. 1979;55:328–33.

339. Carbonic_Anhydrase_-_CSRD Assay.pdf.

340. Gardner PR, Nguyen DD, White CW. Aconitase is a sensitive and critical target of oxygen poisoning in cultured mammalian cells and in rat lungs. Proc. Natl. Acad. Sci. U.S.A. 1994 Dec 6;91(25):12248–52.

341. LOWRY OH, ROSEBROUGH NJ, FARR AL, RANDALL RJ. Protein measurement with the Folin phenol reagent. J. Biol. Chem. 1951 Nov;193(1):265–75.

342. Buffoli B, Pechánová O, Kojsová S, Andriantsitohaina R, Giugno L, Bianchi R, et al. Provinol prevents CsA-induced nephrotoxicity by reducing reactive oxygen species, iNOS, and NF-κB expression. J. Histochem. Cytochem. 2005 Dec;53(12):1459–68.

343. Devaux Y, Seguin C, Grosjean S, De Talancé N, Schwartz M, Burlet A, et al. Retinoic acid and lipopolysaccharide act synergistically to increase prostanoid concentrations in rats in vivo. J. Nutr. 2001 Oct;131(10):2628–35.

344. Broadbelt NV, Chen J, Silver RB, Poppas DP, Felsen D. Pressure activates epidermal growth factor receptor leading to the induction of iNOS via NFkappaB and STAT3 in human proximal tubule cells. Am. J. Physiol. Renal Physiol. 2009 Jul;297(1):F114–124.

345. Le Berre L, Bruneau S, Naulet J, Renaudin K, Buzelin F, Usal C, et al. Induction of T Regulatory Cells Attenuates Idiopathic Nephrotic Syndrome. J Am Soc Nephrol. 2009 Jan;20(1):57–67.

346. Taal MW, Zandi-Nejad K, Weening B, Shahsafaei A, Kato S, Lee KW, et al. Proinflammatory gene expression and macrophage recruitment in the rat remnant kidney. Kidney Int. 2000 Oct;58(4):1664–76.

347. Grochot-Przeczek A, Lach R, Mis J, Skrzypek K, Gozdecka M, Sroczynska P, et al. Heme Oxygenase-1 Accelerates Cutaneous Wound Healing in Mice. PLoS ONE [Internet]. 2009 Jun 4

[cited 2013 Sep 22];4(6). Available from: http://www.ncbi.nlm.nih.gov/pmc/articles/PMC2686151/

348. Mazzei L, García IM, Cacciamani V, Benardón ME, Manucha W. WT-1 mRNA expression is modulated by nitric oxide availability and Hsp70 interaction after neonatal unilateral ureteral obstruction. Biocell. 2010 Dec;34(3):121–32.

349. Ding Y, Zou J, Li Z, Tian J, Abdelalim S, Du F, et al. Study of Histopathological and Molecular Changes of Rat Kidney under Simulated Weightlessness and Resistance Training Protective Effect. PLoS One [Internet]. 2011 May 23 [cited 2013 Sep 22];6(5). Available from: http://www.ncbi.nlm.nih.gov/pmc/articles/PMC3100312/

350. Maitra SR, Jacob A, Zhou M, Wang P. Modulation of matrix metalloproteinase-9 and tissue inhibitor of matrix metalloproteinase-1 in sepsis. Int J Clin Exp Med. 2010;3(3):180–5.

351. Schmittgen TD, Livak KJ. Analyzing real-time PCR data by the comparative C(T) method. Nat Protoc. 2008;3(6):1101–8.

352. Gallant JE, DeJesus E, Arribas JR, Pozniak AL, Gazzard B, Campo RE, et al. Tenofovir DF, emtricitabine, and efavirenz vs. zidovudine, lamivudine, and efavirenz for HIV. N. Engl. J. Med. 2006 Jan 19;354(3):251–60.

353. Quimby D, Brito MO. Fanconi syndrome associated with use of tenofovir in HIV-infected patients: a case report and review of the literature. AIDS Read. 2005 Jul;15(7):357–64.

354. Hall AM, Kleta R. The Renal Fanconi Syndrome. In: Barrat J, Harris K, Topham P, editors. Oxford Desk Reference in Nephrology. New York: Oxford University Press; 2009:204–7.

355. Lewis W, Haase CP, Raidel SM, Russ RB, Sutliff RL, Hoit BD, et al. Combined antiretroviral therapy causes cardiomyopathy and elevates plasma lactate in transgenic AIDS mice. Lab. Invest. 2001 Nov;81(11):1527–36.

356. Dalakas MC, Illa I, Pezeshkpour GH, Laukaitis JP, Cohen B, Griffin JL. Mitochondrial myopathy caused by long-term zidovudine therapy. N. Engl. J. Med. 1990 Apr 19;322(16):1098–105.

357. Reagan-Shaw S, Nihal M, Ahmad N. Dose translation from animal to human studies revisited. FASEB J. 2008 Mar;22(3):659–61.

358. Gilead Sciences Inc. Drug approval package for NDA 21–356: VIREAD (tenofovir disoproxil fumarate). U S Food and Drug Administration FDA Report. 2001. Pharmacology review. Available at: http://www.fda.gov/cder/foi/nda/2001–21-356_Viread_pharmr_P1.pdf. Accessed October 15, 2008.

359. Naito A, Hasegawa H, Kurasawa T, Ohtake Y, Matsukawa H, Ezure Y, et al. Histopathological study of kidney abnormalities in an experimental SIADH rat model and its application to the evaluation of the pharmacologic profile of VP-343, a selective vasopressin V2 receptor antagonist. Biol. Pharm. Bull. 2001 Aug;24(8):897–901.

360. Zhang C, Liu J, Pan H, Yang X, Bian K. [Mitochondrial dysfunction induced by excessive ROS/RNS-metabolic cardiovascular disease and traditional Chinese medicines intervention]. Zhongguo Zhong Yao Za Zhi. 2011 Sep;36(17):2423–8.

361. Kinai E, Hanabusa H. Renal tubular toxicity associated with tenofovir assessed using urine-beta 2 microglobulin, percentage of tubular reabsorption of phosphate and alkaline phosphatase levels. AIDS. 2005 Nov 18;19(17):2031–3.

362. Norden AG, Scheinman SJ, Deschodt-Lanckman MM, Lapsley M, Nortier JL, Thakker RV, et al. Tubular proteinuria defined by a study of Dent's (CLCN5 mutation) and other tubular diseases. Kidney Int. 2000 Jan;57(1):240–9.

363. Boesken WH. Diagnostic significance of SDS-PAA-electrophoresis of urinary proteins: different forms of proteinuria and their correlation to renal diseases. Curr Probl Clin Biochem. 1979;(9):235–48.

364. Boesken WH, Kopf K, Schollmeyer P. Differentiation of proteinuric diseases by discelectrophoretic molecular weight analysis of urinary proteins. Clin. Nephrol. 1973 Oct;1(5):311–8.

365. Papaleo A, Warszawski J, Salomon R, Jullien V, Veber F, Dechaux M, et al. Increased beta-2 microglobulinuria in human immunodeficiency virus-1-infected children and adolescents treated with tenofovir. Pediatr. Infect. Dis. J. 2007 Oct;26(10):949–51.

366. Gatanaga H, Tachikawa N, Kikuchi Y, Teruya K, Genka I, Honda M, et al. Urinary beta2-microglobulin as a possible sensitive marker for renal injury caused by tenofovir disoproxil fumarate. AIDS Res. Hum. Retroviruses. 2006 Aug;22(8):744–8.

367. Lieberthal W, Menza SA, Levine JS. Graded ATP depletion can cause necrosis or apoptosis of cultured mouse proximal tubular cells. Am. J. Physiol. 1998 Feb;274(2 Pt 2):F315–327.

368. Kanno T, Utsumi T, Ide A, Takehara Y, Saibara T, Akiyama J, et al. Dysfunction of mouse liver mitochondria induced by 2,2'-azobis-(2-amidinopropane) dihydrochloride, a radical initiator, in vitro and in vivo. Free Radic. Res. 1994 Sep;21(4):223–34.

369. Ishiyama M, Tominaga H, Shiga M, Sasamoto K, Ohkura Y, Ueno K. A combined assay of cell viability and in vitro cytotoxicity with a highly water-soluble tetrazolium salt, neutral red and crystal violet. Biol. Pharm. Bull. 1996 Nov;19(11):1518–20.

370. Reddy PVB, Rama Rao KV, Norenberg MD. Inhibitors of the mitochondrial permeability transition reduce ammonia-induced cell swelling in cultured astrocytes. J. Neurosci. Res. 2009 Sep;87(12):2677–85.

371. Han D, Williams E, Cadenas E. Mitochondrial respiratory chain-dependent generation of superoxide anion and its release into the intermembrane space. Biochem. J. 2001 Jan 15;353(Pt 2):411–6.

372. Zorov DB, Juhaszova M, Sollott SJ. Mitochondrial ROS-induced ROS release: an update and review. Biochim. Biophys. Acta. 2006 Jun;1757(5-6):509–17.

373. Lenaz G. The mitochondrial production of reactive oxygen species: mechanisms and implications in human pathology. IUBMB Life. 2001 Nov;52(3-5):159–64.

374. Holley AK, Bakthavatchalu V, Velez-Roman JM, St Clair DK. Manganese superoxide dismutase: guardian of the powerhouse. Int J Mol Sci. 2011;12(10):7114–62.

375. Squadrito GL, Pryor WA. The formation of peroxynitrite in vivo from nitric oxide and superoxide. Chem. Biol. Interact. 1995 May 19;96(2):203–6.

376. Johnson F, Giulivi C. Superoxide dismutases and their impact upon human health. Mol. Aspects Med. 2005 Oct;26(4-5):340–52.

377. Trump BF, Berezesky IK, Laiho KU, Osornio AR, Mergner WJ, Smith MW. The role of calcium in cell injury. A review. Scan Electron Microsc. 1980;(Pt 2):437–62, 492.

378. Torikai S. Dependency of microdissected nephron segments upon oxidative phosphorylation and exogenous substrates: a relationship between tubular anatomical location in the kidney and metabolic activity. Clin. Sci. 1989 Sep;77(3):287–95.

379. Bagnasco S, Good D, Balaban R, Burg M. Lactate production in isolated segments of the rat nephron. Am. J. Physiol. 1985 Apr;248(4 Pt 2):F522–526.

380. Ackrell BA. Progress in understanding structure-function relationships in respiratory chain complex II. FEBS Lett. 2000 Jan 21;466(1):1–5.

381. Nakatani T, Nakashima T, Kita T, Hirofuji C, Itoh K, Itoh M, et al. Succinate dehydrogenase activities of fibers in the rat extensor digitorum longus, soleus, and cardiac muscles. Arch. Histol. Cytol. 1999 Oct;62(4):393–9.

382. Ludwig B, Bender E, Arnold S, Hüttemann M, Lee I, Kadenbach B. Cytochrome C oxidase and the regulation of oxidative phosphorylation. Chembiochem. 2001 Jun 1;2(6):392–403.

383. Fernandez-Checa JC, Kaplowitz N. Hepatic mitochondrial glutathione: transport and role in disease and toxicity. Toxicol. Appl. Pharmacol. 2005 May 1;204(3):263–73.

384. Mallis RJ, Hamann MJ, Zhao W, Zhang T, Hendrich S, Thomas JA. Irreversible thiol oxidation in carbonic anhydrase III: protection by S-glutathiolation and detection in aging rats. Biol. Chem. 2002 Apr;383(3-4):649–62.

385. Santos NAG, Catão CS, Martins NM, Curti C, Bianchi MLP, Santos AC. Cisplatin-induced nephrotoxicity is associated with oxidative stress, redox state unbalance, impairment of energetic metabolism and apoptosis in rat kidney mitochondria. Arch. Toxicol. 2007 Jul;81(7):495–504.

386. O'Toole JF, Patel HV, Naples CJ, Fujioka H, Hoppel CL. Decreased cytochrome c mediates an age-related decline of oxidative phosphorylation in rat kidney mitochondria. Biochem. J. 2010 Apr 1;427(1):105–12.

387. Smith RAJ, Murphy MP. Mitochondria-targeted antioxidants as therapies. Discov Med. 2011 Feb;11(57):106–14.

388. Linares V, Alonso V, Albina ML, Bellés M, Sirvent JJ, Domingo JL, et al. Lipid peroxidation and antioxidant status in kidney and liver of rats treated with sulfasalazine. Toxicology. 2009 Feb 27;256(3):152–6.

389. Abraham P, Ramamoorthy H, Isaac B. Depletion of the cellular antioxidant system contributes to tenofovir disoproxil fumarate - induced mitochondrial damage and increased oxido-nitrosative stress in the kidney. J. Biomed. Sci. 2013;20(1):61.

390. Zimmerman BJ, Granger DN. Reperfusion injury. Surg. Clin. North Am. 1992 Feb;72(1):65–83.

391. Queiroz-Junior CM, Pacheco CM da F, Fonseca AH, Klein A, Caliari MV, De Francischi JN. Myeloperoxidase content is a marker of systemic inflammation in a chronic condition: the example given by the periodontal disease in rats. Mediators Inflamm. 2009;2009:760837.

392. Inoue H, Akiyama S, Maeda-Yamamoto M, Nesumi A, Tanaka T, Murakami A. High-dose green tea polyphenols induce nephrotoxicity in dextran sulfate sodium-induced colitis mice by down-regulation of antioxidant enzymes and heat-shock protein expressions. Cell Stress Chaperones. 2011 Nov;16(6):653–62.

393. Feder ME, Hofmann GE. Heat-shock proteins, molecular chaperones, and the stress response: evolutionary and ecological physiology. Annu. Rev. Physiol. 1999;61:243–82.

394. De Maio A. Heat shock proteins: facts, thoughts, and dreams. Shock. 1999 Jan;11(1):1–12.

395. Yoo CG, Lee S, Lee CT, Kim YW, Han SK, Shim YS. Anti-inflammatory effect of heat shock protein induction is related to stabilization of I kappa B alpha through preventing I kappa B kinase activation in respiratory epithelial cells. J. Immunol. 2000 May 15;164(10):5416–23.

396. Abraham NG, Cao J, Sacerdoti D, Li X, Drummond G. Heme oxygenase: the key to renal function regulation. Am J Physiol Renal Physiol. 2009 Nov;297(5):F1137–F1152.

397. Nath KA. Heme oxygenase-1: a provenance for cytoprotective pathways in the kidney and other tissues. Kidney Int. 2006 Aug;70(3):432–43.

398. Rivett AJ. The effect of mixed-function oxidation of enzymes on their susceptibility to degradation by a nonlysosomal cysteine proteinase. Arch. Biochem. Biophys. 1985 Dec;243(2):624–32.

399. Klebanoff SJ, Clark RA: The Neutrophil. Amsterdam, North-Holland Publishing Co., 1978.

400. Güngör N, Godschalk RWL, Pachen DM, Van Schooten FJ, Knaapen AM. Activated neutrophils inhibit nucleotide excision repair in human pulmonary epithelial cells: role of myeloperoxidase. FASEB J. 2007 Aug;21(10):2359–67.

401. Sekizuka E, Grisham MB, Li MA, Deitch EA, Granger DN. Inflammation-induced intestinal hyperemia in the rat: role of neutrophils. Gastroenterology. 1988 Dec;95(6):1528–34.

402. Pattison DI, Davies MJ. Reactions of myeloperoxidase-derived oxidants with biological substrates: gaining chemical insight into human inflammatory diseases. Curr. Med. Chem. 2006;13(27):3271–90.

403. Winterbourn CC, Kettle AJ. Biomarkers of myeloperoxidase-derived hypochlorous acid. Free Radic. Biol. Med. 2000 Sep 1;29(5):403–9.

404. Pattison DI, Davies MJ. Absolute rate constants for the reaction of hypochlorous acid with protein side chains and peptide bonds. Chem. Res. Toxicol. 2001 Oct;14(10):1453–64.

405. Buss IH, Darlow BA, Winterbourn CC. Elevated protein carbonyls and lipid peroxidation products correlating with myeloperoxidase in tracheal aspirates from premature infants. Pediatr. Res. 2000 May;47(5):640–5.

406. Sies H. Glutathione and its role in cellular functions. Free Radic. Biol. Med. 1999 Nov;27(9-10):916–21.

407. Kolli VK, Kanakasabapathy I, Faith M, Ramamoorthy H, Isaac B, Natarajan K, et al. A preclinical study on the protective effect of melatonin against methotrexate-induced small intestinal damage: effect mediated by attenuation of nitrosative stress, protein tyrosine nitration, and PARP activation. Cancer Chemotherapy and Pharmacology. 2013 Feb 19;71(5):1209–18.

408. Babiak RM, Campello AP, Carnieri EG, Oliveira MB. Methotrexate: pentose cycle and oxidative stress. Cell Biochem. Funct. 1998 Dec;16(4):283–93.

409. Radi R. Nitric oxide, oxidants, and protein tyrosine nitration. Proc. Natl. Acad. Sci. U.S.A. 2004 Mar 23;101(12):4003–8.

410. Pacher P, Beckman JS, Liaudet L. Nitric oxide and peroxynitrite in health and disease. Physiol. Rev. 2007 Jan;87(1):315–424.

411. Greenacre SA, Ischiropoulos H. Tyrosine nitration: localisation, quantification, consequences for protein function and signal transduction. Free Radic. Res. 2001 Jun;34(6):541–81.

412. Bian K, Davis K, Kuret J, Binder L, Murad F. Nitrotyrosine formation with endotoxin-induced kidney injury detected by immunohistochemistry. Am. J. Physiol. 1999 Jul;277(1 Pt 2):F33–40.

413. Collins T, Read MA, Neish AS, Whitley MZ, Thanos D, Maniatis T. Transcriptional regulation of endothelial cell adhesion molecules: NF-kappa B and cytokine-inducible enhancers. FASEB J. 1995 Jul;9(10):899–909.

414. Tugcu V, Ozbek E, Tasci AI, Kemahli E, Somay A, Bas M, et al. Selective nuclear factor kappa-B inhibitors, pyrolidium dithiocarbamate and sulfasalazine, prevent the nephrotoxicity induced by gentamicin. BJU Int. 2006 Sep;98(3):680–6.

415. Orfila C, Lepert J-C, Alric L, Carrera G, Béraud M, Pipy B. Immunohistochemical distribution of activated nuclear factor kappaB and peroxisome proliferator-activated receptors in carbon tetrachloride-induced chronic liver injury in rats. Histochem. Cell Biol. 2005 Jun;123(6):585–93.

416. Kim YM, Tzeng E, Billiard TR. Role of NO and nitrogen intermediates in regulation of cell functions. In: Goligorsky, MS.; Gross, SS., editors. Nitric Oxide and the Kidney: Physiology and Pathophysiology. Chapman and Hall; New York: 1997. p. 22-51.

417. Honma S, Takahashi N, Shinohara M, Nakamura K, Mitazaki S, Abe S, et al. Amelioration of cisplatin-induced mouse renal lesions by a cyclooxygenase (COX)-2 selective inhibitor. Eur. J. Pharmacol. 2013 Sep 5;715(1-3):181–8.

418. Khan Z, Khan N, Tiwari RP, Sah NK, Prasad GBKS, Bisen PS. Biology of Cox-2: an application in cancer therapeutics. Curr Drug Targets. 2011 Jun;12(7):1082–93.

419. Ramesh G, Reeves WB. TNF-alpha mediates chemokine and cytokine expression and renal injury in cisplatin nephrotoxicity. J. Clin. Invest. 2002 Sep;110(6):835–42.

420. Gu Z, Kaul M, Yan B, Kridel SJ, Cui J, Strongin A, et al. S-nitrosylation of matrix metalloproteinases: signaling pathway to neuronal cell death. Science. 2002 Aug 16;297(5584):1186–90.

421. Frears ER, Zhang Z, Blake DR, O'Connell JP, Winyard PG. Inactivation of tissue inhibitor of metalloproteinase-1 by peroxynitrite. FEBS Lett. 1996 Feb 26;381(1-2):21–4.

422. Traenckner EB, Pahl HL, Henkel T, Schmidt KN, Wilk S, Baeuerle PA. Phosphorylation of human I kappa B-alpha on serines 32 and 36 controls I kappa B-alpha proteolysis and NF-kappa B activation in response to diverse stimuli. EMBO J. 1995 Jun 15;14(12):2876–83.

423. Zoja C, Garcia PB, Remuzzi G. The role of chemokines in progressive renal disease. Front Biosci (Landmark Ed). 2009;14:1815–22.

424. Abraham E. Nuclear factor-kappaB and its role in sepsis-associated organ failure. J. Infect. Dis. 2003 Jun 15;187 Suppl 2:S364–369.

425. Guijarro C, Egido J. Transcription factor-kappa B (NF-kappa B) and renal disease. Kidney Int. 2001 Feb;59(2):415–24.

426. Arenzana-Seisdedos F, Turpin P, Rodriguez M, Thomas D, Hay RT, Virelizier JL, et al. Nuclear localization of I kappa B alpha promotes active transport of NF-kappa B from the nucleus to the cytoplasm. J. Cell. Sci. 1997 Feb;110 (Pt 3):369–78.

427. Viatour P, Merville M-P, Bours V, Chariot A. Phosphorylation of NF-kappaB and IkappaB proteins: implications in cancer and inflammation. Trends Biochem. Sci. 2005 Jan;30(1):43–52.

428. Hoffmann A, Levchenko A, Scott ML, Baltimore D. The IkappaB-NF-kappaB signaling module: temporal control and selective gene activation. Science. 2002 Nov 8;298(5596):1241–5.

429. Meyer M, Schreck R, Baeuerle PA. H2O2 and antioxidants have opposite effects on activation of NF-kappa B and AP-1 in intact cells: AP-1 as secondary antioxidant-responsive factor. EMBO J. 1993 May;12(5):2005–15.

430. Rahman I, Marwick J, Kirkham P. Redox modulation of chromatin remodeling: impact on histone acetylation and deacetylation, NF-kappaB and pro-inflammatory gene expression. Biochem. Pharmacol. 2004 Sep 15;68(6):1255–67.

431. Bonnard M, Mirtsos C, Suzuki S, Graham K, Huang J, Ng M, et al. Deficiency of T2K leads to apoptotic liver degeneration and impaired NF-kappaB-dependent gene transcription. EMBO J. 2000 Sep 15;19(18):4976–85.

432. Hansen JM, Harris C. A novel hypothesis for thalidomide-induced limb teratogenesis: redox misregulation of the NF-kappaB pathway. Antioxid. Redox Signal. 2004 Feb;6(1):1–14.

433. Chung HY, Kim HJ, Kim KW, Choi JS, Yu BP. Molecular inflammation hypothesis of aging based on the anti-aging mechanism of calorie restriction. Microsc. Res. Tech. 2002 Nov 15;59(4):264–72.

434. Hamanaka RB, Chandel NS. Mitochondrial reactive oxygen species regulate cellular signaling and dictate biological outcomes. Trends Biochem. Sci. 2010 Sep;35(9):505–13.

435. Dautzenberg M, Keilhoff G, Just A. Modulation of the myogenic response in renal blood flow autoregulation by NO depends on endothelial nitric oxide synthase (eNOS), but not neuronal or inducible NOS. J. Physiol. (Lond.). 2011 Oct 1;589(Pt 19):4731–44.

436. Xie QW, Kashiwabara Y, Nathan C. Role of transcription factor NF-kappa B/Rel in induction of nitric oxide synthase. J. Biol. Chem. 1994 Feb 18;269(7):4705–8.

437. Kone BC, Baylis C. Biosynthesis and homeostatic roles of nitric oxide in the normal kidney. Am. J. Physiol. 1997 May;272(5 Pt 2):F561–578.

438. Cooper AJ, Pinto JT, Callery PS. Reversible and irreversible protein glutathionylation: biological and clinical aspects. Expert Opin Drug Metab Toxicol. 2011 Jul;7(7):891–910.

439. Sun J, Morgan M, Shen R-F, Steenbergen C, Murphy E. Preconditioning results in S-nitrosylation of proteins involved in regulation of mitochondrial energetics and calcium transport. Circ. Res. 2007 Nov 26;101(11):1155–63.

440. Kim SF, Huri DA, Snyder SH. Inducible nitric oxide synthase binds, S-nitrosylates, and activates cyclooxygenase-2. Science. 2005 Dec 23;310(5756):1966–70.

441. Di Paola R, Genovese T, Impellizzeri D, Ahmad A, Cuzzocrea S, Esposito E. The renal injury and inflammation caused by ischemia-reperfusion are reduced by genetic inhibition of TNF-αR1: a comparison with infliximab treatment. Eur. J. Pharmacol. 2013 Jan 30;700(1-3):134–46.

442. Taubitz A, Schwarz M, Eltrich N, Lindenmeyer MT, Vielhauer V. Distinct contributions of TNF receptor 1 and 2 to TNF-induced glomerular inflammation in mice. PLoS ONE. 2013;8(7):e68167.

443. Kohan DE. Role of endothelin and tumour necrosis factor in the renal response to sepsis. Nephrol. Dial. Transplant. 1994;9 Suppl 4:73–7.

444. Baud L, Perez J, Friedlander G, Ardaillou R. Tumor necrosis factor stimulates prostaglandin production and cyclic AMP levels in rat cultured mesangial cells. FEBS Lett. 1988 Oct 24;239(1):50–4.

445. Dinarello CA, Cannon JG, Wolff SM, Bernheim HA, Beutler B, Cerami A, et al. Tumor necrosis factor (cachectin) is an endogenous pyrogen and induces production of interleukin 1. J. Exp. Med. 1986 Jun 1;163(6):1433–50.

446. Mullin JM, Laughlin KV, Marano CW, Russo LM, Soler AP. Modulation of tumor necrosis factor-induced increase in renal (LLC-PK1) transepithelial permeability. Am. J. Physiol. 1992 Nov;263(5 Pt 2):F915–924.

447. Reiter RJ, Tan D, Burkhardt S. Reactive oxygen and nitrogen species and cellular and organismal decline: amelioration with melatonin. Mech. Ageing Dev. 2002 Apr 30;123(8):1007–19.

448. Rodriguez C, Mayo JC, Sainz RM, Antolín I, Herrera F, Martín V, et al. Regulation of antioxidant enzymes: a significant role for melatonin. J. Pineal Res. 2004 Jan;36(1):1–9.

449. Reiter RJ, Paredes SD, Korkmaz A, Jou M-J, Tan D-X. Melatonin combats molecular terrorism at the mitochondrial level. Interdiscip Toxicol. 2008 Sep;1(2):137–49.

450. Xu J, Sun S, Wei W, Fu J, Qi W, Manchester LC, et al. Melatonin reduces mortality and oxidatively mediated hepatic and renal damage due to diquat treatment. J. Pineal Res. 2007 Mar;42(2):166–71.

451. Martín M, Macías M, León J, Escames G, Khaldy H, Acuña-Castroviejo D. Melatonin increases the activity of the oxidative phosphorylation enzymes and the production of ATP in rat brain and liver mitochondria. Int. J. Biochem. Cell Biol. 2002 Apr;34(4):348–57.

452. Ferraz FF, Kos AG, Janino P, Homsi E. Effects of melatonin administration to rats with glycerol-induced acute renal failure. Ren Fail. 2002 Nov;24(6):735–46.

453. Liang Y-L, Zhang Z-H, Liu X-J, Liu X-Q, Tao L, Zhang Y-F, et al. Melatonin protects against apoptosis-inducing factor (AIF)-dependent cell death during acetaminophen-induced acute liver failure. PLoS ONE. 2012;7(12):e51911.

454. Virág L, Szabó E, Gergely P, Szabó C. Peroxynitrite-induced cytotoxicity: mechanism and opportunities for intervention. Toxicol. Lett. 2003 Apr 11;140-141:113–24.

455. Tator CH. Update on the pathophysiology and pathology of acute spinal cord injury. Brain Pathol. 1995 Oct;5(4):407–13.

456. McTigue DM, Tani M, Krivacic K, Chernosky A, Kelner GS, Maciejewski D, et al. Selective chemokine mRNA accumulation in the rat spinal cord after contusion injury. J. Neurosci. Res. 1998 Aug 1;53(3):368–76.

457. Tyor WR, Avgeropoulos N, Ohlandt G, Hogan EL. Treatment of spinal cord impact injury in the rat with transforming growth factor-beta. J. Neurol. Sci. 2002 Aug 15;200(1-2):33–41.

458. Harlan JM. Consequences of leukocyte-vessel wall interactions in inflammatory and immune reactions. Semin. Thromb. Hemost. 1987 Oct;13(4):434–44.

459. Gitto E, Karbownik M, Reiter RJ, Tan DX, Cuzzocrea S, Chiurazzi P, et al. Effects of melatonin treatment in septic newborns. Pediatr. Res. 2001 Dec;50(6):756–60.

460. Li Z, Nickkholgh A, Yi X, Bruns H, Gross M-L, Hoffmann K, et al. Melatonin protects kidney grafts from ischemia/reperfusion injury through inhibition of NF-κB and apoptosis after experimental kidney transplantation. J. Pineal Res. 2009 May;46(4):365–72.

461. Pascua P, Camello-Almaraz C, Camello PJ, Martin-Cano FE, Vara E, Fernandez-Tresguerres JA, et al. Melatonin, and to a lesser extent growth hormone, restores colonic smooth muscle physiology in old rats. J. Pineal Res. 2011 Nov;51(4):405–15.

462. Yip H-K, Chang Y-C, Wallace CG, Chang L-T, Tsai T-H, Chen Y-L, et al. Melatonin treatment improves adipose-derived mesenchymal stem cell therapy for acute lung ischemia-reperfusion injury. J. Pineal Res. 2013 Mar;54(2):207–21.

463. Korhonen R, Lahti A, Kankaanranta H, Moilanen E. Nitric oxide production and signaling in inflammation. Curr Drug Targets Inflamm Allergy. 2005 Aug;4(4):471–9.

464. Szczepanik M. Melatonin and its influence on immune system. J. Physiol. Pharmacol. 2007 Dec;58 Suppl 6:115–24.

465. Jung KH, Hong S-W, Zheng H-M, Lee D-H, Hong S-S. Melatonin downregulates nuclear erythroid 2-related factor 2 and nuclear factor-kappaB during prevention of oxidative liver injury in a dimethylnitrosamine model. J. Pineal Res. 2009 Sep;47(2):173–83.

466. . Koopman, M. C., Minors, D. S., and Waterhouse, J. M. (1989) Urinary and renal circadian rhythms. In Biological Rhythms in Clinical Practice (Arendt, J., Minors, I).S. Waterhouse, J. M., Eds); pp. 83-98, Wnght.London.

467. Kemp GJ, Blumsohn A, Morris BW. Circadian changes in plasma phosphate concentration, urinary phosphate excretion, and cellular phosphate shifts. Clin. Chem. 1992 Mar;38(3):400–2.

468. Richardson BA, Studier EH, Stallone JN, Kennedy CM. Effects of melatonin on water metabolism and renal function in male Syrian hamsters (Mesocricetus auratus). J. Pineal Res. 1992 Sep;13(2):49–59.

469. Adaramoye OA, Adewumi OM, Adesanoye OA, Faokunla OO, Farombi EO. Effect of tenofovir, an antiretroviral drug, on hepatic and renal functional indices of Wistar rats: protective role of vitamin E. J Basic Clin Physiol Pharmacol. 2012;23(2):69–75.

Publications

1. **Hemalatha Ramamoorthy**, Bina Isaac and Premila Abraham. Oxidative Stress, Decreased Activities Of Anti-Oxidant Enzymes, And Neutrophil Infiltration Contribute To Tenofovir Induced Renal Damage In Rats. ***Int. Res. J.Pharmacy and Pharmacology 2011, 1(9); 259-270.***

2. **Hemalatha Ramamoorthy**, Bina Isaac and Premila Abraham. Evidence For The Roles Of Oxidative Stress, Nitrosative Stress And NF-κB Activation In Tenofovir Disoproxil Fumarate (TDF) Induced Renal Damage In Rats. ***BMC Infectious Diseases 2012, 12 (Supp1):P6.***

3. Premila Abraham, **Hemalatha Ramamoorthy**, Bina Isaac. Depletion of the cellular antioxidant system contributes to tenofovir disoproxil fumarate - induced mitochondrial damage and increased oxido-nitrosative stress in the kidney**.** ***Journal of Biomedical Science*** 2013, **20**:61 ***(19 August 2013).***

4. **Hemalatha Ramamoorthy**, Premila Abraham and Bina Isaac. Effectiveness of melatonin in the amelioration of tenofovir nephrotoxicity by the attenuation of oxidative stress, nitrosative stress, and inflammation- a preclinical study in rats. **(submitted to Journal of physiology and Biochemistry)**

5. Premila Abraham**,** **Hemalatha Ramamoorthy,** Bina Isaac. A reliable and reproducible preclinical model of Tenofovir disoproxil fumarate (TDF) nephrotoxicity. **(submitted to Indian Journal of Pharmacology)**

6. Premila Abraham, **Hemalatha Ramamoorthy**, Bina Isaac. Role of NF k B signalling pathway and PARP activation in TDF nephrotoxicity **(manuscript under preparation).**

Papers presented at conferences

1. **80th Annual meeting of the society of Biological Chemists (India)** held in CIMAP, Lucknow between 12 th and 15 th November 2011 . Theme: Metabolic pathway modulations- applications in health and Agriculture .

   Hemalatha R., Isaac B and Abraham P. Oxidative stress, decreased activities of antioxidant enzymes, and neutrophil infiltration contribute to tenofovir induced renal damage in rats.

2. **International Science symposium on HIV & infectious diseases** (HIV Science 2012) held in Chennai between 20-22 nd January 2012

   Hemalatha R., Isaac B,and Abraham P. Evidence for the roles of oxidative stress, nitrosative stress and NF-κB activation in tenofovir induced renal damage in rats.

   WON THE BEST POSTER AWARD

3. **81th Annual meeting of the society of Biological Chemists (India)** held in CIMAP, Kolkatta between 8 th and 11 th November 2012 .

   Hemalatha R., Isaac B and Abraham P. **Possible Role Of Mitochondrial Damage in Tenofovir induced Nephrotoxicity.**

Appendix

APPENDIX-I

Optimization of PCR assays for target genes by generation of standard curves and melting curve analysis:

The log fluorescence data graphs, standard curves and melting curves were generated for each gene of interest using the Opticon Monitor software, on completion of the PCR assay for each gene studied. The efficiencies of the PCR for the genes studied were found to be similar and were in the range of 1.80 to 2.05.

NF-κB

Figures 1: (A-B) show the log fluorescence data graph, standard curve and melting curves respectively for **NF-κB** . The melting curve analysis showed the presence of a single peak (figure 1 C).

IκB-α

Figures 2: (A-B) show the log fluorescence data graph, standard curve and melting curves respectively for **IκB-α**. The melting curve analysis showed the presence of a single peak. (figure **2** C).

iNOS

Figures 3: (A-B) show the log fluorescence data graph, standard curve and melting curves respectively for **iNOS**. The melting curve analysis showed the presence of a single peak (figure **3** C).

COX-2

Figures 4: (A-B) show the log fluorescence data graph, standard curve and melting curves respectively for **COX-2**. The melting curve analysis showed the presence of a single peak. (figure **4** C).

TNF-α

Figures 5: (A-B) show the log fluorescence data graph, standard curve and melting curves respectively for **TNF-α**. The melting curve analysis showed the presence of a single peak (figure **5 C**).

Heat Shock Protein (HSP 70)

Figures 6: (A-B) show the log fluorescence data graph, standard curve and melting curves respectively for HSP 70. The melting curve analysis showed the presence of a single peak. (figure **6** C).

Heme oxygenase-1 (HO-1)

Figures 7: (A-B) shows the log fluorescence data graph, standard curve and melting curves respectively for HO-1. The melting curve analysis showed the presence of a single peak (figure **7** C).

Caspase-3

Figures 8: (A-B) show the log fluorescence data graph, standard curve and melting curves respectively for Caspase-3. The melting curve analysis showed the presence of a single peak (figure **8** C).

MMP-9

Figures 9: (A-B) show the log fluorescence data graph, standard curve and melting curves respectively for Caspase-3. The melting curve analysis showed the presence of a single peak (figure **9** C).

Beta-actin

Figures 10: (A-B) show the log fluorescence data graph, standard curve and melting curve respectively for Beta-actin. The melting curve analysis showed the presence of a single peak (figure **10 C**)

GAPDH

Figures 11: (A-B) show the log fluorescence data graph, standard curve and melting curves respectively for GAPDH. The melting curve analysis showed the presence of a single peak . (figure **11 C**)

(a) NF-κB :

Figures : 1 A, B and C show the log fluorescence data, standard curve and melting curves respectively for NF-κB . The average efficiency of the PCR for NF-κB was found to be 100%. The melting curve analysis showed the presence of a single peak at 80^{o}C.

.

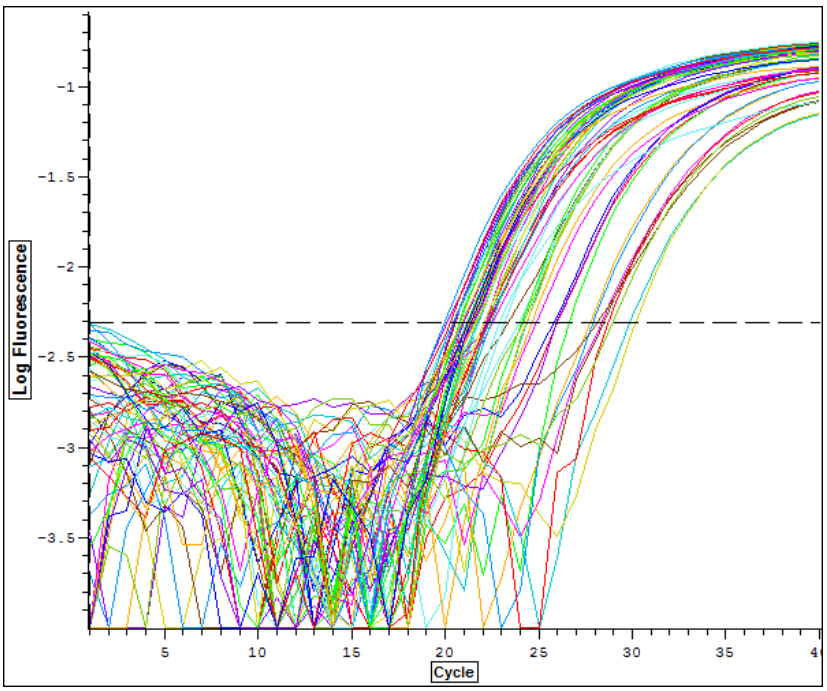

Figure : 1 A Log fluorescence data graph for NF-κB . The graph depicts the PCR cycle number on the x-axis and relative log fluorescence units on the y-axis. The dotted line shows the cycle threshold set at a point above baseline fluorescence.

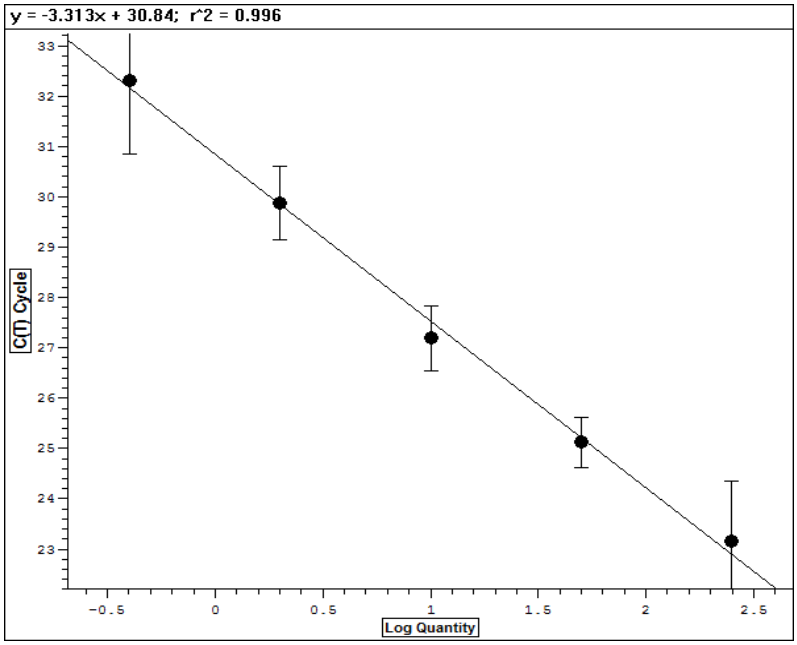

Figure: 1 B Standard curve for NF-κB . The graph depicts log of the quantity of cDNA on the x-axis and cycle threshold value on the y-axis for each of the standard samples used.

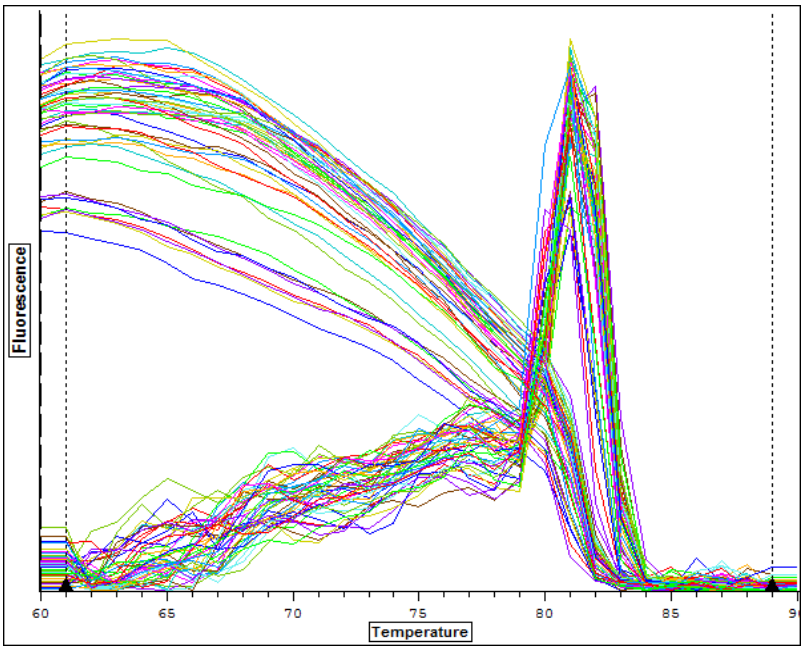

Figure: 1 C Melting curve for NF-κB . The graphical plot of the melting curve was obtained after the PCR, using NF-κB specific primers. The presence of a single peak at 80^{o} C is suggestive of the generation of a specific product during the PCR.

(b) IκB -α :

Figures: 2 A, B and C show the log fluorescence data, standard curve and melting curves respectively for IκB -α . The average efficiency of the PCR for IκB -α was found to be 85%. The melting curve analysis showed the presence of a single peak at 78^{o}C .

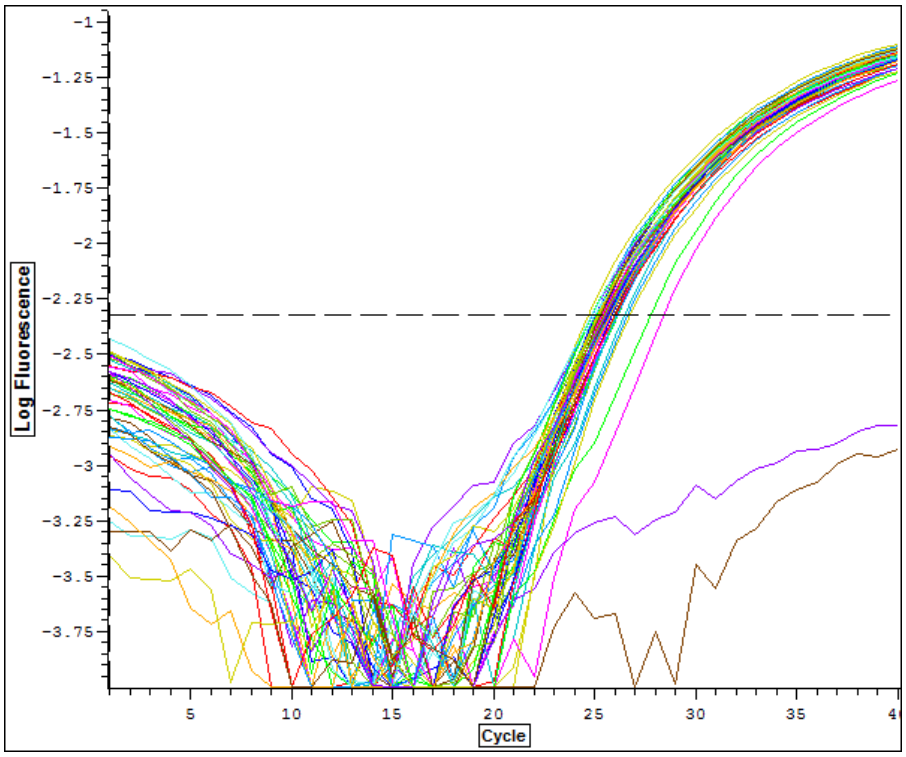

Figure: 2 A. Log fluoresscence data graph for IκB-α. The graph depicts the PCR cycle number on the x-axis and relative log fluorescence units on the y-axis. The dotted line shows the cycle threshold set at a point above baseline fluorescence.

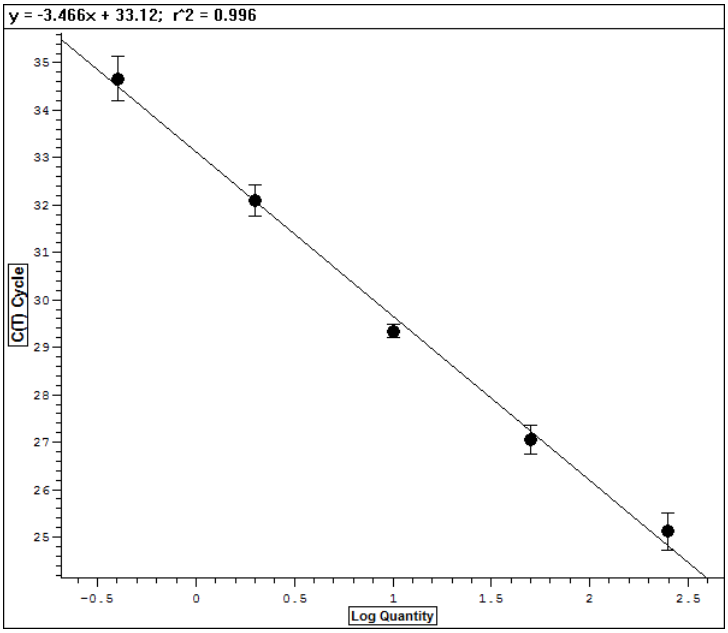

Figure: 2 B Standard curve for IκB-α. The graph depicts log of the quantity of cDNA on the x-axis and cycle threshold value on the y-axis for each of the standard samples used.

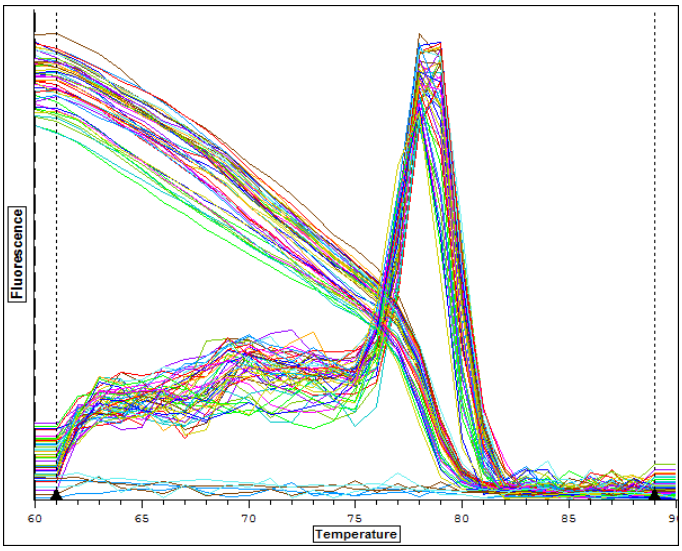

Figure: 2 C Melting curve for IκB-α. The graphical plot of the melting curve was obtained after the PCR, using IκB-α specific primers. The presence of a single peak at 78^{o} C is suggestive of the generation of a specific product during the PCR.

(c) iNOS :

Figures: 3 A, B and C show the log fluorescence data, standard curve and melting curves respectively for iNOS. The average efficiency of the PCR for iNOS was found to be 80-85%. The melting curve analysis showed the presence of a single peak at 83^{o}C.

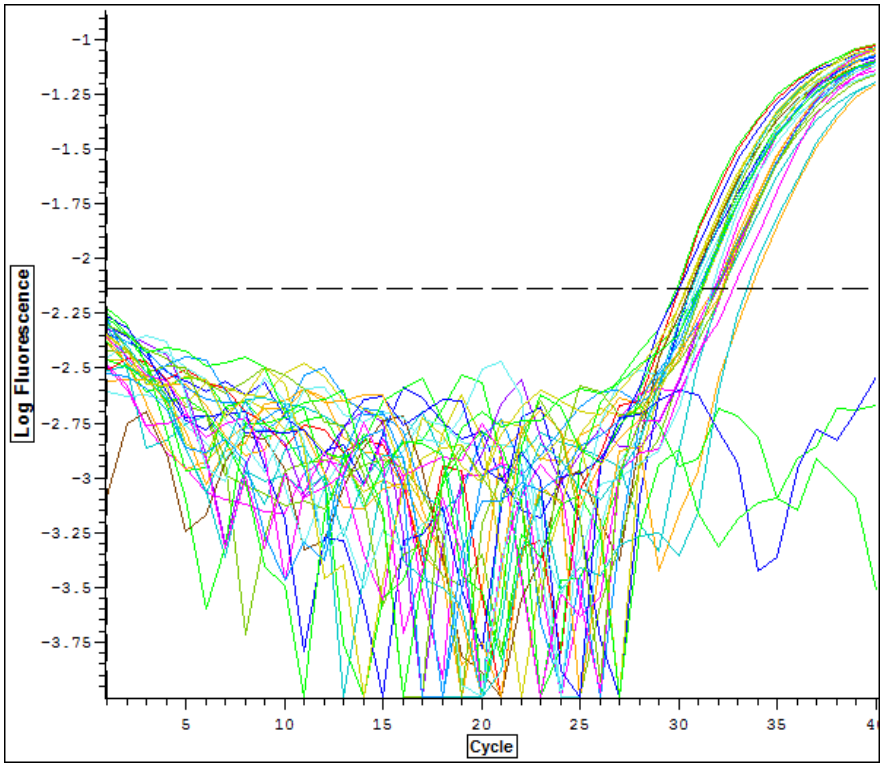

Figure: 3 A Log fluoresscence data graph for iNOS. The graph depicts the PCR cycle number on the x-axis and relative log fluorescence units on the y-axis. The dotted line shows the cycle threshold set at a point above baseline fluorescence.

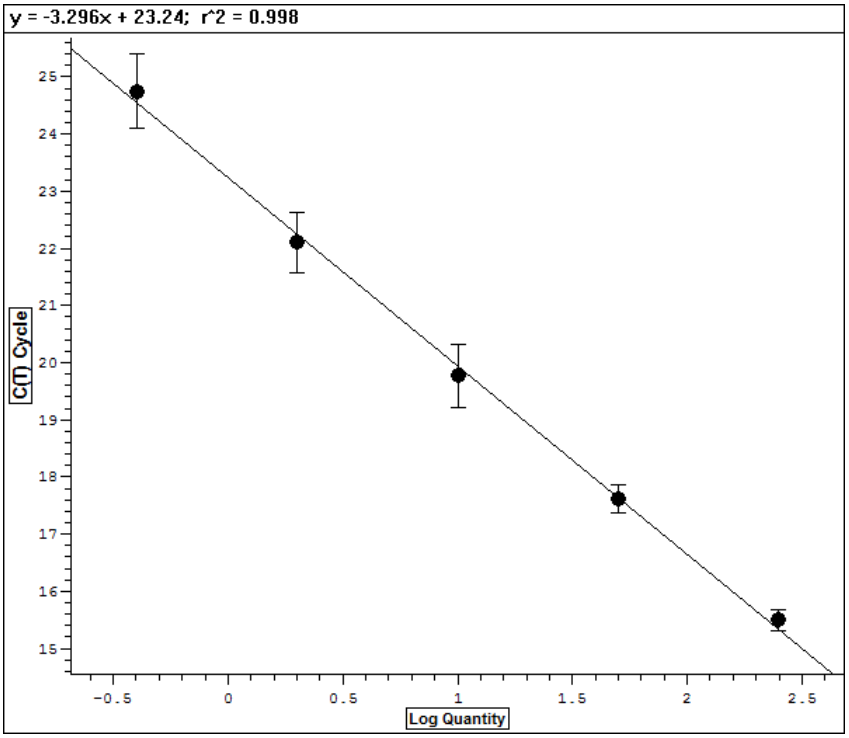

Figure: 3 B Standard curve for iNOS. The graph depicts log of the quantity of cDNA on the x-axis and cycle threshold value on the y-axis for each of the standard samples used.

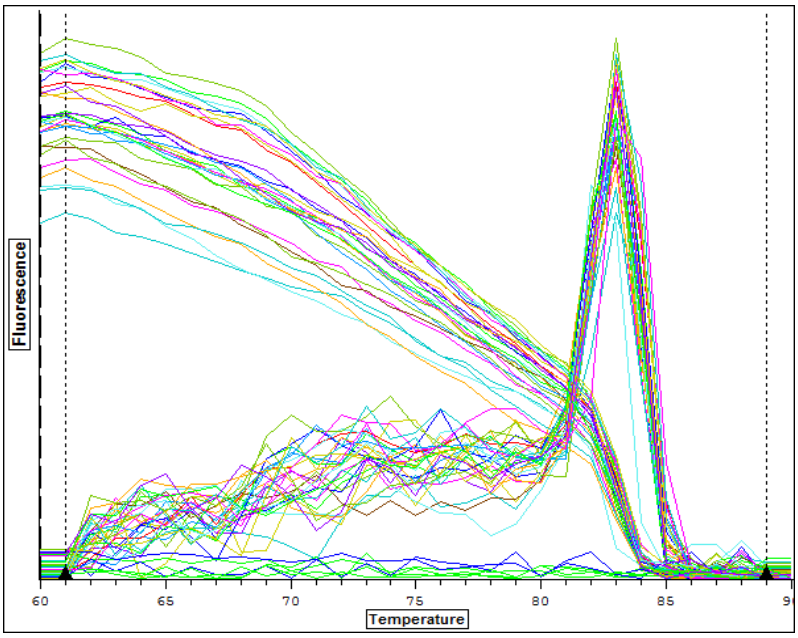

Figure: 3 C Melting curve for iNOS. The graphical plot of the melting curve was obtained after the PCR, using iNOS specific primers. The presence of a single peak at 83-85^{o} C is suggestive of the generation of a specific product during the PCR.

(d) COX 2 :

Figures: 4 A, B and C show the log fluorescence data, standard curve and melting curves respectively for COX 2. The average efficiency of the PCR for COX 2 was found to be 90%. The melting curve analysis showed the presence of a single peak at 84^{o}C.

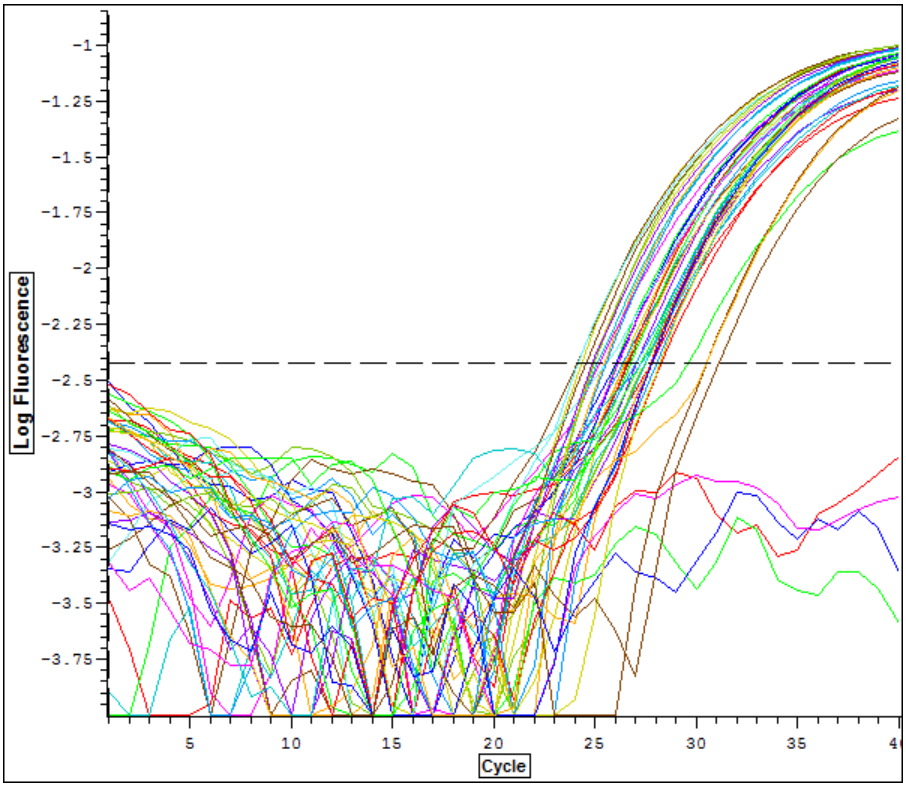

Figure: 4 A. Log fluoresscence data graph for COX 2. The graph depicts the PCR cycle number on the x-axis and relative log fluorescence units on the y-axis. The dotted line shows the cycle threshold set at a point above baseline fluorescence.

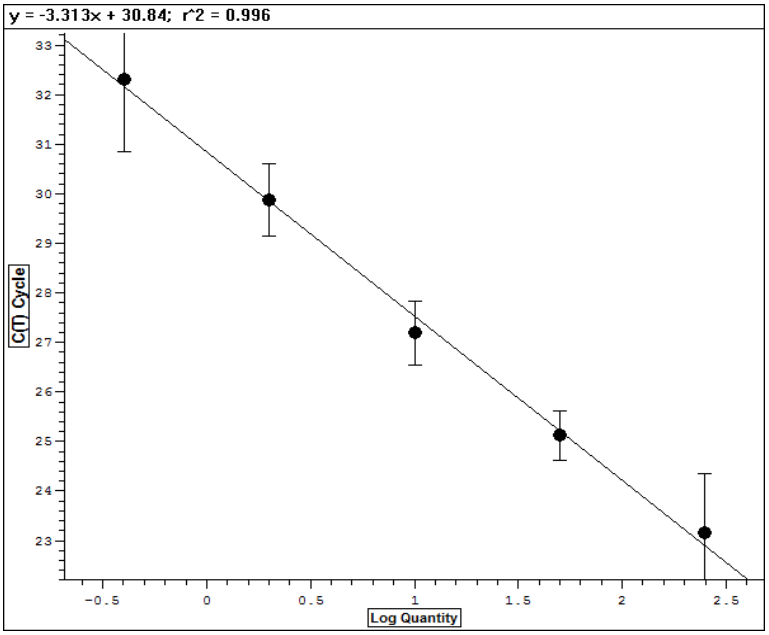

Figure: 4 B Standard curve for COX 2. The graph depicts log of the quantity of cDNA on the x-axis and cycle threshold value on the y-axis for each of the standard samples used.

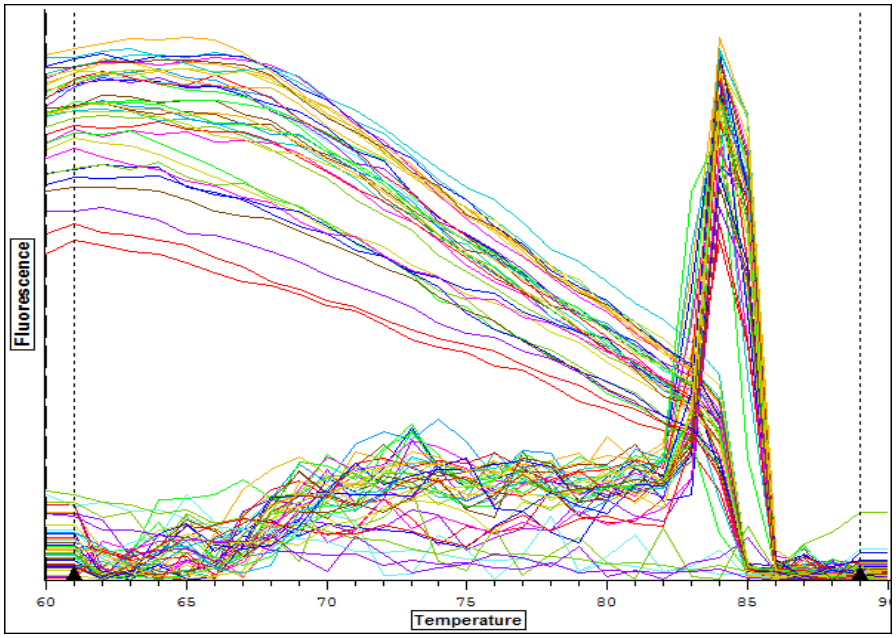

Figure: 4 C Melting curve for COX 2. The graphical plot of the melting curve was obtained after the PCR, using COX 2 specific primers. The presence of a single peak at 84^{o} C is suggestive of the generation of a specific product during the PCR.

(e) TNF α :

Figures: 5 A, B,C show the log fluorescence data, standard curve and melting curves respectively for TNF α. The average efficiency of the PCR for TNF α was found to be 75-90 %. The melting curve analysis showed the presence of a single peak at 78-79^{o}C.

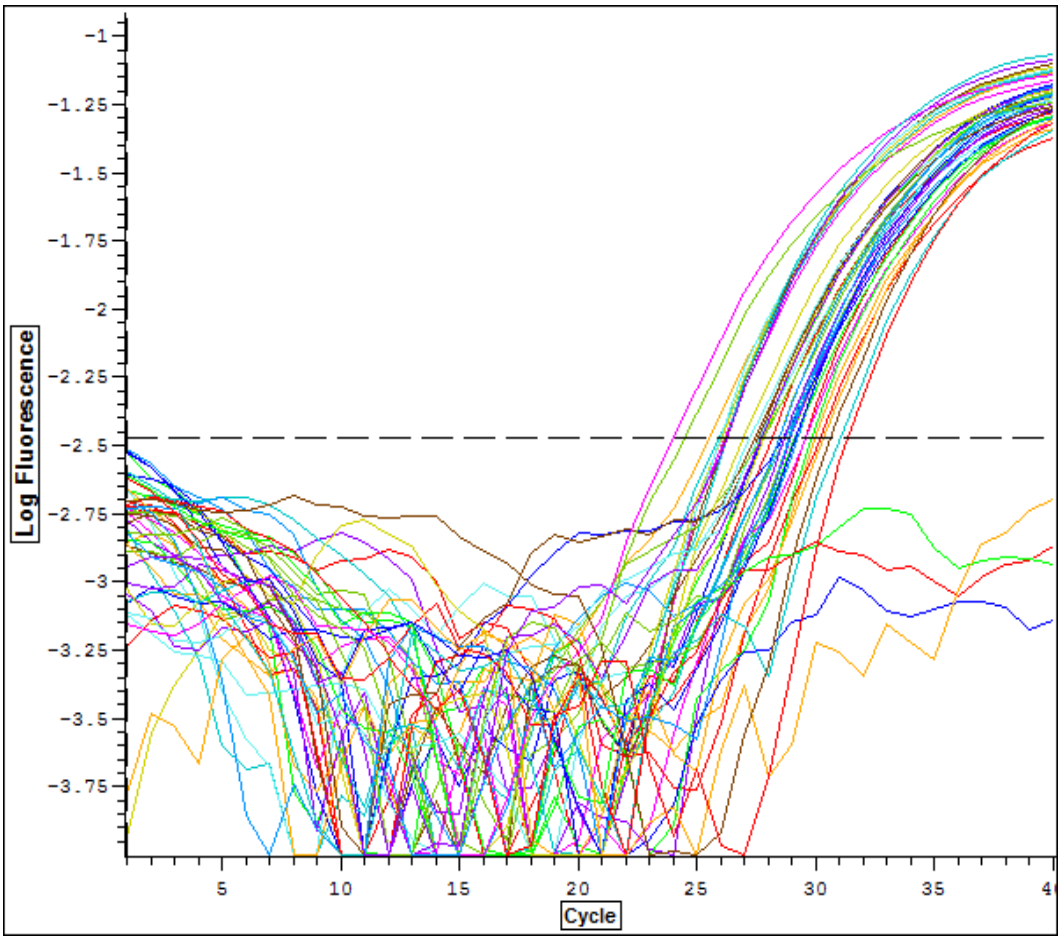

Figure: 5 A Log fluoresscence data graph for TNF α. The graph depicts the PCR cycle number on the x-axis and relative log fluorescence units on the y-axis. The dotted line shows the cycle threshold set at a point above baseline fluorescence.

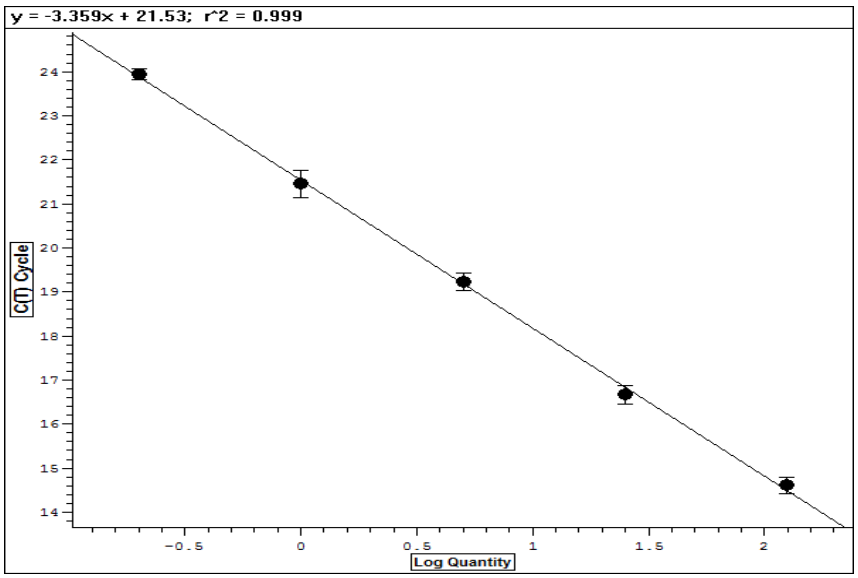

Figure: 5 B Standard curve for TNF α. The graph depicts log of the quantity of cDNA on the x-axis and cycle threshold value on the y-axis for each of the standard samples used.

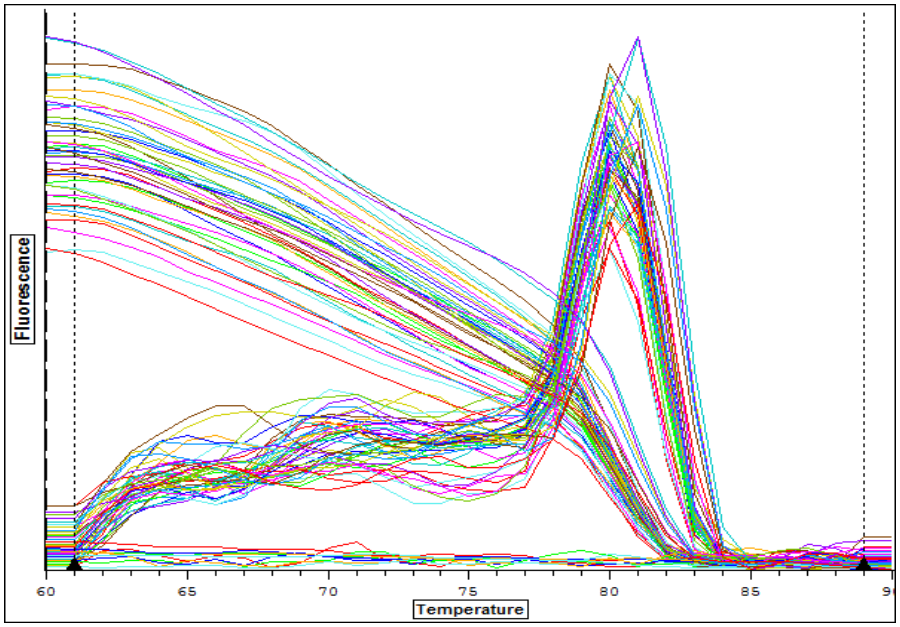

Figure: 5 C Melting curve for TNF α. The graphical plot of the melting curve was obtained after the PCR, using TNF α specific primers. The presence of a single peak at 79-80degree C is suggestive of the generation of a specific product during the PCR.

(f) HSP 70:

Figures: 6 A, B and C show the log fluorescence data, standard curve and melting curves respectively for HSP 70 . The average efficiency of the PCR for HSP 70 was found to be 80-100%. The melting curve analysis showed the presence of a single peak at 78-79^{o}C.

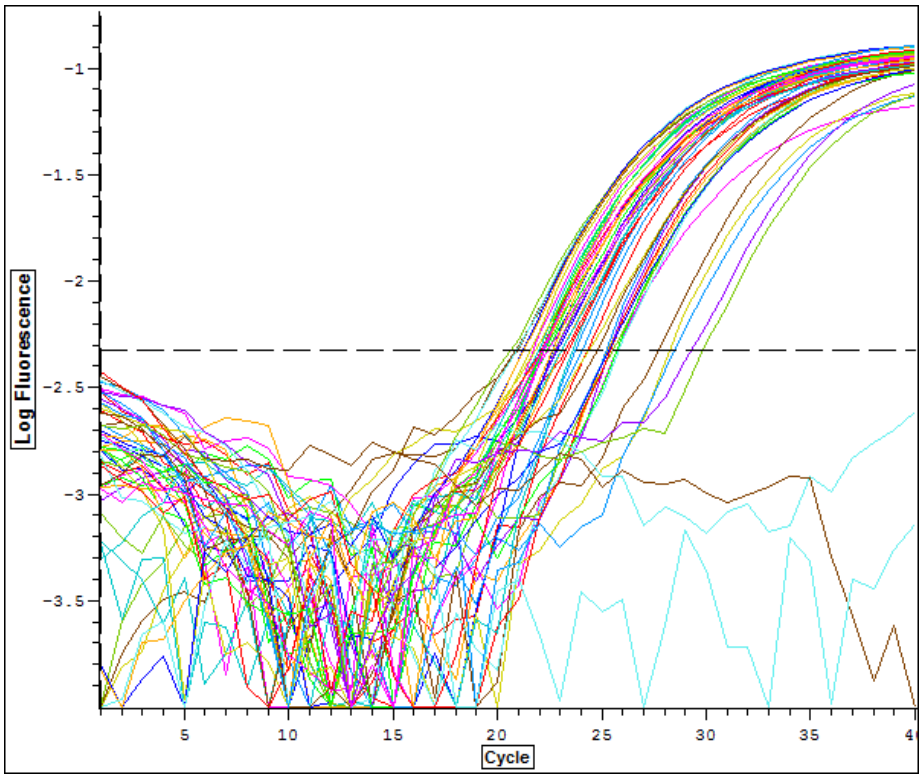

Figure: 6 A Log fluoresscence data graph for HSP 70. The graph depicts the PCR cycle number on the x-axis and relative log fluorescence units on the y-axis. The dotted line shows the cycle threshold set at a point above baseline fluorescence.

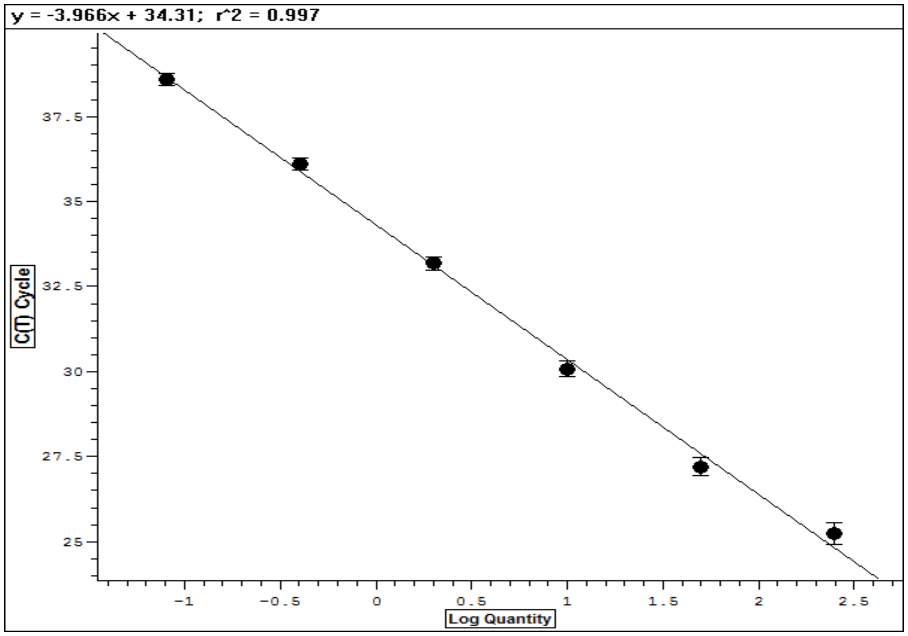

Figure: 6 B Standard curve for HSP 70. The graph depicts log of the quantity of cDNA on the x-axis and cycle threshold value on the y-axis for each of the standard samples used.

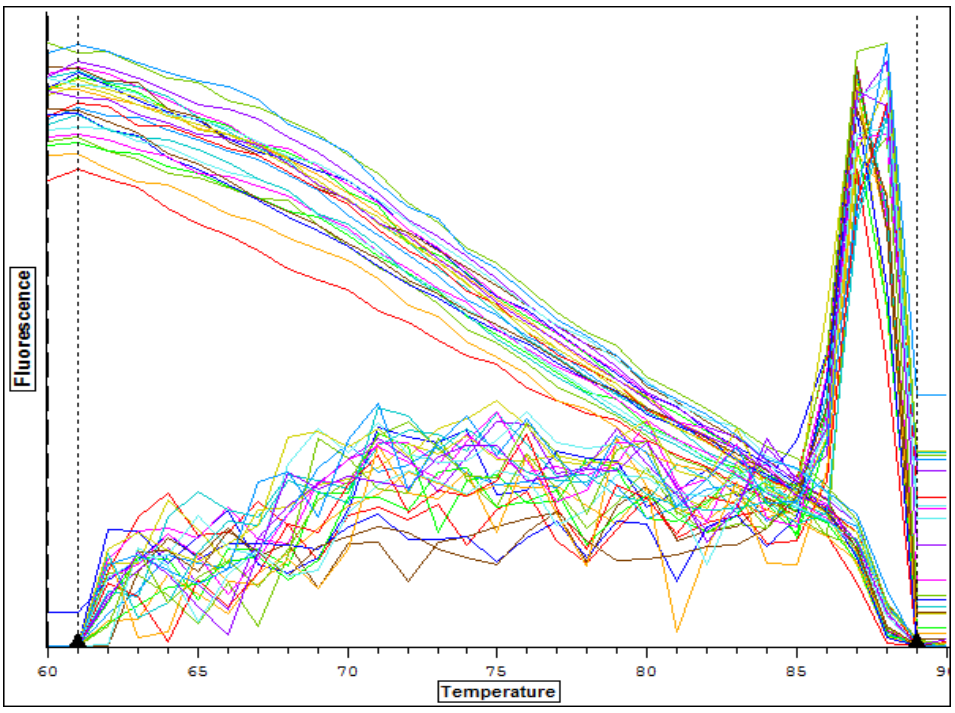

Figure: 6 C . Melting curve for HSP 70. The graphical plot of the melting curve was obtained after the PCR, using HSP 70 specific primers. The presence of a single peak at 86^{o} C is suggestive of the generation of a specific product during the PCR.

(g) Heme oxygenase-1 (HO-1)

Figures: 7 A and B show the log fluorescence data, standard curve and melting curves respectively for HO-1. The average efficiency of the PCR for HO-1 was found to be 90%. The melting curve analysis showed the presence of a single peak at 83^{o}C .

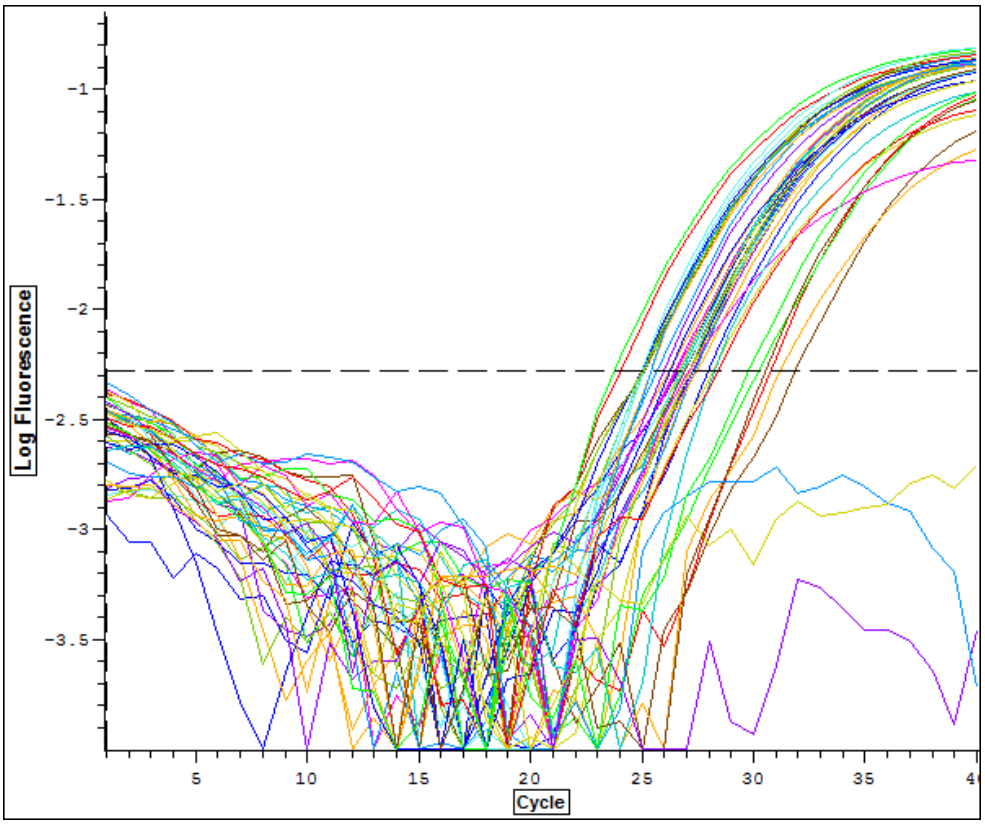

Figure: 7 A Log fluoresscence data graph for HO-1. The graph depicts the PCR cycle number on the x-axis and relative log fluorescence units on the y-axis. The dotted line shows the cycle threshold set at a point above baseline fluorescence.

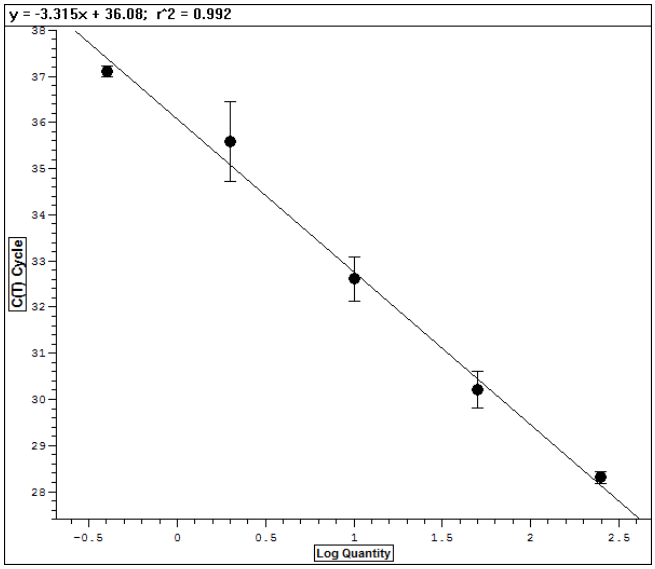

Figure: 7 B Standard curve for HO-1. The graph depicts log of the quantity of cDNA on the x-axis and cycle threshold value on the y-axis for each of the standard samples used.

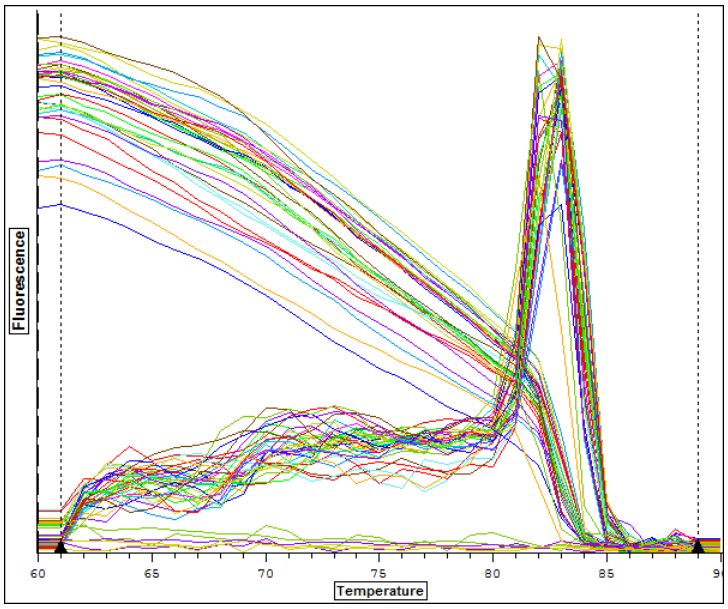

Figure: 7 C Melting curve for HO-1. The graphical plot of the melting curve was obtained after the PCR, using HO-1 specific primers. The presence of a single peak at 83^{o} C is suggestive of the generation of a specific product during the PCR.

(h) CASPASE 3:

Figures: 8 A and c show the log fluorescence data, standard curve and melting curves respectively for caspase 3. The average efficiency of the PCR for caspase-3 was found to be 100%. The melting curve analysis showed the presence of a single peak at 78-79^{o}C.

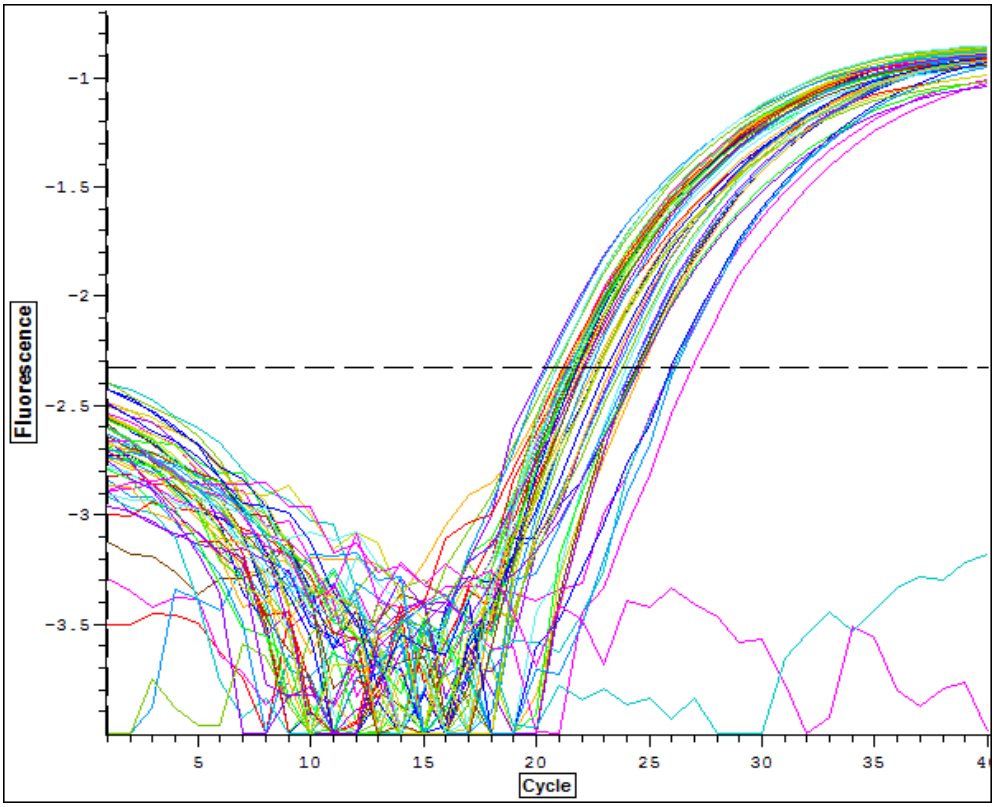

Figure: 8 A Log fluoresscence data graph for caspase 3. The graph depicts the PCR cycle number on the x-axis and relative log fluorescence units on the y-axis. The dotted line shows the cycle threshold set at a point above baseline fluorescence.

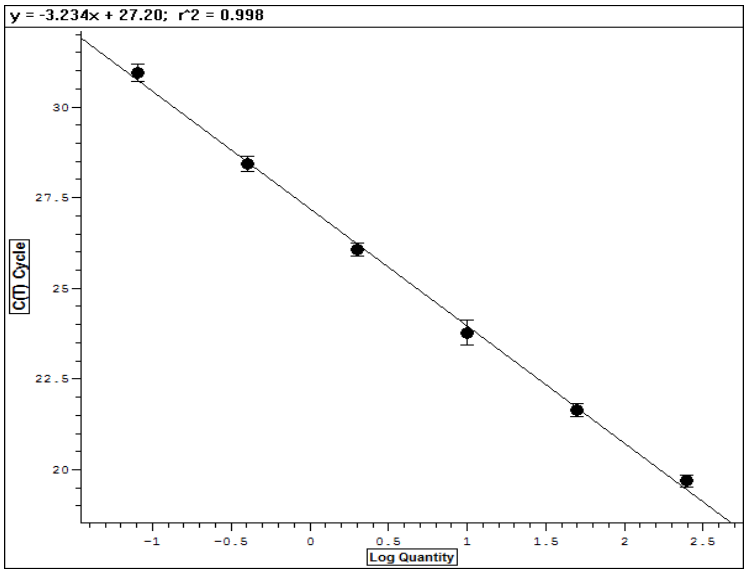

Figure: 8 B Standard curve for Caspase 3. The graph depicts log of the quantity of cDNA on the x-axis and cycle threshold value on the y-axis for each of the standard samples used.

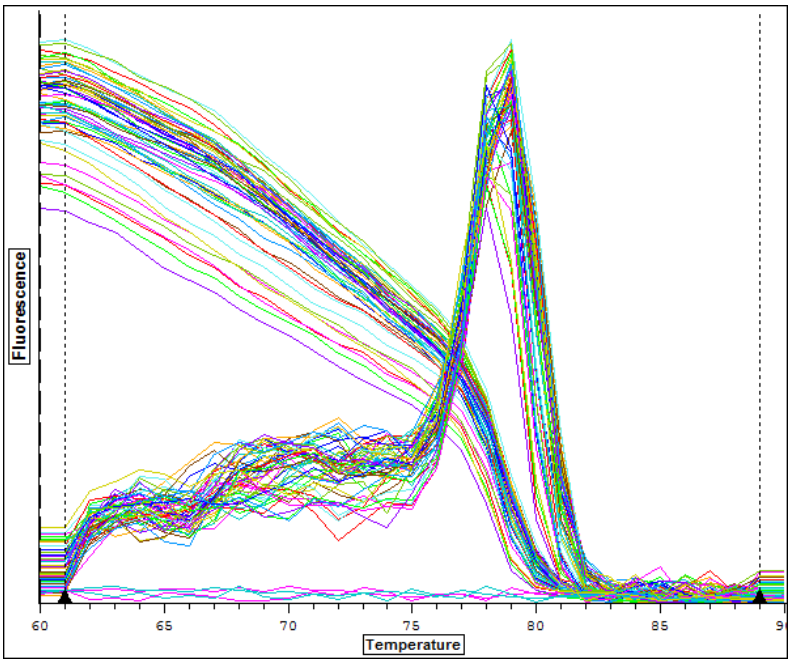

Figure: 8 C Melting curve for Caspase 3. The graphical plot of the melting curve was obtained after the PCR, using Caspase 3 specific primers. The presence of a single peak at 79-80degree C is suggestive of the generation of a specific product during the PCR.

(i) MMP 9:

Figures: 9 A and c show the log fluorescence data, standard curve and melting curves respectively for MMP 9. The average efficiency of the PCR for MMP 9 was found to be 80%. The melting curve analysis showed the presence of a single peak at 75- 79^{o}C .

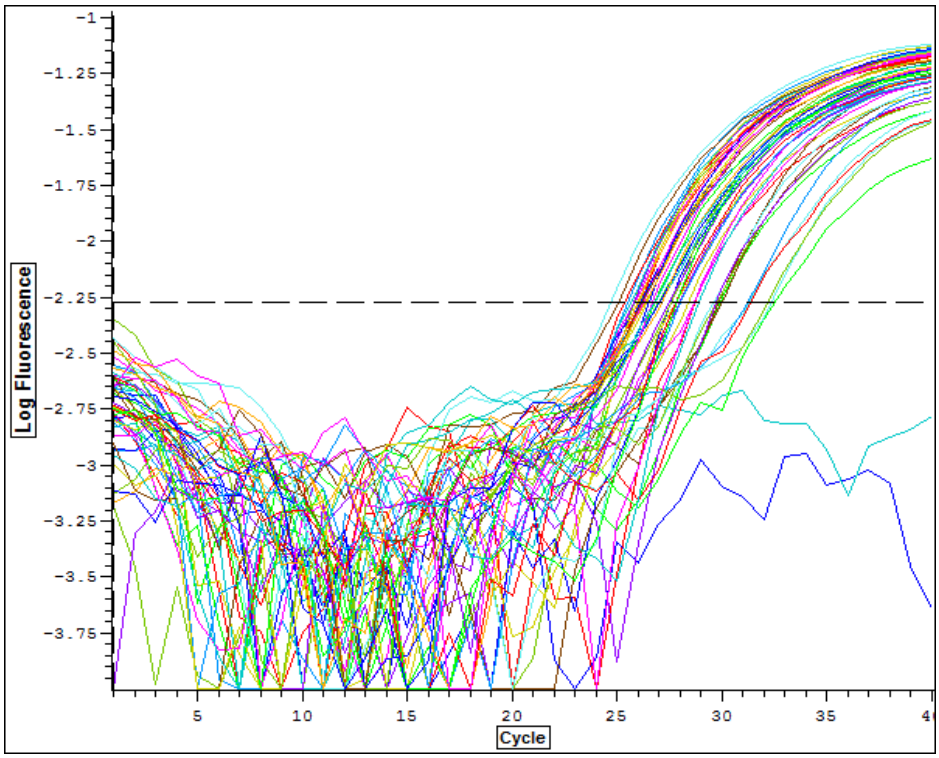

Figure: 9 A. Log fluoresscence data graph for MMP 9. The graph depicts the PCR cycle number on the x-axis and relative log fluorescence units on the y-axis. The dotted line shows the cycle threshold set at a point above baseline fluorescence.

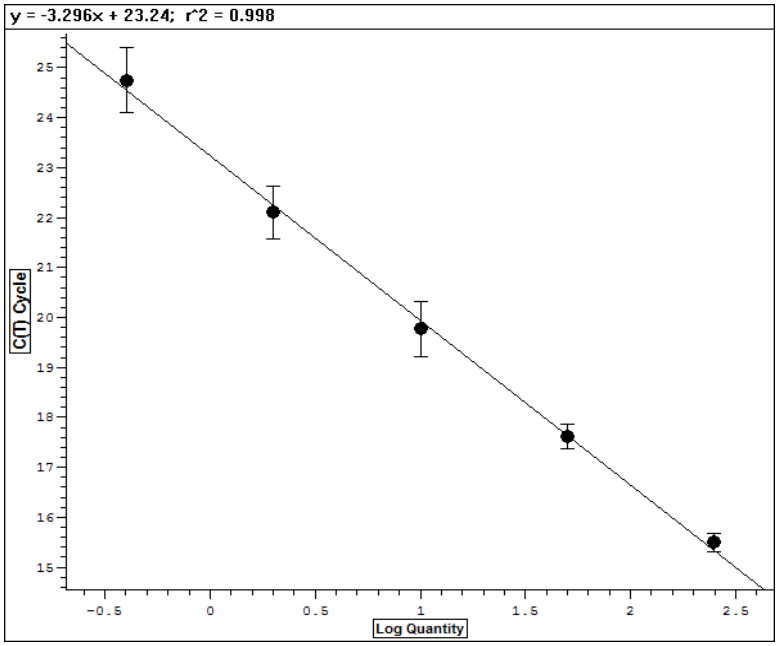

Figure: 9 B Standard curve for MMP 9. The graph depicts log of the quantity of cDNA on the x-axis and cycle threshold value on the y-axis for each of the standard samples used.

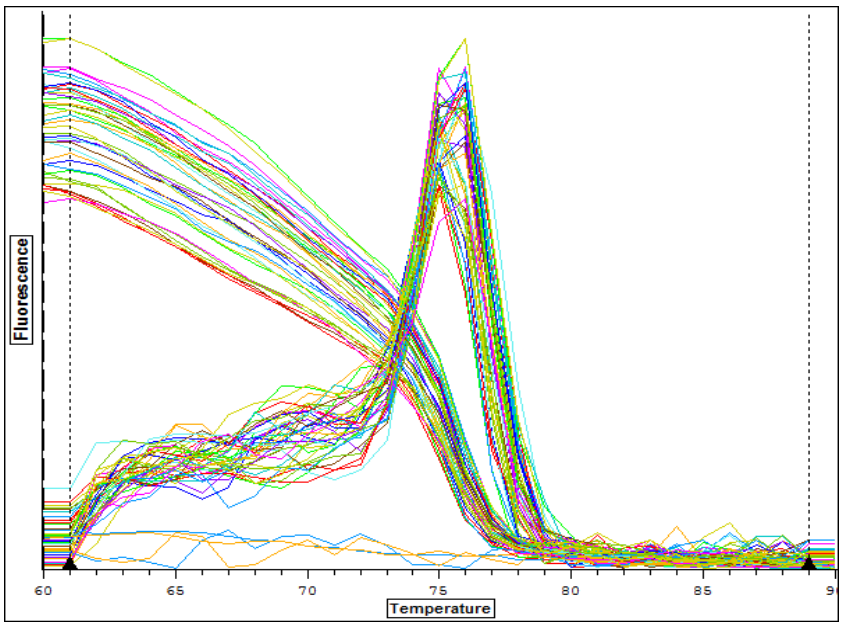

Figure: 9 C Melting curve for MMP 9. The graphical plot of the melting curve was obtained after the PCR, using MMP 9 specific primers. The presence of a single peak at 78^{o} C is suggestive of the generation of a specific product during the PCR.

(j) BETA ACTIN:

Figures: 10 A show the log fluorescence data, standard curve and melting curves respectively for Beta actin . The average efficiency of the PCR for beta actin was found to be 100%. The melting curve analysis showed the presence of a single peak at 78-79^{o}C .

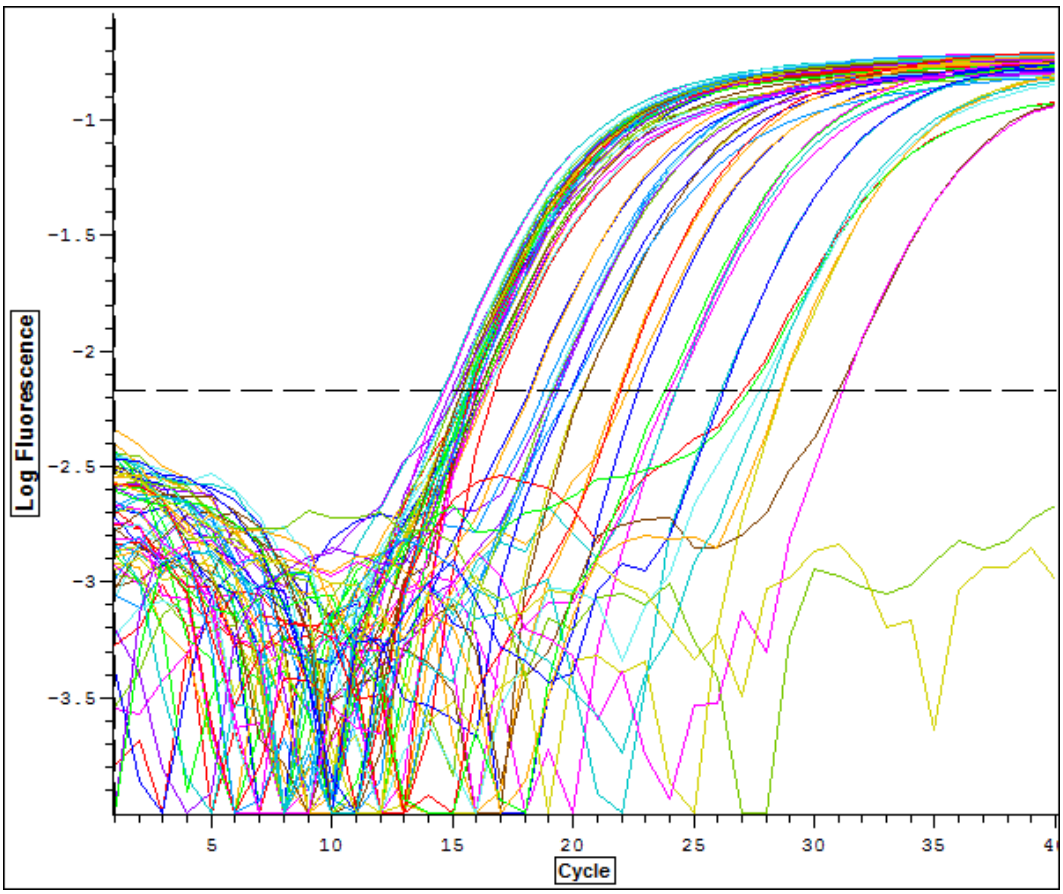

Figure: 10 A Log fluoresscence data graph for Beta Actin. The graph depicts the PCR cycle number on the x-axis and relative log fluorescence units on the y-axis. The dotted line shows the cycle threshold set at a point above baseline fluorescence.

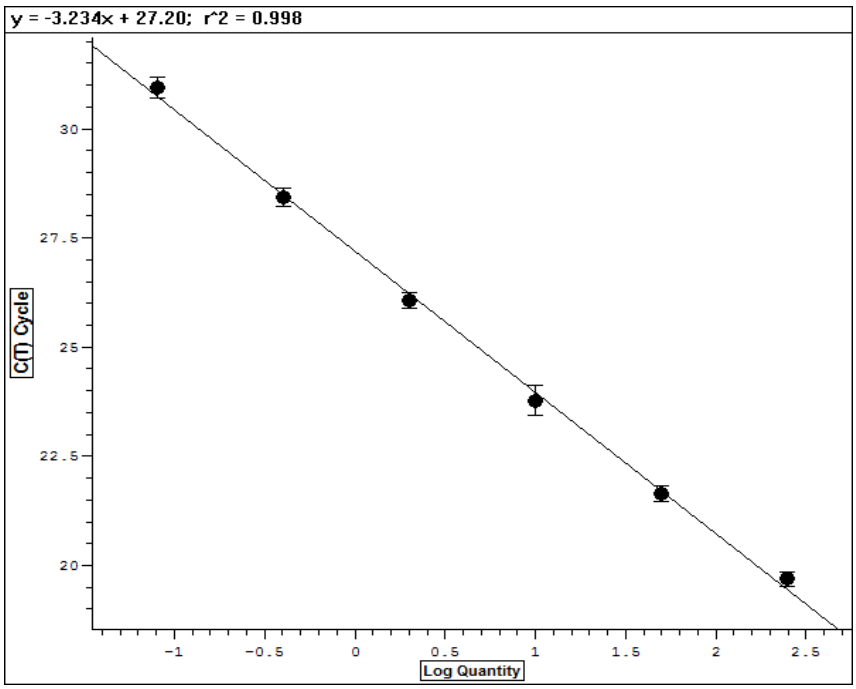

Figure: 10 B Standard curve for Beta actin. The graph depicts log of the quantity of cDNA on the x-axis and cycle threshold value on the y-axis for each of the standard samples used.

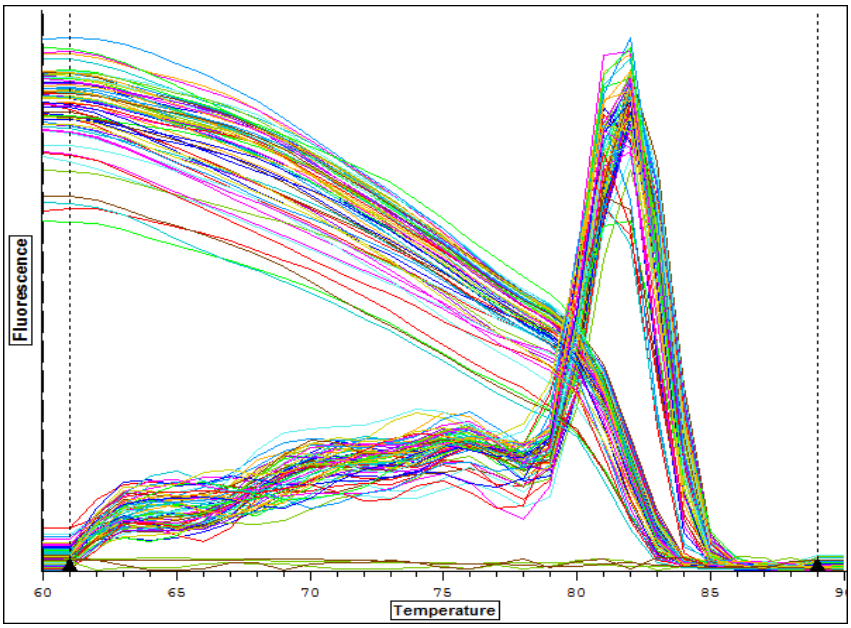

Figure: 10 C Melting curve for Beta actin. The graphical plot of the melting curve was obtained after the PCR, using Beta actin specific primers. The presence of a single peak at 79-80degree C is suggestive of the generation of a specific product during the PCR

GAPDH :

Figures: 11 A,B and C, w the log fluorescence data, standard curve and melting curves respectively for GAPDH. The average efficiency of the PCR for beta actin was found to be 70-80%. The melting curve analysis showed the presence of a single peak at 78-79^{o}C .

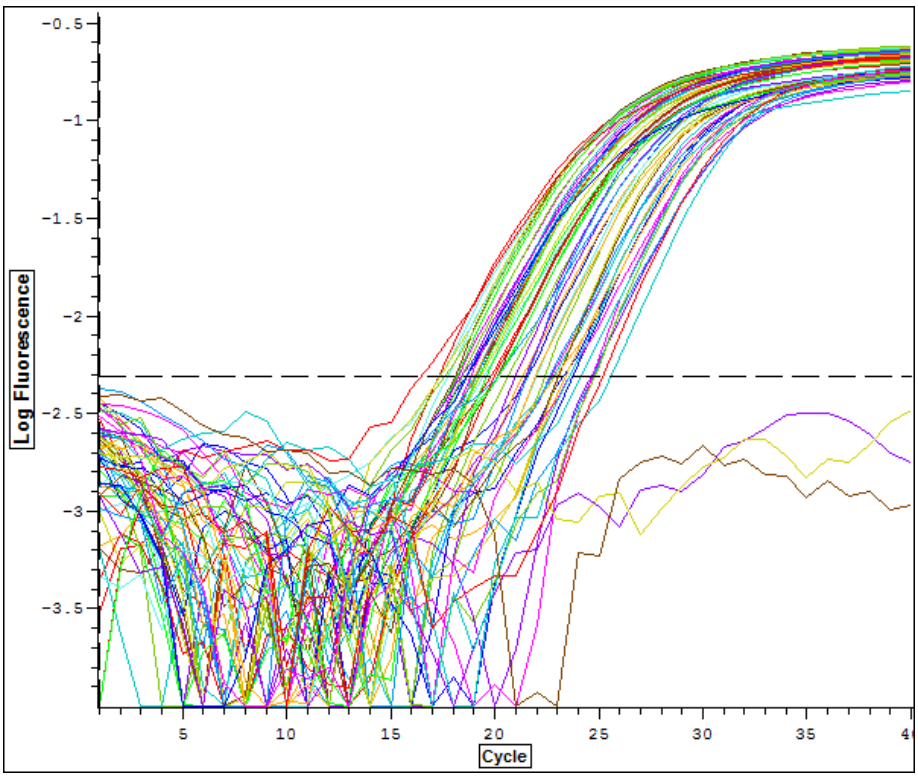

Figure: 11 A. Log fluoresscence data graph for GAPDH. The graph depicts the PCR cycle number on the x-axis and relative log fluorescence units on the y-axis. The dotted line shows the cycle threshold set at a point above baseline fluorescence.

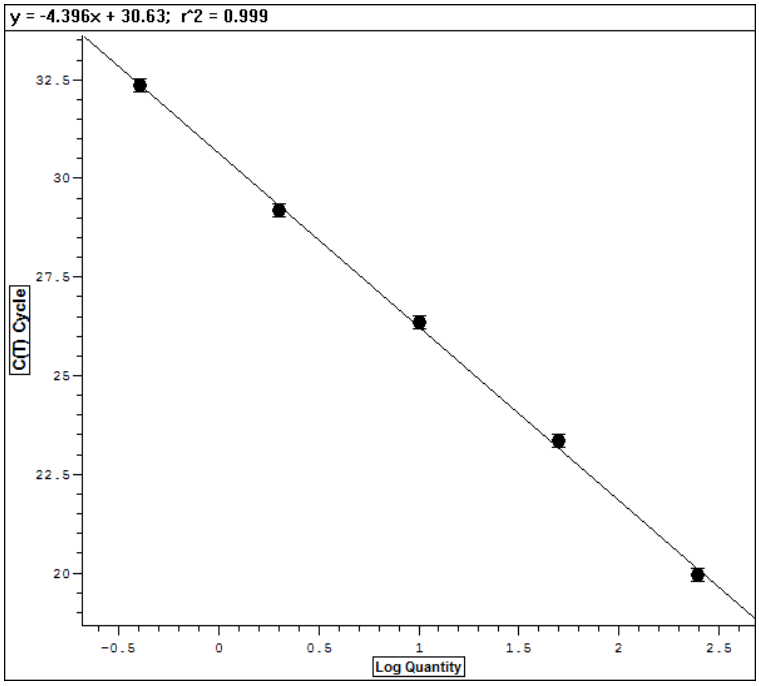

Figure: 11 B Standard curve for GAPDH. The graph depicts log of the quantity of cDNA on the x-axis and cycle threshold value on the y-axis for each of the standard samples used.

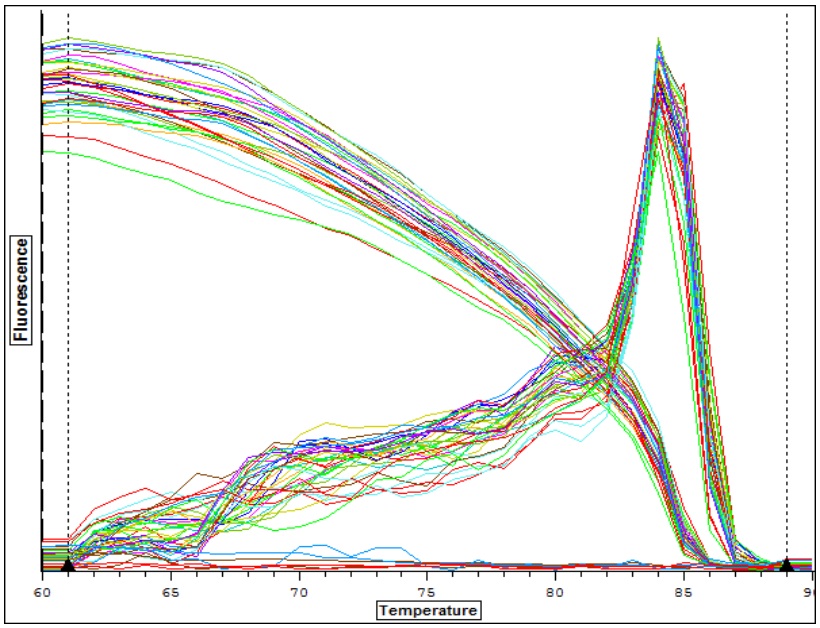

Figure: 11 C Melting curve for GAPDH. The graphical plot of the melting curve was obtained after the PCR, using GAPDH specific primers. The presence of a single peak at 80-85^{o} C is suggestive of the generation of a specific product during the PCR.